

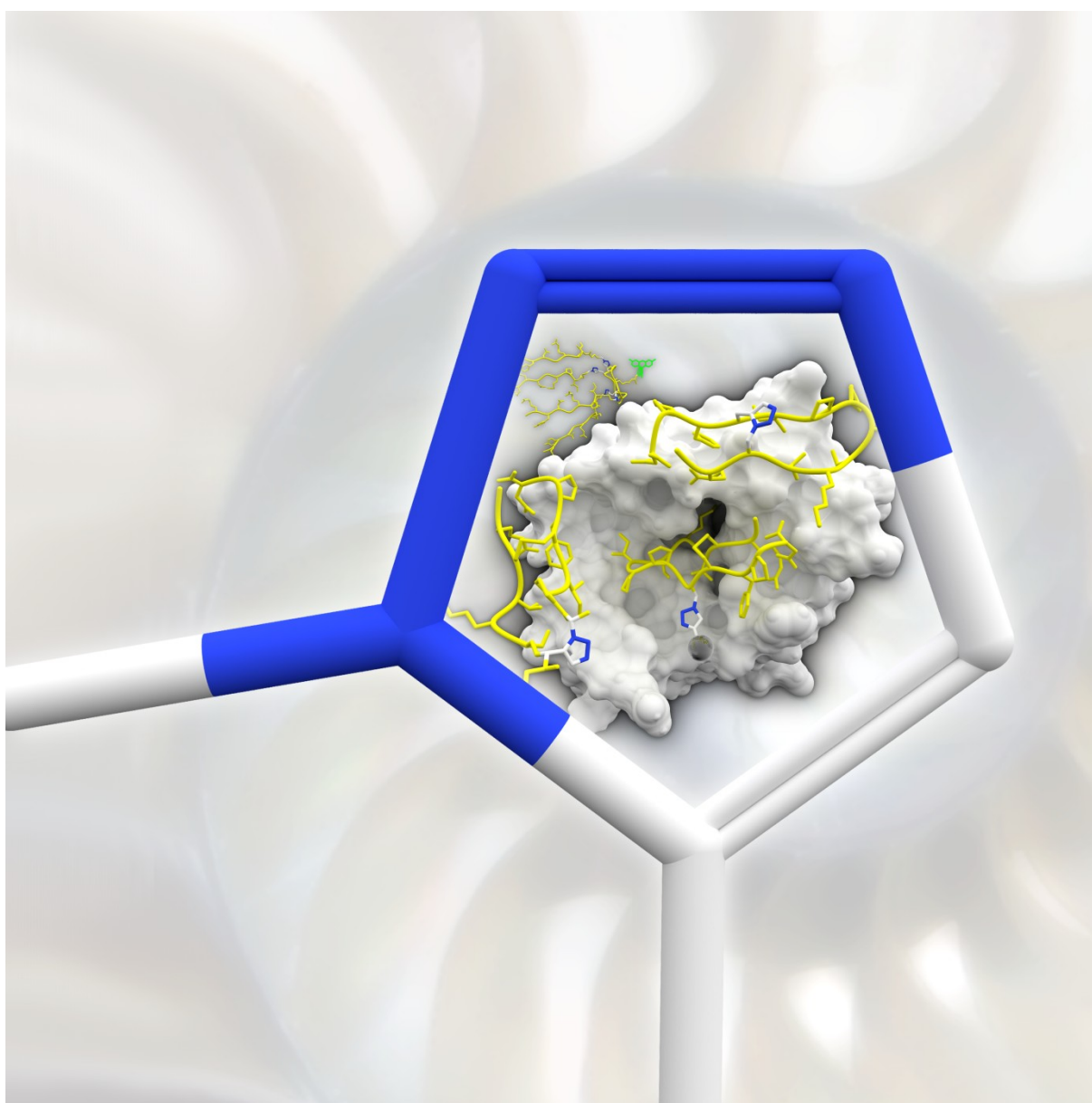
# Disubstituted 1,2,3-Triazoles: A Multitool for Biomolecular Chemistry

Dissertation  
Martin Empting



TECHNISCHE  
UNIVERSITÄT  
DARMSTADT

Clemens-Schöpf-Institut für  
Organische Chemie und Biochemie







# Disubstituted 1,2,3-Triazoles: A Multitool for Biomolecular Chemistry



TECHNISCHE  
UNIVERSITÄT  
DARMSTADT

**Clemens-Schöpf-Institut für  
Organische Chemie und Biochemie**

*Vom Fachbereich Chemie*  
**der Technischen Universität Darmstadt**

**zur Erlangung des akademischen Grades eines  
Doktor-Ingenieurs (Dr.-Ing.)**

**genehmigte  
kumulative Dissertation**

**vorgelegt von**

**Dipl. Ing. Martin Empting  
aus Königs Wusterhausen**

Referent: Prof. Dr. Harald Kolmar  
Korreferenten: Prof. Dr. Gerd Buntkowsky  
Prof. Dr. U. Diederichsen (Universität Göttingen)

Tag der Einreichung: 02. November 2012  
Tag der mündlichen Prüfung: 17. Dezember 2012

Darmstadt 2013

---

Die vorliegende Arbeit wurde unter der Leitung von Herrn Prof. Dr. Harald Kolmar am Clemens Schöpf-Institut für Organische Chemie und Biochemie der Technischen Universität Darmstadt von März 2009 bis November 2012 angefertigt.

---

---

**Teile der vorliegenden Arbeit sind bereits veröffentlicht oder wurden zur Veröffentlichung eingereicht:**

---

1. Heiko Fittler, Olga Avrutina, Bernhard Glotzbach, **Martin Empting\***, & Harald Kolmar\*, Combinatorial Tuning of Peptidic Drug Candidates: High-Affinity Matriptase Inhibitors through Incremental Structure-Guided Optimization. *Submitted September 2012*.
2. **Martin Empting\***, 1,2,3-Triazole: Multifunktionswerkzeuge für die Peptidchemie. *Nachrichten aus der Chemie* (2012/13), *in press*.
3. Olga Avrutina, Heiko Fittler, Bernhard Glotzbach, Harald Kolmar, & **Martin Empting\***, Between Two Worlds: a Comparative Study on In Vitro and In Silico Inhibition of Trypsin and Matriptase by Redox-Stable SFTI-1 Variants at Near Physiological pH. *Org. Biomol. Chem.* (2012), *10*, 7753-7762.
4. Marco Tischler<sup>†</sup>, Daichi Nasu<sup>†</sup>, **Martin Empting<sup>†</sup>**, Stefan Schmelz, Dirk W. Heinz, Philip Rottmann, Harald Kolmar, Gerd Buntkowsky\*, Daniel Tietze\*, & Olga Avrutina\*, Braces for the peptide backbone: Insights into structure-activity relationships of protease inhibitor mimics with locked amide conformations. *Angew. Chem. Int. Ed.* (2012), *51*, 3708-3712.  

See also: Peptid in Ketten: Einblicke in die Struktur-Aktivitäts-Beziehungen von Proteaseinhibitormimetika mit fixierten Amidkonformationen. *Angew. Chem.* (2012), *124*, 3768-3772.
5. **Martin Empting<sup>†</sup>**, Olga Avrutina, Reinhard Meusinger, Sebastian Fabritz, Michael Reinwarth, Markus Biesalski, Stephan Voigt, Gerd Buntkowsky, & Harald Kolmar\*, "Triazole Bridge": Disulfide-Bond Replacement by Ruthenium-Catalyzed Formation of 1,5-Disubstituted 1,2,3-Triazoles. *Angew. Chem. Int. Ed.* (2011), *50*, 5207-5211.  

See also: "Triazolbrücke": ein Disulfidbrückenersatz durch Ruthenium-katalysierte Bildung von 1,5-disubstituierten 1,2,3-Triazolen. *Angew. Chem.* (2011), *123*, 5313-5317.
6. Olga Avrutina<sup>†</sup>, **Martin Empting<sup>†</sup>**, Sebastian Fabritz, Martin Daneschdar, Holm Frauendorf, Ulf Diederichsen, & Harald Kolmar\*, Application of copper(I) catalyzed azide-alkyne [3+2] cycloaddition to the synthesis of template-assembled multivalent peptide conjugates. *Org. Biomol. Chem.* (2009), *7*, 4177-4185.

---

<sup>†</sup>Gemeinsame Erstautorenschaft

\*Korrespondenzautor(en)

---

---

---

## Weitere Publikationen, die im Rahmen dieser Doktorarbeit veröffentlicht wurden:

---

7. Sebastian Fabritz<sup>‡</sup>, Sebastian Hörner<sup>‡</sup>, Doreen Könning, **Martin Empting**, Michael Reinwarth, Christian Dietz, Bernhard Glotzbach, Holm Frauendorf, Harald Kolmar\*, & Olga Avrutina\*, From Pico to Nano: Biofunctionalization of Cube-octameric Silsesquioxanes by Peptides and Miniproteins. *Org. Biomol. Chem.* (2012), 10, 6287-6293.
8. Sebastian Fabritz, Dirk Heyl, Viktor Bagutski, **Martin Empting**, Eckhard Rikowski, Holm Frauendorf, Ildiko Balog, Wolf-Dieter Fessner, Jörg J. Schneider, Olga Avrutina, & Harald Kolmar\*, Towards click bioconjugations on cube-octameric silsesquioxane scaffolds. *Org. Biomol. Chem.* (2010), 8, 2212-2218.

---

## Tagungsbeiträge

---

9. **Martin Empting** (2011), *Kurzvortrag und Poster*, "'Triazole bridge": an adequate synthetic disulfide surrogate?', 10th German Peptide Symposium, Berlin, Germany.
10. **Martin Empting** (2009), *Poster*, 'Application of Copper(I)-Catalyzed Azide-Alkyne [3+2] Cycloaddition to the Synthesis of Template-Assembled Multivalent Peptide Conjugates.', 9th German Peptide Symposium, Göttingen, Germany.

---

<sup>‡</sup>Gemeinsame Erstautorenschaft

\*Korrespondenzautor(en)

---

---

---

## Zusammenfassung

---

Der zentrale chemische Baustein der vorliegenden kumulativen Dissertation ist der 1,2,3-Triazol und dessen unterschiedliche Anwendungsmöglichkeiten in der Peptidchemie. Die hier präsentierten Studien können grob in zwei Teilgebiete eingeordnet werden: Gerüstmolekül-basierte Multimerisierung peptidischer Liganden durch Kupfer(I)-katalysierte Azid-Alkin Cycloaddition (CuAAC) und der Einsatz von 1,2,3-Triazolen als nichtnatürliche Strukturbausteine von Peptidomimetika. Der zweite Themenkomplex umfasst sowohl den biomimetischen Ersatz von Peptidrückgratelementen als auch die Substitution von makrozyklischen und linearen Seitenkettenmotiven. Hierfür kam zusätzlich zu der genannten CuAAC-Chemie auch eine Ruthenium(II)-katalysierte Variante (RuAAC) zum Einsatz. Die genannten synthetischen Methoden wurden erfolgreich für die Synthese verschiedener Triazol-haltiger peptidischer Substanzen angewendet und hinsichtlich der Durchführung in Lösung vor allem aber auch an der festen Phase vorangebracht.

Experimente zur Konstruktion wohldefinierter multivalenter Biokonjugate wurden mit fünf unterschiedlichen Peptidliganden und zwei regioselektiv adressierbaren funktionalisierten Plattformmolekülen – so genannten RAFT (*regioselectively addressable functionalized template*) – durchgeführt. Die CuAAC-Kupplung gelang mit stöchiometrischer Konversion der Edukte zu den gewünschten verzweigten Peptidoligomeren und lieferte moderate bis gute Ausbeuten. Eines der synthetisierten Konstrukte beinhaltete vier Kopien einer „RGD“ Sequenz und zusätzlich einen Fluoreszenzmarker. Die genannten bioaktiven Peptidliganden können den GPIIb/IIIa Rezeptor binden und dadurch die Aggregation von Blutplättchen inhibieren. Somit könnte dieses Gerüstmolekül-basierte multivalente Konstrukt für Fluoreszenzmikroskopie von GPIIb/IIIa-exprimierenden Zellen geeignet sein. Allerdings wurden keine detaillierten biologischen Untersuchungen mit diesem Biokonjugat durchgeführt, da ohnehin nur mit einem sehr geringen therapeutischen bzw. diagnostischen Nutzen zu rechnen ist. Desweiteren bleibt anzumerken, dass bis zum heutigen Zeitpunkt fortschrittlichere Biokonjugationsmethoden entwickelt worden sind, die nicht der Übergangsmetallkatalyse bedürfen. Dennoch stellt die beschriebene Studie eine Blaupause für die erfolgreiche Synthese heteromultivalenter Peptidkonjugate dar. Die berichtete Methode wird unter anderem weiterhin in der Arbeitsgruppe von Prof. Kolmar in verschiedenen Projekten zum Aufbau Gerüstmolekül-basierter Konstrukte mit anderen Peptidliganden verwendet, die therapeutisches oder diagnostisches Potential besitzen.

Eine weitere sehr vielversprechende Anwendung von 1,2,3-Triazolen beruht auf den besonderen physikochemischen Eigenschaften dieser stickstoffhaltigen aromatischen Heterozyklen. Sie können in Wasserstoffbrückenbindungen sowohl als Akzeptoren als auch Donatoren wirken, sind polar und besitzen eine gute Wasserlöslichkeit. Diese Faktoren und die Möglichkeit, selektiv 1,4- oder 1,5-disubstituierte 1,2,3-Triazole durch die Wahl des Übergangsmetallkatalysators der verwendeten Azid-Alkin Zykoaddition auszubauen, machen diese Baueinheit zu einem geeigneten nichtnatürlichen Ersatz von Amidbindungen. Es ist somit möglich, das Peptidrückgrat durch ein Hydrolyse-resistentes Biomimetikum zu ersetzen und darüber hinaus entweder in der *trans*- oder der *cis*-Konformation einzufrieren. Dieses Konzept wurde für das Design und die Synthese von peptidomimetischen Varianten des monozyklischen *sunflower trypsin inhibitor*-1 (SFTI-1[1,14]) herangezogen. Zu diesem Zweck wurde eine Strategie verwendet, welche Mikrowellen-unterstützte Fmoc-basierte Peptidfestphasensynthese (Fmoc-SPPS) mit CuAAC- oder RuAAC-Kupplungen an der festen Phase kombinierte. Die gewünschten Verbindungen konnten so in ausreichenden Mengen synthetisiert werden, um damit sowohl strukturelle Untersuchungen als auch *in vitro* Inhibitionstests durchzuführen. Die gelösten Kristallstrukturen von Trypsin-Inhibitor-Komplexen durch Röntgenbeugungsexperimente beweisen die erfolgreiche Synthese der funktionalen Peptidomimetika mit nichtnatürlichen Rückgratelementen. Desweiteren konnte

---

gezeigt werden, dass mit diesem Ansatz auch die der nativen Struktur entgegenstehenden Amidkonformationen erzwungen werden können. Somit kann zum Beispiel an einer ausgewählten Stelle in der Aminosäuresequenz ein *cis*-Mimetikum installiert werden. Dieses ist insofern bemerkenswert, als *cis*-Peptidbindungen sehr selten in der Natur zu finden sind und meist nur vor Prolinresten auftreten. Diese Technik ermöglicht es demnach, neue peptidische Strukturen zu erzeugen, die mit dem kanonischen Repertoire nicht erreichbar wären. Wie erwartet führte das „Einfrieren“ einer dem natürlichen Rückgrat gegensätzlichen Amidkonformation beim SFTI-1 zu einer signifikant verminderten Bioaktivität. Schließlich gibt einem diese Methode die Möglichkeit an die Hand, bestimmte Peptidsegmente in einem Molekül gegen enzymatische Degradation zu schützen, was zu einer verbesserten *in vivo* Stabilität führen sollte.

Zwei weitere Studien hatten zum Inhalt, den Effekt von 1,2,3-Triazol-basierten Disulfidaustauschen auf die Bioaktivität von SFTI-1 [1,14] zu untersuchen. Zu diesem Zweck wurden vier Seitenkettenmakrozyklisierungsmotive unterschiedlicher Länge und Form anstatt des natürlichen Cystins mittels kommerziell erhältlicher Bausteine installiert. Wieder kam einer Kombination aus Fmoc-SPPS und CuAAC oder RuACC an der festen Phase zum Einsatz. Die intramolekulare Reaktion ergab die gewünschten Triazole-verbrückten peptidomimetischen Verbindungen mit einem 1,4- oder einem 1,5-Disubstitutionsmuster. Die reinen Produkte wurden sowohl mittels Infrarot- und 2D-Kernresonanzspektroskopie als auch durch Massenspektrometrie (Elektrospray-Ionisation) charakterisiert. *In vitro* Inhibitionsuntersuchungen zeigten, dass die Substitutionsart des Makrozyklisierungsmotivs einen dramatischen Einfluss auf die Bioaktivität hatte. Interessanterweise waren die Varianten mit einem 1,5-Muster potente Trypsininhibitoren und besaßen Substrat-unabhängige Inhibitionskonstanten  $K_i$  im einstellig nanomolaren bis subnanomolaren Bereich. Die 1,4-Gegenstücke hingegen zeigten eine signifikant verminderte Bioaktivität im Vergleich zum Wildtyp. Die Länge der verbrückenden Einheit zwischen dem Peptidrückgrat und dem Triazolebaustein hatte einen nicht so entscheidenden Einfluss. Diese *in vitro*-Ergebnisse wurden durch molekulare Modellierung bestätigt, da in diesen *in silico* Experimenten eine bessere Übereinstimmung mit der Struktur des nativen Peptids für das RuAAC-Produkt beobachtet wurde. Somit wird die Verwendung von 1,5-disubstituierten 1,2,3-Triazolen als Disulfidbrückenersatz empfohlen. Allerdings sollte die geeignete Länge des Makrozyklisierungsmotivs für jeden biologischen Kontext neu evaluiert werden.

Sowohl die vier SFTI-1-Derivate mit „Triazolbrücken“ als auch die beiden nativen mono- und bityklischen Varianten wurden auf ihre Aktivität gegen die pharmazeutisch relevante Protease Matriptase getestet. Überraschenderweise wurde für alle sechs genannten Peptide eine dramatisch schlechtere Affinität als gegen Trypsin gemessen. Diese Beobachtung war unerwartet, da ein negatives elektrostatisches Oberflächenpotential am aktiven Zentrum von Matriptase Anlass für ausgeprägte attraktive Wechselwirkungen zwischen dem positiv geladenen SFTI-1-Gerüst und dem Enzym geben sollte. Um dieses kontraintuitive Ergebnis weiter zu untersuchen, wurde ein *in silico* Experiment mit Hilfe der Software YASARA *structure* und einem angepassten AMBER-basierten Kraftfeld in zwei Schritten durchgeführt. Zuerst, wurde eine Molekulardynamik Simulation durchgeführt. Danach wurden 100 Einzelstrukturen aus den erhaltenen Trajektorien für ein lokales Docking Experiment extrahiert. Durch den zugrundeliegenden AUTODOCK-Algorithmus konnten so die freien Bindungsenergien für alle Inhibitor-Enzym-Komplexe berechnet werden. In der Tat deuteten die *in silico* Affinitäten auf eine stärkere Interaktion zwischen dem SFTI-1-Gerüst und Matriptase im Vergleich zur Bindung an Trypsin hin. Allerdings wurde im Vergleich zu Trypsin eine erheblich reduzierte Rate, die obligatorische canonische Orientierung im aktiven Zentrum des Enzyms zu treffen, bei den Docking Experimenten gegen Matriptase ermittelt. Eine Normalisierung der berechneten freien Bindungsenergien mit Hilfe dieses Hitfaktors gab die tatsächlich gemessenen Affinitäten aus den *in vitro* Assays relativ gut wieder. Eine

---

anschließende Strukturanalyse der simulierten Trajektorien und die Berechnung der Wurzel der mittleren quadratischen Abweichung (*root-mean-square deviation*, RMSD) einzelner Segmente der jeweiligen SFTI-1-Varianten gaben Anlass zu der Vermutung, dass negative entropische Beiträge, die ihren Ursprung in den terminalen Regionen der Peptide haben, die generell reduzierte Bioaktivität gegen Matriptase verursachen.

Die Ergebnisse der *in silico* Untersuchungen lieferten wertvolle Hinweise für mögliche Strategien zur Optimierung des Inhibitors gegen die pharmazeutisch relevante Serinprotease, welche in einer weiteren Studie untersucht wurden. Es wurde beobachtet, dass die offenkettige Variante von SFTI-1 (SFTI-1[1,14]) eine leichte Präferenz in ihrer Anti-Matriptase-Wirkung gegen über dem bizyklischen Wildtyp zeigte. Somit war dieses monozyklische Peptid ein geeigneter Startpunkt für die weiteren Versuche. Struktur-geleitete Überlegungen führten zu der Identifikation von drei Positionen innerhalb der Aminosäuresequenz, die potentiell für inkrementelle verteilhafte Modifikationen geeignet waren. Zwei dieser Reste wurden jeweils mit Azid-funktionalisierten nichtnatürlichen Baueinheiten ausgestattet, um eine divergente Synthese mittels eines kombinatorischen Ansatzes zu ermöglichen. Zusätzlich wurden auch Substitutionen mit ausgewählten kanonischen Aminosäuren durchgeführt. Zusammen ermöglichte dies den raschen Aufbau einer kleinen Molekülbibliothek mit 22 Peptiden, die sich durch jeweils eine einzelne andere Seitenkettenmodifikation unterschieden. Matriptaseinhibitionstests wiesen auf mehrere vorteilhafte Seitenkettenaustausche hin. Diejenigen Modifikationen mit den ausgeprägtesten Verbesserungen wurden in einer Verbindung vereint, welche eine  $K_i$  im einstellig nanomolaren Bereich besaß. Dieses Peptid wurde *SFTI-1-derived matriptase inhibitor-1* (SDMI-1) genannt und beinhaltete ausschließlich Standardaminosäuren. Dennoch wurden auch signifikante Affinitätsverbesserungen für einzelne Triazol-haltige Verbindungen gegen Matriptase beobachtet. Dies zeigte die Nützlichkeit dieses Ansatzes einer „Click-Bibliothek“ für die rasche Sondierung diverser Seitenkettenfunktionalitäten hinsichtlich bestimmter gewünschter Eigenschaften.

Wie bereits erwähnt könnte ein möglicher nachteilbehafteter entropischer Beitrag durch die Sekundärschleife von SFTI-1 die Bindung an Matriptase beeinflussen haben. Deshalb wurden die zwei C-terminalen Reste von SDMI-1 in einer weiteren Variante trunziert. Dieses Dodecapeptid wurde SDMI-2 genannt und besaß eine vergleichbare Aktivität wie SDMI-1. Darüber hinaus wurde ein verbessertes Selektivitätsprofil für das kürzere Peptid festgestellt, da es eine sechsfach schlechtere Aktivität gegen Trypsin als gegen Matriptase zeigte. Die entwickelten Verbindungen könnten wertvolle Peptidliganden für weitere Biokonjugationsexperimente darstellen und werden derzeit auf eine mögliche Patentanmeldung geprüft. So zum Beispiel würde die direkte Ankopplung von Radionukliden, welche für Positronenemissions- oder Einzelphotonen-Emissionscomputertomographie (*positron emission tomography* – PET, *single-photon emission computed tomography* – SPECT) geeignet sind, evtl. eine Anwendung als diagnostische Werkzeuge für *in vivo* Bildgebung ermöglichen. Desweiteren ist das Potential für weitere Affinitäts- und Selektivitätsverbesserungen in Bezug auf Matriptase oder auch andere Proteasen von pharmazeutischer Relevanz noch nicht erschöpft.

Die in dieser kumulativen Dissertation vorgestellten und durch Fachleute begutachteten Artikel tragen dazu bei einen vielseitigen Werkzeugkasten für das Design und die Synthese von peptidomimetischen Verbindungen mit Hilfe von disubstituierten 1,2,3-Triazolen aufzubauen. Die vorgestellten Ergebnisse sind von Interesse für die biomolekulare Chemie im Allgemeinen und die Peptidchemie im Speziellen sein.





---

---

## Danksagung

---

Den folgenden Personen möchte ich meinen aufrichtigen Dank aussprechen:

Meinem Doktorvater, **Prof. Dr. Harald Kolmar**, möchte ich für die vielen Dinge danken, die er mir im Hinblick auf meine Doktorarbeit und darüberhinaus ermöglicht hat. So durfte ich interessante Themen bearbeiten und hatte dennoch genügend Freiräume um eigene Ideen umzusetzen. Ich habe dies immer als ein Privileg angesehen, welches mich bei meiner Arbeit motiviert und gefördert hat. Vielen Dank dafür!

**Dr. Olga Avrutina**, möchte ich für ihre Geduld und Sorgfalt danken, mit der sie stets das Potential der Chemikerrasselbande in produktive Bahnen kanalisiert. Durch Dich habe ich sehr viel über Peptidchemie und wissenschaftliches Schreiben gelernt und bin motiviert diese wertvollen Hinweise auch weiterhin umzusetzen.

Meiner Lebensgefährtin und Ehefrau *in spe*, **Dr. Pia Ockelmann**, bin ich zu besonderem Dank verpflichtet. Du hast mir auch in schwierigen Phasen mit Deiner Liebe und Deinem Zuspruch immer den Rücken gestärkt. Durch Dich kenne ich was die wahre Bedeutung von Loyalität und Rückhalt ist. Ich konnte mehrfach beobachten, dass dies nicht selbstverständlich ist, und bin so glücklich, dass es Dich gibt!

Mit absoluter Sicherheit kann ich sagen, dass diese Dissertation niemals ohne meine Eltern, **Renate und Thomas Empting**, möglich gewesen wäre! Ihr habt mein Interesse an der Chemie gefördert, mir das Studium ermöglicht, mich stets ohne zu viel Kontrolle begleitet und somit den Weg geebnet, der hierher geführt hat. Ich hoffe, dass ich die guten Voraussetzungen, die Ihr mir in den Schoß gelegt habt, auch zu eurer Zufriedenheit umsetzen konnte.

Weiterhin möchte ich meiner Schwiegermutter *in spe*, **Inge André-Ockelmann**, als auch meinem Schwager *in spe*, **Alexander Ockelmann**, für ihr Verständnis und nachhaltige Hilfe Tag ein Tag aus herzlich danken. Auch meinem Bruder **Christian Empting** und seiner frisch gebackenen kleinen Familie möchte ich danken, da Blut einfach dicker als Wasser ist. Mein Leben wird durch euch alle bereichert und wäre einfach nicht dasselbe ohne euch.

Was wäre die Laborzeit ohne **Björn Steinmann** und **Stefan Zielonka** gewesen? Ich möchte es nicht herausfinden. Sicherlich werden sich jetzt unsere Wege in gewisserweise trennen. Umso mehr denke ich mit Freude an die lustigen Jahre zurück. Ich hoffe sehr, wir werden uns nicht aus den Augen verlieren! Oder nicht?

**Heiko Fittler** und **Daichi Nasu** möchte ich für das Engagement und die ausgesprochen gute Zusammenarbeit in den gemeinsamen Projekten danken, in denen ihr einen großen Teil beigetragen habt. Tollerweise blieb dabei der Spass auch nicht auf der Strecke.

Dem **Rest des Arbeitskreises** von Prof. Kolmar möchte ich für die vielen Hilfen und das allseitige Miteinander danken.

Herrn **Prof. Dr. Buntkowsky** danke ich für die Übernahme des Korreferats und seiner stets freundlichen und überaus hilfsbereiten Art.

**Marco Körner** (ehemals Tischler) und **Daniel Tietze** aus dem Arbeitskreis Buntkowsky möchte ich ebenfalls für die unkomplizierte und angenehme Zusammenarbeit danken.



---

**Table of Contents**

---

<b>1</b>	<b>Introduction</b>	<b>1</b>
1.1	1,2,3-Triazoles and the Azide-Alkyne 1,3-Dipolar Cycloaddition (AAC)	3
1.1.1	Copper(I)-Catalyzed AAC – the Archetype of “Click” Reactions	4
1.1.2	Ruthenium(II)-Catalyzed AAC	5
1.2	Triazoles as Versatile Tools for Selective Bioconjugation	7
1.2.1	Complementary Selective Bioconjugation Reactions	7
1.2.2	Direct Linkage of Functional Units	9
1.2.3	The Scaffold-Based Approach to Molecular Complexity	11
1.3	Molecular Prosthesis: Triazoles as Artificial Structural Elements	15
1.3.1	The Ideal Test System: SFTI-1 – a Canonical Inhibitor of Trypsin-like Serine Proteases	15
1.3.2	Locked <i>trans</i> - and <i>cis</i> -Amide Surrogates	17
1.3.3	The “Triazole Bridge” – a Disulfide Replacement	19
1.3.4	Triazoles as an Interface for Side Chain Variability	21
1.4	Aims and Scope	23
<b>2</b>	<b>Cumulative Part</b>	<b>25</b>
2.1	Heteromultivalent Scaffold-based Peptide Tetramers <i>via</i> CuAAC	29
2.2	Locked <i>trans</i> - and <i>cis</i> -Amide Surrogates within the SFTI-1 Backbone	39
2.3	Disulfide Replacement <i>via</i> 1,5-disubstituted 1,2,3-Triazoles	45
2.4	<i>In vitro</i> & <i>in silico</i> Studies of Matriptase Inhibition by SFTI-1 Variants	51
2.5	Combinatorial “Click Libraries” for the Optimization of Matriptase Inhibition	63
<b>3</b>	<b>Summary</b>	<b>75</b>
<b>4</b>	<b>References</b>	<b>79</b>
<b>5</b>	<b>Abbreviations</b>	<b>87</b>
<b>6</b>	<b>Supporting Information</b>	<b>91</b>
6.1	Supporting Information for Chapter 2.1	93
6.1.1	RP-HPLC traces for scaffolds and peptide ligands	93
6.1.2	RP-HPLC Traces for the Macrocyclization of Cyclic Decapeptide Scaffolds	106
6.1.3	ESI-MS Spectra of Bioconjugates	110
6.1.4	GFC traces of Bioconjugates	116
6.2	Supporting Information for Chapter 2.2	125
6.2.1	Synthetic Procedures	125
6.2.2	Trypsin Inhibition Assays	129
6.2.3	3. Crystallography	131
6.2.4	<i>In silico</i> methods	134
6.2.5	Analytical Data	135
6.2.6	Supporting References	144
6.3	Supporting Information for Chapter 2.3	145
6.3.1	1. 3D Modeling and Calculations	145
6.3.2	Experimental Section	146
6.3.3	Plotted Kinetic Data	151
6.3.4	RP-HPLC	154

6.3.5	ESI-MS	160
6.3.6	IR Spectra	170
6.3.7	NMR Spectra	173
6.4	Supporting Information for Chapter 2.4	183
6.4.1	Experimental Procedures	183
6.4.2	In Silico Methods	185
6.4.3	Supporting Figures	187
6.4.4	Supporting Tables	190
6.5	Supporting Information for Chapter 2.5	195
6.5.1	ESI-MS	195
6.5.2	RP-HPLC	196
6.5.3	Plotted Kinetic Data	201

## 1 Introduction

The divine proportion is often claimed to be a universal design principle ubiquitously found in Nature. It is believed to entail both function and form (beauty).<sup>[1]</sup> In its simplest representation this “golden ratio”, also referred to as  $\phi$  (phi), describes the sectioning of one length “a+b” into two segments “a” and “b” fulfilling one basic requirement:  $\frac{a}{b} = \frac{a+b}{a} \equiv \phi$  (Figure 1).<sup>[1]</sup> When solved, this equation yields  $\phi$  as the irrational number “1.618...”; a proportionality constant that is also the limit of consecutive quotients of the famous Fibonacci series. Certain geometric structures like the golden tri- and rectangle contain  $\phi$  as the ratio of their edges and are considered as aesthetic and harmonic shapes.

These basic forms appear in other more complex structural units. The pentagon, for example, is one of the regular polygons which form the faces of platonic bodies. It intrinsically contains  $\phi$  as it can be sectioned into golden triangles by connecting opposite corners. Fascinatingly, architectures derived from these mathematical shapes have been described to be excessively utilized by Nature.<sup>[1]</sup> Designs like the blossom of the sunflower or the segmentation of the human body are believed to contain  $\phi$  and the Fibonacci series in one way or another (Figure 2). They are attributed with an intrinsic beauty and have inspired artists and scientists alike.<sup>[2-4]</sup> Observation of the divine ratio has even been

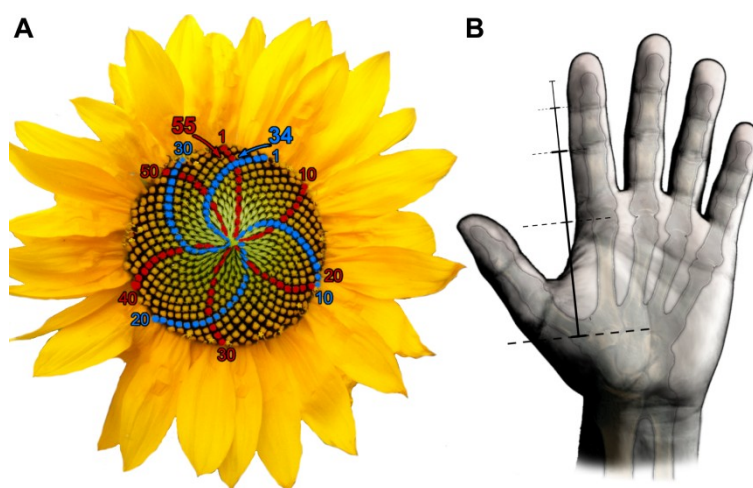


Figure 2. (A) The Fibonacci numbers found in the blossom of a sunflower: the seeds are arranged in 34 (blue) or 55 (red) logarithmic spirals. (B) Sectioning of the human hand by the golden ratio.

1,2,3-triazole: **One** planar  $\pi$ -system is built through the connection of **two** carbons and **three** nitrogens forming a **five**-membered ring (pentagon). The presented work will provide an overview on applications of this remarkably versatile structural unit in peptide chemistry that,

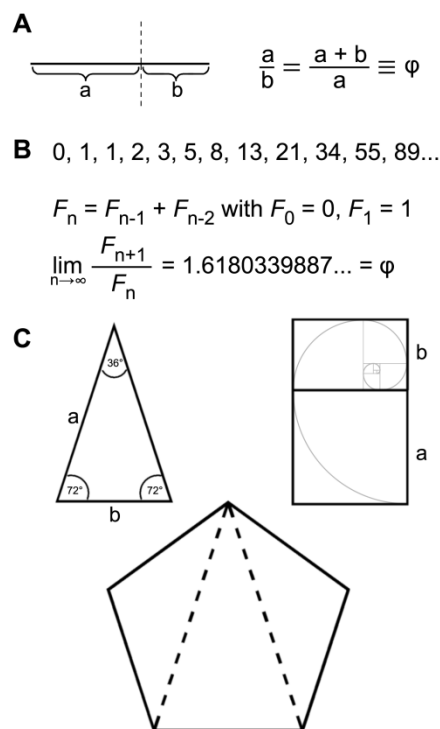


Figure 1. (A) Sectioning of a length (a+b) by the golden ratio. (B) The Fibonacci numbers, definition of the Fibonacci sequence, and the limit of consecutive quotients -  $\phi$ . (C) A golden tri- and rectangle as well as a regular pentagon with imprinted golden triangle.

reported on the atomic and molecular levels.<sup>[2-4]</sup> An article published in the renowned journal “Science” describes the occurrence of  $\phi$  upon certain quantum phase transitions in cobalt niobate.<sup>[2]</sup> Other scientific publications bear evidence of relations between  $\phi$  and the human genome.<sup>[3-4]</sup>

Whether this concept of the ideal proportion is truly a universal design principle or not, will not be further discussed here. Nevertheless, the Fibonacci numbers and  $\phi$  can be found within the central molecular building block relevant for this thesis – the

at least in my opinion, combines function and form.



Figure 3. Illustration by M. Empting.

*"I suspect that the generative faculty in seeds is formed in the likeness of this self-propagating proportion (the Fibonacci series) and that the pentagon, which is the genuine flag of the generative faculty of seeds, is displayed in the flower"*

– Johannes Kepler

## 1.1 1,2,3-Triazoles and the Azide-Alkyne 1,3-Dipolar Cycloaddition (AAC)

Nitrogen-containing aromatic pentacycles are fundamental molecular structures in organic synthesis and related disciplines, among them bioorganic, medicinal, or organometallic chemistry.<sup>[5-12]</sup>

Derivatives of pyrrole and imidazole are frequently found in natural products like indoles, purines, and other alkaloids, as well as heme groups or the side chains of the amino acids histidine and tryptophan.<sup>[13-17]</sup>

Pyrazoles, triazoles, and tetrazoles are considerably less abundant in nature. Nevertheless, they constitute integral synthetic structural motifs for the generation of functional moieties and molecules like coordinating ligands or pharmacophores.<sup>[18-21]</sup> A significant impact on organic chemistry in general can be ascribed to 1,2,3-triazoles. Since the establishment of the “click chemistry” concept by Sharpless and coworkers in 2001,<sup>[22]</sup> this compound class is gaining more and more popularity. The constantly increasing interest is essentially related to the success of one type of reaction: the azid-alkyne 1,3-dipolar cycloaddition (AAC, Figure 5).<sup>[20, 23-25]</sup>

Put in a nutshell, the AAC refers to the reaction of an azide with an alkyne under formation of a 1,2,3-triazole. Its basic form, which proceeds under thermal activation and without regio control, was initially described in detail by Rolf Huisgen.<sup>[26-27]</sup> However, a number of cognate reactions have been reported to date eliminating the necessity of elevated temperatures and allowing for the selective synthesis of 1,4- or 1,5-disubstituted 1,2,3-triazoles, respectively

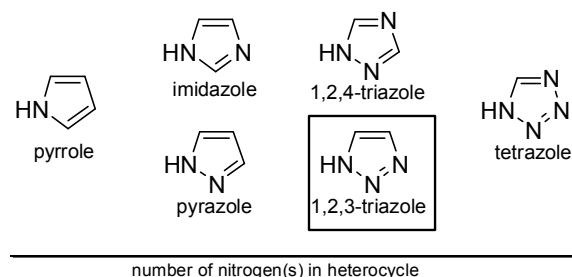


Figure 4. Series of nitrogen-containing pentagonal heterocycles sorted according to the number of nitrogens within the ring.

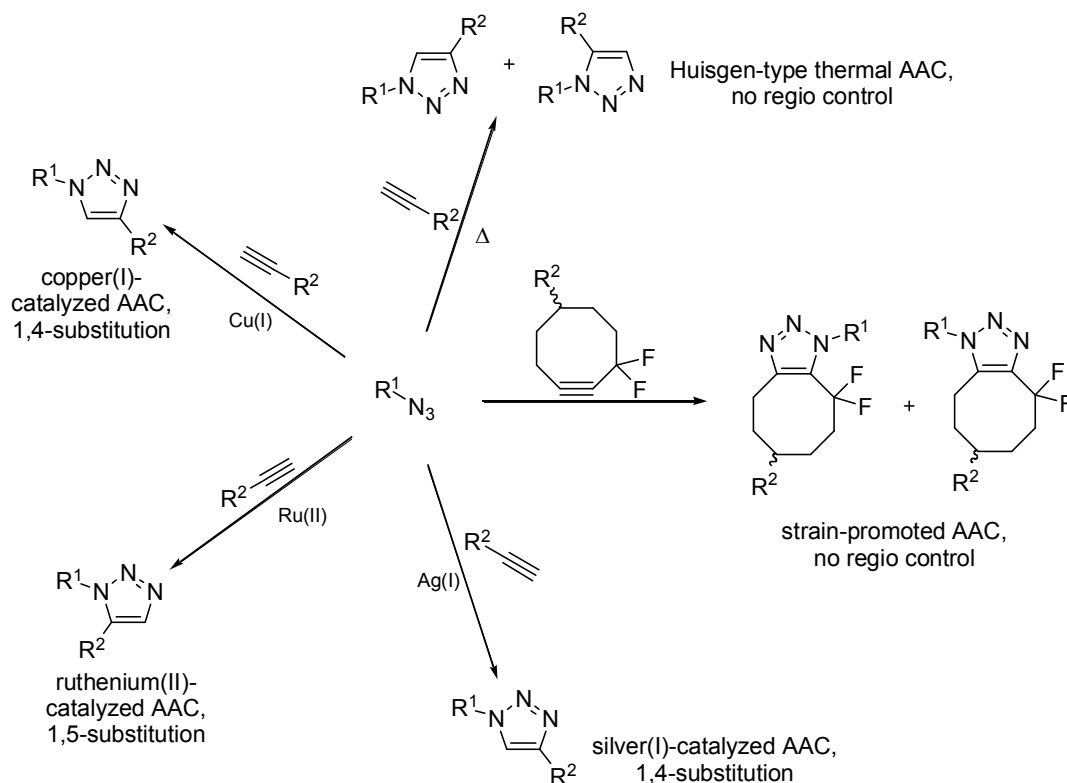


Figure 5. Schematic depiction of common azide-alkyne 1,3-dipolar cycloadditions (AAC). The name of each reaction type and the substitution pattern of the expected product(s) are given.

(Figure 5). The copper(I)-catalyzed (CuAAC), ruthenium(II)-catalyzed (RuAAC), silver(I)-catalyzed (AgAAC), and strain-promoted (SPAAC) variants possess significantly improved reaction rates at room temperature compared to the Huisgen-type thermal AAC through activation of the alkyne component.<sup>[24, 28-31]</sup>

The work presented in this thesis essentially relies on two of the addressed reaction types: the CuAAC and the RuAAC. Thus, they will be discussed in detail in the following sections.

---

### 1.1.1 Copper(I)-Catalyzed AAC – the Archetype of “Click” Reactions

---

The chemical modification of highly functionalized compounds such as peptides or carbohydrates usually meets two main problems: selectivity and reactivity. Due to the high abundance of nucleophiles like amine, alcohol, or thiol groups as well as the sensitivity of biomolecules towards harsh environment, a selective chemical modification procedure must fulfill several key features in order to generate the desired products in a controllable fashion. The reaction should proceed smoothly in aqueous media under mild conditions, give high yields, result in no or at least inoffensive side products, and be chemo- as well as stereoselective. Ideally, reaction partners can be used without protecting groups. These requirements are typically unmet by the standard repertoire of classical organic synthesis relying on carbonyl chemistry and nucleophile/electrophile reactivity.<sup>[32]</sup>

One of the most successful endeavors to address the problem of biocompatibility in a systematic way is certainly the aforementioned concept of “click chemistry.”<sup>[22]</sup> In the course of this doctrine, the CuAAC emerged as the archetype of this type of reactions.<sup>[33]</sup> Indeed, it were the working groups of Meldal and Sharpless who discovered (at the same time and independently) that azide-alkyne 1,3-dipolar cycloadditions are significantly accelerated by copper(I) species.<sup>[28-29]</sup> Additionally, it was found that only the 1,4-disubstituted regioisomer of the 1,2,3-triazole is formed, whereas under Huisgen conditions a product mixture is generated (Figure 5). Finally, a perfect atom economy is maintained upon conversion of azides and alkynes to 1,2,3-triazoles as all atoms of the starting materials are conserved within the product(s). This feature accounts also for the other AAC types.

The mechanism of copper(I)-catalysis, however, is not fully elucidated to date. Initial studies based on DFT calculations proposed a straight-forward catalytic cycle involving only one copper center.<sup>[34]</sup> But recent publications hint towards a more complex behavior of the copper(I) catalyst. Kinetic studies demonstrated a second order dependence of the CuAAC on the concentration of copper catalyst under ligand-free conditions.<sup>[35-36]</sup> Additionally, depending on the experimental setup upon addition of rate-accelerating ligands or bases, the kinetic behavior of the reaction varied considerably.<sup>[37-39]</sup> Thus, the presence of either two separate copper centers, binuclear species or higher order aggregates have been proposed to be involved in some point of the catalytic cycle. However, it is generally accepted that formation of a copper acetylide intermediate is the key step in the beginning of this reaction that is responsible for the intrinsic regioselectivity of the CuAAC, ultimately leading to 1,4-disubstituted 1,2,3-triazoles.<sup>[34]</sup> Additionally, the second metal center involved is proposed to function as an auxiliary activator of the copper acetylide complex through  $\pi$ -coordination of the alkyne triple bond.<sup>[31]</sup> A simplified reaction mechanism is depicted in Figure 6.

Since 2002, a considerable number of articles has been published covering applications of the CuAAC in all areas of organic chemistry demonstrating the impressive scope of this reaction.<sup>[36]</sup> Nevertheless, one significant restriction of the CuAAC is caused by the catalyst itself. Copper is a cytotoxic agent, which hampers the application of this chemistry in living systems.<sup>[40]</sup> There are several methods known for the preparation of the copper(I) species. One of the most commonly used strategies is the *in situ* generation from copper(II) salts like CuSO<sub>4</sub> through reduction (e.g. with sodium ascorbate).<sup>[36]</sup> However, removing residual copper species is a challenging task. Another restriction of the CuAAC is that it only proceeds with



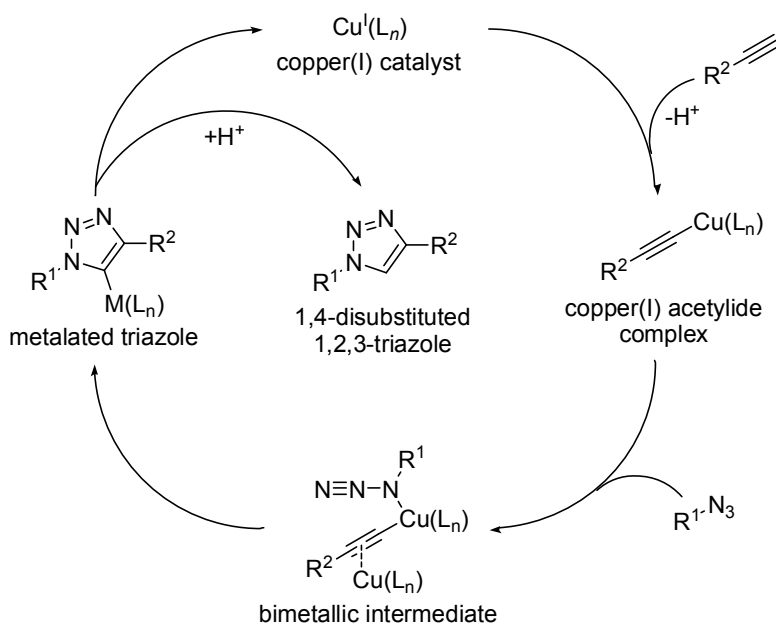


Figure 6. Generalized reaction mechanism of the CuAAC.

chemical strategies.<sup>[43-44]</sup>

Recently, it has been shown that certain silver(I) complexes catalyze the azide-alkyne cycloaddition very similar to copper(I) species with respect to the proposed reaction mechanism.<sup>[31]</sup> Thus, 1,4-disubstituted 1,2,3-triazoles are also selectively generated *via* the so-called AgAAC (Figure 5). Additionally, recent advances in the design of novel biocompatible ligands for the CuAAC reaction may allow for the *in vivo* application of certain complexed copper(I) species.<sup>[45]</sup> This would significantly improve the scope of this bioconjugation technique and eliminate one of its main restrictions. In the future, these novel strategies and other catalyst formulations might enable to circumvent the usage of toxic copper species retaining the regioselectivity.<sup>[31, 40]</sup>

### 1.1.2 Ruthenium(II)-Catalyzed AAC

While copper(I)- and silver(I)-catalyzed azide-alkyne cycloadditions allow for the exclusive generation of 1,4-disubstituted 1,2,3-triazoles from a wide range of azides and terminal alkynes, a robust chemistry towards the 1,5-substituted counterparts is also available. Ruthenium(II) complexes of the  $[\text{Cp}^*\text{RuCl}]$ -type (Figure 7) have been shown to selectively accelerate the AAC reaction with complementary regioselectivity at room temperature.<sup>[30, 43-44, 46]</sup> Thus, 1,5-disubstituted 1,2,3-triazoles can be effectively synthesized *via* the RuAAC using the same starting materials as in the CuAAC reaction. The proposed mechanism of ruthenium(II) catalysis is depicted in Figure 8.<sup>[30]</sup> In the first step, both azide and alkyne components coordinate the ruthenium center through displacement of two spectator ligands. While the azide group binds through the nitrogen proximal to the carbon, the alkyne is coordinated in a  $\pi$ -fashion. Then, a ruthenacycle is formed, which directs the

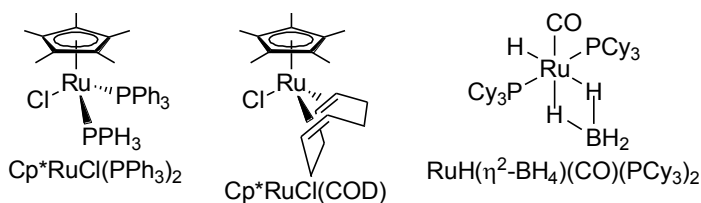


Figure 7. Structures of suitable RuAAC catalysts.  $\text{Cp}^*$ : pentamethylcyclopentadienyl,  $\text{PPh}_3$ : triphenylphosphine,  $\text{COD}$ : cyclooctadienyl,  $\text{PCy}_3$ : tricyclohexylphosphine.

terminal alkynes as the required copper acetylide species cannot be formed with internal triple bonds.

In the context of peptide synthesis and modifications, this reaction shows its full potential. Practically all side-chain functionalities of the 20 canonical amino acids are tolerated without the need for protection groups. Generally, fast conversion rates as well as comparably high yields can be achieved in aqueous media.<sup>[41-42]</sup> Additionally, the reaction can be conducted in solution as well as on the solid support during solid phase peptide synthesis (SPPS), thus allowing for versatile and modular

formation of the 1,2,3-triazole with the described regioselectivity.<sup>[30]</sup> Reductive elimination of the formed triazole and recoordination of the spectator ligands complete the catalytic cycle. As this reaction proceeds *via* a  $\pi$ -coordinated alkyne and not a metal acetylide, the RuAAC is applicable to internal alkynes. The pentamethylcyclopentadienyl (Cp\*) ligand is considered to be essential for high reaction rates as its steric demand facilitates the initial displacement of spectator ligands like, for example, bidentate cyclo-octadien (COD).<sup>[30]</sup>

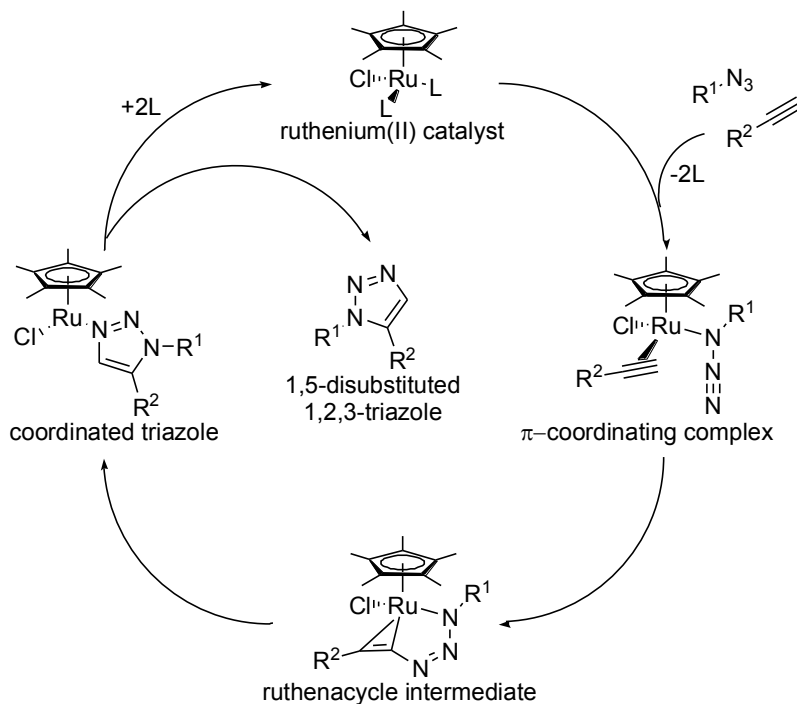


Figure 8. Proposed reaction mechanism of the RuAAC. L: spectator ligand.

Although frequently referred to as “ruthenium-click”, this reaction falls short of some essential criteria for click reactions: it is not compatible with aqueous solvents, many reactive functionalities like, for example, carboxy or amine groups are not tolerated, and usage of inert gas atmosphere is often required for clean and smooth conversions. Thus, the applicability of the RuAAC reaction in peptide chemistry is usually limited to reaction partners with full terminal and side-chain protection. This requirement, however, can be easily fulfilled when performing reactions on the solid support.<sup>[43-44]</sup> Finally, precisely dosed microwave irradiation can further facilitate RuAAC conversion leading to fast and efficient reaction rates.<sup>[43-44]</sup>

Interestingly, the described preference of the 1,5-pattern can be inverted in favor of 1,4-disubstituted 1,2,3-triazoles through variation of the coordination shell at the ruthenium center.<sup>[47-48]</sup> Catalysts lacking cyclopentadienyl (Cp) or pentamethylcyclopentadienyl (Cp\*) ligands have been shown to react *via* ruthenium acetylide species similar to the CuAAC mechanism.<sup>[47]</sup> Thus, usage of, for example,  $\text{RuH}(\eta^2\text{-BH}_4)(\text{CO})(\text{PCy}_3)_2$  (Figure 7) instead of  $\text{Cp}^*\text{RuCl}(\text{COD})$  exclusively yields the 1,4-disubstituted AAC product.<sup>[47]</sup> Nevertheless, it remains to be proven whether this type of reaction can approach the scope and practicability of the copper(I)-catalyzed method with the same regioselectivity.

---

## 1.2 Triazoles as Versatile Tools for Selective Bioconjugation

---

Synergy – the effect of two or more functions collaborating in a beneficial manner when combined appropriately – is a concept that can be applied to the construction of biomolecular assemblies.<sup>[49-50]</sup> One facile strategy to achieve such a “more-than-additive-behavior” with a synthetic construct relies on the utilization of modular design principles.<sup>[51]</sup> For example, a moiety of moderate binding capabilities can be converted into a highly affine entity by incorporating multiple copies in one molecule.<sup>[52-53]</sup> If the architecture of such a homooligo- or homomultimer is convenient, multivalent interaction modes become available decisively improving binding kinetics as well as thermodynamics (avidity).<sup>[49, 54]</sup> Furthermore, a cleverly arranged unification of dissimilar modules gives rise to novel molecular features which none of the used components would possess as singular compounds.<sup>[55]</sup> Thus, the covalent combination of a selective binding moiety, for example an antibody, with a bioactive substance results in a hetero(multi)valent construct suitable for targeted drug delivery.<sup>[56]</sup> Such assemblies are known as antibody-drug conjugates (ADC) and their efficiency is currently investigated in several clinical trials.<sup>[56-57]</sup>

For the design of synthetic or semi-synthetic higher ordered multimeric compounds several aspects have to be considered. First, the modules of interest and their associated features should be identified.<sup>[58]</sup> Second, a suitable molecular architecture for the arrangement of the involved components should be evaluated considering spatial and chemical requirements as well as expected modes of action of the resulting construct.<sup>[51, 54, 59]</sup> Last, an appropriate synthetic strategy for the covalent (or sometimes non-covalent) linkage of the described elements should be laid out.<sup>[60-62]</sup>

In the presented work, peptidic modules were used as binding and interacting moieties.<sup>[41]</sup> Thus, a conjugation chemistry was needed that is compatible with biomolecules. It has been shown that the CuAAC reaction described in chapter 1.1 is a valuable tool applicable to this kind of synthetic problem. Nevertheless, a few other coupling techniques have been developed that fulfill the requirements for the selective conjugation of peptides.<sup>[60, 63-78]</sup> These reactions can be used as complementary instruments in addition to the CuAAC and will be reviewed shortly in section 1.2.1.

In general, strategies for the construction of bioconjugates can be divided into two categories: direct linkage and scaffold-based approaches.<sup>[41, 79]</sup> The former type refers to the straightforward covalent connection of (in most cases) two molecules possessing the desired properties *via* relatively short linker segments. This approach is very useful for the construction of labeled biomolecules and is reviewed in section 1.2.2.<sup>[80]</sup> The second strategy relies on the generation of more complex architectures using the addressed functional modules and an additional platform molecule. This method is commonly used for the well-ordered assembly of constructs containing more than two bioactive components and will be discussed in detail in section 1.2.3.<sup>[61]</sup>

---

### 1.2.1 Complementary Selective Bioconjugation Reactions

---

The scope of chemical reactions suitable for the selective modifications of unprotected biomolecules is rather limited. Synthetic techniques that are truly innocuous to living systems and functional *in vivo* are even fewer in number. Carolyn Bertozzi defined this type of methods as “bioorthogonal”.<sup>[70-71]</sup> Indeed, the classic CuAAC does not belong to this elected group of reactions due to the toxicity of the involved copper species. Nevertheless, chemistry that is not perfectly bioorthogonal may also be of great value when a general compatibility with peptide functionality is provided.

Table 1 shows a selection of reactions suitable for selective bioconjugation.

**Table 1.** Chemical reactions commonly employed in or suitable for bioconjugations of peptides except the CuAAC (reaction schemes are simplified).

Name	Reaction Scheme	Type
maleimide-thiol coupling		Michael-type addition
thioether coupling		nucleophilic substitution
thiol-ene click		radical reaction
oxime ligation		carbonyl chemistry
Staudinger ligation		Staudinger-type reaction, bioorthogonal
strain-promoted azide-alkyne cycloaddition (SPAAC)		[3+2] cycloaddition, bioorthogonal
strain-promoted nitron cycloaddition (SPANC)		[3+2] cycloaddition, switchable
inverse electron-demand Diels-Alder		[4+2] cycloaddition, bioorthogonal

The chemoselective modification of free thiol groups is a well-established methodology.<sup>[62-67, 81]</sup> Usually, a stable thioether linkage is formed through different chemical approaches like the maleimide-thiol coupling<sup>[62-63, 81]</sup> or the thiol-ene click reaction.<sup>[66-67]</sup> Haloalkane-thiol nucleophilic substitutions are also possible but precise pH control is required in order to favor the sulfur nucleophile over, for example, amine or alcohol functionalities.<sup>[64-65]</sup> Additionally, naturally occurring cysteines in peptide sequences might interfere with all thiol-based conjugation techniques.

Another functionality frequently used for bioconjugation is the carbonyl group. An aldehyde, for example, can be easily installed in a peptide in form of a glyoxal moiety *via* oxidation of an *N*-terminal serine.<sup>[82]</sup> This carbonyl can then be reacted with aminoxy groups to give an

oxime.<sup>[68-69, 83]</sup> This bond is far more stable than a hydrazone or a thiazolidine linkage that are prone to hydrolysis and, thus, less advisable for such application.<sup>[82, 84-86]</sup>

In 2000, Bertozzi and coworkers presented the first truly bioorthogonal conjugation chemistry in the form of their variant of the Staudinger reduction.<sup>[72]</sup> A key component in this reaction is the azide functionality, which is usually not found in biological systems and provides a soft nucleophile.<sup>[87]</sup> Its reaction partner is a phosphine group which is abiotic and non-toxic, as well. In aqueous environments the resulting aza-ylide intermediate is finally trapped as a stable amide and a phosphine oxide moieties.<sup>[72, 88]</sup> The applicability of this reaction to *in vivo* experiments has been demonstrated in murine models revealing its extraordinary selectivity.<sup>[89]</sup> A “traceless” variant of the Staudinger ligation has also been developed suitable for the synthesis of native peptide bonds under benign conditions.<sup>[90-91]</sup> In this case, the involved phosphine moiety is entirely removed from the product during the coupling process leaving nothing behind but the sole amide.

Besides the CuAAC, other cycloaddition reactions have become more and more important for selective modification of biomolecules.<sup>[70-71, 73-74, 80, 92]</sup> The strain-promoted azide-alkyne cycloaddition (SPAAC) is another bioorthogonal conjugation technique developed by the Bertozzi group.<sup>[71]</sup> It basically operates with the same building blocks like the CuAAC, but eliminates the need for the copper(I) catalyst through the utilization of the pre-activated triple bond found in strained cyclooctynes.<sup>[92]</sup> Thus, the SPAAC proceeds with second-order rate constants around  $0.1 \text{ M}^{-1}\text{s}^{-1}$  at room temperature sufficient for rapid conversions. Nevertheless, the water solubility of the used alkyne component is a major issue impairing the performance of the SPAAC in living systems.<sup>[71, 93]</sup> However, cyclooctynes optimized with respect to reactivity and solubility may be applicable for selective *in vivo* experiments in vertebrates.

The strain-promoted alkyne-nitrone cycloaddition (SPANC) also involves cyclooctynes.<sup>[73-75]</sup> In this reaction a nitrone moiety is used as the dipolar component instead of an azide. It can be effectively generated from carbonyls *in situ* (e.g. *N*-terminal glyoxals in peptides).<sup>[74]</sup> As the cycloaddition proceeds only in the presence of the nitrone, this reaction can be switched on through addition of alkylhydroxylamine to a non-reacting mixture of the cyclooctyne and carbonyl components giving the desired dipolar functionality for SPANC coupling.<sup>[74]</sup>

Finally, a variant of the Diels-Alder reaction suitable for selective bioconjugate chemistry has been developed.<sup>[76-78]</sup> This type of cycloaddition involves a tetrazine as an electron-poor diene and an electron-rich dienophile (e.g. the Reppe anhydride or certain cyclooctynes). Thus, the electron demand of the reaction partners is inverse compared to a “regular” Diels-Alder cycloaddition. This chemistry performs well in living systems and can be, therefore, considered as a bioorthogonal one.<sup>[77]</sup>

In theory, all of the selective bioconjugation techniques described in this section can be combined with the CuAAC either following the one-pot or sequential reaction schemes. For example, thiol- and carbonyl-based procedures have been shown to be perfectly orthogonal to the “copper-click” methodology,<sup>[61-62]</sup> while the inverse-electron demand Diels-Alder should proceed cleanly in the presence of free alkynes or azides. Furthermore, strained cyclooctynes can be selectively addressed prior to terminal alkynes, although both moieties basically undergo cycloadditions with azide groups.<sup>[62]</sup> A similar strategy would rely on the Staudinger ligation in the presence of non-activated triple bonds, which can be addressed in a second step using the CuAAC. This array of selective chemical reactions allows for the assembly of complex heteromultivalent molecular constructs suitable for all kinds of applications in chemical biology.<sup>[61]</sup>

---

### 1.2.2 Direct Linkage of Functional Units

---

The CuAAC conjugation methodology has been excessively used to directly link two biomolecules together or to attach functional molecules like fluorophores or radio labels to

proteins, peptides, nucleic acids, etc.<sup>[94-96]</sup> The biggest challenge in this context is to find reaction conditions that suit educts and products alike. Thus, different CuAAC protocols have been elaborated with catalyst concentrations ranging from about 1 to 500 mol% compared to the alkyne component.<sup>[41, 97-98]</sup> The copper(I) source can be Cu<sup>0</sup> wires or powder, as well as Cu<sup>I</sup> or Cu<sup>II</sup> salts, while the latter variant is more frequently used.<sup>[36, 41, 99-100]</sup> The addition of accelerating ligands or bases can improve reaction rates and facilitate quantitative conversions.<sup>[36, 38]</sup> Furthermore, several solvent systems are available including aqueous buffers with or without organic modifiers like *tert*-butanol (*t*BuOH), as well as pure organic solutions or even neat reactions.<sup>[36, 97-98]</sup>

As the CuAAC proceeds fastest in aqueous environments,<sup>[98]</sup> this medium is highly recommended for the dimerization or modification of biomolecules, which usually possess an adequate to excellent water solubility and have to be handled under mild conditions. Representative conditions for this type of reactions are given in Figure 9.

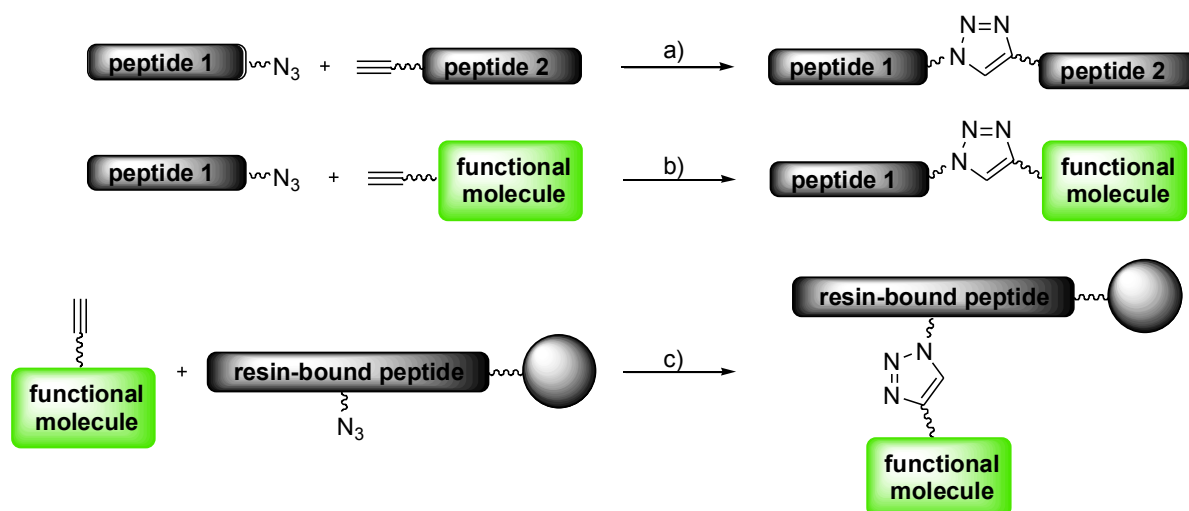


Figure 9. Typical conjugation schemes for the direct modification of peptides using CuAAC. Functional molecules could be fluorescence or radio labels, as well as bioactive organic compounds. Conditions: a) 1 eq peptide 1 and 1 eq peptide 2 in H<sub>2</sub>O/*t*BuOH (2:1, v/v), 3-10 eq CuSO<sub>4</sub>, 3-10 eq sodium ascorbate (NaAsc), r.t., 1-24 h. b) 1 eq peptide 1 and 1.2 eq “clickable” functional molecule in H<sub>2</sub>O/*t*BuOH (2:1, v/v), 5 eq CuSO<sub>4</sub>, 5 eq NaAsc, 20 eq of *N,N*-diisopropylethylamine (DIEA), r.t., 1-24 h. c) 1 eq resin-bound peptide and 5 eq “clickable” functional molecule in degassed and argon-flushed DMF, 1 eq CuSO<sub>4</sub>, 1 eq NaAsc, 8 eq of DIEA, r.t., overnight.

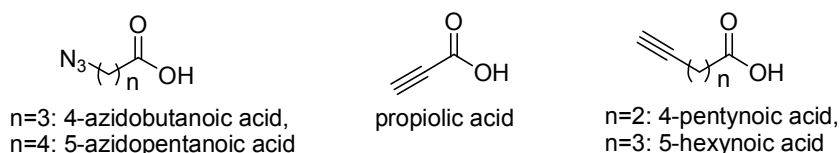
Usually, the amount of copper(I)-catalyst needed for clean and smooth conversions upon bioconjugation reactions is quite high. Equimolar stoichiometries or even ten-fold excess of the transition metal compared to the alkyne component are not seldom found in common CuAAC protocols.<sup>[41, 97]</sup> In contrast, only 0.1-10 mol% of the copper(I) species is often sufficient to conduct catalyzed cycloadditions with small organic compounds.<sup>[36]</sup> Thus, chromatographic work-up of crude bioconjugates is mandatory to remove residual copper salts.

In general, azide and alkyne functionalities can be efficiently introduced either in the side chains or at the *N*-terminus of peptides. Typical carbon-carbon triple bond containing building blocks are stable and do not react under the conditions of Fmoc-based solid phase peptide synthesis (Fmoc-SPPS).<sup>[43-44, 101]</sup> Thus, they are perfectly suited for installation of alkyne moieties at any desired position in the amino acid sequence. Azides located in side chains, however, have been reported to cause side reactions in some cases.<sup>[102]</sup> Nevertheless, this functionality also possesses a sufficient tolerance towards active-ester coupling and basic deprotection chemistry to allow for a wide range of applications in Fmoc-SPPS.<sup>[41]</sup>

A typical strategy to install the addressable functionalities into peptides is to couple azide- or alkyne-bearing carboxylic acids to free amino groups during peptide synthesis on the solid support.<sup>[41, 101]</sup> The respective nitrogen nucleophile could either be the *N*-terminus that is

available at every amino acid residue after Fmoc-deprotection or the side chain functionality of, for example, lysine or ornithine.<sup>[41-42, 101]</sup> The latter approach requires certain orthogonal protecting groups that are selectively cleavable without interfering with the Fmoc-strategy. A very decent way to introduce azides or alkynes into peptides is to utilize non-natural amino acids already bearing the desired functionalities in their side chains.<sup>[44, 97]</sup> Some commercially available or easily accessible building blocks are depicted in Figure 10. The presented compounds are commonly used as vehicles for the facile introduction of the desired functionalities into biomolecules in general and peptides in particular.

#### functionalized carboxylic acids:



#### Fmoc-protected amino acids:

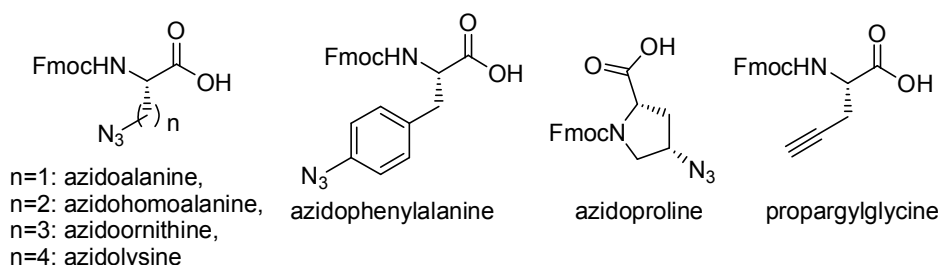


Figure 10. A collection of building blocks suitable for the facile installation of azide- and alkyne functionalities in peptides.

This repertoire of azide- and alkyne-bearing building blocks enables the direct covalent linkage of two biomolecules possessing desired features. Additionally, modular synthetic approaches and combinatorial chemistry become possible. Hence, compound libraries of reasonable size can be constructed from a relatively small set of clickable components using divergent synthetic routes.<sup>[103]</sup> The resulting collection of different molecular constructs can be screened for beneficial properties. This may facilitate the identification of tailor-made conjugates for an aspired biochemical application.

### 1.2.3 The Scaffold-Based Approach to Molecular Complexity

Higher ordered molecular assemblies are frequently observed in Nature.<sup>[49]</sup> The immunoglobulin M (IgM) pentamer, for example, possesses a well-defined architecture and orientation of the functional units.<sup>[104]</sup> This special geometry is established through covalent linkage of five singular antibodies *via* certain “joining peptides” and allows for enhanced target binding through multivalent interactions.

Scaffold-based bioconjugates can be regarded as artificial analogues of such complex natural architectures. Nevertheless, functional modules of synthetic constructs are usually considerably smaller in size (between 0.5 and 5 kDa) compared to their biological ancestors (180 kDa for IgM monomer).<sup>[41-42, 61, 101]</sup> As a consequence, the shape and physical characteristics of artificial assemblies are significantly influenced by the structural unit which links all functional modules together. This scaffold defines the orientation of bioactive ligands as well as other attached moieties and acts as a structural template for the resulting conjugate.

Suitable molecules for such framework units are rich in number and may originate from every category of chemical compounds. Peptides, carbohydrates, smaller organic molecules, as well

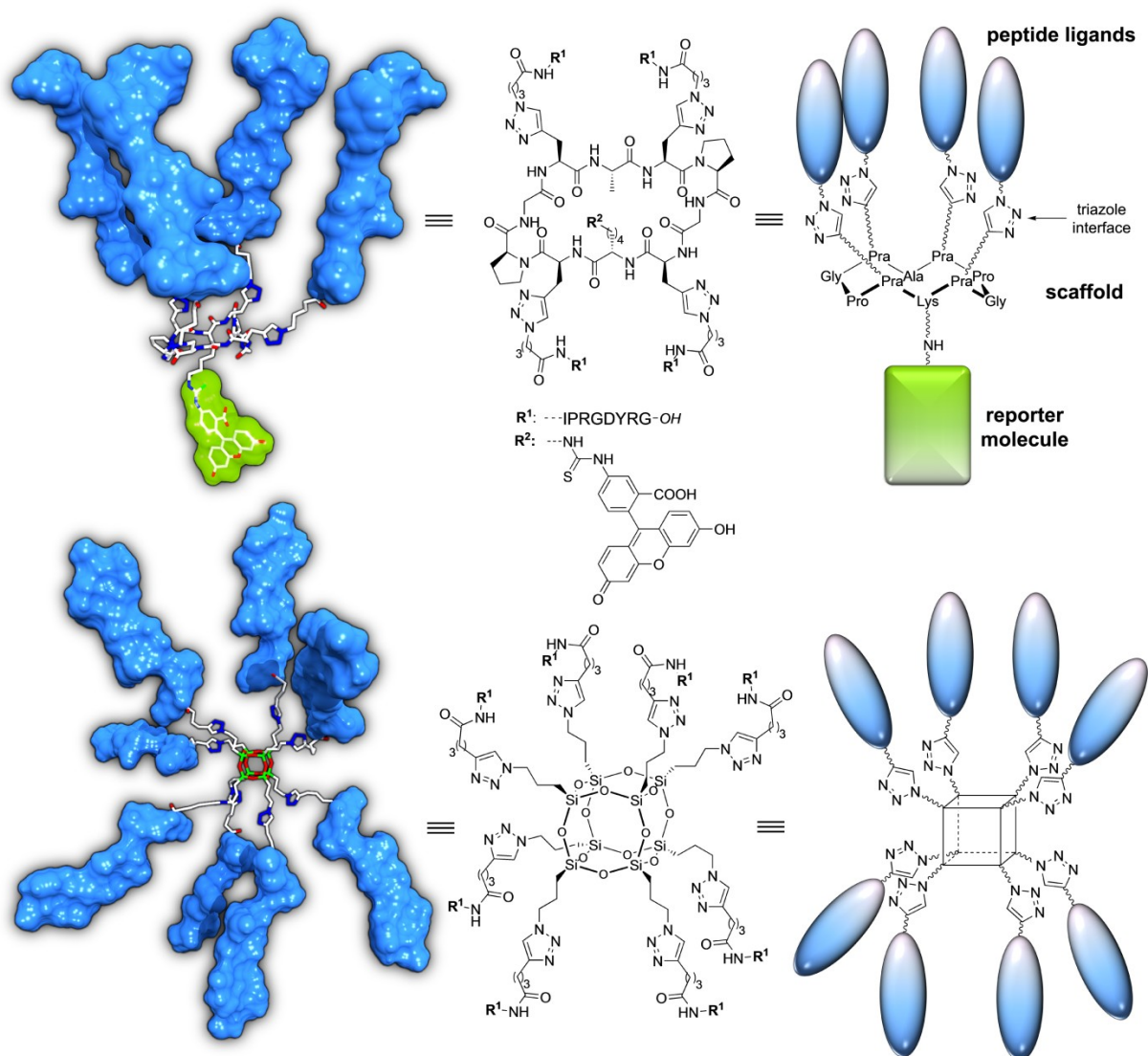


Figure 11. Peptide multimers synthesized *via* CuAAC in different representations (3D model, chemical structure, and schematic representation). (Top) A heteromultivalent bioconjugate consisting of a cyclic decapeptide scaffold, four attached peptide ligands, and one fluorescent label. Pra: propargylglycine. (Bottom) A homooctamer of the same peptide ligand attached to a cube-octameric silsesquoxane scaffold.

as inorganic pico- or nanoparticles are possible materials for a scaffold unit.<sup>[51, 59, 105-109]</sup> Two exemplary CuAAC conjugates possessing four or eight identical peptide ligands, respectively, are depicted in Figure 11.<sup>[41, 101]</sup>

One of these constructs is based on a peptidic scaffold which possesses the shape of two short anti-parallel  $\beta$ -sheets that are joined together *via* two terminal proline-glycine turns.<sup>[105]</sup> This macrocyclic structure provides a versatile conformationally restrained template that directs the functionalizable side chains of two amino acids into oppositely to the four remaining coupling sites. In principle, any desired reactive group can be installed at each of the six possible positions of this versatile framework. This allows for a wide range of combinations of different functional modules in various relative orientations.<sup>[41, 61, 105]</sup> Chapter 2.1 of the cumulative section describes the synthesis of the conjugate shown in the top of Figure 11. Interestingly, the peptidic ligand which was displayed in a four-fold manner contained a so-called RGD motif.<sup>[110-111]</sup> These sequences of arginine, glycine, and aspartate have been shown to bind transmembrane receptor molecules known as integrins.<sup>[110, 112]</sup> This attribute makes them interesting for tumor therapy as inhibitors of angiogenesis.<sup>[111-112]</sup>



The synthesis of such scaffold-based multivalent constructs *via* CuAAC is possible using the same protocols as described in section 1.2.2 for the direct linkage approach.<sup>[41-42]</sup> However, a pronounced tendency towards precipitation of resulting bioconjugates in aqueous solvent systems has been observed.<sup>[41]</sup> Nevertheless, successful resolution of formed solids was achieved through addition of diluted ammonia allowing for chromatographic isolation.<sup>[41]</sup>

The full potential of the CuAAC methodology can be unlocked through combination with the complementary bioconjugation techniques described in section 1.2.1 (Figure 12).<sup>[61-62]</sup> This strategy opens avenues towards regioselectively addressable functionalized templates (RAFT) perfectly suitable for the facile construction of heteromultivalent biomolecular constructs.<sup>[113]</sup> Boturny and coworkers have provided an impressive example of a sequential one-pot triple conjugation using three different ligation strategies at within the same procedure.<sup>[61]</sup> Through successive oxime, maleimide-thiol, and CuAAC coupling of peptides and carbohydrates to a well-defined cyclic decapeptide framework, highly-ordered assemblies were synthesized chemo- and regioselectively (Figure 12). Constructs based on this scaffold have already been tested *in vivo* and showed promising results for the application as molecular imaging devices in living systems.<sup>[113]</sup>

Presenting bioactive modules in such a multivalent manner can have several beneficial effects. Most importantly, singular modules may cooperate in a synergistic way through simultaneous interaction with one or multiple molecular target(s), significantly improving overall binding affinity.<sup>[49-50]</sup> This phenomenon is termed

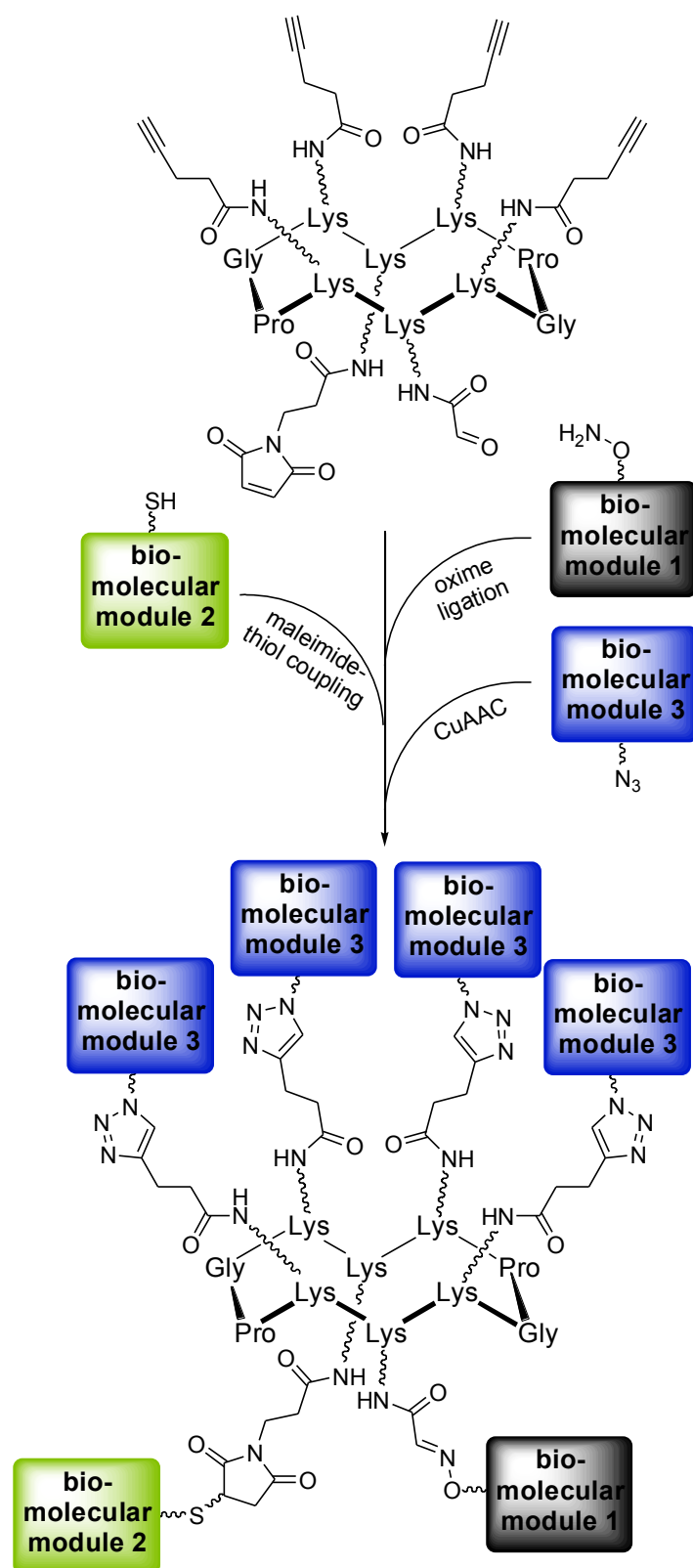


Figure 12. Scheme of a sequential one-pot triple bioconjugation of three different biomolecular modules to a cyclic decapeptide scaffold.

avidity and includes thermodynamic as well as kinetic effects.<sup>[49]</sup> In addition to the mere sum of the individual enthalpic terms to the free energy of binding, a beneficial entropic contribution occurs when the spatial orientation and fixation of the ligands promotes concerted interaction. The latter effect can also be considered from a kinetic perspective as multiple binding-competent units are brought to close proximity, thereby increasing their local concentration, which significantly decreases the rates of dissociation. However, shape and rigidity of the scaffold molecule have a significant influence on these effects.<sup>[49]</sup>

The presentation of ligands on an appropriate template compound may give rise to new modes of action. For example, a multivalent binder of certain cell-surface receptors may facilitate receptor dimerization leading to an initiation of the related signal transduction cascade triggering specific cellular responses.<sup>[54]</sup> Other interesting effects of complex architectures with multiple effector regions have been described for antibody-based therapeutics. These new biological entities (NBE) are capable of recruiting parts of the immune system to tumor cells and, thus, induce antibody-dependent cell-mediated cytotoxicity (ADCC) or complement-dependent cytotoxicity (CDC).<sup>[114-115]</sup> These principles may also be applied for the design of artificial ADCC- or CDC-competent bioconjugates as well as constructs suitable for targeted drug delivery.

Another beneficial property of higher ordered molecular assemblies is their enhanced resistance towards enzymatic degradation and, thus, increased serum stability.<sup>[116]</sup> In combination with an attenuated renal clearance, prolonged circulation times can be achieved with bioconjugates larger than approximately 15 kDa.<sup>[117-118]</sup>

### 1.3 Molecular Prosthesis: Triazoles as Artificial Structural Elements

“Protein prosthesis” – a term coined by Tam *et al.* in 2007 – was used to describe the utilization of 1,2,3-triazoles as backbone surrogates in amino acid sequences.<sup>[119]</sup> Indeed, several other applications of this versatile nitrogen-containing pentacycle as substitutes of different structural elements within peptides or proteins have been reported.<sup>[43-44, 119-124]</sup> Among them are triazole-based disulfide mimics,<sup>[44, 121]</sup> locked *trans*- and *cis*-amide surrogates,<sup>[43, 119]</sup> as well as constrained side chain replacements (Figure 13).<sup>[124-125]</sup> The first two types of bioisosterism have been thoroughly investigated in the frame of this thesis. Additionally, the possibility of using 1,2,3-triazoles as an interface for the rapid generation of small biomimetic side chain libraries was studied.

For all of these applications and concepts, a naturally occurring peptide called sunflower trypsin inhibitor-1 (SFTI-1) was used as a model compound for *in vitro* validation.<sup>[126-131]</sup> SFTI-1 and relevant target serine proteases will be introduced shortly in section 1.3.1 prior to brief descriptions of triazole-based backbone mimics (section 1.3.2) and disulfide replacements (section 1.3.3). Finally, the utilization of azide-alkyne cycloadditions for the installation of diverse side-chain functionalities in peptide frameworks will be discussed (section 1.3.4).

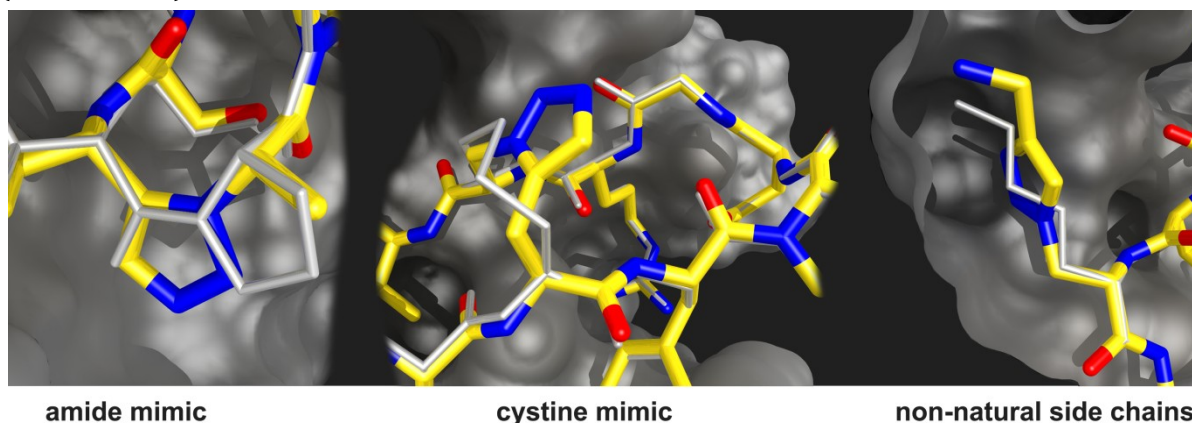


Figure 13. Different possibilities for the application of disubstituted 1,2,3-triazoles as mimics or replacements of important structural elements of peptides and proteins.

#### 1.3.1 The Ideal Test System: SFTI-1 – a Canonical Inhibitor of Trypsin-like Serine Proteases

Serine proteases constitute an important class of hydrolases and are very common in all kinds of organisms and tissues.<sup>[132-133]</sup> One prototypic serine-protease is trypsin.<sup>[134]</sup> This digestive enzyme is present in the intestines of most vertebrates and invertebrates.<sup>[134-135]</sup> Together with the structurally similar chymotrypsin, it defines a category of endopeptidases that possess the trypsin or chymotrypsin fold.<sup>[132]</sup> These enzymes are rich in number and fulfill various important tasks in healthy organisms.<sup>[136-137]</sup> However, some serine proteases play also crucial roles in pathological processes, which renders them interesting pharmaceutical targets.<sup>[136, 138]</sup> They all share a common tertiary structure of the catalytic domain with a key feature called “catalytic triad”.<sup>[139]</sup> An aspartate, a histidine, and a serine residue operate together enabling the nucleophilic attack of the activated hydroxylic group of the latter amino acid on the backbone carbonyl atom of a peptidic substrate positioned in the active site. This facilitates breakage of the amide bond followed by hydrolysis of the enzyme-peptide ester intermediate. Due to substrate-specific pockets at the active site, serine proteases can be very selective towards certain amino acid sequences, especially concerning the residue after which the amide bond is cleaved. A selection of serine proteases with pharmaceutical importance in an overlay with trypsin is shown in Figure 14.<sup>[140-149]</sup>

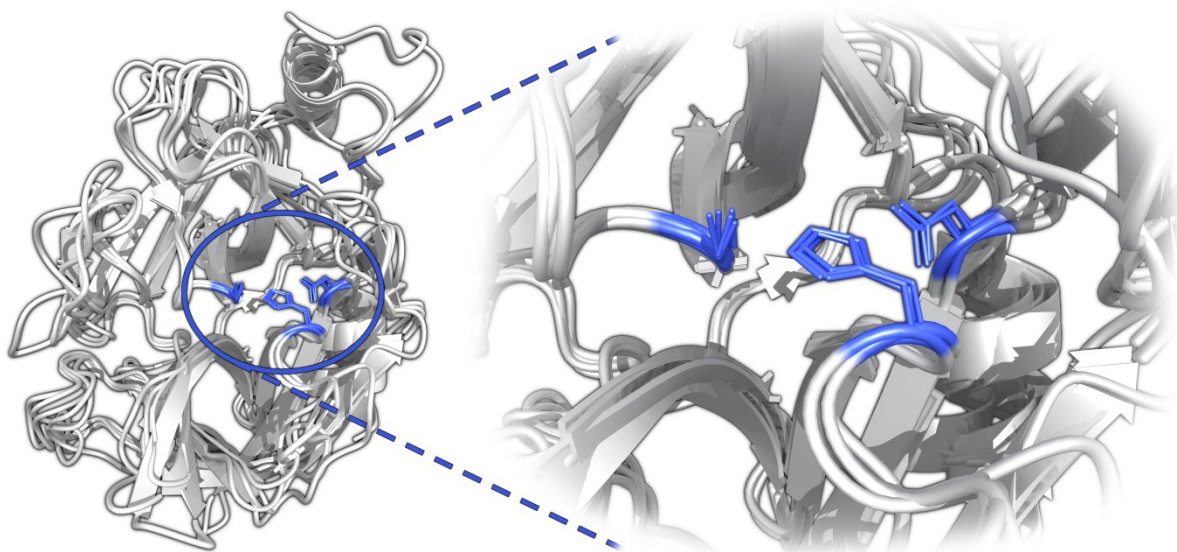


Figure 14. (Left) Overlay of 3D structures of the catalytic domains of trypsin, matriptase, urokinase-type plasminogen activator (uPA), hepsin, mast cell tryptase, and neutrophil elastase. (Right) Close-up of the catalytic triad (blue).

One trypsin-like enzyme that selectively cleaves peptide bonds after the basic residues lysine or arginine is matriptase (other names: MT-SP1, TADG-15, and ST14/SNC19).<sup>[150]</sup> It has been thoroughly studied as a potential drug target and is also an integral part of research articles presented in this thesis.<sup>[125, 140-141, 151]</sup> Unlike soluble trypsin, it is anchored to the basolateral membrane of epithelial cells *via* an *N*-terminal stem region.<sup>[141, 143]</sup> This surface immobilization is typical for type II transmembrane serine proteases (TTSP).<sup>[152-153]</sup> In healthy tissue the proteolytic activity of matriptase is precisely regulated by its cognate inhibitors hepatocyte growth factor activator inhibitor-1 and 2 (HAI-1, HAI-2).<sup>[154-155]</sup> Enzymatic processing of extracellular components by this TTSP is important for development, growth, differentiation, and remodeling of the surrounding tissue.<sup>[156-159]</sup> However, a dysregulation of this natural activity by, for example, overexpression of matriptase can have severe pathological outcomes and has been correlated with the development and progression of epithelial tumors, inflammation-related diseases, as well as osteoarthritis and atherosclerosis.<sup>[140-141, 160]</sup> As a consequence, a number of synthetic compounds has been designed for *in vivo* blockade of matriptase activity.<sup>[161-162]</sup>

A promising approach towards the development of efficient serine protease inhibitors is the optimization of naturally occurring peptides with intrinsic anti-proteolytic activity.<sup>[163-164]</sup> Previously mentioned SFTI-1 is such a molecule (Figure 15).<sup>[164]</sup> It consists of 14 amino acids and binds to trypsin-like enzymes predominantly *via* the seven *N*-terminal residues.<sup>[127-129, 131]</sup> This

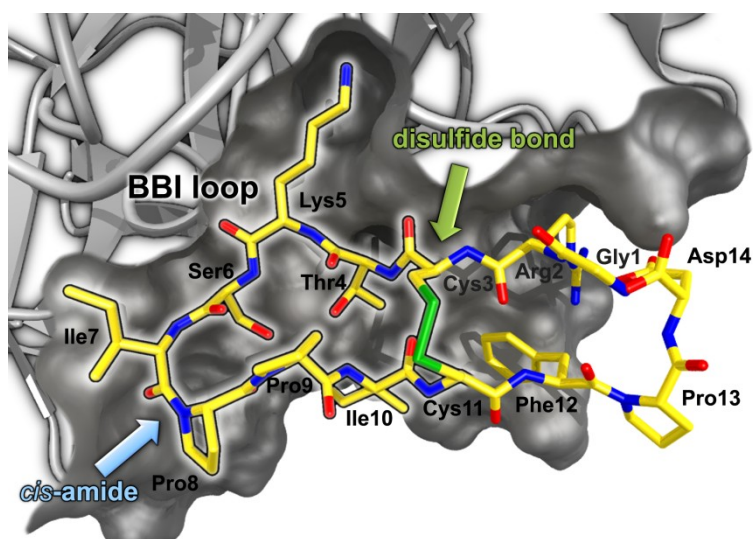


Figure 15. 3D model of SFTI-1 upon interaction with trypsin (PDB-ID: 1SFI). A cut surface of trypsin is shown. The Bowman-Birk inhibitor loop is highlighted and the disulfide bond as well as the *cis*-amide are indicated.

region is shaped like the peptide substrate upon binding, facilitating a favorable interaction with serine proteases.<sup>[163]</sup> This canonical conformation is achieved and maintained through the so-called Bowman-Birk inhibitor (BBI) loop.<sup>[165-166]</sup> This rigid and constrained structure comprises a *cis*-proline motive, a disulfide bridge, and an extended hydrogen-bond network.<sup>[167]</sup> In addition to the BBI segment, a secondary loop is present at the terminal regions of native bicyclic SFTI-1. However, this backbone macrocyclization motif is not mandatory for protease inhibition.<sup>[128]</sup>

All of these structural features render native SFTI-1 as a very potent inhibitor of trypsin with an inhibition constant  $K_i$  in the subnanomolar range.<sup>[128, 151]</sup> As the addressed *cis*-amide and the cystine motifs are essential for biological activity, this peptide is perfectly suited as a model compound for the validation of the non-natural replacements described in sections 1.3.2 and 1.3.3. Additionally, SFTI-1 shows a latent activity against other serine proteases, e.g. matriptase.<sup>[130]</sup> This gives rise to a possible optimization of this fascinating framework towards the pharmaceutically relevant TTSP *via* side chain modifications explained in section 1.3.4.

Substantial data on SFTI-1 comprising X-ray coordinates of enzyme-inhibitor complexes, NMR solution structures, and structure-activity relationships (SAR) have already been reported in the literature.<sup>[128, 130, 143, 168]</sup> Additionally, a straight-forward synthetic access *via* Fmoc-SPPS and a routine measurement of inhibition constants of SFTI-1 variants facilitate structure-guided studies.

### 1.3.2 Locked *trans*- and *cis*-Amide Surrogates

Biological macromolecules, as all polymers, are constructed of smaller structural units, whereas the central monomeric building blocks of proteins and peptides are amino acids. Linking two amino acids together *via* the  $\alpha$ -amino and carboxy groups results in a peptide bond. Together with the  $\alpha$ -carbon atoms, this special form of an amide linkage constitutes the backbone of every proteinaceous substance. This group has several important properties; among them the ability to act as a hydrogen bond donor and acceptor. Resonance structures illustrate its partial double bond character that leads to two possible conformers (*cis* and *trans*).<sup>[169-170]</sup> Finally, it is susceptible to hydrolysis in a strong basic or acidic environment as well as enzymatic degradation.

An ideal biomimicry of a peptide bond possesses all relevant structural characteristics of amides, is stable under harsh conditions, and is easy to synthesize. Some possible isosters are shown in Figure 16.<sup>[171]</sup> Thioamides, for example, are suitable amide replacements in terms of shape and general chemical properties.<sup>[171]</sup> However, they only tolerate mild reagents and conditions due to the intrinsic reactivity of the carbon-sulfur double bond.

Interestingly, it has been shown that 1,2,3-triazoles can be installed within the peptide backbone without significantly disturbing structure and, thus, maintaining biological function.<sup>[43, 119-120, 172]</sup> More importantly, these amide mimics are capable of locking defined backbone conformations depending on the substitution pattern present on the aromatic heterocycle. Hence, 1,4-disubstituted 1,2,3-triazoles are similar to *trans*-amides, while the 1,5-disubstituted counterpart corresponds to a *cis*-isomer.

Synthesis proceeds *via* the Fmoc-SPPS methodology in combination with on-resin CuAAC or RuAAC steps using non-natural azide- and alkyne-bearing amino acid analogs (Figure 17).<sup>[43]</sup>

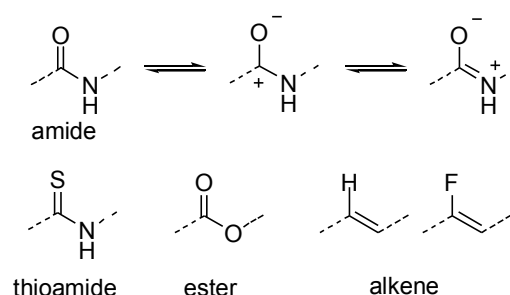


Figure 16. (Top) Amide bond and resonance structures. (Bottom) A few functionalities that have been used as isosteric to amide bonds.

The residue on the *N*-terminal side of the respective dipeptide is replaced by a building block possessing a triple bond instead of a carboxy group. It is accessible from the Weinreb amide (aldehyde) derivative of the respective amino acid *via* a Seyferth-Gilbert homologation using the Bestmann-Ohira reagent.<sup>[172]</sup>

The *C*-terminal residue possesses an azide functionality instead of the free  $\alpha$ -amino group, which can be directly introduced *via* diazotransfer using trifluoromethanesulfonyl azide (triflyl azide).<sup>[172]</sup>

A preferable synthetic route towards the installation of triazole-based backbone replacements involves AAC chemistry on the solid support in the course of Fmoc-SPPS.<sup>[43, 172]</sup>

The azide-bearing building block is coupled to the peptide resin at the desired position in the amino acid sequence using active ester strategies. Then the triazole is formed using the alkyne component and AAC methodologies. Through choice of the catalyst (copper(I) or ruthenium(II)) a defined substitution pattern of the non-natural backbone element is achieved which reflects either the *cis* or the *trans* conformer of the native amide bond.

The two isomers of the peptide bond are interconvertible with a strong emphasis on the *trans* conformation.<sup>[169-170]</sup> This is caused by a more favourable orientation of amino acid side-chain functionalities. Thus, *cis*-amides are very rarely observed in nature. They are usually restricted to positions followed by a proline residue, where the preference of the *trans* conformation is less pronounced compared to all other canonical amino acids.<sup>[169, 173]</sup> However, if a *cis*-amide is present, it is usually an important structural feature in the biological context and mandatory for bioactivity.<sup>[119, 174-176]</sup> Thus, the ability to literally lock the peptide backbone in one of the two possible conformations using triazole mimics bears great potential for structure-guided approaches towards tailor-made peptides. In theory, this strategy allows for the installation of any amino acid side chain after a *cis*-amide bond.<sup>[43, 119]</sup> Hence, new possibilities for rational design approaches are provided, otherwise not accessible using only the 20 canonical amino acid building blocks.

Finally, this concept has been successfully applied to SFTI-1 which possesses a *cis*-prolyl motif

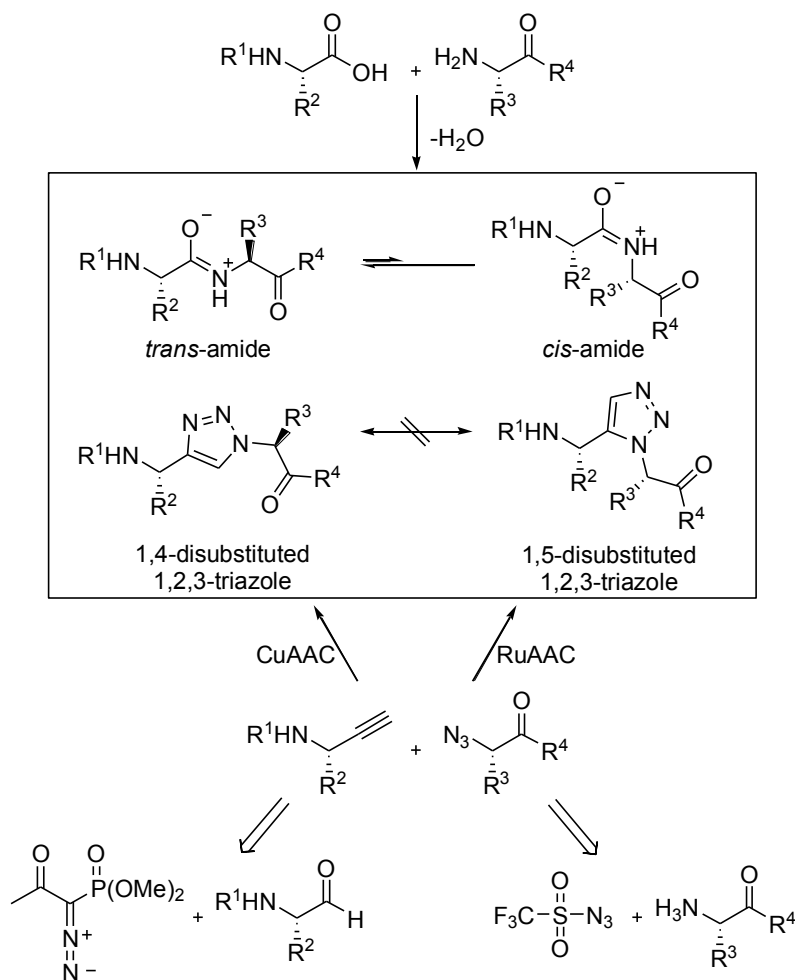


Figure 17. Schematic depiction of triazole-based *trans*- and *cis*-amide mimics. (Top) Condensation of two amino acids forming a dipeptide with a *trans*- and *cis*-amide equilibrium. (Bottom) Synthetic route to 1,4- and 1,5-disubstituted 1,2,3-triazoles installed within the peptide backbone using CuAAC or RuAAC methodologies. This step is preferably conducted on the solid support in the course of Fmoc-SPPS. Alkyne components can be synthesized from corresponding aldehydes using the Bestmann-Ohira reagent. The azide component is accessible from the corresponding free amine through diazotransfer using trifluoromethanesulfonyl azide.



within the BBI loop important for biological activity.<sup>[43]</sup> Hence, peptidomimetic variants with locked backbone amides have been assembled and tested for bioactivity. The synthesized compounds allowed for functional and structural analysis of inhibitor-trypsin complexes using X-ray diffraction crystallography, which undoubtedly proved the structural similarity between the triazole-containing peptidomimetics and the native peptide (Figure 18).<sup>[43]</sup> Chapter 2.2 in the cumulative section of this thesis provides more detail on this topic.

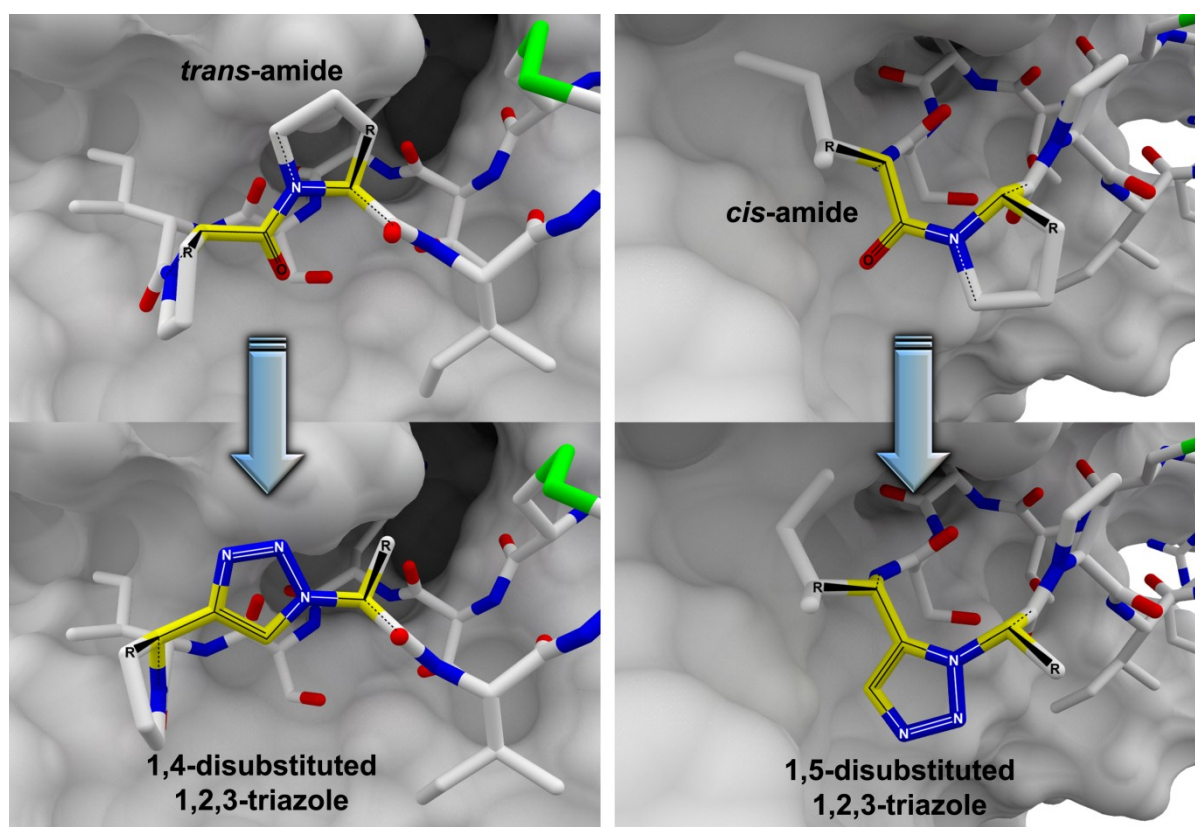


Figure 18. 3D representations of inhibitor-enzyme complexes between trypsin (white surface) and SFTI-1 (top, PDB-ID: 1SFI) and peptidomimetics containing either a 1,4-disubstituted 1,2,3-triazole (bottom left, PDB-ID: 4ABI) or a 1,5-disubstituted 1,2,3-triazole (bottom right, PDB-ID: 4ABJ). Replaced amide bonds as well as the corresponding triazole-based backbone elements are highlighted.

### 1.3.3 The “Triazole Bridge” – a Disulfide Replacement

Disulfide bonds are very common structural elements of proteins and peptides. They are readily formed from free thiol groups of two cysteine residues in oxidative environments.<sup>[177]</sup> This side-chain-to-side-chain linkage provides the possibility for a reversible covalent connection of amino acids that are not adjacent in the primary structure. Thus, it contributes significantly to protein stability and rigidity. Indeed, extraordinary temperature and proteolysis resistant miniproteins usually contain at least three disulfide bridges forming a special “knotted” tertiary structure.<sup>[178-179]</sup> These cystine knots comprise typically 30-50 amino acids and constitute an extreme type of side-chain macrocyclization motifs. However, singular disulfide bonds are also frequently found in smaller bioactive peptides.<sup>[44, 121, 180-182]</sup> They are usually essential structural constraints limiting the conformational freedom and, thus, improve biological activity through reduced unfavorable entropic contributions. Nevertheless, some disulfide-containing peptides like, for example, amylin-(18) still suffer from stability issues.<sup>[183-184]</sup> It has been shown that the utilization of redox-stable cysteine replacements can significantly increase the resistance of such peptides towards

degradation.<sup>[183-184]</sup> A number of strategies for disulfide mimics have been described in the literature. Two very common replacements are thioether or alkene analogs (Figure 19).<sup>[185-189]</sup> However, multiple synthetic steps and the need for orthogonal protection as well as the occurrence of *cis/trans* isomers hamper their broader application.

Interestingly, it has been shown that disubstituted 1,2,3-triazoles are versatile side-chain macrocyclization motifs that can be installed in peptides on the solid support without additional protecting groups.<sup>[190]</sup> This is made possible by the usage of commercially available non-natural amino acids bearing the functional groups required for AAC reactions introduced in section 1.2.2. Hence, cysteine residues are replaced by azide- and alkyne-bearing building blocks.

Then, an intramolecular triazole linkage with either a 1,4- or a 1,5-substitution pattern can be generated *via* on-support CuAAC or RuAAC reactions.<sup>[44, 121]</sup> However, careful choice of the SPPS resin is crucial for clean conversions and the amount of peptide loaded onto the solid support must be low in order to suppress unwanted side reactions. Notably, CuAAC macrocyclization can also be performed in diluted solution. However, chromatographic isolation is in any case mandatory for pure products.<sup>[44]</sup>

Both types of “triazole bridges” have been successfully applied to the generation of bioactive peptidomimetic compounds. Meldal and coworkers reported the installation of triazole bridges *via* CuAAC in tachyplesin-I (TP-I) analogs and reported a conservation of antibacterial activity.<sup>[121]</sup> However, Kowalczyk *et al.* used the same approach for triazole-containing amylin-(18) peptidomimetics, but could not detect the desired anabolic effect on primary foetal rat bone-forming cells or osteoblasts.<sup>[184]</sup>

A similar result using 1,4-disubstituted 1,2,3-triazoles as disulfide replacements was observed for SFTI-1.<sup>[44]</sup> *In vitro* studies revealed a dramatic loss of inhibitory activity compared to the native peptide for the CuAAC product. However, using ruthenium(II) catalysis for the intramolecular azide-alkyne cycloaddition yielded potent peptidomimetics with anti-tryptic activity in the range of the parent compound.<sup>[44]</sup> Interestingly, it was observed that the addressed substitution pattern had a more dramatic effect on bioactivity than the length of the linker between the peptide backbone and the azide functionality.<sup>[44, 151]</sup> Thus, both combinations of propargylglycine with either azidoalanine or azidohomoalanine result in adequate disulfide replacements using RuAAC macrocyclization (Figure 20).<sup>[44, 151]</sup>

These results have been corroborated by molecular dynamics simulations and additional in-

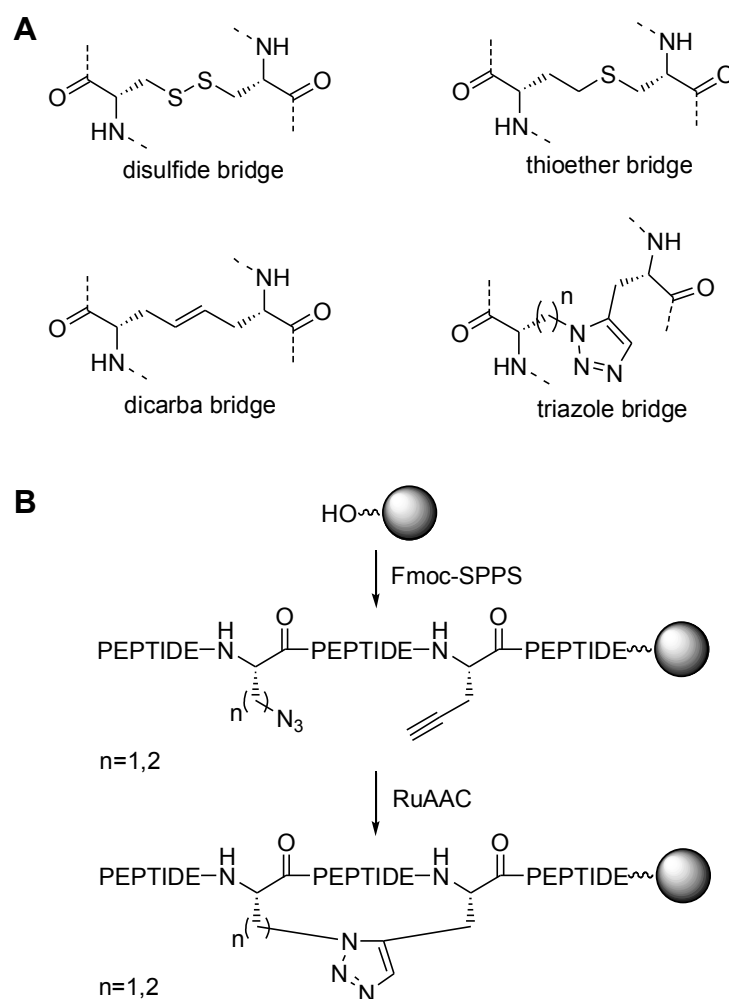


Figure 19. (A) A disulfide bridge and examples of suitable disulfide replacements. (B) Synthetic route towards a 1,5-disubstituted 1,2,3-triazole side chain macrocyclization motif.



depth *in silico* experiments showing that side-chain-to-side-chain linkages using a 1,5-substitution pattern match the structural requirements of a disulfide bond better than the 1,4-patterned counterparts.<sup>[44, 151]</sup> Nevertheless, it has to be evaluated individually for every particular biological context which of the possible triazole bridges is the preferable design in terms of activity. Chapters 2.3 and 2.4 in the cumulative section of this thesis provide more detail on *in vitro* and *in silico* studies of triazole-containing SFTI-1-based inhibitors of trypsin as well as matriptase.

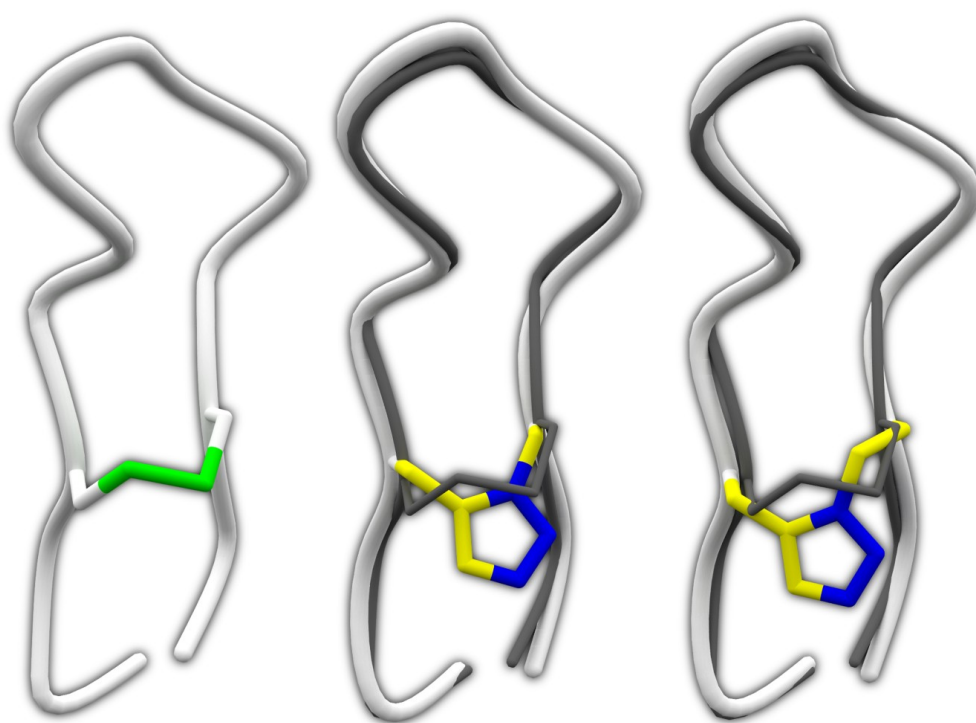


Figure 20. Tube representations of the monocyclic cystine-containing variant of SFTI-1 (left) in an overlay with triazole-bridged derivatives (middle and right) possessing the 1,5-substitution pattern and different linker lengths.

### 1.3.4 Triazoles as an Interface for Side Chain Variability

The natural repertoire of 20 canonical amino acids provides a profound selection of diverse side chain functionalities. This variability is dramatically increased when the singular building blocks are combined to linear oligo- or polymers which in turn are able to fold into complex three-dimensional architectures. A simple random sequence of only 14 canonical amino acids describes a totality of  $14^{20}$  individual molecules, which in quantity corresponds to the number of stars within the observable Universe.<sup>[191]</sup> At least by today's standards, the structure space that is reflected by this gigantic amount of compounds cannot be completely explored in reasonable time scales.<sup>[192]</sup> However, Nature evolved additional mechanisms to generate even more possibilities for functional biomacromolecules. Thus, two extra amino acids – selenocysteine and pyrrolysine – are used for protein synthesis in certain organisms, while post-translational modification of the standard repertoire adds another dimension of complexity.<sup>[193-195]</sup> Hydroxylation, phosphorylation, glycosylation, ubiquitination, or covalent cross-linking of amino acid side chains are only a few examples of Nature's intrinsic modular design beyond mere protein synthesis.<sup>[195-197]</sup> Nevertheless, these biological processes require intricate enzymatic machineries to operate with desired accuracy.

A feasible method to achieve a similar efficiency in peptide chemistry is the utilization of biocompatible reactions.<sup>[198-199]</sup> Burk and coworkers, for example, used oxime ligation to

decorate a moderate binder of polo-like kinase 1 (Plk1) with non-natural building blocks as functional side-chain groups.<sup>[199]</sup> They were able to identify peptide derivatives with significantly improved interaction profiles unmatched by variants containing only the standard amino acid repertoire. This strategy is reminiscent of the direct bioconjugation methodology described in section 1.2.2.

A similar approach was used to optimize SFTI-1 towards matriptase. In this study presented in chapter 2.5 of the cumulative section non-natural azide-bearing amino acids were used as anchor points for the installation of diverse side-chain functionalities *via* CuAAC (Figure 21).<sup>[125]</sup> Additionally, also amino acid substitutions using the canonical repertoire were performed. The positions within the peptide sequence suitable for modification were identified through structure-guided considerations prior to synthesis. Indeed, several triazole-containing SFTI-1-derivatives with improved matriptase affinities were identified. However, the best inhibition constant was determined for a peptide containing only natural amino acids. Nevertheless, the modular approach using the CuAAC methodology allowed for a divergent synthetic route towards peptidomimetic variants. Thus, a targeted compound library of reasonable size was generated which enabled to probe the SFTI-1 framework for beneficial side-chain modifications (Figure 22). A big challenge in this context is to refine the gigantic structure space of conceivable variants to a reasonable number of potentially functional modifications. This can be achieved *via* rational molecular design principles including ligand- or structure-based virtual screening or general considerations using structure-activity relationships (SAR).

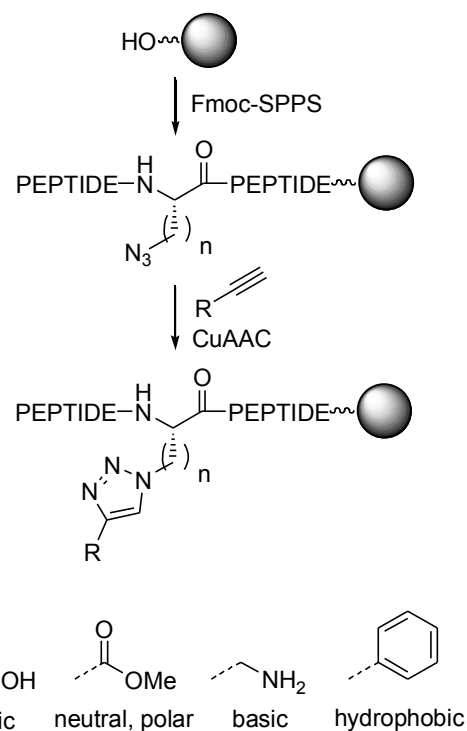


Figure 21. Scheme of a divergent synthetic route towards a targeted compound library containing different side chain functionalities.

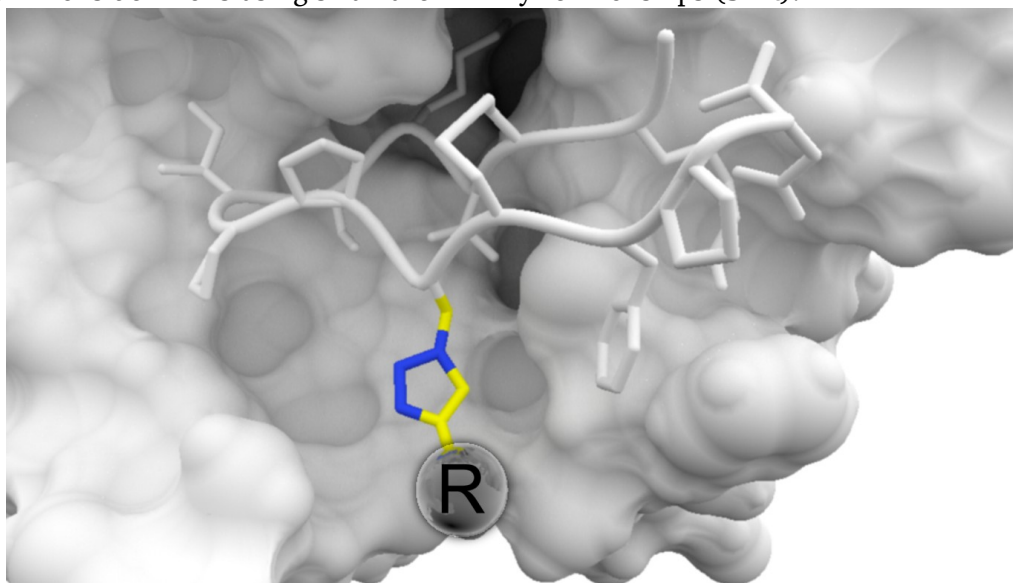


Figure 22. 3D illustration of triazole-based side chain modifications installed in one position of the monocyclic variant of SFTI-1 enabling to probe for residues R possessing beneficial interaction profiles with matriptase (white surface).

## 1.4 Aims and Scope

The application of synthetic peptides and peptide conjugates in modern life sciences is an emerging field with promising perspectives.<sup>[200]</sup> Compounds like Cilengitide or DOTATOC (Figure 23) demonstrate the potential of this type of compounds for therapy or diagnosis of various cancer types and other diseases.<sup>[111, 201-203]</sup> High affinities and sufficient selectivities towards desired target molecules, good solubility, as well as low toxicity are beneficial attributes for a possible pharmaceutical application.<sup>[204-205]</sup>

Nevertheless, many peptides suffer from certain unfavorable properties impairing their use as drugs:

1. Most peptides are susceptible to enzymatic degradation resulting in low serum stability.<sup>[206-207]</sup>
2. Even small peptides usually violate three criteria of the Lepinski's rule of five: They easily exceed a molecular mass of 500 Da, possess more than 5 hydrogen bond donors, and have more than 10 hydrogen bond acceptors. Thus, they commonly show a low "druglikeness" and are not orally bioavailable.<sup>[208]</sup>
3. Peptides below 15 kDa typically undergo fast renal clearance significantly reducing circulation times.<sup>[118]</sup>

Some of these drawbacks, especially regarding the drug-like properties (point 2), cannot be eliminated without sacrificing essential characteristics of peptides. However, stability issues and renal clearance rates can be addressed through chemical modifications.<sup>[116-118]</sup> Hence, PEGylation, PASylation, or simply increase of molecular weight, e.g. via multimerization, have been shown to significantly attenuate filtration of 23iological by the kidneys.<sup>[116-118]</sup> Furthermore, the use of non-natural building blocks like D-amino acids or peptoid structures, as well as side-chain-to-side-chain or head-to-tail cyclization can improve the tolerance of

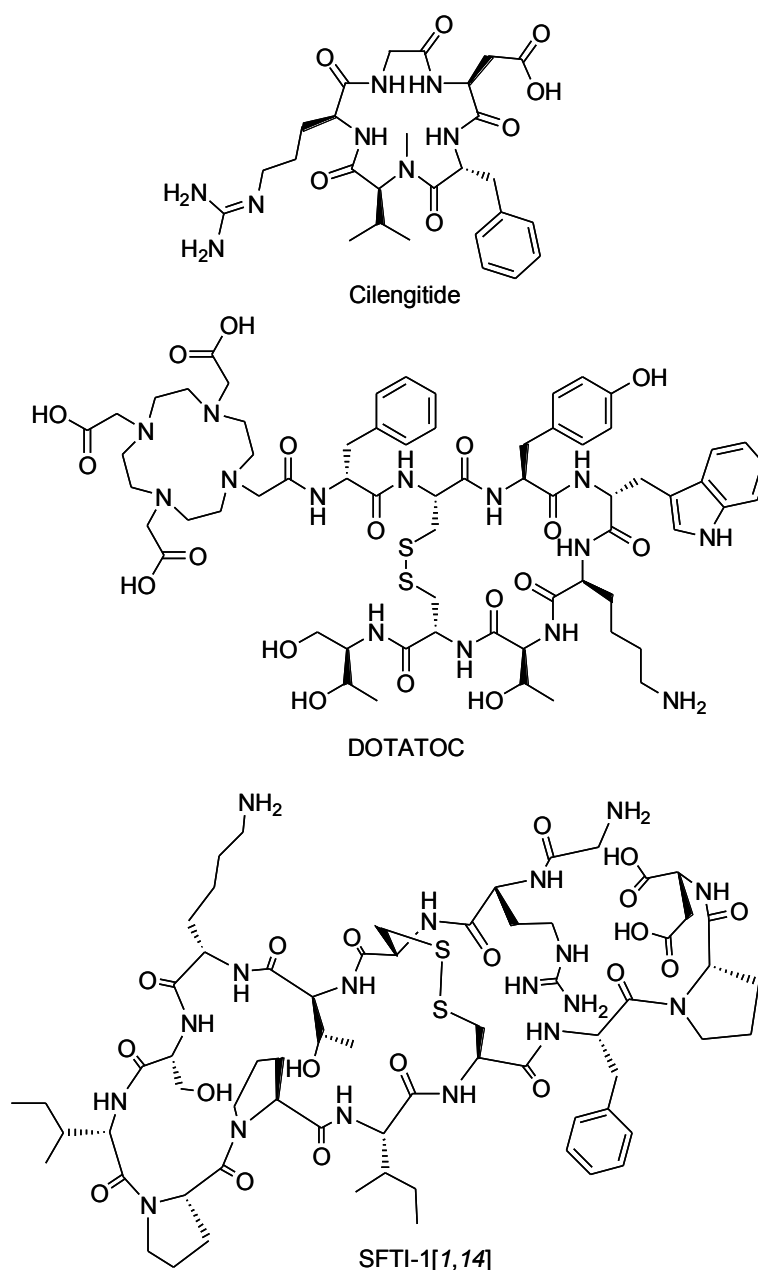


Figure 23. Chemical structures of Cilengitide, DATOTOC, and the monocyclic variant of the sunflower trypsin inhibitor-1 (SFTI-1[1,14]).

peptides towards degradation *in vivo*.<sup>[206, 209-210]</sup> Hence, the advancement of bioconjugation techniques as well as the development of non-natural mimics of structural elements of peptides are important and challenging tasks which have been pursued in the frame of this work.

The applicability of azide-alkyne cycloaddition methodologies and resulting 1,2,3-triazoles for peptide modification and optimization was investigated with respect to the following objectives:

1. An efficient synthetic route towards the assembly of heteromultivalent constructs using peptidic ligands, a suitable scaffold, and additional reporter molecules *via* CuAAC had to be established.
2. The possibility of replacing essential structural elements of the monocyclic variant of the sunflower trypsin inhibitor-1 (SFTI-1[1,14]) by non-natural 1,2,3-triazole-based building blocks had to be investigated. These studies included modification of *cis*- and *trans*-amide bonds as well as mimicking the cystine motive.
3. Establishing and advancing the on-support CuAAC and RuAAC methodologies was necessary to gain access to desired peptidomimetic compounds.
4. The impact of these modifications in structure and anti-tryptic activity of the resulting peptidomimetic compounds had to be examined by enzyme inhibition assays, molecular dynamics simulations, docking experiments, as well as X-ray diffraction crystallography of enzyme-inhibitor complexes.
5. Finally, the SFTI-1[1,14] framework had to be optimized towards the pharmacologically relevant target protease matriptase. For this purpose a small “click library” had to be designed using structure-guided principles, synthesized *via* a combinatorial approach, and screened for beneficial modifications.

---

## 2 Cumulative Part

---

This section contains the following articles that have been published in peer-reviewed journals or are currently under review.

- 2.1 Olga Avrutina<sup>†</sup>, **Martin Empting**<sup>†</sup>, Sebastian Fabritz, Matin Daneschdar, Holm Frauendorf, Ulf Diederichsen, & Harald Kolmar\*, Application of copper(I) catalyzed azide-alkyne [3+2] cycloaddition to the synthesis of template-assembled multivalent peptide conjugates. *Org. Biomol. Chem.* (2009), 7, 4177-4185.  
– Reproduced by permission of the Royal Society of Chemistry (RSC).
- 2.2 Marco Tischler<sup>†</sup>, Daichi Nasu<sup>†</sup>, **Martin Empting**<sup>†</sup>, Stefan Schmelz, Dirk W. Heinz, Philip Rottmann, Harald Kolmar, Gerd Buntkowsky\*, Daniel Tietze\*, & Olga Avrutina\*, Braces for the peptide backbone: Insights into structure-activity relationships of protease inhibitor mimics with locked amide conformations. *Angew. Chem. Int. Ed.* (2012), 51, 3708-3712.  
– Reproduced by permission of John Wiley and Sons.
- 2.3 **Martin Empting**, Olga Avrutina, Reinhard Meusinger, Sebastian Fabritz, Michael Reinwarth, Markus Biesalski, Stephan Voigt, Gerd Buntkowsky, & Harald Kolmar\*, "Triazole Bridge": Disulfide-Bond Replacement by Ruthenium-Catalyzed Formation of 1,5-Disubstituted 1,2,3-Triazoles. *Angew. Chem. Int. Ed.* (2011), 50, 5207-5211.  
– Reproduced by permission of John Wiley and Sons.
- 2.4 Olga Avrutina, Heiko Fittler, Bernhard Glotzbach, Harald Kolmar, & **Martin Empting**\*, Between Two Worlds: a Comparative Study on In Vitro and In Silico Inhibition of Trypsin and Matriptase by Redox-Stable SFTI-1 Variants at Near Physiological pH. *Org. Biomol. Chem.* (2012), 10, 7753-7762.  
– Reproduced by permission of the Royal Society of Chemistry (RSC).
- 2.5 Heiko Fittler, Olga Avrutina, Bernhard Glotzbach, **Martin Empting**\*, & Harald Kolmar\*, Combinatorial Tuning of Peptidic Drug Candidates: High-Affinity Matriptase Inhibitors through Incremental Structure-Guided Optimization.  
– Submitted in September 2012.

Figures from the following article have been reused in the introduction (section 1) by permission of the Gesellschaft Deutscher Chemiker (GDCh):

- **Martin Empting**\*, 1,2,3-Triazole: Multifunktionswerkzeuge für die Peptidchemie. *Nachrichten aus der Chemie* (2012/13), in press.

---

<sup>†</sup>shared primary authorship, \*corresponding author(s)

Additionally, the following articles have also been published between 2009 and 2012:

- Sebastian Fabritz<sup>‡</sup>, Sebastian Hörner<sup>‡</sup>, Doreen Könnig, **Martin Empting**, Michael Reinwarth, Christian Dietz, Bernhard Glotzbach, Holm Frauendorf, Harald Kolmar\*, & Olga Avrutina\*, From Pico to Nano: Biofunctionalization of Cube-octameric Silsesquioxanes by Peptides and Miniproteins. *Org. Biomol. Chem.* (2012), 10, 6287-6293.
- Sebastian Fabritz, Dirk Heyl, Viktor Bagutski, **Martin Empting**, Eckhard Rikowski, Holm Frauendorf, Ildiko Balog, Wolf-Dieter Fessner, Jörg J. Schneider, Olga Avrutina, & Harald Kolmar\*, Towards click bioconjugations on cube-octameric silsesquioxane scaffolds. *Org. Biomol. Chem.* (2010), 8, 2212-2218.

---

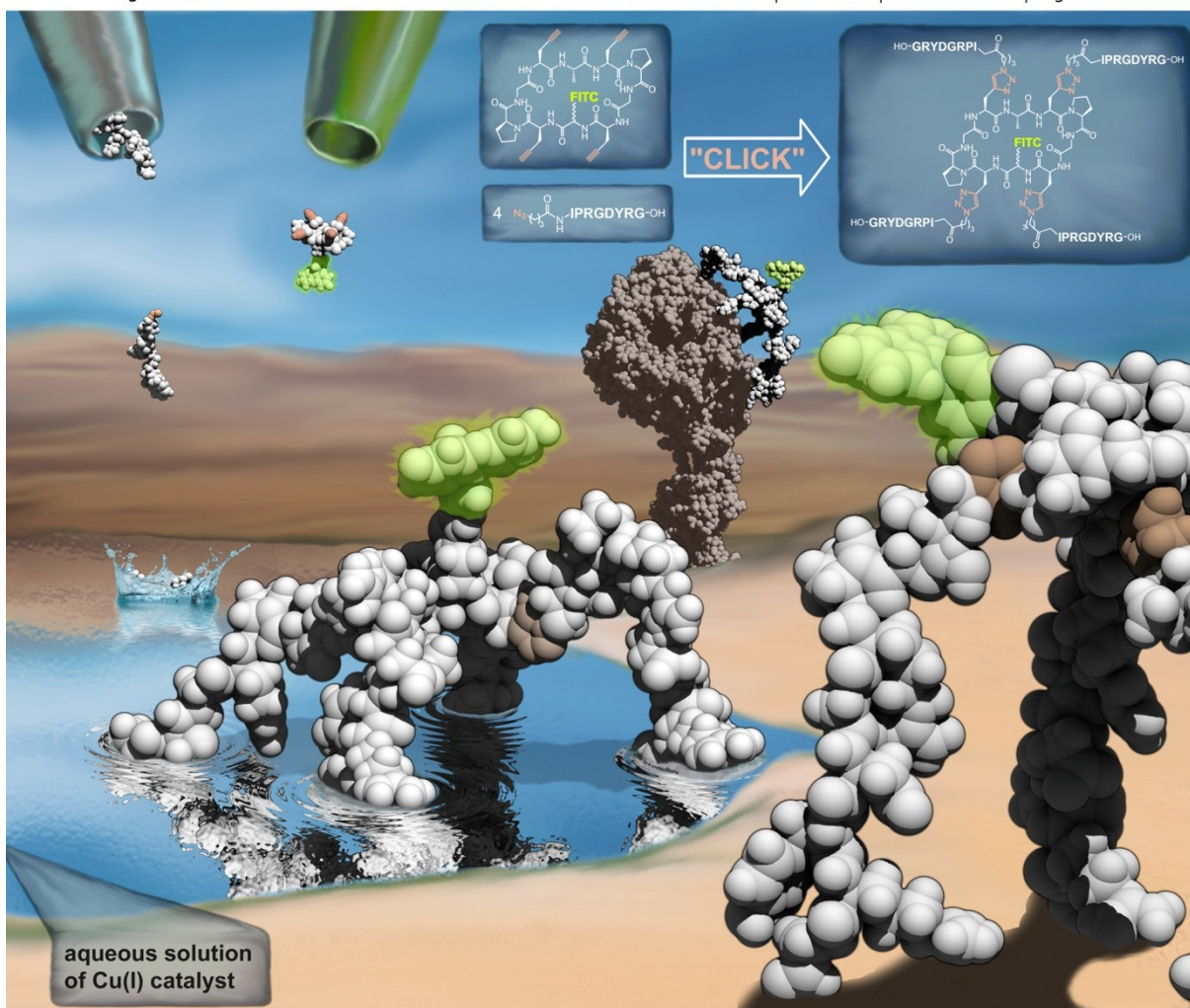
<sup>‡</sup>shared primary authorship, \*corresponding author(s)

---

# Organic & Biomolecular Chemistry

www.rsc.org/obc

Volume 7 | Number 20 | 21 October 2009 | Pages 4133–4320



ISSN 1477-0520

RSC Publishing

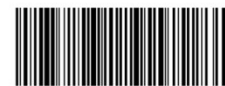
**FULL PAPER**Harald Kolmar *et al.*

Application of copper(I) catalyzed azide-alkyne [3+2] cycloaddition to the synthesis of template-assembled multivalent peptide conjugates

Highlights in

**Chemical Science**

In this issue



1477-0520(2009)7:20;1-E

Front cover of issue 20, volume 7, Organic & Biomolecular Chemistry 2009  
 – Reproduced by permission of the Royal Society of Chemistry (RSC).





## 2.1 Heteromultivalent Scaffold-based Peptide Tetramers *via* CuAAC

### Title:

Application of copper(I) catalyzed azide–alkyne [3+2] cycloaddition to the synthesis of template-assembled multivalent peptide conjugates

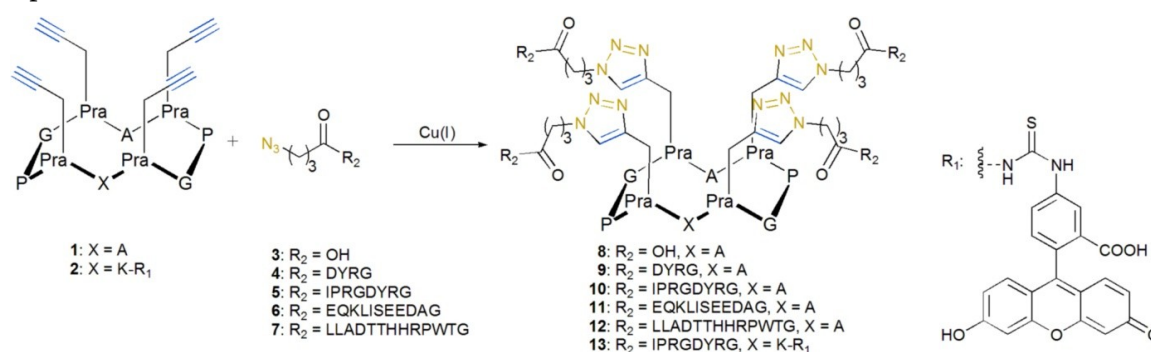
### Authors:

Olga Avrutina, Martin Empting, Sebastian Fabritz, Martin Daneschdar, Holm Frauendorf, Ulf Diederichsen, Harald Kolmar

### Bibliographic Data:

*Organic & Biomolecular Chemistry*,  
Volume 7, Issue 20, Pages 4177-4185, October 21, 2009.  
DOI: 10.1039/B908261A.  
First published online: August 25, 2009.

### Graphical Abstract:



Tetravalent peptide conjugates were synthesized from unprotected peptide monomers on a cyclic decapeptide as a conjugation scaffold using “click” azide–alkyne cycloaddition in water at room temperature within comparatively short reaction times.

### Contributions by M. Empting:

- Synthesized and isolated all peptidic compounds
- Performed HPLC and GFC analysis
- Wrote experimental section of the article and created all figures
- Created cover artwork

# Application of copper(I) catalyzed azide–alkyne [3+2] cycloaddition to the synthesis of template-assembled multivalent peptide conjugates†

Olga Avrutina,<sup>‡a</sup> Martin Empting,<sup>‡a</sup> Sebastian Fabritz,<sup>a</sup> Matin Daneschdar,<sup>a</sup> Holm Frauendorf,<sup>b</sup> Ulf Diederichsen<sup>b</sup> and Harald Kolmar<sup>\*a</sup>

Received 27th April 2009, Accepted 2nd July 2009

First published as an Advance Article on the web 25th August 2009

DOI: 10.1039/b908261a

Here we describe the facile generation of tetravalent peptide conjugates *via* a copper(I) catalyzed azide–alkyne cycloaddition (CuAAC) using a cyclic peptide template as a versatile conjugation scaffold. This stable and rigid framework is a conformationally constrained cyclic  $\beta$ -sheet decorated with spatially defined alkyne moieties that serve as selectively addressable coupling sites. The proposed method allows for the effective coupling of unprotected peptide monomers in water at room temperature within comparatively short reaction times. The resulting conjugates display the ligands in an oriented manner, thus allowing for multivalent interactions with given target molecules, which may contribute to enhanced affinity and specificity. In addition, the selected scaffold offers an orthogonal coupling site for the incorporation of fluorescent labels or radioligands.

## Introduction

A number of interactions taking place in nature occur in multivalent mode.<sup>1</sup> It is known that a multivalent display created through multiplication of biologically active monomers on an appropriate scaffold can significantly enhance the net affinity of a resulting construct towards its target in comparison to the interactions of individual monomers.<sup>1,2</sup> Linear or branched polymers, dendrimers, and peptides placed on various scaffold structures have already been used *e.g.* to enhance antigen immunogenicity, binding affinity, or selectivity.<sup>3–6</sup> Better understanding of the nature and mechanisms of multivalent interactions between the interplay partners is of particular research interest. Enhanced binding affinity towards desired targets, probably due to an improved steric orientation, make them potentially attracting objects in the design of antibodies, receptors, and inhibitors of proteases.<sup>7,8</sup>

Two different mechanistic models can be considered for the explanation of increased binding affinity of multimeric systems.<sup>9</sup> First, when a simultaneous binding to the corresponding receptors cannot take place, an increase in receptor–ligand binding can be explained by an apparent increase in local ligand concentration. Second, in cases of polyvalent binding, *e.g.* by interacting with receptors that are located on cell surfaces in several copies, cooperative interactions between multiple ligands and receptors can occur resulting in increased net affinity (avidity) of the receptor–ligand interaction.

In the context of multivalent peptide conjugation, the choice of a proper structural framework is of particular importance.<sup>10</sup> This

scaffold should possess a three dimensional architecture providing free access to reactive moieties and making, therefore, possible the coupling of the ligands of choice without steric hindrance. Moreover, it is highly desirable for the scaffold to offer not only the possibility to oligomerize functional monomers but also to give an option for the introduction of other substituents, *e.g.* fluorescent dyes, lipophilic molecules for membrane association, chelators for incorporation of radionuclides, or additional orthogonal reactive moieties for the introduction of other bioactive ligands as shown schematically in Fig. 1.

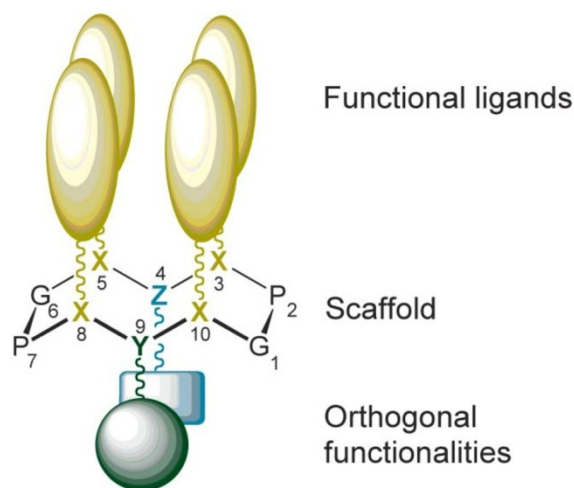


**Fig. 1** Schematic representation of cyclic decapeptide scaffold decorated with different types of ligands. P, proline; G, glycine; X, chemo- and regioselectively addressable conjugation sites; Y, Z, sites for alternative (orthogonal) functionalization.

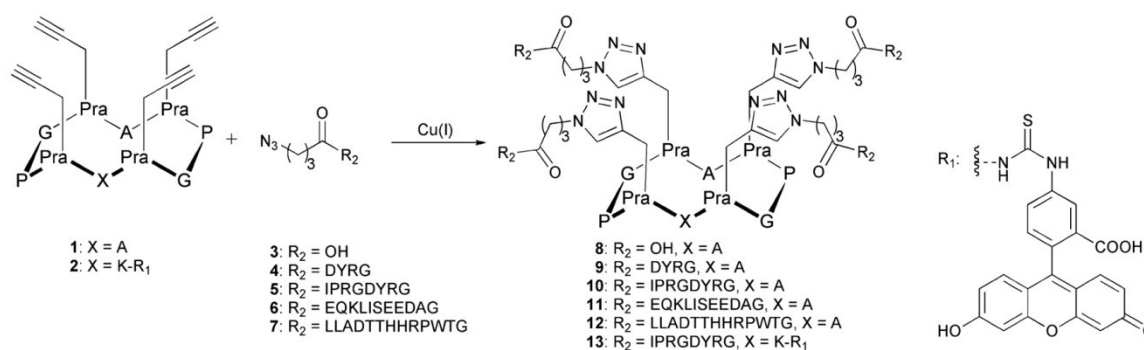
Cyclic peptides and their mimics are versatile molecules with particular properties. It was shown that cyclic decapeptides developed by Mutter and colleagues in the frame of their concept

<sup>a</sup>Clemens-Schöpf Institute of Organic Chemistry and Biochemistry, Darmstadt University of Technology, Petersenstr. 22, 64287, Darmstadt, Germany

<sup>b</sup>Institut für Organische und Biomolekulare Chemie, Georg-August Universität Göttingen, Tamannstraße 2, 37077, Göttingen, Germany

† Electronic supplementary information (ESI) available: RP-HPLC for peptides 1–13, RP-HPLC traces of template 2 cyclization under activation with HBTU and PyBOP, ESI-MS for peptides 8–13, GFC traces for conjugates 9–13 and corresponding monomers. See DOI: 10.1039/b908261a

‡ These authors contributed equally to this work.



**Scheme 1** Synthetic strategy for the preparation of multivalent peptide conjugates on alkyne functionalized cyclic decapeptide scaffolds using copper(I) catalyzed azide-alkyne [3+2] cycloaddition.

of template assembled synthetic proteins (TASP)<sup>11–21</sup> possess due to the presence of two glycine-proline turns an architecture of an antiparallel  $\beta$ -sheet<sup>21–23</sup> that can also serve as scaffolds for coupling of a wide spectrum of ligands with diverse functionalities.<sup>10,24–31</sup>

Herein, we report the synthesis of tetravalent peptide conjugates by copper(I) catalyzed azide-alkyne [3+2] cycloaddition on a decameric peptide template bearing alkyne groups that were introduced using the commercially available non-natural amino acid building block Fmoc-L-propargylglycine (Pra). We show that unprotected peptide ligands can be effectively assembled on the framework alone or in combination with an orthogonally attached fluorescent reporter group (Scheme 1). Our presented strategy provides a short route towards efficient generation of multimeric compounds.

## Results and discussion

### General strategy

Cyclic decapeptides have been widely used in protein *de novo* design and drug discovery<sup>32–42</sup> due to their well-defined architecture furnishing a topological arrangement with sterically defined active groups, which provides a possibility for coupling of functional building blocks. A variety of synthetic strategies based on orthogonal protecting groups in combination with chemoselective ligations has been reported to date.<sup>10,25,26,29–31,43,44</sup> The concept of regioselectively addressable templates (RAFT) conventionally employs two main approaches aimed at the conjugation of unprotected peptides onto the functional scaffold. One involves the formation of amide bonds between the  $\gamma$ -amines of lysine side chains and linker molecules bearing reactive groups suitable for successive chemoselective ligations (Scheme 2A). The other exploits the particular reactivity of thiol functions of cysteine residues (Scheme 2B). Both approaches require the proper protection of the reactive moieties not only during assembly of linear precursors on the solid support but also in the course of head-to-tail cyclization. Lysine based templates also require additional steps for the introduction of selectively addressable moieties, usually aldehydes or aminoxy groups, for oxime bond formation<sup>30</sup> and recently reported alkynes and azides for the click coupling.<sup>31</sup> Cysteine based cyclic decapeptide scaffolds, though allowing for the direct chemoselective ligation *via* thio-ether bonds, are predisposed to the formation of undesired disulfides. Moreover,

the regioselective conjugation is not possible with peptides or proteins containing unprotected cysteine residues.

Obviously very simple, our design was based on a construct derived from the well established *cyclo*-(Xaa-Ala-Xaa-Pro-Gly)<sub>2</sub> sequence. We reasoned that the incorporation of alkyne moieties in the desired positions (Xaa) of the decapeptide framework could be easily accomplished using Fmoc protected propargylglycine (Scheme 2C). This commercially available alkyne bearing building block could be easily incorporated in the growing peptide without side chain protection, therefore significantly reducing complexity of the whole procedure.

### Synthesis of alkyne and azide building blocks

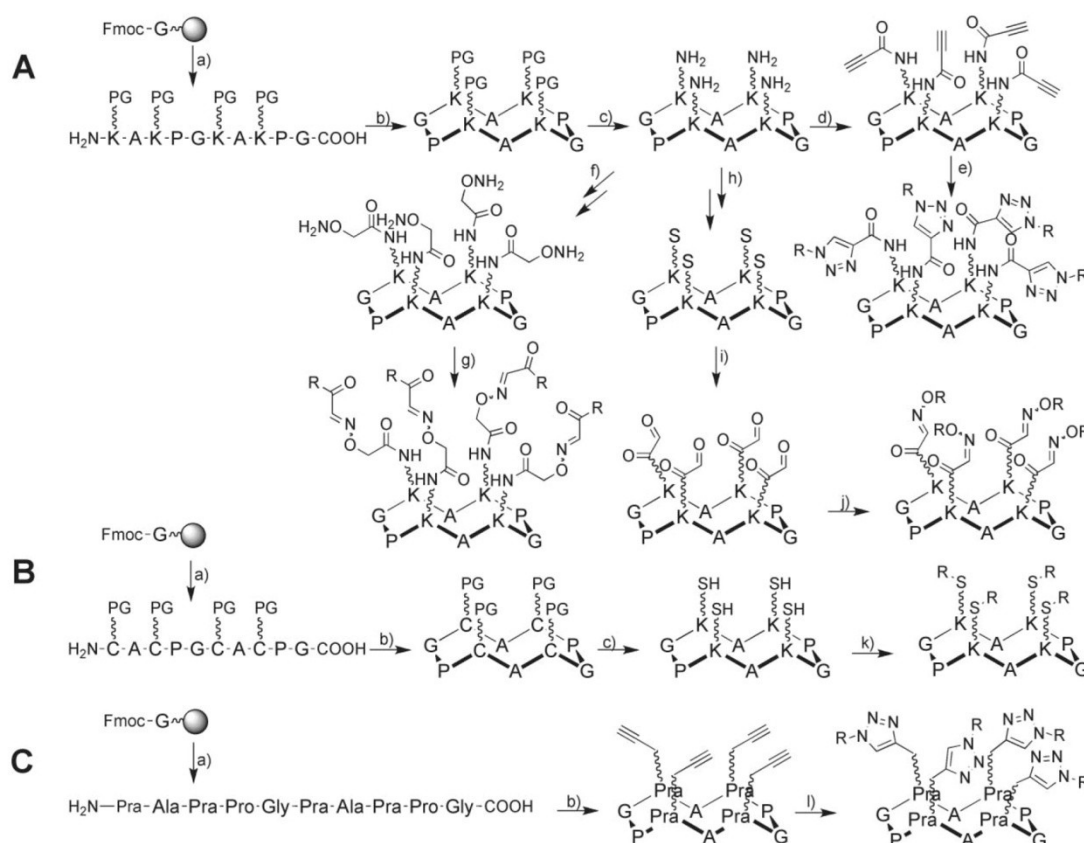
As alkyne components, two different decameric cyclopeptides were synthesized, **1** and **2**. Sharing the same topological features, they differ in the amino acid residue at position 9 (Fig. 1). While scaffold **1** contains no coupling sites other than the desired propargyl side chains, cyclopeptide **2** possesses an orthogonal reactivity in the form of a lysine  $\gamma$ -amino group that is labeled with FITC to demonstrate its utility for the coupling of additional ligands like fluorescent dyes, metal chelators, cell penetrating peptides, *etc.* prior to peptide conjugation *via* click reaction.

Solid phase synthesis of both templates, due to the influence of applied microwave irradiation, was fast and resulted in crude linear precursors of remarkable quality and in excellent yields. They were converted into the cyclic successors without further purification *via* active ester activation of the carboxy terminus. Our experiments corroborated the known fact<sup>45</sup> of *N*-terminal guanidination caused by uronium based reagent HBTU during head-to-tail cyclization. Therefore, phosphonium activator PyBOP was applied to the macrocyclization of template **2** (for further details refer to the supplemental material†).

Introduction of FITC as a model ligand for orthogonal coupling was carried out after macrocyclization of the corresponding precursor followed by cleavage of the Boc protecting group. Similar to previous synthetic steps, this transformation yielded a labeled alkyne functionalized RAFT scaffold in excellent yield (73% after four synthetic steps) and quality. Interestingly, no chromatographic purification was necessary during the whole course of the synthesis for template **2**.

Azide functionality was effectively introduced into model peptide ligands **4–7** during solid phase synthesis using





**Scheme 2** Comparison of homo-tetramerization strategies using different RAFT scaffolds. A, selected approaches for the peptide conjugation using a lysine based template. B, general approach for the homo-multimerization through cysteine based templates. C, general scheme for the peptide conjugation *via* a proargylglycine based scaffold used in this study. PG, protecting group; R, unprotected bioactive ligand; (a) Fmoc SPPS and acidic cleavage from the support, (b) head-to-tail cyclization *via* C-terminal activation, (c) side chain deprotection, (d) propionic acid, DCC,<sup>31</sup> (e) R-N<sub>3</sub>, CuSO<sub>4</sub>, sodium ascorbate, t-BuOH-H<sub>2</sub>O (1 : 1),<sup>31</sup> (f) BocNHCH<sub>2</sub>COOSu, DIEA, DMF, then Boc deprotection,<sup>29</sup> (g) CHO-CO-R, buffer pH = 4.6,<sup>29</sup> (h) Boc-Ser(t-Bu)OH, PyBOP, DIEA, DMF, then Boc deprotection,<sup>30</sup> (i) NaIO<sub>4</sub>, H<sub>2</sub>O,<sup>30</sup> (j) R-O-NH<sub>2</sub>, 10% AcOH,<sup>30</sup> (k) R-Br, pH = 7.5,<sup>43</sup> (l) R-N<sub>3</sub>, CuSO<sub>4</sub>, Cu(0), sodium ascorbate, DIEA, H<sub>2</sub>O.

4-azidobutanoic acid **3** as an *N*-terminal building block under standard coupling conditions generally applied in this work.

### Click ligations

As a conjugation strategy, copper(I) catalyzed azide-alkyne cycloaddition [3+2] was chosen (Scheme 1). It is a highly efficient coupling method, orthogonal to most known ligation techniques, which gives an option to link together peptidic ligands as well as other functional substituents.<sup>46–49</sup>

To demonstrate the utility of the novel cyclic decapeptide scaffolds **1** and **2** towards the conjugation of unprotected peptide ligands and to investigate steric effects on ligation efficacy, azido-functionalized peptides of different length ranging from four to fourteen residues were used for coupling onto the presented scaffolds. Prior to the coupling of bulky peptidic building blocks, initial studies towards general applicability and optimization of reaction conditions were conducted using the small non-peptidic azido building block **3**. For this purpose, different click systems were tested such as iodo(trimethylphosphite)copper(I)/DIEA in

MeOH–acetonitrile, CuSO<sub>4</sub>/sodium ascorbate/DIEA in water, Cu-wire in water, CuSO<sub>4</sub>/Cu wire/sodium ascorbate/DIEA in water. Combined addition of Cu(II) and Cu(0) in the presence of sodium ascorbate comprised the optimal system characterized with faster and cleaner conversions. We reasoned that as for bulky biological ligands reaction times could be prolonged, a continuous Cu(I) source in the form of a redox pair of Cu(II) and Cu(0) should be installed. The chromatographic traces of the chosen reaction system revealed the formation of synthesis intermediates already 5 min after catalyst addition. Complete conversion was reached within 50 min (Fig. 2). Conjugation of peptides **4–7** onto template **1** were accomplished in the same way. HPLC traces of the reaction components and conjugation products are shown in Fig. 3. Though HPLC monitoring proved that educts were completely consumed, the yields of the resulting conjugates decreased according to the length of the ligands, probably due to the tendency of particular peptides to aggregate in concentrated solutions (see Table 2). The irregular low yield of conjugate **11** could be explained by losses during preparative purification focused on obtaining a high quality product.

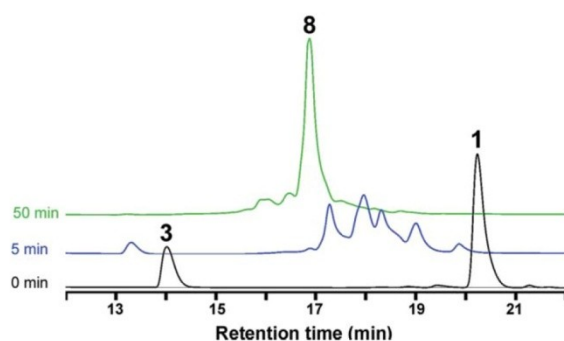


**Fig. 2** HPLC monitoring of CuAAC reaction between alkyne **1** and azide **4** at 220 nm. Gradient: 9→45% acetonitrile in 0.1% aq. TFA over 30 minutes at flow rate 1 mL/min.

High resolution ESI-MS analysis proved the formation of tetrameric conjugates. Exemplary high resolution ESI-MS spectra for conjugate **12** are shown in Fig. 4; for the complete data set see the supplemental material.† Formation of the tetrapeptide conjugates **9–12** was further proved by analytical gel filtration. This analysis was of particular importance for the cases when the click conjugates and their corresponding monomeric peptide ligands showed similar elution behaviour under RP-HPLC conditions (Fig. 3B and C). Size exclusion chromatography made it possible to doubtlessly distinguish between the tetramers and monomers as shown exemplary for compounds **10** and **11** in Fig. 5. Click coupling onto additionally derivatized scaffold **2** differed

from that for **1** carrying only alkyne moieties. Introduction of a bulky hydrophobic FITC substituent affected water solubility of template **2** significantly. Two modifications of the proposed click protocol were employed. Since it was not possible to dissolve the cyclic decapeptide **2** in water, a water–acetonitrile mixture was used. After two days of reaction the presence of click conjugation intermediates could still be detected in the HPLC trace (Fig. 6A), and the yield of the final product was significantly lower in comparison to the reactions carried out in pure water (13% and 30% after purification, respectively). Therefore, we increased the amount of tertiary amino base (DIEA) in the reaction system that made it possible to avoid the use of an organic co-solvent. This resulted in a remarkable acceleration of the reaction rate and yielded the target conjugation product within 5 h.

Nevertheless, taking into consideration the solubility problems caused by bulky substituents, it seems reasonable to introduce a solubilizing moiety like PEG into templates carrying hydrophobic ligands through one of the possible ligation sites (Fig. 1, *e.g.* position 4). This can be easily achieved *via* an incorporation of an additional orthogonal amino group or thiol function.

## Experimental

### General procedures

All chemicals and solvents purchased from Acros, Roth, Novabiochem, Aldrich or Sigma were of highest grade available. Fmoc-L-Pra-OH was obtained from Anaspec. All comprising a PrepStar

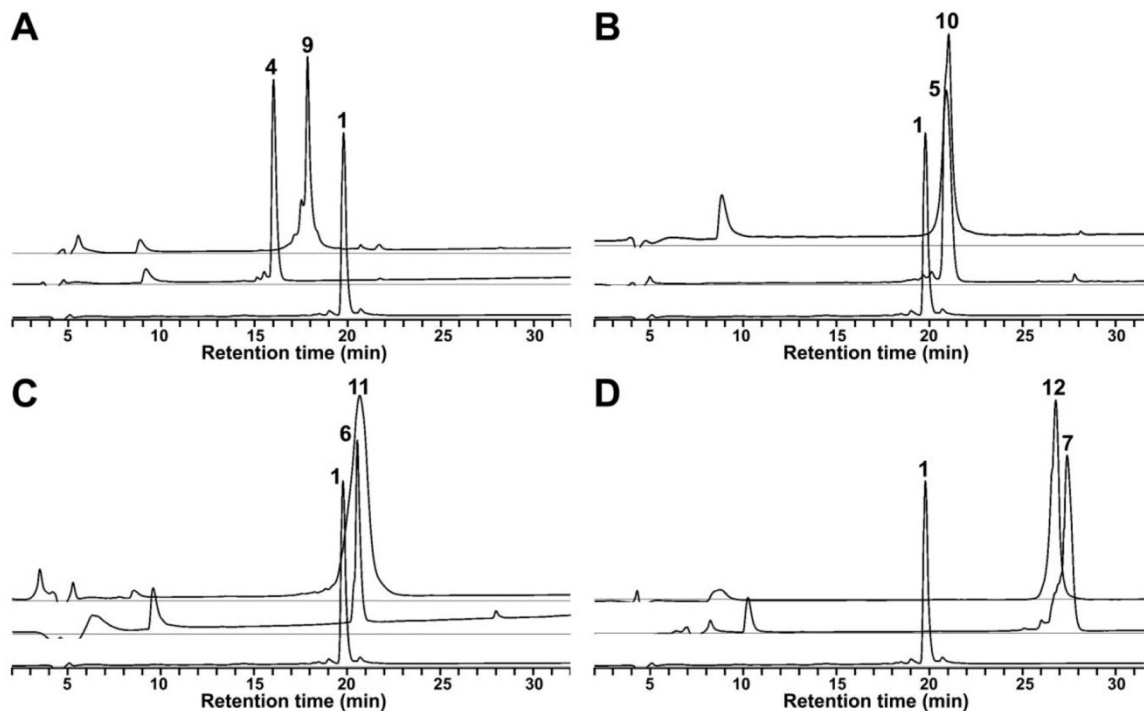


**Fig. 3** HPLC traces of click reaction components and the resulting conjugates at 220 nm. Gradient: 9→45% acetonitrile in 0.1% aq. TFA over 30 minutes at flow rate 1 mL/min.

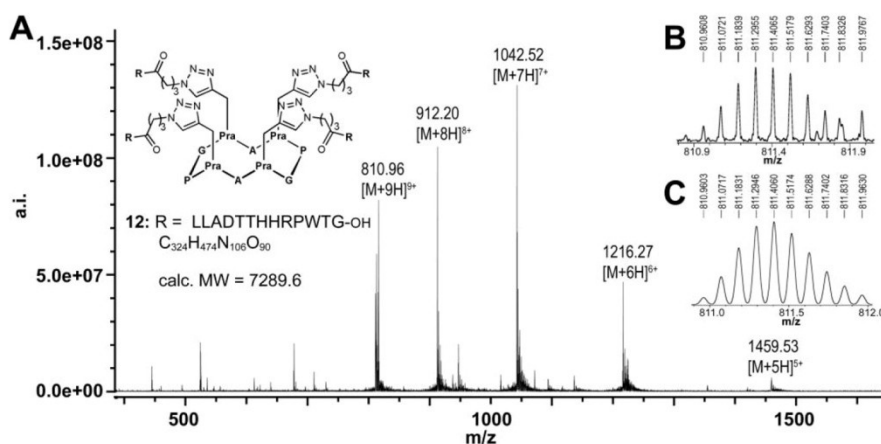


**Fig. 4** Mass spectra of conjugate **12**. A, ESI-MS spectrum; B, high resolution spectrum recorded for  $[M + 9H]^{9+}$ ; C, mass distribution calculated for  $C_{324}H_{483}N_{106}O_{90}$  ( $9+$ ).

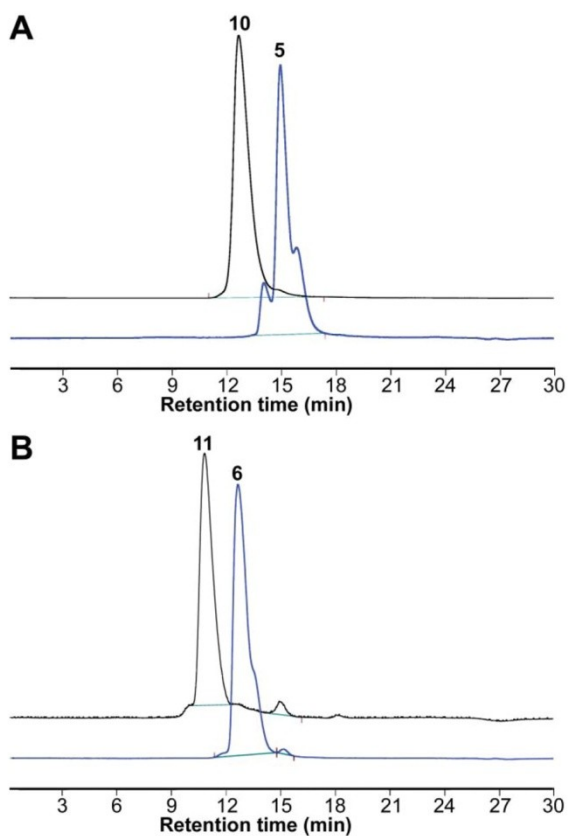


**Fig. 5** GFC traces of monomeric peptide ligands and corresponding tetra-conjugates at 220 nm. Eluent: 150 m aq. NaCl at flow rate 0.75 mL/min.

218 Solvent Delivery Module, a ProStar 410 HPLC AutoSampler and a ProStar 325 Dual Wavelength UV-Vis HPLC Detector using a Phenomenex Synergi 4u Hydro-RP 80 Å (250 × 4.6 mm, 4 μm, 8 nm) column for analytical runs and a YMC J'sphere ODS-H80,

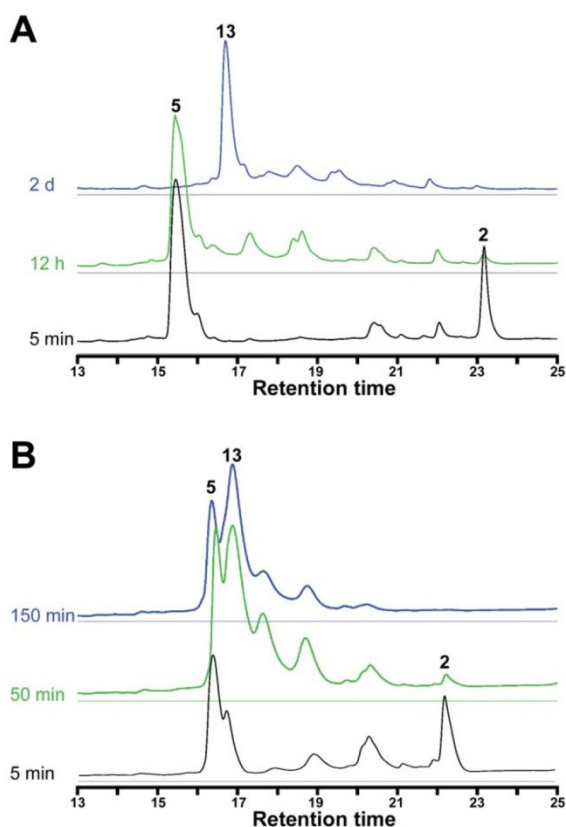


**Fig. 6** HPLC monitoring of CuAAC reaction between alkyne **2** and azide **5** at 220 nm. Gradient: 9 → 72% acetonitrile in 0.1% aq. TFA over 30 minutes at flow rate 1 mL/min. A, click reaction in water-acetonitrile (2 : 1); B, click reaction in water with excess DIEA (2 eq. according to copper catalyst).

RPC-18 (250 × 20 mm, 4 μm, 8 nm) for semi-preparative ones. The solvent system consisted of eluent A (0.1% aq. TFA) and eluent B (90% aq. acetonitrile containing 0.1% TFA). ESI mass spectra

**Table 1** Building blocks synthesized in the presented study

Entry	Sequence	Calculated Mol. Wt.	Observed <i>m/z</i>	R <sub>f</sub> <sup>b</sup>	Yield <sup>c</sup> [%]
Alkyne	<b>1</b> 	830.4	853.6	20.29	36
	<b>2</b> 	1276.6	1299.6	22.71	73
Azide	<b>3</b> 	129.1	n.d. <sup>a</sup>	13.54	78
	<b>4</b> 	620.3	621.3	16.04	33
	<b>5</b> 	1043.5	1044.6	20.92	17
	<b>6</b> 	1328.6	1329.7	20.54	5
	<b>7</b> 	1614.8	1616.0	27.41	23

<sup>a</sup> Characterized by <sup>1</sup>H- and <sup>13</sup>C-NMR.<sup>32, b</sup> Compounds **1** and **3–7**: gradient: 9→45% acetonitrile in 0.1% TFA over 30 minutes at 1 mL/min; compound **2**: gradient: 9→72% acetonitrile in 0.1% TFA over 30 minutes at 1 mL/min. <sup>c</sup> Overall yield calculated from initial loading of the resin.

were recorded on a Bruker-Franzen Esquire LC and a Bruker Apex-Q IV FT-ICR mass spectrometer. <sup>1</sup>H-NMR and <sup>13</sup>C-NMR spectra were obtained with a Bruker DRX300 instrument (300 MHz). Peptides were synthesized on a manual Discover SPS Microwave Peptide Synthesizer (CEM) using the Fmoc strategy. Amino acids were employed in 4 eq. excess according to resin. HBTU (3.9 eq) and DIEA (8 eq.) were applied as coupling reagents. Coupling microwave conditions were 55 °C and 20 W within 10 min. Fmoc deprotection was performed by treatment with piperidine (20% in NMP) at 50 °C by 20 W microwave power and within 5 min. Cleavage from the Wang resin was done either at room temperature within 2 h or in the microwave at 40 °C, other amino acids were supplied by CEM; preloaded Fmoc-Gly-Wang-resin by Novabiochem; preloaded H-Gly-2Cl-Trt-resin by Iris Biotech. Both analytical and semi-preparative RP-HPLC were performed on a Varian modular system 20 W within 30 min using TFA/H<sub>2</sub>O/anisole/TES (36:2:1:1, v/v/v/v) cleavage cocktail. Cleavage from 2-Cl-Trt resin was performed with acetic acid/DCM/MeOH (5:4:1, v/v/v) mixture within 2–3 h.

#### Synthesis of scaffold 1

The linear precursor peptide NH<sub>2</sub>-Pra-Ala-Pra-Pro-Gly-Pra-Ala-Pra-Pro-Gly-OH was synthesized *via* microwave assisted Fmoc

SPPS on Wang resin preloaded with Fmoc-Gly (loading capacity 0.61 mmol/g). Coupling efficacy was controlled by the Kaiser test. Both Fmoc-Ala-OH building blocks were double coupled as well as the C-terminal proline. After cleavage from the resin with 95% aq. TFA and lyophilization, cyclization was performed without further purification by treatment with HBTU (1 eq.) and DIEA (2 eq.) in diluted solution (1 mg peptide/1 mL DMF) overnight at ambient temperature. After solvent removal under reduced pressure, the crude cyclic decapeptide was purified by preparative HPLC to yield 55 mg of pure *cyclo*-(Pra-Ala-Pra-Pro-Gly)<sub>2</sub> **1** (Table 1).

#### Synthesis of scaffold 2

The linear precursor peptide NH<sub>2</sub>-Pra-Lys(Boc)-Pra-Pro-Gly-Pra-Ala-Pra-Pro-Gly-OH was synthesized *via* microwave assisted Fmoc SPPS on a 2-Cl-Trt resin preloaded with Fmoc-Gly. Coupling efficacy was controlled by the Kaiser test. All amino acids were double coupled except for the Fmoc-Pra-OH building blocks. After cleavage from the resin with a cleavage cocktail containing 50% acetic acid, 40% DCM and 10% methanol followed by lyophilization, cyclization was performed directly with the crude linear peptide by treatment with PyBOP (1.2 eq.) and DIEA (3 eq.) in diluted solution (1 mg peptide/1 mL DMF) overnight

**Table 2** Peptide tetra-conjugates 8–13

Entry	Educts		HPLC <sup>a</sup> R <sub>t</sub> /min	GFC <sup>b</sup> R <sub>t</sub> /min	Yield <sup>c</sup> /%
	Alkyne	Azide			
<b>8</b>	1	3	17.50	—	—
<b>9</b>	1	4	17.87	12.32	75
<b>10</b>	1	5	20.9	12.76	50
<b>11</b>	1	6	20.69	11.02	14
<b>12</b>	1	7	25.85	13.52	28
<b>13</b>	2	5	16.27	12.81	30

<sup>a</sup> Compounds **8–12**: gradient: 9→45% acetonitrile in 0.1% TFA over 30 minutes at 1 mL/min; compound **13**: gradient: 9→72% acetonitrile in 0.1% TFA over 30 minutes at 1 mL/min. <sup>b</sup> Eluent: 150 mM NaCl at flow rate 0.75 mL/min. <sup>c</sup> Pure yield after purification *via* HPLC; the loss of substance during routine monitoring of reaction progress and analytical purposes is not considered.

at ambient temperature. The solvent was removed under reduced pressure and the crude cyclic decapeptide *cyclo*-(Pra-Lys(Boc)-Pra-Pro-Gly-Pra-Ala-Pra-Pro-Gly) was treated with 95% aq. TFA to remove the Boc protecting group. Precipitation and washing with MTBE yielded crude *cyclo*-(Pra-K-Pra-P-G-Pra-A-Pra-P-G) in excellent quality that enabled its labelling with amino reactive FITC (2 eq.) in the presence of DIEA (2 eq.) in DMF without additional purification. After DMF removal under reduced pressure the excess of FITC was extracted with ether from a water–methanol (5:1) solution of labelled cyclic decapeptide **2**. This yielded FITC labelled alkyne functionalized RAFT scaffold **2** in excellent yield and quality (19 mg, Table 1).

#### Synthesis of *N*-terminal azido functionalized peptides 4–7

Peptide ligands were synthesized using microwave assisted Fmoc SPPS on Fmoc-Gly preloaded Wang resin using HBTU/DIEA activation in NMP. Each coupling cycle took 10 min, and the Fmoc deprotection was accomplished within 5 min. To introduce the *N*-terminal azido-group, 4 eq. of 4-azidobutanoic acid **3** synthesized from methyl 4-bromobutanoate following a reported procedure<sup>50</sup> were coupled onto the terminal amino group under the same coupling conditions. Cleavage from the solid support

was conducted in the microwave oven within 30 min using 95% TFA at 38 °C. After microwave assisted cleavage from the solid support followed by MTBE precipitation, purification was done by preparative HPLC to yield pure azide functionalized peptide ligands **4–7** (see Table 1).

#### Copper(I) catalyzed azide–alkyne [3+2] cycloaddition (CuAAC) reaction

The click ligations of the alkyne scaffold **1** and the azido building blocks **3–7** were accomplished by treatment of an aqueous solution of **1** (2.4 μmol) and the corresponding azide (9.6 μmol) with CuSO<sub>4</sub> (28.8 μmol), sodium ascorbate (28.8 μmol), DIEA (28.8 μmol) and 15 mg of HNO<sub>3</sub>-treated Cu-wire. Reaction progress was monitored by analytical HPLC (Fig. 2, 3 and 6) until conversion of both the azide and alkyne components was complete (50 min–4 h). The solvation of occasional precipitate was performed by addition of 0.3% ammonia. Conjugates **8–13** were isolated *via* semi-preparative RP-HPLC and characterized *via* RP-HPLC, GFC and ESI-MS as mentioned in Tables 2 and 3.

The click reaction between FITC labeled alkyne scaffold **2** and the azido building block **5** was conducted by treatment of the solution of **2** (1.56 μmol) and the azide (6.28 μmol) in water with CuSO<sub>4</sub> (18.72 μmol), sodium ascorbate (18.72 μmol) and DIEA (37.44 μmol). The reaction was continuously shaken at ambient temperature. Reaction progress was monitored by analytical RP-HPLC (Fig. 6B). The conjugation product was isolated by semi-preparative RP-HPLC yielding 2.6 mg of **13** as a yellow powder (Tables 2, 3). The formation of the desired conjugate was proven by GFC and ESI-MS.

#### Conclusions

We demonstrate the utility of the CuAAC reaction for the synthesis of tetravalent peptide conjugates on a cyclic peptide template. Unprotected biologically relevant azido peptides are efficiently converted into the corresponding cycloaddition products. The introduction of an azide moiety into the growing peptide chain by pre-activated 4-azidobutanoic acid is easy, efficient and needs no protecting groups or harsh reaction conditions. Alternatively,

**Table 3** Summarized ESI-MS data for the synthesized peptidic tetra-conjugates 9–13

	Entry	9	10	11	12	13	
		Calc. MW	3311.4	5004.5	6144.9	7289.6	5450.6
		Formula	C <sub>140</sub> H <sub>194</sub> N <sub>50</sub> O <sub>46</sub>	C <sub>216</sub> H <sub>326</sub> N <sub>78</sub> O <sub>62</sub>	C <sub>256</sub> H <sub>402</sub> N <sub>74</sub> O <sub>102</sub>	C <sub>324</sub> H <sub>474</sub> N <sub>106</sub> O <sub>90</sub>	C <sub>240</sub> H <sub>344</sub> N <sub>80</sub> O <sub>67</sub> S
Measured	[M + H] <sup>+</sup>	3312.45	5005.51	6145.92	7290.63	5451.6	
	[M + 2H] <sup>2+</sup>	—	—	—	—	—	
	[M + 3H] <sup>3+</sup>	1104.83	—	—	2430.88	—	
	[M + 4H] <sup>4+</sup>	828.87	1252.13	1537.74	—	—	
	[M + 5H] <sup>5+</sup>	663.30	1001.91	—	1459.53	—	
	[M + 6H] <sup>6+</sup>	—	835.0863 <sup>a</sup>	—	1216.27	—	
	[M + 7H] <sup>7+</sup>	—	715.9316 <sup>a</sup>	—	1042.52	—	
	[M + 8H] <sup>8+</sup>	—	626.5661 <sup>a</sup>	—	912.2046 <sup>a</sup>	—	
	[M + 9H] <sup>9+</sup>	—	—	—	810.9598 <sup>a</sup>	—	

<sup>a</sup> High resolution spectra (see Fig. 4 and supplementary information†).



azide bearing peptides and proteins are also readily accessible not only *via* Fmoc SPPS using the commercially available building blocks, *e.g.* Fmoc-L-azidohomoalanine, but through several selective protein modifications.<sup>51,52</sup> Azido group bearing proteins can be obtained by recombinant expression methods *via* growing *E. coli* strains deficient in methionine synthesis in the presence of azido homoalanine (AZH) resulting in the incorporation of AZH in place of methionine in proteins.<sup>51</sup> Moreover, a recently reported single-step azide introduction *via* an aqueous diazo transfer provides another possibility to functionalize native proteins with a clickable moiety.<sup>52</sup>

The alkyne functionalized cyclic peptide templates used in this study can be easily synthesized from commercially available building blocks and encompass two important features: (a) they have defined three dimensional architecture that provides free access to reactive moieties and allows for the coupling of bulky ligands without hindrance and (b) they enable conjugation of unprotected peptides in water using the simple, inexpensive and effective copper catalyst also providing an option for the oligomerization of native folded proteins. Click cycloaddition is fast and highly selective; the resulting conjugates are easily separable *via* HPLC or GFC.

It will be interesting to see whether larger peptides exceeding the length of 14 residues used in this study, miniproteins<sup>53</sup> or even proteins can be placed in fourfold copies onto the decapeptide scaffold and if steric constraints exist that might negatively influence conjugation efficiency. In this case, flexible linkers like polyethylene glycol<sup>54</sup> or oligoglycine could be introduced for enhancing conformational flexibility.

Peptide **5** of the model peptides used in this study (IPRGDYRG) contains an RGD motif and is known to bind GPIIb/IIIa receptor on the surface of platelets, thereby inhibiting platelet aggregation.<sup>55</sup> Systematic studies to compare biological activity of tetravalent peptide conjugates compared to their monomeric counterparts are currently underway aimed at obtaining a better understanding of the avidity effects imposed by the particular spatial orientation of peptide ligands induced by the conjugation onto a cyclic decapeptide scaffold.

## Acknowledgements

This work was supported by the Deutsche Forschungsgemeinschaft through grant KO 1390/9-1 and by BMBF.

## References

- M. Mammen, S. K. Choi and G. M. Whitesides, *Angew. Chem., Int. Ed.*, 1998, **37**, 2754–2794.
- V. Martos, P. Castreno, J. Valero and J. de Mendoza, *Curr. Opin. Chem. Biol.*, 2008, **12**, 698–706.
- R. J. Kok, A. J. Schraa, E. J. Bos, H. E. Moorlag, S. A. Åsgeirsdóttir, M. Everts, D. K. F. Meijer and G. Molema, *Bioconjugate Chem.*, 2002, **13**, 128–135.
- G. Thumshirn, U. Hersel, S. L. Goodman and H. Kessler, *Chem.–Eur. J.*, 2003, **9**, 2717–2725.
- S. E. Cwirla, P. Balasubramanian, D. J. Duffin, C. R. Wagstrom, C. M. Gates, S. C. Singer, A. M. Davis, R. L. Tansik, L. C. Mattheakis, C. M. Boytos, P. J. Schatz, D. P. Baccanari, N. C. Wrighton, R. W. Barrett and W. J. Dower, *Science*, 1997, **276**, 1696–1699.
- O. Vadas, O. Hartley and K. Rose, *Biopolymers*, 2008, **90**, 496–502.
- Z. Fan, Y. Lu, X. Wu and J. Mendelsohn, *J. Biol. Chem.*, 1994, **269**, 27595–27602.
- Z. Hayouka, J. Rosenbluh, A. Levin, S. Loya, M. Lebendiker, D. Veprintsev, M. Kotler, A. Hizi, A. Loyter and A. Friedler, *Proc. Natl. Acad. Sci. U. S. A.*, 2007, **104**, 8316–8321.
- H. J. Wester and H. Kessler, *J. Nucl. Med.*, 2005, **46**, 1940–1945.
- Y. Singh, G. T. Dolphin, J. Razkin and P. Dumy, *ChemBioChem*, 2006, **7**, 1298–1314.
- M. Mutter, R. Hersperger, K. Gubernator and K. Muller, *Proteins*, 1989, **5**, 13–21.
- G. Tuchscherer, C. Servis, G. Corradin, U. Blum, J. Rivier and M. Mutter, *Protein Sci.*, 1992, **1**, 1377–1386.
- R. Floegel and M. Mutter, *Biopolymers*, 1992, **32**, 1283–1310.
- K. H. Altmann and M. Mutter, *Int. J. Biochem.*, 1990, **22**, 947–956.
- G. Tuchscherer, V. Steiner, K. H. Altmann and M. Mutter, *Methods Mol. Biol.*, 1994, **36**, 261–285.
- G. Tuchscherer and M. Mutter, *J. Biotechnol.*, 1995, **41**, 197–210.
- G. Tuchscherer and M. Mutter, *J. Pept. Sci.*, 1995, **1**, 3–10.
- M. Mutter and G. Tuchscherer, *Cell Mol. Life Sci.*, 1997, **53**, 851–863.
- G. Tuchscherer, D. Grell, M. Mathieu and M. Mutter, *J. Pept. Res.*, 1999, **54**, 185–194.
- D. Grell, J. S. Richardson and M. Mutter, *J. Pept. Sci.*, 2001, **7**, 146–151.
- S. Peluso, T. Ruckle, C. Lehmann, M. Mutter, C. Peggion and M. Crisma, *ChemBioChem*, 2001, **2**, 432–437.
- Z. H. Peng, *Biopolymers*, 1999, **49**, 565–574.
- P. Dumy, I. M. Eggleston, G. Esposito, S. Nicula and M. Mutter, *Biopolymers*, 1996, **39**, 297–308.
- A. S. Causton and J. C. Sherman, *J. Pept. Sci.*, 2002, **8**, 275–282.
- H. K. Rau, N. DeJonge and W. Haehnel, *Angew. Chem., Int. Ed.*, 2000, **39**, 250–253.
- R. Schnepf, P. Horth, E. Bill, K. Wieghardt, P. Hildebrandt and W. Haehnel, *J. Am. Chem. Soc.*, 2001, **123**, 2186–2195.
- J. Hauert, J. Fernandez-Carneado, O. Michielin, S. Mathieu, D. Grell, M. Schapira, O. Spertini, M. Mutter, G. Tuchscherer and T. Kovacsovic, *ChemBioChem*, 2004, **5**, 856–864.
- M. P. Glenn, L. K. Pattenden, R. C. Reid, D. P. Tyssen, J. D. Tyndall, C. J. Birch and D. P. Fairlie, *J. Med. Chem.*, 2002, **45**, 371–381.
- D. Boturyn, J. L. Coll, E. Garanger, M. C. Favrot and P. Dumy, *J. Am. Chem. Soc.*, 2004, **126**, 5730–5739.
- D. Boturyn, E. Defrancq, G. T. Dolphin, J. Garcia, P. Labbe, O. Renaudet and P. Dumy, *J. Pept. Sci.*, 2008, **14**, 224–240.
- J. Wang, H. Li, G. Zou and L. X. Wang, *Org. Biomol. Chem.*, 2007, **5**, 1529–1540.
- R. Hirschmann, K. C. Nicolau, S. Pietranico, E. M. Leahy, J. Salvino, B. Arison, M. A. Cichy, P. G. Spoors, W. C. Shakespeare, P. A. Sprengler, P. Hamley, A. B. Smith, T. Reisine, K. Raynor, L. Maechler, C. Donaldson, W. Vale, R. M. Freidinger, M. R. Cascieri and C. D. Strader, *J. Am. Chem. Soc.*, 1993, **115**, 12550–12568.
- R. Boyce, G. Li, H. P. Nestler, T. Suenaga and W. C. Still, *J. Am. Chem. Soc.*, 1994, **116**, 7955–7956.
- T. Sasaki and E. T. Kaiser, *J. Am. Chem. Soc.*, 1989, **111**, 380–381.
- M. Lieberman and T. Sasaki, *J. Am. Chem. Soc.*, 1991, **113**, 1470–1471.
- C. T. Choma, J. D. Lear, M. J. Nelson, P. L. Dutton, D. E. Robertson and W. F. DeGrado, *J. Am. Chem. Soc.*, 1994, **116**, 856–865.
- M. R. Ghadiri, C. Soares and C. Choi, *J. Am. Chem. Soc.*, 1992, **114**, 825–831.
- R. Hirschmann, P. A. Sprengler, T. Kawasaki, J. W. Leahy, W. C. Shakespeare and A. B. Smith, *Tetrahedron*, 1993, **49**, 3665–3676.
- M. Kahn, *Synlett*, 1993, 821–826.
- J. Eichler, A. W. Lucka and R. A. Houghten, *Pept. Res.*, 1994, **7**, 300–307.
- J. M. Ostresh, G. M. Husar, S. E. Blondelle, B. Dorner, P. A. Weber and R. A. Houghten, *Proc. Natl. Acad. Sci. U. S. A.*, 1994, **91**, 11138–11142.
- M. Mutter and S. Villeumier, *Angew. Chem., Int. Ed. Engl.*, 1989, **28**, 535–554.
- H. K. Rau and W. Haehnel, *J. Am. Chem. Soc.*, 1998, **120**, 468–476.
- B. H. Monien, F. Drepper, M. Sommerhalter, W. Lubitz and W. Haehnel, *J. Mol. Biol.*, 2007, **371**, 739–753.
- S. C. Story and J. V. Aldrich, *Int. J. Pept. Protein Res.*, 1994, **43**, 292–296.
- C. W. Tornøe, C. Christensen and M. Meldal, *J. Org. Chem.*, 2002, **67**, 3057–3064.
- V. V. Rostovtsev, L. G. Green, V. V. Fokin and K. B. Sharpless, *Angew. Chem., Int. Ed.*, 2002, **41**, 2596–2599.

- 48 D. T. Rijkers, G. W. van Esse, R. Merks, A. J. Brouwer, H. J. Jacobs, R. J. Pieters and R. M. Liskamp, *Chem. Commun.*, 2005, 4581–4583.
- 49 B. Jagadish, R. Sankaranarayanan, L. Xu, R. Richards, J. Vagner, V. J. Hruby, R. J. Gillies and E. A. Mash, *Bioorg. Med. Chem. Lett.*, 2007, **17**, 3310–3313.
- 50 N. Khoukhi, M. Vautier and R. Carrié, *Tetrahedron*, 1987, **43**, 1811–1822.
- 51 K. L. Kiick, E. Saxon, D. A. Tirrell and C. R. Bertozzi, *Proc. Natl. Acad. Sci. U. S. A.*, 2002, **99**, 19–24.
- 52 S. F. van Dongen, R. L. Teeuwen, M. Nallani, S. S. van Berkel, J. J. Cornelissen, R. J. Nolte and J. C. van Hest, *Bioconjugate Chem.*, 2009, **20**, 20–23.
- 53 H. Kolmar, *FEBS J.*, 2008, **275**, 2684–2690.
- 54 A. Abuchowski, J. R. McCoy, N. C. Palczuk, T. van Es and F. F. Davis, *J. Biol. Chem.*, 1977, **252**, 3582–3586.
- 55 S. Reiss, M. Sieber, V. Oberle, A. Wentzel, P. Spangenberg, R. Claus, H. Kolmar and W. Losche, *Platelets*, 2006, **17**, 153–157.

## 2.2 Locked *trans*- and *cis*-Amide Surrogates within the SFTI-1 Backbone

### Title:

**Braces for the Peptide Backbone: Insights into Structure–Activity Relationships of Protease Inhibitor Mimics with Locked Amide Conformations**

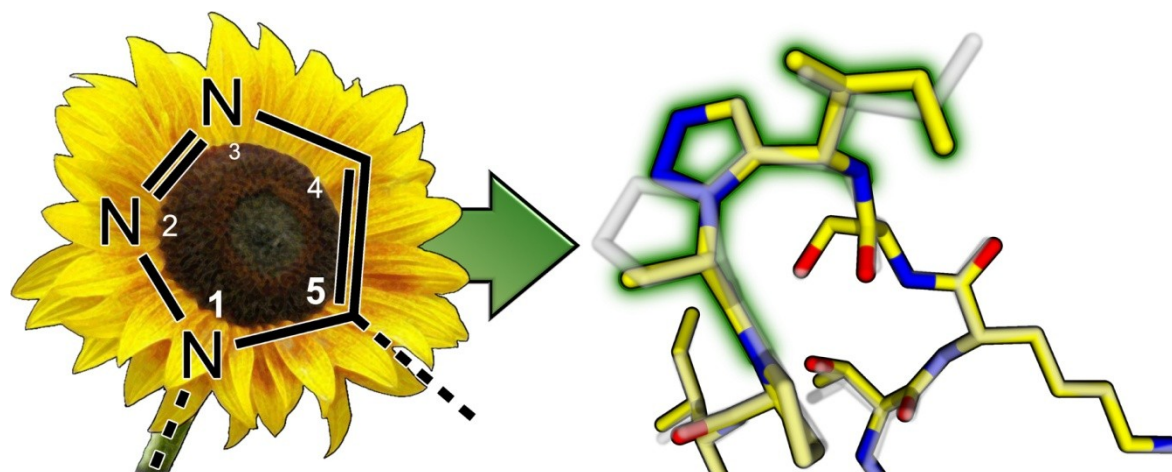
### Authors:

Marco Tischler, Daichi Nasu, Martin Empting, Stefan Schmelz, Dirk W. Heinz, Philipp Rottmann, Harald Kolmar, Gerd Buntkowsky, Daniel Tietze, Olga Avrutina

### Bibliographic Data:

*Angewandte Chemie International Edition*,  
Volume 51, Issue 15, Pages 3708–3712, April 10, 2012.  
DOI: 10.1002/anie.201108983.  
First published online: February 28, 2012.

### Graphical Abstract:



Flower power: Potent protease inhibitors containing triazolyl mimics of *cis* and *trans* backbone amides were engineered based on the structure of the sunflower trypsin inhibitor 1. The biologically relevant *cis*-Pro motif was successfully replaced with a non-prolyl unit. High-resolution crystal structures of 1,4- and 1,5-disubstituted 1,2,3-triazolyl peptidomimetics can serve in the design of tailor-made Bowman–Birk inhibitors.

### Contributions by M. Empting:

- Developed concept together with MT, DT, and OA
- Synthesized and isolated peptidic compounds **3**, **4**, and wild-type SFTI-1[1,14]
- Performed HPLC and ESI-MS analysis of **3**, **4**, and wild-type SFTI-1[1,14]
- Performed trypsin-inhibition assays with **3**, **4**, and wild-type SFTI-1[1,14]
- Wrote the article together with MT, DT, and OA
- Created all figures of the maintext

## Braces for the Peptide Backbone: Insights into Structure–Activity Relationships of Protease Inhibitor Mimics with Locked Amide Conformations\*\*

Marco Tischler, Daichi Nasu, Martin Empting, Stefan Schmelz, Dirk W. Heinz, Philipp Rottmann, Harald Kolmar, Gerd Buntkowsky,\* Daniel Tietze,\* and Olga Avrutina\*

The architecture of protein macromolecules fundamentally depends on the sequential arrangement of peptide backbone bonds in defined conformations. Among the three torsion angles ( $\varphi$ ,  $\psi$ , and  $\omega$ ) present at each amino acid, it is the amide bond ( $\omega$ ) which is intrinsically hindered as a result of its partial double-bond character and it is thus more or less restricted to either a *trans* or a *cis* conformation (Figure 1).<sup>[1]</sup> Generally, amide bonds occur predominantly in the *trans* conformation as it minimizes unfavorable contacts between adjacent amino acids.<sup>[1d]</sup> Nevertheless, *cis* amides, if present, are usually an imperative for bioactivity.<sup>[2]</sup>

The distribution of *cis/trans* conformations drastically changes from about 0.03% for non-prolyl peptide bonds to about 6% for Xaa-Pro motifs.<sup>[1a-c]</sup> This is directly linked to the propensity of proline with its cyclic side chain to form a sterically hindered backbone motif which strongly affects the preceding peptide bond.<sup>[3]</sup>

Beyond the structural features that *cis* amide bonds induce in proteins, *cis–trans* isomerization (CTI) adds a kinetic dimension to biomolecular systems. In fact, it is not only one of the rate-determining steps in protein folding,<sup>[4]</sup> but CTI also provides the possibility for a time-dependent conformational switch, thus allowing for a dynamic modulation of structure and activity.<sup>[5]</sup>

During the last decade, a few structural mimics of *cis* amides in peptides and proteins have been reported, among

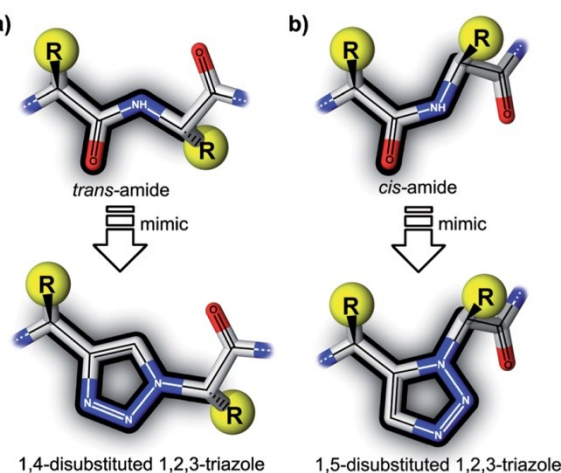


**Figure 1.** Representation of triazolyl amide mimics incorporated into a generic peptide backbone. a) *trans* amide mimic based on a 1,4-disubstituted 1,2,3-triazole, b) *cis* amide mimic based on a 1,5-disubstituted 1,2,3-triazole. Backbone atoms are depicted as sticks and side-chain moieties as balls. An overlay of the Lewis structure with stereo information is given. N blue, C light gray, O red, side chains yellow; hydrogen atoms omitted for clarity. The dihedral angles defining the *trans* and *cis* amide bonds ( $\omega$  torsion angles) and the respective triazole-based mimics are highlighted by black outlines.

\*] M. Tischler,<sup>[1]</sup> P. Rottmann, Prof. Dr. G. Buntkowsky, Dr. D. Tietze Eduard-Zintl-Institut für Anorganische und Physikalische Chemie Technische Universität Darmstadt Petersenstrasse 22, 64287 Darmstadt (Germany) E-mail: Gerd.Buntkowsky@chemie.tu-darmstadt.de tietze@chemie.tu-darmstadt.de

Homepage: <http://www.tu-darmstadt.de/fb/ch/akbuntkowsky>  
 D. Nasu,<sup>[1]</sup> M. Empting,<sup>[1]</sup> Prof. Dr. H. Kolmar, Dr. O. Avrutina Clemens-Schöpfung-Institut für Organische Chemie und Biochemie Technische Universität Darmstadt Petersenstrasse 22, 64287 Darmstadt (Germany) E-mail: Avrutina@Biochemie-TUD.de  
 Dr. S. Schmelz, Prof. Dr. D. W. Heinz Abteilung Molekulare Strukturbiologie Helmholtz-Zentrum für Infektionsforschung (HZI) Inhoffenstrasse 7, 38124 Braunschweig (Germany)

[†] These authors contributed equally to this work.

[\*\*] This research was supported by the Deutsche Forschungsgemeinschaft (grant Ko 1390/9-1) and LOEWE—Soft Control.

Supporting information for this article is available on the WWW under <http://dx.doi.org/10.1002/anie.201108983>.

them pseudo-prolines,<sup>[2f,5]</sup> disubstituted tetrazoles,<sup>[6]</sup> and triazoles.<sup>[2a,c,7]</sup> Thus, an Asn-*cis*-Pro bond in bovine pancreatic ribonuclease was successfully replaced by a triazolyl unit through expressed protein ligation<sup>[8]</sup> without loss of catalytic activity.<sup>[2e]</sup> In fact, disubstituted 1,2,3-triazoles have been shown to be viable surrogates for *cis* and *trans*-amide bonds, depending on their substitution pattern (Figure 1).<sup>[2c,9]</sup> To our knowledge, no detailed insights into the molecular architecture and structural requirements of a bioactive *cis* amide mimic containing a 1,5-disubstituted 1,2,3-triazole upon binding to its target have been reported.

Herein, we demonstrate the applicability of modular triazole-based backbone elements for locking *cis* and *trans* amides within the functional loop of a Bowman–Birck protease inhibitor (BBI).<sup>[10]</sup> High-resolution crystal structures revealed the detailed structural features of both *cis* and *trans* triazolyl amide surrogates in highly potent peptidomimetics bound to bovine trypsin. Our results provide new information on the behavior of triazolyl units within active biomolecules,



and lead to a re-evaluation of their steric and electronic homology to the native peptide bond.

As a model peptide the highly potent sunflower trypsin inhibitor 1 (SFTI-1) from *Helianthus annuus* was chosen.<sup>[11]</sup> In the native form, its 14 amino acid backbone GRCKTSIP-PICFPD is cystine bridged and head-to-tail cyclized, and contains an Ile-*cis*-Pro amide bond as an indispensable prerequisite for bioactivity.<sup>[12]</sup> Recently we demonstrated the utility of its open-chain variant (SFTI-1[1,14]) to study the influence of subtle changes within shape-defining regions, like the disulfide bridge, on structure–activity relationships.<sup>[13]</sup> Because of to the highly conserved canonical conformation of the functional loop of protease inhibitors, even minor steric alterations on the sub-Ångstrom range have significantly affected the bioactivity of the investigated peptidomimetics.<sup>[13]</sup>

Besides the cystine motif, the *cis* amide bond between Ile7 and Pro8 is a prominent structural element within the inhibitor loop of SFTI-1[1,14] crucial for its bioactivity (Figure 2).<sup>[12]</sup> Consequently, the replacement of this intriguing conformational archetype by a 1,5-disubstituted 1,2,3-triazole mimic appeared to be a promising concept, although previous attempts to mimic this particular motif with non-natural surrogates were not successful.<sup>[14]</sup> Thus, a *cis* amide mimic must not only match the steric requirements of the parent perfectly, but also provide a similar chemical environment.

It has been shown that replacement of Pro8 by an alanine residue (Figure 2, compound **1**) led to a drastic decrease of inhibitory activity against trypsin.<sup>[12]</sup> This was apparently caused by an induced conformational heterogeneity resulting from the loss of the *cis* amide stabilizing effect of proline. To

validate our results and to assure consistency within the test system used, we included the corresponding Pro→Ala mutants **1** and **2** in this work. Efforts were made to exchange the subsequent *trans* amide bond with a corresponding 1,4-disubstituted counterpart **6** and to synthesize SFTI-1[1,14] derivatives bearing the respective mismatched substitution patterns of the triazolyl moiety at each position (**4** and **5**). To precisely refer to each peptidomimetic compound, we assigned a three-letter code for the introduced dipeptide surrogates. Thus, the one-letter code was used to reflect the mimicked amino acid sequence. A “*c*” or “*t*” indicates the conformation of the amide bond locked by the triazole counterfeit.

Based on 1,5-disubstituted 1,2,3-triazoles, conformationally defined non-prolyl backbone motifs are easily accessible by solid-phase peptide synthesis. All peptides were assembled on a solid support either using commercially available building blocks or synthetic precursors (Scheme 1 and the Supporting Information). (*S*)-2-Azidopropanoic acid (**7**) and the Fmoc-protected alkyne components **8** and **9** were synthesized according to previously reported procedures.<sup>[15]</sup>

Azide **7** was introduced at position 8 or 9 in the growing peptide chain using in situ activation under gentle microwave irradiation. The subsequent generation of 1,4- or 1,5-disubstituted 1,2,3-triazoles **14**–**17** was achieved by Cu<sup>I</sup>- or Ru<sup>II</sup>-catalyzed azide–alkyne cycloaddition (CuAAC or RuAAC, respectively) on the solid support.<sup>[2a,7b,13,16]</sup> Microwave-assisted Fmoc-SPPS was continued until the peptide chain was assembled. After acidolytic cleavage, precipitation, and DMSO- or air-mediated oxidation of crude products, chromatographic purification yielded the cyclic target compounds **1**–**6** on a multi-milligram scale.

In order to gain insights into the spatial aspects of the active loop conformation upon binding to a serine protease, in silico calculations (Supporting Information) and crystallographic analysis were conducted using a modified procedure,<sup>[17]</sup> which resulted in high-resolution crystal structures (1.45–1.55 Å) for the complex of bovine trypsin with [IcA<sup>7,8</sup>]SFTI-1[1,14] **4** and [PtA<sup>8,9</sup>]SFTI-1[1,14] **6** (Figure 3). The inhibitory potency of all synthesized SFTI derivatives was evaluated in enzyme kinetic studies with active-site-titrated trypsin using the chromogenic substrate *Boc*-QAR-*p*NA, and the apparent and substrate-independent inhibitory constants ( $K_i^{\text{app}}$  and  $K_i$ ) were determined as previously reported.<sup>[10b,13]</sup>

As seen from Table 1, the presence of the undesirable conformation at each of the two examined positions led to a drastic decrease of inhibitory activity. Thus, the alanine exchange at position 8 (SFTI derivative **1**) resulted in the loss of the *cis*-stabilizing effect of proline, hence, dynamic disorder of the inhibitory loop by CTI. Locking the *trans* conformation at this position by a 1,4-disubstituted 1,2,3-triazole had an even more dramatic effect: peptidomimetic **4** possessed the lowest activity of all studied compounds. Vice versa, the variant with a locked *cis* conformation through the use of a 1,5-disubstituted triazolyl building block between Ile7 and Ala8 (compound **3**) showed a significant improvement in bioactivity over compound **1**, although not in the range of the parent peptide SFTI-1[1,14]. This can be explained considering the crystal structures of the wild-type inhibitor and **3** in

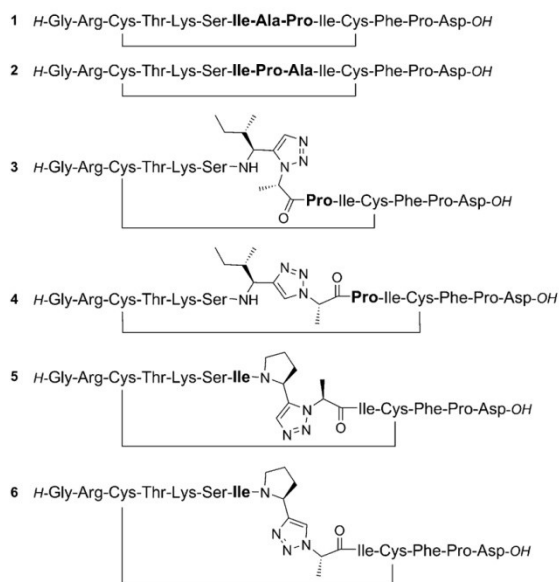
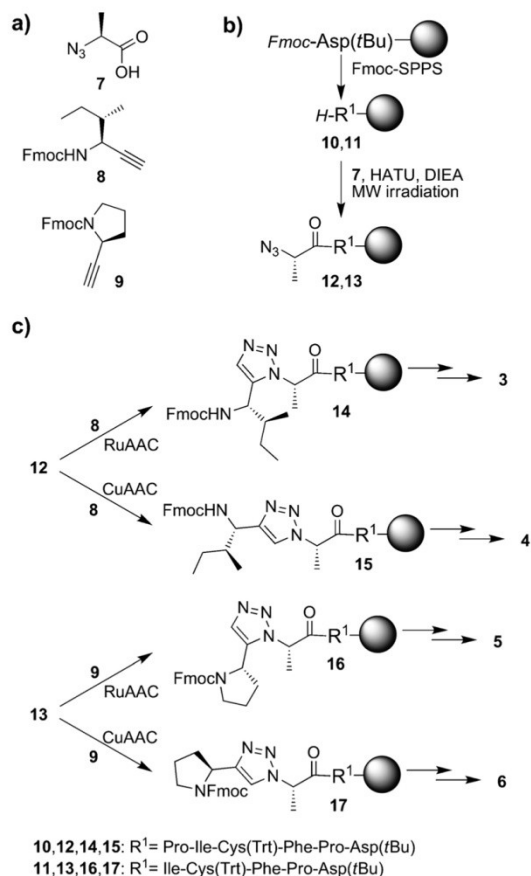


**Figure 2.** Overview of synthesized compounds: [Ala<sup>8</sup>]SFTI-1[1,14] (**1**), [Ala<sup>9</sup>]SFTI-1[1,14] (**2**), [IcA<sup>7,8</sup>]SFTI-1[1,14] (**3**), [PtA<sup>7,8</sup>]SFTI-1[1,14] (**4**), [PcA<sup>8,9</sup>]SFTI-1[1,14] (**5**), [PtA<sup>8,9</sup>]SFTI-1[1,14] (**6**). The investigated *cis* (between Ile7 and Pro8) and *trans* amides (between Pro8 and Pro9) are highlighted in bold.



**Scheme 1.** a) Azide- and alkyne-bearing building blocks (2S)-2-azido-propanoic acid (**7**), (2S,3S)-N-(9-fluorenylmethoxycarbonyl)-1-ethynyl-2-methylbutylamine (**8**), and (2S)-N-(9-fluorenylmethoxycarbonyl)-2-ethynylpyrrolidine (**9**). b) Synthesis of azide-bearing peptide resins **12** and **13**. c) Synthesis of oxidized peptidomimetics **3–6**. Fmoc-SPPS: Fmoc-assisted solid-phase peptide synthesis; HATU: 2-(1*H*-7-azabenzotriazol-1-yl)-1,1,3,3-tetramethyluronium hexafluorophosphate; DIEA: *N,N*-diisopropylethylamine; MW: microwave; RuAAC: ruthenium(II)-catalyzed azide–alkyne cycloaddition using [Cp\*<sub>2</sub>Ru(cod)Cl] (Cp\* = C<sub>5</sub>Me<sub>5</sub>, cod = cyclooctadiene) as catalyst; CuAAC: copper(I)-catalyzed azide–alkyne cycloaddition using CuSO<sub>4</sub>, sodium ascorbate, and DIEA for catalysis; multiple reaction arrows at the end of the synthetic sequence: Fmoc-SPPS, acidolytic cleavage, precipitation, DMSO- or air-mediated oxidation, and chromatographic isolation.

complex with trypsin (Figure 3). It is evident that SFTI-1 is able to form a hydrogen bond with the phenolic hydroxy group of Tyr39 near the binding pocket of the protease through the carbonyl oxygen of Ile7. This finding is supported by in silico experiments, as an energy-minimization procedure (AMBER force field) applied to the crystal structure (1SFI) resulted in formation of the aforementioned hydrogen bond, which may contribute to the binding enthalpy of SFTI-1[1,14]. Indeed, the N2 and N3 atoms of 1,2,3-triazoles have been reported to possess hydrogen-bond-accepting abilities<sup>[18]</sup> and, thus, may partly compensate for the missing interactions.

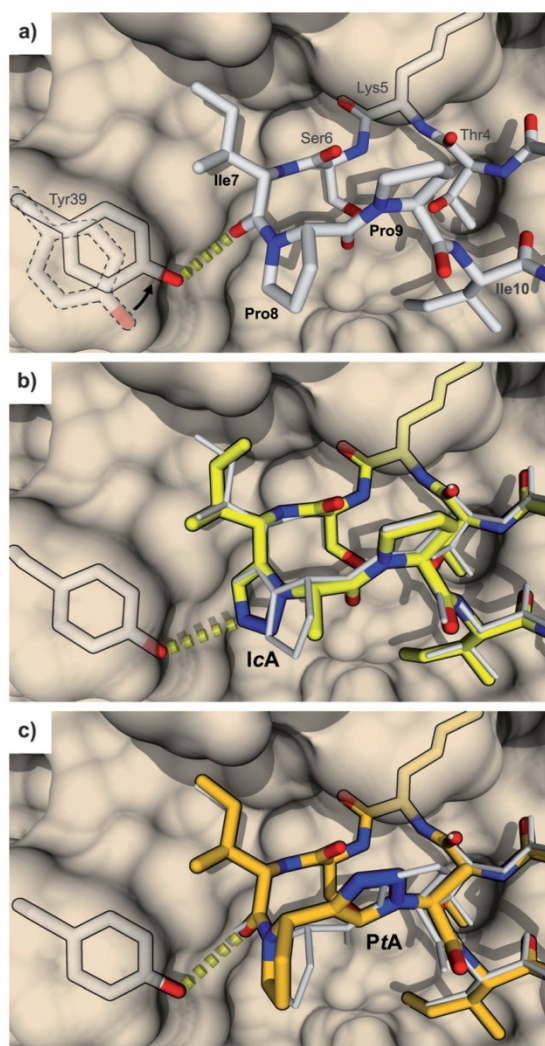


**Figure 3.** Comparison of the inhibitor loops of SFTI-1 and peptidomimetics **3** and **6** in the corresponding protease/inhibitor complexes. Structures aligned at Lys5 of inhibitors. The orientation of the side chain of Tyr39 from trypsin (surface) before (dashed outline) and after energy minimization (solid outline) and the formed hydrogen bonds are shown (Software: YASARA structure with AMBER03 force field, POVRay). Inhibitors shown as stick representations; N blue, O red; hydrogen atoms omitted for clarity. a) Native bicyclic SFTI-1 (C white, PDB ID code: 1SFI). b) [IcA<sup>7,8</sup>]SFTI-1[1,14] **3** (solid outlines, C lemon yellow, PDB ID code: 4ABJ) in an overlay with 1SFI (thin white). c) [PtA<sup>8,9</sup>]SFTI-1[1,14] **6** (solid outlines, C orange, PDB ID code: 4ABI) in an overlay with 1SFI (thin white).

In full agreement with our expectations, the alanine exchange at residue 9 (**2**) locked the *trans* conformation with a 1,4-disubstituted 1,2,3-triazole between Pro8 and Ala9 (**6**) and also had no pronounced effect on bioactivity. This finding can easily be explained taking into consideration that no alterations have been made relative to the native conforma-



**Table 1:** Inhibitory activity of compounds 1–6 and monocyclic SFTI-1[1,14] (wild-type, wt).<sup>[13]</sup>

Entry	Sequence	$K_i$ [nM] <sup>[a]</sup>	Relative activity
1	GRCTKSIAPICFPD	178 ± 25	1 <sup>[b]</sup>
2	GRCTKSIPIAICFPD	3.2 ± 0.5	1 <sup>[c]</sup>
3	GRCTKS[ <b>IcA</b> ]PICFPD	34 ± 5	0.2 <sup>[b]</sup>
4	GRCTKS[ <b>IhA</b> ]PICFPD	302 ± 50	1.7 <sup>[b]</sup>
5	GRCTKS[ <b>PcA</b> ]ICFPD	255 ± 42	80 <sup>[c]</sup>
6	GRCTKS[ <b>PtA</b> ]ICFPD	6.3 ± 1.8	2 <sup>[c]</sup>
wt	GRCTKSIPICFPD	0.2 ± 0.03	–

[a] Error calculated by propagation of error for  $K_i^{app}$  and  $K_M$  (see the Supporting Information); relative activities are calculated as the ratios of the  $K_i$  values for the respective compound to that of [b] 1 or [c] 2.

tion, and no relevant contacts between residue 9 and trypsin were observed in the crystal structure (Figure 3c). In contrast, an induced conformational mismatch (5) caused a drastic reduction of binding affinity.

Nevertheless, it must be mentioned that as a result of its intrinsic architecture, the 1,4-disubstituted 1,2,3-triazole unit as a *trans* amide backbone element increases the distance between the  $\alpha$ -carbons of adjacent residues by 1.3 Å. In contrast, the 1,5-disubstituted 1,2,3-triazolyl *cis* amide mimic preserves bond length and spatial arrangement almost perfectly (increase of distance between  $\alpha$ -carbons: 0.376 Å). Interestingly, the crystal structure of peptidomimetic 6 revealed that the predominant orientation of the incorporated 1,4-disubstituted 1,2,3-triazole significantly differed from the geometry predicted from the hydrogen-bond profile (see the Supporting Information).<sup>[9b]</sup>

In summary, we have demonstrated that 1,4- and 1,5-disubstituted 1,2,3-triazoles can easily be introduced into the backbone of synthetic peptides as viable amide surrogates for the generation of locked *trans* or *cis* conformations. Only peptidomimetics resembling the native-like amide isomers showed high inhibition potency (two-digit nanomolar  $K_i$  values). Our approach allowed for the establishment of the rather uncommon *cis* conformation in sensitive, structure-defining regions of the functional loop of BBI SFTI-1 through the introduction of non-prolyl backbone motifs. The exchange of a proline residue following a *cis* amide bond by any of the other 19 natural amino acids usually leads to a formation of the undesired *trans* isomer. The presented synthetic strategy, in principle, enables the installation of each desired side chain without violating the backbone structure, thus, providing access to tailor-made *cis* amide mimics previously excluded from rational design.

Generally, SFTI-1 is a valuable framework for the development of selective protease inhibitors of diagnostic and therapeutic relevance.<sup>[11a,19]</sup> Since all BBIs share a conserved *cis*-Pro motif in their functional loop, data and structural insights validated for the SFTI-1 scaffold may be extrapolated to the whole inhibitor family.<sup>[20]</sup> Nevertheless, as other trypsin-like proteases of pharmaceutical relevance may differ in their amino acid composition close to the enzyme active pocket, the loss of binding affinity for the *cis* amide mimic 3, presumably caused by changes in the intermolecular hydrogen-bonding pattern, might not be a general problem.

To conclude, our facile preparation of peptidomimetics bearing triazolyl backbone units may find utility in various biochemical applications, as, in contrast to the native amide bond, a triazole does not undergo proteolytic hydrolysis. Therefore, enhanced metabolic stability can be expected.<sup>[21]</sup> Gathered crystallographic data provide fundamental information important for ongoing research aimed at the improvement of peptidomimetic protease inhibitors through implementation of non-natural (triazole) units in their activity-defining regions.

Received: December 20, 2011

Published online: February 28, 2012

**Keywords:** amide mimics · Bowman–Birk inhibitors · protease inhibitors · structure elucidation

- [1] a) J. Song, K. Burrage, Z. Yuan, T. Huber, *BMC Bioinf.* **2006**, *7*, 124; b) A. Jabs, M. S. Weiss, R. Hilgenfeld, *J. Mol. Biol.* **1999**, *286*, 291–304; c) D. Pal, P. Chakrabarti, *J. Mol. Biol.* **1999**, *294*, 271–288; d) D. E. Stewart, A. Sarkar, J. E. Wampler, *J. Mol. Biol.* **1990**, *214*, 253–260; e) M. S. Weiss, A. Jabs, R. Hilgenfeld, *Nat. Struct. Biol.* **1998**, *5*, 676.
- [2] a) W. S. Horne, C. A. Olsen, J. M. Beierle, A. Montero, M. R. Ghadiri, *Angew. Chem.* **2009**, *121*, 4812–4818; *Angew. Chem. Int. Ed.* **2009**, *48*, 4718–4724; b) K. P. Exarchos, T. P. Exarchos, G. Rigas, C. Papaloukas, D. I. Fotiadis, *BMC Bioinf.* **2011**, *12*, 142; c) C. Freund, P. Gehrig, A. Baici, T. A. Holak, A. Plückthun, *Folding Des.* **1998**, *3*, 39–49; d) M. Keller, C. Boissard, L. Patiny, N. N. Chung, C. Lemieux, M. Mutter, P. W. Schiller, *J. Med. Chem.* **2001**, *44*, 3896–3903; e) A. Tam, U. Arnold, M. B. Soellner, R. T. Raines, *J. Am. Chem. Soc.* **2007**, *129*, 12670–12671; f) S. Chierici, M. Jourdan, M. Fiquet, P. Dumy, *Org. Biomol. Chem.* **2004**, *2*, 2437–2441.
- [3] K. P. Lu, G. Finn, T. H. Lee, L. K. Nicholson, *Nat. Chem. Biol.* **2007**, *3*, 619–629.
- [4] a) R. L. Stein, *Adv. Protein Chem.* **1993**, *44*, 1–24; b) F. X. Schmid, L. M. Mayr, M. Mücke, E. R. Schönbrunner, *Adv. Protein Chem.* **1993**, *44*, 25–66.
- [5] a) Y. Che, G. R. Marshall, *Biopolymers* **2006**, *81*, 392–406; b) M. Keller, C. Sager, P. Dumy, M. Schutkowski, G. S. Fischer, M. Mutter, *J. Am. Chem. Soc.* **1998**, *120*, 2714–2720.
- [6] a) J. Zabrocki, G. D. Smith, J. B. Dunbar, H. Iijima, G. R. Marshall, *J. Am. Chem. Soc.* **1988**, *110*, 5875–5880; b) G. D. Smith, J. Zabrocki, T. A. Flak, G. R. Marshall, *Int. J. Pept. Protein Res.* **1991**, *37*, 191–197; c) J. Zabrocki, J. B. Dunbar, K. W. Marshall, M. V. Toth, G. R. Marshall, *J. Org. Chem.* **1992**, *57*, 202–209; d) R. J. Nachman, J. Zabrocki, J. Olczak, H. J. Williams, G. Moyna, A. Ian Scott, G. M. Coast, *Peptides* **2002**, *23*, 709–716.
- [7] a) Y. Hitotsuyanagi, S. Motegi, H. Fukaya, K. Takeya, *J. Org. Chem.* **2002**, *67*, 3266–3271; b) D. Tietze, M. Tischler, S. Voigt, D. Imhof, O. Ohlenschläger, M. Görlach, G. Buntkowsky, *Chem. Eur. J.* **2010**, *16*, 7572–7578.
- [8] T. W. Muir, *Annu. Rev. Biochem.* **2003**, *72*, 249–289.
- [9] a) M. Nahrwold, T. Bogner, S. Eissler, S. Verma, N. Sewald, *Org. Lett.* **2010**, *12*, 1064–1067; b) E. Valverde, F. Lecaille, G. Lalmanach, V. Aucagne, F. Delmas, *Angew. Chem.* **2012**, *124*, 742–746; *Angew. Chem. Int. Ed.* **2012**, *51*, 718–722.
- [10] a) A. Clemente, G. Sonnante, C. Domoney, *Curr. Protein Pept. Sci.* **2011**, *12*, 358–373; b) J. D. McBride, A. B. Brauer, M. Nieve, R. J. Leatherbarrow, *J. Mol. Biol.* **1998**, *282*, 447–458.
- [11] a) P. Li, S. Jiang, S. L. Lee, C. Y. Lin, M. D. Johnson, R. B. Dickson, C. J. Michejda, P. P. Roller, *J. Med. Chem.* **2007**, *50*,

- 5976–5983; b) U. C. Marx, M. L. Korsinczky, H. J. Schirra, A. Jones, B. Condie, L. Otvos, Jr., D. J. Craik, *J. Biol. Chem.* **2003**, *278*, 21782–21789; c) M. L. Korsinczky, H. J. Schirra, K. J. Rosengren, J. West, B. A. Condie, L. Otvos, M. A. Anderson, D. J. Craik, *J. Mol. Biol.* **2001**, *311*, 579–591; d) M. L. Korsinczky, H. J. Schirra, D. J. Craik, *Curr. Protein Pept. Sci.* **2004**, *5*, 351–364.
- [12] A. B. E. Brauer, G. J. Domingo, R. M. Cooke, S. J. Matthews, R. J. Leatherbarrow, *Biochemistry* **2002**, *41*, 10608–10615.
- [13] M. Empting, O. Avrutina, R. Meusinger, S. Fabritz, M. Reinwarth, M. Biesalski, S. Voigt, G. Buntkowsky, H. Kolmar, *Angew. Chem.* **2011**, *123*, 5313–5317; *Angew. Chem. Int. Ed.* **2011**, *50*, 5207–5211.
- [14] D. Scarpi, E. G. Occhiato, A. Trabocchi, R. J. Leatherbarrow, A. B. Brauer, M. Nievo, A. Guarna, *Bioorg. Med. Chem.* **2001**, *9*, 1625–1632.
- [15] a) H. D. Dickson, S. C. Smith, K. W. Hinkle, *Tetrahedron Lett.* **2004**, *45*, 5597–5599; b) J. T. Lundquist IV, J. C. Pelletier, *Org. Lett.* **2001**, *3*, 781–783; c) S. Ohira, *Synth. Commun.* **1989**, *19*, 561–564.
- [16] a) K. Holland-Nell, M. Meldal, *Angew. Chem.* **2011**, *123*, 5310–5312; *Angew. Chem. Int. Ed.* **2011**, *50*, 5204–5206; b) M. Roice, I. Johannsen, M. Meldal, *QSAR Comb. Sci.* **2004**, *23*, 662–673; c) B. C. Boren, S. Narayan, L. K. Rasmussen, L. Zhang, H. Zhao, Z. Lin, G. Jia, V. V. Fokin, *J. Am. Chem. Soc.* **2008**, *130*, 8923–8930.
- [17] S. Lockett, R. S. Garcia, J. J. Barker, A. V. Konarev, P. R. Shewry, A. R. Clarke, R. L. Brady, *J. Mol. Biol.* **1999**, *290*, 525–533.
- [18] a) M. Juricek, P. H. J. Kouwer, A. E. Rowan, *Chem. Commun.* **2011**, *47*, 8740–8749; b) R. M. Meudtner, M. Ostermeier, R. Goddard, C. Limberg, S. Hecht, *Chem. Eur. J.* **2007**, *13*, 9834–9840.
- [19] C. Yuan, L. Chen, E. J. Meehan, N. Daly, D. J. Craik, M. Huang, J. C. Ngo, *BMC Struct. Biol.* **2011**, *11*, 30.
- [20] A. B. Brauer, J. D. McBride, G. Kelly, S. J. Matthews, R. J. Leatherbarrow, *Bioorg. Med. Chem.* **2007**, *15*, 4618–4628.
- [21] O. Hartley, H. Gaertner, J. Wilken, et al., *Proc. Natl. Acad. Sci. USA* **2004**, *101*, 16460–16465.



## 2.3 Disulfide Replacement *via* 1,5-disubstituted 1,2,3-Triazoles

### Title:

“Triazole Bridge”: Disulfide-Bond Replacement by Ruthenium-Catalyzed Formation of 1,5-Disubstituted 1,2,3-Triazoles

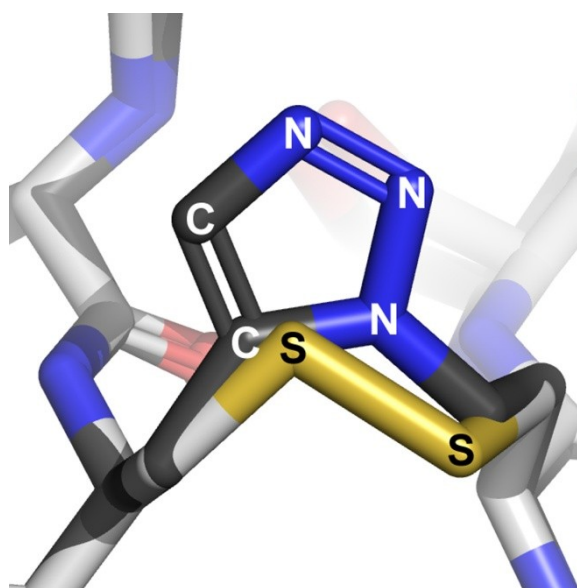
### Authors:

Martin Empting, Olga Avrutina, Reinhard Meusinger, Sebastian Fabritz, Michael Reinwarth, Markus Biesalski, Stephan Voigt, Gerd Buntkowsky, Harald Kolmar

### Bibliographic Data:

*Angewandte Chemie International Edition*,  
Volume 50, Issue 22, Pages 5207–5211, May 23, 2011.  
DOI: 10.1002/anie.201008142.  
First published online: May 04, 2012.

### Graphical Abstract:



A good impression: A modular approach using a ruthenium(II) catalyst during peptide synthesis gives rigid and well-defined triazole bridges as tailor-made substitutes for natural disulfide bridges (see structures). The corresponding modification of the monocyclic sunflower trypsin inhibitor-1 yielded an equally potent peptidomimetic containing a redox stable 1,5-disubstituted 1,2,3-triazole bridge.

### Contributions by M. Empting:

- Developed concept together with OA
- Synthesized and isolated all peptidic compounds
- Performed HPLC, ESI-MS, and IR-analysis as well as trypsin-inhibition assays of all peptidic compounds
- Wrote the article and created all figures

**Disulfide Mimics****“Triazole Bridge”: Disulfide-Bond Replacement by Ruthenium-Catalyzed Formation of 1,5-Disubstituted 1,2,3-Triazoles\*\***

Martin Empting, Olga Avrutina, Reinhard Meusinger, Sebastian Fabritz, Michael Reinwarth, Markus Biesalski, Stephan Voigt, Gerd Buntkowsky, and Harald Kolmar\*

About one fourth of the peptidic macromolecular structures deposited in the protein data base (PDB) contain at least one disulfide bridge.<sup>[1]</sup> In nature, disulfide bonds are formed in a milieu where oxidizing conditions prevail, for example, on the cell surface or in the extracellular matrix. Many proteins benefit from disulfide contributions to their conformational stability. In particular, the defined tertiary folding of oligopeptides smaller than 30 residues essentially relies on macrocyclization through the cystine motif because of the restricted number of noncovalent intramolecular interactions available. Moreover, formation of the disulfide pattern results in structural rigidity of the peptidic framework, as for example, in the family of cystine knot miniproteins,<sup>[2]</sup> leading to conformationally constrained scaffolds with extraordinary thermal stability and resistance against proteolytic degradation.<sup>[2a]</sup> Hence, the discovery and development of disulfide-bridged peptides suitable for diagnostic and therapeutic applications remains a field of intense research.<sup>[3]</sup>

The in-vitro generation of disulfide bonds in peptides is usually achieved post-synthetically and mediated by DMSO, air oxygen, or other oxidizing agents. Although this reaction step can be achieved under relatively mild conditions in solution, it remains one of the most demanding obstacles towards high-yield peptide synthesis, especially for disulfide-rich species in which the controlled regiospecific formation of several disulfide bonds is not trivial to control.<sup>[4]</sup> In addition, to suppress unwanted intermolecular reactions of the thiol groups of individual peptides, oxidative folding usually has to be conducted in highly diluted solutions. In spite of the use of

glutathione-based redox buffers, polymer-supported oxidation systems, macrocyclization on the solid support and/or orthogonal protecting groups, control over the topology of the disulfide bridges formed is still a challenge.<sup>[4a,e,f,5]</sup>

In view of these difficulties and to improve the redox stability of bridged peptides, several routes towards synthetic disulfide surrogates have been developed.<sup>[6]</sup> Straightforward approaches usually employ thioether, olefin, or alkane-based isosters.<sup>[6a,b,d-f]</sup> However, cystathione bridges require multiple synthetic steps and careful choice of orthogonal protection, and dicarba bridges give *cis/trans* isomers during ring-closing metathesis (RCM).<sup>[6a,b,f]</sup> Only an additional purification step or the subsequent palladium-catalyzed hydrogenation of the unsaturated species to the corresponding alkane leads to a construct with defined configuration.<sup>[6b,f]</sup>

In 2004, Meldal et al. described the utility of copper(I)-catalyzed azide-alkyne cycloaddition (CuAAC) for a triazole-based disulfide replacement.<sup>[6c]</sup> Owing to the compelling characteristics of this prototypic “click” reaction, it has been extensively applied in peptide chemistry exploiting the almost perfect orthogonality to side-chain reactivities.<sup>[7]</sup> The introduction of 1,4-disubstituted 1,2,3-triazoles into peptides has also been used to mimic and rigidify conformations of the amide backbone.<sup>[7d,8]</sup> Moreover, a variety of examples of CuAAC-based macrocyclizations of peptides in solution and on solid supports has been reported.<sup>[6c,8d,9]</sup>


Using the same azide- and alkyne-functionalized building blocks, 1,5-disubstituted 1,2,3-triazoles can be generated in the ruthenium(II)-catalyzed variant (RuAAC) of the CuAAC.<sup>[10]</sup> This reaction expands the range of peptidomimetic structures selectively accessible from the same precursor and having different biological activities governed by the architecture of the incorporated triazole.<sup>[10c,f-h]</sup>

To our knowledge, 1,5-disubstituted 1,2,3-triazoles have not been taken into consideration as disulfide mimics to date. Herein, we report the facile introduction of 1,4- and 1,5-disubstituted 1,2,3-triazoles into a monocyclic variant of the sunflower trypsin inhibitor-I (SFTI-1[*I,I*], **1**;<sup>[11]</sup> Figure 1) and show that the macrocyclic peptidomimetic **2** with the “1,5” substitution pattern retains nearly full biological activity in contrast to the “1,4” variants **3** and **4**.

The choice of **1** as the model peptide for the investigation of triazole-based disulfide replacements had several reasons. SFTI-1 is a small, though very potent, inhibitor of trypsin.<sup>[11,12]</sup> Therefore, the influence of different modes of macrocyclization on the bioactivity of the corresponding synthetic variant can be routinely examined by serine protease inhibition assays.<sup>[3e,6e,11,12c,13]</sup>

[\*] M. Empting, Dr. O. Avrutina, Dr. R. Meusinger, S. Fabritz, M. Reinwarth, Prof. Dr. H. Kolmar  
Clemens-Schöpf-Institut für Organische Chemie und Biochemie  
Technische Universität Darmstadt  
Petersenstrasse 22, 64287 Darmstadt (Germany)  
Fax: (+49) 6151-16-5399  
E-mail: kolmar@biochemie-tud.de  
Homepage: <http://www.chemie.tu-darmstadt.de/kolmar>  
Prof. Dr. M. Biesalski  
Ernst-Berl-Institute für Technische und Makromolekulare Chemie  
Technische Universität Darmstadt (Germany)  
S. Voigt, Prof. Dr. G. Buntkowsky  
Eduard-Zintl-Institut für Anorganische und Physikalische Chemie  
Technische Universität Darmstadt  
Petersenstrasse 22, 64287 Darmstadt (Germany)

[\*\*] This research was supported by the Deutsche Forschungsgemeinschaft through grant Ko 1390/9-1, LOEWE—Soft Control and by BMBF.

 Supporting information for this article is available on the WWW under <http://dx.doi.org/10.1002/anie.201008142>.



## Communications

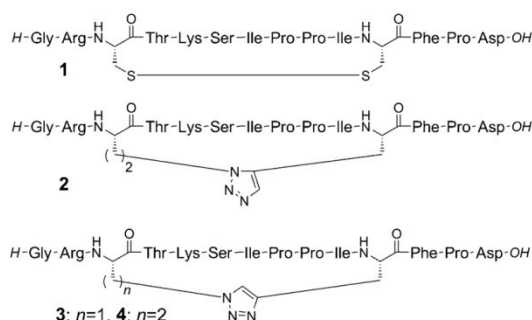


**Figure 1.** Chemical formula of monocyclic SFTI-1[7,14] (**1**),<sup>[11]</sup> [Ala<sup>3</sup>(&sup1),Ala<sup>11</sup>(&sup2)]SFTI-1[7,14][(&sup1-CH<sub>2</sub>-1,5-[1,2,3]triazolyl-&sup2)] (**2**), [Ala<sup>3</sup>(&sup1),Ala<sup>11</sup>(&sup2)]SFTI-1[7,14][(&sup1-1,4-[1,2,3]triazolyl-&sup2)] (**3**), and [Ala<sup>3</sup>(&sup1),Ala<sup>11</sup>(&sup2)]SFTI-1[7,14][(&sup1-CH<sub>2</sub>-1,4-[1,2,3]triazolyl-&sup2)] (**4**). & = Conjunction of peptide backbone and the corresponding macrocyclization motif.

Craik and co-workers intensely investigated the structure and proteolytic stabilities of monocyclic and linear variants of SFTI-1 and demonstrated the importance of the disulfide bridge in maintaining the inhibitory activity of open-chain species.<sup>[12a,b,14]</sup> Furthermore, Roller et al. and Rolka et al. have shown that disulfide replacements are tolerated depending on the steric demand at residue 3 (Figure 1).<sup>[6c,12c,15]</sup>

A solution structure of SFTI-1[1,14] (PDB code: 1JBN)<sup>[12a]</sup> enabled possible triazole-based linkages within the peptide chain to be modeled and to evaluate their fit into the parent disulfide-bridged template **1** (Figure 2).

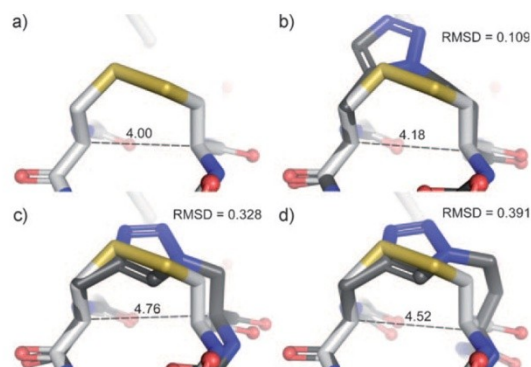


**Figure 2.** Structure and overlays of energy-minimized 3D models of SFTI-1 variants 1–4 showing the region of the disulfide bridge and the corresponding triazole-based substitutes. a) **1**, b) **1** and **2**, c) **1** and **3**, d) **1** and **4**.<sup>[12a]</sup> Models were aligned at the respective carbonyl, C<sub>α</sub>, C<sub>β</sub>, and amide nitrogen atoms of residue 11. The root mean square deviations (RMSD) calculated for the respective carbonyl, C<sub>α</sub>, C<sub>β</sub>, and amide nitrogen atoms of residues 3 and 11 at the compared structures are given in Å. Measured distances between the C<sub>α</sub> atoms of residues 3 and 11 of the corresponding model are shown as dashed lines and values are given in Å. Blue nitrogen, light gray carbon atoms of **1**, dark gray carbon atoms of **2–4**, red oxygen, yellow sulfur, hydrogen atoms are omitted for clarity (for details see the Supporting Information).

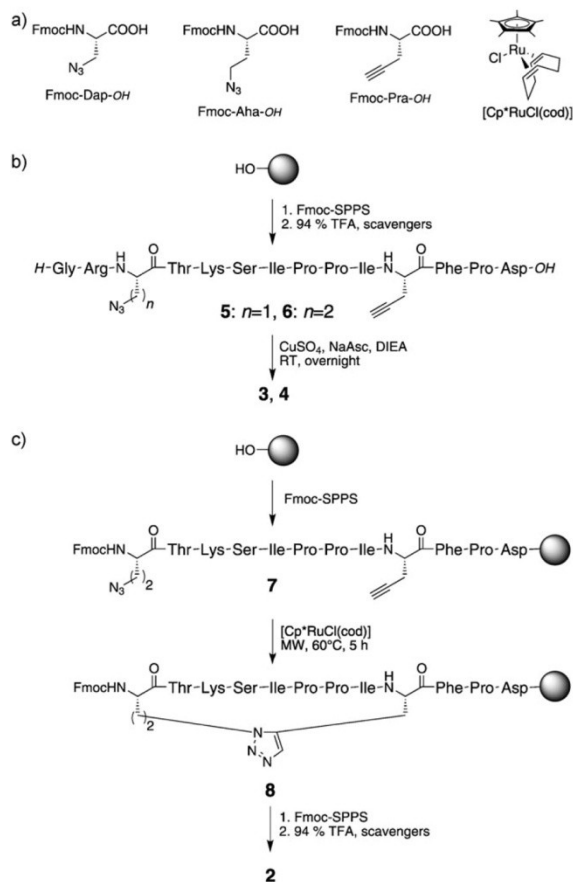
The alignment of the deduced structures of peptidomimetics **2–4** with disulfide-bridged peptide **1** gave insight into the steric requirements of the proposed triazole bridges and allowed their tendency to disturb the parent backbone conformation to be investigated (Figure 2b–d). The incorporation of 1,4-disubstituted 1,2,3-triazoles led to increased distances between the C<sub>α</sub> atoms of residues 3 and 11 compared to those of the corresponding cysteines in **1** (Figure 2c,d). In the case of the 1,5-disubstituted species the spacing remained essentially the same (Figure 2a,b). Owing to the planar and rigid architecture resulting in low degrees of structural freedom for the aromatic heterocycle, the “1,4” substitution pattern renders compounds **3** and **4** unable to adopt the native conformation of **1** properly, thereby forcing the residues 3 and 11 into more remote positions. In contrast, the “1,5” pattern of **2** seems to be compatible with the intrinsic geometry of **1**. Therefore, a significant difference between the inhibitory activities of compounds **2**, **3**, and **4** depending on the mode of macrocyclization was expected.

SFTI-1[1,14] (**1**) was synthesized by microwave-assisted Fmoc-SPPS with subsequent DMSO mediated oxidation (Supporting Information). Compounds **3** and **4** were synthesized in a similar way using commercially available SPPS building blocks Fmoc-L-propargylglycine (Fmoc-Pra-OH) and Fmoc-L-azidoalanine (Fmoc-Aza-OH) or Fmoc-L-azido-homoalanine (Fmoc-Aha-OH) yielding the linear precursors **5** ([Aza<sup>3</sup>,Pra<sup>11</sup>]SFTI-1[1,14]) and **6** ([Aha<sup>3</sup>,Pra<sup>11</sup>]SFTI-1[1,14]), respectively (Scheme 1a,b). CuAAC-mediated macrocyclization of unprotected peptides **5** and **6** was performed in diluted solution after acidic cleavage from the support.

As expected, RuAAC conditions appeared incompatible to solution-phase macrocyclization of unprotected peptide **6** leading to an undefined mixture of side products. Instead, the 1,5-disubstituted 1,2,3-triazole was successfully installed during SPPS using [Cp\*<sub>2</sub>RuCl(cod)] as the catalyst and microwave irradiation to give compound **2**, though in low yield (2.1% according to initial resin load, Scheme 1c). Purified peptides **1–6** were characterized by RP-HPLC, ESI-MS, IR-, and NMR-spectroscopy.

Though a formation of an intramolecular triazole bridge proceeds without change of the molecular mass and cannot be detected by standard mass spectrometry, the azide group gives a prominent IR absorption band around 2100 cm<sup>-1</sup>.<sup>[16]</sup> This band is sufficiently separated from the main IR signals commonly found in peptides, and its absence in products **2**, **3**, and **4** thus indicates the generation of triazoles (Figure 3a). 2D HSQC NMR spectroscopy enabled to discriminate 1,4- from 1,5-disubstituted 1,2,3-triazoles by measuring the chemical shifts of the <sup>1</sup>H,<sup>13</sup>C coupling signal assigned to the unique carbon-bound proton found in both heterocycles (Figure 3b).

The signals correlating to the single proton and the corresponding carbon nucleus at position 5 or 4 in the 1,4- or 1,5-disubstituted 1,2,3-triazole bridges of compounds **2**, **3**, and **4** were found in the aromatic region between δ = 7.8–7.3 ppm (<sup>1</sup>H) and δ = 135–120 ppm (<sup>13</sup>C). The 2D NMR spectroscopy procedure enabled them to be distinguished from protons not bound to carbon and from the intrinsic phenyl multiplet arising from the side chain of residue 12. The measured <sup>1</sup>H



**Scheme 1.** a) Non-natural amino acid building blocks Fmoc-L-azidoalanine (Fmoc-Aza-OH), Fmoc-L-azidohomoalanine (Fmoc-Aha-OH), Fmoc-L-propargylglycine (Fmoc-Pra-OH) and the catalyst for RuAAC mediated macrocyclization. b) Synthesis of peptidomimetics **3** and **4** bridged by 1,4-disubstituted 1,2,3-triazole. c) Synthesis of peptidomimetic **2** bridged by 1,5-disubstituted 1,2,3-triazole. DIEA = *N,N*-diisopropylethylamine, Fmoc = Fluorenylmethoxycarbonyl, NaAsc = sodium ascorbate, TFA = trifluoroacetic acid, Cp\* = C<sub>5</sub>Me<sub>5</sub>, cod = cyclooctadiene, SPPS = solid-phase peptide synthesis.

and <sup>13</sup>C chemical shifts were in good agreement with reported data<sup>[10d]</sup> and displayed a significant difference between the “1,4” and “1,5” substitution pattern confirming the proposed constitution of RuAAC and CuAAC products **2**, **3**, and **4** (Figure 3b).

The inhibitory activity of peptides **1–6** was determined by kinetic studies using active-site titrated trypsin (see Figure 4 and the Supporting Information).<sup>[17]</sup>

The determined *K<sub>i</sub><sup>app</sup>* values for compounds **1–6** are summarized in Table 1. Peptidomimetic **2** with the “1,5” substitution pattern displayed an inhibitory potency in nanomolar range, which is comparable to that of the disulfide-bridged parent peptide **1**. In contrast, monocyclic SFTI-1 variants **3** and **4** produced by CuAAC macrocyclization showed a dramatic decline in inhibitory activity against trypsin. Two main issues could provide a plausible explanation

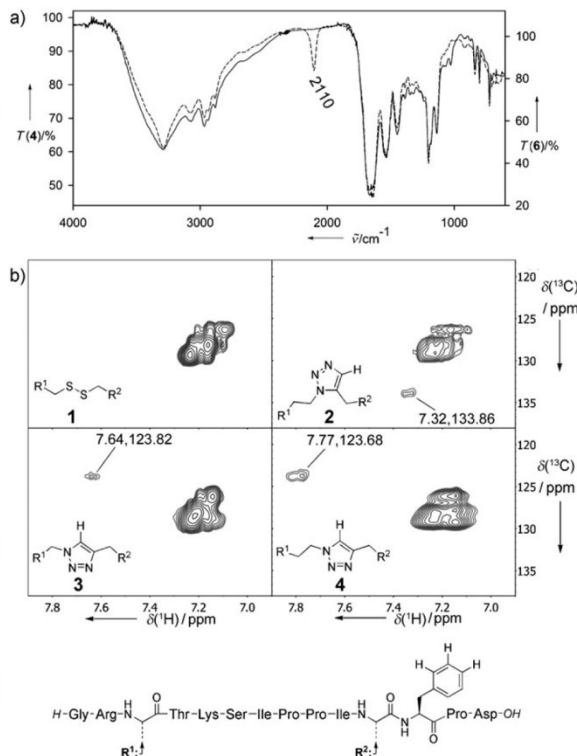


**Figure 3.** a) Superimposed IR transmission spectra of peptides **4** (—) and **6** (----), respectively, and assigned asymmetric NNN stretch band of the azide group of **6** at 2110 cm<sup>-1</sup>. b) 2D HSQC NMR spectra (<sup>1</sup>H, <sup>13</sup>C heteronuclear correlations) showing the aromatic region of the peptides **1–4**. Corresponding structural formula and <sup>1</sup>H, <sup>13</sup>C chemical shifts for signals assigned to the unique carbon-bound proton of 1,4- and 1,5-disubstituted 1,2,3-triazoles are shown.

**Table 1:** Summary of *K<sub>i</sub><sup>app</sup>* values determined for compounds **1–6**.

Entry	Bridging motif	<i>K<sub>i</sub><sup>app</sup></i> [nM] <sup>[a]</sup>	Relative activity <sup>[b]</sup>
1	cystine	1.48 ± 0.1	1
2	1,5-disubstituted 1,2,3-triazole	2.4 ± 0.14	1.6
3	1,4-disubstituted 1,2,3-triazole	1908 ± 261	1288
4	1,4-disubstituted 1,2,3-triazole	742 ± 88	501
5	–	1916 ± 205	1293
6	–	13 845 ± 1835	9347

[a] Standard error of the nonlinear regression is given. [b] Relative activities are calculated as the ratios of the *K<sub>i</sub><sup>app</sup>* values for the respective compound to that of peptide **1**.

for this finding. First, the rigidity of the 1,2,3-triazole formed prevents the “1,4” pattern from having a proper fit into the parent structure, thereby increasing the bridging distance of the peptide backbone. Though significant tolerance of the monocyclic SFTI-1 backbone towards the length of the connecting element has been recently reported for non-rigid, flexible linkers,<sup>[15]</sup> the impact of structurally constrained



## Communications

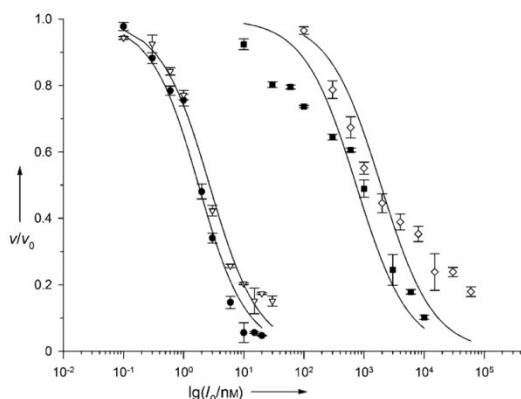


**Figure 4.** Kinetic data for the inhibition of trypsin-catalyzed proteolysis of chromogenic substrate Boc-QAR-pNA (Bachem) by SFTI-1 analogues **1** (●), **2** (▽), **3** (○), and **4** (■) and corresponding curves of the Morrison equation (fitted by the Marquardt–Levenberg algorithm of SigmaPlot 11). Error bars indicating the standard deviation of each data point (triple determination).

disulfide substitutes could be dramatic, as shown herein. As another reason for the reduced activity of compounds **3** and **4** the steric demand in proximity to or at the  $C_{\beta}$  atom of residue 3 can be considered, since it has been shown that bulky moieties at this position cause a drastic decrease of the inhibitory effect.<sup>[15a]</sup>

In conclusion, we demonstrated the utility of a 1,5-disubstituted 1,2,3-triazole bridge as a disulfide replacement. Owing to its redox stability and dissimilarity to common building blocks of nature, improved pharmacokinetic properties can be expected for this disulfide surrogate. Since, for a range of bioactive molecules the preference of 1,5-disubstituted 1,2,3-triazoles over the 1,4 species may turn out to be not so explicit as for the structures described, a modular approach towards tailor-made heterodetic compounds can be achieved through the variation of RuAAC and CuAAC macrocyclization strategies using commercially available building blocks. Experiments towards generation of peptides containing both a triazole bridge and disulfide bonds are currently under way. This strategy may help to overcome the difficulties that often arise during oxidative folding of cysteine-rich peptides in vitro.

Received: December 23, 2010

Revised: February 21, 2011

Published online: May 4, 2011

**Keywords:** click chemistry · disulfide bridges · peptidomimetics · SFTI-1 · trypsin inhibition

[1] H. M. Berman, J. Westbrook, Z. Feng, G. Gilliland, T. N. Bhat, H. Weissig, I. N. Shindyalov, P. E. Bourne, *Nucleic Acids Res.* **2000**, *28*, 235–242.

[2] a) H. Kolmar, *Curr. Opin. Pharmacol.* **2009**, *9*, 608–614; b) D. J. Craik, J. S. Mylne, N. L. Daly, *Cell. Mol. Life Sci.* **2010**, *67*, 9–16.

- [3] a) A. Berezov, H. T. Zhang, M. I. Greene, R. Murali, *J. Med. Chem.* **2001**, *44*, 2565–2574; b) A. Shrivastava, M. A. von Wronski, A. K. Sato et al., *Protein Eng. Des. Sel.* **2005**, *18*, 417–424; c) M. A. Fázio, V. X. Oliveira, Jr., P. Bulet, M. T. Miranda, S. Daffre, A. Miranda, *Biopolymers* **2006**, *84*, 205–218; d) T. S. Han, M. M. Zhang, A. Walewska, P. Gruszczynski, C. R. Robertson, T. E. Cheatham III, D. Yoshikami, B. M. Olivera, G. Bulaj, *ChemMedChem* **2009**, *4*, 406–414; e) R. G. Boy, W. Mier, E. M. Nothelfer, A. Altmann, M. Eisenhut, H. Kolmar, M. Tomaszowski, S. Kramer, U. Haberkorn, *Mol. Imaging Biol.* **2010**, *12*, 377–385.
- [4] a) L. Moroder, D. Besse, H. J. Musiol, S. Rudolph-Bohner, F. Siedler, *Biopolymers* **1996**, *40*, 207–234; b) I. Annis, B. Hargittai, G. Barany, *Methods Enzymol.* **1997**, *289*, 198–221; c) C. J. Armishaw, J. L. Dutton, D. J. Craik, P. F. Alewood, *Biopolymers* **2009**, *94*, 307–313; d) J. Zhang, S. Diamond, T. Arvedson, B. J. Sasu, L. P. Miranda, *Biopolymers* **2010**, *94*, 257–264; e) M. Muttenthaler, S. T. Nevin, A. A. Grishin et al., *J. Am. Chem. Soc.* **2010**, *132*, 3514–3522; f) A. M. Steiner, G. Bulaj, *J. Pept. Sci.* **2011**, *17*, 1–7.
- [5] a) I. Annis, L. Chen, G. Barany, *J. Am. Chem. Soc.* **1998**, *120*, 7226–7238; b) B. Hargittai, G. Barany, *J. Pept. Res.* **1999**, *54*, 468–479.
- [6] a) L. Yu, Y. Lai, J. Wade, S. M. Coutts, *Tetrahedron Lett.* **1998**, *39*, 6633–6636; b) A. K. Galande, J. O. Trent, A. F. Spatola, *Biopolymers* **2003**, *71*, 534–551; c) M. Roice, I. Johannsen, M. Meldal, *QSAR Comb. Sci.* **2004**, *23*, 662–673; d) J. Elaridi, J. Patel, W. R. Jackson, A. J. Robinson, *J. Org. Chem.* **2006**, *71*, 7538–7545; e) S. Jiang, P. Li, S. L. Lee, C. Y. Lin, Y. Q. Long, M. D. Johnson, R. B. Dickson, P. P. Roller, *Org. Lett.* **2007**, *9*, 9–12; f) M. A. Hossain, K. J. Rosengren, S. Zhang, R. A. Bathgate, G. W. Tregear, B. J. van Lierop, A. J. Robinson, J. D. Wade, *Org. Biomol. Chem.* **2009**, *7*, 1547–1553.
- [7] a) C. W. Tornøe, M. Meldal, Peptides: The Wave of the Future, Proceedings of the Second International and the Seventeenth American Peptide Symposium **2001**, pp. 263–264; b) V. V. Rostovtsev, L. G. Green, V. V. Fokin, K. B. Sharpless, *Angew. Chem.* **2002**, *114*, 2708–2711; *Angew. Chem. Int. Ed.* **2002**, *41*, 2596–2599; c) C. W. Tornøe, C. Christensen, M. Meldal, *J. Org. Chem.* **2002**, *67*, 3057–3064; d) Y. L. Angell, K. Burgess, *Chem. Soc. Rev.* **2007**, *36*, 1674–1689; e) G. C. Tron, T. Pirali, R. A. Billington, P. L. Canonico, G. Sorba, A. A. Genazzani, *Med. Res. Rev.* **2008**, *28*, 278–308; f) J. F. Lutz, Z. Zarafshani, *Adv. Drug Delivery Rev. Adv. Drug Deliv. Rev.* **2008**, *60*, 958–970; g) O. Avrutina, M. Empting, S. Fabritz, M. Daneschdar, H. Frauendorf, U. Diederichsen, H. Kolmar, *Org. Biomol. Chem.* **2009**, *7*, 4177–4185.
- [8] a) W. S. Horne, M. K. Yadav, C. D. Stout, M. R. Ghadiri, *J. Am. Chem. Soc.* **2004**, *126*, 15366–15367; b) A. Brik, J. Alexandratos, Y. C. Lin, J. H. Elder, A. J. Olson, A. Wlodawer, D. S. Goodsell, C. H. Wong, *ChemBioChem* **2005**, *6*, 1167–1169; c) K. Oh, Z. Guan, *Chem. Commun.* **2006**, 3069–3071; d) J. M. Beierle, W. S. Horne, J. H. van Maarseveen, B. Waser, J. C. Reubi, M. R. Ghadiri, *Angew. Chem.* **2009**, *121*, 4819–4823; *Angew. Chem. Int. Ed.* **2009**, *48*, 4725–4729.
- [9] a) J. H. van Maarseveen, W. S. Horne, M. R. Ghadiri, *Org. Lett.* **2005**, *7*, 4503–4506; b) Y. Angell, K. Burgess, *J. Org. Chem.* **2005**, *70*, 9595–9598; c) V. D. Bock, R. Perciaccante, T. P. Jansen, H. Hiemstra, J. H. van Maarseveen, *Org. Lett.* **2006**, *8*, 919–922; d) R. A. Turner, A. G. Oliver, R. S. Lokey, *Org. Lett.* **2007**, *9*, 5011–5014; e) V. Goncalves, B. Gautier, A. Regazzetti, P. Coric, S. Bouaziz, C. Garbay, M. Vidal, N. Inguibert, *Bioorg. Med. Chem. Lett.* **2007**, *17*, 5590–5594; f) V. D. Bock, D. Speijer, H. Hiemstra, J. H. van Maarseveen, *Org. Biomol. Chem.* **2007**, *5*, 971–975; g) S. Cantel, C. Isaad Ale, M. Scrima et al., *J. Org. Chem.* **2008**, *73*, 5663–5674; h) R. Jagasia, J. M. Holub, M. Bollinger, K. Kirshenbaum, M. G. Finn, *J. Org. Chem.* **2009**, *74*,

- 2964–2974; i) A. Le Chevalier Isaad, A. M. Papini, M. Chorev, P. Rovero, *J. Pept. Sci.* **2009**, *15*, 451–454; j) M. Nahrwold, T. Bogner, S. Eissler, S. Verma, N. Sewald, *Org. Lett.* **2010**, *12*, 1064–1067.
- [10] a) L. Zhang, X. Chen, P. Xue, H. H. Sun, I. D. Williams, K. B. Sharpless, V. V. Fokin, G. Jia, *J. Am. Chem. Soc.* **2005**, *127*, 15998–15999; b) L. K. Rasmussen, B. C. Boren, V. V. Fokin, *Org. Lett.* **2007**, *9*, 5337–5339; c) G. Appendino, S. Bacchiega, A. Minassi, M. G. Cascio, L. De Petrocellis, V. Di Marzo, *Angew. Chem.* **2007**, *119*, 9472–9475; *Angew. Chem. Int. Ed.* **2007**, *46*, 9312–9315; d) A. Tam, U. Arnold, M. B. Soellner, R. T. Raines, *J. Am. Chem. Soc.* **2007**, *129*, 12670–12671; e) B. C. Boren, S. Narayan, L. K. Rasmussen, L. Zhang, H. Zhao, Z. Lin, G. Jia, V. V. Fokin, *J. Am. Chem. Soc.* **2008**, *130*, 8923–8930; f) A. R. Kelly, J. Wei, S. Kesavan, J. C. Marie, N. Windmon, D. W. Young, L. A. Marcaurrelle, *Org. Lett.* **2009**, *11*, 2257–2260; g) W. S. Horne, C. A. Olsen, J. M. Beierle, A. Montero, M. R. Ghadiri, *Angew. Chem.* **2009**, *121*, 4812–4818; *Angew. Chem. Int. Ed.* **2009**, *48*, 4718–4724; h) D. Tietze, M. Tischler, S. Voigt, D. Imhof, O. Ohlenschlager, M. Grolach, G. Buntkowsky, *Chem. Eur. J.* **2010**, *16*, 7572–7578.
- [11] M. L. Korsinczky, H. J. Schirra, D. J. Craik, *Curr. Protein Pept. Sci.* **2004**, *5*, 351–364.
- [12] a) M. L. Korsinczky, H. J. Schirra, K. J. Rosengren, J. West, B. A. Condie, L. Otvos, M. A. Anderson, D. J. Craik, *J. Mol. Biol.* **2001**, *311*, 579–591; b) U. C. Marx, M. L. Korsinczky, H. J. Schirra, A. Jones, B. Condie, L. Otvos, Jr., D. J. Craik, *J. Biol. Chem.* **2003**, *278*, 21782–21789; c) P. Li, S. Jiang, S. L. Lee, C. Y. Lin, M. D. Johnson, R. B. Dickson, C. J. Michejda, P. P. Roller, *J. Med. Chem.* **2007**, *50*, 5976–5983.
- [13] E. Zablorna, K. Kazmierczak, A. Jaskiewicz, M. Stawikowski, G. Kupryszewski, K. Rolka, *Biochem. Biophys. Res. Commun.* **2002**, *292*, 855–859.
- [14] a) M. L. Korsinczky, R. J. Clark, D. J. Craik, *Biochemistry* **2005**, *44*, 1145–1153; b) M. L. Colgrave, M. J. Korsinczky, R. Clark, F. Foley, D. J. Craik, *Biopolymers* **2010**, *0*, 0.
- [15] a) A. Legowska, D. Debowski, R. Lukajtis, M. Wysocka, C. Czaplowski, A. Lesner, K. Rolka, *Bioorg. Med. Chem.* **2010**, *18*, 8188–8193; b) A. Legowska, E. Bulak, A. Jaskiewicz, I. Maluch, M. Sieracki, M. Wysocka, A. Lesner, K. Rolka, *Protein Pept. Lett.* **2010**, *17*, 1223–1227.
- [16] a) C. J. Nielsen, C. E. Sjøgfogren, *J. Mol. Struct. (THEOCHEM)* **1987**, *150*, 361–379; b) F. F. Chen, F. Wang, *Molecules* **2009**, *14*, 2656–2668.
- [17] a) O. Avrutina, H. U. Schmoltd, D. Gabrijelcic-Geiger, D. Le Nguyen, C. P. Sommerhoff, U. Diederichsen, H. Kolmar, *Biol. Chem.* **2005**, *386*, 1301–1306; b) J. F. Morrison, *Biochim. Biophys. Acta Enzymol.* **1969**, *185*, 269–286.

## 2.4 *In vitro* & *in silico* Studies of Matriptase Inhibition by SFTI-1 Variants

### Title:

Between two worlds: a comparative study on *in vitro* and *in silico* inhibition of trypsin and matriptase by redox-stable SFTI-1 variants at near physiological pH

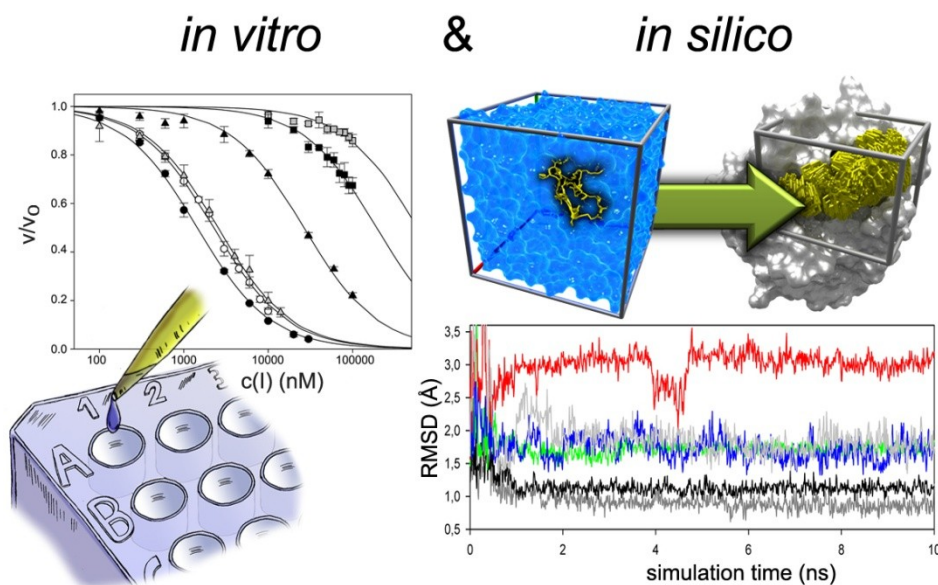
### Authors:

Olga Avrutina, Heiko Fittler, Bernhard Glotzbach, Harald Kolmar, Martin Empting

### Bibliographic Data:

*Organic & Biomolecular Chemistry*,  
Volume 10, Issue 38, Pages 7753-7762, September 12, 2012.  
DOI: 10.1002/anie.201008142.  
First published online: August 06, 2012.

### Graphical Abstract:



Derivatives of sunflower trypsin inhibitor-1 possessing native cystine as well as triazolyl side-chain macrocyclization motifs were studied *in vitro* and *in silico* for matriptase inhibition.

### Contributions by M. Empting:

- Developed concept
- Performed all *in silico* experiments
- Wrote the article
- Created all figures



# Organic & Biomolecular Chemistry

Cite this: *Org. Biomol. Chem.*, 2012, **10**, 7753

www.rsc.org/obc

PAPER

## Between two worlds: a comparative study on *in vitro* and *in silico* inhibition of trypsin and matriptase by redox-stable SFTI-1 variants at near physiological pH<sup>†</sup>

Olga Avrutina, Heiko Fittler, Bernhard Glotzbach, Harald Kolmar and Martin Empting\*

Received 18th June 2012, Accepted 3rd August 2012

DOI: 10.1039/c2ob26162f

A comparative study on *in vitro* and *in silico* inhibition of trypsin and matriptase by derivatives of the sunflower trypsin inhibitor-1 at near physiological pH is reported. Besides wild-type bicyclic SFTI-1, monocyclic variants possessing native cystine as well as redox-stable triazolyl side-chain macrocyclization motifs were studied for the first time in matriptase inhibition assays. Interestingly, monocyclic SFTI-1[1,14] demonstrated higher potency against this pharmacologically relevant protease compared to its bicyclic counterpart. Structural analysis of binding/inhibition of investigated SFTI-1 derivatives was performed using a combination of molecular dynamics simulations and docking experiments. *In silico* data were in good accordance with *in vitro* results, indicating the importance of the terminal inhibitor regions for the affinity towards matriptase. Presented work gives new perspectives for the optimization of the SFTI-1 framework towards *in vivo* applications.

### Introduction

Very often interesting scientific findings arise from unexpected or even counterintuitive results. Recently, a comparison between the crystal structures of the sunflower trypsin inhibitor-1 (SFTI-1), a bicyclic tetradecapeptide, in complex with two closely related serine proteases revealed a surprising biochemical peculiarity.<sup>1,2</sup> By analyzing the binding geometry of SFTI-1 matriptase and trypsin aggregates, Yuan *et al.* confirmed a high similarity between both structures.<sup>1,2</sup> Though the homologous interaction profile of these serine proteases with SFTI-1 was expected, it appeared rather astonishing that this smallest naturally occurring Bowman–Birk Inhibitor (BBI)<sup>3,4</sup> favors trypsin over matriptase in retrospect.<sup>1–3,5</sup> Under the basic conditions (pH 8.2–8.5) commonly applied to *in vitro* inhibition assays for these enzymes, the electrostatic surface potential around the active site of matriptase shows, compared to the environment around the catalytic center of trypsin, a significantly

higher negative polarization (Fig. 1). This provides a better overall charge complementarity with SFTI-1. It has been proposed that this anticipated enthalpic preference is overcompensated by an entropic penalty predominantly originating from the secondary binding loop of SFTI-1.<sup>1</sup> This might explain the surprising difference between its inhibitory activity against trypsin ( $K_i$  0.1 nM) and matriptase ( $K_i$  1–100 nM).<sup>1–3,5</sup>

However, selective binding and/or inhibition of matriptase under physiological conditions is of great pharmacological interest as this type II transmembrane serine protease (TTSP) is involved in a variety of pathological processes like progression and metastasis of epithelial tumors, as well as osteoarthritis and atherosclerosis.<sup>6–10</sup> A number of potent inhibitors of this serine protease based either on small organic molecules or large antibody fragments and exhibiting single digit nanomolar or even picomolar inhibition constants, respectively, have already been reported.<sup>11,12</sup> Nevertheless, attempts to tune the peptidic SFTI-1 framework towards matriptase resulted in inhibitors with enhanced selectivity but dramatically decreased potency.<sup>5</sup> Besides monocyclic variants lacking the disulfide connectivity and possessing substantially worsened kinetic properties, matriptase inhibition by side-chain cyclized SFTI-1 derivatives having free N- and C-termini has not been reported to date.

Recently, we developed potent inhibitors of trypsin based on monocyclic SFTI-1 derivatives containing redox-stable triazole bridges of different length and shape.<sup>13</sup> The impact of the macrocyclization motif in their bioactivity was demonstrated as well.<sup>13</sup> Herein, we report an unexpected change of the relative potency within the set of matriptase inhibitors **1–6** (Fig. 2) and evaluate

Clemens-Schöpf Institute of Organic Chemistry and Biochemistry, Technische Universität Darmstadt, Petersenstr. 22, 64287 Darmstadt, Germany. E-mail: Empting@Biochemie-TUD.de

<sup>†</sup> Electronic supplementary information (ESI) available: Detailed synthetic procedures of compounds **1** and **3**, experimental details of enzyme assays, Fig. S1–S9 (SDS-Page analysis of inclusion body production, refolding/autoactivation, and purification of recombinant matriptase, as well as RP-HPLC traces, ESI-MS spectra, and dose–response curves against trypsin for previously uncharacterized inhibitors **1** and **3**), and Tables S1–S7 (determination of  $K_i$  values using alternative equations and the full set of used force field parameters). See DOI: 10.1039/c2ob26162f



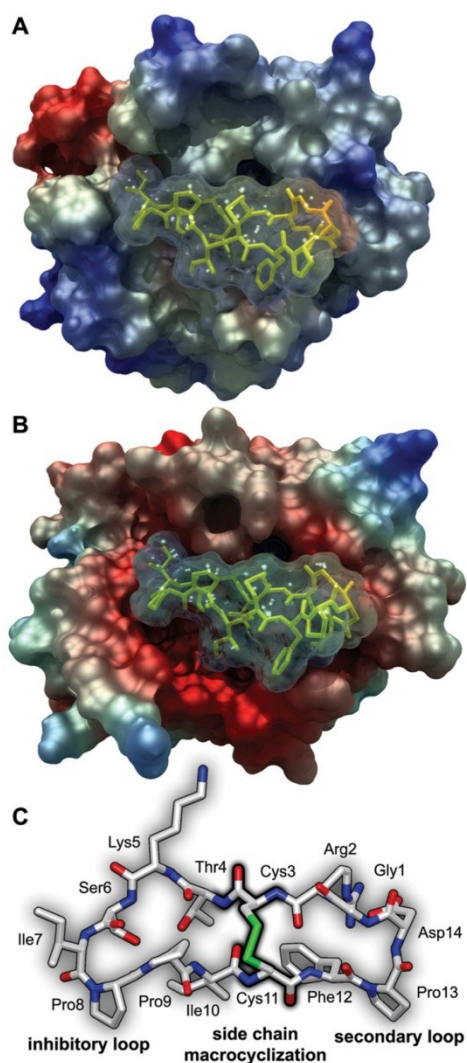


**Fig. 1** Molecular surfaces of bicyclic SFTI-1 (transparent surface and yellow sticks) in complex with (A) trypsin (PDB ID: 1SFI) and (B) matriptase (PDB ID: 3P8F). Color gradients (red to blue) indicate electrostatic surface potentials (negative to positive) at pH 8.5 calculated *via* the Particle Mesh Ewald method with a maximum value of 500 kJ mol<sup>-1</sup>.<sup>14</sup> (C) Stick representation of SFTI-1 structure. Blue: nitrogen, red: oxygen, green: sulfur, white: carbon, hydrogen omitted for clarity.

this finding on a structural basis using a two-step *in silico* method.

Recently, Swedberg and coworkers have used molecular dynamics (MD) simulations to predict beneficial amino acid exchanges for SFTI-1-derived inhibitors of kallikrein-related peptidase 4 (KLK4).<sup>15</sup> Our computational approach combines an MD calculation with subsequent semi-flexible and rigid docking experiments using a customized AMBER-derived force field (YASARA2) with embedded parameters for the calculation of non-natural triazolyl moieties within peptides.<sup>16–18</sup> This procedure enabled us to investigate the structural characteristics of

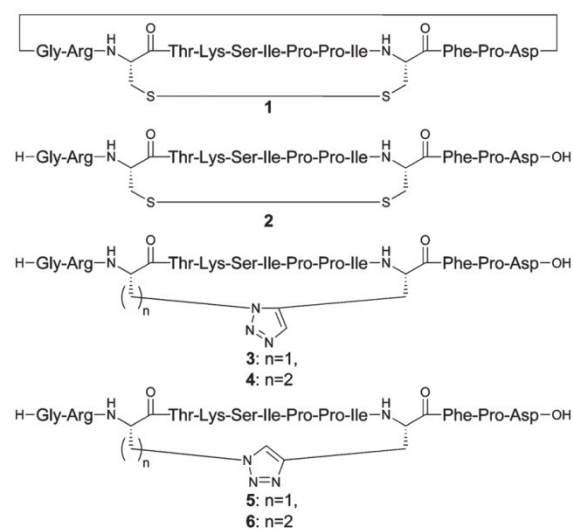


**Fig. 2** Structures of investigated peptides and peptidomimetics. Bicyclic SFTI-1 (1), monocyclic SFTI-1[1,14] (2), monocyclic peptidomimetics containing either a 1,5-disubstituted 1,2,3-triazole (3, 4) or a 1,4-disubstituted 1,2,3-triazole (5, 6) as the macrocyclization motif.

each peptidic ligand in solution and upon binding to both trypsin and matriptase. *In silico* binding affinities were calculated and compared with the *in vitro* results. Thus, the role of the secondary loop as well as the impact of different macrocyclization motifs in matriptase inhibition of variants 1–6 were elucidated.

## Results and discussion

### *In vitro* inhibition of trypsin and matriptase

Trypsin is a prominent digestive protease commonly found in the small intestine of vertebrates<sup>19</sup> and operating most effectively under the mild basic conditions of its native environment (pH ~ 8).<sup>20</sup> Membrane-anchored matriptase, on the other hand, is usually expressed in epithelial cells and regulates cellular adhesion and growth by hydrolyzing proteins bound to cell surfaces or present in the extracellular matrix.<sup>21</sup> Thus, it functions in an environment controlled by homeostasis in healthy tissues (pH 7.4). Furthermore, tumors in general are known to generate hypoxic regions leading even to acidic microenvironments.<sup>22–24</sup> However, cancer-related matriptase possesses a pH optimum of about 9, therefore, the majority of reported inhibition assays have been carried out at a pH range between 8 and 9.<sup>3,5,11,12,25,26</sup>

We evaluated the potency of synthesized inhibitors through the determination of the fractional activity of the respective enzyme ( $v/v_0$ ) in the presence of an inhibitor at various concentrations [I]. A number of mathematical methods are commonly used for the calculation of apparent inhibition constants  $K_i^{\text{app}}$  or  $IC_{50}$  values (concentration of the inhibitor to achieve a half-maximal degree of inhibition) for competitive inhibitors like SFTI-1.<sup>27–32</sup>

Therefore, we used the following equations for the non-linear fit of observed dose–response curves ( $[E]$  meaning active concentration of the enzyme).

$$v = \frac{1}{v_0 \left( 1 + \frac{[I]}{IC_{50}} \right)} \quad (1)$$

$$\frac{v}{v_0} = \frac{([E] - [I] - K_i^{app}) + \sqrt{([E] + K_i^{app} - [E])^2 + 4K_i^{app}[E]}}{2[E]} \quad (2)$$

$$\frac{v}{v_0} = 1 - \frac{([E] - [I] + K_i^{app}) - \sqrt{([E] + [I] + K_i^{app})^2 - 4[E][I]}}{2[E]} \quad (3)$$

In the case of reversible competitive inhibition  $IC_{50}$  values calculated using eqn (1) can be converted into the substrate-independent  $K_i$  using eqn (4) ( $[S]$  is the concentration of the chromogenic substrate used within the enzyme assay and  $K_M$  is the corresponding Michaelis–Menten constant).<sup>27</sup>

$$K_i = \frac{IC_{50}}{1 + \frac{[S]}{K_M}} \quad (4)$$

In the case of tight-binding inhibition, eqn (5) has to be used instead of eqn (4).<sup>28</sup>

$$K_i = \frac{IC_{50} - \frac{E}{2}}{1 + \frac{[S]}{K_M}} \quad (5)$$

Eqn (2) and (3) are both adaptations of the Morrison equation for the determination of the substrate-dependent (apparent) inhibition constants for tight-binding inhibitors.<sup>29–32</sup> They can be transformed into each other *via* simple arithmetic conversions (see ESI†). Substrate-independent inhibition constant  $K_i$  can be calculated from  $K_i^{app}$  through eqn (6).<sup>30</sup>

$$K_i = \frac{K_i^{app}}{1 + \frac{[S]}{K_M}} \quad (6)$$

However, all used methods yielded essentially the same  $K_i$  values (see ESI†). For the sake of comparability with our previous studies, the results generated *via* eqn (3) and (6) are summarized in Table 1.

To investigate the effect of near physiological pH on matriptase inhibition by SFTI-1 (**1**) and SFTI-1[1,14] (**2**), we determined  $K_i$  values for both compounds at pH 7.6 and 8.5 (Fig. 3A, Table 1). A significant decrease in inhibitory activity for **1** and **2** at lower pH was observed. However, the detected inhibitory potency of bicyclic SFTI-1 under more basic conditions was in accordance with reported data (0.1  $\mu$ M – Li *et al.*, 0.15  $\mu$ M – this work).<sup>5</sup> Interestingly, the monocyclic variant SFTI-1[1,14] (**2**) possessing only a disulfide bond as the macrocyclization motif showed a better inhibition of matriptase compared to its backbone-cyclized counterpart **1**. To our knowledge, this unexpected finding has not been reported to date.

In the case of trypsin, the highly constrained bicyclic wild-type peptide (**1**) was the most potent inhibitor within the set of

**Table 1** Determined  $K_i$  for compounds **1–6**

Entry	Trypsin/nM pH 7.6	Matriptase/ $\mu$ M	
		pH 7.6	pH 8.5
1	0.07 $\pm$ 0.01	1.1 $\pm$ 0.14	0.15 $\pm$ 0.03
2	0.21 $\pm$ 0.03 <sup>a</sup>	0.7 $\pm$ 0.09	0.1 $\pm$ 0.02
3	5.1 $\pm$ 1.0	1.24 $\pm$ 0.16	n.d.
4	0.34 $\pm$ 0.05 <sup>a</sup>	12.9 $\pm$ 1.6	n.d.
5	273 $\pm$ 51 <sup>a</sup>	285 $\pm$ 37	n.d.
6	106 $\pm$ 18 <sup>a</sup>	94.1 $\pm$ 12	n.d.

All experiments were performed in triplicate. n.d. means not determined. <sup>a</sup> Values calculated from previously reported  $K_i^{app}$ .<sup>13</sup>

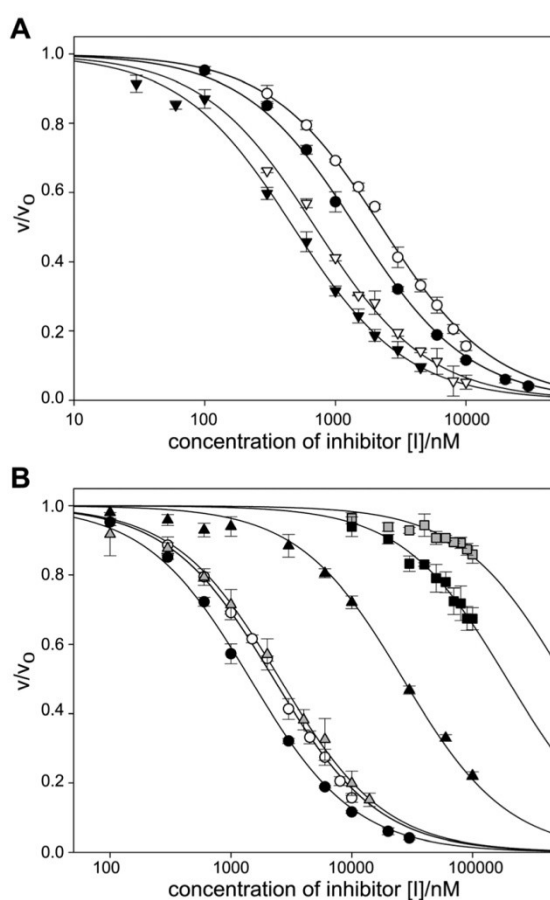


**Fig. 3** Dose–response curves for the inhibition of matriptase-catalyzed proteolysis of chromogenic substrate Boc-QAR-*p*NA with the X-axis on a logarithmic scale. (A) Comparison of bicyclic SFTI-1 (**1**) with monocyclic SFTI-1[1,14] (**2**) at pH 7.6 (white and black circles, respectively) and 8.5 (white and black triangles, respectively). (B) Comparison of disulfide-bridged inhibitors **1** (white circles) and **2** (black circles) with triazole-bridged peptidomimetics **3** (grey triangles), **4** (black triangles), **5** (grey squares), and **6** (black squares) at pH 7.6. Data points are arithmetic means of three experiments and error bars are given as the standard deviation.



tested compounds 1–6. Each modification of the SFTI-1 scaffold resulted in the loss of bioactivity against trypsin (Table 1). Nevertheless, the decrease in potency was quite marginal for open-chain variants 2 and 4. The substitution pattern within the macrocyclization motif of peptidomimetics 3–6 had a dramatic influence on their bioactivity.<sup>13</sup> Inhibitors 3 and 4 containing a 1,5-disubstituted 1,2,3-triazole were significantly more potent compared to variants 5 and 6 possessing the 1,4-isomer.

However, novel compound 3 lacking one methylene unit within the side chain of the third residue (Fig. 2) was not as active as variant 4.

To study the effect of the described SFTI-1 framework modifications on matriptase inhibition, we determined  $K_i$  values for all compounds at pH 7.6 (Fig. 3B, Table 1). Similarly to trypsin inhibition, peptidomimetics 3 and 4 showed better performance than 5 and 6 in matriptase assays as well. Surprisingly, comparison of variants 3 and 4 showed that 3 was more active against matriptase, while 4 was the better trypsin inhibitor.

The collected *in vitro* data shown in Table 1 emphasize that the native SFTI-1 scaffold has a general preference for trypsin over matriptase, especially at near physiological pH. The discrimination between trypsin and matriptase upon changing the target enzyme must have intrinsic structural reasons. Moreover, the unexpected inversion of relative affinities (1 *versus* 2, and 3 *versus* 4) has to be explained.

#### MD simulation of SFTI-1 (1), SFTI-1[1,14] (2) and peptidomimetic compounds 3–6

To elucidate in atomic detail the impact of every single modification, we simulated compounds 1–6 as shown in Fig. 4 (see also the Experimental section).

A significant amount of structural data on SFTI-1 in solution as well as in complex with relevant proteases is available in the protein data base.<sup>1,2,33</sup> Thus, for the simulation of monocyclic variants 3–6 initial coordinates were derived from the reported ones (1JBN). However, preliminary studies revealed that the extensive hydrogen bond network of the SFTI-1 framework is able to compensate the steric strain on the peptide backbone generated by rigid, planar triazole bridges. This resulted in unnaturally bent heterocyclic structures within compounds 5 and 6 (ESI†). Thus, we decreased the scaling factor for non-bonded interactions and applied increased temperature during the initial phase of simulation (Fig. 4). This procedure allowed respective structures to leave the local minimum of the template coordinates. After incremental rescaling of parameters within 1 ns and an additional relaxation period of 8 ns no significant fluctuations in backbone root mean square deviations (RMSD) were observed (Fig. 5A). Hence, stable trajectories were analyzed in detail revealing fundamental structural differences between compounds 1–6 (Fig. 5B, C, and Table 2). The most dramatic effect on the peptide structure is caused by the 1,4-disubstituted 1,2,3-triazole bridge within variant 5. Fig. 5B clearly illustrates a significant distortion of the inhibitory loop compared to crystal structures of wild-type SFTI-1 in complex with trypsin and matriptase. A similar, although not so dramatic, effect was observed for compound 6 which contained the 1,4-substitution pattern as well.

The applied simulation procedure resulted in significantly larger distances between the  $\alpha$ -carbons of residues 3 and 11 for both compounds (5 and 6) compared to our previous study where only an energy minimization step was used.<sup>13</sup> Thus, the two opposing  $\beta$ -strands within the respective peptide frameworks are more remote from each other than within the structures of inhibitors 1–4. Consequently, the possibility to form intramolecular hydrogen bonds is reduced for peptides 5 and 6 (Table 2). Since the hydrogen bond network is a structural prerequisite for the stability of the BBI loop conformation and, thus, biological activity,<sup>15</sup> these findings could explain the observed loss of potency for SFTI-1 variants possessing the 1,4-substitution pattern within their macrocyclization motif.

Bicyclic wild type 1 and monocyclic compound 2, as well as 1,5-disubstituted 1,2,3-triazole containing peptidomimetics 3 and 4, did not show a significant disorder of the inhibitor loop (Fig. 5B). Nevertheless, considerable structural changes within the N- and C-terminal regions of compounds 2–6 compared to the secondary loop of SFTI-1 occurred (Fig. 5C). This result, however, was highly anticipated as the conformational constraints caused by the additional backbone macrocyclization of peptide 1 are missing within the open-chain variants. The structural deviation of residues 1, 2 and 12–14 within highly potent trypsin inhibitor 4 was the most prominent one, while the values for compounds 3, 5, and 6 were in the range of monocyclic SFTI-1[1,14] (Fig. 5C). Considering the decreased relative activity of 4 against matriptase, our structural data support the notion that the N- and C-terminal regions are responsible for enzyme specificity rather than for the general capability to inhibit trypsin-like proteases. Thus, the observed structural changes and increased flexibility of these backbone segments in open-chain variants most likely are the reason for the improved activity of monocyclic compound 2 compared to bicyclic 1 against matriptase.

#### Docking of SFTI-1 (1), SFTI-1[1,14] (2) and peptidomimetic compounds 3–6 to trypsin and matriptase

To investigate the impact of described framework modifications in the binding geometries of inhibitor–protease complexes, docking experiments were performed (see the Experimental section, Fig. 4). The collected data are summarized in Table 3.

As all of the investigated compounds 1–6 inhibit trypsin and matriptase in a concentration-dependent manner (Fig. 3 and Table 1), we rationalized that interaction of open-chain variant 2 and peptidomimetics 3–6 with these proteases must follow a similar binding geometry to wild-type SFTI-1. This postulation is supported by recently solved inhibitor–trypsin complex structures of monocyclic SFTI-based peptidomimetics.<sup>34</sup> Thus, in order to exhibit observed biological activities, each compound must penetrate the S1 site of a respective protease with the side chain of Lys5. Consequently, we screened the set of generated inhibitor–protease complexes for structures that fulfilled this requirement. The ratio of counted aggregates matching the expected binding geometry to the number of all calculated structures (100 each) is given as  $P_{hit}$  (Table 3). Interestingly, in our docking experiments this value was significantly higher for trypsin than for matriptase. Furthermore, all potent inhibitors



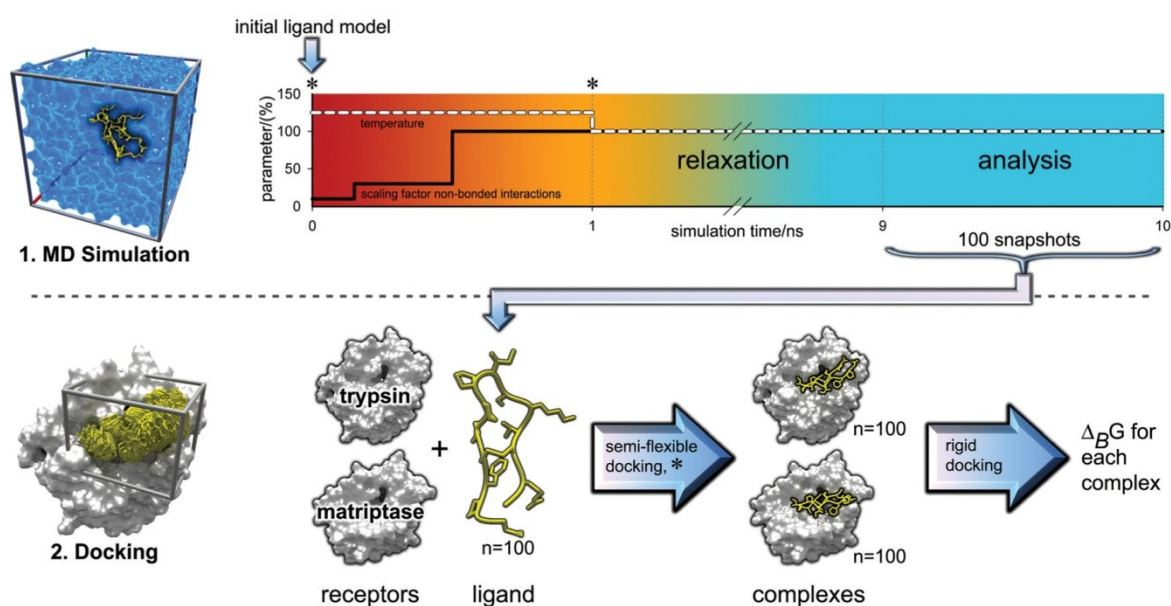


**Fig. 4** Design of the two-step *in silico* experiment. Illustrative images (left) show a simulation cell containing water and a peptidic ligand (top left), as well as a number of ligand poses generated in a local docking experiment restricted by a simulation cell around the active site of the receptor (bottom left). The MD simulation procedure (top) is depicted as time-lapsed absolute temperature (dashed, white) and scaling factor curves for non-bonded interactions (black, solid). Both parameters are given in percent to 298 K and 1, respectively. The color gradient (red to blue) qualitatively illustrates the resulting stress applied to the simulated structure; red means harsh and blue means normalized conditions. The 8 ns period for relaxation is shortened. Snapshots between nanosecond nine and ten are analyzed using a docking procedure (bottom). Free energies of binding  $\Delta_B G$  are calculated by sequential semi-flexible and rigid docking steps. Receptor molecules trypsin and matriptase are shown as white surfaces. The ligand is depicted as yellow tubes and sticks. The star symbol indicates an energy minimization step.

1–4 consistently showed a higher probability  $P_{hit}$  to interact with both proteases in a mode similar to the reported complexes of SFTI-1, compared to weak binders 5 and 6.

We also investigated the capability of compounds 1–6 to form intermolecular hydrogen bonds with each of the target proteases.

Thus, the number of corresponding interactions was counted for each complex with the ligand docked following the described binding mode. As expected, peptidomimetic 5 showed the lowest number of hydrogen bonds within the set of examined structures. However, the amount of measured intermolecular proton donor–acceptor interactions of compound 6 with trypsin and matriptase was in the same range as for inhibitors 1–4.

The analysis of the structural and thermodynamic properties of the generated docking results was of particular importance. The applied procedure enabled us to determine the free energy of binding  $\Delta_B G$  for each ligand–receptor complex (Table 3). Calculated structures of compounds 1–6 bound to matriptase and possessing the highest absolute value of  $\Delta_B G$  are shown in Fig. 6. These models exhibited the most favorable interaction profiles observed, therefore were the best predicted structures for the actual binding geometry within our *in silico* experiment. Complexes 1 and 2 were found to interact with matriptase in a very similar manner compared to the reported crystal structure (Fig. 6A, B). Due to the highly distorted BBI loop of peptidomimetic 5, this variant showed the most deviating docking geometry (Fig. 6E). The N- and C-terminal regions were drastically displaced, considerably reducing the possibility for attractive

interactions. Indeed, only a moderate increase of the backbone RMSD values was observed for compounds 3, 4, and 6. Similar data were extracted from docking experiments with trypsin (Fig. S9, ESI<sup>†</sup>). However, a more prominent deviation between predicted binding geometries and the crystal structure was measured for the residues corresponding to the secondary loop of SFTI-1. The stability of the investigated aggregates was evaluated by averaging calculated  $\Delta_B G$  for every structure with expected binding geometry resulting in  $\Delta_B G^{dock}$  (Table 3).

In general, the calculated mean values indicated a significantly more favorable interaction between matriptase and inhibitors 1–6 compared to respective complexes with trypsin. This finding corroborated the expected influence of charge complementarity between the SFTI-1 scaffold and the surface around the active site of matriptase on overall complex stability.

The most prominent deviations upon docking to trypsin are observed in the N- and C-terminal regions of compounds 1–6. This indicates less conformational constraints compared to the respective matriptase complexes. Thus, an increased flexibility of bound SFTI ligands is provided, while the amount of attractive electrostatic interactions is reduced. A tighter, but also more constrained binding of SFTI-1 to matriptase had already been postulated by Yuan *et al.* and was corroborated by our experiments.<sup>1</sup>

Surprisingly, the ability to bind similarly to the reported crystal structures did not necessarily lead to high values of mean  $\Delta_B G^{dock}$ . Thus, for variant 6 the best docking complexes were characterized by rather low backbone RMSD values (Fig. 6F and

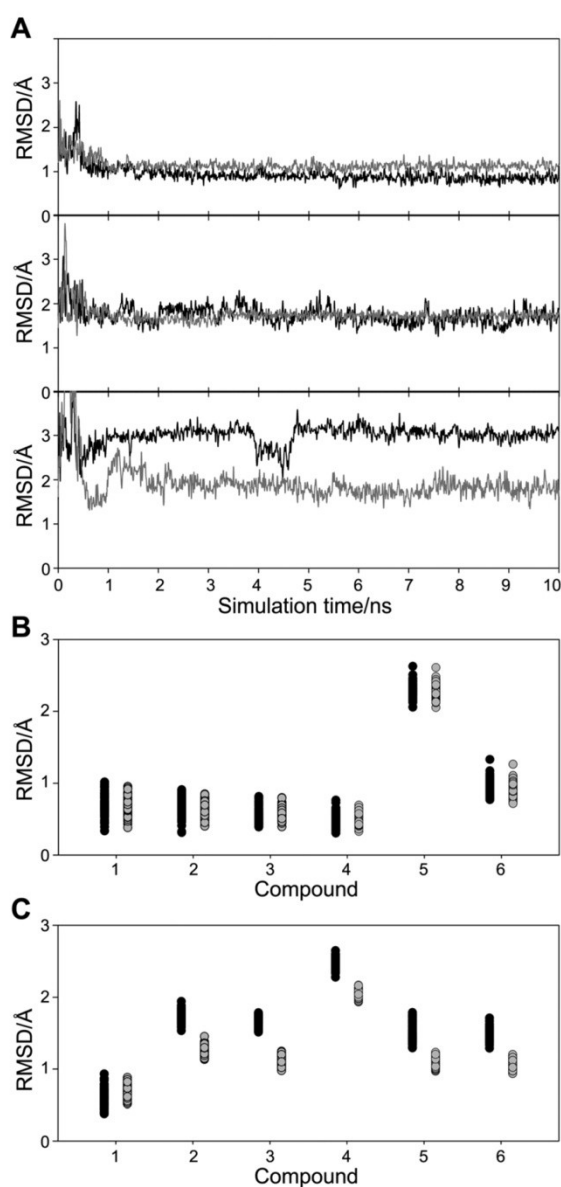


**Fig. 5** (A) Backbone RMSD values of **1** (top, black), **2** (top, grey), **3** (middle, black), **4** (middle, grey), **5** (bottom, black), and **6** (bottom, grey) compared to SFTI-1 solution structure 1JBL plotted against the simulation time. Dot plots of backbone RMSD values of the inhibitory loop (B) and the secondary loop/N- and C-terminal regions (C) of compounds **1–6** compared to SFTI-1 in complexes with trypsin (black) and matriptase (grey) showing 100 values determined every 10 ps during the last nanosecond of simulation.

S9F). Nevertheless, more distorted structures with significantly lower affinities were also observed. This heterogeneity of interaction profiles was reflected by the highest errors (standard deviations) of corresponding  $\Delta_B G^{\text{dock}}$  within the set of investigated compounds (Table 3). This probably originates from the described moderate distortion of the inhibitory loop during

**Table 2** Data collected from the simulation experiments for compounds **1–6**

Entry	Backbone RMSD <sup>a,b</sup> /Å	Distance Cα3–Cα11 <sup>b</sup> /Å	Intramol. H-bonds <sup>b,c</sup>
1	0.87 ± 0.09	3.93 ± 0.08	6.08 ± 1.08
2	1.13 ± 0.07	3.95 ± 0.07	6.12 ± 1.14
3	1.72 ± 0.15	3.90 ± 0.06	5.85 ± 1.15
4	1.74 ± 0.06	4.29 ± 0.10	5.67 ± 0.96
5	3.02 ± 0.10	5.66 ± 0.12	2.63 ± 0.91
6	1.79 ± 0.15	5.16 ± 0.14	4.36 ± 0.82

<sup>a</sup> Compared to solution structure 1JBL. <sup>b</sup> Values are arithmetical means of 100 structures taken from the last nanosecond of simulation. Errors are given as standard deviation. <sup>c</sup> Measured using a threshold of 6.25 kJ mol<sup>-1</sup>.

simulation (Fig. 5B). Nevertheless, the applied two-step docking procedure allowed a number of the *in silico* samples of peptidomimetic **6** to reconfigure the backbone conformation to the original BBI geometry upon interaction with the target enzymes.

In our docking experiments, compound **4** showed average values of  $\Delta_B G^{\text{dock}}$  very similar to **6** (Table 3). In this case, the pronounced deviation within the N- and C-terminal regions can be considered as the reason for the reduced complex stability (Fig. 5C). Thus, within the predicted inhibitor **4**–matriptase complex the aromatic side chain of Phe12 is positioned considerably different to inhibitors **1–3** (Fig. 6D). In the corresponding crystal structure this residue is highly constrained, being flanked by two benzyl groups of Phe97 and Phe99 of the protease molecule.<sup>1</sup> Thus, affinity of peptidomimetic **4** towards matriptase might be reduced due to a loss of favorable hydrophobic interactions within this region. Upon docking to trypsin, the C-terminal residues were even more displaced (Fig. S9D†). Nevertheless, the observed loss of free binding energy was still only of moderate magnitude for compound **4**. Interestingly, this inhibitor demonstrated the highest probability to interact with both proteases in the BBI geometry within the set of peptidomimetics **3–6** (Table 3).

Compound **3** showed significantly lower  $P_{\text{hit}}$  values compared to **4**. However, if bound in the BBI modality, **3** formed far more stable complexes. The determined absolute values of  $\Delta_B G^{\text{dock}}$  were even higher than those of monocyclic **2**. As, compared to **4**, peptidomimetic **3** lacks one methylene unit within the macrocyclization motif (Fig. 2), this structure possesses less degrees of conformational freedom. As a result, the proximity of  $\alpha$ -carbons between residues 3 and 11 in compound **3** matches the corresponding distance within the wild-type peptides **1** and **2** almost perfectly (Table 2). Nevertheless, the discussed structural constraints also caused the loss of backbone flexibility. Thus, compound **3** is held within a defined range of conformations displaying high stabilities of complexes with both proteases, once the inhibitor is positioned accordingly. However, the applied docking algorithm did not always succeed to fit compound **3** into the BBI geometry. This indicates that the latitude between perfect fit and steric clashes for SFTI-1 variants in complex with matriptase is rather limited.

A similar effect was observed for wild type **1**. This very constrained bicyclic inhibitor consistently showed the highest



**Table 3** Data collected from the docking experiments for compounds 1–6 against trypsin and matriptase and corresponding *in vitro* free energies of binding  $\Delta_B G^{\text{exp}}$ 

Entry	Trypsin					Matriptase				
	$P_{\text{hit}}/(\%)$	Intermol. H-bonds <sup>a,b</sup>	$\Delta_B G^{\text{dock } a/}$ (kJ mol <sup>-1</sup> )	$\Delta_B G^{\text{calc } c/}$ (kJ mol <sup>-1</sup> )	$\Delta_B G^{\text{exp } d/}$ (kJ mol <sup>-1</sup> )	$P_{\text{hit}}/(\%)$	Intermol. H-bonds <sup>a</sup>	$\Delta_B G^{\text{dock } a/}$ (kJ mol <sup>-1</sup> )	$\Delta_B G^{\text{calc } c/}$ (kJ mol <sup>-1</sup> )	$\Delta_B G^{\text{exp } d/}$ (kJ mol <sup>-1</sup> )
1	96	10.3 ± 1.9	61.3 ± 6.3	58.9 ± 6.1	58.0 ± 0.4	51	9.2 ± 1.8	71.0 ± 8.1	36.2 ± 4.1	34.0 ± 0.3
2	99	11.3 ± 1.5	51.6 ± 4.9	51.1 ± 4.8	55.2 ± 0.4	67	10.1 ± 2.1	63.2 ± 4.9	42.3 ± 5.8	35.1 ± 0.3
3	87	10.9 ± 1.4	54.8 ± 6.9	47.7 ± 6.0	47.3 ± 0.5	51	11.0 ± 1.6	69.0 ± 6.9	35.2 ± 4.4	33.7 ± 0.3
4	100	10.0 ± 1.7	48.6 ± 5.4	48.6 ± 5.4	54.0 ± 0.3	61	9.1 ± 1.9	56.4 ± 5.4	34.4 ± 7.1	27.9 ± 0.3
5	69	8.9 ± 1.4	33.6 ± 3.9	23.2 ± 2.7	37.5 ± 0.5	47	8.4 ± 1.5	42.6 ± 3.9	20.0 ± 3.0	20.2 ± 0.3
6	81	9.8 ± 1.6	43.8 ± 9.8	35.4 ± 8.0	39.8 ± 0.4	43	9.3 ± 2.2	56.1 ± 9.8	24.1 ± 4.8	23.0 ± 0.3

<sup>a</sup> Values are arithmetical means of all inhibitor–protease complexes following BBI modality and errors are standard deviations. <sup>b</sup> Measured using a threshold of 6.25 kJ mol<sup>-1</sup>. <sup>c</sup> Calculated using  $\Delta_B G^{\text{calc}} = P_{\text{hit}} \times \Delta_B G^{\text{dock}}$ . <sup>d</sup> Calculated using eqn (7). Errors of  $\Delta_B G^{\text{exp}}$  were calculated by propagation of errors (ESI†).

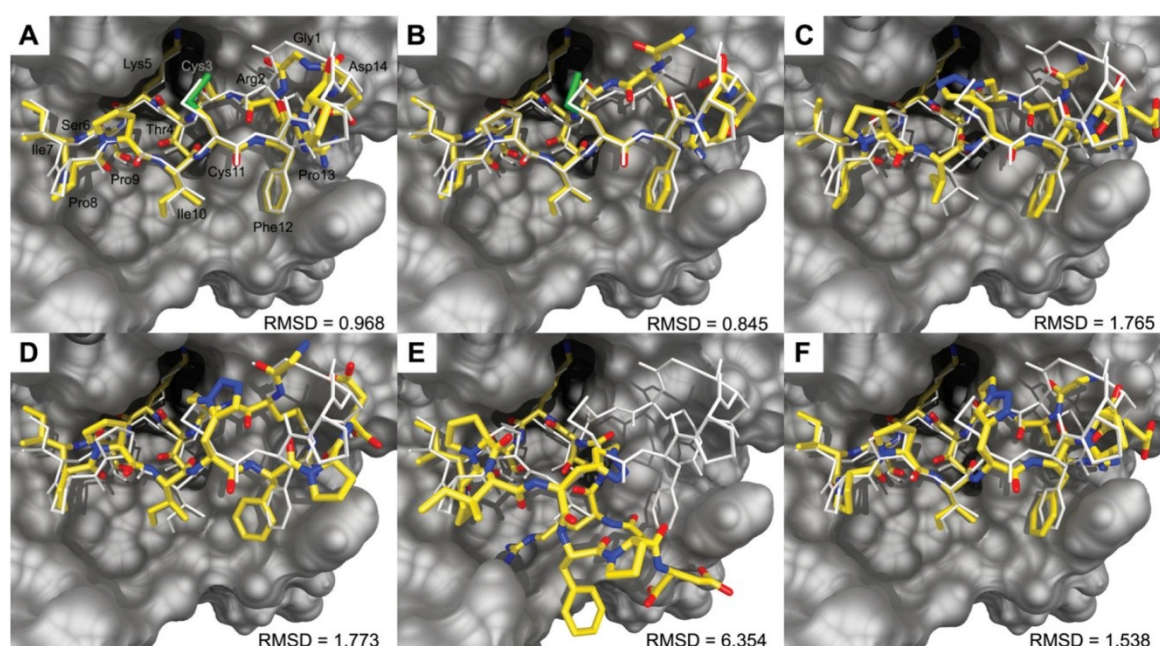


**Fig. 6** Predicted structures of compounds 1 (A), 2 (B), 3 (C), 4 (D), 5 (E), and 6 (F) in complex with matriptase (grey surface) as an overlay with reported crystal structure 3P8F (white sticks).<sup>1</sup> Blue: nitrogen, green: sulfur, red: oxygen, yellow: carbon, hydrogen is omitted for clarity. Measured RMSD values for inhibitor backbones compared to 3P8F are given in Å.

values of  $\Delta_B G^{\text{dock}}$  upon binding to both enzymes. Nevertheless, the probability of 1 to actually interact under the mode revealed by crystal structures was significantly lower than for compounds 2 and 4. Thus, flexibility within the region of the secondary loop might be crucial for the inhibitor to be effectively transferred from solution (simulation) into the active site of the proteases (docking). This effect is far more pronounced in the case of matriptase, probably due to the mentioned reduced space around residue 12 of inhibitors 1–6.

Monocyclic inhibitor 2 seems to provide a good compromise between flexibility and proper backbone arrangement. Hence, it forms very stable complexes with both proteases at a high probability.

#### Comparison of *in vitro* and *in silico* data

To take into account the reduced probabilities for SFTI-1 derivatives to bind to matriptase according to elucidated crystal structures, we directly weighted all  $\Delta_B G^{\text{dock}}$  by corresponding  $P_{\text{hit}}$  to calculate *in silico* binding affinities  $\Delta_B G^{\text{calc}}$  (Table 3). This procedure allowed evaluating relative potencies of the investigated compounds towards examined proteases. Additionally, experimental inhibition constants  $K_i$  were used to calculate free energies of binding  $\Delta_B G^{\text{exp}}$  using eqn (7) ( $R$  meaning the universal gas constant and  $T$  the absolute temperature).

$$\Delta_B G^{\text{exp}} = -RT \ln K_i \quad (7)$$

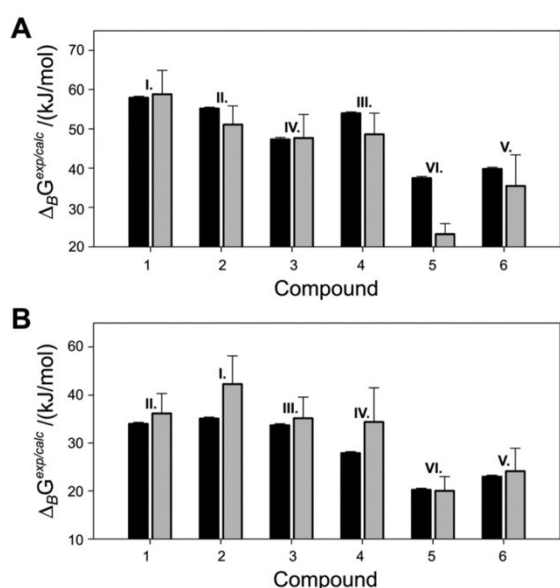


**Fig. 7** Bar chart of *in vitro*  $\Delta_B G^{\text{exp}}$  (black) and *in silico*  $\Delta_B G^{\text{calc}}$  (grey) for complexes of compounds 1–6 with trypsin (A) and matriptase (B). Rankings of binding affinities for both *in vitro* and *in silico* experiments are indicated by attic numerals (best to worst: I–VI).

Thus, the collected *in silico* data were compared with corresponding *in vitro* results (Fig. 7).

The applied simulation/docking procedure enabled to fully reproduce the outcome of the enzyme assays qualitatively. Thus, ranking investigated inhibitors 1–6 according to their affinity ( $\Delta_B G^{\text{calc}}$  or  $\Delta_B G^{\text{exp}}$ ) resulted in the same relative order for both proteases (Fig. 7). Generally, absolute values of  $\Delta_B G^{\text{calc}}$  for the inhibition of matriptase were higher compared to those determined by *in vitro* experiments. Since calculated binding affinities can only be regarded as rough estimates, both  $\Delta_B G^{\text{calc}}$  and  $\Delta_B G^{\text{exp}}$  are in astonishingly good agreement.

A similar result was achieved for trypsin inhibition. However, the most significant difference between *in vitro* and *in silico* data was observed for the weakest inhibitor 5 (Fig. 7A). Thus, it is probable that the applied docking procedure overestimates the influence of the massive distortion of the BBI loop in solution on trypsin affinity. The dramatic displacement of the peptide backbone may actually be attenuated through dynamic interactions of 5 with the surface of the protease. Nevertheless, the possibility for minor backbone readjustments was provided by energy minimization between the semi-flexible and the rigid docking steps. An additional time-intensive MD simulation procedure might be required to cover the dynamic nature of ligand–receptor interactions as well as the influence of solvent molecules on the investigated complex structures. Furthermore, effects of transient or permanent breakage and formation of covalent bonds have to be ignored within the classical force field approach. Such reactions might have a significant impact in the investigated system, as dynamic hydrolysis/recyclization equilibrium has been reported for trypsin inhibition by SFTI-1.<sup>35</sup>

## Conclusion

Our *in vitro* data show that the *in vivo* application of the wild-type SFTI-1 as a therapeutic agent targeting matriptase is limited due to its drastically reduced potency at physiological pH. Nevertheless, as reported in previous works, the SFTI-1 framework provides an appropriate starting point for lead compound optimization towards inhibition of pharmacologically relevant proteases.<sup>15,36–38</sup> With the focus on matriptase as the target enzyme, we suggest the open-chain variant SFTI-1[1,14] as a promising scaffold rather than its bicyclic ancestor. Based on these findings, we developed SFTI-1[1,14] derivatives with significantly improved affinity and selectivity towards the addressed TTSP; these results will be published elsewhere.

Additionally, triazole-bridged matriptase inhibitor 3 provides the best kinetic properties within the set of peptidomimetics 3–6. Its highly constrained side-chain macrocyclic motif might also be a valuable asset when redox stability is of particular importance within the pharmaceutical context.

Our *in silico* experiments provided a plausible explanation for the potencies observed *in vitro*. Despite the intrinsic limitations and simplifications of the force field approach, computed binding affinities  $\Delta_B G^{\text{calc}}$  represented satisfactory qualitative estimates of values determined by enzyme assays. Structural analysis of the simulation and docking experiments indicated the importance of the terminal regions of SFTI-1 derivatives upon matriptase binding/inhibition. Higher conformational constraints lead to better interaction profiles while lowering the overall probability to bind matriptase following the expected modality. Nevertheless, changes within the structure of the BBI macrocycle affected inhibitory potency in the most severe manner. However, further refinement of force field parameters for triazolyl moieties within peptidic molecules using additional X-ray and/or NMR experiments might be necessary for more precise calculations. Additionally, to confirm the predicted entropic effects on inhibitory potency, isothermal calorimetry could be conducted.<sup>39</sup>

## Experimental

### Chemicals

All Fmoc-protected amino acids, resins for solid phase peptide synthesis (SPPS), solvents, and other chemicals were purchased from Agilent (Varian), Bachem, Fischer Chemicals, Iris Biotech, Novabiochem, Roth and Sigma-Aldrich.

### Peptide synthesis

Linear peptide precursors were assembled by automated microwave-assisted SPPS using the Fmoc strategy.<sup>40,41</sup>

Bicyclic SFTI-1 (1) was synthesized *via* solution-phase backbone macrocyclization of linear precursor H-Arg(Pbf)-Cys(Trt)-Thr(*t*Bu)-Lys(Boc)-Ser(*t*Bu)-Ile-Pro-Pro-Ile-Cys(Trt)-Phe-Pro-Asp(*t*Bu)-Gly-OH using C-terminal PyBOP/HOBt activation followed by acidolytic side-chain deprotection, oxidative disulfide bond formation and chromatographic isolation.

Synthesis and characterization of monocyclic SFTI-1[1,14] (2) and triazole-containing peptidomimetics 4–6 have been



previously reported.<sup>13</sup> New peptidomimetic compound **3** possessing a 1,5-disubstituted 1,2,3-triazolyl side chain macrocyclization motif was synthesized using a similar approach.<sup>13</sup> First, the peptide resin containing unnatural amino acids azidoalanine (Aza) and propargylglycine (Pra) (Fmoc-Aza-Thr(*t*Bu)-Lys (Boc)-Ser(*t*Bu)-Ile-Pro-Pro-Ile-Pra-Phe-Pro-Asp(*t*Bu)-resin) was synthesized. Then, the triazole bridge was installed *via* on-support ruthenium(II)-catalyzed azide-alkyne cycloaddition (RuAAC) followed by coupling of N-terminal residues Gly1 and Arg2. Acidolytic cleavage and chromatographic isolation followed.

For experimental details and analytical data on bicyclic SFTI-1 (**1**) and new triazole-bridged compound **3** refer to ESI.†

### Recombinant production of matriptase

BL21-CodonPlus (DE3)-RP competent *E. coli* cells (Stratagene) were transformed with expression vector pET42dest-His-hMatI (cd)596–855. This vector was constructed for overexpression of the zymogen sequence of the catalytic domain of matriptase as the following fusion: Met-Ser-Tyr-Tyr-His6-aa596–855. Inclusion body production, protein denaturation, purification and refolding/autoprotolytic activation were conducted according to reported procedures (see ESI, Fig. S1 and S2† for details).<sup>11,25,42</sup> Substrate-specific catalytic activity of the purified enzyme was verified through the hydrolysis of chromogenic substrate Boc-QAR-*p*NA and quantified *via* active-site titration using 4-methylumbelliferyl-*p*-guanidinobenzoate (MUGB) (see ESI, Fig. S3†).<sup>43,44</sup>

### Inhibition assays

Apparent (substrate-dependent) inhibition constants  $K_i^{\text{app}}$  of SFTI-1-derivatives **1–6** against active-site-titrated bovine trypsin ( $[E] = 0.5 \text{ nM}$ ) and matriptase ( $[E] = 0.9 \text{ nM}$ ) were determined by recording kinetic curves of the enzymatic hydrolysis of chromogenic substrate Boc-QAR-*p*NA ( $[S] = 250 \text{ }\mu\text{M}$ ) at different concentrations of inhibitor  $[I]$  (pH 7.6 or pH 8.5) using a Tecan GENios microplate reader.<sup>13</sup> Calculated relative initial velocities of the residual proteolytic reaction ( $v/v_0$ ) were plotted against  $[I]$ . Eqn (3) for tight-binding inhibitors was fitted by non-linear regression to the resulting dose–response curves using the Marquardt–Levenberg algorithm of Sigma Plot 11.<sup>29</sup>

Substrate-independent inhibition constants  $K_i$  were calculated from  $K_i^{\text{app}}$  and the Michaelis–Menten constants  $K_M$  for the corresponding enzyme–substrate complex using eqn (6).<sup>25,34</sup>

$K_M$  for Boc-QAR-*p*NA in complex with matriptase at pH 7.6 and pH 8.5 were calculated by Lineweaver–Burk plots as  $236.8 \pm 56.1 \text{ }\mu\text{M}$  and  $66.6 \pm 16.0 \text{ }\mu\text{M}$ , respectively.  $K_M$  for trypsin as well as the method for the estimation of errors for each individual  $K_i$  have been recently reported.<sup>34</sup>

In the case of reversible competitive inhibition  $K_i$  equals the dissociation constant  $K_d$  of the inhibitor–enzyme complex.<sup>45</sup> Thus, the free energy of binding  $\Delta_B G$  can be calculated from  $K_i$  using eqn (7).

### Force field customization

All *in silico* experiments were performed with the YASARA structure package (YASARA Biosciences). For the precise handling of triazole-bridged peptides during *in silico* calculations, new topology entries and atom types for the involved carbon and nitrogen species have been implemented into the YASARA2 force field description file. Thus, amino acid residues with 1,4- and 1,5-disubstituted 1,2,3-triazoles in the side chain of compounds **3–6** were covered. Corresponding equilibrium bond lengths, bond angles and dihedrals have been deduced from reported crystal structures.<sup>46,47</sup> Values for force constants and scaling factors were adopted from similar aromatic and hetero-aromatic structures (*e.g.* imidazole) within the original force field. The full set of parameters used to calculate disubstituted 1,2,3-triazoles is given in the ESI.†

### Molecular dynamics simulation and docking

Solution NMR structures of SFTI-1 (PDB ID: 1JBL) and SFTI-1 [1,14] (PDB ID: 1JBN) were used as initial templates for compounds **1–6**.<sup>33</sup> Triazole bridges of peptidomimetics **3–6** were modelled into 1JBN to match the topology entry within the customized force field. Each compound was then subjected to a two-step simulation and docking procedure performed *via* a self-written command sequence (macro). The design of the *in silico* experiment is sketched in Fig. 4.

Following point charge assignment *via* semi-quantitative quantum mechanics,<sup>48</sup> an energy minimization was conducted with initial structures of compounds **1–6** in 0.9% (m/v) NaCl (aq.) at pH 7.6. To prevent structures from being trapped in the local minimum of the template coordinates, all compounds were then simulated at 373 K and the scaling factor for non-bonded interactions was reduced to 10%. This parameter was stepwise re-adjusted to 100% within 500 ps. After 1 ns of simulation, the temperature was set to 298 K and energy-minimized structures were simulated for another 9 ns. Trajectories (snapshots) were saved every 10 ps. Thus, 100 models for each individual compound **1–6** from the last nanosecond of the simulation were extracted and used for the docking experiment. Semi-flexible docking to the active sites of trypsin and matriptase with fixed ligand backbones and adjusted side-chain atoms of Lys5 was performed to identify the most probable binding geometry using the AutoDock 4 algorithm with 999 runs.<sup>18</sup> The highest ranked complex structure was subjected to an energy minimization with fixed receptor atoms followed by another energy minimization step with a fully unrestrained ligand–receptor complex. The resulting structures were then used for the rigid docking experiment (additional 999 runs) to compute virtual free energies of binding  $\Delta_B G$  with AutoDock.

### Acknowledgements

This work was supported by the Deutsche Forschungsgemeinschaft through grant Ko 1390/9-1 and by BMBF. We thank Prof. Dr Kay Hamacher (AG Computational Biology & Simulation, Technische Universität Darmstadt) for discussion concerning *in silico* experiments and for reading the manuscript.



## References

- 1 C. Yuan, L. Q. Chen, E. J. Meehan, N. Daly, D. J. Craik, M. D. Huang and J. C. Ngo, *BMC Struct. Biol.*, 2011, **11**.
- 2 S. Lockett, R. S. Garcia, J. J. Barker, A. V. Konarev, P. R. Shewry, A. R. Clarke and R. L. Brady, *J. Mol. Biol.*, 1999, **290**, 525–533.
- 3 Y. Q. Long, S. L. Lee, C. Y. Lin, I. J. Enyedy, S. M. Wang, P. Li, R. B. Dickson and P. P. Roller, *Bioorg. Med. Chem. Lett.*, 2001, **11**, 2515–2519.
- 4 M. L. J. Korsinczyk, R. J. Clark and D. J. Craik, *Biochemistry*, 2005, **44**, 1145–1153.
- 5 P. Li, S. Jiang, S. L. Lee, C. Y. Lin, M. D. Johnson, R. B. Dickson, C. J. Michejda and P. P. Roller, *J. Med. Chem.*, 2007, **50**, 5976–5983.
- 6 Y. E. Shi, J. Torri, L. Yieh, A. Wellstein, M. E. Lippman and R. B. Dickson, *Cancer Res.*, 1993, **53**, 1409–1415.
- 7 K. Uhland, *Cell. Mol. Life Sci.*, 2006, **63**, 2968–2978.
- 8 K. List, *Future Oncol.*, 2009, **5**, 97–104.
- 9 J. M. Milner, A. Patel, R. K. Davidson, T. E. Swingler, A. Desilets, D. A. Young, E. B. Kelso, S. T. Donell, T. E. Cawston, I. M. Clark, W. R. Ferrell, R. Plevin, J. C. Lockhart, R. Leduc and A. D. Rowan, *Arthritis Rheum.*, 2010, **62**, 1955–1966.
- 10 I. Seitz, S. Hess, H. Schulz, R. Eckl, G. Busch, H. P. Montens, R. Brandl, S. Seidl, A. Schomig and I. Ott, *Arterioscler., Thromb., Vasc. Biol.*, 2007, **27**, 769–775.
- 11 T. Steinmetzer, A. Schweinitz, A. Sturzebecher, D. Donnecke, K. Uhland, O. Schuster, P. Steinmetzer, F. Muller, R. Friedrich, M. E. Than, W. Bode and J. Sturzebecher, *J. Med. Chem.*, 2006, **49**, 4116–4126.
- 12 C. J. Farady, J. Sun, M. R. Darragh, S. M. Miller and C. S. Craik, *J. Mol. Biol.*, 2007, **369**, 1041–1051.
- 13 M. Empting, O. Avrutina, R. Meusinger, S. Fabritz, M. Reinwarth, M. Biesalski, S. Voigt, G. Buntkowsky and H. Kolmar, *Angew. Chem., Int. Ed.*, 2011, **50**, 5207–5211.
- 14 U. Essmann, L. Perera, M. L. Berkowitz, T. Darden, H. Lee and L. G. Pedersen, *J. Chem. Phys.*, 1995, **103**, 8577–8593.
- 15 J. E. Swedberg, S. J. de Veer, K. C. Sit, C. F. Reboul, A. M. Buckle and J. M. Harris, *PLOS One*, 2011, **6**.
- 16 E. Krieger, K. Joo, J. Lee, J. Lee, S. Raman, J. Thompson, M. Tyka, D. Baker and K. Karplus, *Proteins: Struct., Funct., Bioinf.*, 2009, **77**, 114–122.
- 17 W. Brandt, T. Herberg and L. Wessjohann, *Biopolymers*, 2011, **96**, 651–668.
- 18 G. M. Morris, D. S. Goodsell, R. S. Halliday, R. Huey, W. E. Hart, R. K. Belew and A. J. Olson, *J. Comput. Chem.*, 1998, **19**, 1639–1662.
- 19 W. R. Rypniewski, A. Perrakis, C. E. Vorgias and K. S. Wilson, *Protein Eng., Des. Sel.*, 1994, **7**, 57–64.
- 20 S. N. S. Murthy, J. Kostman and V. P. Dinoso, *Dig. Dis. Sci.*, 1980, **25**, 289–294.
- 21 T. H. Bugge, T. M. Antalis and Q. Y. Wu, *J. Biol. Chem.*, 2009, **284**, 23177–23181.
- 22 J. L. Wike-Hooley, J. Haveman and H. S. Reinhold, *Radiother. Oncol.*, 1984, **2**, 343–366.
- 23 I. F. Tannock and D. Rotin, *Cancer Res.*, 1989, **49**, 4373–4384.
- 24 P. Montcourrier, I. Silver, R. Farnoud, I. Bird and H. Rochefort, *Clin. Exp. Metastasis*, 1997, **15**, 382–392.
- 25 A. Desilets, J. M. Longpre, M. E. Beaulieu and R. Leduc, *FEBS Lett.*, 2006, **580**, 2227–2232.
- 26 F. Beliveau, A. Desilets and R. Leduc, *FEBS J.*, 2009, **276**, 2213–2226.
- 27 Y. Cheng and W. H. Prusoff, *Biochem. Pharmacol.*, 1973, **22**, 3099–3108.
- 28 R. A. Copeland, D. Lombardo, J. Giannaras and C. P. Decicco, *Bioorg. Med. Chem. Lett.*, 1995, **5**, 1947–1952.
- 29 J. F. Morrison, *Biochim. Biophys. Acta, Enzymol.*, 1969, **185**, 269–286.
- 30 J. W. Williams and J. F. Morrison, *Methods Enzymol.*, 1979, **63**, 437–467.
- 31 W. R. Greco and M. T. Hakala, *J. Biol. Chem.*, 1979, **254**, 12104–12109.
- 32 D. J. Murphy, *Anal. Biochem.*, 2004, **327**, 61–67.
- 33 M. L. J. Korsinczyk, H. J. Schirra, K. J. Rosengren, J. West, B. A. Condie, L. Otvos, M. A. Anderson and D. J. Craik, *J. Mol. Biol.*, 2001, **311**, 579–591.
- 34 M. Tischler, D. Nasu, M. Empting, S. Schmelz, D. W. Heinz, P. Rottmann, H. Kolmar, G. Buntkowsky, D. Tietze and O. Avrutina, *Angew. Chem., Int. Ed.*, 2012, **51**, 3708–3712.
- 35 U. C. Marx, M. L. J. Korsinczyk, H. J. Schirra, A. Jones, B. Condie, L. Otvos and D. J. Craik, *J. Biol. Chem.*, 2003, **278**, 21782–21789.
- 36 A. Lesner, A. Legowska, M. Wysocka and K. Rolka, *Curr. Pharm. Des.*, 2011, **17**, 4308–4317.
- 37 E. Zablotna, A. Jaskiewicz, A. Legowska, H. Miecznikowska, A. Lesner and K. Rolka, *J. Pept. Sci.*, 2007, **13**, 749–755.
- 38 J. D. McBride, H. N. M. Freeman and R. J. Leatherbarrow, *Eur. J. Biochem.*, 1999, **266**, 403–412.
- 39 S. Leavitt and E. Freire, *Curr. Opin. Struct. Biol.*, 2001, **11**, 560–566.
- 40 M. Amblard, J. A. Fehrentz, J. Martinez and G. Subra, *Mol. Biotechnol.*, 2006, **33**, 239–254.
- 41 S. Park, S. Gunasekera, T. L. Aboye and U. Goransson, *Int. J. Pept. Res. Ther.*, 2010, **16**, 167–176.
- 42 T. Takeuchi, M. A. Shuman and C. S. Craik, *Proc. Natl. Acad. Sci. U. S. A.*, 1999, **96**, 11054–11061.
- 43 T. Chase and E. Shaw, *Biochemistry*, 1969, **8**, 2212–2224.
- 44 G. W. Jameson, D. V. Roberts, R. W. Adams, W. S. A. Kyle and D. T. Elmore, *Biochem. J.*, 1973, **131**, 107–117.
- 45 W. R. Greco and M. T. Hakala, *J. Biol. Chem.*, 1979, **254**, 2104–2109.
- 46 M. R. Krause, R. Goddard and S. Kubik, *J. Org. Chem.*, 2011, **76**, 7084–7095.
- 47 A. Brik, J. Alexandratos, Y. C. Lin, J. H. Elder, A. J. Olson, A. Wlodawer, D. S. Goodsell and C. H. Wong, *ChemBioChem*, 2005, **6**, 1167–1169.
- 48 A. Jakalian, D. B. Jack and C. I. Bayly, *J. Comput. Chem.*, 2002, **23**, 1623–1641.



## 2.5 Combinatorial "Click Libraries" for the Optimization of Matriptase Inhibition

Title:

**Combinatorial Tuning of Peptidic Drug Candidates: High-Affinity Matriptase Inhibitors through Incremental Structure-Guided Optimization**

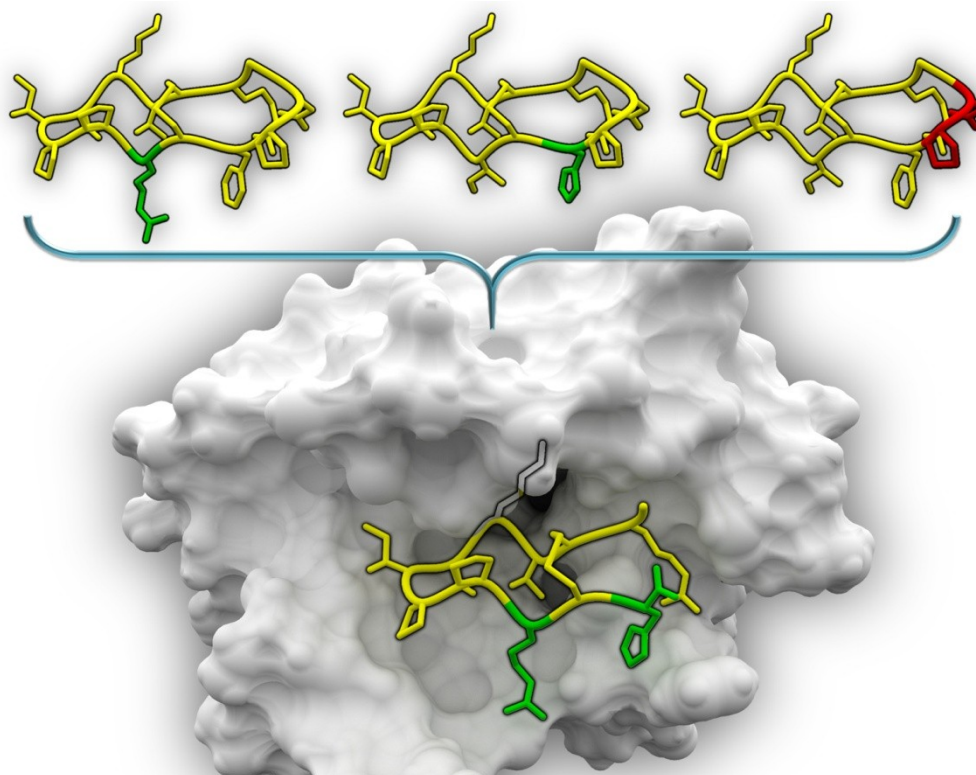
Authors:

Heiko Fittler, Olga Avrutina, Bernhard Glotzbach, Martin Empting, Harald Kolmar

Bibliographic Data:

Submitted for publication in September 2012.

Graphical Abstract:



The combination of incremental improvements of the sunflower trypsin inhibitor-1 (SFTI-1) yields single-digit nanomolar inhibitors of matriptase. Beneficial modifications of the peptidic framework were identified *via* a small "click" library and allowed for the establishment of additional favorable interactions between the enzyme and the inhibitor.

Contributions by M. Empting:

- Developed concept
- Performed all *in silico* experiments
- Wrote the article
- Created all figures

# Combinatorial Tuning of Peptidic Drug Candidates: High-Affinity Matriptase Inhibitors through Incremental Structure-Guided Optimization†

Heiko Fittler,<sup>a</sup> Olga Avrutina,<sup>a</sup> Bernhard Glotzbach,<sup>a</sup> Martin Empting,<sup>\*a</sup> and Harald Kolmar<sup>\*a</sup>

<sup>5</sup> Received (in XXX, XXX) Xth XXXXXXXXX 20XX, Accepted Xth XXXXXXXXX 20XX

DOI: 10.1039/b000000x

Herein we report a convenient strategy for the development of novel, highly-potent peptidic inhibitors of the trypsin-like serine protease matriptase based on the monocyclic variant of the sunflower trypsin inhibitor-1 (SFTI-1[1,14]). We screened SFTI-1[1,14] variants possessing incremental modifications of the parent peptide for beneficial binding properties. This compound library comprising 6 peptides and 16 triazole-containing peptidomimetics was established *via* structure-guided rational design and synthesized using a divergent strategy employing "copper-click" chemistry. The most favorable amino acid substitutions were combined in one framework yielding potent SFTI-1-derived matriptase inhibitor-1 (SDMI-1) and the truncated dodecapeptide variant (SDMI-2) with single-digit nanomolar inhibition constants. *In silico* studies indicated that the improved matriptase affinity compared to the parent peptide is caused by the successful establishment of additional favorable proton donor-acceptor interactions between basic inhibitor side chains and acidic residues on the surface of the target enzyme. SDMI-1 and 2 are potent inhibitors of the pharmaceutically relevant protease matriptase at a near physiological pH and, thus, may find applications in therapy or diagnostics.

## 20 Introduction

Trypsin is one of the most prominent digestive enzymes ubiquitously found in the small intestine of vertebrates.<sup>1</sup> Its intriguing molecular framework includes the famous triad Asp-His-Ser as a core feature implementing its proteolytic activity.<sup>2</sup> This prototypic architecture and the ability to cleave peptide bonds after basic residues constitutes the structural and functional groundwork of a whole class of biocatalysts referred to as trypsin-like serine proteases.<sup>3</sup> Members of this enzyme family are involved in diverse biological processes and occur in soluble form or as membrane-anchored entities.<sup>4</sup> Type II transmembrane serine proteases (TTSP), for instance, are bound to the cell surface *via* the *N*-terminus and have been characterized as important mediators of the pericellular procession and activation of various effector molecules.<sup>3-7</sup> Active forms of peptide hormones, growth and differentiation factors, receptors, enzymes, and adhesion molecules are generated from inactive precursors through endoproteolytic cleavage by specific TTSPs.<sup>4</sup> Hence,

they play crucial roles in the cellular development and maintenance of homeostasis.<sup>3</sup>

<sup>40</sup> A well-studied example of a membrane-anchored trypsin-like serine protease with pharmaceutical relevance is matriptase.<sup>8-18</sup> It is widely expressed on the surface of epithelial cells in healthy tissue where its proteolytic activity is precisely regulated by natural protease inhibitors like the hepatocyte growth factor activator inhibitor-1 and 2 (HAI-1, HAI-2).<sup>10, 13</sup> However, dysregulation of this physiological inhibitor-protease balance is believed to facilitate pathological processes. Indeed, a number of studies associate matriptase overexpression with the development and progression of epithelial tumors, as well as osteoarthritis and atherosclerosis.<sup>14-18</sup> Furthermore, Napp *et al.* observed pronounced *in vivo* matriptase activity in a murine orthotopic pancreatic tumor model and showed that the administration of active-site inhibitors significantly reduces proteolysis of the substrate analyte.<sup>11</sup> Hence, potent and selective matriptase inhibitors are of great therapeutic importance, and their development is a challenging task. To date, a number of small synthetic organic compounds as well as large antibody fragments exhibiting single-digit nanomolar to subnanomolar inhibition constants have been reported.<sup>19-21</sup> Very recently, Marsault and <sup>60</sup>coworkers have demonstrated the applicability of peptidomimetics bearing a benzothiazole-based "serine trap" for the development of very potent matriptase inhibitors.<sup>21</sup> Reactive carbonyl functionality at the P1 position allowed for the

<sup>a</sup> Clemens-Schöpf Institute of Organic Chemistry and Biochemistry, Technische Universität Darmstadt, Petersenstr. 22, 64287 Darmstadt, Germany. E-mail: M.Empting@Biochemie-TUD.de, Kolmar@Biochemie-TUD.de

†Electronic Supplementary Information (ESI) available: Tabulated data of ESI-MS analysis, RP-HPLC chromatograms, and plotted kinetic data of enzyme inhibition assays for all compounds. See DOI: 10.1039/b000000x/



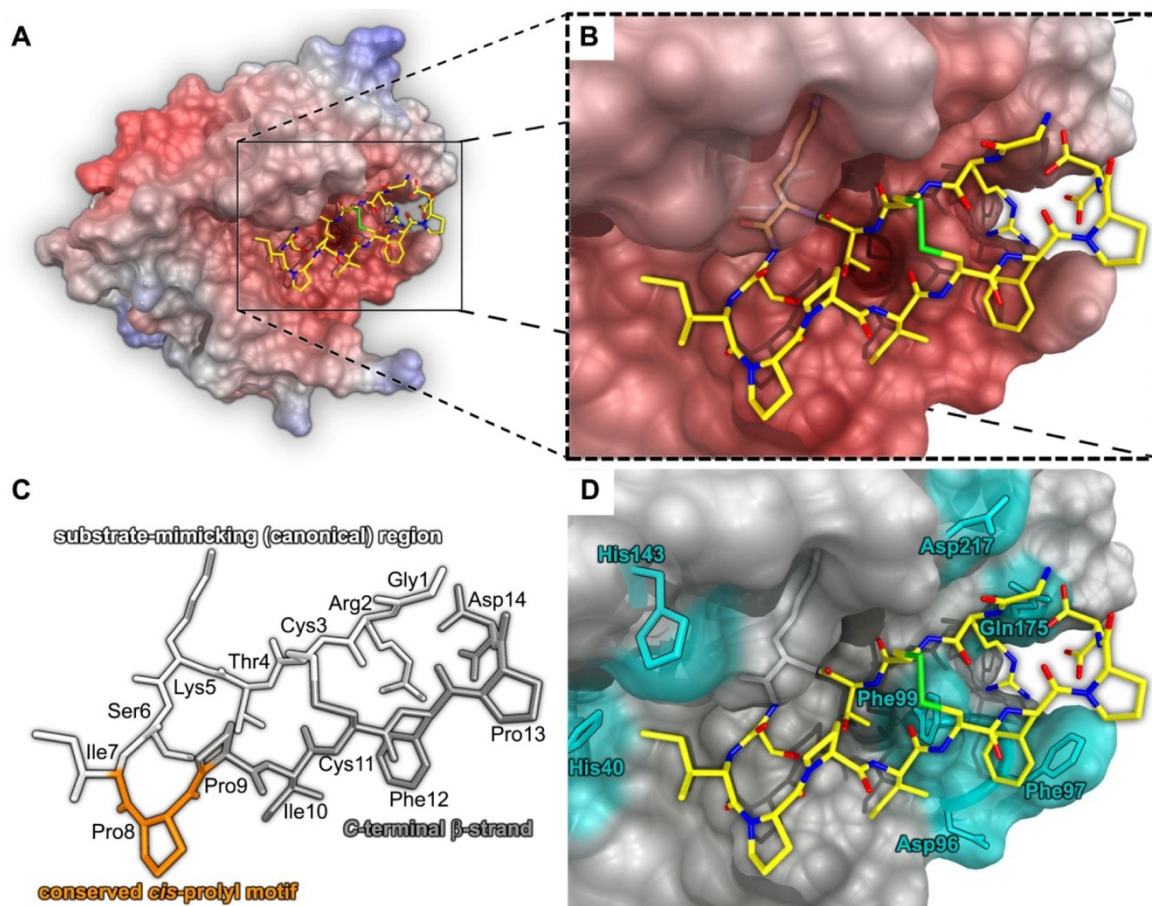


**Fig. 1** Predicted structure of the SFTI-1[1,14] (1)-matriptase complex generated *via* molecular dynamics simulations followed by a two-step docking procedure.<sup>22</sup> Blue: nitrogen, green: sulfur, red: oxygen, yellow: carbon, hydrogen is omitted for clarity. Reported X-ray/NMR structures 3P8F and 1JBN were used as initial coordinates.<sup>12, 23</sup> (A) Molecular surface of the catalytic domain of matriptase in complex with 1 (sticks). Color gradients (red to blue) indicate electrostatic surface potentials (negative to positive) at pH 7.4 calculated *via* the Particle Mesh Ewald method with a maximum value of 500 kJ/mol.<sup>24</sup> (B) Enlarged depiction of the active site. Regions concealing parts of the ligand are shown transparently. Bound inhibitor 1 is highlighted by a black outline. (C) Sequence and schematic representation of SFTI-1[1,14] (1). (D) Depiction of the active site indicating side chains of matriptase residues (cyan sticks, black outline) which have been considered within the presented approach for the structure-guided optimization of the SFTI-1 framework (sticks, black outline).

10 establishment of a transient covalent linkage between the ligand and the active-site serine.<sup>21, 25, 26</sup>

In this study, we present a convenient strategy for the development of non-covalent high-affinity matriptase inhibitors starting from a naturally occurring peptidic framework 15 comprising a canonical protease inhibitor loop (Fig. 1). We used the rigid and well-defined tetradecapeptide framework of the sunflower trypsin inhibitor-1 (SFTI-1) as a starting point for structure-guided lead compound optimization. This molecular scaffold possesses a canonical (substrate-mimicking) loop for 20 anti-proteolytic activity and has already been successfully used for the generation of inhibitors of chymotrypsin, elastase, cathepsin G,  $\beta$ -trypsin, proteinase K or kallikrein-related peptidase.<sup>27-31</sup> Additionally, a latent inhibitory activity against matriptase in the nanomolar range ( $K_i = 1-150$  nM) has been 25 reported for the bicyclic peptide at the pH optimum of the TTSP (pH ~8.5-9).<sup>22, 32-35</sup> Very recently, we showed that this moderate

potency is essentially decreased in an environment with near physiological parameters ( $K_i = 1.1$   $\mu$ M at pH 7.6).<sup>22</sup> This is of particular importance for potential *in vivo* applications. A 30 therapeutic/diagnostic agent must possess high activity under homeostasis or – in case of tumor as well as inflammation-induced hypoxia – more acidic conditions.<sup>36-40</sup>

Using a structure-guided incremental optimization strategy we were able to generate SFTI-1 derivatives with single-digit 35 nanomolar  $K_i$  as well as an improved trypsin/matriptase selectivity profile.

## Results and Discussion

In our previous study, we reported that the monocyclic variant SFTI-1[1,14] possesses a slightly improved inhibition constant 40 compared to the bicyclic wild type.<sup>22</sup> Thus, the open-chain derivative represents a promising starting point for the design of

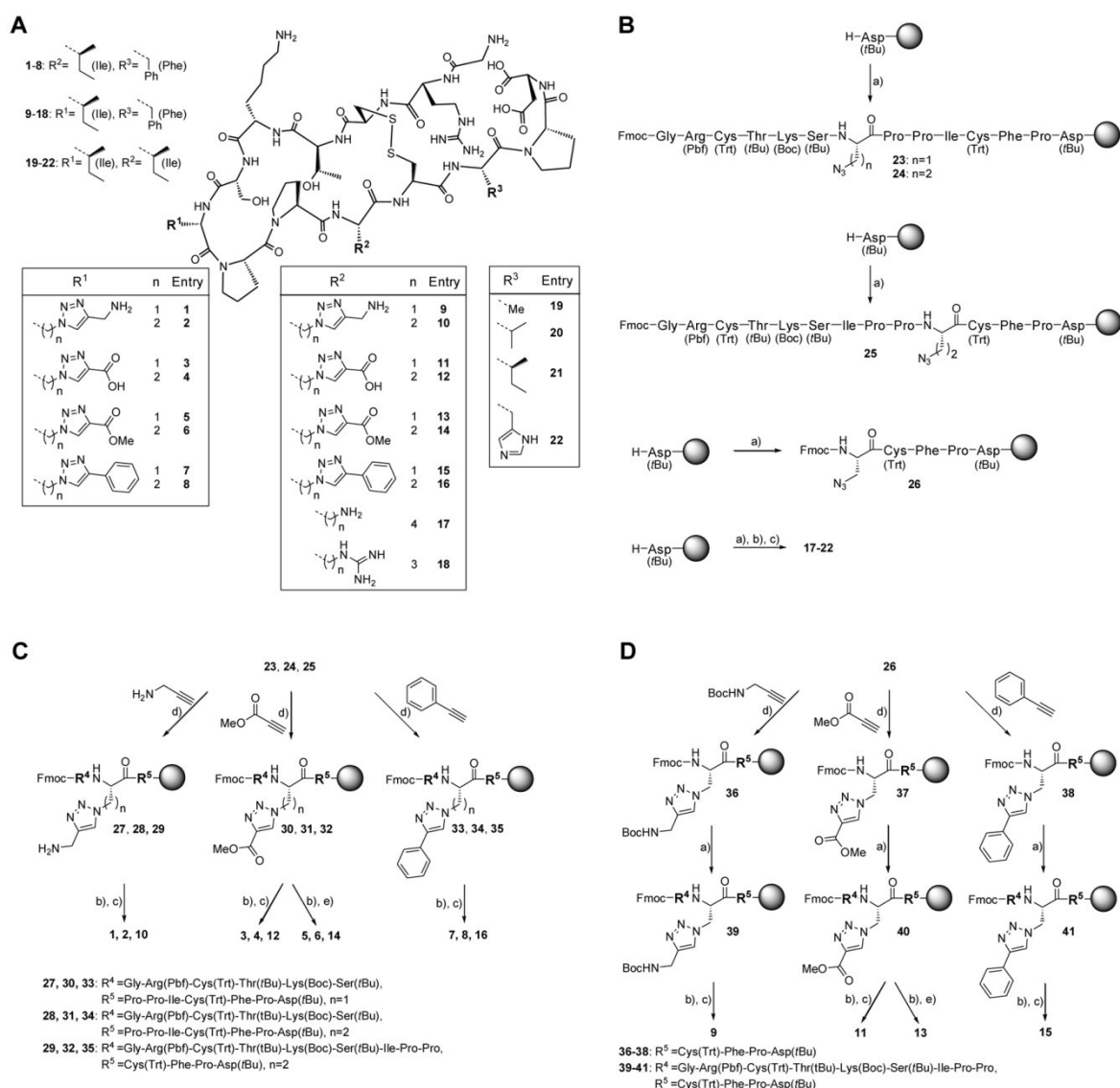


**Fig. 2** Design and synthesis of a small compound library comprising SFTI-1[1,14] derivatives **1–22**. (A) Collection of triazolyl-containing peptides **1–16** as well as variants **17–22** with a singular substitutions at positions 10 and 12 using canonical amino acids lysine, arginine, alanine, valine, isoleucine, or histidine. (B) Synthesis of precursors **23, 24, 25**, and **26** as well as inhibitors **17–22**. (C) and (D) Schematic depictions of synthetic routes yielding triazolyl-containing peptides **1–16**. Conditions: a) microwave-assisted Fmoc-SPPS; b) acidolytic cleavage from the solid support using TFA/H<sub>2</sub>O/anisole/TES (47:1:1:1, v:v:v:v) and dithiothreitol (DTT), c) air-mediated oxidative macrocyclization in 100 mM (NH<sub>4</sub>)<sub>2</sub>CO<sub>3</sub> aq (pH=8.4) at 1 mg peptide/mL; d) on-resin CuAAC using given alkyne component (5 eq), CuSO<sub>4</sub>·5H<sub>2</sub>O (20 mol %), sodium ascorbate (20 mol %), and *N,N*-diisopropylethylamine (DIEA, 8 eq) in DMF at ambient temperature (overnight) e) air-mediated oxidative macrocyclization in 100 mM (NH<sub>4</sub>)<sub>2</sub>CO<sub>3</sub> aq (pH=7.7) at 1 mg peptide/mL. All compounds **1–22** were isolated through preparative reversed-phase HPLC.

novel matriptase inhibitors. A combination of molecular dynamics simulation and docking experiments yielded an *in silico* SFTI-1[1,14]-matriptase complex, very similar to the reported wild-type inhibitor-protease X-ray structure (Fig. 1).<sup>12,22</sup>

Using this structural data and considering suggestions made by Yuan *et al.*,<sup>12</sup> we designed a minimal compound library **1–22** suitable for an initial search for incremental enhancements of the lead structure (step 1, Fig. 2). In a second step we investigated whether a combination of the individual beneficial modifications of the SFTI-1 framework results in an additive effect (step 2).

Finally, we truncated the most promising variant to study the influence of the C-terminal residues on matriptase affinity and selectivity (step 3).

### Step 1: Tuning Affinity of Singular Residues (Increments)

Trypsin and matriptase share a very similar substrate spectrum.

Thus, we rationalized that substitutions within the canonical region of SFTI-1[1,14] (Fig. 1C) would be detrimental towards improved affinity. However, we included the P2' position (Ile7) as a site for side-chain replacements within our molecular design

(Fig. 2A). Histidines 40 and 143 of matriptase are in close proximity to this residue, therefore they might provide the possibility for favourable hydrogen bonding interactions with the ligand (Fig. 1D).

To reduce the synthetic expense and to cover an adequate structural and functional space, we set up a divergent synthetic procedure. Azide-bearing peptidic scaffolds **23** and **24** were assembled on the solid support using commercially available building blocks Fmoc-L-azidoalanine (Fmoc-Aza-OH) and Fmoc-L-azidohomoalanine (Fmoc-Aha-OH) (Fig. 2B). On-resin copper(I)-catalyzed azide-alkyne cycloaddition (CuAAC) with different alkyne components allowed for the facile installation of an amine, a carboxylic acid, the corresponding methyl ester and a phenyl functionality at position 7. This combinatorial approach is quite similar to the “tethered fragment” strategy previously described by Burke Jr. and coworkers.<sup>41, 42</sup> Acidolytic cleavage from the solid support, oxidative macrocyclization and chromatographic isolation gave SFTI-1[1,14] derivatives **1–8** (Fig. 2C). Interestingly, both free carboxylic acids **3** and **4** as well as corresponding methyl esters **5** and **6** were selectively accessible from the respective open-chain methyl ester precursor peptides through the choice of macrocyclization conditions. The methyl carboxylate was hydrolyzed during disulfide bond formation at pH 8.4 giving free acids **3** and **4**. Setting the pH to 7.7, however, allowed for the preservation of the methyl ester group yielding the corresponding cystine-bridged products **5** and **6**.

Unfortunately, none of the position 7 variants **1–8** showed an improved matriptase affinity over SFTI-1[1,14] in enzyme inhibition assays (Table 1). Thus, we focused our further experiments on the optimization of positions 10 and 12.

In the ligand-receptor complex, the side chain of residue 10 of SFTI-1[1,14] is oriented towards a surface area of matriptase with a pronounced negative polarization (Fig. 1). The  $\beta$ -carboxylic group of the Asp96 contributes significantly to this environment. Yuan *et al.* suggested installing short basic side chain functionalities with low degrees of conformational freedom like aminoalanine or aminohomoalanine at position 10 of the inhibitor to establish favorable electrostatic interactions.<sup>12</sup> Nevertheless, initial molecular modeling implied that a linker of about four to five methylene units is needed to position a basic functionality in proximity to the  $\beta$ -carboxylic group of Asp96 in its native conformation present in the crystal structure (PDB-ID: 3P8F). Thus, we designed SFTI-1[1,14] derivatives **9–16** possessing planar and rigid triazolyl linkers of appropriate length to investigate the possibility for new favorable interactions between the ligand and the receptor (Fig. 2A).

Initially, synthetic routes for **9–16** were devised as modifications of to the approach used for SFTI-1[1,14] variants **1–8**. While variants **10, 12, 14, and 16** were readily accessible *via* this strategy (Fig. 2C), compounds **9, 11, 13, and 15** could not be synthesized in this manner. An attempt to assemble the Aza10 analog of peptide-resin **25** on the solid support resulted in an undefined mixture of side products (data not shown). Nevertheless, we were able to synthesize compounds **9, 11, 12, and 15** *via* the resin-bound pentapeptide intermediate **26** as depicted in Fig. 2D.

Interestingly, a significant increase of matriptase affinity over SFTI-1[1,14] was observed for four of the eight triazolyl-

**Table 1** Determined inhibition constants of compounds **1–22** against matriptase at pH 7.6 and calculated differences in free energies of binding/dissociation compared to SFTI-1[1,14].

Entry	$K_i$ / nM	Relative Activity <sup>b</sup>	$\Delta_B G_{(x)} - \Delta_B G_{(SFTI-1[1,14])}$ / (kJ·mol <sup>-1</sup> ) <sup>c</sup>
SFTI-1[1,14]	703 ± 87 <sup>d</sup>	1	0
Pos. 7 <sup>e</sup>	<b>1</b>	4892 ± 663	7.0
	<b>2</b>	3822 ± 494	5.4
	<b>3</b>	13886 ± 1711	19.8
	<b>4</b>	2380 ± 291	3.4
	<b>5</b>	1629 ± 200	2.3
	<b>6</b>	10857 ± 1349	15.4
	<b>7</b>	3342 ± 414	4.8
	<b>8</b>	1252 ± 155	1.8
Pos. 10 <sup>e</sup>	<b>9</b>	148 ± 19	0.21
	<b>10</b>	513 ± 66	0.73
	<b>11</b>	46287 ± 5728	65.8
	<b>12</b>	8096 ± 1011	11.5
	<b>13</b>	208 ± 27	0.30
	<b>14</b>	2224 ± 277	3.2
	<b>15</b>	556 ± 70	0.79
	<b>16</b>	4750 ± 585	6.8
Pos. 12 <sup>e</sup>	<b>17</b>	232 ± 29	0.33
	<b>18</b>	50.6 ± 6.5	0.072
	<b>19</b>	1614 ± 206	2.3
	<b>20</b>	580 ± 72	0.83
	<b>21</b>	319 ± 40	0.45
	<b>22</b>	206 ± 27	0.29

<sup>a</sup> Determined as described in the Experimental Section. <sup>b</sup> Relative activity given as the ratio  $K_i$  of the corresponding compound /  $K_i$  of SFTI-1[1,14]. <sup>c</sup>  $\Delta_B G_{(x)}$  refers to the free energy of binding/dissociation of compound x. <sup>d</sup>  $\Delta_B G$  were calculated from respective  $K_i$  using  $\Delta_B G = -RT \ln K_i$ .<sup>22, 43</sup> Errors of the given differences  $\Delta_B G_{(x)} - \Delta_B G_{(SFTI-1[1,14])}$  were calculated by propagation of errors. <sup>e</sup> As published before.<sup>22</sup> <sup>f</sup> The modified position of the SFTI-1[1,14] framework is given.

containing peptidomimetics **9–16** (Table 1).

The most pronounced enhancement within the set of inhibitors **9, 10, 13, and 15** was detected for the aminomethyl-functionalized 1,2,3-triazole **9**. The difference of the free energies of binding/dissociation  $\Delta_B G$  between compound **9** and SFTI-1[1,14] was calculated as 3.9 kJ/mol. Thus, additional favorable electrostatic inhibitor-enzyme interactions were successfully established by furnishing the peptide with a basic functionality at position 10. However, if length of the triazolyl linker is increased by only one methylene unit (**10**), the attractive contribution is significantly reduced. Furthermore, the installation of an acidic carboxy group at this position (**11, 12**) is detrimental for matriptase inhibition. Noteworthy, a significant increase of inhibitor potency compared to SFTI-1[1,14] is also observed for the formally uncharged methyl ester derivative **13** although not as pronounced as in the case of the amino-functionalized variant **9**.

Additionally, we investigated the impact of basic canonical amino acids, lysine and arginine, at position 10 (**17, 18**) on matriptase affinity. Surprisingly, compound **18** equipped with a flexible aliphatic linker demonstrated the highest potency of SFTI-1[1,14] variants **1–22** listed in Table 1. Due to the inherent degrees of conformational freedom of the respective amino acid side chains, a pronounced entropic penalty has been expected for compounds **17** and **18**.<sup>12</sup> Indeed,  $\epsilon$ -amino-functionalized derivative **17** was slightly less potent than inhibitor **9** possessing a more rigid and restrained linker motif of comparable length. However, a double-digit nanomolar  $K_i$  corresponding to an increase of  $\Delta_B G$  by 6.5 kJ/mol resulted from a singular amino



acid substitution (**18**).

Finally, we investigated the impact of modifications at position 12 of the SFTI-1[1,14] framework on matriptase affinity. Yuan *et al.* described a pronounced undesirable entropic effect on Phe12 of SFTI-1 due to conformational restraints caused by Phe97 and Phe99 side chains forming the S4 subsite of the enzyme (Fig. 1D).<sup>12</sup> As a consequence, substitution of Phe12 by non-natural amino acids possessing larger aromatic side chains has a detrimental effect on bioactivity.<sup>33</sup> Thus, we decided to replace the native phenylalanine residue by smaller aliphatic, hydrophobic, as well as heteroaromatic amino acids alanine, valine, isoleucine, and histidine (Fig. 2A). Respective compounds **19–22** were synthesized through routine microwave-assisted Fmoc-SPPS followed by oxidative macrocyclization and chromatographic isolation (see Supporting Information).

Indeed, we observed a beneficial effect of Phe12Ile (**21**) as well as Phe12His (**22**) substitutions on matriptase inhibition in our *in vitro* assays. In particular, the imidazole functionality at position 12 (**22**) facilitated an improved interaction between the SFTI-1 framework and the surface of the enzyme of about 3 kJ/mol.

### Step 2: Combination of Beneficial Increment Modifications

Encouraged by the enhanced matriptase affinities observed for compounds **9**, **18** and **22**, we combined the singular modifications of position 10 (**9**, **18**) with the described Phe12His substitution (**22**). The resulting constructs **42** and **43** (Fig. 3) were synthesized either *via* microwave-assisted Fmoc-SPPS (**42**) or by using a strategy analogous to that described for compounds **9–16** (**42**) (compare Fig. 2D).

Inhibitors **42** and **43** demonstrated a further increased matriptase affinity compared to SFTI-1[1,14] derivatives **9**, **18**, and **22** (Table 2). Our calculations suggest that the observed improvement in  $\Delta_B G$  relies predominantly on an additive effect. The determined individual favorable contributions of compounds **18** and **22** sum up to  $9.6 \pm 0.6$  kJ/mol, whereas, the difference of free energies of binding/dissociation between **43** and SFTI-1[1,14] was calculated as  $10.3 \pm 0.4$  kJ/mol. The difference between these two values could be accounted to a synergistic behavior.<sup>43</sup> However, the observed effect is negligible considering the respective estimated uncertainties. In case of inhibitor **42** even an unfavorable non-additive portion was detected for the installed modifications as the calculated increase of  $\Delta_B G$  was smaller than the sum of the incremental improvements (Table 2).

Nevertheless, tetradecapeptide **43** which we refer to as the

SFTI-1-derived matriptase inhibitor-1 (SDMI-1) possesses a low inhibition constant of 11 nM near the physiological pH. Furthermore, in the enzyme assay conducted near the pH optimum of matriptase (pH = 8.5) a single-digit nanomolar  $K_i$  (1.1 nM) was observed.

### Step 3: Truncation of Most Promising Variant

In a very recent study we performed a structural analysis of several monocyclic triazole-bridged SFTI-1 derivatives *in silico*.<sup>22</sup> The yielded results indicated a pronounced influence of the terminal regions on matriptase affinity. An entropic penalty caused by the fixation of the Phe12 residue of the parent bicyclic peptide through aromatic side chains of the enzyme has already been described and addressed in the presented work.<sup>12</sup> However, additional conformational constraints of residues Pro13 and Asp14 forming the secondary loop may cause unfavourable entropic contributions upon binding to matriptase. According to our calculations interaction with trypsin is not affected in this manner. As a consequence, the truncation of the two C-terminal residues might have a beneficial effect on matriptase inhibition. Additionally, we rationalized that removing the negative charge of the terminal carboxy group by introduction of a C-terminal amide might enhance the overall charge complementarity between the target enzyme and the inhibitor.

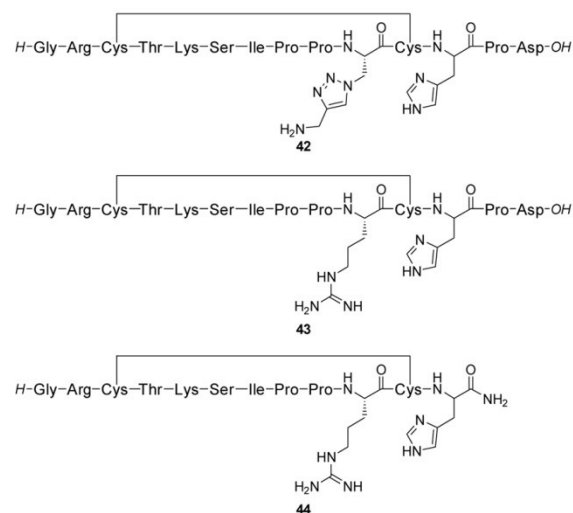


**Fig. 3** Structures of triazolyl-containing SFTI-1[1,14] derivative **42**, SFTI-1 derived matriptase inhibitor-1 (SDMI-1) **43** and SFTI-1 derived matriptase inhibitor-2 (SDMI-2) **44**.

**Table 2.** Determined inhibition constants of compounds **42–44** against matriptase at pH 7.6 (8.5), calculated differences in free energies of binding/dissociation compared to SFTI-1[1,14] as well as trypsin affinity and selectivity at pH 7.6.<sup>[a]</sup>

Entry	Matriptase $K_i$ <sup>b</sup> / nM	Relative Activity	$\Delta_B G_{(n)} - \Delta_B G_{(SFTI-1[1,14])}$ / (kJ·mol <sup>-1</sup> )	Sum of Increment Contributions <sup>c</sup> / kJ·mol <sup>-1</sup>	Trypsin $K_i$ / nM	Selectivity <sup>d</sup>
SFTI-1[1,14]	703 ± 87 <sup>e</sup>	1	0	n.a.	0.21 ± 0.03 <sup>e</sup>	0.0003
<b>42</b>	89.5 ± 11.1	0.13	5.1 ± 0.4	6.9 ± 0.6	9.2 ± 2.1	0.1
<b>43</b> (SDMI-1)	11.0 ± 1.4 (1.1 ± 0.3)	0.016	10.3 ± 0.4	9.6 ± 0.6	11.2 ± 2.0	1.0
<b>44</b> (SDMI-2)	6.2 ± 1.2 (2.3 ± 0.8)	0.009	11.7 ± 0.6	n.a.	38.0 ± 11.1	6.1

<sup>a</sup> Experiments were performed as described in the footnote of Table 1 and in the Experimental Section. <sup>b</sup> Values in brackets correspond to  $K_i$  determined at pH 8.5. <sup>c</sup> Errors were calculated by propagation of errors. <sup>d</sup> Calculated as the ratio of  $K_i$  against matriptase (pH 7.6) /  $K_i$  against trypsin (pH 7.6). <sup>e</sup> As published before.<sup>22</sup>

Inspired by these considerations, we synthesized the monocyclic dodecapeptide **44** as described in the Experimental Section (Fig. 3). Indeed, we observed an additional minor improvement of inhibitor potency resulting in a  $K_i$  of  $6.2 \pm 1.2$  nM. This SFTI-1-derived matriptase inhibitor-2 (SDMI-2) exhibits a  $2.3 \pm 0.8$  nM inhibition constant at pH 8.5 and shows an improved selectivity towards matriptase over trypsin (6-fold). To our knowledge, **43** and **44** are to date the most potent Bowmann-Birk matriptase inhibitors described.

Finally, we modeled the inhibitor-protease complex for SDMI-2 (**44**) based on the *in silico* coordinates of SFTI-1[1,14] and matriptase described above (see Fig. 1).<sup>22</sup> First, the amino acid exchanges Ile10Arg and Phe12His were introduced into the parent model. Then, residues Pro13 and Asp14 were replaced by a C-terminal amide. Optimization of side-chain geometry and subsequent energy minimization yielded a structure quite similar to the corresponding SFTI-1 co-crystal (3P8F, Fig. 4A). Nevertheless, additional favorable interactions between **44** and matriptase were observed (Fig. 4B). The side chain of Asp96 was reoriented to form a bidentate hydrogen bond with the guanidyl functionality of Arg10. Furthermore, the possibility for a proton donor-acceptor interaction between the backbone carbonyl oxygen of Asp96 and the  $\epsilon^2$ -nitrogen of His12 was detected. However, an X-ray structure of the SDMI-2-matriptase complex is needed to undoubtedly prove whether the predicted *in silico* coordinates are valid. Yuan *et al.* suggested to use short basic residues like aminohomoalanine at position 10 to establish an effective electrostatic interaction with Asp96 while attenuating entropic penalties arising from extended flexible linkers.<sup>12</sup> However, it remains to be tested whether such a short side chain is sufficient to position a basic functionality in proximity to the carboxylic group of Asp96.

## Conclusion

In this study we present a convenient strategy for the development of novel, highly potent inhibitors of matriptase based on the SFTI-1 framework. Using a divergent synthetic route we screened 22 compounds for beneficial modifications of the parent peptide. Combination of the most favorable amino acid substitutions and subsequent C-terminal truncation yielded SFTI-1 derived matriptase inhibitors-1 and 2 (SDMI-1 and 2) with inhibition constants in the low nanomolar to single-digit nanomolar range. The structure-guided design of the initial peptide/peptidomimetic library as well as the shortening of the amino acid sequence were inspired by *in silico* experiments which were used as an idea generator towards beneficial modifications of the wild-type compound.<sup>12, 22</sup> Thus, an inhibitor possessing only twelve residues as well as an inverted trypsin-matriptase selectivity in favor of the latter enzyme was developed.

Although the applied synthetic strategy using “copper-click” chemistry was applicable for the assembly of the majority of the triazolyl-containing peptidomimetics **1–16**, it was incompatible with the use of non-natural amino acid azidoalanine at position 10 (compounds **9**, **11**, **13**, and **15**). In our previous works, we did not observe significant limitations using Fmoc-Aza-OH as a building block for microwave assisted Fmoc-SPPS.<sup>44</sup> However, the unexpected restricted applicability of the unprotected azide

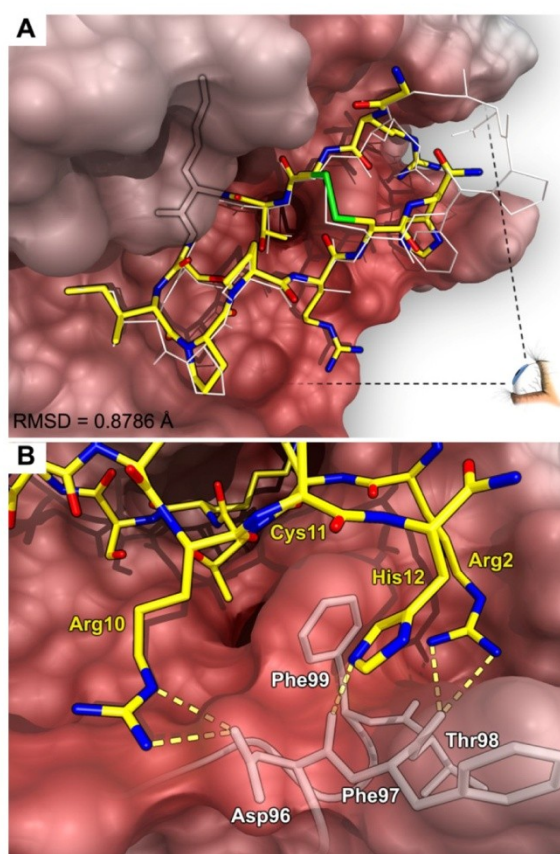


**Fig. 4** (A) Predicted structure of SFTI-1 derived matriptase inhibitor-1 (SDMI-2) **44** (thick coloured sticks) upon binding to matriptase (surface). The SFTI-1-matriptase X-ray structure (3P8F) is shown as thin white sticks and the calculated peptide backbone root mean square deviation (RMSD) is given for both complexes. The angle of view for the picture below is indicated. (B) Close-up of the predicted inhibitor **44**-enzyme complex. Important matriptase residues are depicted as transparent white sticks with black outlines and putative hydrogen bond interactions are shown as dashed yellow lines. Blue: nitrogen, green: sulfur, red: oxygen, yellow: carbon, hydrogen is omitted for clarity. Color gradients (red to blue) indicate electrostatic surface potentials (negative to positive) at pH 7.6 calculated *via* the Particle Mesh Ewald method with a maximum value of  $500 \text{ kJ mol}^{-1}$ .<sup>24</sup>

functionality under the described conditions was circumvented through a modified synthetic route.

Novel compounds **43** and **44** are potent inhibitors of matriptase in a pH range near the physiological one and, thus, may find applications in therapy or diagnostics. Notably, the activity of these SFTI-1 derivatives composed exclusively of natural amino acids is not in the range of recently reported peptidomimetics bearing reactive carbonyl functionalities.<sup>21</sup> Since only two residues have been furnished with new side-chain functionalities, the SFTI-1 framework provides further potential for the establishment of unique attractive interactions with matriptase and, therefore, improvement of affinity and selectivity. Additionally, our ongoing studies show that **43** and **44** can serve as versatile platforms for conjugation with reporter molecules without sacrificing bioactivity. This strategy would allow for *in vivo* imaging experiments using for example PET/SPECT or

NIRF methodologies.<sup>45-48</sup>

Nevertheless, further selectivity tests using an extended set of relevant trypsin-like proteases as well as characterization of these two peptidic inhibitors *in vivo* are issues that have to be addressed in the future.

## Experimental

### General

All chemicals and solvents were purchased from Bachem, Iris Biotech, Novabiochem, Sigma-Aldrich, Rapp Polymere, Roth or Varian (Agilent).

Analytical and semi-preparative RP-HPLC were performed on a Varian 920-LC system and a Varian 940-LC system, respectively. A Phenomenex Hypersil 5u BDS C18 LC column (150 x 4.6 mm, 5  $\mu$ m, 130 Å) and a Phenomenex Luna 5u C18 LC column (250 x 12.20 mm, 5  $\mu$ m, 100 Å) were used as stationary phases. The eluent system consisted of eluent A (0.1% aq. TFA) and eluent B (90 % aq. acetonitrile containing 0.1% TFA).

ESI mass spectra were recorded with a Shimadzu LCMS-2020 using a Phenomenex Jupiter 5u C4 LC column (50 x 1 mm, 5  $\mu$ m, 300 Å) as well as a binary eluent system consisting of eluent A (0.1% aq. formic acid, LC-MS grade) and eluent B (100 % acetonitrile containing 0.1% formic acid, LC-MS grade).

Peptides were synthesized using a Liberty 12-channel automated peptide synthesizer on a Discover SPS microwave peptide synthesizer platform (CEM) following the Fmoc strategy.

### Chemistry

**General Procedures of Peptide Synthesis.** All peptide bearing a C-terminal carboxy acid were assembled on a TentaGel S AC resin (Rapp Polymere) or a 2-chlorotrityl chloride resin (Iris Biotech) preloaded with Fmoc-L-Asp(*t*Bu). Corresponding peptide amides were assembled on AmphiSpheres 40 RAM resin (Agilent).

Loading of 2-chlorotrityl chloride resin was performed manually as follows. A solution of 103 mg Fmoc-L-Asp(*t*Bu)-OH (0.25 mmol) and 34  $\mu$ L N,N-diisopropylethylamine (DIEA, 1 mmol) in a minimal amount of dichloromethane (DCM) was added to the resin. The resulting mixture was shaken for 2 h at ambient temperature. The solution was removed by filtration and the loaded resin was washed with DCM/methanol/DIEA (17:2:1; 3 $\times$ ), DCM (3 $\times$ ), dimethylformamide (DMF, 3 $\times$ ) and DCM (3 $\times$ ).

Canonical amino acids were attached by double or triple coupling using 4 eq of the corresponding amino acid, 3.9 eq of 2-(1H-benzotriazol-1-yl)-1,1,3,3-tetramethyluronium hexafluorophosphate (HBTU) and 8 eq of DIEA, or, in case of cysteine, 3-4 eq of 2,4,6-trimethylpyridine (collidine). Arginine and cysteine were coupled using a two-step microwave program: 1. RT, 0 W, 25 min; 2. 75 °C, 25 W, 0.5 min (Arg) and 1. RT, 0 W, 2. min; 2. 50 °C, 25 W, 4 min (Cys), respectively. All other amino acids were coupled using a standard microwave program: 75 °C, 21 W, 5 min.

Non-natural azide-bearing building blocks Fmoc-L-Aza-OH and Fmoc-L-Aha-OH were attached *via* double coupling using 2 eq of the corresponding amino acid, 1.9 eq HATU, and 4 eq DIEA and a two-step microwave program (1. 60°C, 30 W, 45 min, 2. 75 °C, 20 W, 5 min).

Fmoc deprotection was achieved in two steps by reaction with 20% piperidine in DMF at 75 °C, 42 W for 0.5 min (initial deprotection) followed by a second deprotection step with 20% piperidine in DMF at 75 °C, 42 W for 3 min.

Cleavage of peptides from the solid support and removal of side-chain protecting groups was achieved *via* acidolysis using a standard cleavage cocktail consisting of trifluoroacetic acid (TFA)/H<sub>2</sub>O/anisole/triethylsilane (TES) (47:1:1:1, v:v:v:v) and DTT to suppress unwanted oxidation. The resulting reaction mixture was shaken for 3 h at RT followed by precipitation and subsequent washing (3 $\times$ ) with methyl tertiary butyl ether (MTBE) to yield crude linear peptides.

Air-mediated oxidative macrocyclization of the crude peptides was conducted in 100 mM (NH<sub>4</sub>)<sub>2</sub>CO<sub>3</sub> aq (1 mg/mL, pH = 8.4) and monitored by analytical RP-HPLC. After complete conversion (1-7 days) the solvent was removed by freeze-drying to yield the crude peptides. To suppress unwanted saponification of the methyl ester of compounds **5**, **6**, **13**, and **14**, a 100 mM (NH<sub>4</sub>)<sub>2</sub>CO<sub>3</sub> aq buffer (pH 7.7) was used (Fig. 2).

**Triazolyl-containing peptides 1–8, 10, 12, 14, and 16.** Azide-bearing peptide resins **23**, **24**, and **25** were assembled on a TentaGel S AC-Asp(*t*-Bu) Fmoc resin (loading: 0.21 mmol/g) according to the described procedures on a 0.25 mmol scale, washed (3 $\times$  with DCM and 3 $\times$  with ether) and dried in an exsiccator.

On-support copper(I)-catalyzed azide-alkyne cycloaddition (CuAAC) was conducted with 0.05 mmol of intermediates **23**, **24**, and **25** and the respective alkyne component (propargylamine, methyl propiolate, or phenylacetylene) according to the scheme laid out in Fig. 2C. A solution of 5 eq alkyne, 1 eq copper(II) sulfate pentahydrate (CuSO<sub>4</sub>·5H<sub>2</sub>O), 1 eq sodium ascorbate (NaAsc) and 8 eq DIEA in 5 mL argon-flushed DMF was added to the peptide resin and shaken at ambient temperature overnight. Then, the solution was removed by filtration and the peptide resin was washed with methanol (3 $\times$ ), 0.5 % sodium diethyldithiocarbamate in DMF (w/v, 3 $\times$ ), DMF (3 $\times$ ) and DCM (3 $\times$ ) yielding intermediates **27–35**.

After Fmoc deprotection, acidolytic cleavage from the solid support, ether precipitation, and oxidative disulfide formation, macrocyclic peptides were isolated *via* semi-preparative RP-HPLC. This gave compounds **1–8**, **10**, **12**, **14**, and **16** as white solids in the following yields. **1**: 13.5 mg (17 %); **2**: 14.9 mg (18.6 %); **3**: 9.3 mg (11.6 %); **4**: 6.3 mg (7.8 %); **5**: 2.4 mg (3 %); **6**: 2 mg (2.5 %); **7**: 0.5 mg (0.6 %); **8**: 5.1 mg (6.2 %); **10**: 4.6 mg (5.8 %); **12**: 4 mg (5 %); **14**: 4 mg (4.9 %); **16**: 2 mg (2.4 %). For analytical data, please refer to the supporting information.

**Triazolyl-containing peptides 9, 11, 13, and 15.** Azide-bearing peptide resin **26** was assembled on a TentaGel S AC-Asp(*t*-Bu) Fmoc resin (loading: 0.21 mmol/g) according to the described procedures on a 0.25 mmol scale, washed (3 $\times$  with DCM and 3 $\times$  with ether) and dried in an exsiccator.

On-support copper(I)-catalyzed azide-alkyne cycloaddition (CuAAC) was conducted with 0.05 mmol of intermediates **26** and the respective alkyne component (*N*-Boc-propargylamine, methyl propiolate, or phenylacetylene) according to the scheme laid out in Fig. 2D. A solution of 5 eq alkyne, 1 eq copper(II) sulfate pentahydrate (CuSO<sub>4</sub>·5H<sub>2</sub>O), 1 eq sodium ascorbate (NaAsc) and 8 eq DIEA in 5 mL argon-flushed DMF was added to the peptide



resin and shaken at ambient temperature overnight. Then, the solution was removed by filtration and the peptide resin was washed with methanol (3×), 0.5 % sodium diethyldithiocarbamate in DMF (w/v, 3×), DMF (3×) and DCM (3×) yielding intermediates **36–38**.

The Fmoc protecting group was removed according to the described procedure. The remaining *N*-terminal residues were attached to each triazolyl-containing peptide resin yielding intermediates **39–41**. After Fmoc deprotection, acidolytic cleavage from the solid support, ether precipitation, and oxidative disulfide formation, macrocyclic peptides were isolated *via* semi-preparative RP-HPLC. This gave compounds **9**, **11**, **13**, and **15** as white solids in the following yields: **9**: 16.8 mg (21.2 %); **11**: 6.6 mg (8.2 %); **13**: 4.1 mg (5.1 %); **15**: 4.2 mg (5.1 %). For analytical data, please refer to the supporting information.

**Triazolyl-containing peptide 42.** Inhibitor **42** was synthesized following a strategy similar to that described for compounds **9**, **11**, **13**, and **15**. First peptide-resin intermediate Fmoc-Aza-Cys(Trt)-His(Trt)-Pro-Asp(*t*Bu)-resin was assembled on a 2-chlorotrityl chloride resin preloaded with Fmoc-Asp(*t*Bu) (loading: 0.23 mmol/g) on a 0.05 mmol scale. Then, a solution of 39 mg *N*-Boc-propargylamine (0.25 mmol), 14 mg CuSO<sub>4</sub>·5H<sub>2</sub>O (0.05 mmol), 10 mg NaAsc (0.05 mmol) and 70 μL DIEA (0.4 mmol) in 5 mL argon-flushed DMF were added to the peptide resin and shaken at ambient temperature overnight. The solution was removed by filtration and the peptide resin was washed with methanol (3×), 0.5 % sodium diethyldithiocarbamate in DMF (w/v, 3×), DMF (3×) and DCM (3×).

The Fmoc protecting group was removed according to the described procedure. The remaining *N*-terminal residues were attached to the triazolyl-containing peptide resin. After Fmoc deprotection, acidolytic cleavage from the solid support, ether precipitation, and oxidative disulfide formation, macrocyclic peptide **42** was isolated *via* semi-preparative RP-HPLC. This gave 0.9 mg (1.2 %) of pure **42** as a white solid. For analytical data, please refer to the supporting information.

**Peptides 17–22, and 43.** Linear precursors were synthesized on a 2-chlorotrityl chloride resin preloaded with Fmoc-Asp(*t*Bu) (loading: 0.23 mmol/g) on a 0.05 mmol scale.

After acidolytic cleavage from the solid support, ether precipitation, and oxidative disulfide formation, macrocyclic peptides were isolated *via* semi-preparative RP-HPLC. This gave compounds **17–22**, and **43** as white solids in the following yields: **17**: 3 mg (3.9 %); **18**: 6.2 mg (7.9 %); **19**: 17.4 mg (23.9 %); **20**: 11.2 mg (15.1 %); **21**: 23.2 mg (31 %); **22**: 9.2 mg (12.1 %); **43**: 0.9 mg (1.2 %). For analytical data, please refer to the supporting information.

**Inhibitor 44.** The linear precursor of **44** was synthesized on an AmphiSpheres 40 RAM resin (0.44 mmol/g) on a 0.1 mmol scale. After acidolytic cleavage from the solid support, ether precipitation, and oxidative disulfide formation, the macrocyclic peptide was isolated *via* semi-preparative RP-HPLC. This gave 10.5 mg (7.8 %) of **44** as a white solid. For analytical data, please refer to the supporting information.

#### **In Vitro Assays**

**Enzymes.** Recombinant production, autocatalytic activation and purification of matriptase were conducted as previously described.<sup>22</sup> Bovine trypsin was purchased from Sigma-Aldrich.

Active-site titration and determination of Michaelis-Menten constants  $K_M$  for the chromogenic substrate Boc-QAR-*p*NA was performed as reported earlier.<sup>22</sup>

**Data Collection and Analysis.** All experiments were performed in triplicate. Active-site titrated matriptase (final concentration:  $[E] = 0.9$  nM) or trypsin (final concentration:  $[E] = 0.5$  nM) were incubated with the respective inhibitor in different concentrations  $[I]$  at pH 7.6 or 8.5 for 30 min. Then, the chromogenic substrate Boc-QAR-*p*NA (final concentration:  $[S] = 250$  μM) was added. The residual proteolytic activity ( $v/v_0$ ) was determined by monitoring the absorption of the corresponding samples in 96-well plates (NUNC, round bottom, clear) at 405 nm in 60 sec intervals over 30 min at RT using the Tecan GENios microplate reader. Slopes of the initial reaction velocities (steady-state) were calculated and normalized to the data of the uninhibited enzymatic hydrolysis of Boc-QAR-*p*NA. The determined  $v/v_0$  values were plotted against the concentration of the inhibitor. The resulting dose-response curves were fitted either by equation 1 or in case of tight-binding inhibition (trypsin: **42**; matriptase: **43** at pH 8.5, **44** at pH 7.6 and 8.5) by equation 2 through non-linear regression.

$$\frac{v}{v_0} = \left(1 + \frac{[I]}{IC_{50}}\right)^{-1} \quad (1)$$

$$\frac{v}{v_0} = 1 - \frac{([E] + [I] + K_i^{app}) - \sqrt{([E] + [I] + K_i^{app})^2 - 4[E][I]}}{2[E]} \quad (2)$$

Substrate-independent inhibition constants  $K_i$  were calculated from respective  $IC_{50}$  values or apparent (substrate-dependent) inhibition constants  $K_i^{app}$  using equations 3 and 4, respectively.

$$K_i = IC_{50} \left(1 + \frac{[S]}{K_M}\right)^{-1} \quad (3)$$

$$K_i = K_i^{app} \left(1 + \frac{[S]}{K_M}\right)^{-1} \quad (4)$$

Errors were calculated through propagation of errors (compare Tischler *et al.*).<sup>49</sup>

#### **In Silico Procedures**

**General.** All *in silico* experiments were performed on an Intel® Core™ i7-2600 workstation with 8 virtual cores using the YASARA structure package (YASARA Biosciences) and the YASARA2 force field.<sup>50</sup> Graphical content was generated with YASARA and POVRay.<sup>50, 51</sup>

**SDMI-2-matriptase complex.** Prediction of a SFTI-1[1,14]-matriptase complex based on the X-ray structure of the SFTI-1-matriptase complex (PDB ID: 3P8F) has been recently described.<sup>12, 22</sup> Ile10 and Phe12 were replaced by Arg10 and His12 within the calculated structure of the open-chain variant. Residues Pro13 and Asp14 were deleted and the *C*-terminal amide functionality was installed. Then, Arg10 and His12 side-chain geometries were optimized using a rotamer library and steepest decent minimization.<sup>52, 53</sup> A global energy minimization with an increased scaling factor for non-bonded interactions (1.2 instead of 1.0) was performed. Finally, a second energy

minimization was performed with a reset scaling factor for non-bonded interactions (1.0) to yield the SDMI-2-matriptase complex depicted in Fig. 4.

## Acknowledgments

<sup>5</sup> This work was supported by the Deutsche Forschungsgemeinschaft through grant Ko 1390/9-1, by BMBF, and LOEWE-Soft Control.

## References

- 1 W. R. Rypniewski, A. Perrakis, C. E. Vorgias and K. S. Wilson, *Protein Eng.*, 1994, **7**, 57-64.
- 2 A. Schmidt, C. Jelsch, P. Ostergaard, W. Rypniewski and V. S. Lamzin, *J. Biol. Chem.*, 2003, **278**, 43357-43362.
- 3 T. M. Antalis, T. H. Bugge and Q. Wu, *Prog. Mol. Biol. Transl. Sci.*, 2011, **99**, 1-50.
- 4 T. M. Antalis, M. S. Buzza, K. M. Hodge, J. D. Hooper and S. Netzel-Arnett, *Biochem. J.*, 2010, **428**, 325-346.
- 5 T. H. Bugge, T. M. Antalis and Q. Wu, *J. Biol. Chem.*, 2009, **284**, 23177-23181.
- 6 J. D. Hooper, J. A. Clements, J. P. Quigley and T. M. Antalis, *J. Biol. Chem.*, 2001, **276**, 857-860.
- 7 S. Netzel-Arnett, J. D. Hooper, R. Szabo, E. L. Madison, J. P. Quigley, T. H. Bugge and T. M. Antalis, *Cancer Metastasis Rev.*, 2003, **22**, 237-258.
- 8 M. S. Buzza, S. Netzel-Arnett, T. Shea-Donohue, A. P. Zhao, C. Y. Lin, K. List, R. Szabo, A. Fasano, T. H. Bugge and T. M. Antalis, *P. Natl. Acad. Sci. USA*, 2010, **107**, 4200-4205.
- 9 K. List, C. C. Haudenschild, R. Szabo, W. J. Chen, S. M. Wahl, W. Swaim, L. H. Engelholm, N. Behrendt and T. H. Bugge, *Oncogene*, 2002, **21**, 3765-3779.
- 10 R. Szabo, J. P. Hobson, K. List, A. Molinolo, C. Y. Lin and T. H. Bugge, *J. Biol. Chem.*, 2008, **283**, 29495-29504.
- 11 J. Napp, C. Dullin, F. Muller, K. Uhland, J. B. Petri, A. van de Locht, T. Steinmetzer and F. Alves, *Int. J. Cancer*, 2010, **127**, 1958-1974.
- 12 C. Yuan, L. Q. Chen, E. J. Meehan, N. Daly, D. J. Craik, M. D. Huang and J. C. Ngo, *Bmc Structural Biology*, 2011, **11**.
- 13 M. D. Oberst, L. Y. Chen, K. Kiyomiya, C. A. Williams, M. S. Lee, M. D. Johnson, R. B. Dickson and C. Y. Lin, *Am. J. Physiol. Cell Physiol.*, 2005, **289**, C462-470.
- 14 K. List, R. Szabo, A. Molinolo, V. Sriuranpong, V. Redeye, T. Murdock, B. Burke, B. S. Nielsen, J. S. Gutkind and T. H. Bugge, *Gene Dev.*, 2005, **19**, 1934-1950.
- 15 K. Uhland, *Cell. Mol. Life Sci.*, 2006, **63**, 2968-2978.
- 16 K. List, *Future Oncol.*, 2009, **5**, 97-104.
- 17 J. M. Milner, A. Patel, R. K. Davidson, T. E. Swinger, A. Desilets, D. A. Young, E. B. Kelso, S. T. Donell, T. E. Cawston, I. M. Clark, W. R. Ferrell, R. Plevin, J. C. Lockhart, R. Leduc and A. D. Rowan, *Arthritis Rheum.-Us*, 2010, **62**, 1955-1966.
- 18 I. Seitz, S. Hess, H. Schulz, R. Eckl, G. Busch, H. P. Montens, R. Brandl, S. Seidl, A. Schomig and I. Ott, *Arterioscl. Throm. Vas.*, 2007, **27**, 769-775.
- 19 T. Steinmetzer, A. Schweinitz, A. Sturzebecher, D. Donnecke, K. Uhland, O. Schuster, P. Steinmetzer, F. Muller, R. Friedrich, M. E. Than, W. Bode and J. Sturzebecher, *J. Med. Chem.*, 2006, **49**, 4116-4126.
- 20 C. J. Farady, J. Sun, M. R. Darragh, S. M. Miller and C. S. Craik, *J. Mol. Biol.*, 2007, **369**, 1041-1051.
- 21 E. Colombo, A. Desilets, D. Duchene, F. Chagnon, R. Najmanovich, R. Leduc and E. Marsault, *ACS Med. Chem. Lett.*, 2012, **3**, 530-534.
- 22 O. Avrutina, H. Fittler, B. Glotzbach, H. Kolmar and M. Empting, *Org. Biomol. Chem.*, 2012, **10**, 7753-7762.
- 23 M. L. J. Korsinczyk, H. J. Schirra, K. J. Rosengren, J. West, B. A. Condie, L. Otvos, M. A. Anderson and D. J. Craik, *J. Mol. Biol.*, 2001, **311**, 579-591.
- 24 U. Essmann, L. Perera, M. L. Berkowitz, T. Darden, H. Lee and L. G. Pedersen, *J. Chem. Phys.*, 1995, **103**, 8577-8593.
- 25 M. J. Costanzo, H. R. Almond, L. R. Hecker, M. R. Schott, S. C. Yabut, H. C. Zhang, P. Andrade-Gordon, T. W. Corcoran, E. C. Giardino, J. A. Kauffman, J. M. Lewis, L. de Garavilla, B. J. Haertlein and B. E. Maryanoff, *J. Med. Chem.*, 2005, **48**, 1984-2008.
- 26 A. D. Kwong, R. S. Kauffman, P. Hurter and P. Mueller, *Nat. Biotechnol.*, 2011, **29**, 993-1003.
- 27 K. Hilpert, G. Hansen, H. Wessner, R. Volkmer-Engert and W. Hohne, *J. Biochem.*, 2005, **138**, 383-390.
- 28 A. Lesner, A. Legowska, M. Wysocka and K. Rolka, *Curr. Pharm. Design.*, 2011, **17**, 4308-4317.
- 29 A. Legowska, D. Debowski, A. Lesner, M. Wysocka and K. Rolka, *Bioorgan. Med. Chem.*, 2009, **17**, 3302-3307.
- 30 J. E. Swedberg, S. J. de Veer, K. C. Sit, C. F. Reboul, A. M. Buckle and J. M. Harris, *Plos One*, 2011, **6**.
- 31 D. Scarpi, J. D. McBride and R. J. Leatherbarrow, *Bioorgan. Med. Chem.*, 2004, **12**, 6045-6052.
- 32 S. Jiang, P. Li, S. L. Lee, C. Y. Lin, Y. Q. Long, M. D. Johnson, R. B. Dickson and P. P. Roller, *Org. Lett.*, 2007, **9**, 9-12.
- 33 P. Li, S. Jiang, S. L. Lee, C. Y. Lin, M. D. Johnson, R. B. Dickson, C. J. Michejda and P. P. Roller, *J. Med. Chem.*, 2007, **50**, 5976-5983.
- 34 Y. Q. Long, S. L. Lee, C. Y. Lin, I. J. Enyedy, S. M. Wang, P. Li, R. B. Dickson and P. P. Roller, *Bioorg. Med. Chem. Lett.*, 2001, **11**, 2515-2519.
- 35 F. Beliveau, A. Desilets and R. Leduc, *Febs J.*, 2009, **276**, 2213-2226.
- 36 J. L. Wike-Hooley, J. Haveman and H. S. Reinhold, *Radiother. Oncol.*, 1984, **2**, 343-366.
- 37 I. F. Tannock and D. Rotin, *Cancer Research*, 1989, **49**, 4373-4384.
- 38 P. Montcourrier, I. Silver, R. Farnoud, I. Bird and H. Rochefort, *Clin. Exp. Metastasis*, 1997, **15**, 382-392.
- 39 T. Yoshitomi and Y. Nagasaki, *Biointerphases*, 2012, **7**, 7.
- 40 D. Martinez, M. Vermeulen, A. Trevani, A. Ceballos, J. Sabatte, R. Gamberale, M. E. Alvarez, G. Salamone, T. Tanos, O. A. Coso and J. Geffner, *J. Immunol.*, 2006, **176**, 1163-1171.
- 41 F. Liu, J. E. Park, W. J. Qian, D. Lim, A. Scharow, T. Berg, M. B. Yaffe, K. S. Lee and T. R. Burke, Jr., *Chembiochem*, 2012, **13**, 1291-1296.
- 42 F. Liu, J. E. Park, W. J. Qian, D. Lim, A. Scharow, T. Berg, M. B. Yaffe, K. S. Lee and T. R. Burke, Jr., *ACS Chem. Biol.*, 2012, **7**, 805-810.
- 43 M. Nazare, H. Matter, D. W. Will, M. Wagner, M. Urmann, J. Czech, H. Schreuder, A. Bauer, K. Ritter and V. Wehner, *Angew. Chem. Int. Ed.*, 2012, **51**, 905-911.



- 
- 44 M. Empting, O. Avrutina, R. Meusinger, S. Fabritz, M. Reinwarth,  
M. Biesalski, S. Voigt, G. Buntkowsky and H. Kolmar, *Angew.  
Chem. Int. Ed.*, 2011, **50**, 5207-5211.
- 45 L. Melendez-Alafort, P. C. Muzzio and A. Rosato, *Anticancer Agents  
Med. Chem.*, 2012, **12**, 476-499.
- 46 M. Yoshimoto, T. Hayakawa, M. Mutoh, T. Imai, K. Tsuda, S.  
Kimura, I. O. Umeda, H. Fujii and K. Wakabayashi, *J. Nucl. Med.*,  
2012, **53**, 765-771.
- 47 A. Kumar, T. Jindal, R. Dutta and R. Kumar, *Ann. Nucl. Med.*, 2009,  
10 **23**, 745-751.
- 48 W. B. Cai, K. Chen, Z. B. Li, S. S. Gambhir and X. Y. Chen, *J. Nucl.  
Med.*, 2007, **48**, 1862-1870.
- 49 M. Tischler, D. Nasu, M. Empting, S. Schmelz, D. W. Heinz, P.  
Rottmann, H. Kolmar, G. Buntkowsky, D. Tietze and O. Avrutina,  
15 *Angew. Chem. Int. Ed.*, 2012, **51**, 3708-3712.
- 50 E. Krieger, K. Joo, J. Lee, J. Lee, S. Raman, J. Thompson, M. Tyka,  
D. Baker and K. Karplus, *Proteins*, 2009, **77**, 114-122.
- 51 L. F. Pacios, *Comput. Chem.*, 1997, **21**, 25-34.
- 52 A. A. Canutescu, A. A. Shelenkov and R. L. Dunbrack, *Protein Sci.*,  
20 **12**, 2001-2014.
- 53 R. L. Dunbrack and F. E. Cohen, *Protein Sci.*, 1997, **6**, 1661-1681.
-



### 3 Summary

The studies presented in the cumulative section of this thesis illustrate a variety of applications of disubstituted 1,2,3-triazoles for biomolecular chemistry in general and peptide modification in particular. Taken together, these peer-reviewed reports provide a toolbox for the design and synthesis of peptidomimetic compounds. CuAAC and RuAAC methodologies have been established and advanced with respect to feasible conduction of regioselective azide-alkyne cycloadditions in solution as well as on the solid support. In combination with relevant publications by other working groups addressed in the introduction, a detailed knowledge of the scope and limitations of 1,2,3-triazoles and general AAC techniques suitable for peptide modification has been gathered. The described studies can be divided into two main sections: Scaffold-based multimerization of peptide ligands and 1,2,3-triazoles as non-natural structural elements of peptides. The latter topic comprises the design and synthesis of biomimetic backbone segments as well as macrocyclic or linear side-chain motifs.

Bioconjugation experiments towards well-defined multivalent architectures were conducted with five different azide-bearing ligands and two tetra alkyne RAFT molecules. CuAAC coupling resulted in stoichiometric conversions giving desired branched peptide oligomers in moderate to good yields. One construct contained four copies of an RGD sequence and a fluorescent label. The addressed bioactive peptide ligand can bind to GPIIb/IIIa receptor molecules and, thus, inhibit platelet aggregation. This scaffold-based multivalent construct may be suitable for fluorescence microscopy of GPIIb/IIIa-expressing cells and have anticoagulant activity. However, detailed biological assays have not been conducted owing to a low expected therapeutic or diagnostic benefit. Additionally, it has to be stated that to date more advanced bioconjugation techniques are available eliminating the need for transition metal catalysis. Nevertheless, the reported study provides a blueprint for the successful synthesis of heteromultivalent peptide conjugates and the described methodologies still find application in the Kolmar group for the “scaffolding” of other ligand molecules possessing therapeutic and diagnostic potential.

One very promising application of 1,2,3-triazoles relies on their ability to form hydrogen bonds, their polarity, and a good solubility in water. These features render this nitrogen-containing aromatic heterocycle a suitable hydrolysis-resistant mimic of amide bonds. The possibility to synthesize 1,4- or 1,5-disubstituted 1,2,3-triazoles through the choice of transition metal catalyst allows for the generation of amide mimics locked either in *trans* or *cis* conformation, respectively. This concept has been applied to the design and synthesis of peptidomimetic variants of monocyclic sunflower trypsin inhibitor-1 (SFTI-1[1,14]). For this purpose, a combination of microwave-assisted Fmoc-based solid phase peptide synthesis and on-support CuAAC as well as RuAAC was used yielding desired compounds in sufficient amounts for structural analysis and *in vitro* inhibition assays. The solution of crystal structures of trypsin-inhibitor complexes through X-ray diffraction crystallography undoubtedly proved the successful synthesis of functional peptidomimetics. Moreover, it has been shown that a backbone shape corresponding to the sterically unfavorable *cis* isomer can be enforced at positions of choice within a given peptide sequence. This eliminates the need for proline side chains after *cis*-amides and gives rise to novel peptide structures that would not be accessible using only canonical amino acids. As expected, it was observed that locking the opposite conformation to the native structure of SFTI-1 results in a detrimental effect on bioactivity. Additionally, the possibility for protection of certain backbone segments towards enzymatic hydrolysis is provided which gives rise to an enhanced *in vivo* stability.

In two other studies we investigated the effect of 1,2,3-triazole-based disulfide replacements on the biological activity of SFTI-1[1,14]. Four side-chain-to-side-chain macrocyclization motifs differing in length and shape were installed instead of the native cystine using commercially available azide- and alkyne-bearing building blocks. This was achieved *via*

microwave-assisted Fmoc-SPPS followed by intrachain RuAAC or CuAAC on the solid support or in solution, respectively. This yielded “triazole-bridged” peptidomimetic compounds possessing either a 1,4- or a 1,5-disubstitution pattern. Pure products were characterized by IR and 2D NMR spectroscopy as well as ESI-MS analysis. *In vitro* inhibition assays revealed that the substitution pattern of the macrocyclization motif had a dramatic effect on bioactivity. Interestingly, the variants possessing a 1,5-disubstitution pattern were potent inhibitors of trypsin with substrate-independent inhibition constants  $K_i$  in the single-digit nanomolar to subnanomolar range. However, the 1,4-patterned counterparts showed a significantly decreased bioactivity compared to the wild-type peptide. The linker length between the peptide backbone and the triazole moiety did not have such a pronounced influence. The *in vitro* results were corroborated by molecular modeling indicating that the RuAAC products provided a better overall fit to the structure of the parent peptide. Thus, the use of 1,5-disubstituted 1,2,3-triazoles as disulfide replacements is recommended. However, the adequate linker length has to be determined individually for a particular biological context.

The SFTI-1 variants containing “triazole bridges” as well as mono- and bicyclic SFTI-1 have also been tested for activity against the pharmacologically relevant type II transmembrane serine protease matriptase. Surprisingly, all of these six peptides possessed a dramatically decreased affinity towards this pharmacologically relevant enzyme compared to trypsin. This was unexpected as the negative electrostatic surface potential around the active site of matriptase should provide significant attractive contributions to the binding of the positively charged SFTI-1 framework. To further study this counterintuitive result, a two-step *in silico* experiment was set up using the YASARA structure software package and a customized AMBER-based force field. First, a molecular dynamics simulation was performed. Then, 100 snapshots from the resulting trajectories were used for a local docking experiment applying the AUTODOCK algorithm. This allowed for the calculation of free energies of binding for every inhibitor-enzyme complex. Indeed, the yielded *in silico* affinities hinted towards a tighter interaction between the SFTI-1 framework and matriptase compared to trypsin binding. Nevertheless, a significantly reduced success rate to hit the obligatory canonical orientation was observed for docking experiments to matriptase compared to trypsin. Normalization of computed free energies of binding by this hit factor reflected the affinities determined *in vitro* quite well. Subsequent structural analysis of the simulated peptides and calculation of root-mean-square deviations (RMSD) for certain segments of the SFTI-1 variants gave rise to the assumption that entropic penalties originating from the terminal regions caused the reduced potencies of the investigated peptides against matriptase in comparison to trypsin.

These *in silico* results delivered useful information for possible optimization strategies which were addressed in another study. Due to the observation of a slight preference of the monocyclic variant of SFTI-1 (SFTI-1[1,14]) in matriptase inhibition, this peptide was used as a lead compound for further investigations. Initial structure-guided considerations allowed for the identification of three positions within the peptide sequence that provided the potential for incremental beneficial modifications. Two of these residues were individually furnished with azide-bearing non-natural building blocks to facilitate a divergent synthetic strategy *via* a combinatorial approach. Additionally, substitutions with selected canonical amino acids were performed. This procedure enabled to rapidly generate a small compound library of 22 peptides possessing different singular side-chain modifications. Matriptase inhibition assays revealed several beneficial side-chain replacements. The most favorable modifications were merged into one compound, which demonstrated a  $K_i$  in the single-digit nanomolar range. Notably, this variant now referred to as SFTI-1-derived matriptase inhibitor-1 (SDMI-1) contained only standard amino acids, although significant improvements of matriptase affinity were observed for triazole-containing compounds as well. This demonstrates the utility of this

“click-library” approach for the rapid screening of diverse side-chain functionalities for desired effects.

As mentioned before, a possible entropic penalty arising from the secondary loop of SFTI-1 upon binding was assumed to impair matriptase affinity. Thus, the C-terminal region of SDMI-1 was truncated by two residues resulting in the dodecapeptide SDMI-2. This compound possesses a similar activity towards matriptase as SDMI-1 but has an improved selectivity profile as it is sixfold less potent against trypsin. The developed compounds might be valuable platforms for further studies and are currently under consideration for a possible patent application. For example, the direct attachment of radiotracers suitable for PET/SPECT methodologies would enable the utilization as diagnostic tools for *in vivo* imaging. However, the potential for additional improvements of this peptidic framework towards matriptase or other pharmaceutically relevant proteases is not yet exhausted.





## 4 References

- [1] R. M. Ricketts, *Am J Orthod* **1982**, *81*, 351-370.
- [2] R. Coldea, D. A. Tennant, E. M. Wheeler, E. Wawrzynska, D. Prabhakaran, M. Telling, K. Habicht, P. Smeibidl, K. Kiefer, *Science* **2010**, *327*, 177-180.
- [3] J. C. Perez, *Interdiscip Sci* **2010**, *2*, 228-240.
- [4] M. E. Yamagishi, A. I. Shimabukuro, *Bull Math Biol* **2008**, *70*, 643-653.
- [5] T. L. Gilchrist, *J Chem Soc Perk T 1* **2001**, 2491-2515.
- [6] P. J. Steel, *Coordin Chem Rev* **1990**, *106*, 227-265.
- [7] E. Gelensa, W. J. Kootb, W. M. Mengea, H. C. Ottenheijm, H. Timmerman, *Comb Chem High Throughput Screen* **2003**, *6*, 79-99.
- [8] C. J. Andres, D. J. Denhart, M. S. Deshpande, K. W. Gillman, *Comb Chem High Throughput Screen* **1999**, *2*, 191-210.
- [9] J. C. Lewis, R. G. Bergman, J. A. Ellman, *Accounts Chem Res* **2008**, *41*, 1013-1025.
- [10] J. A. R. Navarro, B. Lippert, *Coordin Chem Rev* **2001**, *222*, 219-250.
- [11] A. P. Sadimenko, S. S. Basson, *Coordin Chem Rev* **1996**, *147*, 247-297.
- [12] A. P. Sadimenko, A. D. Garnovskii, N. Retta, *Coordin Chem Rev* **1993**, *126*, 237-318.
- [13] C. T. Walsh, S. Garneau-Tsodikova, A. R. Howard-Jones, *Nat Prod Rep* **2006**, *23*, 517-531.
- [14] H. Hoffmann, T. Lindel, *Synthesis-Stuttgart* **2003**, 1753-1783.
- [15] S. Asperger, B. CetinaCizmek, *Croat Chem Acta* **1996**, *69*, 1305-1328.
- [16] F. R. D. Alves, E. J. Barreiro, C. A. M. Fraga, *Mini-Rev Med Chem* **2009**, *9*, 782-793.
- [17] J. W. Daly, *Cell Mol Life Sci* **2007**, *64*, 2153-2169.
- [18] S. G. Agalave, S. R. Maujan, V. S. Pore, *Chem Asian J* **2011**, *6*, 2696-2718.
- [19] E. McDonald, K. Jones, P. A. Brough, M. J. Drysdale, P. Workman, *Curr Top Med Chem* **2006**, *6*, 1193-1203.
- [20] H. C. Kolb, K. B. Sharpless, *Drug Discovery Today* **2003**, *8*, 1128-1137.
- [21] D. Moderhack, *J Prak Chem-Chem Ztg* **1998**, *340*, 687-709.
- [22] H. C. Kolb, M. G. Finn, K. B. Sharpless, *Angew Chem Int Ed Engl* **2001**, *40*, 2004-2021.
- [23] P. Wu, V. V. Fokin, *Aldrichim Acta* **2007**, *40*, 7-17.
- [24] N. J. Agard, J. A. Prescher, C. R. Bertozzi, *Journal of the American Chemical Society* **2005**, *127*, 11196-11196.
- [25] Q. Wang, T. R. Chan, R. Hilgraf, V. V. Fokin, K. B. Sharpless, M. G. Finn, *Journal of the American Chemical Society* **2003**, *125*, 3192-3193.
- [26] R. Huisgen, *Angew Chem Int Edit* **1963**, *75*, 742-&.
- [27] R. Huisgen, *Angew Chem Int Edit* **1963**, *75*, 604-+.
- [28] V. V. Rostovtsev, L. G. Green, V. V. Fokin, K. B. Sharpless, *Angew Chem Int Ed Engl* **2002**, *41*, 2596-2599.
- [29] C. W. Tornoe, C. Christensen, M. Meldal, *J Org Chem* **2002**, *67*, 3057-3064.
- [30] B. C. Boren, S. Narayan, L. K. Rasmussen, L. Zhang, H. Zhao, Z. Lin, G. Jia, V. V. Fokin, *J Am Chem Soc* **2008**, *130*, 8923-8930.
- [31] J. McNulty, K. Keskar, R. Vemula, *Chemistry* **2011**, *17*, 14727-14730.
- [32] M. D. Best, *Biochemistry-Us* **2009**, *48*, 6571-6584.
- [33] Q. Wang, S. Chittaboina, H. N. Barnhill, *Lett Org Chem* **2005**, *2*, 293-301.
- [34] F. Himo, T. Lovell, R. Hilgraf, V. V. Rostovtsev, L. Noodleman, K. B. Sharpless, V. V. Fokin, *J Am Chem Soc* **2005**, *127*, 210-216.
- [35] P. Ji, J. H. Atherton, M. I. Page, *Org Biomol Chem* **2012**, *10*, 7965-7969.
- [36] M. Meldal, C. W. Tornoe, *Chem Rev* **2008**, *108*, 2952-3015.
- [37] M. G. Finn, S. Presolski, A. A. Accurso, V. O. Rodionov, *Abstr Pap Am Chem S* **2008**, 235.
- [38] V. O. Rodionov, S. I. Presolski, D. D. Diaz, V. V. Fokin, M. G. Finn, *Journal of the American Chemical Society* **2007**, *129*, 12705-12712.
- [39] V. O. Rodionov, V. V. Fokin, M. G. Finn, *Angew Chem Int Edit* **2005**, *44*, 2210-2215.
- [40] D. S. del Amo, W. Wang, H. Jiang, C. Besanceney, A. C. Yan, M. Levy, Y. Liu, F. L. Marlow, P. Wu, *Journal of the American Chemical Society* **2010**, *132*, 16893-16899.

- [41] O. Avrutina, M. Empting, S. Fabritz, M. Daneschdar, H. Frauendorf, U. Diederichsen, H. Kolmar, *Organic & Biomolecular Chemistry* **2009**, *7*, 4177-4185.
- [42] M. Galibert, L. Sancey, O. Renaudet, J. L. Coll, P. Dumy, D. Boturyn, *Organic & Biomolecular Chemistry* **2010**, *8*, 5133-5138.
- [43] M. Tischler, D. Nasu, M. Empting, S. Schmelz, D. W. Heinz, P. Rottmann, H. Kolmar, G. Buntkowsky, D. Tietze, O. Avrutina, *Angew Chem Int Edit* **2012**, *51*, 3708-3712.
- [44] M. Empting, O. Avrutina, R. Meusinger, S. Fabritz, M. Reinwarth, M. Biesalski, S. Voigt, G. Buntkowsky, H. Kolmar, *Angew Chem Int Edit* **2011**, *50*, 5207-5211.
- [45] C. Besanceney-Webler, H. Jiang, T. Zheng, L. Feng, D. Soriano Del Amo, W. Wang, L. M. Klivansky, F. L. Marlow, Y. Liu, P. Wu, *Angew Chem Int Ed Engl* **2011**, *50*, 8051-8056.
- [46] U. Pradere, V. Roy, T. R. McBrayer, R. F. Schinazi, L. A. Agrofoglio, *Tetrahedron* **2008**, *64*, 9044-9051.
- [47] P. N. Liu, J. Li, F. H. Su, K. D. Ju, L. Zhang, C. Shi, H. H. Y. Sung, I. D. Williams, V. V. Fokin, Z. Lin, G. Jia, *Organometallics* **2012**, *31*, 4904-4915.
- [48] P. N. Liu, H. X. Siyang, L. Zhang, S. K. Tse, G. Jia, *J Org Chem* **2012**, *77*, 5844-5849.
- [49] M. Mammen, S. K. Choi, G. M. Whitesides, *Angew Chem Int Edit* **1998**, *37*, 2755-2794.
- [50] D. G. McCafferty, P. Cudic, M. K. Yu, D. C. Behenna, R. Kruger, *Curr Opin Chem Biol* **1999**, *3*, 672-680.
- [51] O. Vadas, O. Hartley, K. Rose, *Biopolymers* **2008**, *90*, 496-502.
- [52] R. J. Kok, A. J. Schraa, E. J. Bos, H. E. Moorlag, S. A. Asgeirsdottir, M. Everts, D. K. F. Meijer, G. Molema, *Bioconjugate Chem* **2002**, *13*, 128-135.
- [53] E. Garanger, D. Boturyn, J. L. Coll, M. C. Favrot, P. Dumy, *Organic & Biomolecular Chemistry* **2006**, *4*, 1958-1965.
- [54] S. E. Cwirla, P. Balasubramanian, D. J. Duffin, C. R. Wagstrom, C. M. Gates, S. C. Singer, A. M. Davis, R. L. Tansik, L. C. Mattheakis, C. M. Boytos, P. J. Schatz, D. P. Baccanari, N. C. Wrighton, R. W. Barrett, W. J. Dower, *Science* **1997**, *276*, 1696-1699.
- [55] E. Garanger, D. Boturyn, P. Dumy, *Anti-Cancer Agent Me* **2007**, *7*, 552-558.
- [56] P. R. Hamann, *Expert Opin Ther Pat* **2005**, *15*, 1087-1103.
- [57] B. A. Teicher, *Curr Cancer Drug Tar* **2009**, *9*, 982-1004.
- [58] U. Haberkorn, M. Eisenhut, *Eur J Nucl Med Mol I* **2005**, *32*, 1354-1359.
- [59] H. Kubas, M. Schafer, U. Bauder-Wust, M. Eder, D. Oltmanns, U. Haberkorn, W. Mier, M. Eisenhut, *Nucl Med Biol* **2010**, *37*, 885-891.
- [60] C. Wangler, S. Maschauer, O. Prante, M. Schafer, R. Schirmacher, P. Bartenstein, M. Eisenhut, B. Wangler, *Chembiochem* **2010**, *11*, 2168-2181.
- [61] M. Galibert, O. Renaudet, P. Dumy, D. Boturyn, *Angew Chem Int Edit* **2011**, *50*, 1901-1904.
- [62] D. M. Beal, V. E. Albrow, G. Burslem, L. Hitchen, C. Fernandes, C. Laphorn, L. R. Roberts, M. D. Selby, L. H. Jones, *Organic & Biomolecular Chemistry* **2012**, *10*, 548-554.
- [63] A. Nefzi, X. C. Sun, M. Mutter, *Tetrahedron Lett* **1995**, *36*, 229-230.
- [64] G. Mezo, M. Manea, A. Jakab, B. Kapuvari, S. Bosze, G. Schlosser, M. Przybylski, F. Hudecz, *J Pept Sci* **2004**, *10*, 701-713.
- [65] N. Fotouhi, P. Joshi, J. W. Tilley, K. Rowan, V. Schwinge, B. Wolitzky, *Bioorganic & Medicinal Chemistry Letters* **2000**, *10*, 1167-1169.
- [66] S. T. Gould, N. J. Darling, K. S. Anseth, *Acta Biomater* **2012**, *8*, 3201-3209.
- [67] M. J. Kade, D. J. Burke, C. J. Hawker, *J Polym Sci Pol Chem* **2010**, *48*, 743-750.
- [68] O. P. Edupuganti, Y. Singh, E. Defrancq, P. Dumy, *Chem-Eur J* **2004**, *10*, 5988-5995.
- [69] D. Forget, D. Boturyn, E. Defrancq, J. Lhomme, P. Dumy, *Chem-Eur J* **2001**, *7*, 3976-3984.
- [70] E. M. Sletten, C. R. Bertozzi, *Angew Chem Int Edit* **2009**, *48*, 6974-6998.
- [71] E. M. Sletten, C. R. Bertozzi, *Accounts Chem Res* **2011**, *44*, 666-676.
- [72] E. Saxon, C. R. Bertozzi, *Science* **2000**, *287*, 2007-2010.
- [73] C. S. McKay, M. Chigrinova, J. A. Blake, J. P. Pezacki, *Organic & Biomolecular Chemistry* **2012**, *10*, 3066-3070.
- [74] X. H. Ning, R. P. Temming, J. Dommerholt, J. Guo, D. B. Ania, M. F. Debets, M. A. Wolfert, G. J. Boons, F. L. van Delft, *Angew Chem Int Edit* **2010**, *49*, 3065-3068.

- [75] A. K. Parhi, R. W. Franck, *Org Lett* **2004**, *6*, 3063-3065.
- [76] R. Pipkorn, W. Waldeck, B. Didinger, M. Koch, G. Mueller, M. Wiessler, K. Braun, *J Pept Sci* **2009**, *15*, 235-241.
- [77] R. Rossin, P. R. Verkerk, S. M. van den Bosch, R. C. Vulders, I. Verel, J. Lub, M. S. Robillard, *Angew Chem Int Ed Engl* **2010**, *49*, 3375-3378.
- [78] Z. K. Wan, G. H. C. Woo, J. K. Snyder, *Tetrahedron* **2001**, *57*, 5497-5507.
- [79] J. H. Kim, J. C. Lim, K. C. Yun, S. J. Choi, Y. D. Hong, *J Labelled Compd Rad* **2012**, *55*, 10-17.
- [80] L. S. Campbell-Verduyn, L. Mirfeizi, A. K. Schoonen, R. A. Dierckx, P. H. Elsinga, B. L. Feringa, *Angew Chem Int Edit* **2011**, *50*, 11117-11120.
- [81] U. S. Toti, B. R. Guru, A. E. Grill, J. Panyam, *Mol Pharmaceut* **2010**, *7*, 1108-1117.
- [82] O. Avrutina, H. U. Schmoldt, D. Gabrijelcic-Geiger, A. Wentzel, H. Frauendorf, C. P. Sommerhoff, U. Diederichsen, H. Kolmar, *Chembiochem* **2008**, *9*, 33-37.
- [83] S. Fabritz, S. Horner, D. Konning, M. Empting, M. Reinwarth, C. Dietz, B. Glotzbach, H. Frauendorf, H. Kolmar, O. Avrutina, *Organic & Biomolecular Chemistry* **2012**, *10*, 6287-6293.
- [84] A. Dirksen, S. Dirksen, T. M. Hackeng, P. E. Dawson, *Journal of the American Chemical Society* **2006**, *128*, 15602-15603.
- [85] D. Forget, D. Boturyn, E. Defrancq, J. Lhomme, P. Dumy, *Chemistry* **2001**, *7*, 3976-3984.
- [86] J. D. Wade, K. Hojo, K. Kawasaki, T. G. Johns, B. Catimel, J. Rothacker, E. C. Nice, *Anal Biochem* **2006**, *348*, 315-317.
- [87] S. S. van Berkel, M. B. van Eldijk, J. C. M. van Hest, *Angew Chem Int Edit* **2011**, *50*, 8806-8827.
- [88] D. J. Vugts, A. Vervoort, M. Stigter-van Walsum, G. W. Visser, M. S. Robillard, R. M. Versteegen, R. C. Vulders, J. K. Herscheid, G. A. van Dongen, *Bioconjug Chem* **2011**, *22*, 2072-2081.
- [89] J. A. Prescher, D. H. Dube, C. R. Bertozzi, *Nature* **2004**, *430*, 873-877.
- [90] R. Merckx, D. T. S. Rijkers, J. Kemmink, R. M. J. Liskamp, *Tetrahedron Lett* **2003**, *44*, 4515-4518.
- [91] R. Kleineweischede, C. P. Hackenberger, *Angew Chem Int Ed Engl* **2008**, *47*, 5984-5988.
- [92] F. Schoenebeck, D. H. Ess, G. O. Jones, K. N. Houk, *Journal of the American Chemical Society* **2009**, *131*, 8121-8133.
- [93] S. T. Laughlin, C. R. Bertozzi, *Acs Chemical Biology* **2009**, *4*, 1068-1072.
- [94] A. J. Dirks, J. J. L. M. Cornelissen, R. J. M. Nolte, *Bioconjugate Chem* **2009**, *20*, 1129-1138.
- [95] P. Daumar, C. A. Wanger-Baumann, N. Pillarsetty, L. Fabrizio, S. D. Carlin, O. A. Andreev, Y. K. Reshetnyak, J. S. Lewis, *Bioconjugate Chem* **2012**, *23*, 1557-1566.
- [96] C. Ligeour, A. Meyer, J. J. Vasseur, F. Morvan, *Eur J Org Chem* **2012**, 1851-1856.
- [97] A. L. Isaad, A. M. Papini, M. Chorev, P. Rovero, *J Pept Sci* **2009**, *15*, 451-454.
- [98] K. Wang, X. H. Bi, S. X. Xing, P. Q. Liao, Z. X. Fang, X. Y. Meng, Q. A. Zhang, Q. Liu, Y. Ji, *Green Chem* **2011**, *13*, 562-565.
- [99] A. Barge, S. Tagliapietra, A. Binello, G. Cravotto, *Curr Org Chem* **2011**, *15*, 189-203.
- [100] E. Lallana, A. Sousa-Herves, F. Fernandez-Trillo, R. Riguera, E. Fernandez-Megia, *Pharm Res-Dordr* **2012**, *29*, 1-34.
- [101] S. Fabritz, D. Heyl, V. Bagutski, M. Empting, E. Rikowski, H. Frauendorf, I. Balog, W. D. Fessner, J. J. Schneider, O. Avrutina, H. Kolmar, *Organic & Biomolecular Chemistry* **2010**, *8*, 2212-2218.
- [102] P. E. Schneggenburger, B. Worbs, U. Diederichsen, *J Pept Sci* **2010**, *16*, 10-14.
- [103] X. P. He, J. Xie, Y. Tang, J. Li, G. R. Chen, *Current Medicinal Chemistry* **2012**, *19*, 2399-2405.
- [104] V. B. Klimovich, *Biochemistry (Mosc)* **2011**, *76*, 534-549.
- [105] Y. Singh, G. T. Dolphin, J. Razkin, P. Dumy, *Chembiochem* **2006**, *7*, 1298-1314.
- [106] Q. Lin, A. D. Hamilton, *Cr Chim* **2002**, *5*, 441-450.
- [107] K. J. Jensen, J. Brask, *Biopolymers* **2005**, *80*, 747-761.
- [108] P. Timmerman, J. Beld, W. C. Puijk, R. H. Meloen, *Chembiochem* **2005**, *6*, 821-+.

- [109] T. Sasaki, E. T. Kaiser, *Journal of the American Chemical Society* **1989**, *111*, 380-381.
- [110] S. Reiss, M. Sieber, V. Oberle, A. Wentzel, P. Spangenberg, R. Claus, H. Kolmar, W. Losche, *Platelets* **2006**, *17*, 153-157.
- [111] C. Mas-Moruno, F. Rechenmacher, H. Kessler, *Anti-Cancer Agent Me* **2010**, *10*, 753-768.
- [112] P. A. Burke, S. J. DeNardo, L. A. Miers, K. R. Lamborn, S. Matzku, G. L. DeNardo, *Cancer Res* **2002**, *62*, 4263-4272.
- [113] L. Sancey, V. Ardisson, L. M. Riou, M. Ahmadi, D. Marti-Battle, D. Boturyn, P. Dumy, D. Fagret, C. Ghezzi, J. P. Vuillez, *Eur J Nucl Med Mol I* **2007**, *34*, 2037-2047.
- [114] R. A. Clynes, T. L. Towers, L. G. Presta, J. V. Ravetch, *Nat Med* **2000**, *6*, 443-446.
- [115] C. W. Shuptrine, R. Surana, L. M. Weiner, *Semin Cancer Biol* **2012**, *22*, 3-13.
- [116] D. H. Na, Y. S. Youn, E. J. Park, J. M. Lee, O. R. Cho, K. R. Lee, S. D. Lee, S. D. Yoo, P. P. Deluca, K. C. Lee, *J Pharm Sci-Us* **2004**, *93*, 256-261.
- [117] J. M. Harris, N. E. Martin, M. Modi, *Clin Pharmacokinet* **2001**, *40*, 539-551.
- [118] T. J. Rutkoski, J. A. Kink, L. E. Strong, R. T. Raines, *Cancer Biol Ther* **2011**, *12*, 208-214.
- [119] A. Tam, U. Arnold, M. B. Soellner, R. T. Raines, *Journal of the American Chemical Society* **2007**, *129*, 12670-+.
- [120] V. D. Bock, D. Speijer, H. Hiemstra, J. H. van Maarseveen, *Org Biomol Chem* **2007**, *5*, 971-975.
- [121] K. Holland-Nell, M. Meldal, *Angew Chem Int Edit* **2011**, *50*, 5204-5206.
- [122] C. F. Wu, X. Zhao, W. X. Lan, C. Y. Cao, J. T. Liu, X. K. Jiang, Z. T. Li, *Journal of Organic Chemistry* **2012**, *77*, 4261-4270.
- [123] D. S. Pedersen, A. Abell, *Eur J Org Chem* **2011**, 2399-2411.
- [124] K. Buysse, J. Farard, A. Nikolaou, P. Vanderheyden, G. Vauquelin, D. S. Pedersen, D. Tourwe, S. Ballet, *Organic Letters* **2011**, *13*, 6468-6471.
- [125] H. Fittler, O. Avrutina, B. Glotzbach, M. Empting, H. Kolmar, *Org Biomol Chem* **2012**, under review.
- [126] R. G. Boy, W. Mier, E. M. Nothelfer, A. Altmann, M. Eisenhut, H. Kolmar, M. Tomaszowski, S. Kramer, U. Haberkorn, *Mol Imaging Biol* **2010**, *12*, 377-385.
- [127] M. L. Korsinczky, H. J. Schirra, D. J. Craik, *Curr Protein Pept Sci* **2004**, *5*, 351-364.
- [128] M. L. Korsinczky, H. J. Schirra, K. J. Rosengren, J. West, B. A. Condie, L. Otvos, M. A. Anderson, D. J. Craik, *J Mol Biol* **2001**, *311*, 579-591.
- [129] Y. Q. Long, S. L. Lee, C. Y. Lin, I. J. Enyedy, S. Wang, P. Li, R. B. Dickson, P. P. Roller, *Bioorg Med Chem Lett* **2001**, *11*, 2515-2519.
- [130] P. Li, S. Jiang, S. L. Lee, C. Y. Lin, M. D. Johnson, R. B. Dickson, C. J. Michejda, P. P. Roller, *J Med Chem* **2007**, *50*, 5976-5983.
- [131] E. Zablotna, K. Kazmierczak, A. Jaskiewicz, M. Stawikowski, G. Kupryszewski, K. Rolka, *Biochem Biophys Res Commun* **2002**, *292*, 855-859.
- [132] L. Hedstrom, *Chemical Reviews* **2002**, *102*, 4501-4523.
- [133] N. D. Rawlings, A. J. Barrett, *Methods Enzymol* **1994**, *244*, 19-61.
- [134] W. R. Rypniewski, A. Perrakis, C. E. Vorgias, K. S. Wilson, *Protein Eng* **1994**, *7*, 57-64.
- [135] A. Muhlia-Almazan, A. Sanchez-Paz, F. L. Garcia-Carreno, *J Comp Physiol B* **2008**, *178*, 655-672.
- [136] T. M. Antalis, T. H. Bugge, Q. Wu, *Prog Mol Biol Transl Sci* **2011**, *99*, 1-50.
- [137] P. Ovaere, S. Lippens, P. Vandenabeele, W. Declercq, *Trends Biochem Sci* **2009**, *34*, 453-463.
- [138] T. M. Antalis, M. S. Buzza, K. M. Hodge, J. D. Hooper, S. Netzel-Arnett, *Biochem J* **2010**, *428*, 325-346.
- [139] A. Schmidt, C. Jelsch, P. Ostergaard, W. Rypniewski, V. S. Lamzin, *Journal of Biological Chemistry* **2003**, *278*, 43357-43362.
- [140] K. List, *Future Oncol* **2009**, *5*, 97-104.
- [141] K. Uhland, *Cell Mol Life Sci* **2006**, *63*, 2968-2978.
- [142] M. Del Rosso, F. Margheri, S. Serrati, A. Chilla, A. Laurenzana, G. Fibbi, *Curr Pharm Des* **2011**, *17*, 1924-1943.
- [143] C. Yuan, L. Q. Chen, E. J. Meehan, N. Daly, D. J. Craik, M. D. Huang, J. C. Ngo, *Bmc Struct Biol* **2011**, *11*.



- [144] L. G. Jiang, H. Y. Yu, C. Yuan, J. D. Wang, L. Q. Chen, E. J. Meehan, Z. X. Huang, M. D. Huang, *Chinese J Struc Chem* **2009**, *28*, 1427-1432.
- [145] A. Angelini, L. Cendron, S. Y. Chen, J. Touati, G. Winter, G. Zanotti, C. Heinis, *Acs Chemical Biology* **2012**, *7*, 817-821.
- [146] J. A. Magee, T. Araki, S. Patil, T. Ehrig, L. True, P. A. Humphrey, W. J. Catalona, M. A. Watson, J. Milbrandt, *Cancer Res* **2001**, *61*, 5692-5696.
- [147] J. R. Somoza, J. D. Ho, C. Luong, M. Ghate, P. A. Sprengeler, K. Mortara, W. D. Shrader, D. Sperandio, H. Chan, M. E. McGrath, B. A. Katz, *Structure* **2003**, *11*, 1123-1131.
- [148] M. J. Costanzo, S. C. Yabut, H. C. Zhang, K. B. White, L. de Garavilla, Y. Wang, L. K. Minor, B. A. Tounge, A. N. Barnakov, F. Lewandowski, C. Milligan, J. C. Spurlino, W. M. Abraham, V. Boswell-Smith, C. P. Page, B. E. Maryano, *Bioorganic & Medicinal Chemistry Letters* **2008**, *18*, 2114-2121.
- [149] M. A. Navia, B. M. McKeever, J. P. Springer, T. Y. Lin, H. R. Williams, E. M. Fluder, C. P. Dorn, K. Hoogsteen, *P Natl Acad Sci USA* **1989**, *86*, 7-11.
- [150] F. Beliveau, A. Desilets, R. Leduc, *Febs J* **2009**, *276*, 2213-2226.
- [151] O. Avrutina, H. Fittler, B. Glotzbach, H. Kolmar, M. Empting, *Organic & Biomolecular Chemistry* **2012**, *10*, 7753-7762.
- [152] T. H. Bugge, T. M. Antalis, Q. Wu, *Journal of Biological Chemistry* **2009**, *284*, 23177-23181.
- [153] J. D. Hooper, J. A. Clements, J. P. Quigley, T. M. Antalis, *Journal of Biological Chemistry* **2001**, *276*, 857-860.
- [154] R. Szabo, J. P. Hobson, K. List, A. Molinolo, C. Y. Lin, T. H. Bugge, *Journal of Biological Chemistry* **2008**, *283*, 29495-29504.
- [155] M. D. Oberst, L. Y. Chen, K. Kiyomiya, C. A. Williams, M. S. Lee, M. D. Johnson, R. B. Dickson, C. Y. Lin, *Am J Physiol Cell Physiol* **2005**, *289*, C462-470.
- [156] M. S. Buzza, S. Netzel-Arnett, T. Shea-Donohue, A. P. Zhao, C. Y. Lin, K. List, R. Szabo, A. Fasano, T. H. Bugge, T. M. Antalis, *P Natl Acad Sci USA* **2010**, *107*, 4200-4205.
- [157] K. List, R. Szabo, A. Molinolo, V. Sriuranpong, V. Redeye, T. Murdock, B. Burke, B. S. Nielsen, J. S. Gutkind, T. H. Bugge, *Gene Dev* **2005**, *19*, 1934-1950.
- [158] J. M. Milner, A. Patel, R. K. Davidson, T. E. Swingler, A. Desilets, D. A. Young, E. B. Kelso, S. T. Donell, T. E. Cawston, I. M. Clark, W. R. Ferrell, R. Plevin, J. C. Lockhart, R. Leduc, A. D. Rowan, *Arthritis Rheum-Us* **2010**, *62*, 1955-1966.
- [159] K. List, C. C. Haudenschild, R. Szabo, W. J. Chen, S. M. Wahl, W. Swaim, L. H. Engelholm, N. Behrendt, T. H. Bugge, *Oncogene* **2002**, *21*, 3765-3779.
- [160] M. D. Roycik, X. Fang, Q. X. Sang, *Curr Pharm Des* **2009**, *15*, 1295-1308.
- [161] T. Steinmetzer, A. Schweinitz, A. Sturzebecher, D. Donnecke, K. Uhland, O. Schuster, P. Steinmetzer, F. Muller, R. Friedrich, M. E. Than, W. Bode, J. Sturzbecher, *Journal of Medicinal Chemistry* **2006**, *49*, 4116-4126.
- [162] E. Colombo, A. Desilets, D. Duchene, F. Chagnon, R. Najmanovich, R. Leduc, E. Marsault, *Acs Med Chem Lett* **2012**, *3*, 530-534.
- [163] J. E. Swedberg, S. J. de Veer, K. C. Sit, C. F. Reboul, A. M. Buckle, J. M. Harris, *Plos One* **2011**, *6*.
- [164] A. Lesner, A. Legowska, M. Wysocka, K. Rolka, *Curr Pharm Design* **2011**, *17*, 4308-4317.
- [165] D. Scarpi, J. D. McBride, R. J. Leatherbarrow, *Bioorgan Med Chem* **2004**, *12*, 6045-6052.
- [166] R. F. Qi, Z. W. Song, C. W. Chi, *Acta Bioch Bioph Sin* **2005**, *37*, 283-292.
- [167] J. D. McBride, A. B. E. Brauer, M. Nievo, R. J. Leatherbarrow, *Journal of Molecular Biology* **1998**, *282*, 447-457.
- [168] S. Luckett, R. S. Garcia, J. J. Barker, A. V. Konarev, P. R. Shewry, A. R. Clarke, R. L. Brady, *J Mol Biol* **1999**, *290*, 525-533.
- [169] D. E. Stewart, A. Sarkar, J. E. Wampler, *J Mol Biol* **1990**, *214*, 253-260.
- [170] J. Song, K. Burrage, Z. Yuan, T. Huber, *BMC Bioinformatics* **2006**, *7*, 124.
- [171] A. Choudhary, R. T. Raines, *Chembiochem* **2011**, *12*, 1801-1807.

- [172] D. Tietze, M. Tischler, S. Voigt, D. Imhof, O. Ohlenschlager, M. Gorlach, G. Buntkowsky, *Chem-Eur J* **2010**, *16*, 7572-7578.
- [173] A. Jabs, M. S. Weiss, R. Hilgenfeld, *J Mol Biol* **1999**, *286*, 291-304.
- [174] W. S. Horne, C. A. Olsen, J. M. Beierle, A. Montero, M. R. Ghadiri, *Angew Chem Int Ed Engl* **2009**, *48*, 4718-4724.
- [175] K. P. Exarchos, T. P. Exarchos, G. Rigas, C. Papaloukas, D. I. Fotiadis, *BMC Bioinformatics* **2011**, *12*.
- [176] M. Keller, C. Boissard, L. Patiny, N. N. Chung, C. Lemieux, M. Mutter, P. W. Schiller, *Journal of Medicinal Chemistry* **2001**, *44*, 3896-3903.
- [177] I. Annis, B. Hargittai, G. Barany, *Methods Enzymol* **1997**, *289*, 198-221.
- [178] H. Kolmar, *Curr Opin Pharmacol* **2009**, *9*, 608-614.
- [179] D. J. Craik, J. S. Mylne, N. L. Daly, *Cell Mol Life Sci* **2010**, *67*, 9-16.
- [180] B. W. Park, H. T. Zhang, C. Wu, A. Berezov, X. Zhang, R. Dua, Q. Wang, G. Kao, D. M. O'Rourke, M. I. Greene, R. Murali, *Nat Biotechnol* **2000**, *18*, 194-198.
- [181] T. S. Han, M. M. Zhang, A. Walewska, P. Gruszczynski, C. R. Robertson, T. E. Cheatham, 3rd, D. Yoshikami, B. M. Olivera, G. Bulaj, *ChemMedChem* **2009**, *4*, 406-414.
- [182] M. A. Fazio, V. X. Oliveira, Jr., P. Bulet, M. T. Miranda, S. Daffre, A. Miranda, *Biopolymers* **2006**, *84*, 205-218.
- [183] R. Kowalczyk, M. A. Brimble, K. E. Callon, M. Watson, J. Cornish, *Bioorg Med Chem* **2012**, *20*, 6011-6018.
- [184] R. Kowalczyk, P. W. Harris, M. A. Brimble, K. E. Callon, M. Watson, J. Cornish, *Bioorg Med Chem* **2012**, *20*, 2661-2668.
- [185] A. K. Galande, K. S. Bramlett, T. P. Burris, J. L. Wittliff, A. F. Spatola, *J Pept Res* **2004**, *63*, 297-302.
- [186] L. Yu, Y. Lai, J. Wade, S. M. Coutts, *Tetrahedron Lett* **1998**, *39*, 6633-6636.
- [187] A. K. Galande, J. O. Trent, A. F. Spatola, *Biopolymers* **2003**, *71*, 534-551.
- [188] M. A. Hossain, K. J. Rosengren, S. Zhang, R. A. Bathgate, G. W. Tregear, B. J. van Lierop, A. J. Robinson, J. D. Wade, *Org Biomol Chem* **2009**, *7*, 1547-1553.
- [189] S. Jiang, P. Li, S. L. Lee, C. Y. Lin, Y. Q. Long, M. D. Johnson, R. B. Dickson, P. P. Roller, *Org Lett* **2007**, *9*, 9-12.
- [190] M. Roice, I. Johannsen, M. Meldal, *QSAR Comb. Sci.* **2004**, *23*, 662-673.
- [191] P. G. van Dokkum, C. Conroy, *Nature* **2010**, *468*, 940-942.
- [192] T. Lindner, H. Kolmar, U. Haberkorn, W. Mier, *Molecules* **2011**, *16*, 1625-1641.
- [193] D. M. Driscoll, P. R. Copeland, *Annu Rev Nutr* **2003**, *23*, 17-40.
- [194] J. A. Krzycki, *Curr Opin Microbiol* **2005**, *8*, 706-712.
- [195] A. E. Bond, P. E. Row, E. Dudley, *Phytochemistry* **2011**, *72*, 975-996.
- [196] K. L. Gorres, R. T. Raines, *Crit Rev Biochem Mol Biol* **2010**, *45*, 106-124.
- [197] M. Yamauchi, M. Sricholpech, *Essays Biochem* **2012**, *52*, 113-133.
- [198] F. Liu, J. E. Park, W. J. Qian, D. Lim, A. Scharow, T. Berg, M. B. Yaffe, K. S. Lee, T. R. Burke, Jr., *Chembiochem* **2012**, *13*, 1291-1296.
- [199] F. Liu, J. E. Park, W. J. Qian, D. Lim, A. Scharow, T. Berg, M. B. Yaffe, K. S. Lee, T. R. Burke, Jr., *ACS Chem Biol* **2012**, *7*, 805-810.
- [200] P. M. Saladin, B. D. Zhang, J. M. Reichert, *IDrugs* **2009**, *12*, 779-784.
- [201] D. L. Bushnell, Jr., T. M. O'Dorisio, M. S. O'Dorisio, Y. Menda, R. J. Hicks, E. Van Cutsem, J. L. Baulieu, F. Borson-Chazot, L. Anthony, A. B. Benson, K. Oberg, A. B. Grossman, M. Connolly, H. Bouterfa, Y. Li, K. A. Kacena, N. LaFrance, S. A. Pauwels, *J Clin Oncol* **2010**, *28*, 1652-1659.
- [202] G. Giovacchini, G. Nicolas, F. Forrer, *Anti-Cancer Agent Me* **2012**, *12*, 526-542.
- [203] G. Tabatabai, M. Weller, B. Nabors, M. Picard, D. Reardon, T. Mikkelsen, C. Ruegg, R. Stupp, *Target Oncol* **2010**, *5*, 175-181.
- [204] A. Giuliani, G. Pirri, S. F. Nicoletto, *Cent Eur J Biol* **2007**, *2*, 1-33.
- [205] L. Jia, G. S. Gorman, L. U. Coward, P. E. Noker, D. McCormick, T. L. Horn, J. B. Harder, M. Muzzio, B. Prabhakar, B. Ganesh, T. K. Das Gupta, C. W. Beattie, *Cancer Chemoth Pharm* **2011**, *68*, 513-524.
- [206] L. T. Nguyen, J. K. Chau, N. A. Perry, L. de Boer, S. A. J. Zaat, H. J. Vogel, *Plos One* **2010**, *5*.

- [207] H. Jenssen, S. I. Aspmo, *Methods Mol Biol* **2008**, *494*, 177-186.
- [208] C. A. Lipinski, F. Lombardo, B. W. Dominy, P. J. Feeney, *Adv Drug Deliv Rev* **2001**, *46*, 3-26.
- [209] D. S. Youngblood, S. A. Hatlevig, J. N. Hassinger, P. L. Iversen, H. M. Moulton, *Bioconjug Chem* **2007**, *18*, 50-60.
- [210] E. M. Molhoek, A. van Dijk, E. J. Veldhuizen, H. P. Haagsman, F. J. Bikker, *Peptides* **2011**, *32*, 875-880.



## 5 Abbreviations

Å	Ångström (10–10 m)
aa	amino acid
ADC	antibody-drug conjugates
ADCC	antibody-dependent cell-mediated cytotoxicity
aq.	aqueous
AgAAC	silver(I)-catalyzed azide-alkyne cycloaddition
AMBER	assisted model building with energy refinement
BBI	Bowman-Birk inhibitor
BOP	benzotriazol-1-yloxytris(dimethylamino)phosphonium hexafluorophosphate
Boc	<i>tert</i> -butyloxycarbonyl
<i>t</i> Bu	<i>tert</i> -butyl
°C	degree Celsius
<i>c</i>	<i>cyclo</i>
calc.	calculated
CDC	complement-dependent cytotoxicity
Cp	cyclopentadienyl
Cp*	pentamethylcyclopentadien
COD	cyclooctadien
COSS	cube-octameric silsesquioxanes
CuAAC	copper(I)-catalyzed azide-alkyne cycloaddition
δ	chemical shift, ppm
Da	Dalton
DCM	dicloromethane (CH <sub>2</sub> Cl <sub>2</sub> )
DIEA	ethyl diisopropyl amine (Hünig base)
DMF	dimethylformamide
DMSO	dimethylsulfoxide
DOTATOC	2-[4-[2-[[[(2R)-1-[[[(4R,7S,10S,13R,16S,19R)-10-(4-aminobutyl)-4-[[[(2R,3R)-1,3-dihydroxybutan-2-yl]carbamoyl]-7-[(1R)-1-hydroxyethyl]-16-[(4-hydroxyphenyl)methyl]-13-(1H-indol-3-ylmethyl)-6,9,12,15,18-pentaoxo-1,2-dithia-5,8,11,14,17-pentazacycloicos-19-yl]amino]-1-oxo-3-phenylpropan-2-yl]amino]-2-oxoethyl]-7,10-bis(carboxymethyl)-1,4,7,10-tetrazacyclododec-1-yl]acetic acid
EI	electron ionization
ELISA	enzyme-linked immunosorbent assay
eq.	equivalent
ESI	electro-spray ionization
et al.	<i>et alii, et aliae, et alia</i>
Fc	fragment, crystallizable (antibody)
Fig.	figure
FITC	fluoresceinisothiocyanate
Fmoc	9-fluorenylmethyloxycarbonyl



GFC	gel filtration chromatography
GPC	gel permeation chromatography
h	hour
HAI-1	hepatocyte growth factor activator inhibitor-1
HAI-2	hepatocyte growth factor activator inhibitor-2
HATU	<i>O</i> -(7-azabenzotriazol-1-yl)-1,1,3,3-tetramethyluroniumhexafluorophosphate
HBTU	<i>O</i> -(1 <i>H</i> -benzotriazol-1-yl)-1,1,3,3-tetramethyluroniumhexafluorophosphate
HCTU	<i>O</i> -(1 <i>H</i> -6-chlorobenzotriazol-1-yl)-1,1,3,3-tetramethyluroniumhexafluorophosphate
HOAt	7-aza-1-hydroxybenzotriazol
HOBt	1-hydroxybenzotriazol
HPLC	high-performance liquid chromatography
HR	high-resolution
IC50	mean inhibitory concentration
IgM	immunoglobulin M
k	kilo ( $10^3$ )
$K_i$	inhibition constant (substrate-independent)
$K_i^{app}$	apparent inhibition constant (substrate-dependent)
L	liter
$\lambda$	wavelength
M	molar concentration (mol/L)
m	milli ( $10^{-3}$ )
Me	methyl
min	minute
MS	mass spectrometry
MTBE	<i>tert</i> -butyl-methylether
MW	molecular weight
MWD	molecular weight distribution
MT-SP1	membrane-type serine protease
$\mu$	micro ( $10^{-6}$ )
m/z	ratio of mass to charge
n	nano ( $10^{-9}$ )
NBE	new biological entities
NCE	new chemical entities
NMP	<i>N</i> -methylpyrrolidinone
NMR	nuclear magnetic resonance
p	pico ( $10^{-12}$ )
Pbf	2,2,4,6,7-pentamethylchromane-6-sulfonyl
PCy <sub>3</sub>	tricyclohexylphosphine
PDB	protein data base
PEG	polyethyleneglycol
PET	positron emission tomography

PG	protecting group
pH	$-\lg[\text{H}^+]$
Plk1	polo-like kinase 1
POSS	polyhedral silsesquioxanes
PPh <sub>3</sub>	triphenylphosphine
PyBOP	benzotriazol-1-yloxy)tripyrrolidinophosphonium hexafluorophosphate
R	residue
RAFT	regioselectively addressable functionalized template
RMSD	root-mean-square deviation
RP	reversed-phase
R <sub>t</sub>	retention time
RuAAC	ruthenium(II)-catalized azide-alkyne cycloaddtion
SAR	structure-activity relation
SDMI-1	SFTI-1-derived matriptase inhibitor-1
SDMI-2	SFTI-1-derived matriptase inhibitor-2
SEC	size exclusion chromatography
SFTI-1	sunflower trypsin inhibitor-1
SPAAC	strain-promoted azide-alkyne cycloaddtion
SPANC	strain-promoted alkyne-nitrone cycloaddtion
SPECT	single-photon emission computed tomography
SPPS	solid phase peptide synthesis
ST14	suppression of tumorigenicity 14 (colon carcinoma)
T	temperature
TASP	template-assembled synthetic peptide
Tab.	table
TFA	trifluoroacetic acid
TES	triethylsilane
TP-I	tachyplesin-I
TPO	thrombopoietin
Trt	trityl
TTSP	Type II transmembrane serine protease
UV/VIS	Ultraviolet-visible
V	volume
v	initial velocity



## 6 Supporting Information

This section contains the supporting information for the studies presented in section 2. It includes relevant additional details on experimental procedures, as well as RP-HPLC or GFC chromatograms, MS, IR and NMR spectra. Furthermore, it provides information on crystallographic and *in silico* procedures.

The data in chapters 6.1 to 6.4 is also available online:

### 6.1 Supporting Information for:

Olga Avrutina, Martin Empting, Sebastian Fabritz, Martin Daneschdar, Holm Frauendorf, Ulf Diederichsen, Harald Kolmar, Application of copper(I) catalyzed azide-alkyne [3+2] cycloaddition to the synthesis of template-assembled multivalent peptide conjugates. *Org. Biomol. Chem.* (2009), 7, 4177-4185.

→<http://www.rsc.org/suppdata/ob/b9/b908261a/b908261a.pdf>

### 6.2 Supporting Information for:

Marco Tischler, Daichi Nasu, Martin Empting, Stefan Schmelz, Dirk W. Heinz, Philip Rottmann, Harald Kolmar, Gerd Buntkowsky, Daniel Tietze, Olga Avrutina, Braces for the peptide backbone: Insights into structure-activity relationships of protease inhibitor mimics with locked amide conformations. *Angew. Chem. Int. Ed.* (2012), 51, 3708-3712.

→[http://onlinelibrary.wiley.com/store/10.1002/anie.201108983/asset/supinfo/anie\\_201108983\\_sm\\_miscellaneous\\_information.pdf?v=1&s=26a6b399ba6d4bb3e9b442c30cc8447fc5ffb5f6](http://onlinelibrary.wiley.com/store/10.1002/anie.201108983/asset/supinfo/anie_201108983_sm_miscellaneous_information.pdf?v=1&s=26a6b399ba6d4bb3e9b442c30cc8447fc5ffb5f6)

### 6.3 Supporting Information for:

Martin Empting, Olga Avrutina, Reinhard Meusinger, Sebastian Fabritz, Michael Reinwarth, Markus Biesalski, Stephan Voigt, Gerd Buntkowsky, Harald Kolmar, "Triazole Bridge": Disulfide-Bond Replacement by Ruthenium-Catalyzed Formation of 1,5-Disubstituted 1,2,3-Triazoles. *Angew. Chem. Int. Ed.* (2011), 50, 5207-5211.

→[http://onlinelibrary.wiley.com/store/10.1002/anie.201008142/asset/supinfo/anie\\_201008142\\_sm\\_miscellaneous\\_information.pdf?v=1&s=d4445de4d7733c392000cf4308075ec4b8c683a2](http://onlinelibrary.wiley.com/store/10.1002/anie.201008142/asset/supinfo/anie_201008142_sm_miscellaneous_information.pdf?v=1&s=d4445de4d7733c392000cf4308075ec4b8c683a2)

### 6.4 Supporting Information for:

Olga Avrutina, Heiko Fittler, Bernhard Glotzbach, Harald Kolmar, Martin Empting, Between Two Worlds: a Comparative Study on In Vitro and In Silico Inhibition of Trypsin and Matriptase by Redox-Stable SFTI-1 Variants at Near Physiological pH. *Org. Biomol. Chem.* (2012), 10, 7753-7762.

→<http://www.rsc.org/suppdata/ob/c2/c2ob26162f/c2ob26162f.pdf>

### 6.5 Supporting Information for:

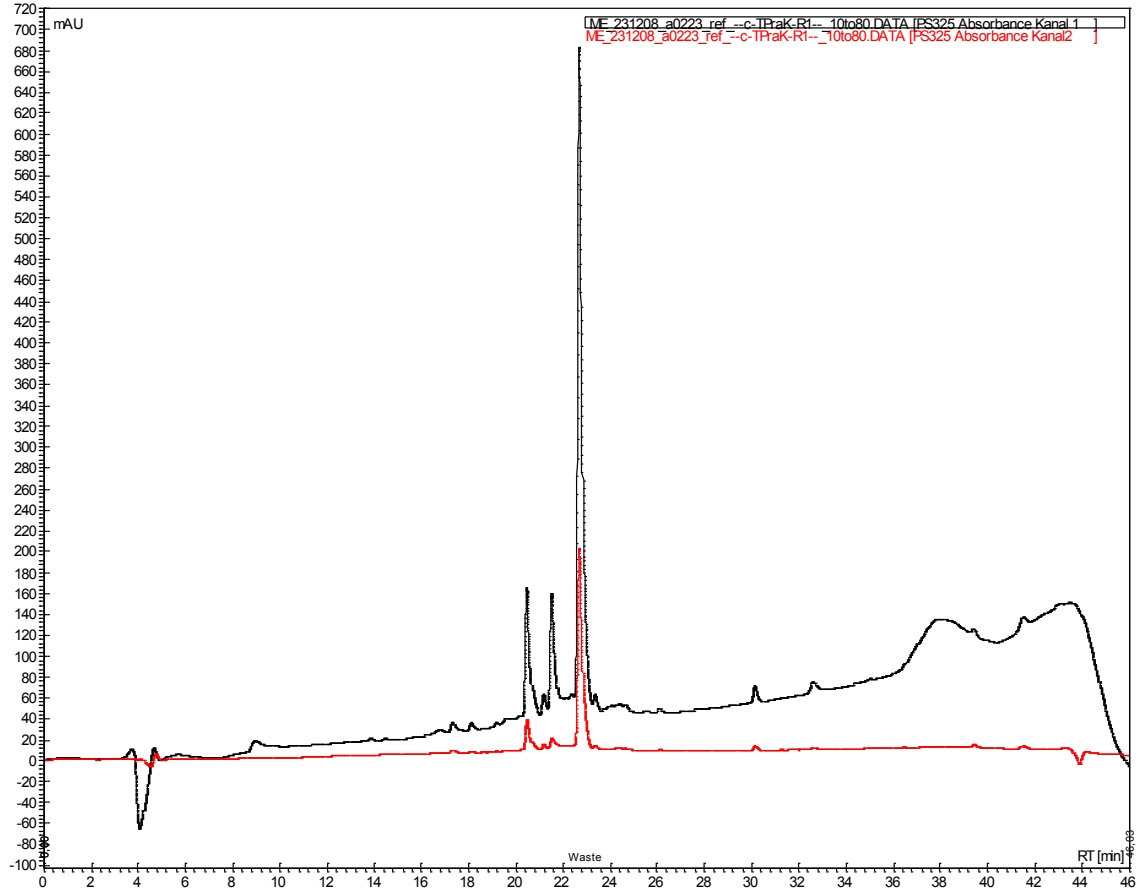
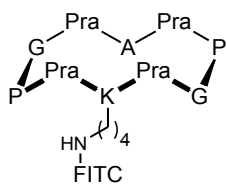
Heiko Fittler, Olga Avrutina, Bernhard Glotzbach, Martin Empting, Harald Kolmar, Combinatorial Tuning of Peptidic Drug Candidates: High-Affinity Matriptase Inhibitors through Incremental Structure-Guided Optimization.

– Submitted for publication in September 2012.

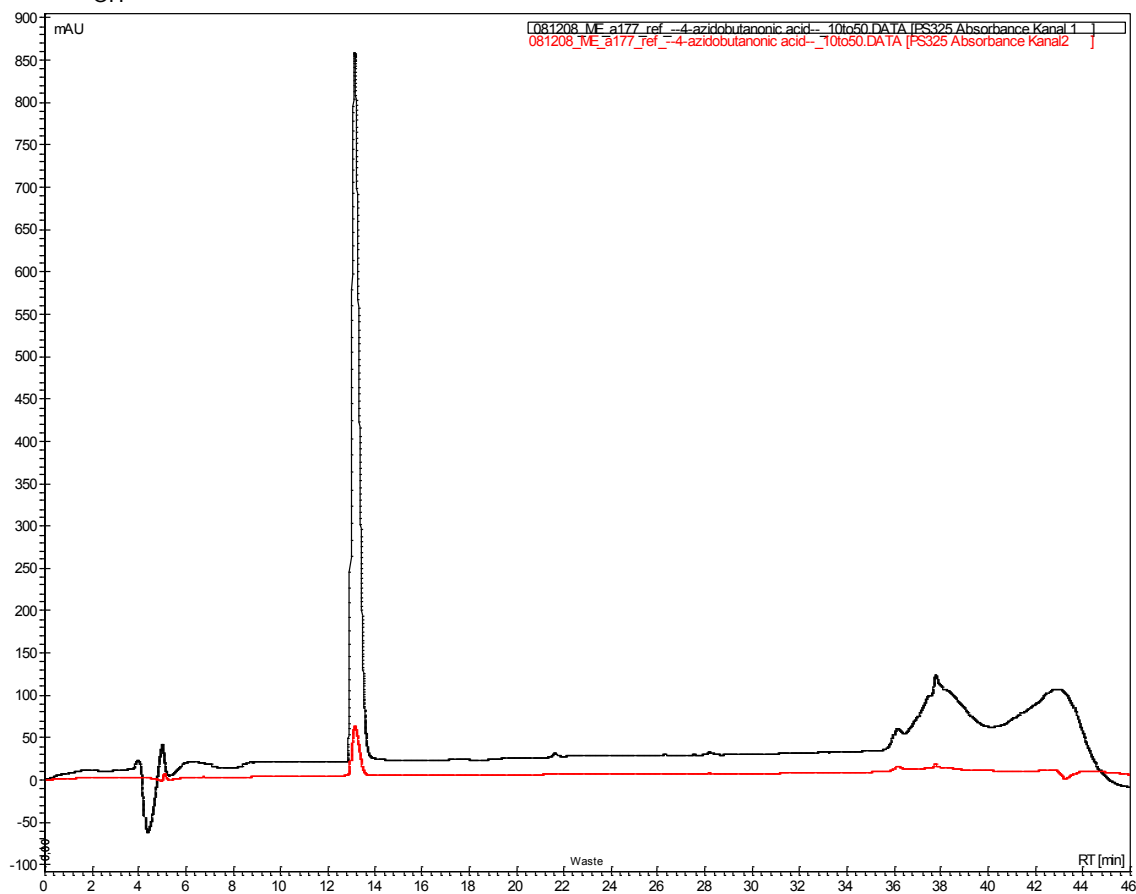
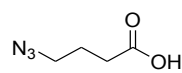




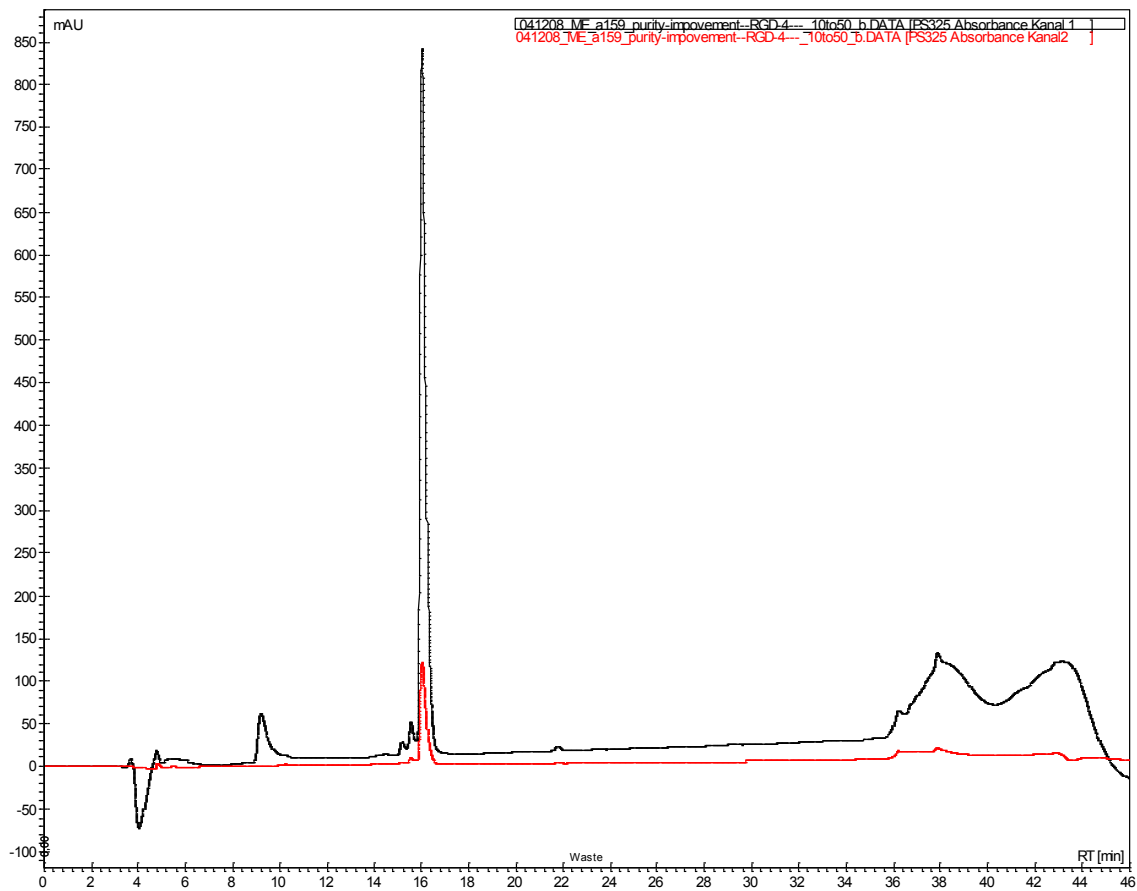
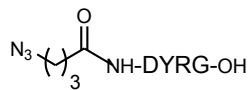




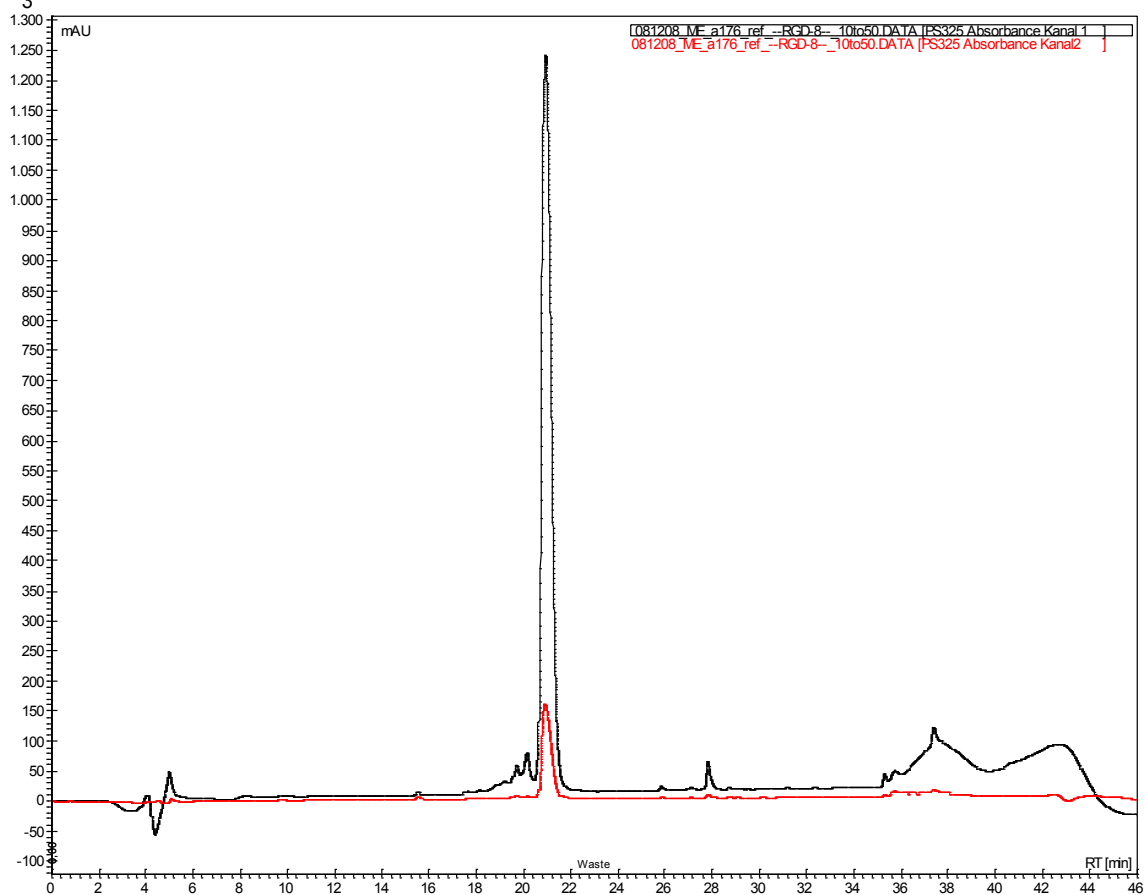
gradient: 9→72% acetonitrile in 0.1% TFA over 30 minutes at 1 mL/min.



gradient: 9→45% acetonitrile in 0.1% TFA over 30 minutes at 1 mL/min



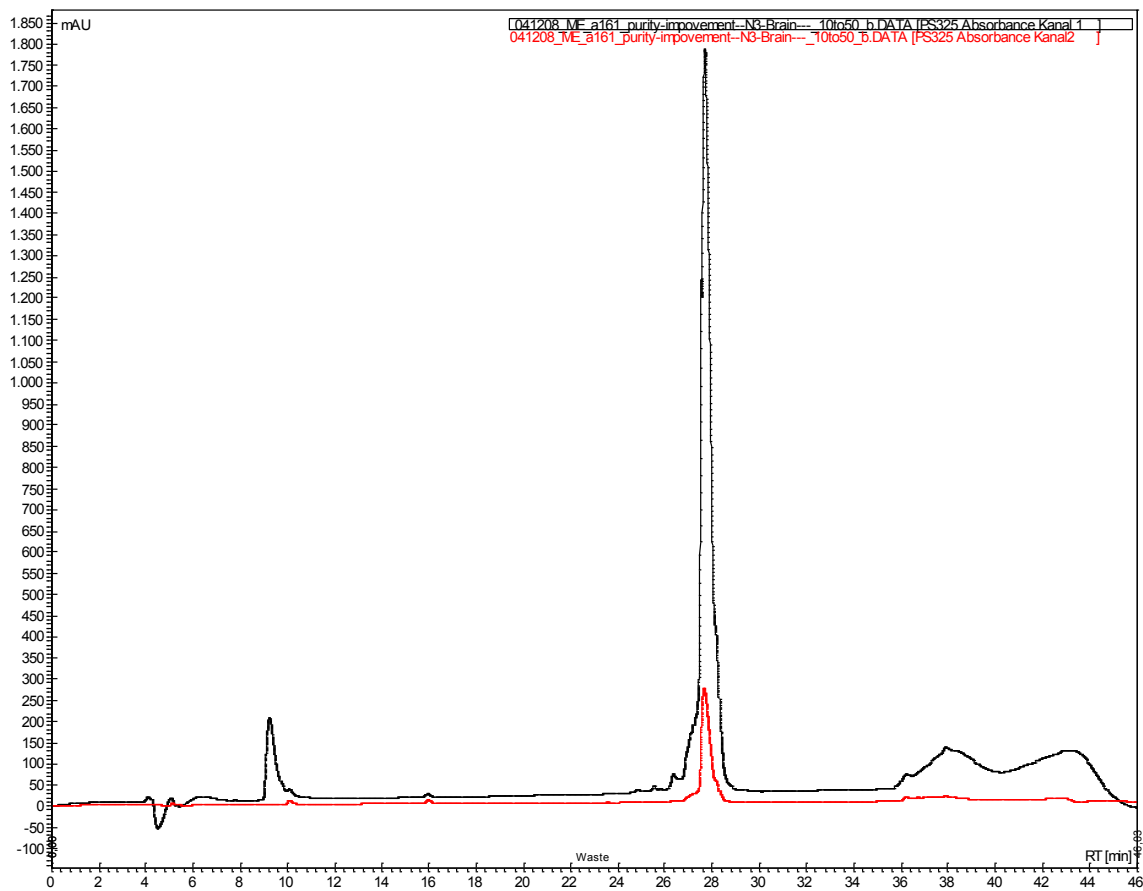
gradient: 9→45% acetonitrile in 0.1% TFA over 30 minutes at 1 mL/min



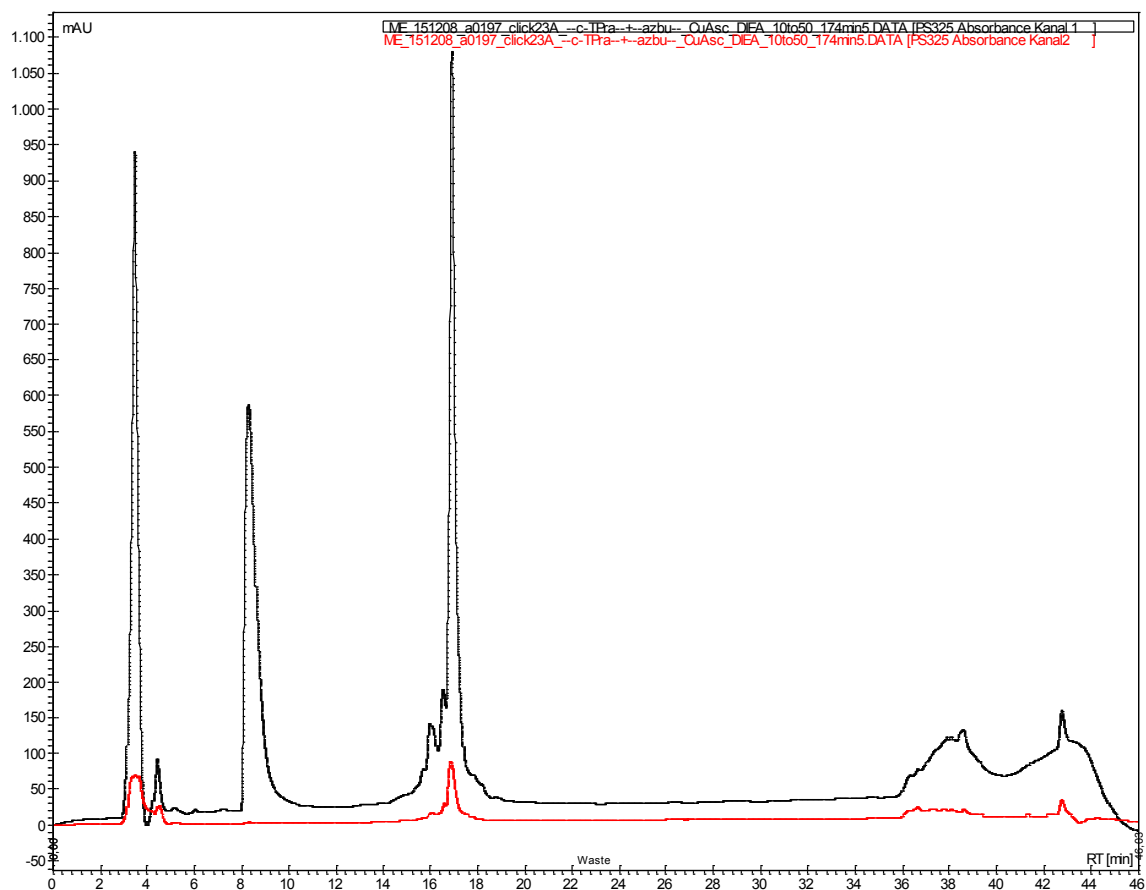
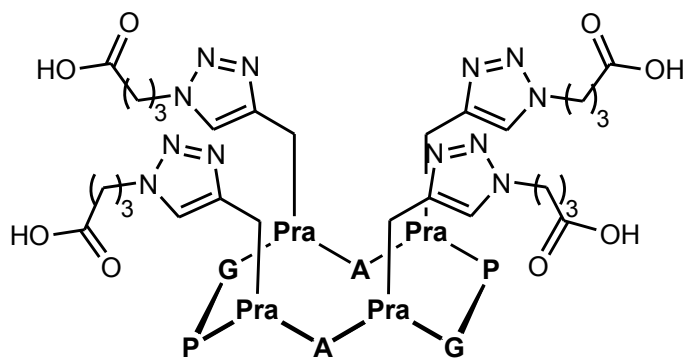
gradient: 9→45% acetonitrile in 0.1% TFA over 30 minutes at 1 mL/min



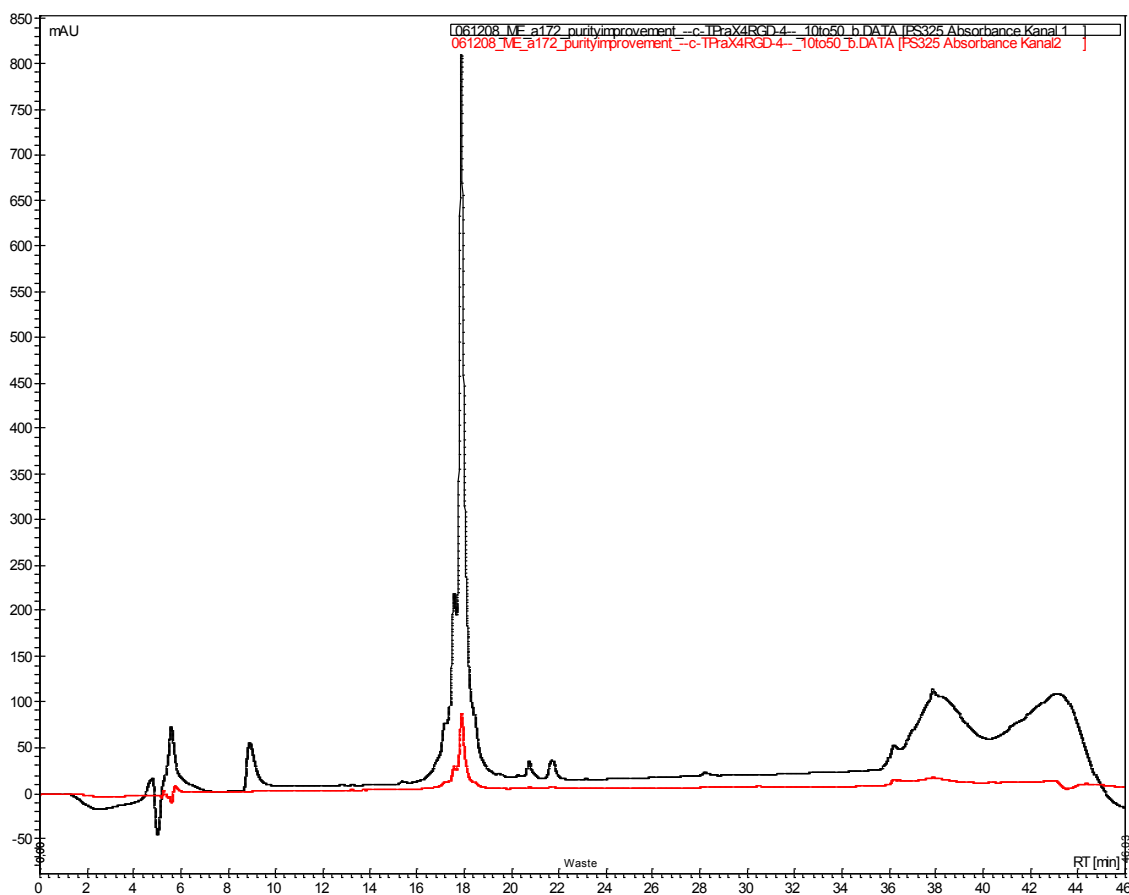
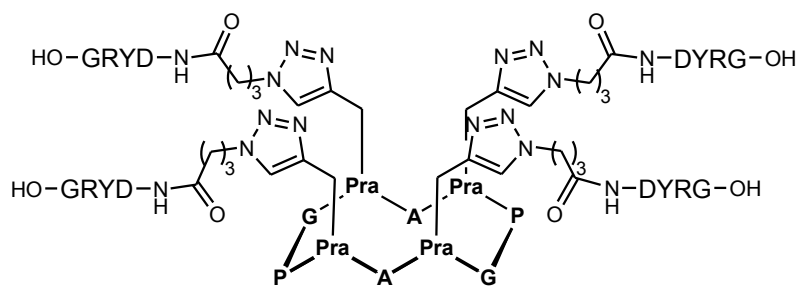




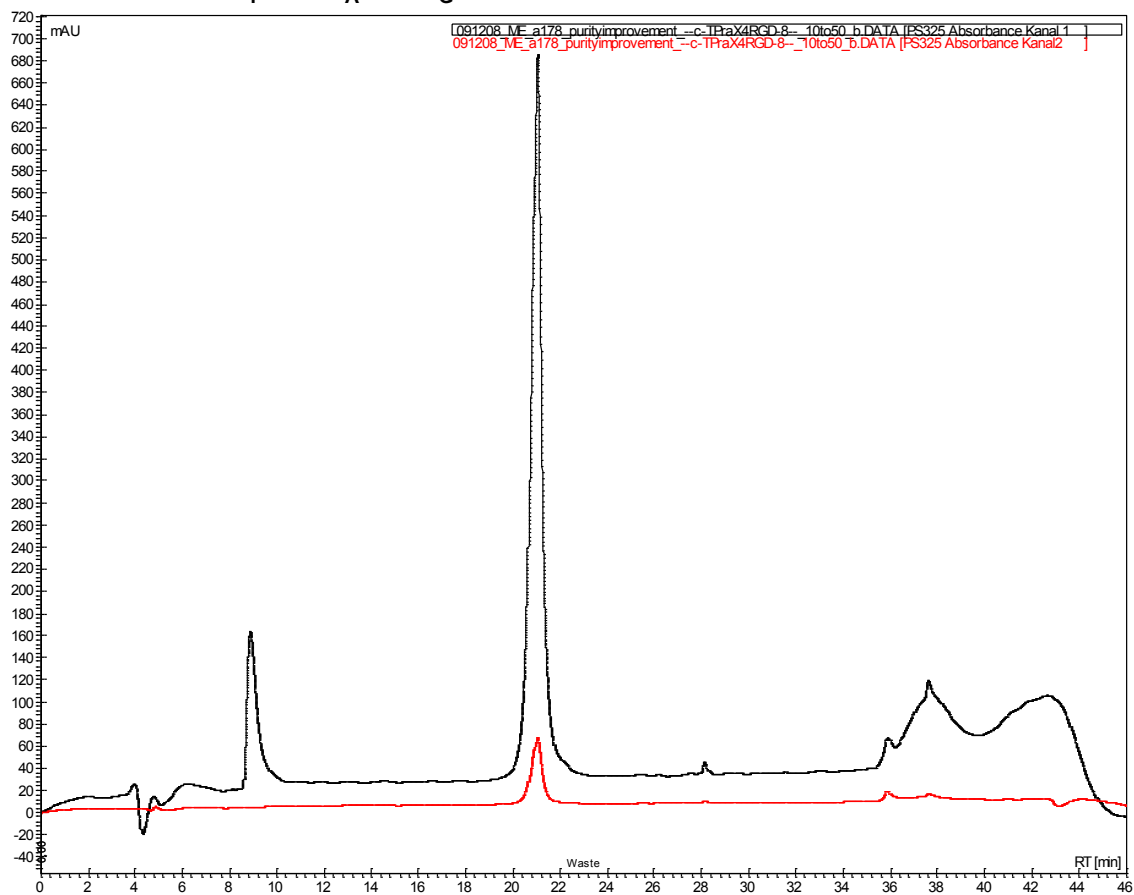
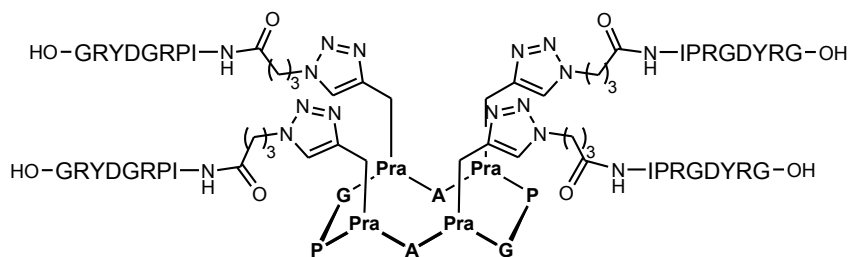
gradient: 9→45% acetonitrile in 0.1% TFA over 30 minutes at 1 mL/min



gradient: 9→45% acetonitrile in 0.1% TFA over 30 minutes at 1 mL/min

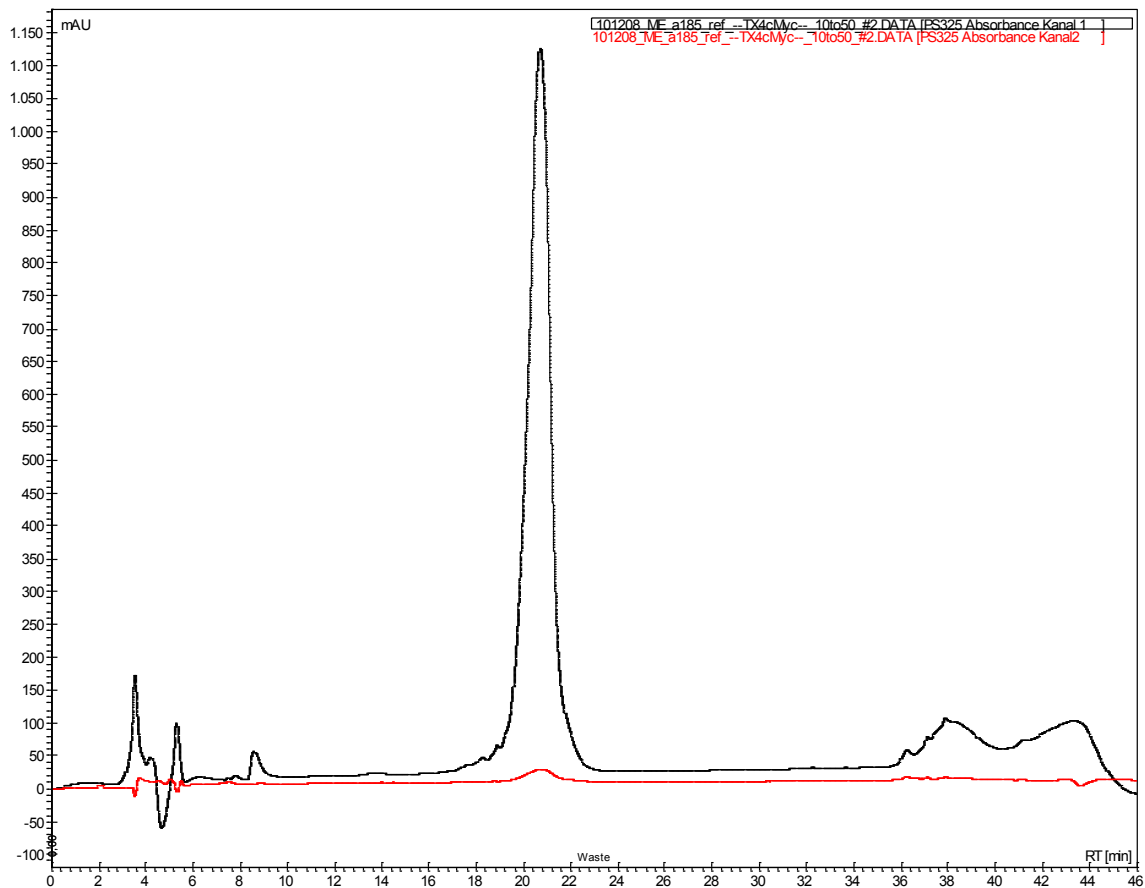
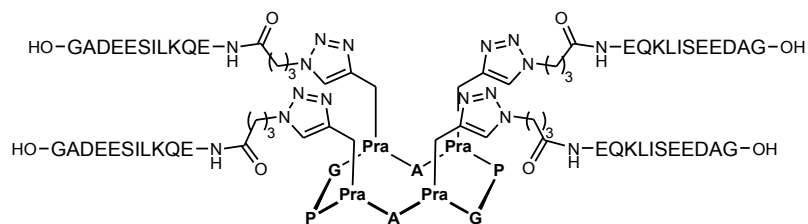


gradient: 9→45% acetonitrile in 0.1% TFA over 30 minutes at 1 mL/min

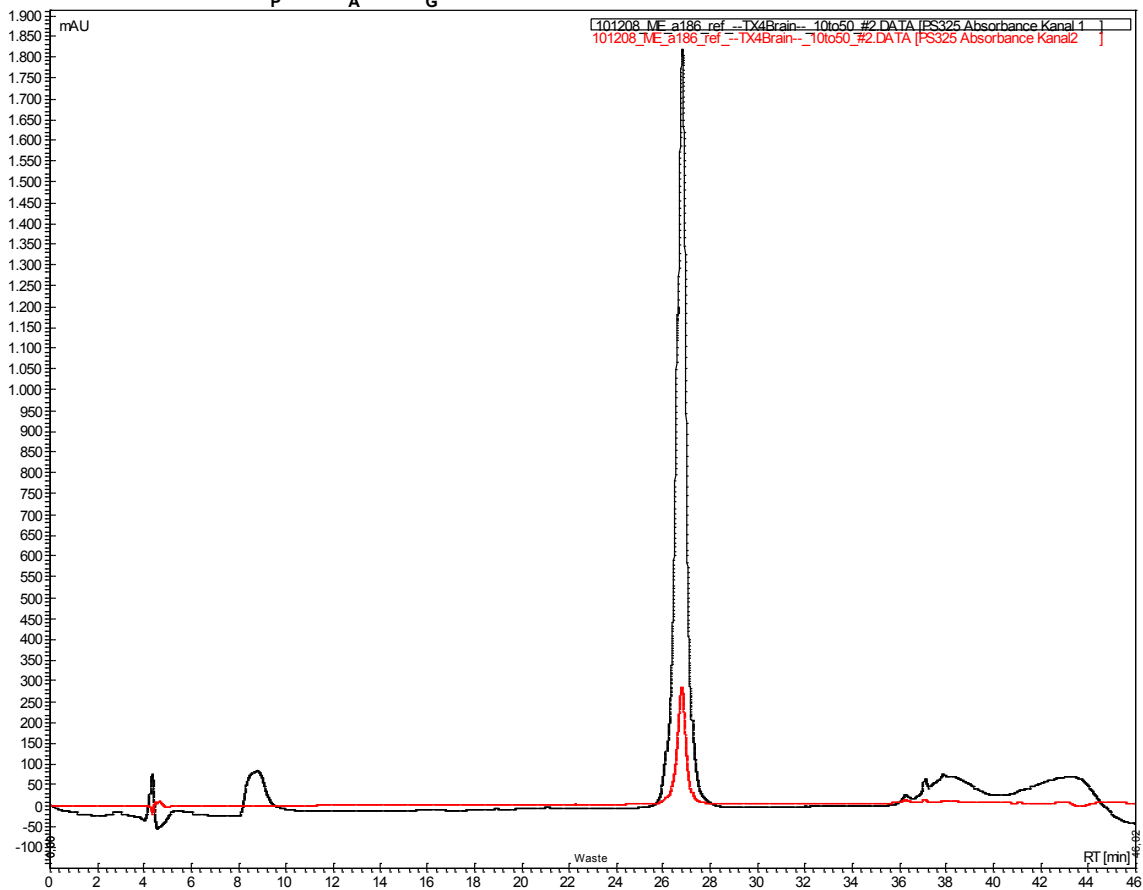
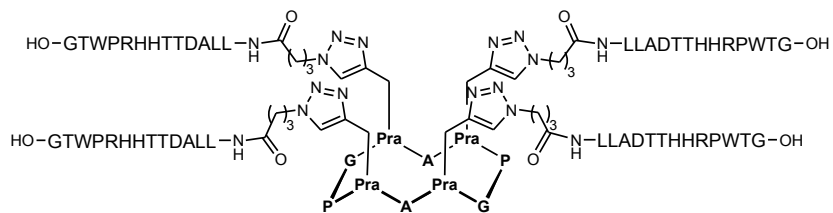


gradient: 9→45% acetonitrile in 0.1% TFA over 30 minutes at 1 mL/min

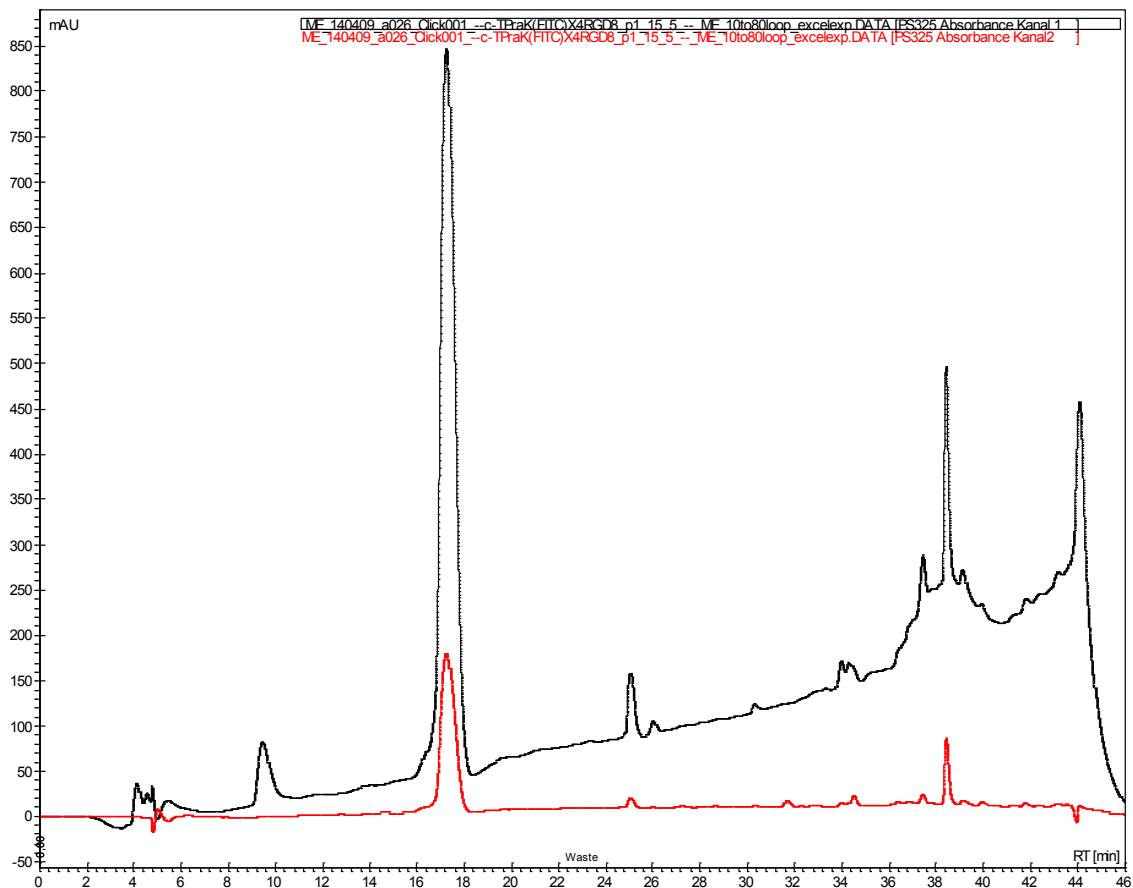
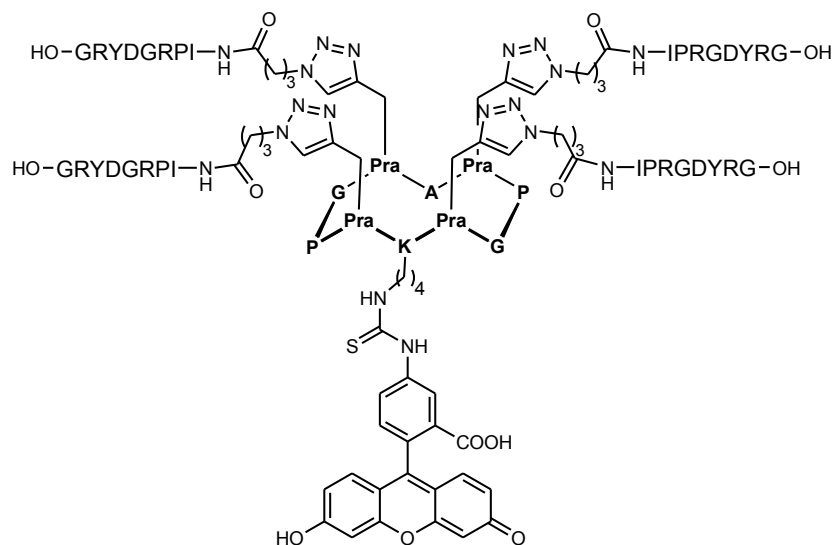




gradient: 9→45% acetonitrile in 0.1% TFA over 30 minutes at 1 mL/min



gradient: 9→45% acetonitrile in 0.1% TFA over 30 minutes at 1 mL/min

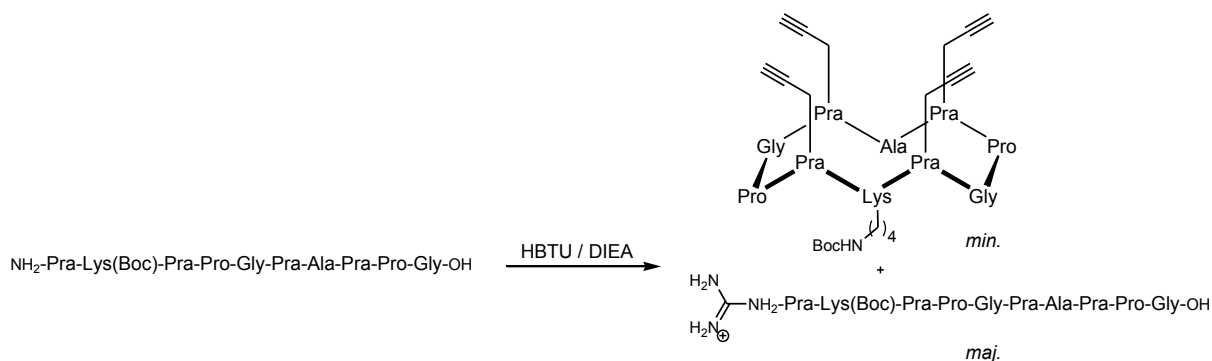


gradient: 9→72% acetonitrile in 0.1% TFA over 30 minutes at 1 mL/min.

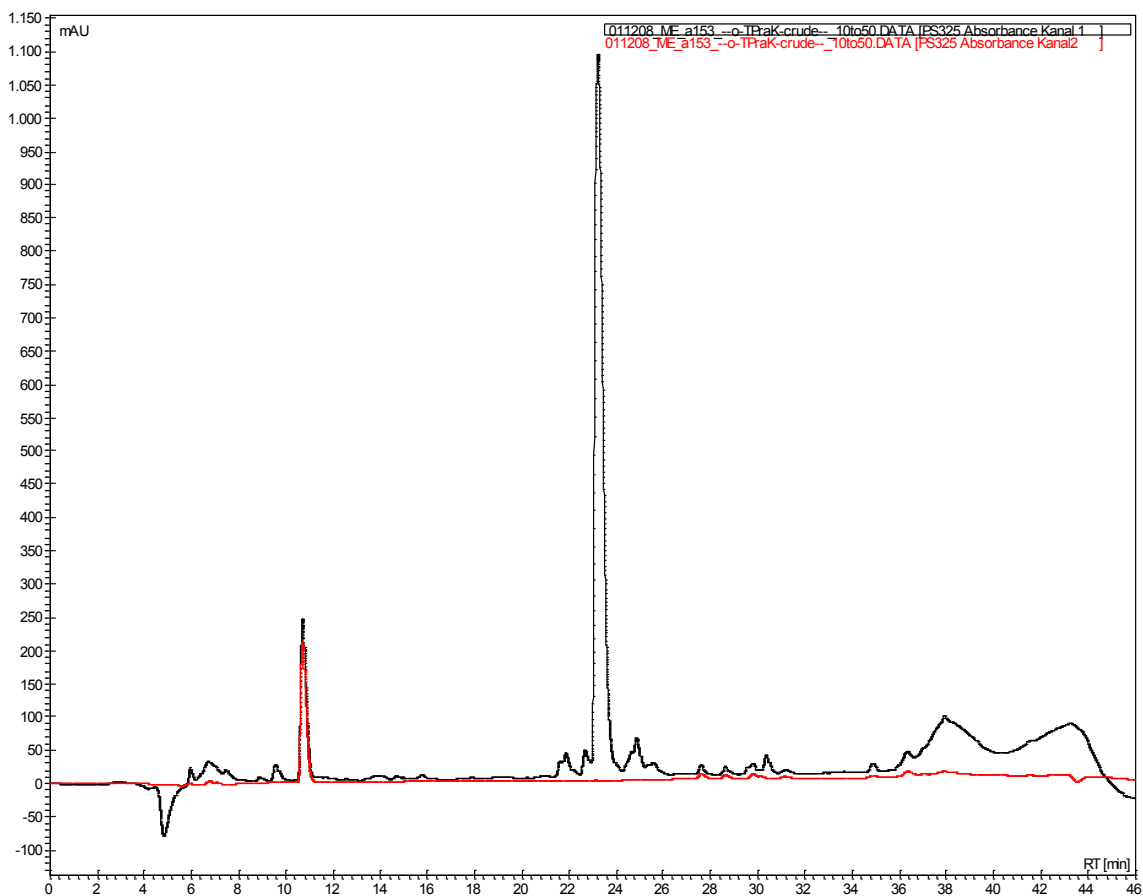
### 6.1.2 RP-HPLC Traces for the Macrocyclization of Cyclic Decapeptide Scaffolds

RP-HPLC traces for the macrocyclization of  $\text{NH}_2\text{-Pra-Lys(Boc)-Pra-Pro-Gly-Pra-Ala-Pra-Pro-Gly-OH}$  to  $\text{cyclo-(Pra-Lys(Boc)-Pra-Pro-Gly-Pra-Ala-Pra-Pro-Gly)}$  using HBTU or PyBOP were recorded at 220 (black) and 280 (red) nm.

#### HBTU activation

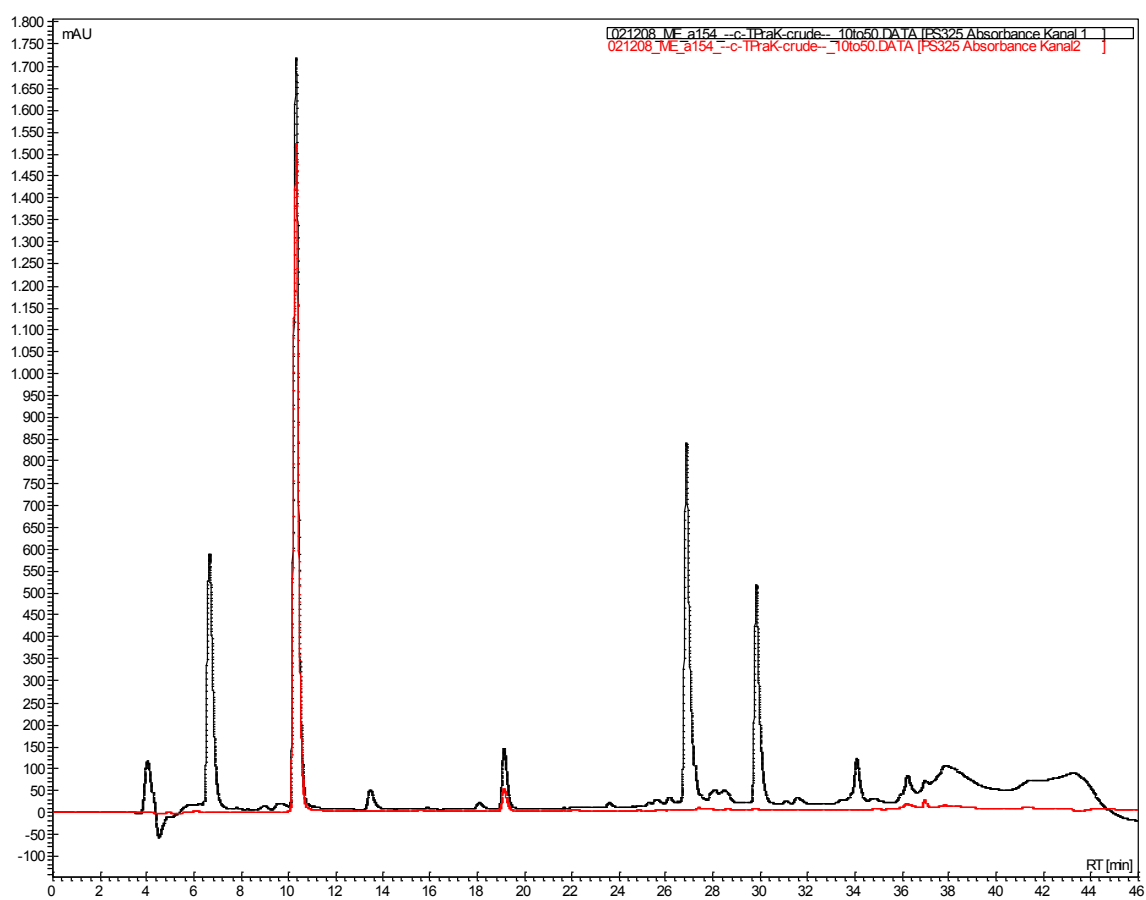


Reference:  $\text{NH}_2\text{-Pra-Lys(Boc)-Pra-Pro-Gly-Pra-Ala-Pra-Pro-Gly-OH}$



gradient: 9→45% acetonitrile in 0.1% TFA over 30 minutes at 1 mL/min

Reaction mixture:



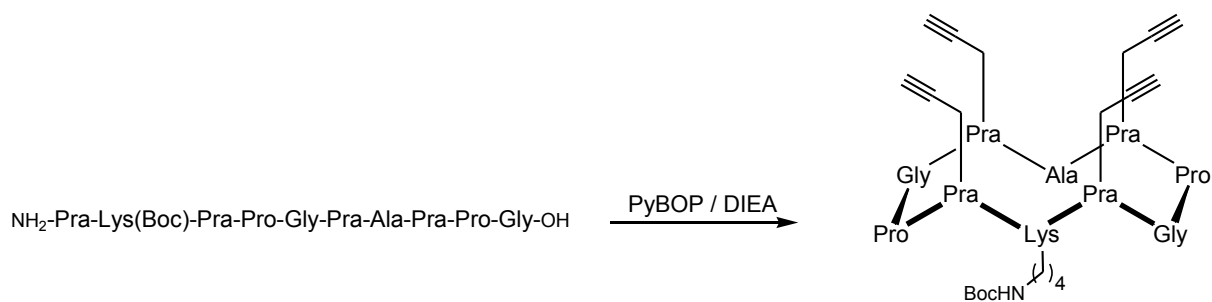
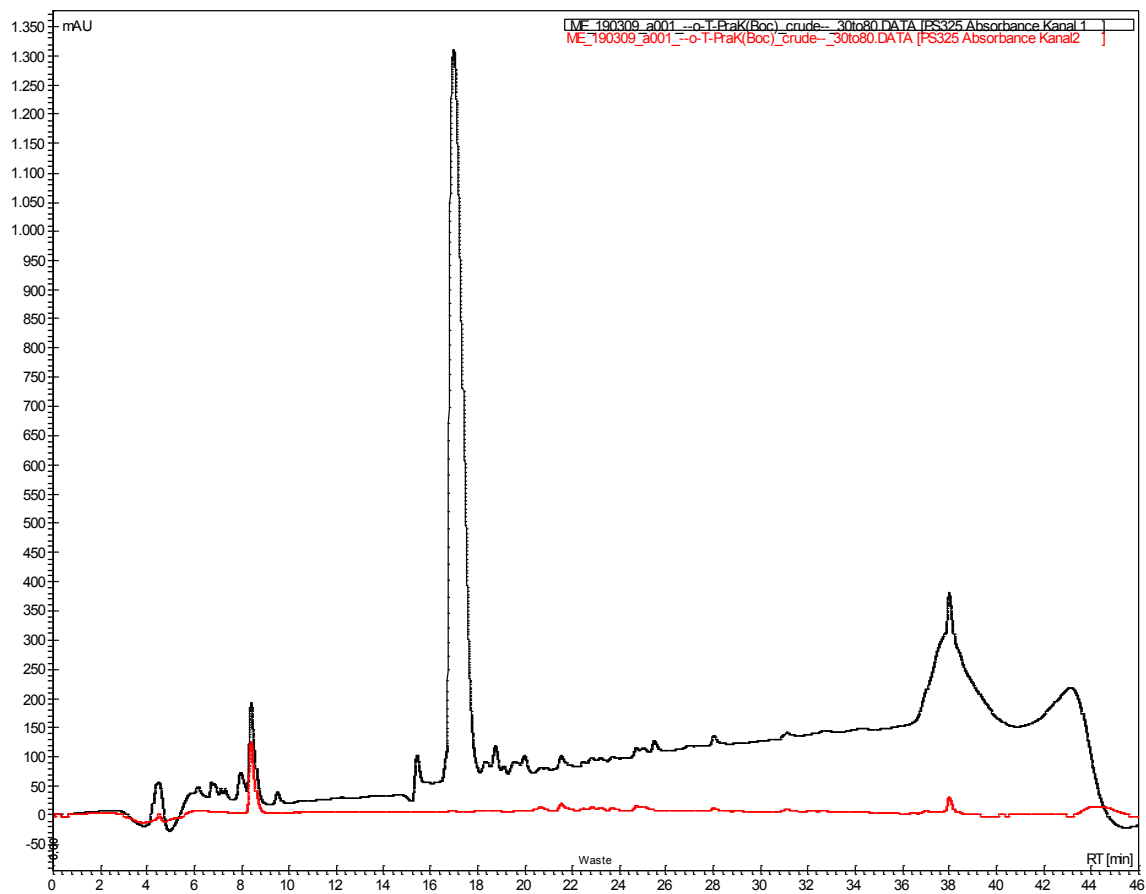
$R_t = 26$  min: guanidinated open chain precursor

$R_t = 30$  min: *cyclo*-(Pra-Lys(Boc)-Pra-Pro-Gly-Pra-Ala-Pra-Pro-Gly)

gradient: 9→45% acetonitrile in 0.1% TFA over 30 minutes at 1 mL/min

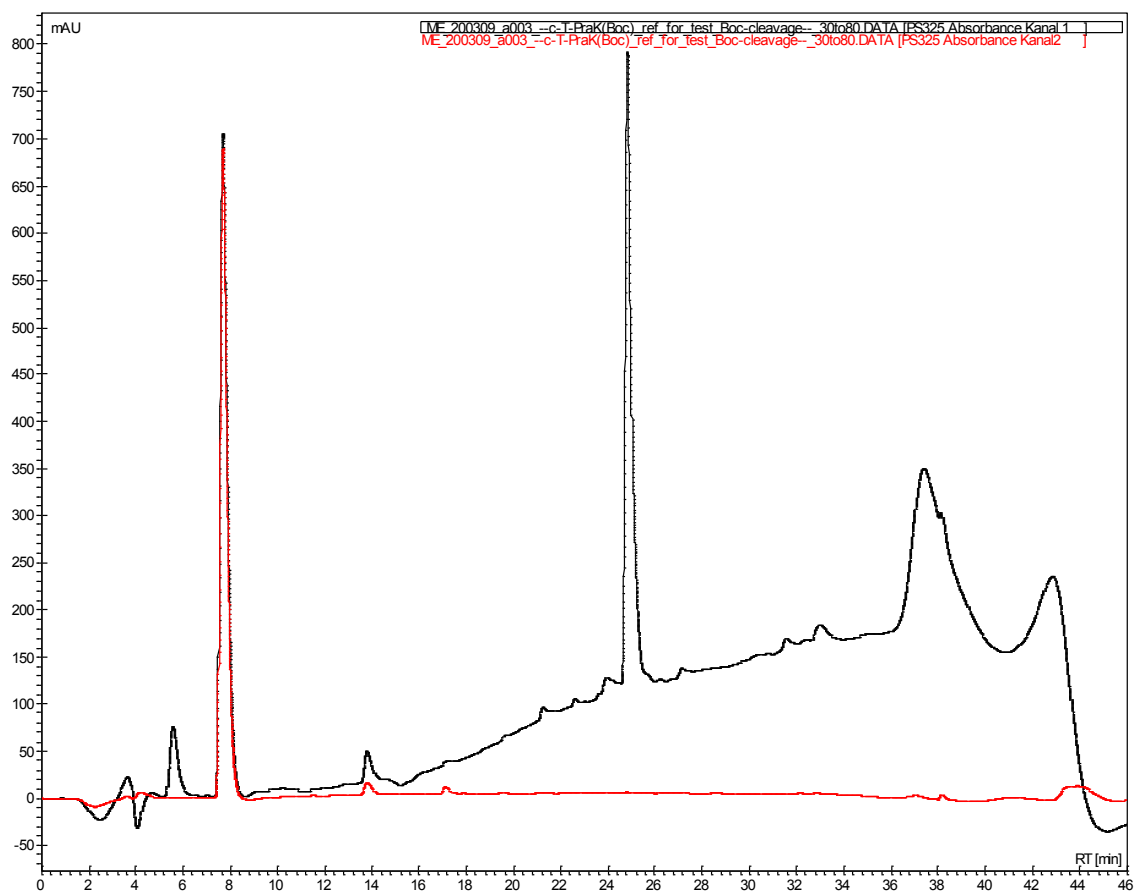


## PyBOP activation

Reference:  $\text{NH}_2\text{-Pra-Lys(Boc)-Pra-Pro-Gly-Pra-Ala-Pra-Pro-Gly-OH}$ 

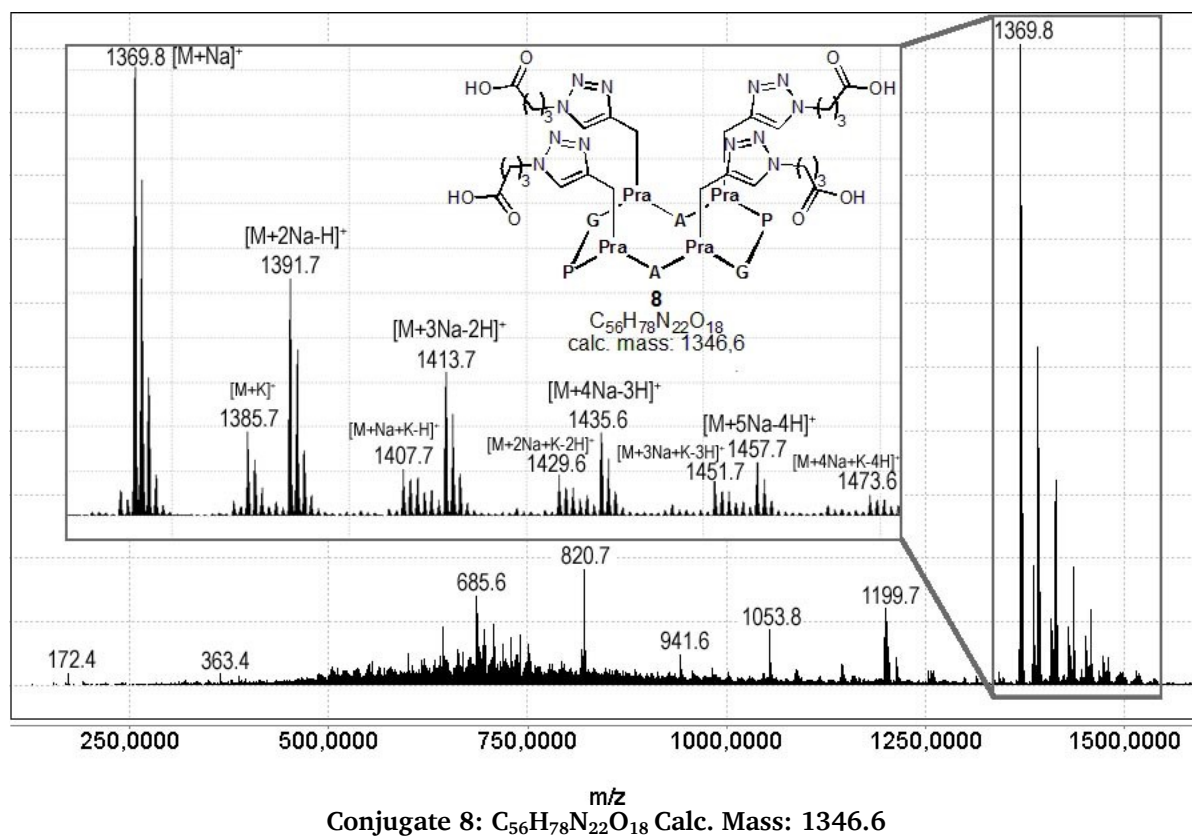
gradient: 30→80% methanol in 0.1% TFA over 30 minutes at 1 mL/min

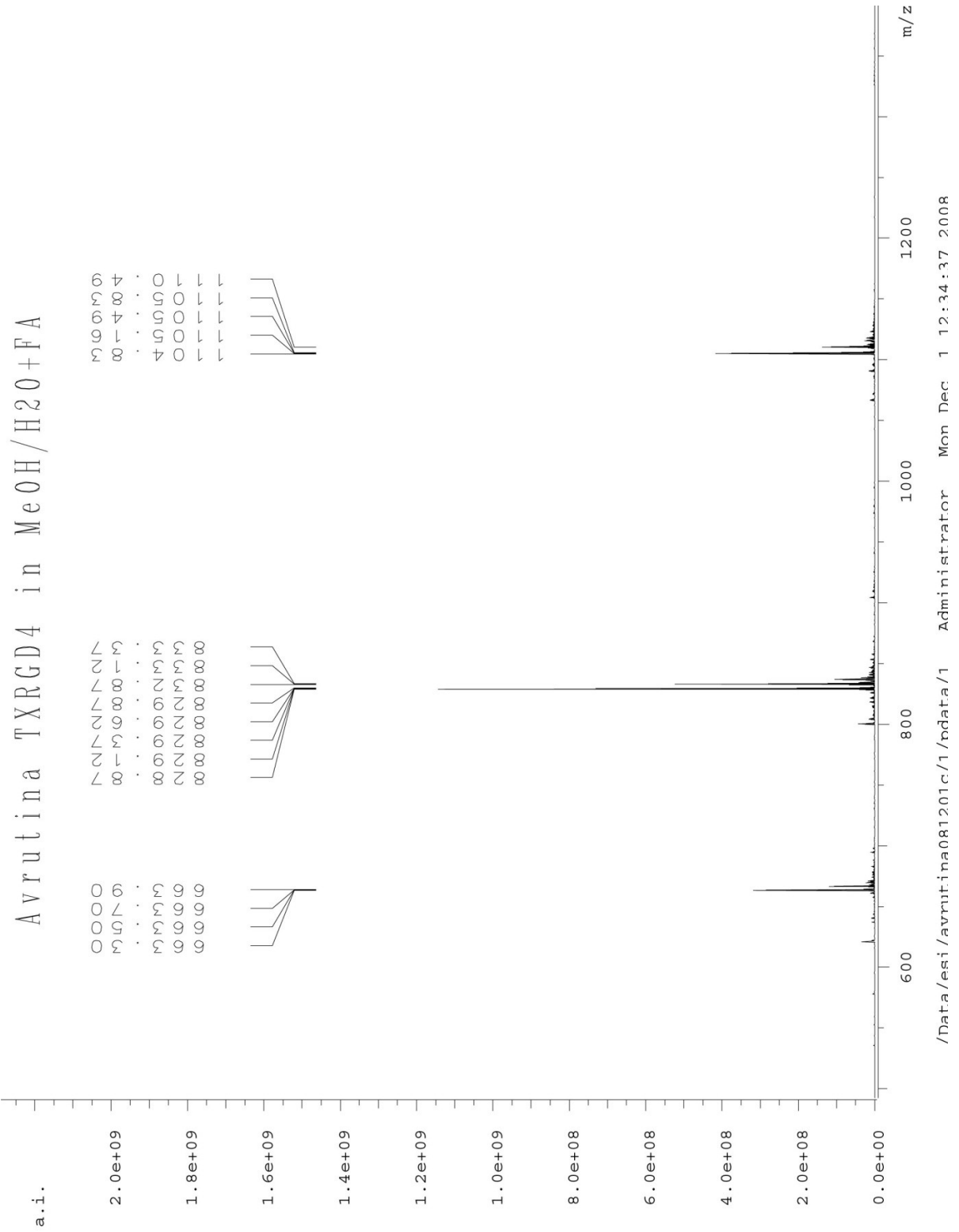
Reaction mixture:



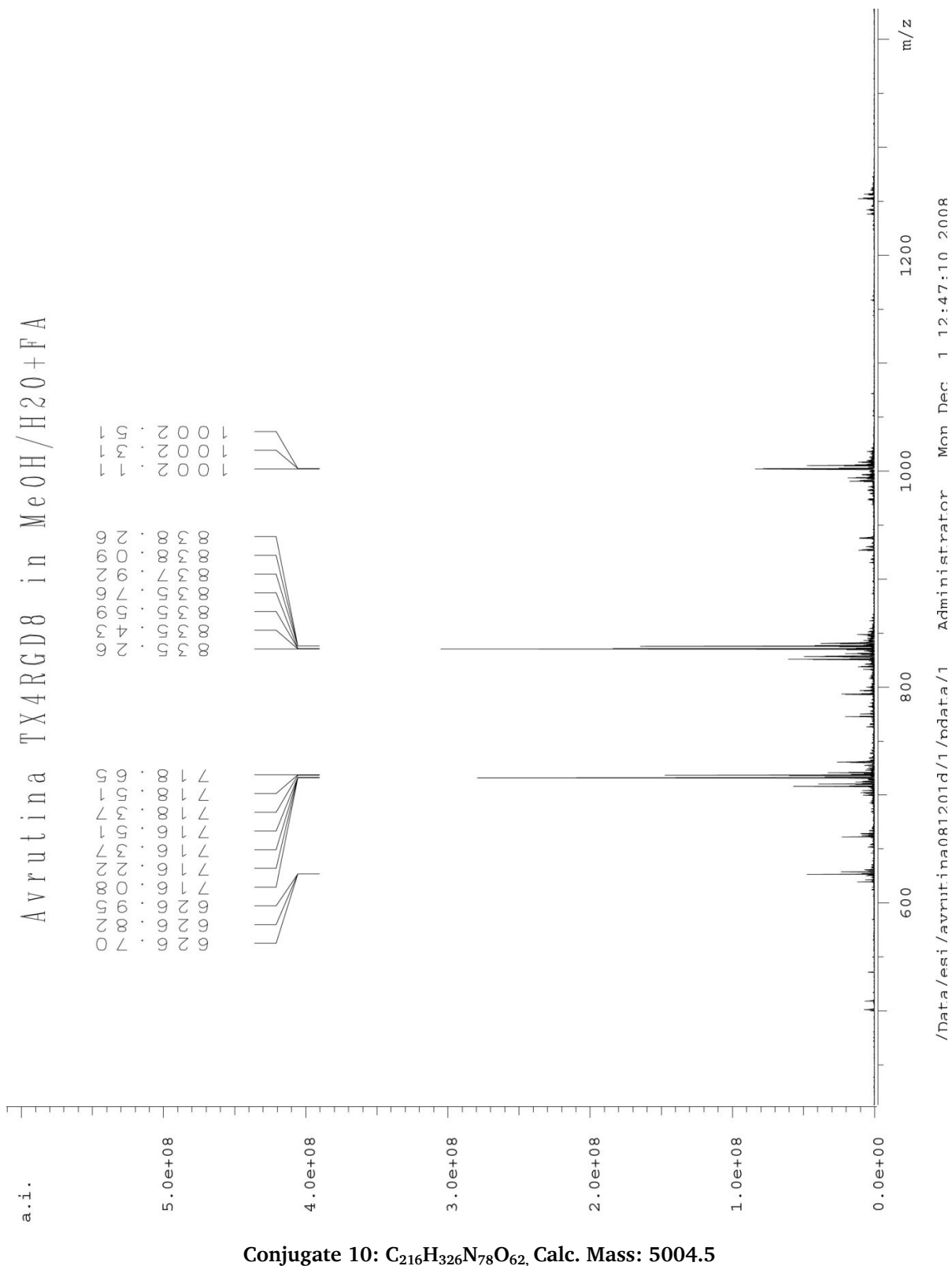
$R_f = 24$  min: *cyclo*-(Pra-Lys(Boc)-Pra-Pro-Gly-Pra-Ala-Pra-Pro-Gly)  
gradient: 30→80% methanol in 0.1% TFA over 30 minutes at 1 mL/min

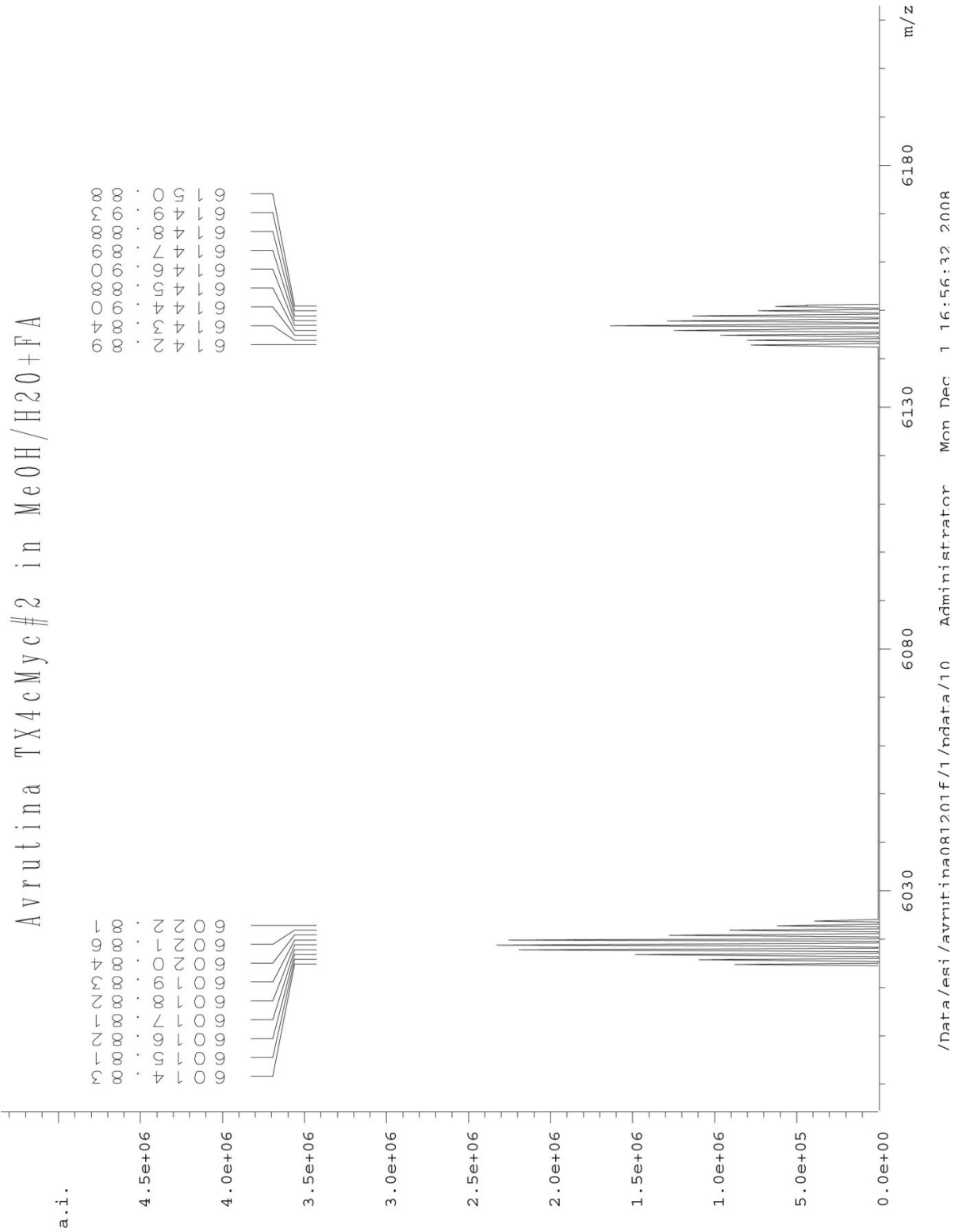
## 6.1.3 ESI-MS Spectra of Bioconjugates





Conjugate 9: C<sub>140</sub>H<sub>194</sub>N<sub>50</sub>O<sub>46</sub>, Calc. Mass: 3311.4

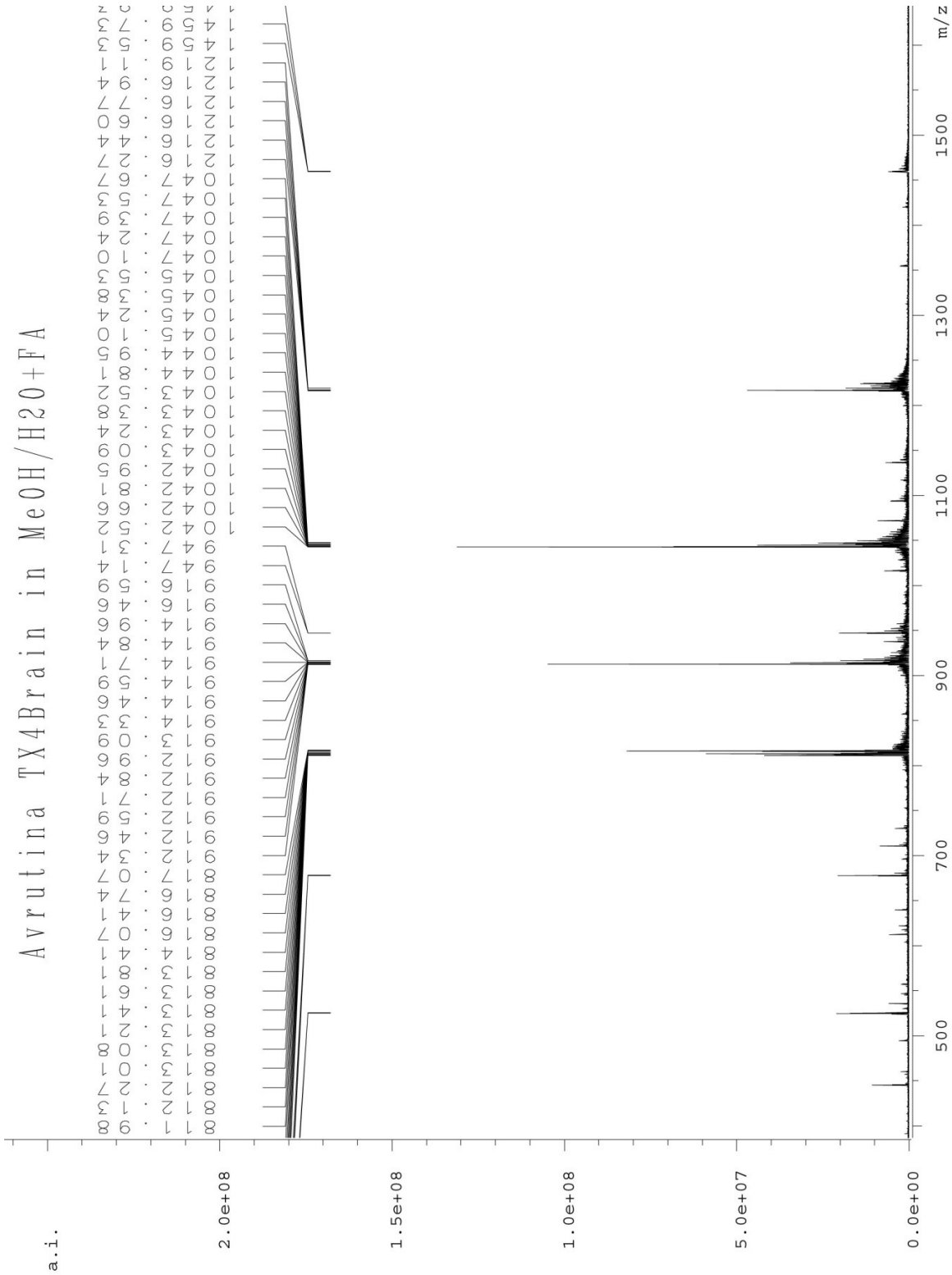




Conjugate 11:  $C_{256}H_{402}N_{74}O_{102}$ , Calc. Mass: 6144.9

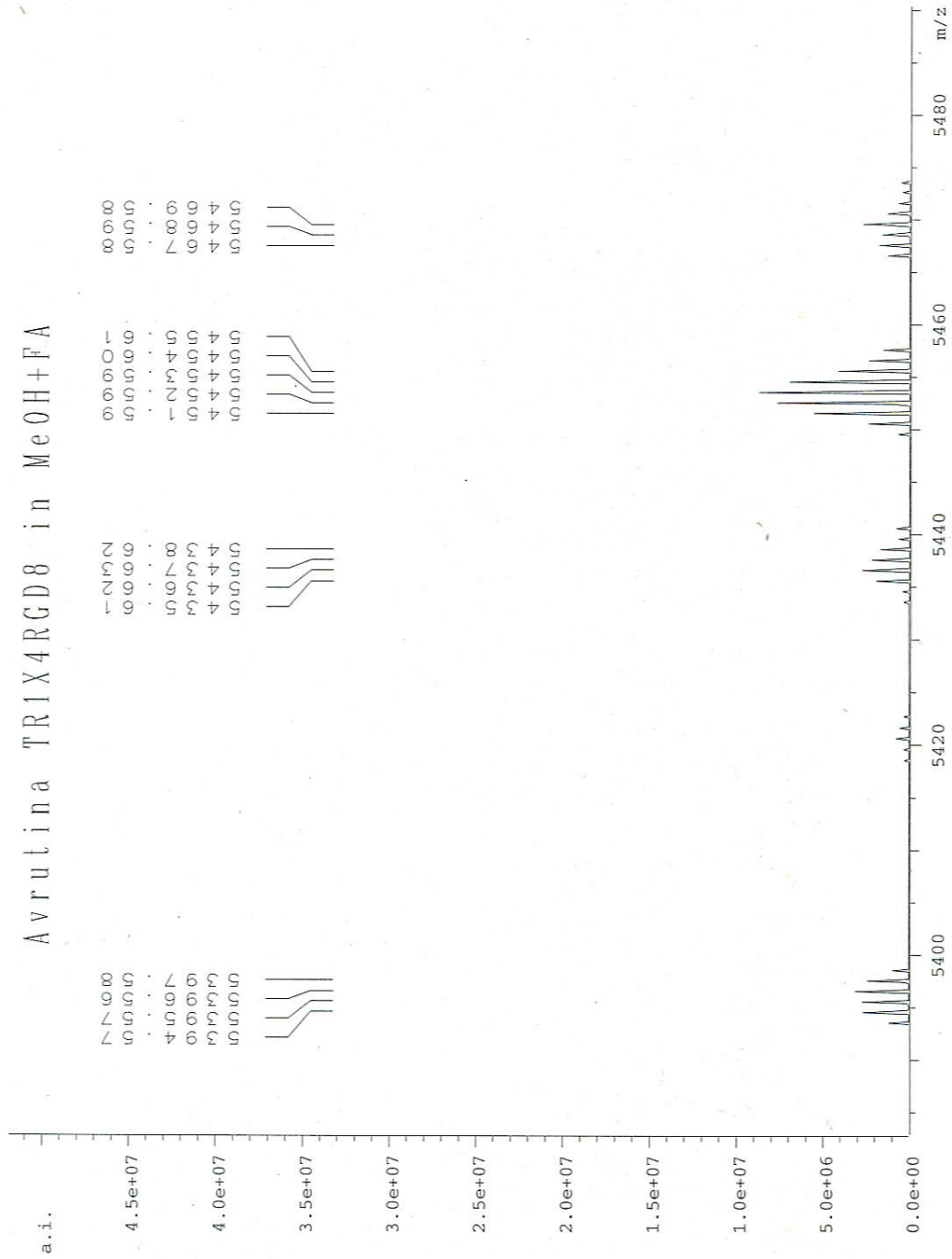


Avrutina TX4Brain in MeOH/H2O+FA



/Data/esi/avrutina081201b/1/odata/1 Administrator Mon Dec 1 12:28:28 2008

Conjugate 12:  $C_{324}H_{474}N_{106}O_{90}$ , Calc. Mass: 7289.6



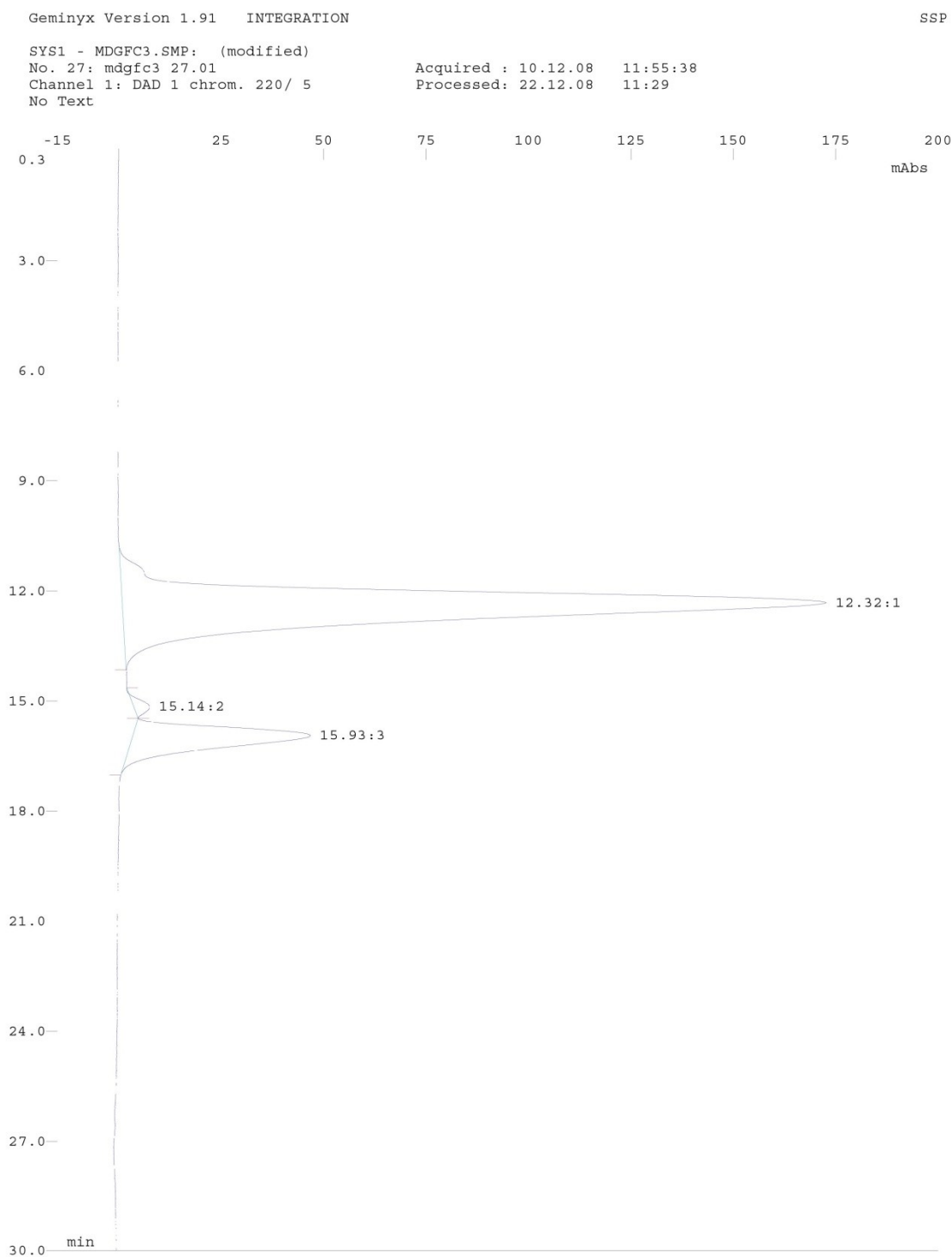
/Data/esi/avrutina090112a/1/pdata/10 Administrator Mon Jan 12 16:20:35 2009

Conjugate 13:  $C_{240}H_{344}N_{80}O_{67}S$ , Calc. Mass: 5450.6

## 6.1.4 GFC traces of Bioconjugates

GFC traces were recorded at 220 nm: (eluent: 150 m aq. NaCl at flow rate 0.75 mL / min).

### Conjugate 9

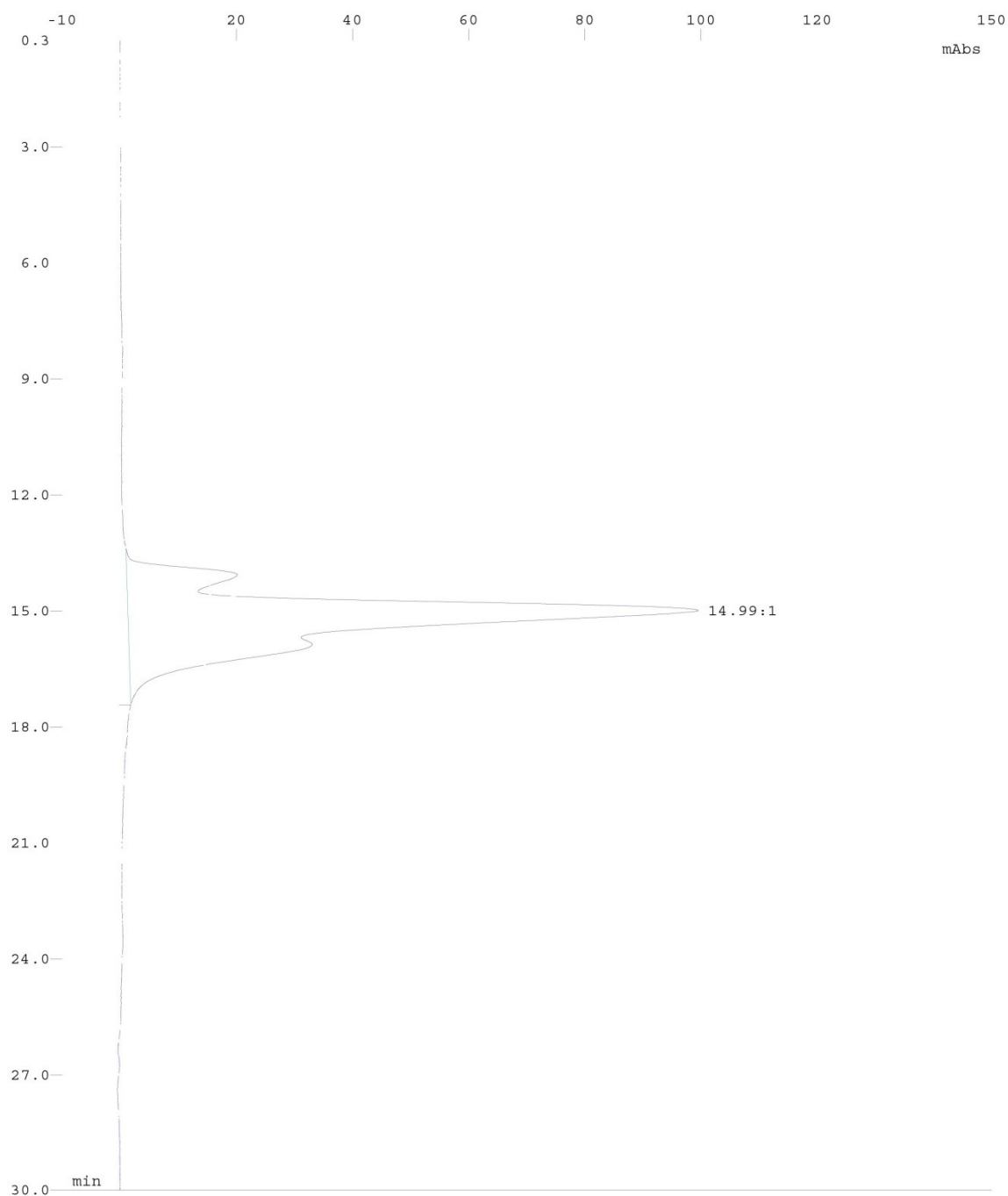


## Conjugate 10

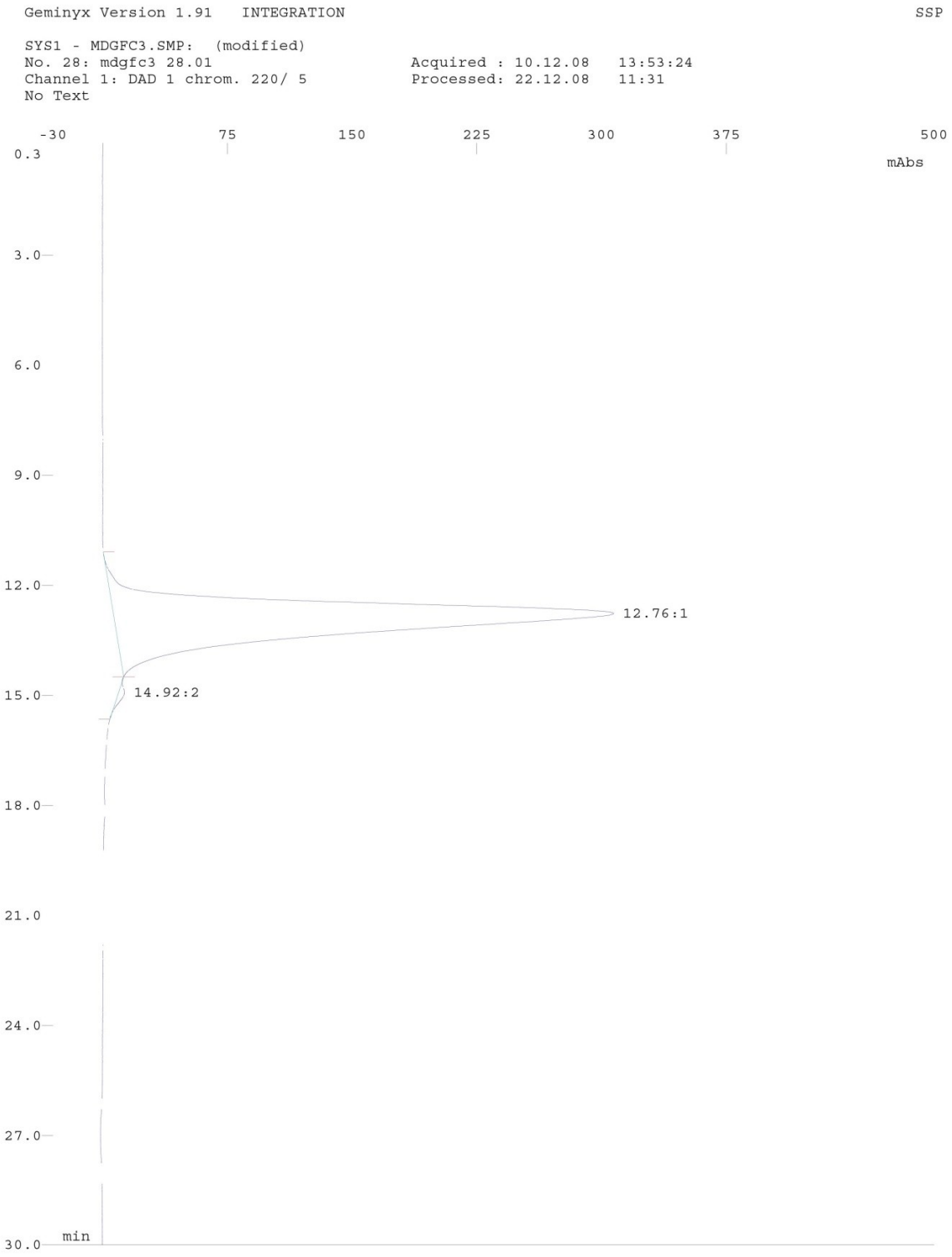
### Peptide ligand 5:

Geminyx Version 1.91 INTEGRATION

SSP

SYS1 - MDGFC3.SMP: (modified)  
No. 23: mdgfc3 23.01  
Channel 1: DAD 1 chrom. 220/ 5  
No TextAcquired : 10.12.08 09:44:56  
Processed: 22.12.08 11:16

Conjugation product 10:



## Conjugate 11

### Peptide ligand 6:

Geminyx Version 1.91 INTEGRATION

SSP

SYS1 - MDGFC3.SMP: (modified)

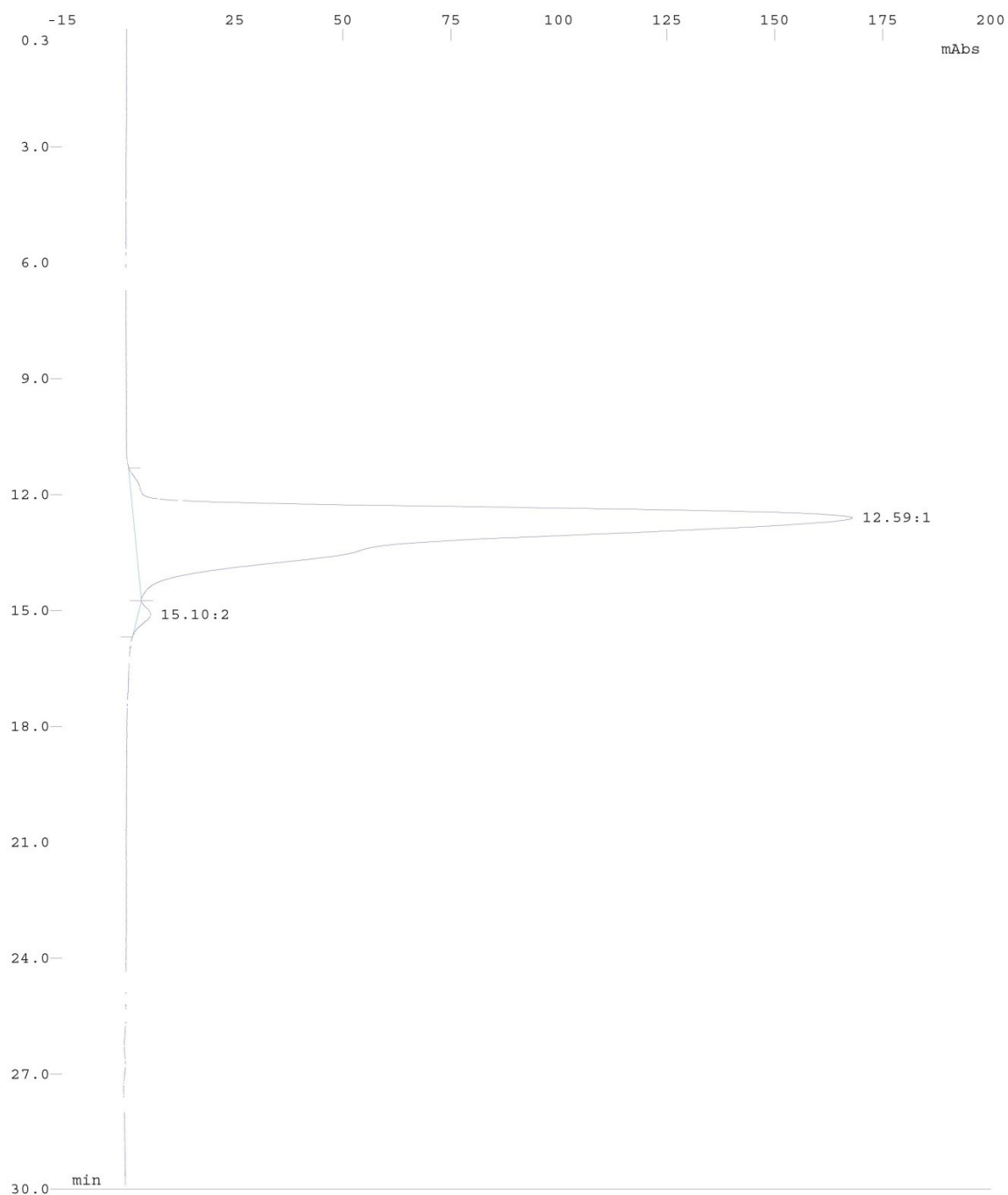
No. 24: mdgfc3 24.01

Channel 1: DAD 1 chrom. 220/ 5

No Text

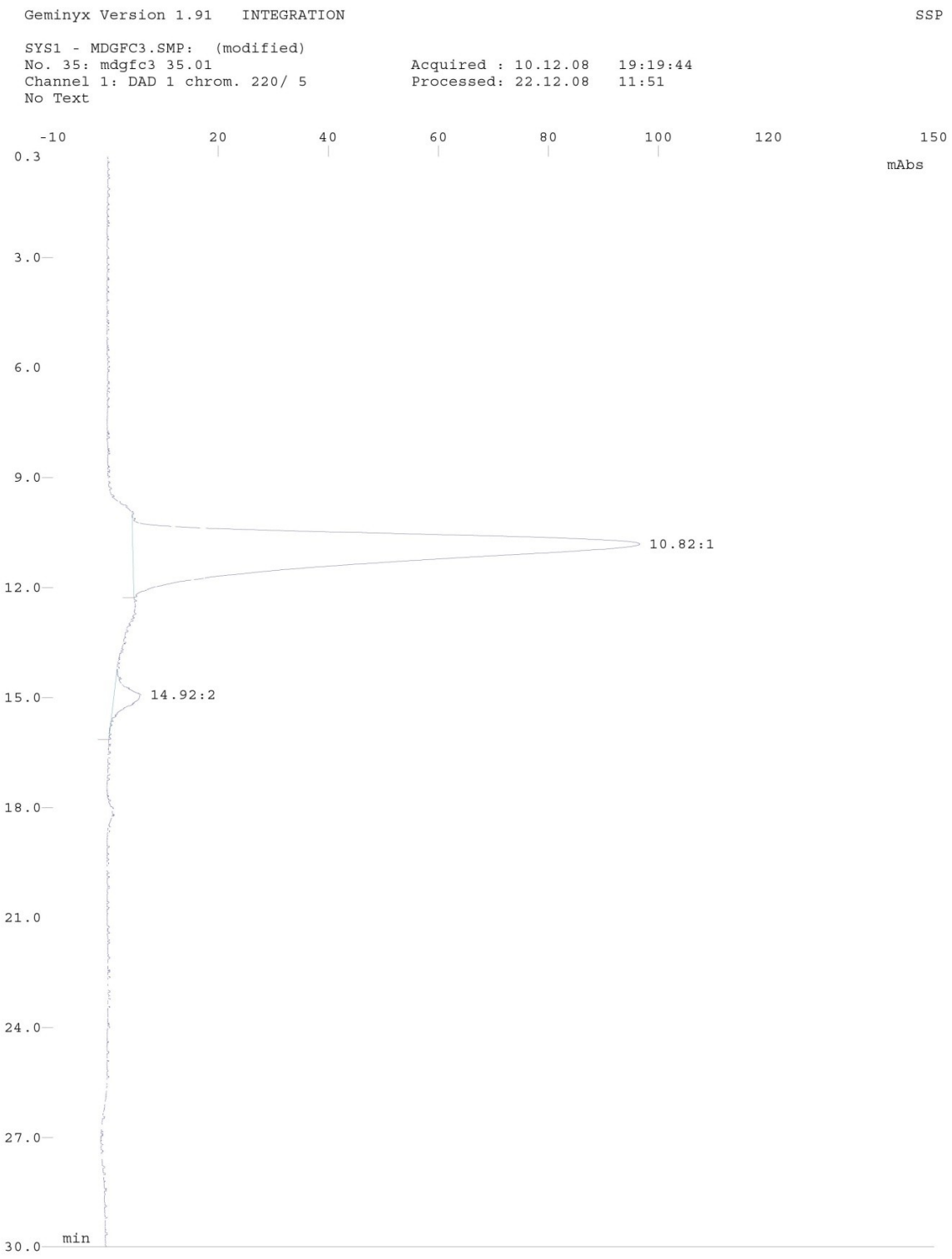
Acquired : 10.12.08 10:17:11

Processed: 22.12.08 11:22





Conjugation product 11:



## Conjugate 12

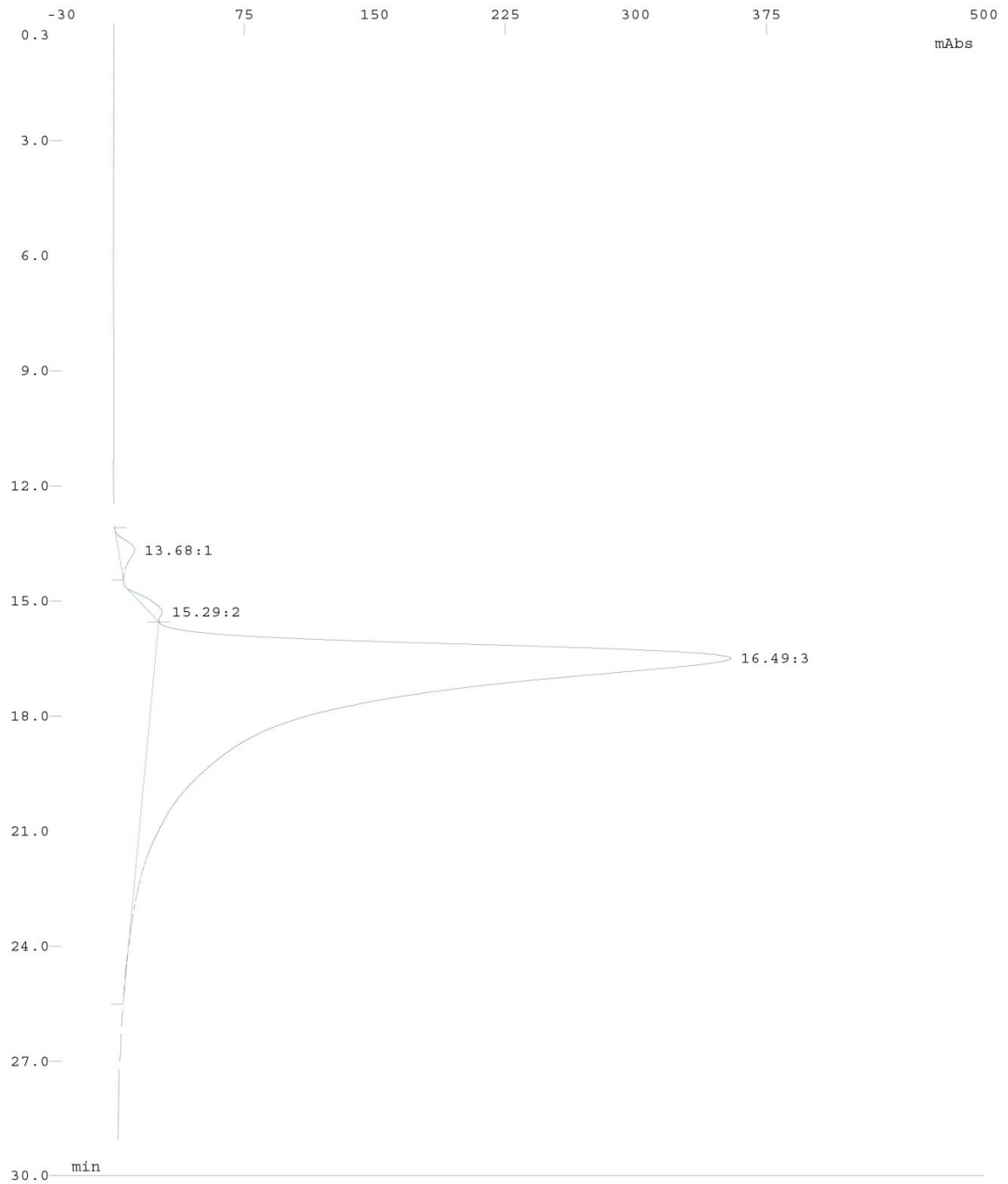
### Peptide ligand 7:

Geminyx Version 1.91 INTEGRATION

SSP

SYS1 - MDGFC3.SMP: (modified)  
No. 25: mdgfc3 25.01  
Channel 1: DAD 1 chrom. 220/ 5  
No Text

Acquired : 10.12.08 10:48:16  
Processed: 22.12.08 11:26



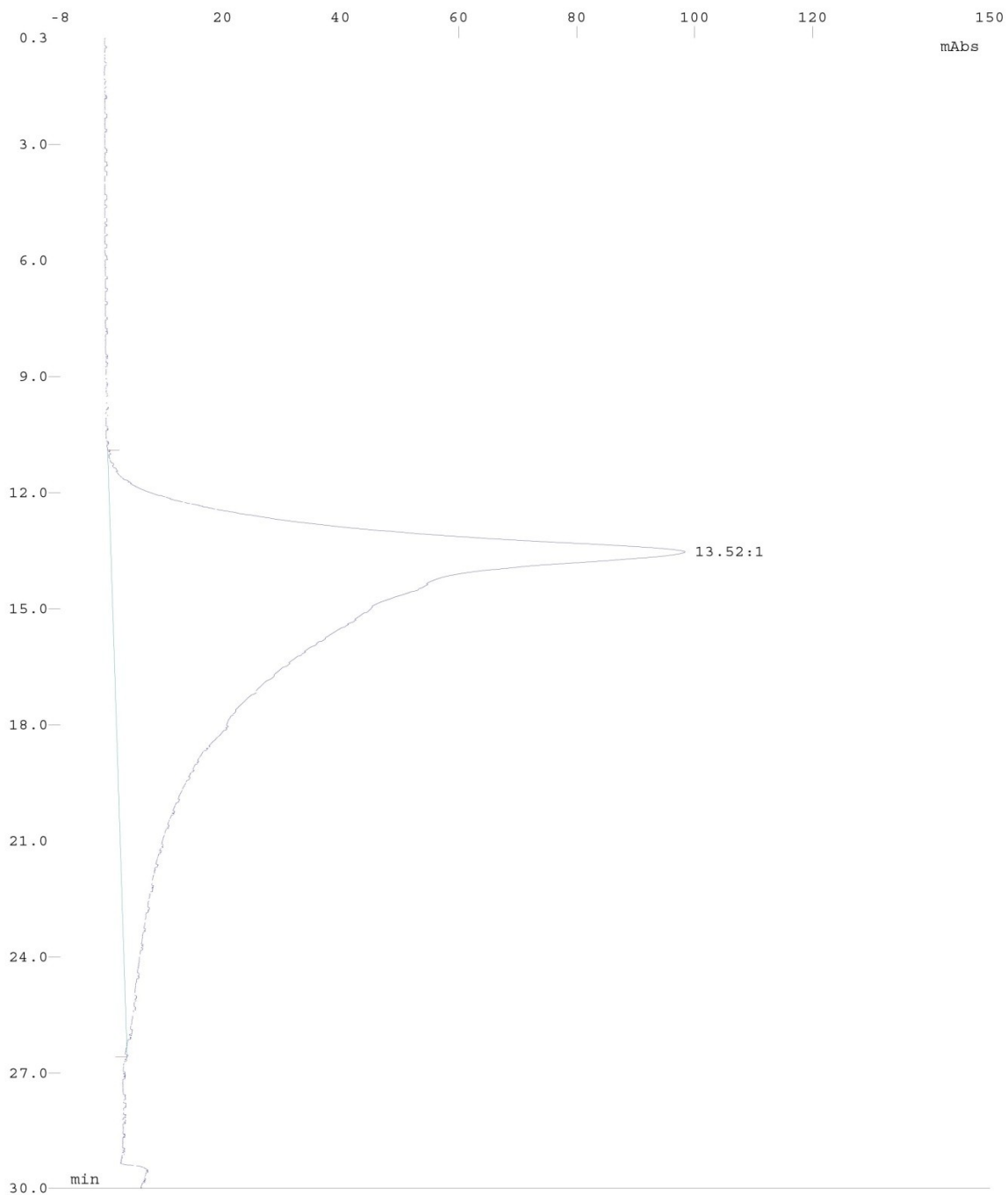
Conjugation product 12:

Geminyx Version 1.91 INTEGRATION

SSP

SYS1 - MDGFC3.SMP: (modified)  
No. 36: mdgfc3 36.01  
Channel 1: DAD 1 chrom. 220/ 5  
No Text

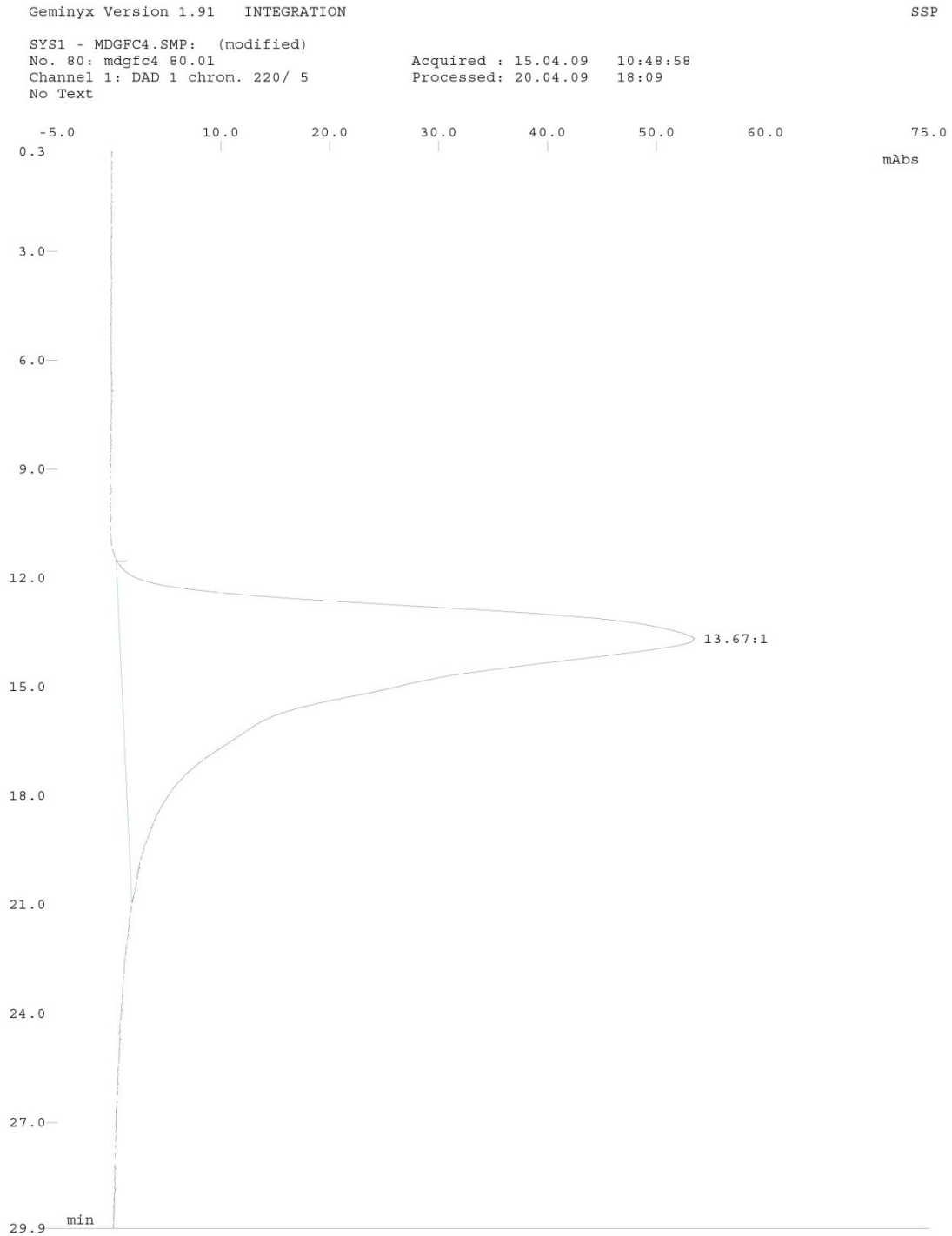
Acquired : 10.12.08 20:03:12  
Processed: 22.12.08 11:53



**Conjugate 13**

Peptide ligand 5 see "conjugate 10"

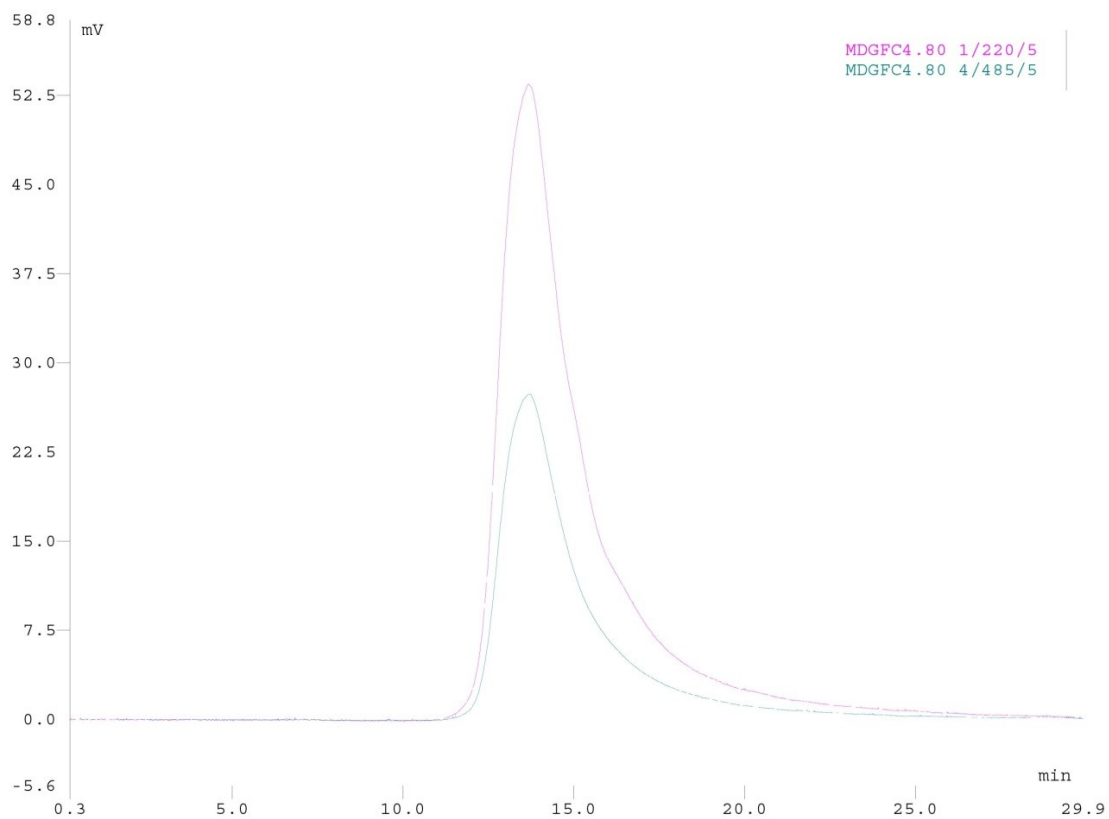
Conjugation product 13:



## GFC trace of 13 at 220 nm and 485 nm:

Geminyx Version 1.91 Chromatogram Overlay

SSP



## 6.2 Supporting Information for Chapter 2.2

### 6.2.1 Synthetic Procedures

#### General Information

Chemicals and solvents were purchased from Bachem, Iris Biotech, Novabiochem, Sigma-Aldrich, Rapp Polymere, Roth, or Varian (Agilent). Azide and alkyne building blocks Fmoc-*L*-propargylglycine (Fmoc-Pra-*OH*), Fmoc-*L*-azidoalanine (Fmoc-Aza-*OH*) and Fmoc-*L*-azidohomoalanine (Fmoc-Aha-*OH*) were obtained from Iris Biotech and chloro(pentamethylcyclopentadienyl)(cyclooctadiene)ruthenium(II) (Cp\**RuCl*(COD)) from Sigma-Aldrich.

Analytical HPLC was conducted with a Varian 920-LC system using a Phenomenex Hypersil 5u BDS C18 LC column (150 x 4.6 mm, 5  $\mu$ m, 130 Å). Semi-preparative RP-HPLC was performed on a Varian modular system comprising a PrepStar 218 Solvent Delivery Module, a ProStar 410 HPLC AutoSampler and a ProStar 325 Dual Wavelength UV-Vis HPLC Detector using a YMC J'sphere ODS-H80 C-18 LC column (250 x 20 mm, 4  $\mu$ m, 8 nm). The eluent system for analytical and semi-preparative HPLC consisted of eluent A (0.1% aq. TFA) and eluent B (90 % aq. acetonitrile containing 0.1% TFA).

ESI mass spectra were recorded with a Shimadzu LCMS-2020 equipped with a Phenomenex Jupiter 5u C4 LC column (50 x 1 mm, 5  $\mu$ m, 300 Å). The eluent system consisted of eluent A (0.1 % aq. formic acid, LC-MS grade) and eluent B (100 % acetonitrile containing 0.1% formic acid, LC-MS grade).

NMR studies were conducted on a Bruker DRX 300 instrument (300 MHz). All samples were dissolved in CD<sub>2</sub>Cl<sub>2</sub>. Resulting spectra were processed and analyzed using the MestReNova software (Mestrelab Research) and are given in section 5.

#### Synthesis of Azide and Alkyne Building Blocks for Fmoc-SPPS

**(2S)-2-Azido-propanoic acid (7).** A solution of sodium azide (5 g, 76.9 mmol) was dissolved in distilled H<sub>2</sub>O (13 mL) with CH<sub>2</sub>Cl<sub>2</sub> (22 mL) and cooled on an ice bath. Triflyl anhydride (2.5 mL, 14.9 mmol) is added slowly over 5 min with stirring continued for 2 h. The mixture was placed in a separatory funnel and the CH<sub>2</sub>Cl<sub>2</sub> phase was removed. The aqueous portion was extracted with CH<sub>2</sub>Cl<sub>2</sub> (2 x 20 mL). The organic fractions containing the triflyl azide were pooled and washed once with saturated Na<sub>2</sub>CO<sub>3</sub> and used without further purification. A mixture of *L*-alanine (715 mg, 8.0 mmol), K<sub>2</sub>CO<sub>3</sub> (1.63 g, 11.8 mmol), CuSO<sub>4</sub> pentahydrate (28 mg, 0.112 mmol) was dissolved in 75 mL H<sub>2</sub>O/methanol solution (1:2, v:v), and the prepared triflyl azide in CH<sub>2</sub>Cl<sub>2</sub> was added. The mixture was stirred at ambient temperature overnight. Subsequently, the organic solvents were removed under reduced pressure and the aqueous slurry was diluted with H<sub>2</sub>O (150 mL), acidified to pH 6 with conc. HCl, diluted with 150 mL phosphate buffer (0.25 M, pH 6.2), and extracted with EtOAc (4 x 80 mL) to remove sulfonamide by-product. The aqueous phase was then acidified to pH 2 with conc. HCl. The product was obtained from another round of EtOAc extractions (3 x 80 mL). These EtOAc extracts were combined, dried over MgSO<sub>4</sub>(s) and evaporated to dryness giving 828 mg of (2S)-2-azido-propanoic acid as a pale oil (90 % yield) with no need for further purification.

<sup>1</sup>H NMR (300 MHz, CD<sub>2</sub>Cl<sub>2</sub>)  $\delta$  = 11.20 (s, 1 H), 4.08 (q, *J* = 6 Hz, 1 H), 1.54 (d, *J* = 6 Hz, 3 H); <sup>13</sup>C NMR (75 MHz, CD<sub>2</sub>Cl<sub>2</sub>)  $\delta$  = 177.2, 57.1, 16.5. EI-MS: *m/z*: [M]<sup>+</sup> obsd. = 115.0 (calc = 115.04).

**(2S,3S)-*N*-(9-Fluorenylmethyloxycarbonyl)-1-ethynyl-2-methyl-butylamine (8) and (2S)-*N*-(9-fluorenylmethyloxycarbonyl)-2-ethynyl-pyrrolidine (9).** The respective Boc-protected Weinreb-amide (9.3 mmol) was dissolved in anhydrous CH<sub>2</sub>Cl<sub>2</sub> (75 mL), and the resulting



solution was cooled to  $-78\text{ }^{\circ}\text{C}$  in a dry ice/acetone bath. Diisobutylaluminum hydride (1 M in  $\text{CH}_2\text{Cl}_2$ , 13 mL, 13 mmol) was added dropwise, and the resulting mixture was stirred at  $-78\text{ }^{\circ}\text{C}$  for 45 min. Excess hydride was quenched by the addition of anhydrous MeOH (20 mL) and the resulting solution was warmed to  $0\text{ }^{\circ}\text{C}$  in ice/water bath. Potassium carbonate (2.8 g, 20 mmol) and dimethyl-(1-diazo-2-oxopropyl)phosphonate (Bestmann-Ohira reagent, 2.09 g, 10.8 mmol) were added to the reaction mixture. The resulting solution was stirred at room temperature for 19 h. The solvents were removed under reduced pressure, and the crude residue was dissolved in 200 mL EtOAc/ $\text{H}_2\text{O}$  mixture (1:1, v:v). The layers were partitioned, and the organic extracts were washed with water and dried over anhydrous  $\text{MgSO}_4(\text{s})$ . The solvent was removed under reduced pressure, and the pale oil purified by column chromatography (silica gel 60 0,040-0,063 mm, 230-300 mesh, eluent  $\text{CHCl}_3/\text{CH}_3\text{OH}$ , 100:1, v:v) to yield the Boc-protected intermediates (2*S*,3*S*)-*N*-(*tert*-butyloxycarbonyl)-1-ethynyl-2-methyl-butylamine (56 %) and (2*S*)-*N*-(*tert*-butyloxycarbonyl)-2-ethynyl-pyrrolidine (57 %), respectively.

Respective Boc-protected alkyne (4.7 mmol) was dissolved in 50 % TFA in  $\text{CH}_2\text{Cl}_2$  (10 mL) and stirred at room temperature for 90 min. The solvent was removed under reduced pressure to yield a pale oil. This oil was dissolved in 50 % acetone in  $\text{H}_2\text{O}$  (20 mL) and  $\text{Na}_2\text{CO}_3$  (611 mg, 5.7 mmol) was added. Fmoc-OSu (1.8 g, 5.3 mmol) was added stepwise while the pH was kept at 9-10 by addition of 1 M aq  $\text{Na}_2\text{CO}_3$ . After stirring overnight, EtOAc (20 mL) was added and the mixture was acidified with 6 M HCl. The organic layer was separated, washed with  $\text{H}_2\text{O}$  (4 times with 10 mL each) and dried over anhydrous  $\text{MgSO}_4$ . The organic solvents were removed under reduced pressure and the crude residue was washed with hexane to give alkynes **8** and **9** as white solids in 1.375 g and 1.459 g (85 % and 82 % yield), respectively.

**8**:  $^1\text{H}$  NMR (300 MHz,  $\text{CD}_2\text{Cl}_2$ )  $\delta$  = 7.82 (d,  $J$  = 9 Hz, 2 H), 7.65 (d,  $J$  = 9 Hz, 2 H), 7.4 (m, 4 H), 5.14 (d,  $J$  = 6 Hz, 1 H), 4.5 (m, 3 H), 4.26 (t,  $J$  = 6 Hz, 1 H), 2.80 (s, residual succinimide), 2.36 (d,  $J$  = 3 Hz, 1 H), 1.69-1.54 (m, 2 H), 1.27 (m, 1 H), 0.99 (m, 6 H);  $^{13}\text{C}$  NMR (75 MHz,  $\text{CD}_2\text{Cl}_2$ )  $\delta$  = 155.3, 144.0, 141.3, 127.7, 127.0, 125.0, 119.9, 81.5, 72.0, 66.7, 47.3, 39.2, 42.1, 25.9, 14.2, 11.3; ESI-MS:  $m/z$ :  $[\text{M}+\text{Na}]^+$  obsd. = 356.3 (calc = 356.16).

**9**:  $^1\text{H}$  NMR (300 MHz,  $\text{CD}_2\text{Cl}_2$ )  $\delta$  = 7.83-7.33 (m, 8 H), 4.59 (d,  $J$  = 3 Hz, 1 H), 4.5-4.30 (m, 3 H), 3.55 (s, 1 H), 3.42 (m, 1 H), 2.35 (s, 1 H), 2.15-1.98 (m, 4 H);  $^{13}\text{C}$  NMR (75 MHz,  $\text{CD}_2\text{Cl}_2$ )  $\delta$  = 154.27, 144.20, 141.27, 127.59, 126.95, 125.12, 119.85, 77.53; 69.91, 67.18, 48.34, 47.33, 45.89, 32.95, 24.45; ESI-MS:  $m/z$ :  $[\text{M}+\text{Na}]^+$  obsd. = 340.3 (calc = 340.13).

## Peptide Synthesis and Macrocyclization

**General Fmoc-SPPS procedure.** Peptides were synthesized in a Liberty 12-channel automated peptide synthesizer on a Discover SPS microwave peptide synthesizer platform (CEM) using the Fmoc strategy. All peptides were synthesized on a *Fmoc*-Asp(*t*Bu) preloaded TentaGel® S AC resin 0.22 mmol/g (Rapp Polymere). All amino acids were attached by double or triple coupling employing 4 eq of the corresponding amino acid, 4 eq of 2-(1H-benzotriazol-1-yl)-1,1,3,3-tetramethyluronium hexafluorophosphate (HBTU) and 8 eq of DIEA, or in case of cysteine 3-4 eq of 2,4,6-trimethylpyridine (collidine). Arginine and cysteine were coupled using a two step microwave program: 1. RT, 0 W, 25 min; 2.  $75\text{ }^{\circ}\text{C}$ , 25 W, 0.5 min (Arg) and 1. RT, 0 W, 2 min; 2.  $50\text{ }^{\circ}\text{C}$ , 25 W, 4 min (Cys), respectively. All other amino acids were coupled using a standard microwave program:  $75\text{ }^{\circ}\text{C}$ , 21 W, 5 min. Fmoc deprotection was achieved in two steps by reaction with 20% piperidine in DMF at  $75\text{ }^{\circ}\text{C}$ , 42 W, for 0.5 min (initial deprotection) followed by a second deprotection step with 20% piperidine in DMF at  $75\text{ }^{\circ}\text{C}$ , 42 W, for 3 min.

Cleavage of peptides from the solid support and removal of side chain protecting groups was achieved *via* acidolysis using a standard cleavage cocktail consisting of trifluoroacetic acid (TFA)/ $\text{H}_2\text{O}$ /anisole/triethylsilane (TES) (47:1:1:1, v:v:v:v) and 1,4-dithio-*D*-threitol (DDT). The resulting reaction mixture was shaken for 3 h at RT followed by precipitation and

subsequent washing (4×) with methyl *tert*-butyl ether (MTBE) to yield crude unprotected peptides.

**[Ala<sup>8</sup>]SFTI-1[1,14] (1).** The linear precursor GRCTKSIAPICFPD was synthesized according to the automated Fmoc-SPPS protocol on a 0.1 mmol scale. Acidolytic cleavage, ether precipitation and washing gave 109.9 mg of crude linear peptide (72.9 %). Oxidative macrocyclization was conducted with 10 mg (6.65 μmol) of reduced peptide in solution (1 mg/mL) in 100 mM (NH<sub>4</sub>)<sub>2</sub>CO<sub>3</sub> aq with 0.5 % (v:v) DMSO over three days at RT. The solvent was removed by freeze-drying followed by semi-preparative purification *via* HPLC to yield 3.7 mg (2.46 μmol, 27.1 % overall yield) of pure disulfide bridged peptide 1. RP-HPLC: Rt = 14.5 min, 18 % acetonitrile over 2 min followed by 18 %→41.5 % acetonitrile over 20 min in 0.1 % aq. TFA at flow rate 1 ml/min. ESI-MS: m/z: [M+2H]<sup>2+</sup> obsd. = 754.06 (calc = 753.37), [M+3H]<sup>3+</sup> obsd. = 503.13 (calc = 502.58), [M-H]<sup>-</sup> obsd. = 1504.09 (calc = 1503.71), [M-2H]<sup>2-</sup> obsd. = 751.85 (calc = 751.35).

**[Ala<sup>9</sup>]SFTI-1[1,14] (2).** The linear precursor GRCTKSIPAICFPD was synthesized according to the automated Fmoc-SPPS protocol on a 0.1 mmol scale. Acidolytic cleavage, ether precipitation and washing gave 137.6 mg of crude linear peptide (86.0 %). Oxidative macrocyclization was conducted with 10 mg (6.65 μmol) of reduced peptide in solution (1 mg/mL) in 100 mM (NH<sub>4</sub>)<sub>2</sub>CO<sub>3</sub> aq with 0.5 % (v:v) DMSO over three days at RT. The solvent was removed by freeze-drying followed by semi-preparative purification *via* HPLC to yield 1.0 mg (665 nmol, 9.1 % overall yield) of pure disulfide bridged peptide 1. RP-HPLC: Rt = 14.9 min, 18 % acetonitrile over 2 min followed by 18 %→41.5 % acetonitrile over 20 min in 0.1 % aq. TFA at flow rate 1 ml/min. ESI-MS: m/z: [M+2H]<sup>2+</sup> obsd. = 754.08 (calc = 753.37), [M+3H]<sup>3+</sup> obsd. = 503.10 (calc = 502.58), [M-H]<sup>-</sup> obsd. = 1504.09 (calc = 1503.71), [M-2H]<sup>2-</sup> obsd. = 751.84 (calc = 751.35).

**[Ica<sup>7,8</sup>]SFTI-1[1,14] (3) and [Ita<sup>7,8</sup>]SFTI-1[1,14] (4).** Peptide resin 10 (*H*-PIC(Trt)FPD(*t*Bu)-resin) was synthesized according to the automated Fmoc-SPPS protocol on a 0.25 mmol scale. Azide acid 7 was attached to the free *N*-terminus using HATU/DIEA activation under microwave irradiation (double coupling; conditions: 60 °C, 30 W, 60 min; 3 eq of acid 7, 2.9 eq HATU, 6 eq DIEA). The resulting peptide resin 12 was dried, weight (1.257 g) and splitted to use one half (0.125 mmol) for on resin RuAAC and the other (0.125 mmol) for on resin CuAAC, respectively.

**RuAAC attachment of alkyne 8.** Peptide resin 12 (0.125 mmol) was placed in a 20 mL syringe barrel suitable for Fmoc-SPPS fitted with a frit (syringe piston removed) and an argon line attached at the outlet nozzle. 166.5 mg of alkyne 8 (4 eq) were added in dry DMF (5 mL) from top, argon was bubbled through the mixture for 10 min. Then 9.5 mg Cp\*RuCl(COD) (20 mol% according to initial loading of the resin) were added from top and the reaction mixture was bubbled with argon for another 10 min. Then the syringe was carefully sealed with the syringe piston from top and with a cover at the outlet nozzle. The sealed syringe and an open reference syringe filled with DMF were placed in the manual Discover SPS microwave peptide synthesizer with the fiber-optic temperature probe measuring the temperature of the reference. After running the microwave program (60 °C, 30 W, 5 h) the solution was removed *via* filtration and the peptide resin was washed with methanol (3 times), 0.5 % sodium diethyldithiocarbamate in DMF (w/v, 3 times) DMF (3 times) and dichloromethane (DCM, 3 times). The peptide resin was dried to yield intermediate 14.

**CuAAC attachment of alkyne 8.** 166.5 mg of alkyne 8 (4 eq) were dissolved in dry DMF (5 mL) and 7 mg copper(II) sulfate pentahydrate (CuSO<sub>4</sub>·5H<sub>2</sub>O, 20 mol% of initial loading of the resin), 5 mg sodium ascorbate (NaAsc) and 170 μL DIEA were added. The yellowish suspension was added to peptide resin 12 (0.125 mmol) and the reaction mixture was shaken

at ambient temperature for 5 h. The solution was removed *via* filtration and the peptide resin was washed with methanol (3 times), 0.5 % sodium diethyldithiocarbamate in DMF (w/v, 3 times) DMF (3 times) and dichloromethane (DCM, 3 times). The peptide resin was dried to yield intermediate **15**.

Triazolyl peptide resins **14** and **15** were subjected to the automated Fmoc-SPPS procedure to assemble the *N*-terminal sequence GRCTKS using the described protocol. Subsequent acidolytic cleavage from the solid support, ether precipitation and washing gave 137 mg of crude linear 1,5-disubstituted 1,2,3-triazole containing peptide GRCTKS[IcA]PICFPD (72 %) and 137 mg of crude linear 1,4-disubstituted 1,2,3-triazole containing peptide GRCTKS[ItA]PICFPD (72 %).

Air-mediated oxidation of GRCTKS[IcA]PICFPD was conducted with 44 mg (26.15  $\mu$ mol) in solution (1 mg/mL) in 100 mM (NH<sub>4</sub>)<sub>2</sub>CO<sub>3</sub> aq over three days at RT. The solvent was removed by freeze-drying followed by semi-preparative purification *via* HPLC to yield 6.3 mg (4.12  $\mu$ mol, 11.3 % overall yield) of pure disulfide bridged peptide **3**. RP-HPLC: Rt = 13.6 min, 18 % acetonitrile over 2 min followed by 18 %→41.5 % acetonitrile over 20 min in 0.1 % aq. TFA at flow rate 1 ml/min. ESI-MS: m/z: [M+1H]<sup>+</sup> obsd. = 1530.01 (calc = 1529.74), [M+2H]<sup>2+</sup> 765.84 (calc = 765.37), [M+3H]<sup>3+</sup> obsd. = 510.87 (calc = 510.58), [M-H]<sup>-</sup> obsd. = 1528.0 (calc = 1527.72), [M-2H]<sup>2-</sup> obsd. = 763.75 (calc = 763.35).

Air-mediated oxidation of GRCTKS[ItA]PICFPD was conducted with 48 mg (31.38  $\mu$ mol) in solution (1 mg/mL) in 100 mM (NH<sub>4</sub>)<sub>2</sub>CO<sub>3</sub> aq over three days at RT. The solvent was removed by freeze-drying followed by semi-preparative purification *via* HPLC to yield 5.3 mg (3.46  $\mu$ mol, 7.9 % overall yield) of pure disulfide bridged peptide **4**. RP-HPLC: Rt = 15.35 min, 18 % acetonitrile over 2 min followed by 18 %→41.5 % acetonitrile over 20 min in 0.1 % aq. TFA at flow rate 1 ml/min. ESI-MS: m/z: [M+2H]<sup>2+</sup> obsd. = 765.80 (calc = 765.37), [M+3H]<sup>3+</sup> obsd. = 510.87 (calc = 510.58), [M-H]<sup>-</sup> obsd. = 1527.96 (calc = 1527.72), [M-2H]<sup>2-</sup> obsd. = 763.74 (calc = 763.35).

**[PcA<sup>8,9</sup>]SFTI-1[1,14] (5) and [PtA<sup>8,9</sup>]SFTI-1[1,14] (6)**. Peptide resin **11** (H-IC(Trt)FPD(tBu)-resin) was synthesized according to the automated Fmoc-SPPS protocol on a 0.2 mmol scale. Azide acid **7** was attached to the free *N*-terminus using HATU/DIEA activation under microwave irradiation (double coupling; conditions: 60 °C, 30 W, 60 min; 3 eq of acid **7**, 2.9 eq HATU, 6 eq DIEA). The resulting peptide resin **13** was dried and split into two charges: one half (0.1 mmol) for on resin RuAAC and the other (0.1 mmol) for on resin CuAAC.

*RuAAC attachment of alkyne 9*. Peptide resin **13** (0.1 mmol) was placed in a 20 mL syringe barrel suitable for Fmoc-SPPS fitted with a frit (syringe piston removed) and an argon line attached at the outlet nozzle. 159 mg of alkyne **9** (5 eq) were added in dry DMF (6 mL) from top, argon was bubbled through the mixture for 20 min. Then 8 mg Cp\**Ru*Cl(COD) (20 mol% of initial loading of the resin) were added from top and the reaction mixture was bubbled with argon for another 10 min. Then the syringe was carefully sealed with the syringe piston from top and with a cover at the outlet nozzle. The sealed syringe and an open reference syringe filled with DMF were placed in the manual Discover SPS microwave peptide synthesizer with the fiber-optic temperature probe measuring the temperature of the reference. After running the microwave program (60 °C, 30 W, 5 h) the solution was removed *via* filtration and the peptide resin was washed with methanol (3 times), 0.5 % sodium diethyldithiocarbamate in DMF (w/v, 3 times) DMF (3 times) and dichloromethane (DCM, 3 times). The peptide resin was dried to yield intermediate **16**.

*CuAAC attachment of alkyne 9*. 159 mg of alkyne **9** (5 eq) were dissolved in dry DMF (5 mL) and 5 mg copper(II) sulfate pentahydrate (CuSO<sub>4</sub>·5H<sub>2</sub>O, 20 mol% of initial loading of the resin), 6 mg sodium ascorbate (NaAsc) and 122  $\mu$ L DIEA were added. The yellowish suspension was added to peptide resin **13** (0.1 mmol) and the reaction mixture was shaken at

ambient temperature for 5 h. The solution was removed *via* filtration and the peptide resin was washed with methanol (3 times), 0.5 % sodium diethyldithiocarbamate in DMF (w/v, 3 times) DMF (3 times) and dichloromethane (DCM, 3 times). The peptide resin was dried to yield intermediate **17**.

Triazolyl peptide resins **16** and **17** were subjected to an automated Fmoc-SPPS procedure to assemble the *N*-terminal sequence GRCTKSI using the described protocol. Subsequent acidolytic cleavage from the solid support, ether precipitation and washing gave 65.1 mg of crude linear 1,5-disubstituted 1,2,3-triazol containing peptide GRCTKSI[PcA]ICFPD (43 %) and 89.2 mg of crude linear 1,4-disubstituted 1,2,3-triazol containing peptide GRCTKSI[PtA]ICFPD (59.2 %).

DMSO-mediated oxidation of GRCTKSI[PcA]ICFPD was conducted with 10 mg (6.54  $\mu$ mol) in solution (1 mg/mL) in 100 mM (NH<sub>4</sub>)<sub>2</sub>CO<sub>3</sub> aq with 0.5 % (v:v) DMSO over three days at RT. The solvent was removed by freeze-drying followed by semi-preparative purification *via* HPLC to yield 1.4 mg (916 nmol, 13.2 % overall yield) of pure disulfide bridged peptide **5**. RP-HPLC: Rt = 15.6 min, 18 % acetonitrile over 2 min followed by 18 %→41.5 % acetonitrile over 20 min in 0.1 % aq. TFA at flow rate 1 ml/min. ESI-MS: m/z: [M+2H]<sup>2+</sup> obsd. = 766.03 (calc = 765.37), [M+3H]<sup>3+</sup> obsd. = 511.12 (calc = 510.58), [M-H]<sup>-</sup> obsd. = 1528.16 (calc = 1527.72), [M-2H]<sup>2-</sup> obsd. = 763.94 (calc = 763.35).

DMSO-mediated oxidation of GRCTKSI[PtA]ICFPD was conducted with 10 mg (6.54  $\mu$ mol) in solution (1 mg/mL) in 100 mM (NH<sub>4</sub>)<sub>2</sub>CO<sub>3</sub> aq with 0.5 % (v:v) DMSO over three days at RT. The solvent was removed by freeze-drying followed by semi-preparative purification *via* HPLC to yield 1.8 mg (3.46  $\mu$ mol, 10.5 % overall yield) of pure disulfide bridged peptide **6**. RP-HPLC: Rt = 15.2 min, 18 % acetonitrile over 2 min followed by 18 %→41.5 % acetonitrile over 20 min in 0.1 % aq. TFA at flow rate 1 ml/min. ESI-MS: m/z: [M+2H]<sup>2+</sup> obsd. = 765.98 (calc = 765.37), [M+3H]<sup>3+</sup> obsd. = 511.15 (calc = 510.58), [M-H]<sup>-</sup> obsd. = 1528.0 (calc = 1527.72), [M-2H]<sup>2-</sup> obsd. = 763.85 (calc = 763.35).

## 6.2.2 Trypsin Inhibition Assays

### General

Kinetic curves were recorded by monitoring the absorption of the corresponding samples in 96-well plates (NUNC, flat bottom, clear) at 405 nm in intervals of 60 sec over 30 min at RT using the Tecan GENios microplate reader. All experiments were performed in triplicate. Trypsin from bovine pancreas (Sigma) was standardized by active-site titration with *p*-nitrophenyl-*p*'-guanidinobenzoate (NPGb) in phosphate buffered saline (PBS: 137 mM NaCl, 2.7 mM KCl, 10.0 mM Na<sub>2</sub>HPO<sub>4</sub>, 1.76 mM KH<sub>2</sub>PO<sub>4</sub>, pH 7.4).

### Determination of Michaelis-Menten Constant (K<sub>M</sub>) for Boc-QAR-pNA

The initial reaction rate ( $v_i$ ) of the proteolytic degradation of Boc-QAR-pNA (Bachem) by bovine Trypsin (100 nM) was determined for a series of concentrations ([S]<sub>i</sub>) of the chromogenic substrate (5000  $\mu$ M – 500  $\mu$ M). The Michaelis-Menten constant (K<sub>M</sub>) was calculated *via* Lineweaver-Burk plot (reciprocal initial reaction rate (1/ $v_i$ ) versus the reciprocal substrate concentration 1/[S]<sub>i</sub>) and linear regression of the resulting data. The experiment was performed in triplicate yielding K<sub>M</sub> as 41.70±6.21  $\mu$ M (arithmetic mean, standard deviation given as error).

### Determination of Apparent Inhibition Constant (K<sub>i</sub><sup>app</sup>) of SFTI Derivatives 1-6

The normalized residual proteolytic activity ( $v/v_0$ ) of trypsin towards the chromogenic

substrate Boc-QAR-pNA (250  $\mu$ M, Bachem) at different concentrations of linear and monocyclic SFTI-1 analogues 1-6 ( $I_0$ ) was determined for  $\sim$  0.5 nM active enzyme ( $E_0$ ) in buffer (50 mM Tris/HCl, 150 mM NaCl, 0.01% Triton X-100, 0.01% sodium azide, pH 7.6). The apparent inhibition constants ( $K_i^{app}$ ) were calculated through fitting the Morrison equation for tight binding inhibitors (1) onto the resulting kinetic data with the Marquardt-Levenberg algorithm of SigmaPlot 11.

$$\frac{v}{v_0} = 1 - \frac{(E_0 + I_0 + K_i^{app}) - \sqrt{(E_0 + I_0 + K_i^{app})^2 - 4E_0I_0}}{2E_0} \quad (1)$$

**Table S1.** Apparent inhibitory constants of compounds 1-6 and monocyclic SFTI-1[1,14] (wt, Ref. 13 from main text).

Entry	Name	Sequence	$K_i^{app}$ / nM <sup>[a]</sup>
1	[Ala <sup>8</sup> ]SFTI-1[1,14]	GRCTKSIAPICFPD	178 $\pm$ 25
2	[Ala <sup>9</sup> ]SFTI-1[1,14]	GRCTKSIPAICFPD	22.2 $\pm$ 2.6
3	[IcA <sup>7,8</sup> ]SFTI-1[1,14]	GRCTKS[IcA]PICFPD	236 $\pm$ 22
4	[ItA <sup>7,8</sup> ]SFTI-1[1,14]	GRCTKS[ItA]PICFPD	2109 $\pm$ 221
5	[PcA <sup>8,9</sup> ]SFTI-1[1,14]	GRCTKSI[PcA]ICFPD	1787 $\pm$ 187
6	[PtA <sup>8,9</sup> ]SFTI-1[1,14]	GRCTKSI[PtA]ICFPD	44.0 $\pm$ 11.4
wt	SFTI-1[1,14]	GRCTKSIPPICFPD	1.48 $\pm$ 0.1

[a] Error of  $K_i^{app}$  is given as the standard error of the global non-linear regression.

### Calculation of Substrate Independent Inhibition Constant ( $K_i$ ) of SFTI Derivatives 1-6

Substrate independent inhibition constant  $K_i$  was calculated from  $K_i^{app}$  and  $K_M$  using the equation (2) (with  $[S] \equiv$  concentration of chromogenic substrate Boc-QAR-pNA used for  $K_i^{app}$  determination).

$$K_i = \frac{K_i^{app}}{\left(1 + \frac{[S]}{K_M}\right)} \quad (2)$$

The error of  $K_i$  ( $\Delta K_i$ ) was calculated by propagation of errors of  $K_i^{app}$  and  $K_M$  using the following approach:

$$\rightarrow \Delta K_i^2 = \left| \frac{\partial K_i}{\partial K_i^{app}} \right|^2 \cdot (\Delta K_i^{app})^2 + \left| \frac{\partial K_i}{\partial K_M} \right|^2 \cdot (\Delta K_M)^2 \quad (3)$$

$$\rightarrow \Delta K_i = \sqrt{\left| \frac{\partial K_i}{\partial K_i^{app}} \right|^2 \cdot (\Delta K_i^{app})^2 + \left| \frac{\partial K_i}{\partial K_M} \right|^2 \cdot (\Delta K_M)^2} \quad (4)$$

Differentiation of  $K_i$  with respect to  $K_i^{app}$  yields:

$$\rightarrow \frac{\partial K_i}{\partial K_i^{app}} = \frac{1}{\left(1 + \frac{[S]}{K_M}\right)} \quad (5)$$

Differentiation of  $K_i$  with respect to  $K_M$ :

using  $K_i = K_i^{app} \left(1 + \frac{[S]}{K_M}\right)^{-1}$  and chain rule for differentiation yields:

$$\frac{\partial K_i}{\partial K_M} = \left( -\frac{K_i^{app}}{\left(1 + \frac{[S]}{K_M}\right)^2} \right) \cdot \left( -\frac{[S]}{K_M^2} \right) \quad \text{and, thus:}$$

$$\rightarrow \frac{\partial K_i}{\partial K_M} = \frac{K_i^{app} \cdot [S]}{\left(1 + \frac{[S]}{K_M}\right)^2 \cdot (K_M)^2} \quad (6)$$

Combination of (4), (5) and, (6) gives the final formula for calculating the error of  $K_i$ :

$$\rightarrow \Delta K_i = \sqrt{\left( \frac{1}{\left(1 + \frac{[S]}{K_M}\right)^2} \right)^2 \cdot (\Delta K_i^{app})^2 + \left( \frac{K_i^{app} \cdot [S]}{\left(1 + \frac{[S]}{K_M}\right)^2 \cdot (K_M)^2} \right)^2 \cdot (\Delta K_M)^2} \quad (7)$$

### 6.2.3 3. Crystallography

#### Trypsin Crystallization, Soaking, and Data Collection

Trypsin crystals for soaking were obtained by mixing equal volumes of protein solution with precipitant solution (1.85-2 M  $(\text{NH}_4)_2\text{SO}_4$ , 50 mM Tris, pH 8.5). To 10  $\mu\text{L}$  of protein solution (30-60 mg/mL bovine pancreas trypsin (Sigma T1426), 0.3 M  $(\text{NH}_4)_2\text{SO}_4$ , 60 mM benzamidine, 6 mM  $\text{CaCl}_2$ , 0.1 M Tris, pH 8.15) 0.5  $\mu\text{L}$  DMF were added prior to crystallization (modified from Luckett, S. et al (1999); Ref. 17 from main text). Crystals grew in hanging-drop vapor-diffusion plates (EasyXtal; QIAGEN) at 19 °C and after 1-2 weeks resulting crystals were used for soaking with  $[\text{IcA}^{7,8}]\text{SFTI-1}[1,14]$  or  $[\text{PtA}^{8,9}]\text{SFTI-1}[1,14]$ . The complexes of trypsin and modified inhibitors were obtained by adding small amounts of lyophilized peptidomimetic directly to crystallization wells which were left overnight at 19 °C. This procedure was repeated twice. In total, crystals were soaked for 8 days with  $[\text{PtA}^{8,9}]\text{SFTI-1}[1,14]$  and 3 weeks with  $[\text{IcA}^{7,8}]\text{SFTI-1}[1,14]$ .

Prior to flash-freezing in liquid nitrogen, crystals were cryoprotected with 25% (v/v) glycerol. X-ray diffraction data were collected at 100 K on a Rigaku MicroMax 7HF Cu anode equipped with a Saturn 944+ detector (home source) using a 2Theta angle with 15-25° to gain a resolution up to 1.4 Å. Data were indexed, integrated, and scaled with HKL2000.<sup>[S1]</sup> Phases were obtained with *Phaser*.<sup>[S2]</sup> using trypsin coordinates (PDB code: 1SFI) as a search model. The coordinates were refined with *Refmac5*<sup>[S3]</sup> from the CCP4 suite<sup>[S4]</sup> and manually checked and corrected with *COOT*.<sup>[S3]</sup> The peptidic inhibitors were manually modeled with *COOT*.<sup>[S3]</sup> Jligand (Version 1.0.25) from the CCP4 suite was used to get initial restraints for each triazole, which were manually optimized based on small molecule data.<sup>[S5]</sup> Crystallographic data collection and refinement statistics are summarized in Table S2. Unbiased  $F_o - F_c$  and final refined  $2F_o - F_c$  electron density maps for  $[\text{IcA}^{7,8}]\text{SFTI-1}[1,14]$  and  $[\text{PtA}^{8,9}]\text{SFTI-1}[1,14]$  are shown in Figure S1 and S2, respectively. Figures were prepared using *PyMOL*.<sup>[S6]</sup>



**Table S3.** Crystallographic data collection (A) and refinement statistics (B) of [IcA<sup>7,8</sup>]SFTI-1[1,14] and [PtA<sup>8,9</sup>]SFTI-1[1,14] co-complex structure with bovine trypsin.

A			B		
	[IcA <sup>7,8</sup> ]SFTI-1[1,14] co-complex with trypsin	[PtA <sup>8,9</sup> ]SFTI-1[1,14] co-complex with trypsin		[IcA <sup>7,8</sup> ]SFTI-1[1,14] co-complex with trypsin	[PtA <sup>8,9</sup> ]SFTI-1[1,14] co-complex with trypsin
Data collection			Refinement		
Space group	P2 <sub>1</sub> 2 <sub>1</sub> 2 <sub>1</sub>	P2 <sub>1</sub> 2 <sub>1</sub> 2 <sub>1</sub>	No. Reflections	40999	36482
Cell dimensions			R <sub>work</sub> /R <sub>free</sub>	19.0/20.4	19.0/21.9
a, b, c (Å)	61.8, 63.4, 69.3	61.1, 63.2, 69.9	R.m.s deviations		
α, β, γ (°)	90.0, 90.0, 90.0	90.0, 90.0, 90.0	Bond lengths (Å)	0.007	0.0087
Resolution (Å)	46.8 - 1.45	46.9-1.55	Bond angles (°)	1.261	1.188
(highest shell (Å))	(1.48 -1.45)	(1.61-1.55)	Ramachandran		
Rmerge	9.6 (45.3)	9.7 (39.0)	favored /outliers	97.8%/0	97.8%/0
I/σI	21.1 (3.7)	12.5 (2.1)	Molprobity score/percentile	1.43/89 <sup>th</sup>	1.4/93 <sup>th</sup>
Completeness (%)	95.5 (84.0)	96.3 (90.4)	PDB Codes	4abj	4abi
Redundancy	11.2(7.0)	3.8 (2.2)			

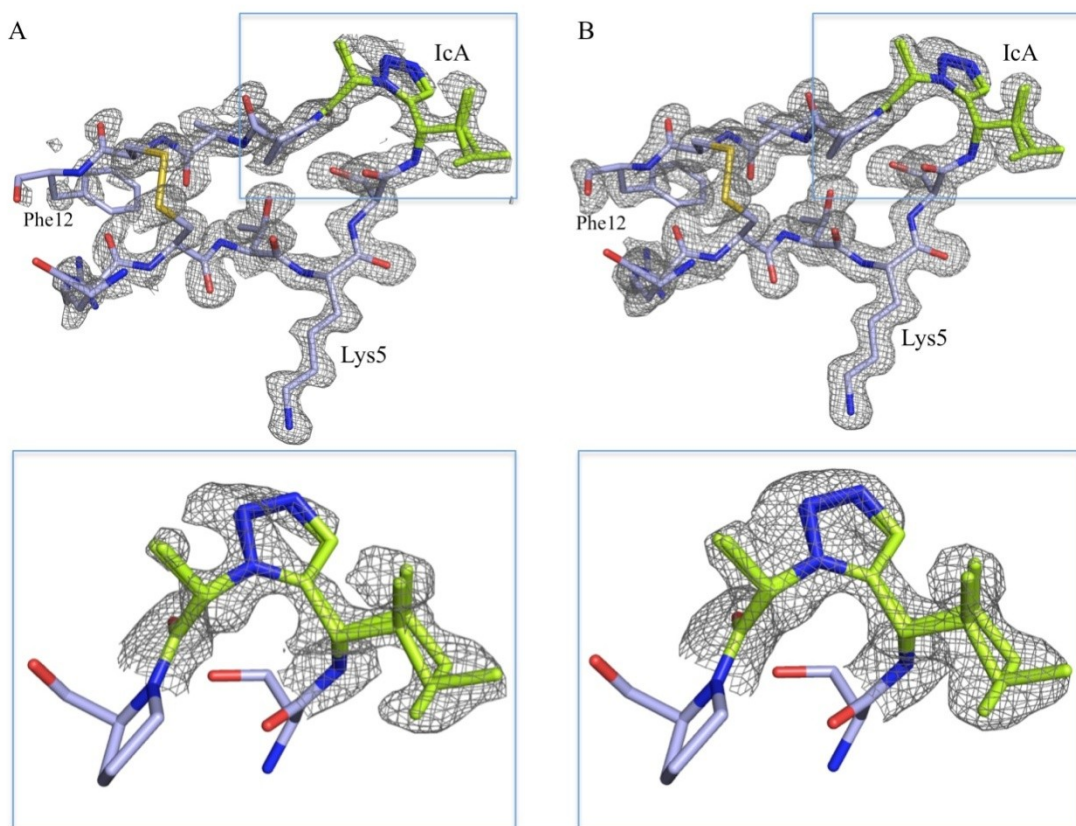


**Figure S1.** Unbiased  $F_o-F_c$  (A) and refined  $2F_o-F_c$  electron density map (B) of [IcA<sup>7,8</sup>]SFTI-1[1,14] contoured at 2.5  $\delta$  and 1.0  $\delta$ , respectively. Insets of A and B show a close-up on the 1,5-disubstituted 1,2,3-triazole [IcA<sup>7,8</sup>].

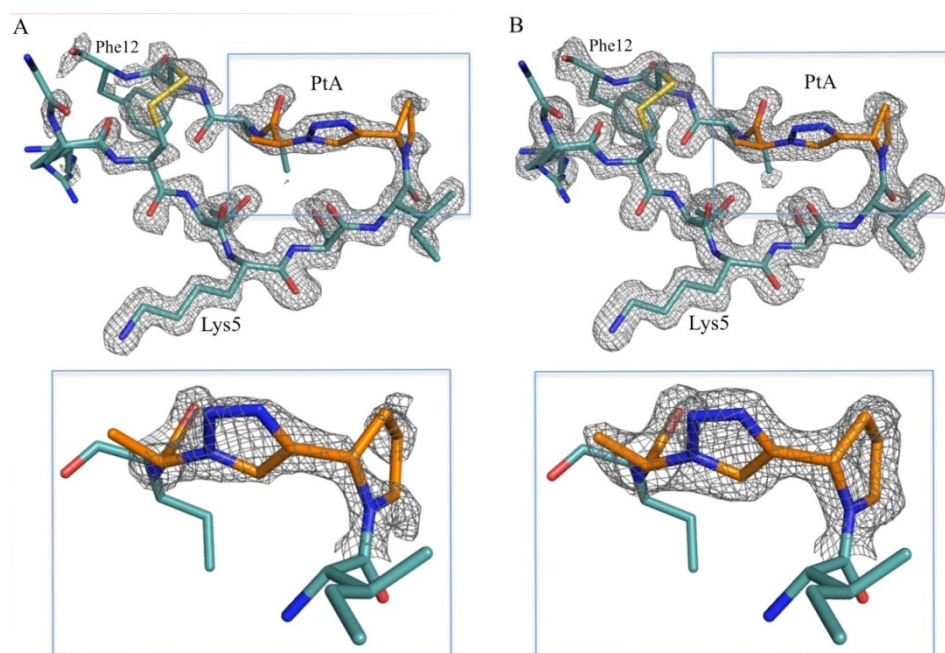


**Figure S2.** Unbiased  $F_o-F_c$  (A) and refined  $2F_o-F_c$  electron density map (B) of  $[\text{PtA}^{8,9}]$ SFTI-1[1,14] contoured at 2.5  $\delta$  and 1.0  $\delta$ , respectively. Insets of A and B show a close-up on the 1,4-disubstituted 1,2,3-triazole  $[\text{PtA}^{8,9}]$ .

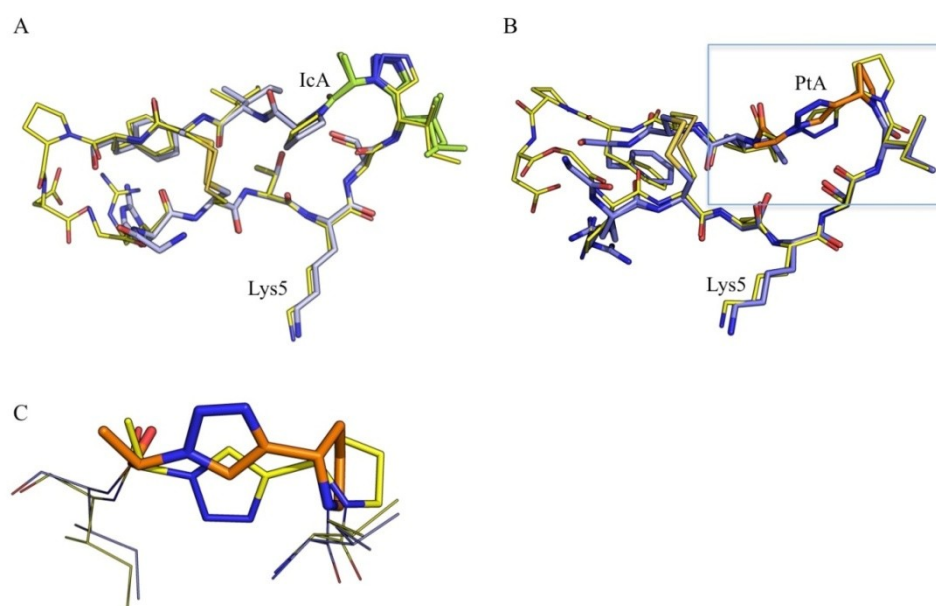


**Figure S3.** Comparison of energy minimized models with those generated from crystallographic data. A Energy minimized model of  $[\text{IcA}^{7,8}]$ SFTI-1[1,14] in yellow, crystallographic coordinates shown in grey,  $[\text{IcA}^{7,8}]$  is highlighted in lemon. B Energy minimized model of  $[\text{PtA}^{8,9}]$ SFTI-1[1,14] in yellow, crystallographic coordinates shown in blue,  $[\text{PtA}^{8,9}]$  is highlighted in orange. C Close-up of B. Note that the 1,4-disubstituted 1,2,3-triazole of  $[\text{PtA}^{8,9}]$  of the crystallographic model has flipped compared to the energy minimized model.

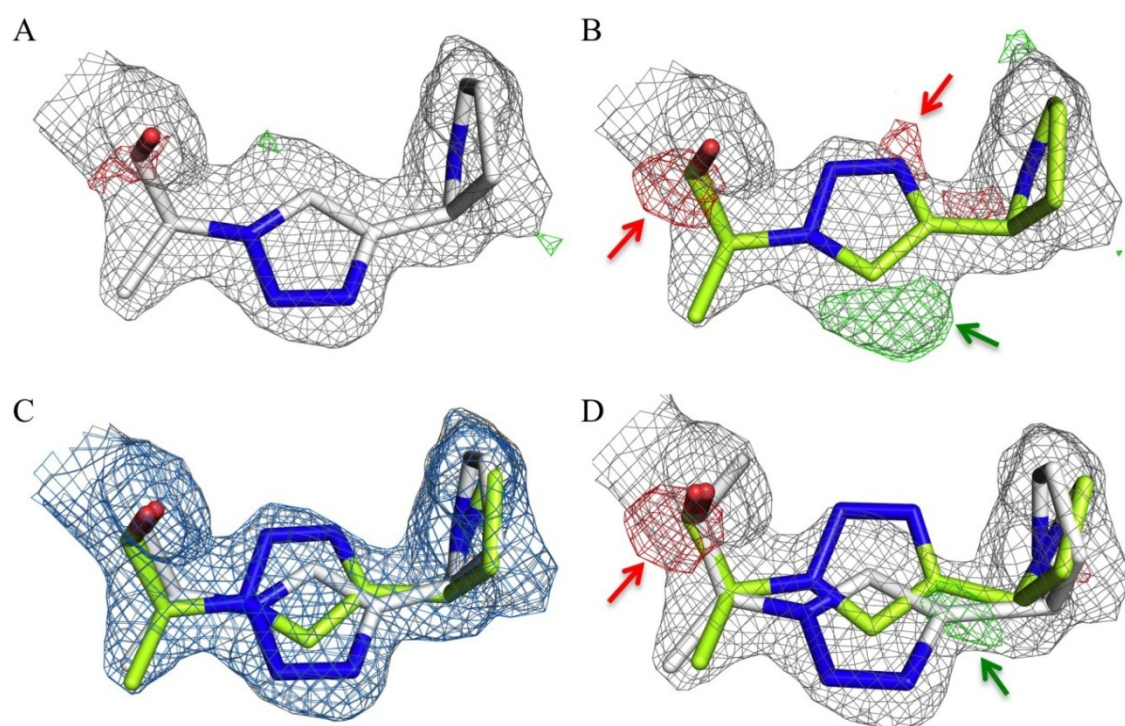


**Figure S4.** Comparison of the two likely conformations of 1,4-disubstituted 1,2,3-triazole of [PtA<sup>8,9</sup>]SFTI-1[1,14]. Each conformation was refined with the same parameters, and its corresponding electron density displayed.  $2F_o-F_c$  maps are shown in grey with a  $\delta$ -level of 1.0.  $F_o-F_c$  maps are shown with  $\delta$ -levels of -4.0 (red) and +4.0 (green). Conformation 1 is shown with white carbons, while conformation 2 of [PtA<sup>8,9</sup>]SFTI-1[1,14] is shown with lemon carbons. **A** Individually refined conformation 1 of [PtA<sup>8,9</sup>]SFTI-1[1,14]. **B** Individually refined conformation 2 of [PtA<sup>8,9</sup>]SFTI-1[1,14]. Places where  $F_o-F_c$  difference map is positive or negative are highlighted with green or red arrows, respectively. Note that the alanine-like side-chain does not fit well into the  $2F_o-F_c$  density. **C** Superposition of conformation 1 (white carbons) and conformation 2 (lemon) with corresponding  $2F_o-F_c$  electron density maps in grey and blue, respectively. **D** Refined [PtA<sup>8,9</sup>]SFTI-1[1,14] with one alternative conformation. Conformation 1 atoms (white carbons) were set to 80 % occupant, while conformation 2 atoms (lemon carbons) were set to 20 % occupant. Places where  $F_o-F_c$  difference map is positive or negative are highlighted with green or red arrows, respectively. Note that conformation 2 is pushed out of  $2F_o-F_c$  electron density, when refined with conformation 1.

#### 6.2.4 *In silico* methods

##### Structures for Figure 3 from the main text

Crystal structures of peptidomimetics **3** and **6** from pdb files 4ABJ and 4ABI were aligned at Lys5 of the inhibitor loop of 1SFI and energy minimized with *YASARA structure* (AMBER03 force field, 298.1 K, pH = 7, coordinates of the respective inhibitor fixed).<sup>[S7]</sup> Graphics were rendered with POVray (www.povray.org).

##### Structures for Figure S3 and S4

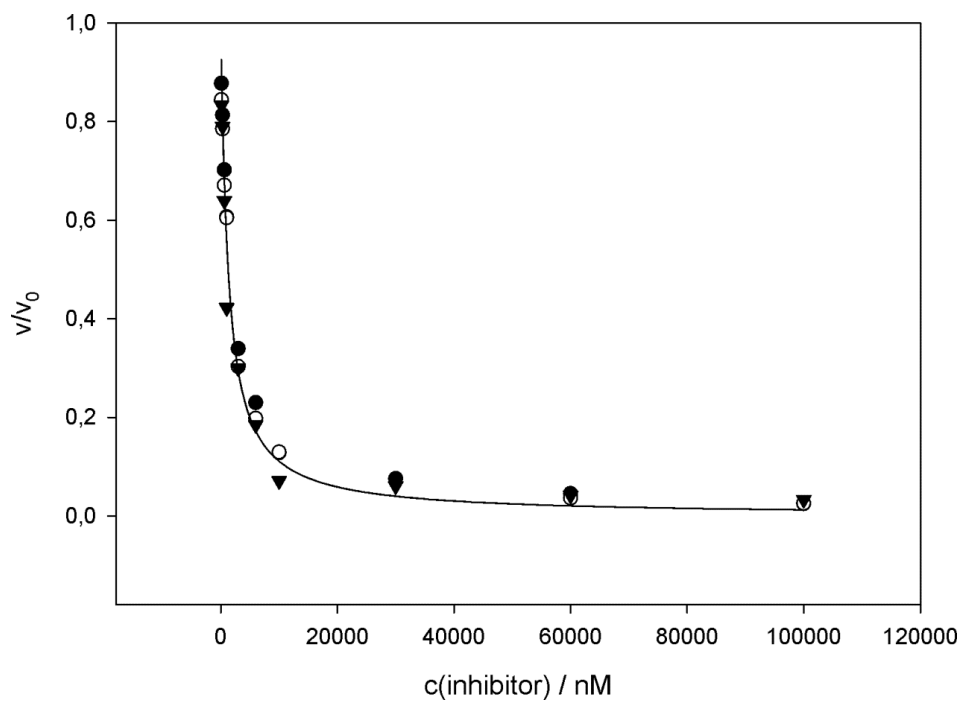
*In silico* models of peptidomimetics **3** and **6** were generated starting from 1SFI using *YASARA structure*.<sup>[S7]</sup> Corresponding 1,5- and 1,4-disubstituted 1,2,3-triazoles were modeled into the backbone, parameterized with AutoSMILES<sup>[S8]</sup> and energy minimized using the AMBER03 force field. The structure of compound **6** was explicitly modeled to match the natural hydrogen bond capabilities of the amide between Pro8 and Pro9 in the inhibitor loop of 1SFI (see Figure S3 C and S4; Ref. 9b from main text). Nevertheless, the predominant orientation of the 1,4-disubstituted 1,2,3-triazole within compound **6** (4ABI) was found to possess a

“flipped” geometry (Figure S3 C).

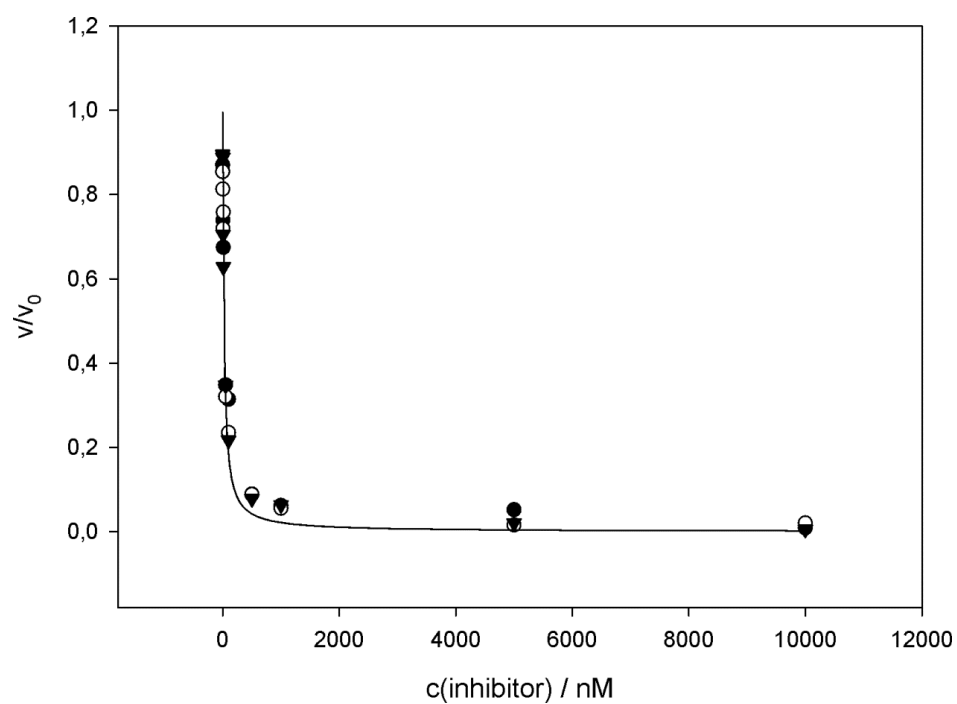
## 6.2.5 Analytical Data

### Plotted Kinetic Data

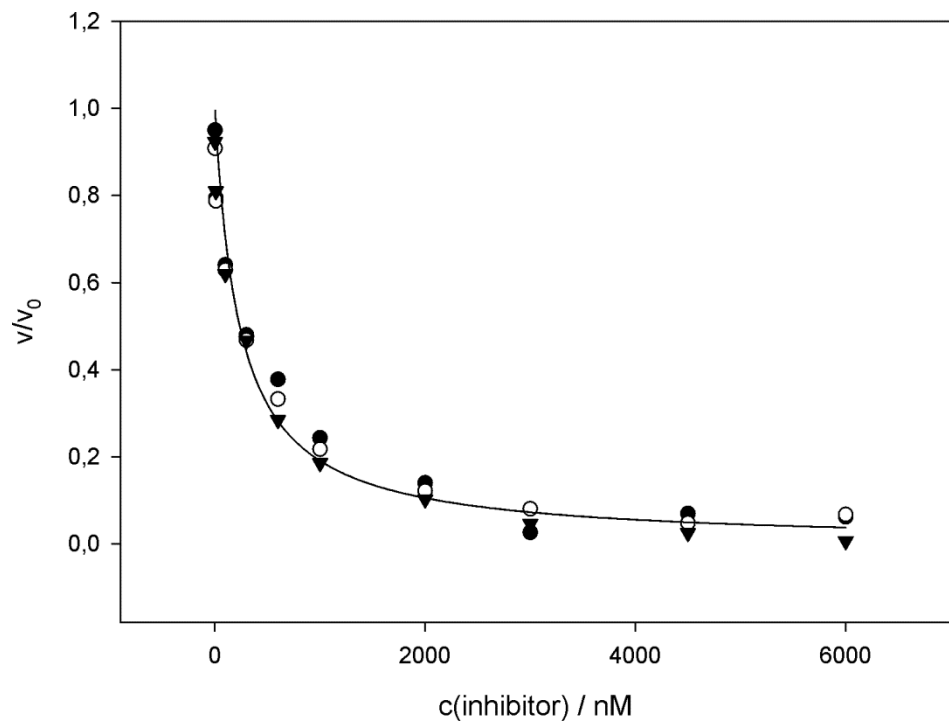
[Ala<sup>8</sup>]SFTI-1[1,14] (1)



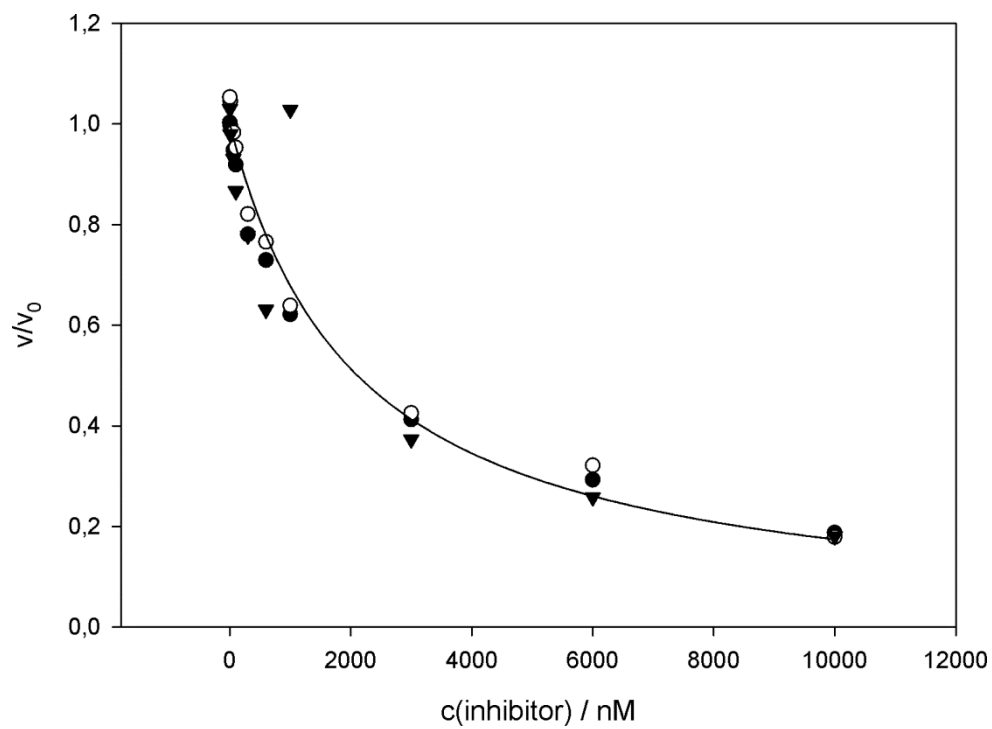
[Ala<sup>9</sup>]SFTI-1[1,14] (2)



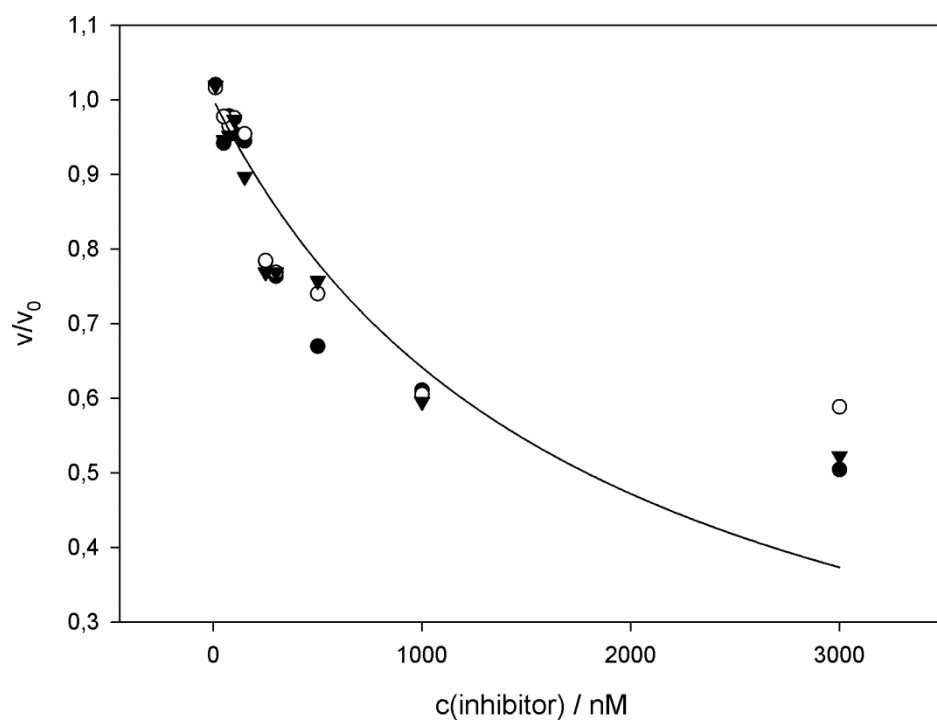
[IcA<sup>7,8</sup>]SFTI-1[1,14] (3)



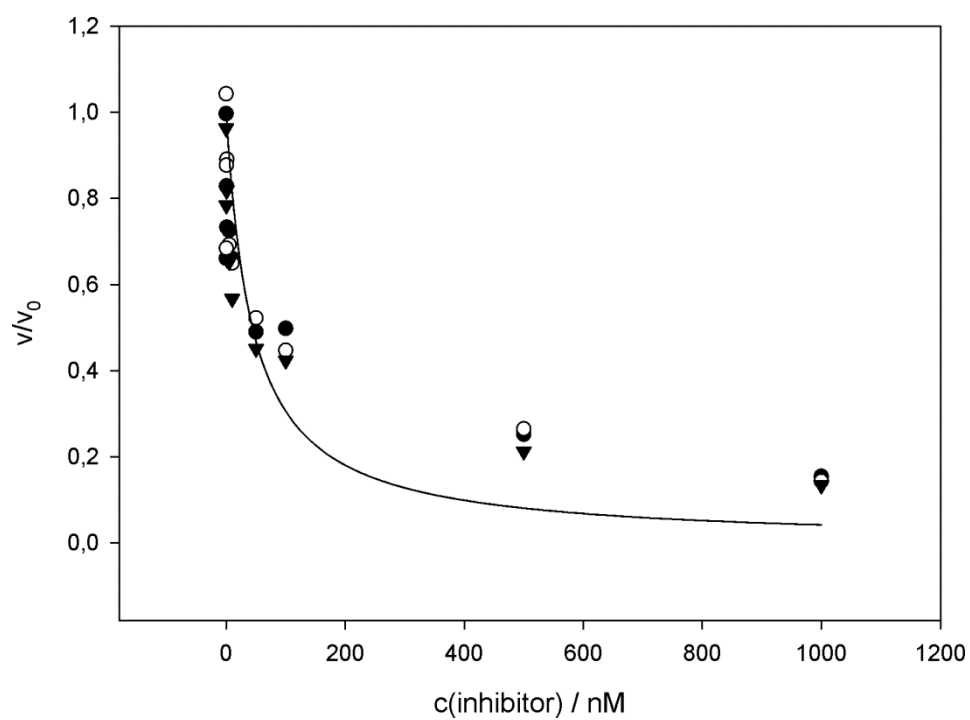
[ItA<sup>7,8</sup>]SFTI-1[1,14] (4)



[PcA<sup>8,9</sup>]SFTI-1[1,14] (5)

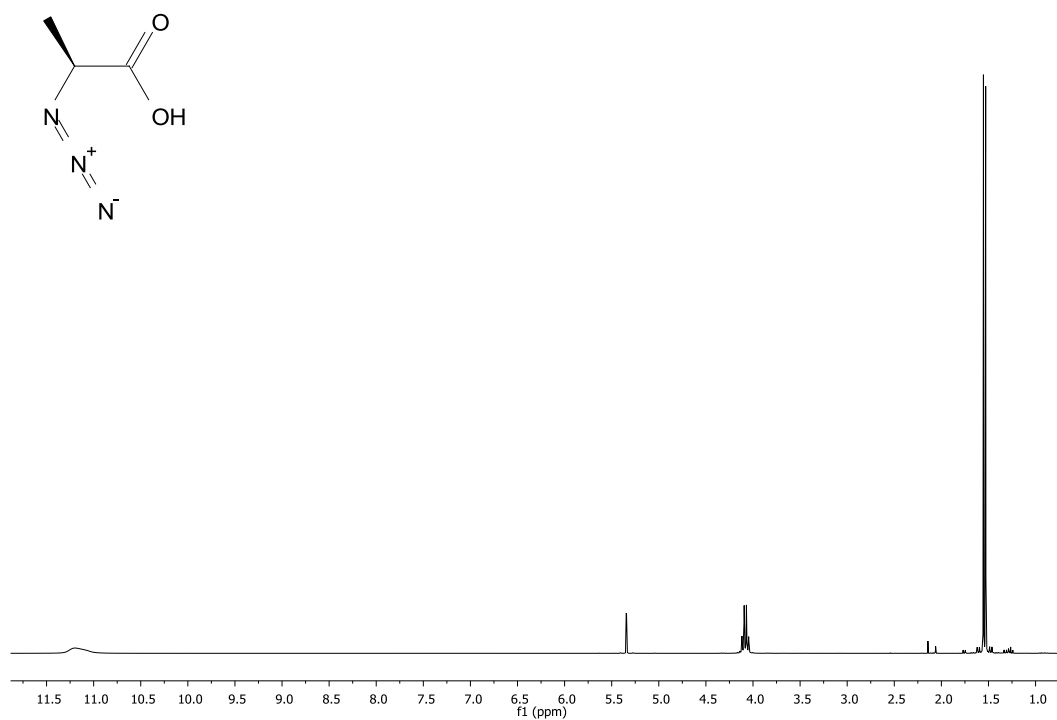


[PtA<sup>8,9</sup>]SFTI-1[1,14] (6)

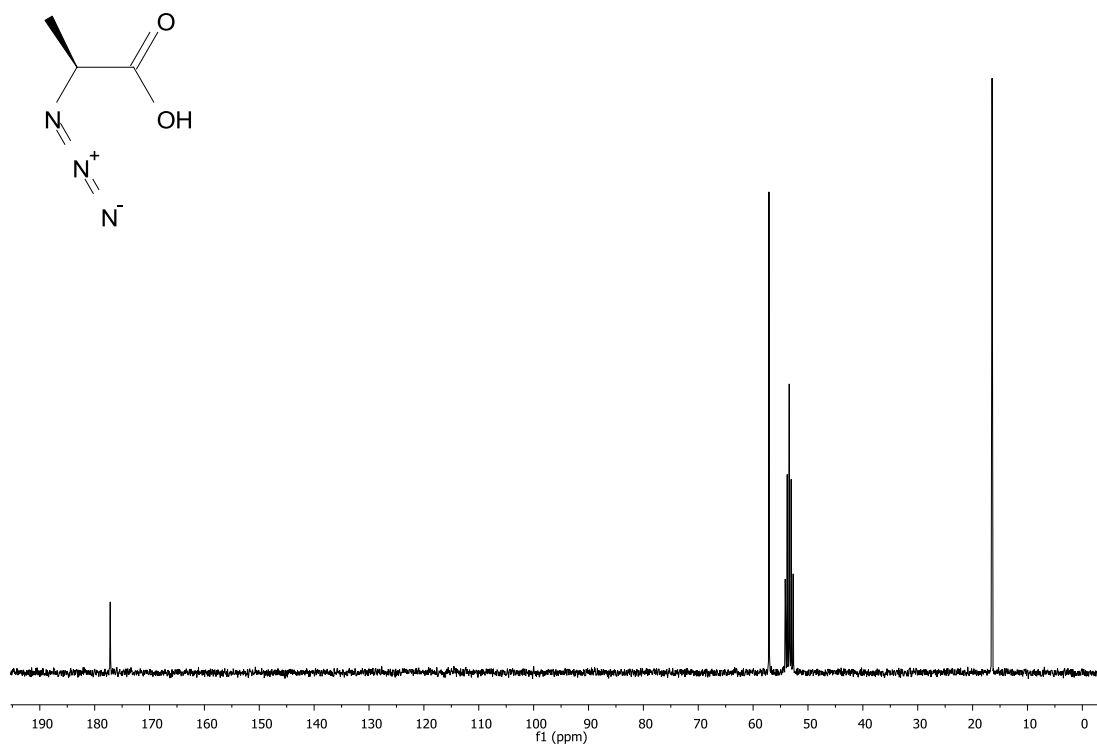




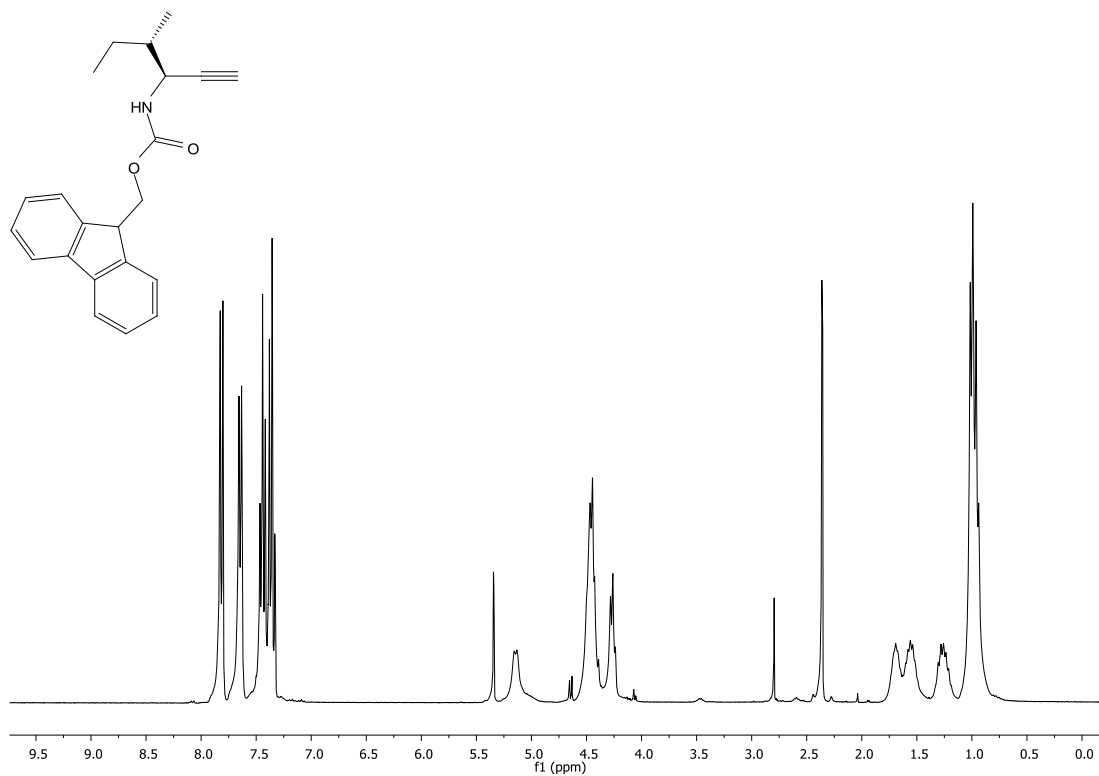
## NMR-spectra of azide and alkyne building blocks



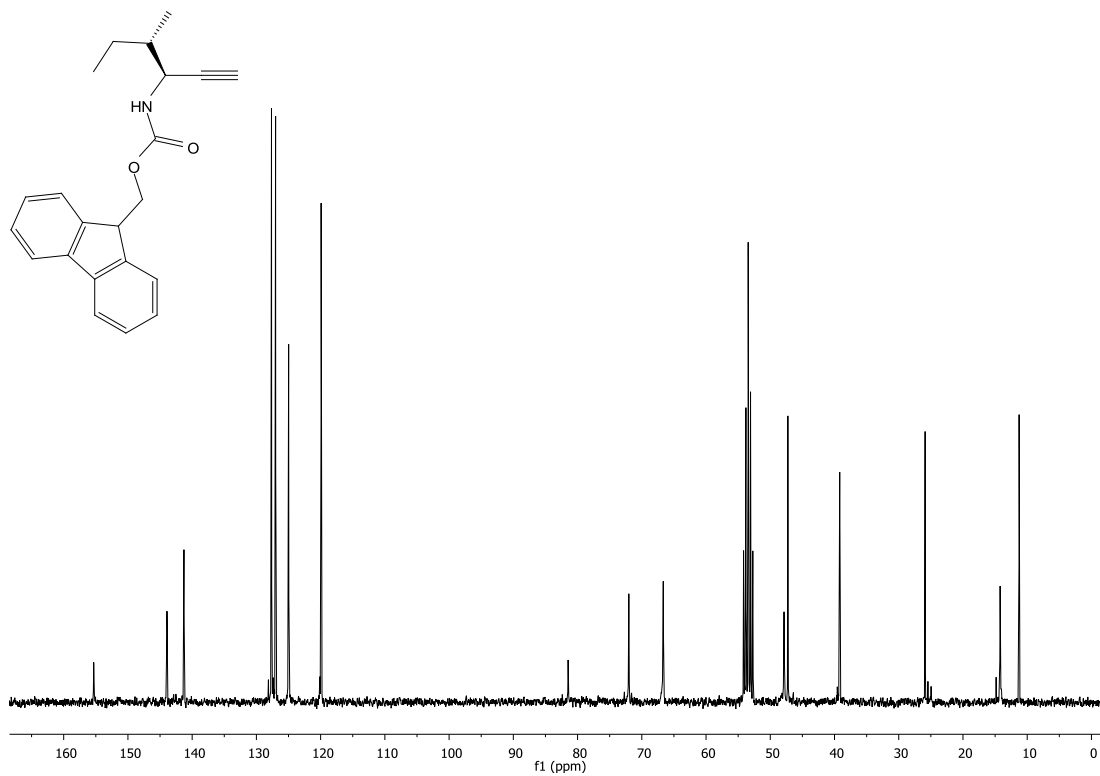
<sup>1</sup>H NMR spectra of (2S)-2-Azido-propanoic acid (7) recorded at 300 MHz.



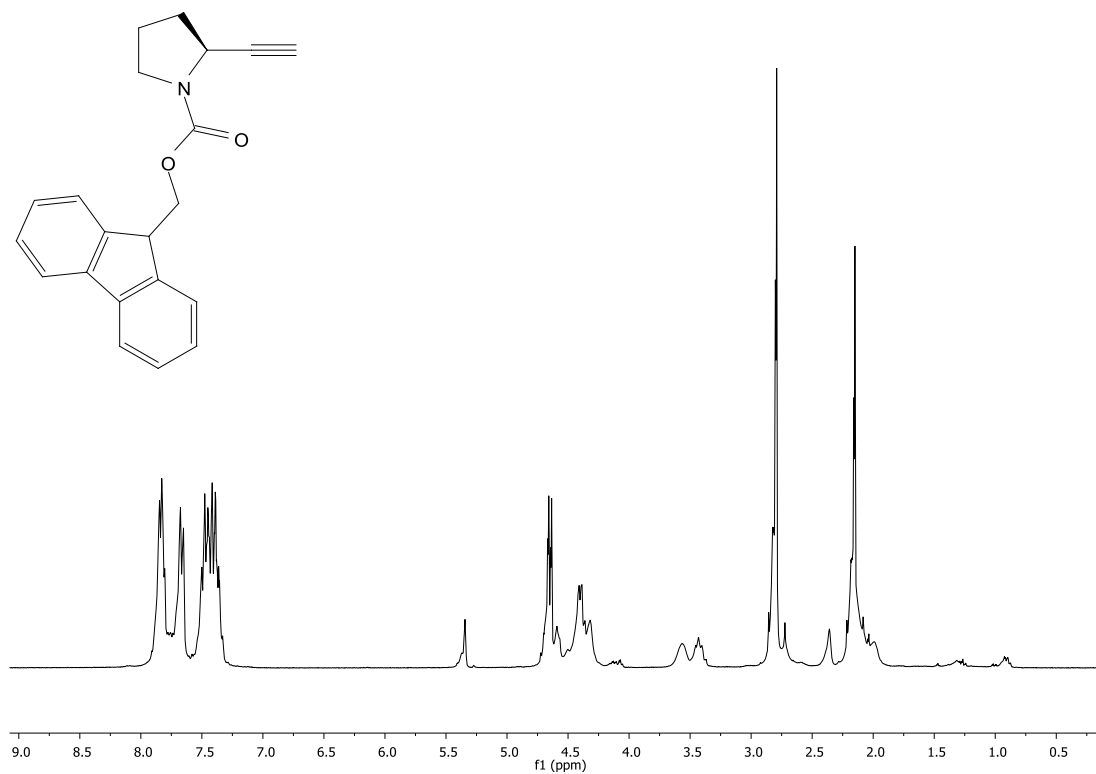
<sup>13</sup>C NMR spectra of (2S)-2-Azido-propanoic acid (7) recorded at 75.4 MHz.



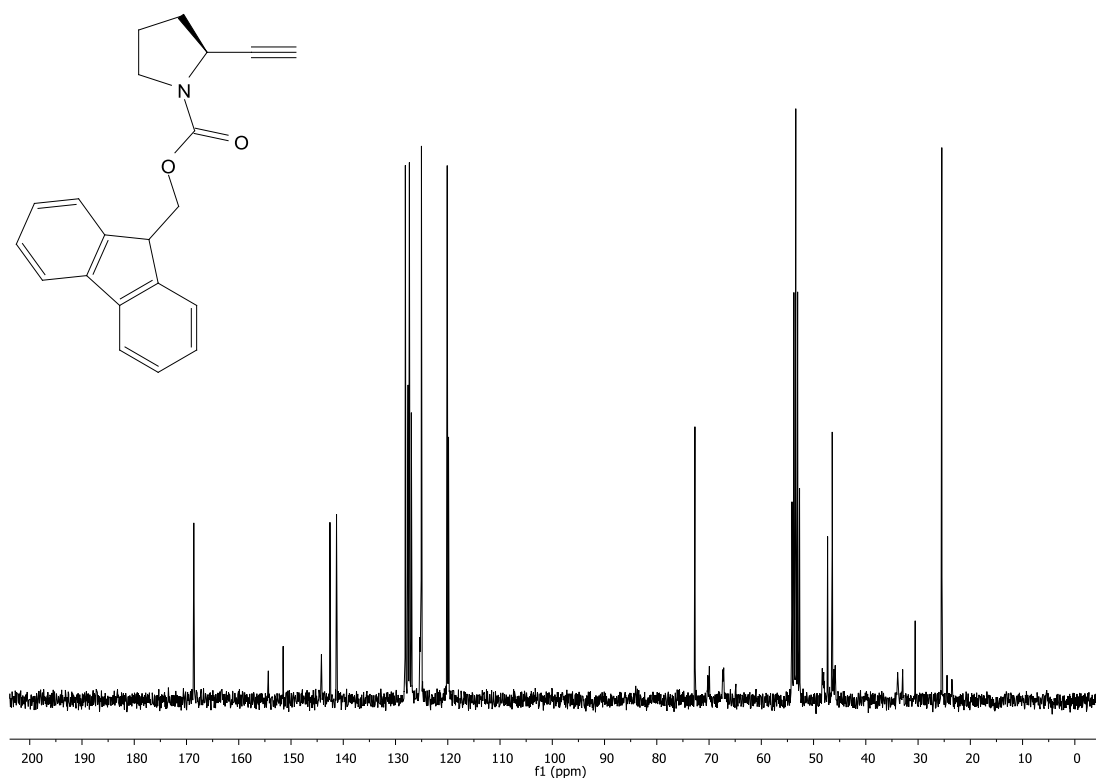
<sup>1</sup>H NMR spectra of (2S,3S)-N-(9-Fluorenylmethoxycarbonyl)-1-ethynyl-2-methyl-butylamine (**8**) recorded at 300 MHz.



<sup>13</sup>C NMR spectra of (2S,3S)-N-(9-Fluorenylmethoxycarbonyl)-1-ethynyl-2-methyl-butylamine (**8**) recorded at 75.4 MHz.

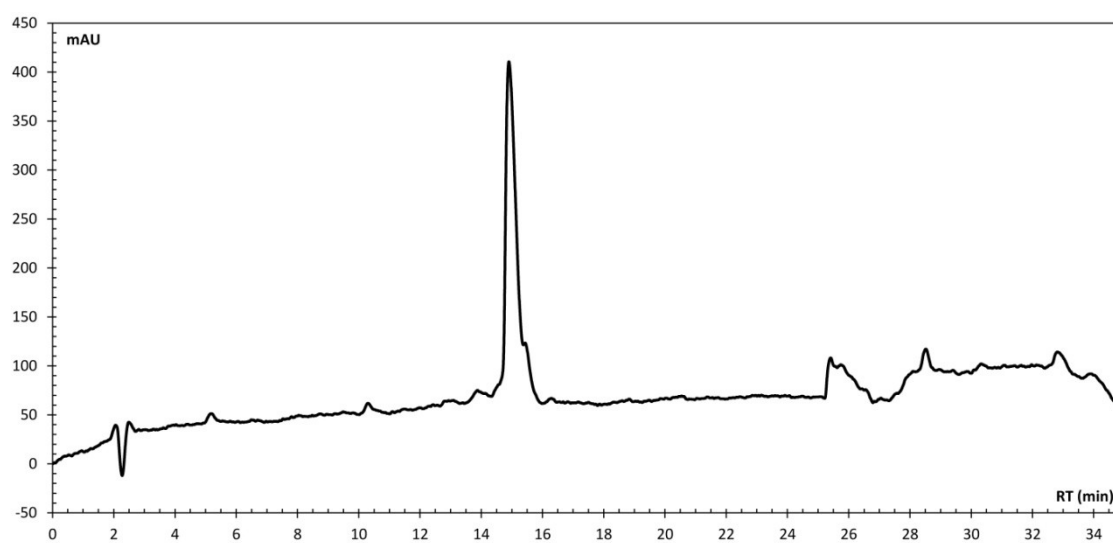


<sup>1</sup>H NMR spectra of (2S)-N-(9-fluorenylmethoxycarbonyl)-2-ethynyl-pyrrolidine (9) recorded at 300 MHz.

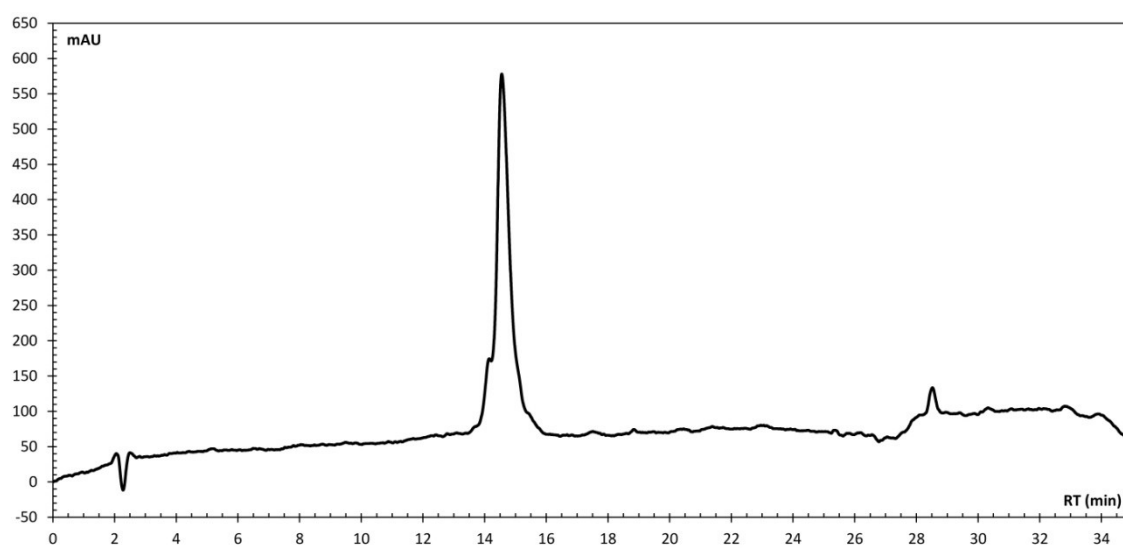


<sup>13</sup>C NMR spectra of (2S)-N-(9-fluorenylmethoxycarbonyl)-2-ethynyl-pyrrolidine (9) recorded at 75.4 MHz.

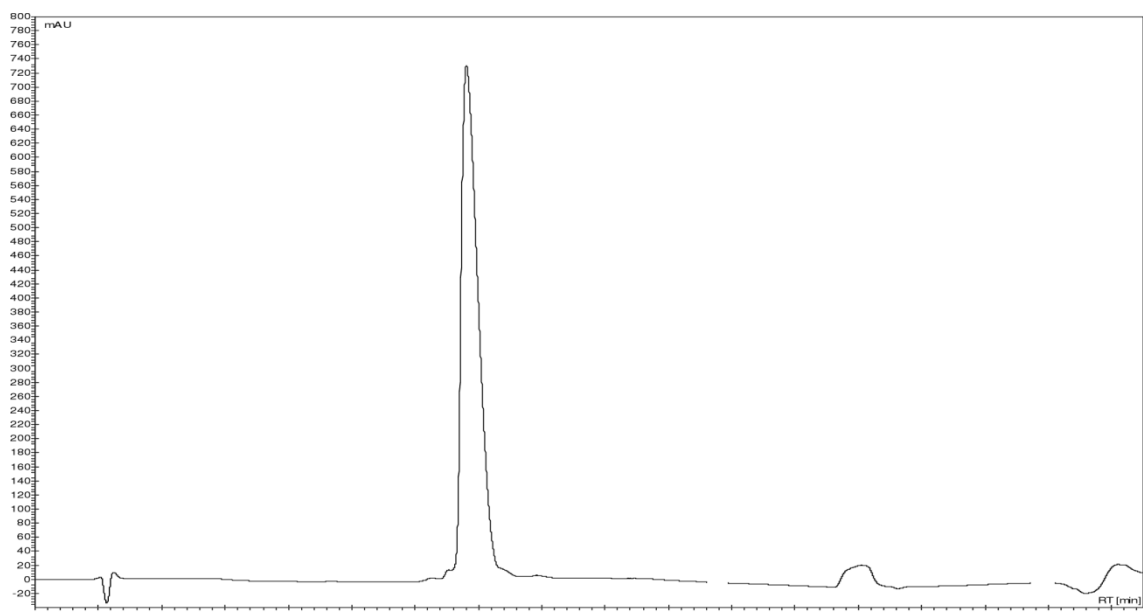
## RP-HPLC

[Ala<sup>8</sup>]SFTI-1[1,14] (1)

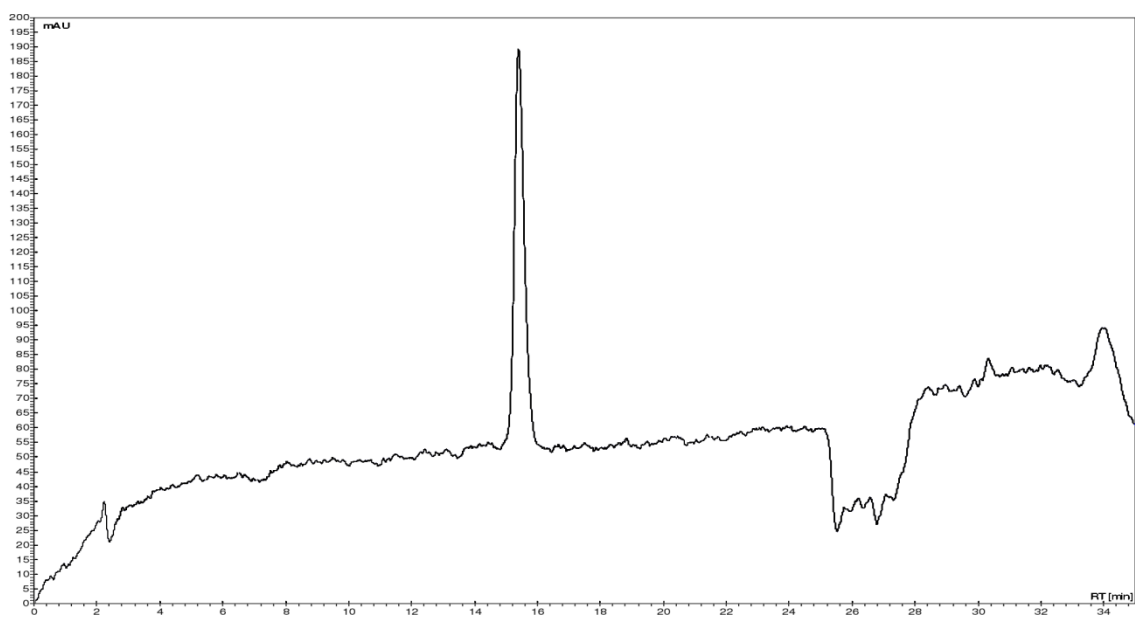
HPLC chromatogram of purified **1** recorded at 220 nm. Gradient: 18→40.5 % acetonitrile in 0.1% aq. TFA over 20 minutes at flow rate 1 mL/min.

[Ala<sup>9</sup>]SFTI-1[1,14] (2)

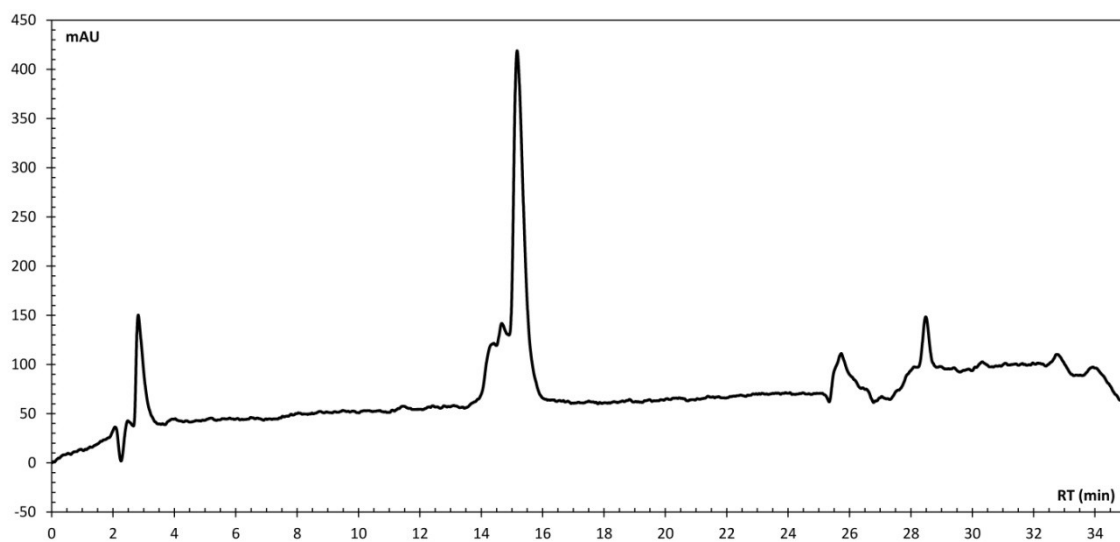
HPLC chromatogram of purified **2** recorded at 220 nm. Gradient: 18→40.5 % acetonitrile in 0.1% aq. TFA over 20 minutes at flow rate 1 mL/min.

$[IcA^{7,8}]SFTI-1[1,14]$  (3)

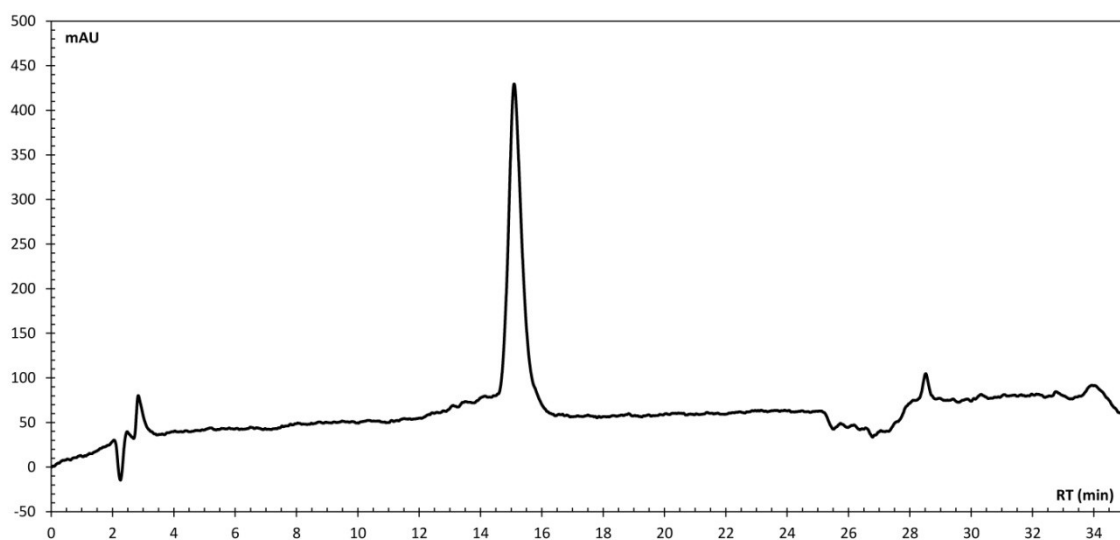
HPLC chromatogram of purified 3 recorded at 220 nm. Gradient: 18→40.5 % acetonitrile in 0.1% aq. TFA over 20 minutes at flow rate 1 mL/min.

 $[ItA^{7,8}]SFTI-1[1,14]$  (4)

HPLC chromatogram of purified 4 recorded at 220 nm. Gradient: 18→40.5 % acetonitrile in 0.1% aq. TFA over 20 minutes at flow rate 1 mL/min.

$[PcA^{8,9}]SFTI-1[1,14]$  (5)

HPLC chromatogram of purified 5 recorded at 220 nm. Gradient: 18→40.5 % acetonitrile in 0.1% aq. TFA over 20 minutes at flow rate 1 mL/min.

 $[PtA^{8,9}]SFTI-1[1,14]$  (6)

HPLC chromatogram of purified 6 recorded at 220 nm. Gradient: 18→40.5 % acetonitrile in 0.1% aq. TFA over 20 minutes at flow rate 1 mL/min.



---

**6.2.6 Supporting References**

---

- [S1] Z. Otwinowski, W. Minor, *Method Enzymol* **1997**, *276*, 307-326.
- [S2] A. J. McCoy, R. W. Grosse-Kunstleve, P. D. Adams, M. D. Winn, L. C. Storoni, R. J. Read, *J Appl Crystallogr* **2007**, *40*, 658-674.
- [S3] G. N. Murshudov, A. A. Vagin, E. J. Dodson, *Acta Crystallogr D* **1997**, *53*, 240-255.
- [S4] N. Collaborative Computational Project, The CCP4 suite: programs for protein crystallography., *Acta Crystallogr D* **1994**, *50*, 760-763.
- [S5] a) M. R. Krause, R. Goddard, S. Kubik, *Journal of Organic Chemistry* **2011**, *76*, 7084-7095; b) A. Brik, J. Alexandratos, Y. C. Lin, J. H. Elder, A. J. Olson, A. Wlodawer, D. S. Goodsell, C. H. Wong, *Chembiochem* **2005**, *6*, 1167-1169.
- [S6] D. W. L., The PyMOL Molecular Graphics System. DeLano Scientific LLC 2002, San Carlos, CA.
- [S7] a) E. Krieger, T. Darden, S. B. Nabuurs, A. Finkelstein, G. Vriend, *Proteins-Structure Function and Bioinformatics* **2004**, *57*, 678-683; b) Y. Duan, C. Wu, S. Chowdhury, M. C. Lee, G. M. Xiong, W. Zhang, R. Yang, P. Cieplak, R. Luo, T. Lee, J. Caldwell, J. M. Wang, P. Kollman, *J Comput Chem* **2003**, *24*, 1999-2012.
- [S8] A. Jakalian, D. B. Jack, C. I. Bayly, *J Comput Chem* **2002**, *23*, 1623-1641.

## 6.3 Supporting Information for Chapter 2.3

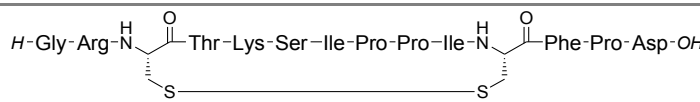
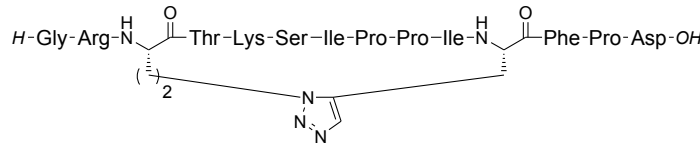
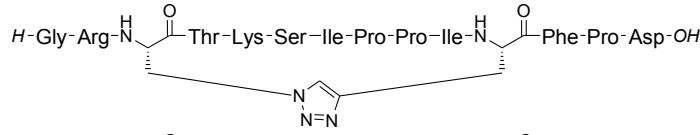
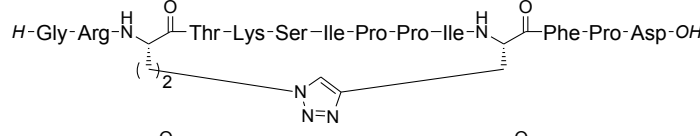
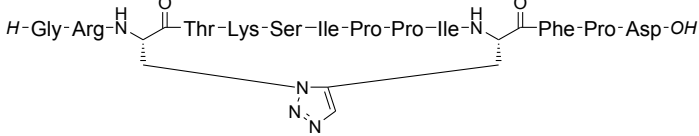
### 6.3.1 1. 3D Modeling and Calculations

3D models of [Ala<sup>3</sup>(&<sup>1</sup>),Ala<sup>11</sup>(&<sup>2</sup>)]SFTI-1[1,14][(&<sup>1</sup>-CH<sub>2</sub>-1,5-[1,2,3]triazolyl-&<sup>2</sup>)] (2), [Ala<sup>3</sup>(&<sup>1</sup>),Ala<sup>11</sup>(&<sup>2</sup>)]SFTI-1[1,14][(&<sup>1</sup>-1,4-[1,2,3]triazolyl-&<sup>2</sup>)] (3) and [Ala<sup>3</sup>(&<sup>1</sup>),Ala<sup>11</sup>(&<sup>2</sup>)]SFTI-1[1,14][(&<sup>1</sup>-CH<sub>2</sub>-1,4-[1,2,3]triazolyl-&<sup>2</sup>)] (4) were derived from the NMR solution structure of monocyclic SFTI-1[1,14] (1) (PDB ID code: 1JBN) and all *in silico* experiments were done with the YASARA structure package applying the YASARA 2 force field.

After loading 1jbn.pdb into YASARA (YASARA Biosciences), an energy minimization was performed (in vacuum). The disulfide connection between residues 3 and 11 was removed retaining the respective C<sub>β</sub> atoms. Then, the corresponding triazole linkages were modelled into the molecule and an energy minimization was performed (in vacuum). The obtained macrocyclic structures of compounds 1-4 were subjected to an energy minimization in 0.9 M NaCl (aq) at pH 7.4 and 298.16 K.

The resulting models were loaded into PyMOL 0.99rc6 (DeLano Scientific LLC) and aligned at the respective carbonyl, C<sub>α</sub>, C<sub>β</sub>, and amide nitrogen atoms of residue 11 using the “Pair Fitting” command wizard. Distances between C<sub>α</sub> atoms of residues 3 and 11 were calculated with the “Measurement” command wizard. The root mean square deviations (RMSD) were calculated for the respective carbonyl, C<sub>α</sub>, C<sub>β</sub>, and amide nitrogen atoms of residues 3 and 11 at the compared structures using the “RMS” command.

**Table S1.** Summary of measured distances between C<sub>α</sub> atoms of residues 3 and 11 (d(C<sub>α3</sub>, C<sub>α11</sub>)) and calculated RMSD values for the respective carbonyl, C<sub>α</sub>, C<sub>β</sub>, and amide nitrogen atoms of residues 3 and 11 for compounds 2, 3, 4 and 9 compared to 1.

Entry	Structure	d(C <sub>α3</sub> , C <sub>α11</sub> ) [Å]	RMSD [Å]
1		4.00	-
2		4.18	0.109
3		4.76	0.328
4		4.52	0.391
9 <sup>a)</sup>		3.69	0.361

[a] Compound 9 was omitted from synthesis.

### 6.3.2 Experimental Section

#### General Information

Chemicals and solvents were purchased from Bachem, Iris Biotech, Novabiochem, Sigma-Aldrich, Rapp Polymere, Roth or Varian (Agilent). Azide and alkyne building blocks Fmoc-L-propargylglycine (Fmoc-Pra-OH), Fmoc-L-azidoalanine (Fmoc-Aza-OH) and Fmoc-L-azidohomoalanine (Fmoc-Aha-OH) were obtained from Iris Biotech and chloro(pentamethylcyclopentadienyl)(cyclooctadiene)ruthenium(II) (Cp\**RuCl(COD)*) from Sigma-Aldrich.

Analytical HPLC was conducted with a Varian 920-LC system using a Phenomenex Hypersil 5u BDS C18 LC column (150 x 4.6 mm, 5  $\mu$ m, 130 Å). Semi-preparative RP-HPLC was performed on a Varian modular system comprising a PrepStar 218 Solvent Delivery Module, a ProStar 410 HPLC AutoSampler and a ProStar 325 Dual Wavelength UV-Vis HPLC Detector using a YMC J'sphere ODS-H80 C-18 LC column (250 x 20 mm, 4  $\mu$ m, 8 nm). The eluent system for analytical and semi-preparative HPLC consisted of eluent A (0.1% aq. TFA) and eluent B (90 % aq. acetonitrile containing 0.1% TFA).

ESI mass spectra were recorded with a Shimadzu LCMS-2020 equipped with a Phenomenex Jupiter 5u C4 LC column (50 x 1 mm, 5  $\mu$ m, 300 Å) and a Bruker-Franzen Esquire LC mass spectrometer. The eluent system consisted of eluent A (0.1% aq. formic acid, LC-MS grade) and eluent B (100 % acetonitrile containing 0.1% formic acid, LC-MS grade).

IR-spectra were measured on a PerkinElmer Spectrum One FT-IR spectrometer. Peptidic samples were dissolved in methanol and applied onto a silicon wafer. After vaporization of the solvent the coated wafer was inserted into the instrument. Recorded raw data was exported to an ASCII file and plotted with SigmaPlot 11.0 (Systat Software, Inc).

NMR studies were conducted on a Bruker DRX 500 instrument (500 MHz). All samples were dissolved in DMSO-*d*<sub>6</sub> and measured using a Shigemi 5mm Symmetrical NMR microtube (magnetic susceptibility matched to DMSO). Resulting spectra were processed and analyzed using the MestReNova software (Mestrelab Research) and are given in section 7. Broad signals in the <sup>1</sup>H and HSQC spectra of 1,4-disubstitued 1,2,3-triazoles **3** and **4** might be caused by paramagnetic contaminations (presumably traces of copper(II) ions) due to the solution CuAAC approach. A detailed signal assignment for <sup>1</sup>H and <sup>13</sup>C chemical shifts was made for compound **1** using HSQC, HMBC, COSY, TOCSY and NOESY experiments; for compounds **2-6** HSQC spectra are given.

#### Peptide Synthesis and Macrocyclization

**General Fmoc-SPPS procedures.** Peptides were synthesized in a Liberty 12-channel automated peptide synthesizer on a Discover SPS microwave peptide synthesizer platform (CEM) using the Fmoc strategy. All amino acids were attached by double or triple coupling employing 4 eq of the corresponding amino acid, 4 eq of 2-(1H-benzotriazol-1-yl)-1,1,3,3-tetramethyluronium hexafluorophosphate (HBTU) and 8 eq of DIEA, or in case of cysteine 3-4 eq of 2,4,6-trimethylpyridine (collidine). Arginine and cysteine were coupled using a two step microwave program: 1. RT, 0 W, 25 min; 2. 75 °C, 25 W, 0.5 min (Arg) and 1. RT, 0 W, 2 min; 2. 50 °C, 25 W, 4 min (Cys), respectively. All other amino acids were coupled using a standard microwave program: 75 °C, 21 W, 5 min. Fmoc deprotection was achieved in two steps by reaction with 20% piperidine in DMF at 75 °C, 42 W for 0.5 min (initial deprotection) followed by a second deprotection step with 20% piperidine in DMF at 75 °C, 42 W for 3 min. Cleavage of peptides from the solid support and removal of side chain protecting groups was achieved *via* acidolysis using a standard cleavage cocktail consisting of trifluoroacetic acid (TFA)/H<sub>2</sub>O/anisole/triethylsilane (TES) (47:1:1:1, v:v:v:v). The resulting reaction mixture was shaken for 3 h at RT followed by precipitation and subsequent washing (4×) with methyl

*tert*-butyl ether (MTBE) to yield crude unprotected peptides.

**SFTI-1[1,14] (1).** The linear precursor peptide *H*-GRCTKSIPPICFPD-*OH* (**9**) was synthesized on a 2-chlorotrityl chloride resin (1.56 mmol/g, Iris Biotech) at 0.25 mmol scale. Loading of the first amino acid was conducted manually by adding a solution of 206 mg Fmoc-Asp(*t*Bu)-*OH* (0.5 mmol, 2 eq) and 342  $\mu$ L *N,N*-diisopropylethylamine (DIEA, 2 mmol, 8 eq) in a minimum amount of DCM to 160 mg resin and shaking the resulting mixture for 2 h at room temperature (RT). The solution was removed by filtration and the loaded resin was washed with DCM/methanol/DIEA (17:2:1; 3 times), DCM (3 times), DMF (3 times) and DCM (3 times) and then subjected to the automated microwave assisted Fmoc-SPPS procedure. All amino acid residues were attached using double coupling. The resulting peptide resin was dried and splitted to keep one half for storage. To suppress unwanted oxidation of thiol groups at residues 3 and 11 during acidolytic cleavage of the other half of the peptide resin, dithiothreitol (DTT) was added to the cleavage cocktail. Ether precipitation and washing yielded 146 mg of crude linear peptide **9** (95  $\mu$ mol, 76 % according to  $\frac{1}{2}$  of the initial loading of the resin). Oxidative macrocyclization of crude **9** was conducted in solution (1 mg/mL) in 100 mM (NH<sub>4</sub>)<sub>2</sub>CO<sub>3</sub> aq with 0.5 % (v:v) DMSO over two days at RT. The solvent was removed by freeze-drying followed by semi-preparative purification *via* HPLC to yield 33 mg of pure disulfide bridged peptide **1** (21.5  $\mu$ mol, 17.2 % according to  $\frac{1}{2}$  of the initial load of the resin). IR (cm<sup>-1</sup>) 3285, 3073, 2966, 2880, 1636, 1556, 1452, 1203, 1138. ESI-MS (m/z) [M+2H]<sup>2+</sup> obsd. = 766.50 (calc = 766.37), [M+H]<sup>+</sup> obsd. = 1531.90 (calc = 1531.74), [M-H]<sup>-</sup> obsd. = 1529.75 (calc = 1529.72), [M+TFA-H]<sup>-</sup> obsd. 1643.70 (calc = 1643.72). For the isotope pattern of [M+H]<sup>+</sup> see spectra in section 5.

In full accordance with the literature[12a], we observed that under the conditions of conducted NMR experiments additional signals from minor conformation(s) occurred. <sup>1</sup>H and <sup>13</sup>C NMR shifts for the main conformer are given in tables S2 and S3.

**Table S2.** Observed <sup>1</sup>H-NMR chemical shifts for main conformer of compound **1**.<sup>a)</sup>

Residue	NH	$\alpha$ -CH	$\beta$ -CH	$\gamma$ -CH	$\delta$ -CH	$\epsilon$ -CH	$\varphi$ -CH	Others
Gly1	n.a.	3.74	-	-	-	-	-	-
Arg2	8.43	4.66	1.72, 1.57	1.52	3.09	-	-	$\epsilon$ -NH 7.75, HH 7.20
Cys3	8.70	5.60	2.90, 2.80	-	-	-	-	-
Thr4	8.54	4.13	4.20	1.27	-	-	-	$\beta$ -OH 5.32
Lys5	8.46	4.26	1.81, 1.46	1.31	1.54	2.77	-	$\epsilon$ -NH <sub>2</sub> n.a.
Ser6	7.20	4.32	3.76, 3.46	-	-	-	-	$\beta$ -OH 5.17
Ile7	8.24	4.24	1.72	1.37, 0.96	0.80	-	-	$\beta$ -CH <sub>3</sub> 0.79
Pro8	-	4.95	2.25, 1.87	1.77, 1.67	3.46, 3.31	-	-	-
Pro9	-	4.17	2.38, 1.66	1.97, 1.25	3.75, 3.49	-	-	-
Ile10	7.55	4.27	1.72	1.34, 1.04	0.72	-	-	$\beta$ -CH <sub>3</sub> 0.62
Cys11	8.79	5.26	2.75, 2.60	-	-	-	-	-
Phe12	8.52	4.79	3.11, 2.80	-	7.25	7.18	7.11	-
Pro13	-	4.44	2.04, 1.95	2.66	3.69, 3.62	-	-	-
Asp14	8.37	4.58	2.88; 2.84	-	-	-	-	-

[a] Parameters: 500 MHz, DMSO-*d*<sub>6</sub>, 300K, <sup>1</sup>H reference: DMSO = 2.50; n.a.: not assigned.

**Table S3.** Observed  $^{13}\text{C}$ -NMR shifts for main conformer of compound **1**.<sup>a)</sup>

Residue	C <sub><math>\alpha</math></sub>	C <sub><math>\beta</math></sub>	C <sub><math>\gamma</math></sub>	C <sub><math>\delta</math></sub>	C <sub><math>\epsilon</math></sub>	C <sub><math>\phi</math></sub>	C=O	Others
Gly1	40.38	-	-	-	-	-	n.a.	-
Arg2	52.00	30.50	24.41	40.45	-	-	171.58	NH2-CN=NH 157.10
Cys3	52.23	45.87	-	-	-	-	169.89	-
Thr4	58.64	67.03	20.31	-	-	-	170.33	-
Lys5	51.48	28.31	22.34	26.75	38.68	-	n.a.	-
Ser6	53.40	63.55	-	-	-	-	n.a.	-
Ile7	53.71	36.68	24.13	10.85	-	-	n.a.	$\beta$ -CH <sub>3</sub> 14.98
Pro8	58.62	30.31	21.62	46.30	-	-	n.a.	-
Pro9	59.54	29.25	24.00	47.11	-	-	170.82	-
Ile10	56.22	35.83	23.90	10.12	-	-	172.86	$\beta$ -CH <sub>3</sub> 15.22
Cys11	52.00	44.72	-	-	-	-	168.47	-
Phe12	51.59	37.84	136.91	129.45	128.02	126.35	170.37	-
Pro13	59.69	28.98	24.00	46.94	-	-	n.a.	-
Asp14	51.71	39.33	-	-	-	-	n.a.	$\beta$ -COO n.a.

[a] Parameters: 500 MHz, DMSO-*d*<sub>6</sub>, 300K,  $^{13}\text{C}$  reference: DMSO = 39.50; n.a.: not assigned.

[Ala<sup>3</sup>(&<sup>1</sup>),Ala<sup>11</sup>(&<sup>2</sup>)]SFTI-1[1,14][(&<sup>1</sup>-CH<sub>2</sub>-1,5-[1,2,3]triazolyl-&<sup>2</sup>)] (**2**). The 12 C-terminal amino acid residues (intermediate **7**: Fmoc-Aha-Thr-Lys-Ser-Ile-Pro-Pro-Ile-Pra-Phe-Pro-Asp-resin) were assembled first on an AmphiSpheres 40 HMP resin (0.4 mmol/g, Varian/Agilent) at 0.25 mmol scale using the automated microwave-assisted Fmoc-SPPS procedure. The described general conditions using triple coupling were applied except for the following changes. Loading of the resin with Fmoc-Asp(*t*Bu)-OH: triple coupling, 2 eq AA, 2 eq 2-(1H-7-azabenzotriazol-1-yl)-1,1,3,3-tetramethyluronium hexafluorophosphate (HATU), 4 eq DIEA, two step microwave program (1. 60 °C, 30 W, 45 min, 2. 75 °C, 20 W, 5 min). Coupling of Fmoc-Aha-OH and Fmoc-Pra-OH: double coupling, 2 eq AA, 2 eq HATU, 4 eq DIEA, two step microwave program (1. 60 °C, 30 W, 45 min, 2. 75 °C, 20 W, 5 min). The resin was dried to yield intermediate **7**.

Ruthenium(II)-catalyzed macrocyclization of intermediate **7** on the solid support was conducted as follows. Dry peptide resin was placed in a 20 mL syringe barrel suitable for Fmoc-SPPS fitted with a frit (syringe piston removed) and an argon line attached at the outlet nozzle. After addition of dry DMF from top, argon was bubbled through the mixture for 30 min. Then 19 mg Cp<sup>\*</sup>RuCl(COD) (20 mol% of initial loading of the resin) were added from top and the reaction mixture was bubbled with argon for another 10 min. Then the syringe was carefully sealed with the syringe piston from top and with a cover at the outlet nozzle. The sealed syringe and an open reference syringe filled with DMF were placed in the manual Discover SPS microwave peptide synthesizer with the fiber-optic temperature probe measuring the temperature of the reference. After running the microwave program (60 °C, 30 W, 5 h) the solution was removed *via* filtration and the peptide resin was washed with methanol (3 times), 0.5 % sodium diethyldithiocarbamate in DMF (w/v, 3 times) DMF (3 times) and dichloromethane (DCM, 3 times). The peptide resin was dried to yield intermediate **8**.

The two N-terminal amino acids, glycine and arginine, were attached manually after standard Fmoc deprotection using double coupling, 4 eq AA, 3.9 eq HBTU, 8 eq DIEA (calculated according to initial loading of the resin) and microwave irradiation (50 °C, 30 W, 30 min). Then the peptide resin was dried and subjected to acidolytic cleavage (standard cleavage cocktail). Ether precipitation, washing and subsequent purification *via* semi-preparative HPLC yielded 8.2 mg macrocyclic peptide **2** (5.3  $\mu\text{mol}$ , 2.1 % according to the initial loading of the resin). IR (cm<sup>-1</sup>) 3281, 3072, 2972, 2880, 1637, 1554, 1449, 1204, 1139. ESI-MS (m/z)

$[M+2H]^{2+}$  obsd. = 775.59 (calc = 774.92),  $[M+H]^+$  obsd. = 1549.03 (calc = 1548.83),  $[M-2H]^{2-}$  obsd. = 773.10 (calc = 772.90),  $[M-H]^-$  obsd. = 1547.20 (calc = 1546.81). For the isotope pattern of  $[M+H]^+$  see spectra in section 5.

**[Ala<sup>3</sup>(&<sup>1</sup>),Ala<sup>11</sup>(&<sup>2</sup>)]SFTI-1[1,14][(&<sup>1</sup>-1,4-[1,2,3]triazolyl-&<sup>2</sup>)] (3).** The linear precursor peptide [Aza<sup>3</sup>,Pra<sup>11</sup>]SFTI-1[1,14] (5) was synthesized on a preloaded TentaGel S AC Asp(*t*Bu) Fmoc resin (0.22 mmol/g, Rapp Polymere) at 0.22 mmol scale using the automated microwave-assisted Fmoc-SPPS procedure. The described general conditions using triple coupling were applied except for the coupling of Fmoc-Aha-*OH* and Fmoc-Pra-*OH*: double coupling, 2 eq AA, 2 eq HATU, 4 eq DIEA, two step microwave program (1. 60 °C, 30 W, 45 min, 2. 75 °C, 20 W, 5 min). The resulting peptide resin was dried and subjected to acidolytic cleavage (standard cleavage cocktail). Ether precipitation, washing and subsequent purification *via* semi-preparative HPLC yielded crude 280 mg linear peptide 5 (182 μmol, 83 % according to the initial loading of the resin). One half of crude 5 was purified *via* semi-preparative HPLC yielding 27 mg pure linear peptide 5 (17.6 μmol, 16 % according to initial load of the resin). IR (cm<sup>-1</sup>) 3287, 3073, 2968, 2880, 2110, 1668, 1531, 1448, 1203, 1137. ESI-MS (m/z)  $[M+2H]^{2+}$  obsd. = 768.16 (calc = 767.91),  $[M-H]^-$  obsd. = 1532.68 (calc = 1532.80),  $[M+TFA-H]^-$  obsd. 1647.79 (calc = 1646.80).

Copper(I) catalyzed macrocyclization of the other half of crude linear peptide 5 was conducted in degassed and argon-flushed H<sub>2</sub>O (1 mg/mL) with 1 eq of copper(II) sulfate pentahydrate (CuSO<sub>4</sub>·5H<sub>2</sub>O), 1 eq sodium ascorbate (NaAsc) and 8 eq DIEA at RT overnight. The solvent was removed by freeze-drying followed by semi-preparative purification *via* HPLC to yield 12.7 mg macrocyclic peptide 3 (8.3 μmol, 7.5 % according to initial load of the resin). IR (cm<sup>-1</sup>) 3287, 3073, 2968, 2880, 1652, 1530, 1449, 1203, 1138. ESI-MS (m/z)  $[M+H]^+$  obsd. = 1535.17 (calc = 1534.81),  $[M+Na]^+$  obsd. = 1557.07 (calc = 1556.79),  $[M-H]^-$  obsd. = 1532.78 (calc = 1532.80),  $[M+TFA-H]^-$  obsd. 1646.79 (calc = 1646.79). For the isotope pattern of  $[M+H]^+$  see spectra in section 5.

**[Ala<sup>3</sup>(&<sup>1</sup>),Ala<sup>11</sup>(&<sup>2</sup>)]SFTI-1[1,14][(&<sup>1</sup>-CH<sub>2</sub>-1,4-[1,2,3]triazolyl-&<sup>2</sup>)] (4).** The linear precursor peptide [Aha<sup>3</sup>,Pra<sup>11</sup>]SFTI-1[1,14] (6) was synthesized on a preloaded TentaGel S AC Asp(*t*Bu) Fmoc resin (0.22 mmol/g, Rapp Polymere) at a scale of 0.22 mmol using the automated microwave-assisted Fmoc-SPPS procedure. The described general parameters using triple coupling were applied except for the coupling of Fmoc-Aha-*OH* and Fmoc-Pra-*OH*: double coupling, 2 eq AA, 2 eq HATU, 4 eq DIEA, two step microwave program (1. 60 °C, 30 W, 45 min, 2. 75 °C, 20 W, 5 min). The resulting peptide resin was dried and subjected to acidolytic cleavage (standard cleavage cocktail). Ether precipitation, washing and subsequent purification *via* semi-preparative HPLC yielded crude 278 mg linear peptide 6 (180 μmol, 82 % according to the initial loading of the resin). 100 mg of crude 6 were purified *via* semi-preparative HPLC yielding 24 mg pure linear peptide 6 (15.5 μmol, 20 % overall yield). IR (cm<sup>-1</sup>) 3288, 3074, 2969, 2880, 2110, 1652, 1538, 1448, 1202, 1137. ESI-MS (m/z)  $[M+2H]^{2+}$  obsd. = 775.26 (calc = 775.38),  $[M+2H]^{2+}$  obsd. = 775.26 (calc = 774.92),  $[M-H]^-$  obsd. = 1546.88 (calc = 1546.81),  $[M+TFA-H]^-$  obsd. 1660.89 (calc = 1660.81).

Copper(I) catalyzed macrocyclization of 50 mg crude linear peptide 6 (32.3 μmol) was conducted in degassed and argon-flushed H<sub>2</sub>O (1 mg/mL) with 1 eq of copper(II) sulfate pentahydrate (CuSO<sub>4</sub>·5H<sub>2</sub>O), 1 eq sodium ascorbate (NaAsc) and 8 eq DIEA at RT over night. The solvent was removed by freeze-drying followed by semi-preparative purification *via* HPLC to yield 7.8 mg macrocyclic peptide 4 (5.04 μmol, 12.8 % overall yield). IR (cm<sup>-1</sup>) 3288, 3074, 2969, 2880, 2110, 1652, 1538, 1448, 1202, 1137. ESI-MS (m/z)  $[M+Na+H]^{2+}$  obsd. = 786.50 (calc = 785.91),  $[M+H]^+$  obsd. = 1549.11 (calc = 1548.83),  $[M+Na]^+$  obsd. = 1571.06 (calc = 1571.82),  $[M-H]^-$  obsd. = 1546.78 (calc = 1546.81),  $[M+TFA-H]^-$  obsd. 1661.39 (calc = 1660.81). For the isotope pattern of  $[M+H]^+$  see spectra in section 5.



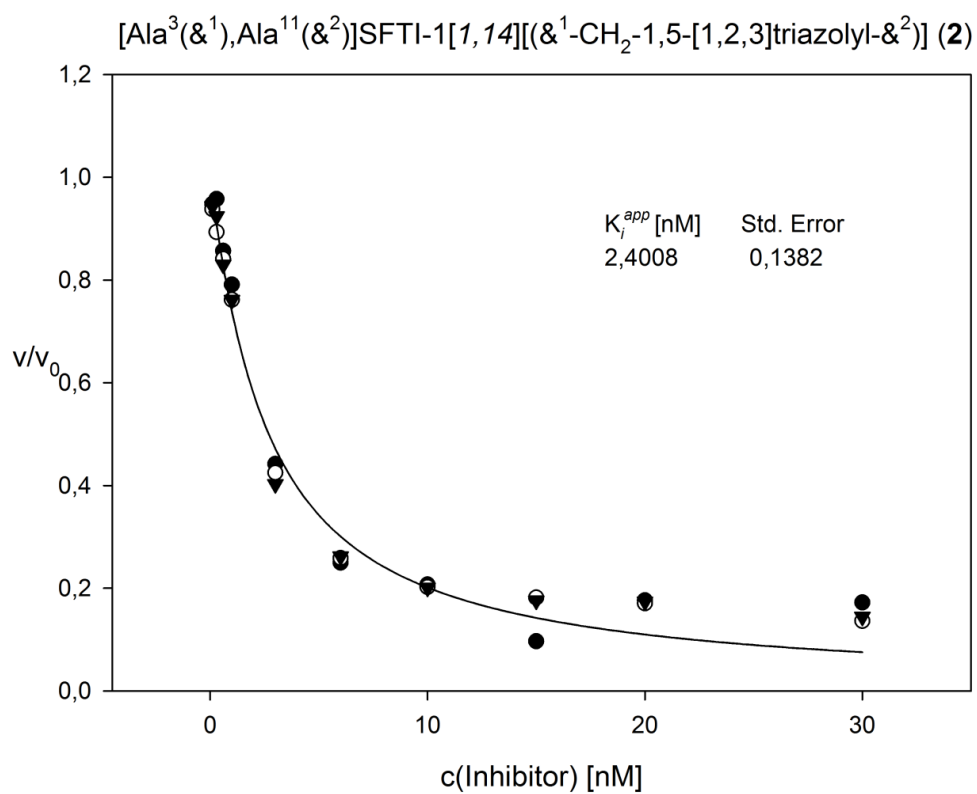
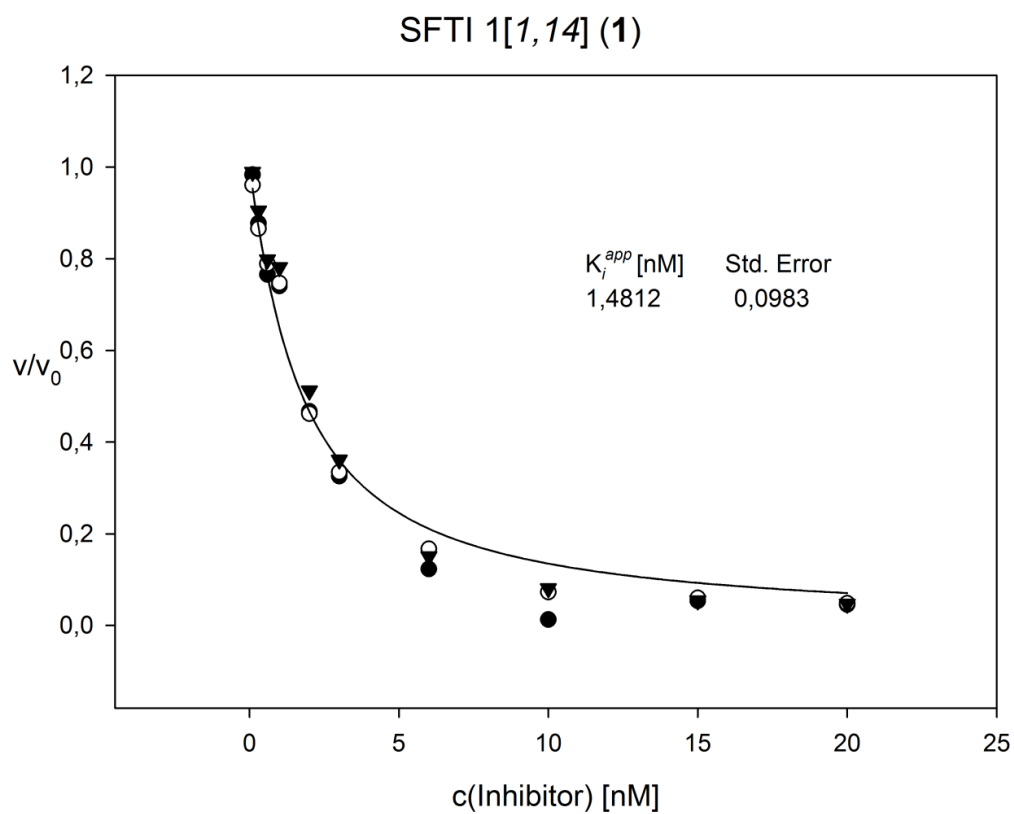
## Trypsin Inhibition

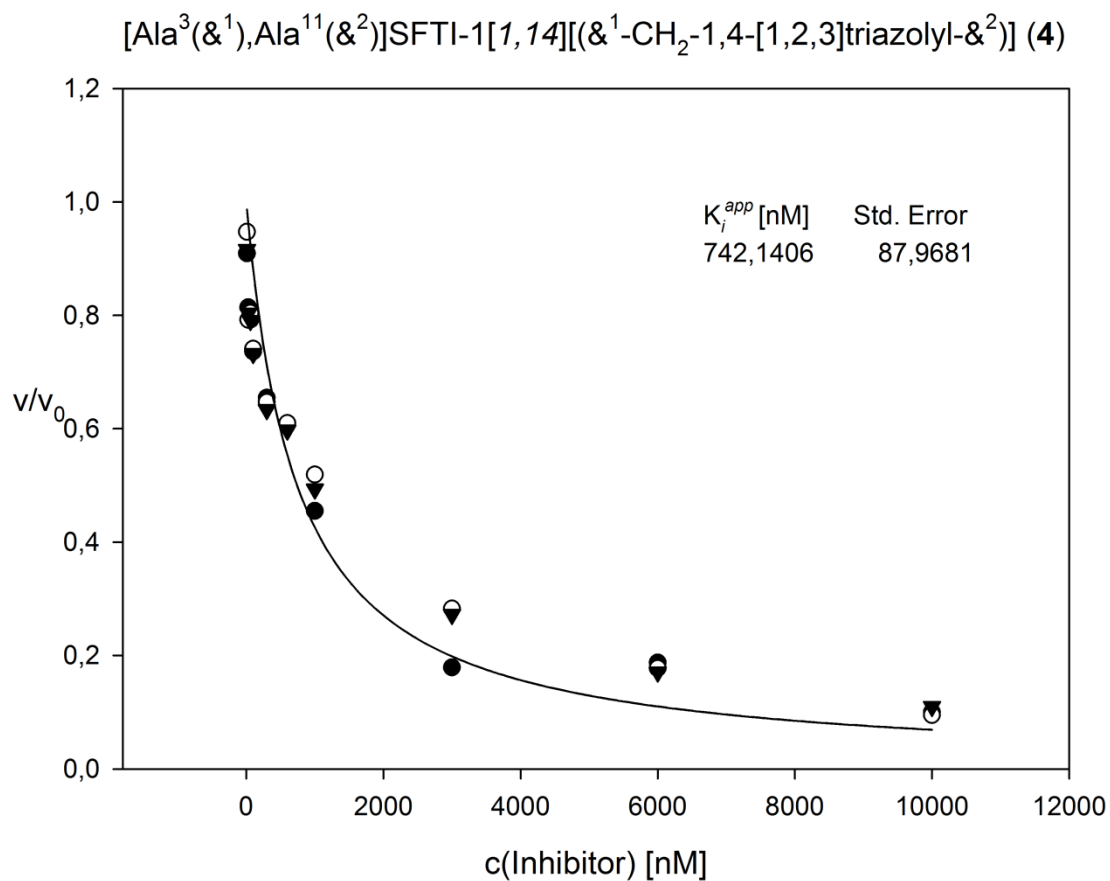
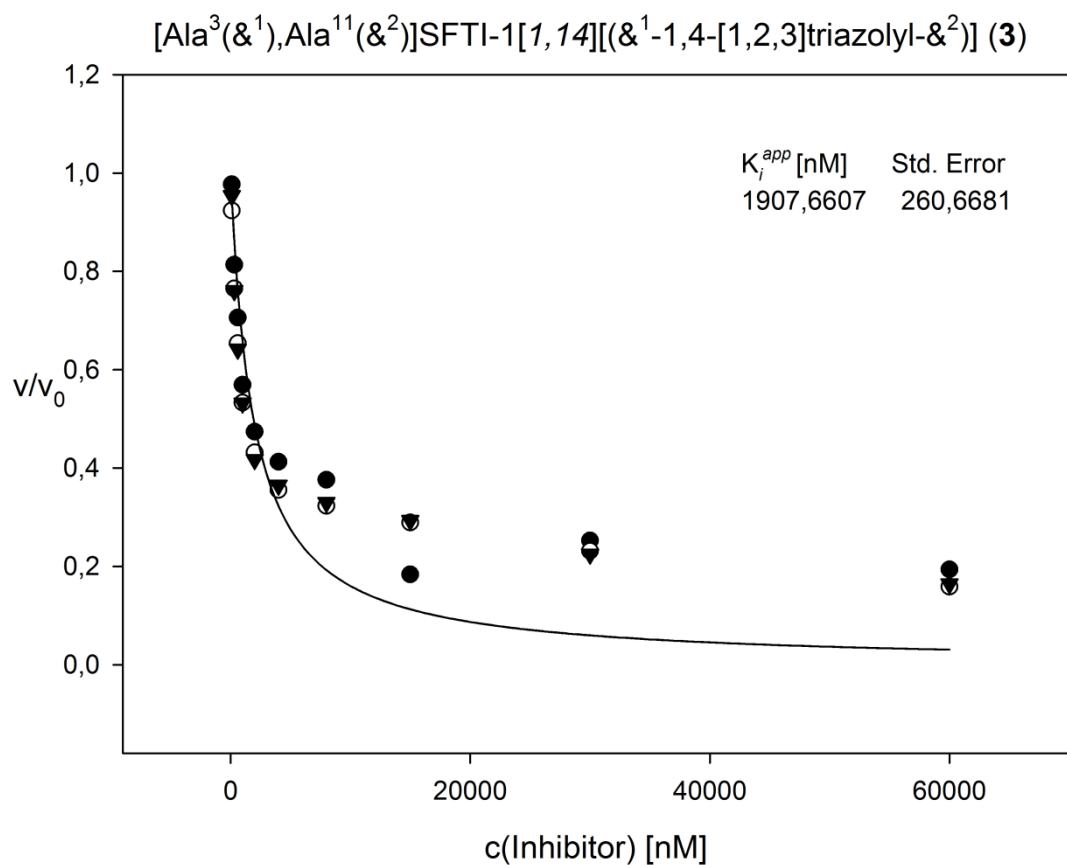
Kinetic curves were recorded by monitoring the absorption of the corresponding samples in 96-well plates (NUNC, flat bottom, clear) at 405 nm in intervals of 60 sec over 30 min at RT using the Tecan GENios microplate reader and all experiments were performed in triplicate.

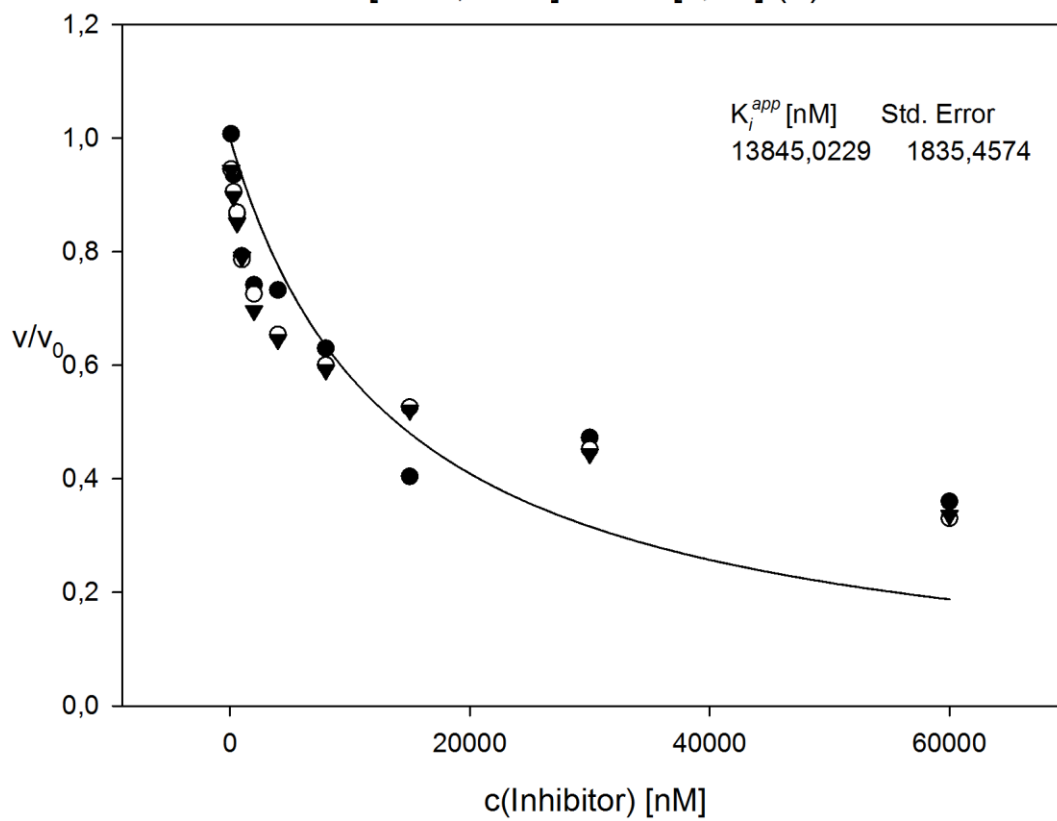
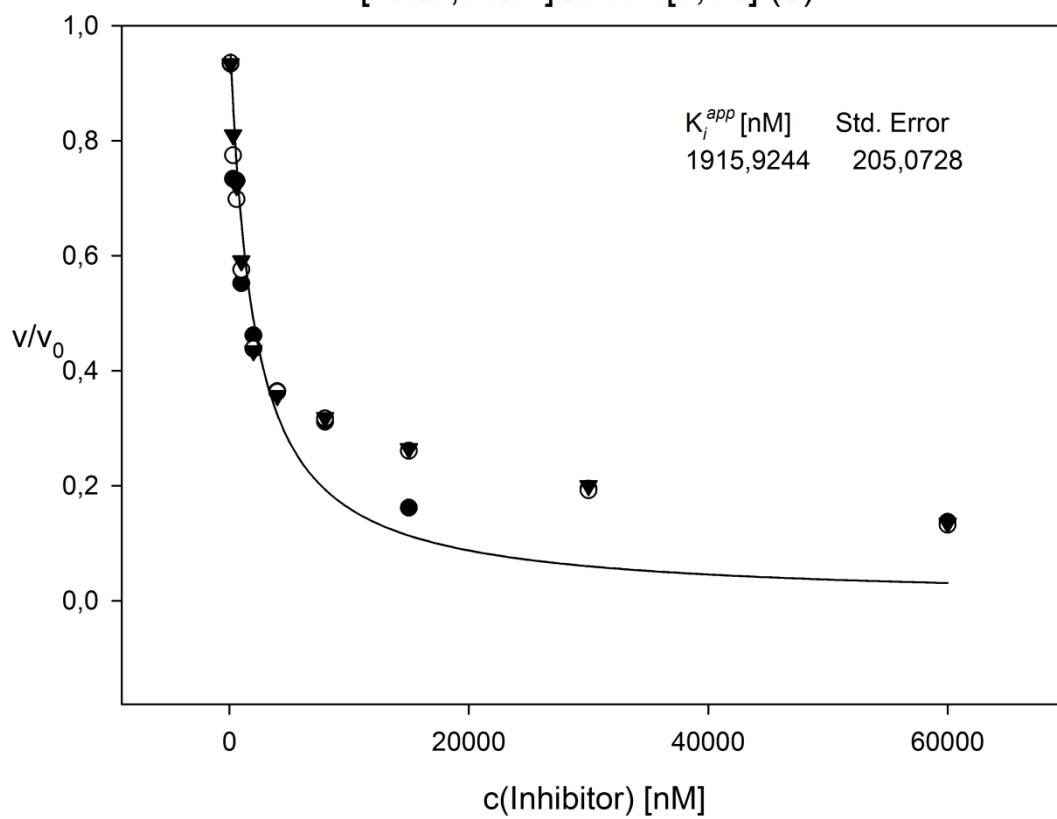
Trypsin from bovine pancreas (Sigma) was standardized by active-site titration with *p*-nitrophenyl-*p*'-guanidinobenzoate (NPGb) in phosphate buffered saline (PBS: 137 mM NaCl, 2.7 mM KCl, 10.0 mM Na<sub>2</sub>HPO<sub>4</sub>, 1.76 mM KH<sub>2</sub>PO<sub>4</sub>, pH 7.4). The normalized residual proteolytic activity ( $v/v_0$ ) of trypsin towards the chromogenic substrate Boc-QAR-pNA (250  $\mu$ M, Bachem) at different concentrations of linear and monocyclic SFTI-1 analogues **1-6** ( $I_0$ ) was determined for  $\sim 0.6$  nM active enzyme ( $E_0$ ) in buffer (50 mM Tris/HCl, 150 mM NaCl, 0.01% Triton X-100, 0.01% sodium azide, pH 7.6). The apparent inhibition constants ( $K_i^{app}$ ) were calculated through fitting the Morrison equation for tight binding inhibitors (1) onto the resulting kinetic data with the Marquardt-Levenberg algorithm of SigmaPlot 11.

$$\frac{v}{v_0} = 1 - \frac{(E_0 + I_0 + K_i^{app}) - \sqrt{(E_0 + I_0 + K_i^{app})^2 - 4E_0I_0}}{2E_0} \quad (1)$$

## 6.3.3 Plotted Kinetic Data

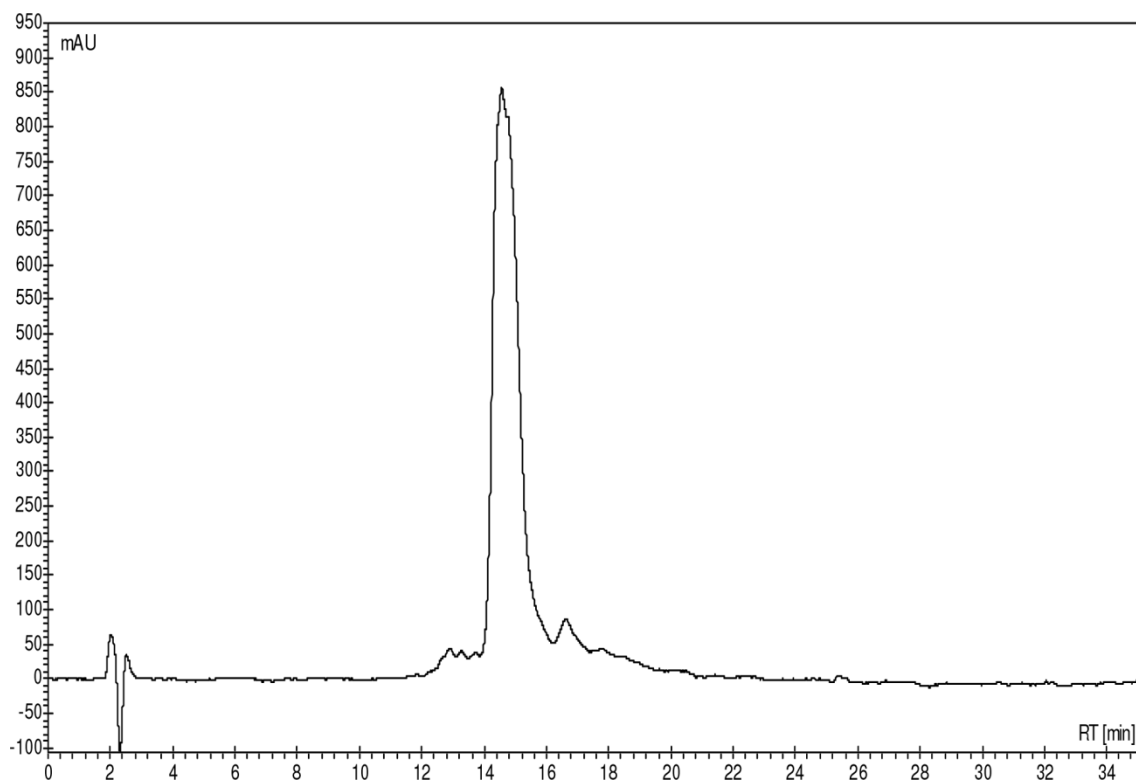




**[Aza<sup>3</sup>,Pra<sup>11</sup>]SFTI 1[1,14] (5)****[Aha<sup>3</sup>,Pra<sup>11</sup>]SFTI 1[1,14] (6)**

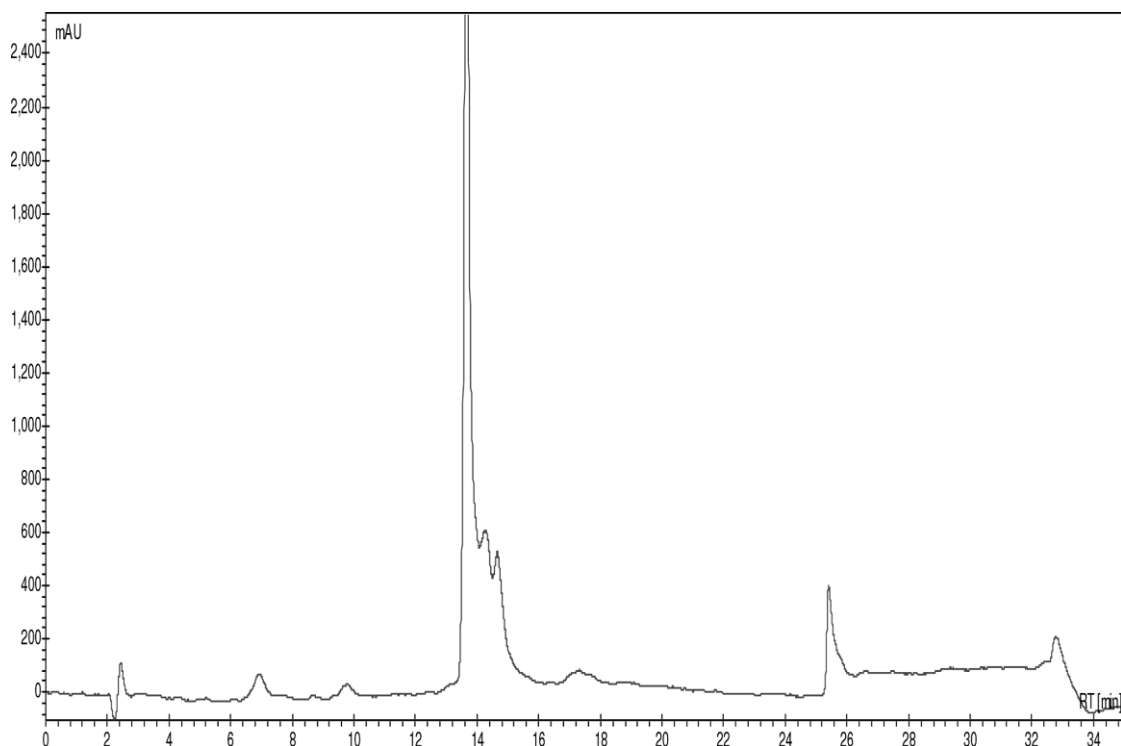
### 6.3.4 RP-HPLC

#### SFTI-1[1,14] (1)

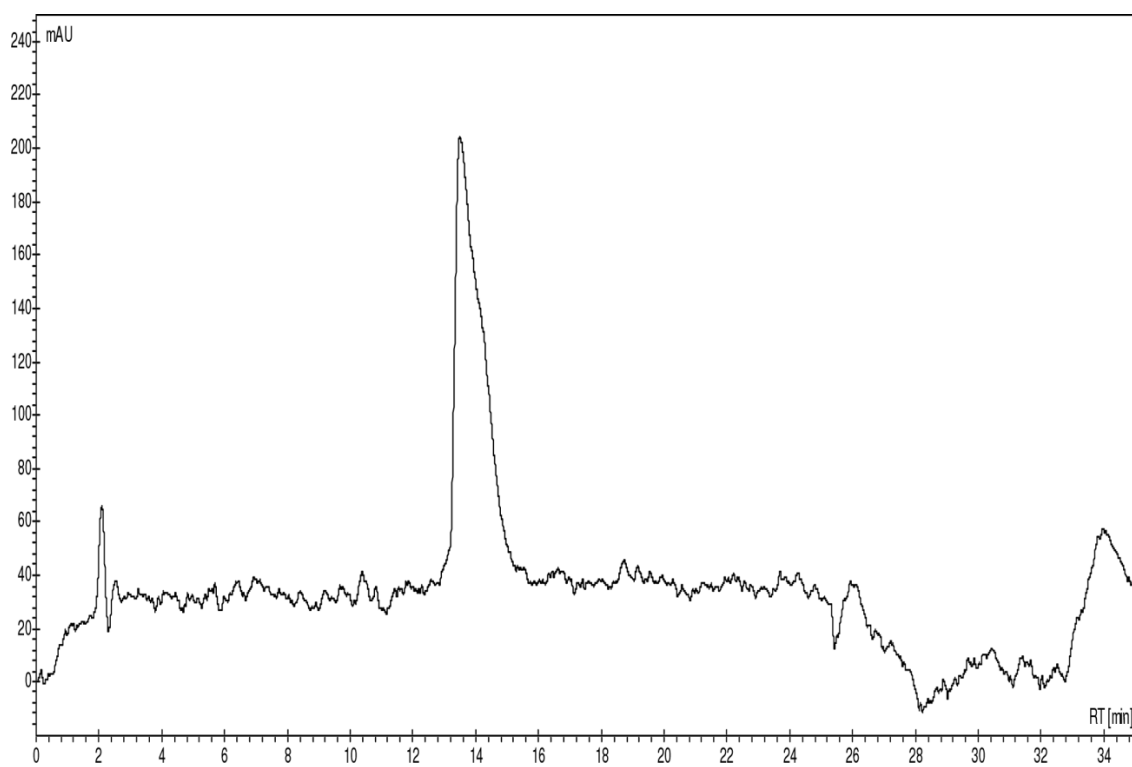


HPLC chromatogram of purified **1** recorded at 220 nm. Gradient: 18→40.5 % acetonitrile in 0.1% aq. TFA over 20 minutes at flow rate 1 mL/min.

[Ala<sup>3</sup>(&<sup>1</sup>),Ala<sup>11</sup>(&<sup>2</sup>)]SFTI-1[1,14][(&<sup>1</sup>-CH<sub>2</sub>-1,5-[1,2,3]triazolyl-&<sup>2</sup>)] (2)

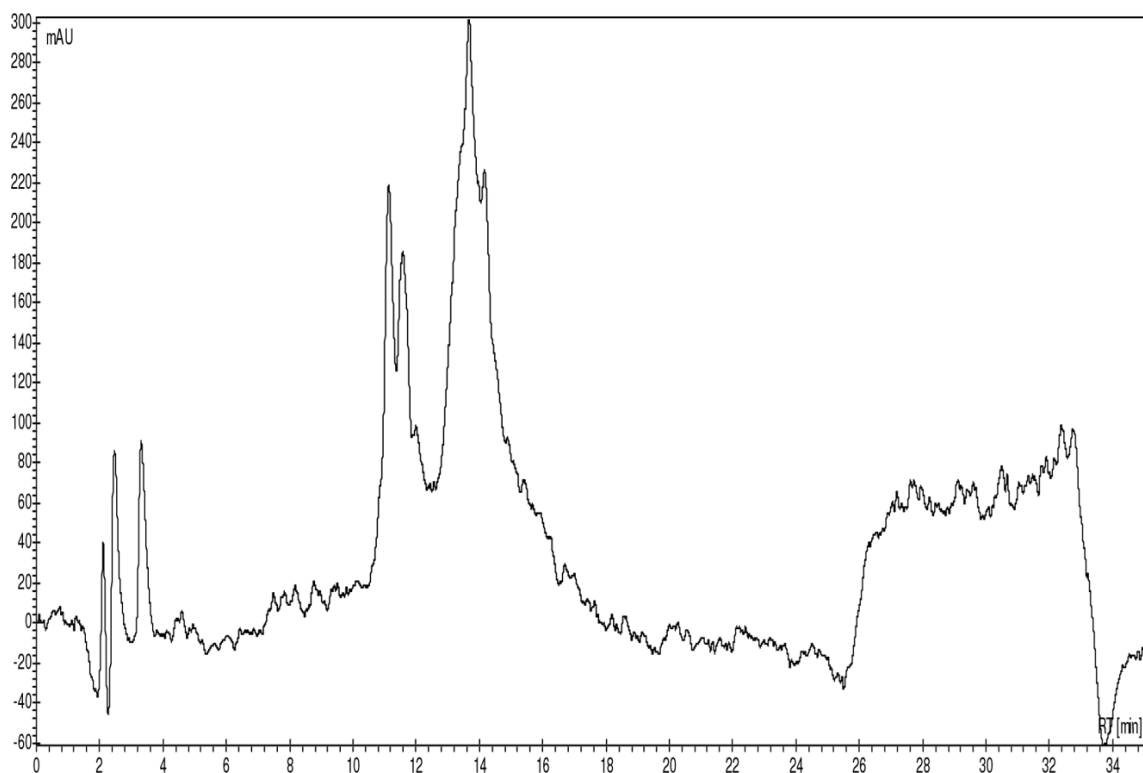


HPLC chromatogram of crude 2 recorded at 220 nm. Gradient: 18→40.5 % acetonitrile in 0.1% aq. TFA over 20 minutes at flow rate 1 mL/min.

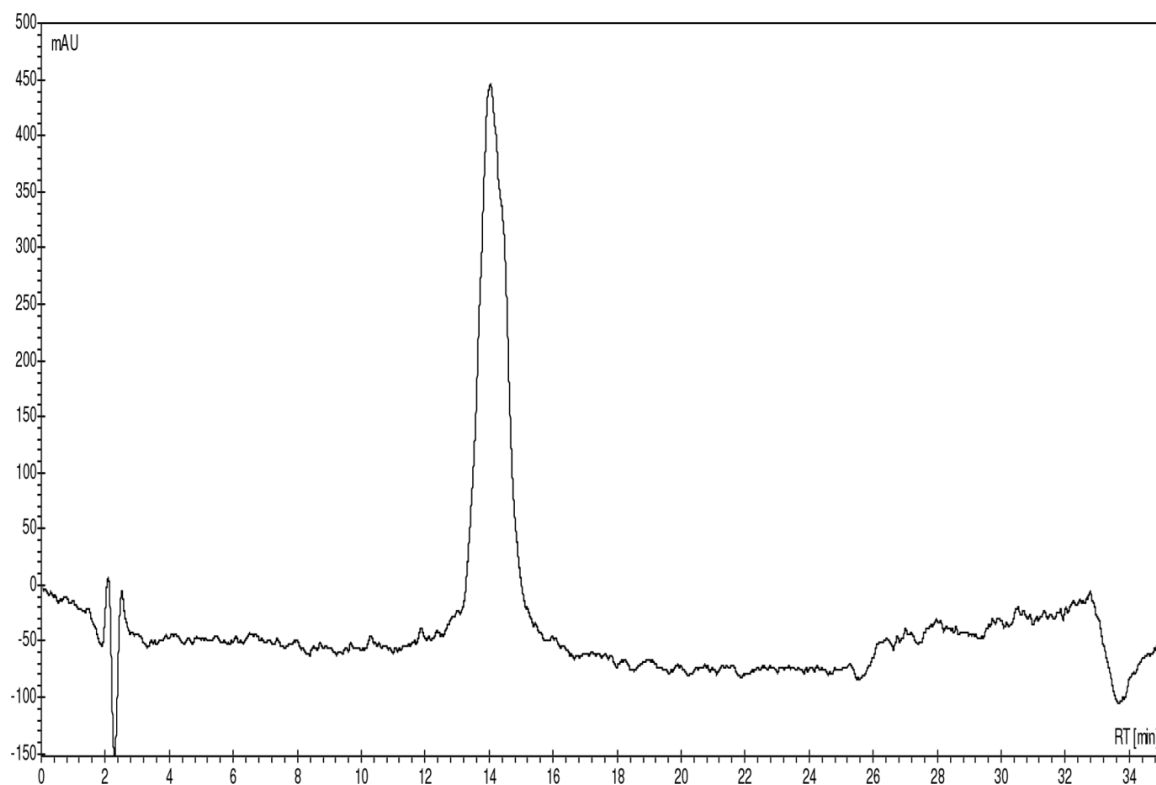


HPLC chromatogram of purified 2 recorded at 220 nm. Gradient: 18→40.5 % acetonitrile in 0.1% aq. TFA over 20 minutes at flow rate 1 mL/min.

[Ala<sup>3</sup>(&<sup>1</sup>),Ala<sup>11</sup>(&<sup>2</sup>)]SFTI-1[1,14][(&<sup>1</sup>-1,4-[1,2,3]triazolyl-&<sup>2</sup>)] (3)



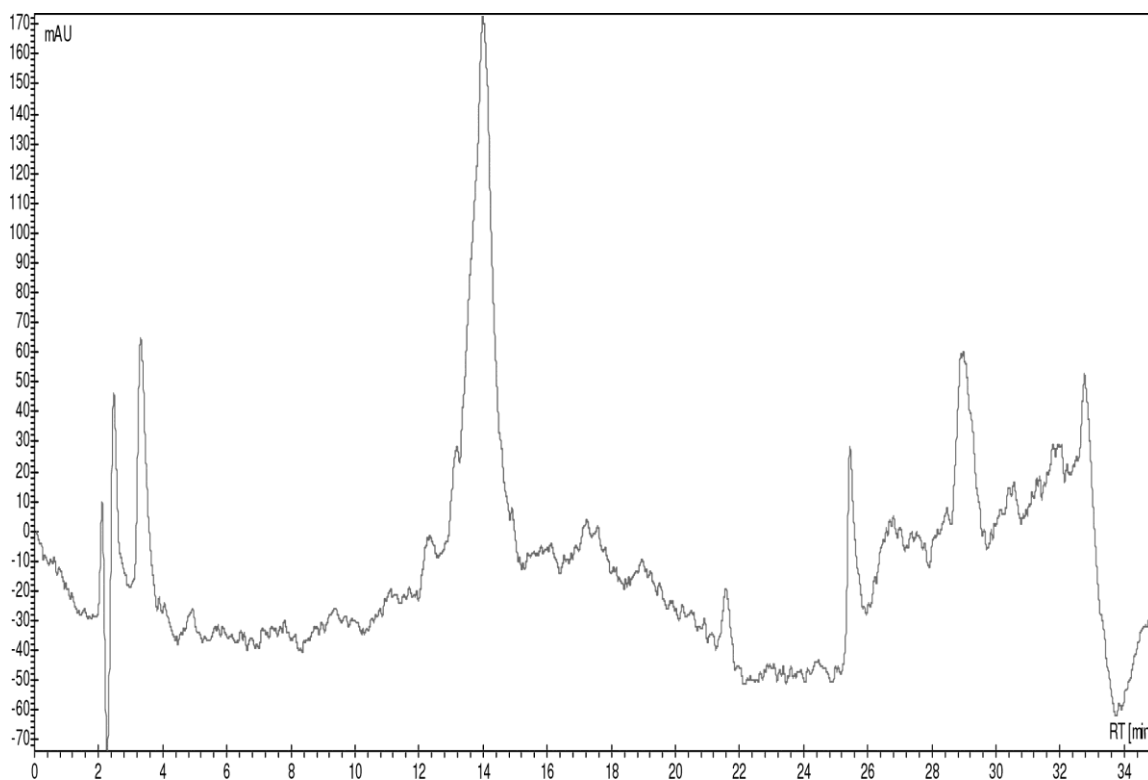
HPLC chromatogram of crude 3 recorded at 220 nm. Gradient: 18→54 % acetonitrile in 0.1% aq. TFA over 20 minutes at flow rate 1 mL/min.



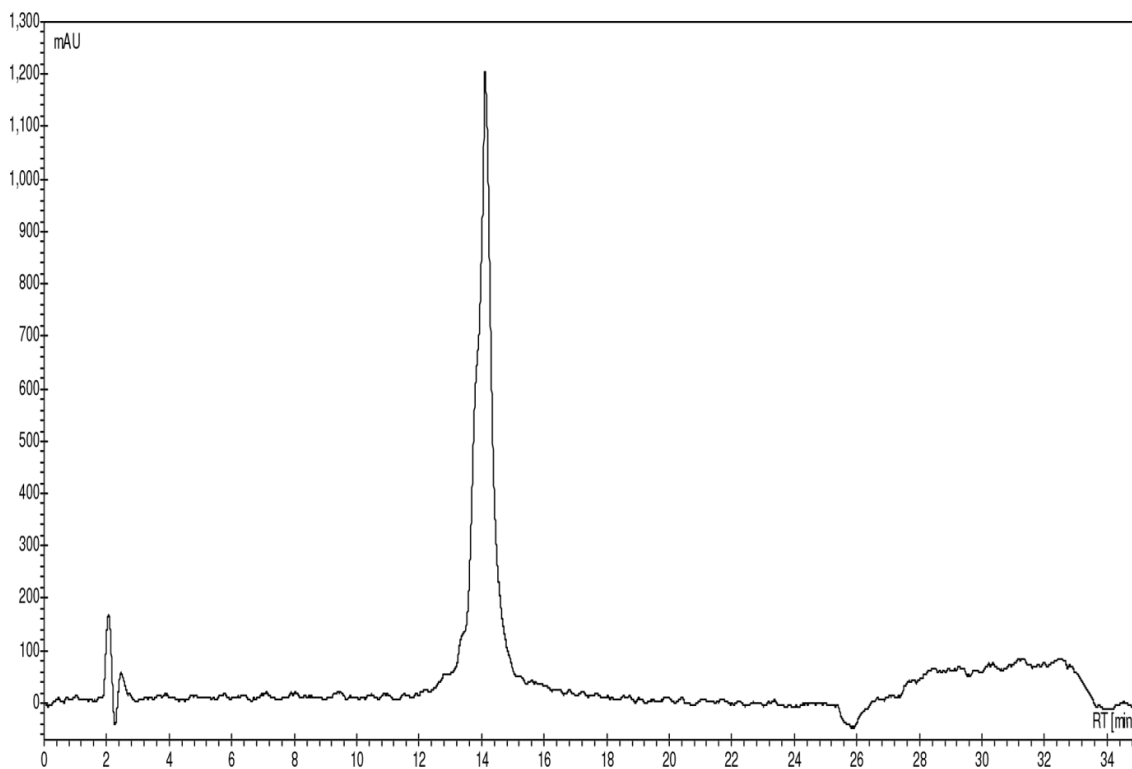
HPLC chromatogram of purified 3 recorded at 220 nm. Gradient: 18→54 % acetonitrile in 0.1% aq. TFA over 20 minutes at flow rate 1 mL/min.



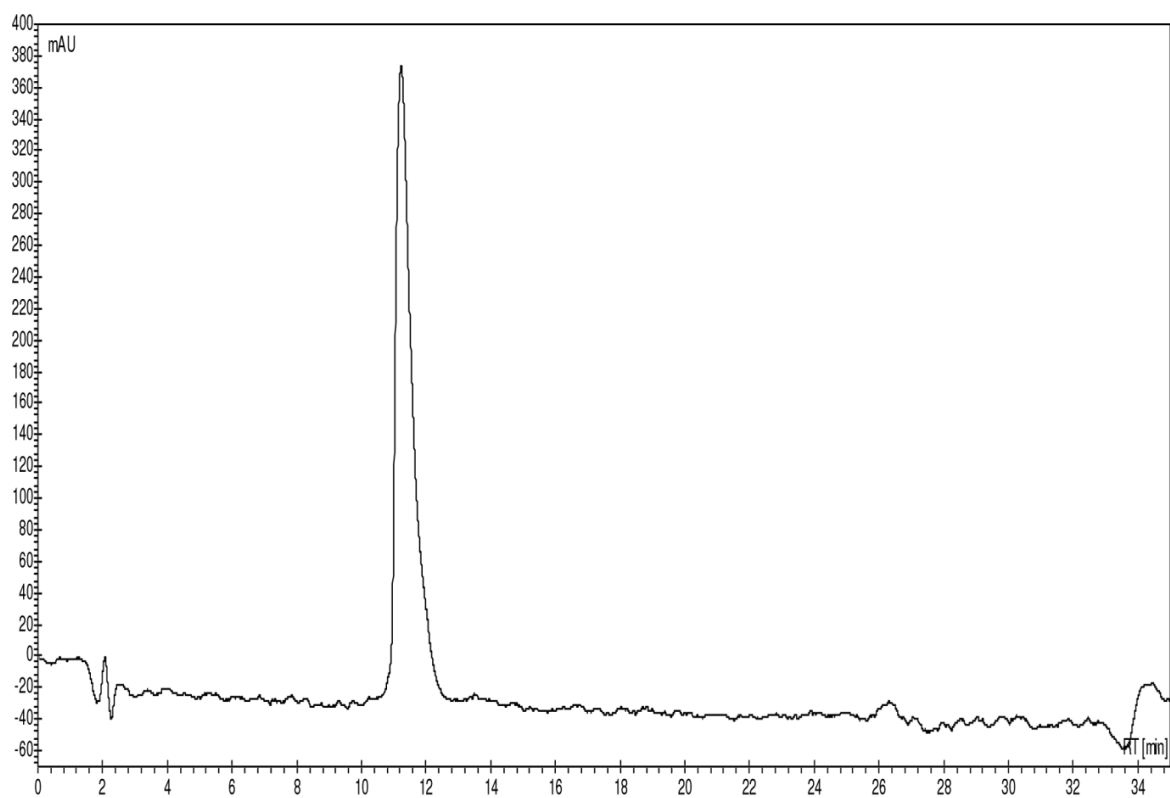
[Ala<sup>3</sup>(&<sup>1</sup>),Ala<sup>11</sup>(&<sup>2</sup>)]SFTI-1[1,14][(&<sup>1</sup>-CH<sub>2</sub>-1,4-[1,2,3]triazolyl-&<sup>2</sup>)] (4)



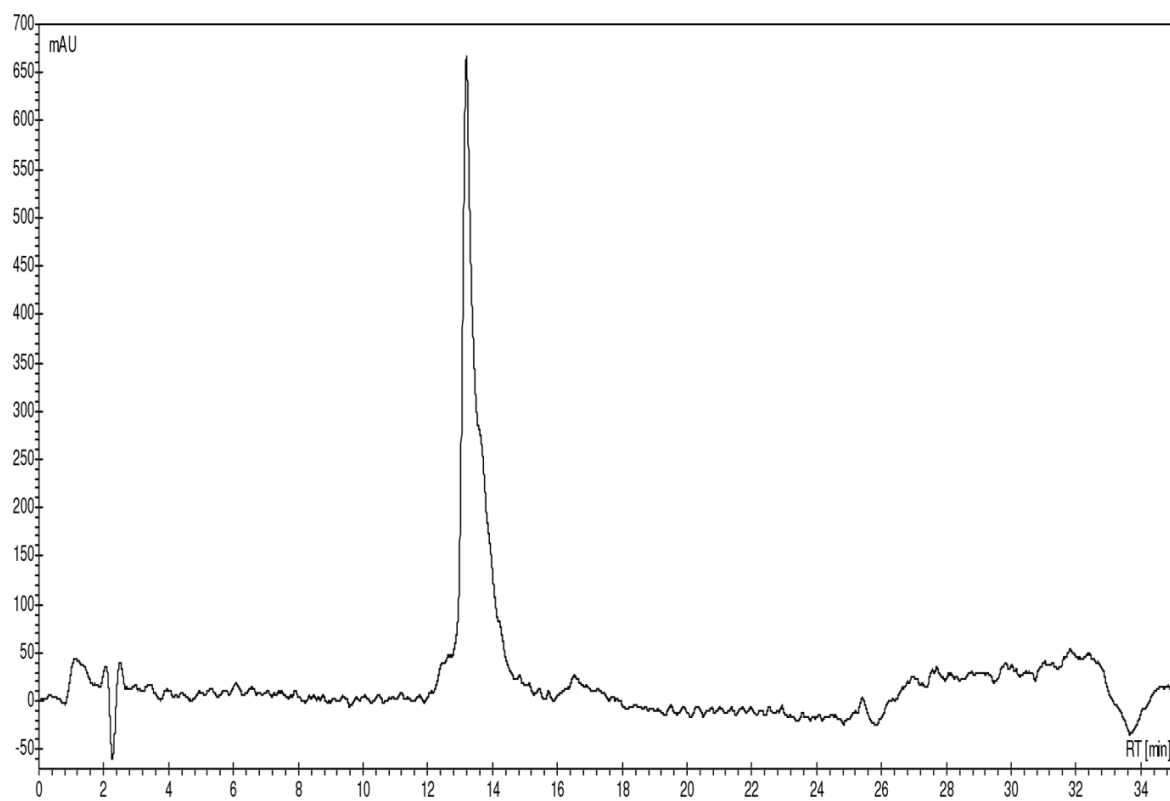
HPLC chromatogram of crude 4 recorded at 220 nm. Gradient: 18→40.5 % acetonitrile in 0.1% aq. TFA over 20 minutes at flow rate 1 mL/min.



HPLC chromatogram of purified 4 recorded at 220 nm. Gradient: 18→40.5 % acetonitrile in 0.1% aq. TFA over 20 minutes at flow rate 1 mL/min.

$[Aza^3, Pra^{11}]SFTI-1[1,14]$  (5)

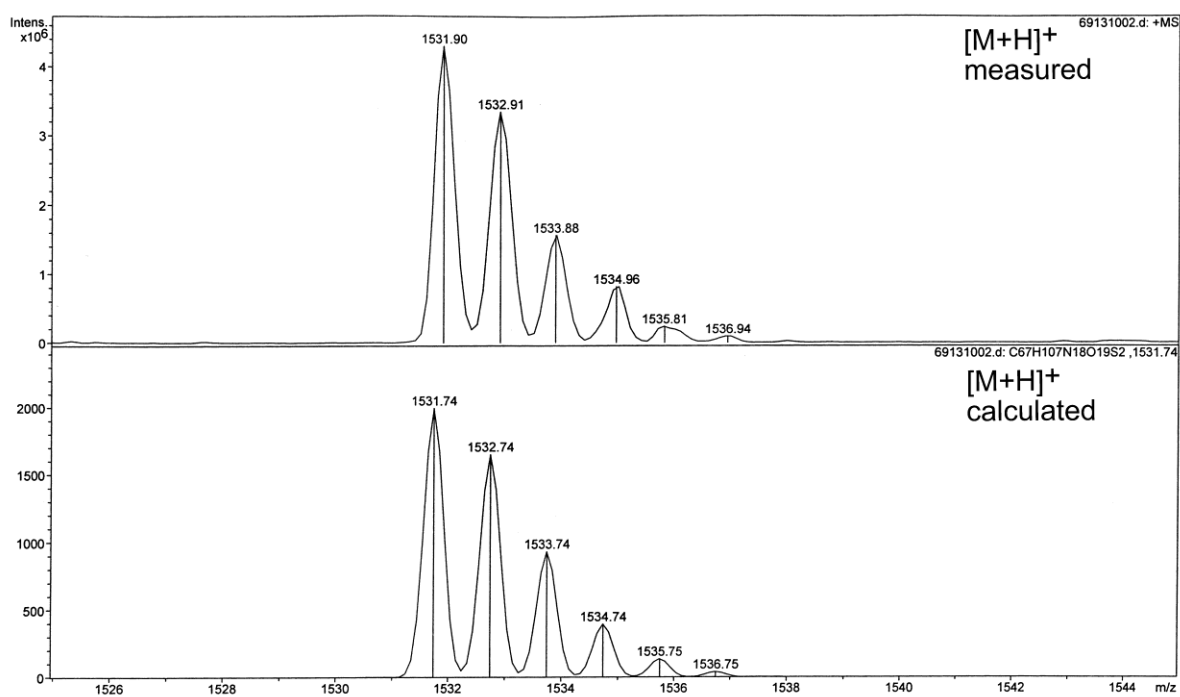
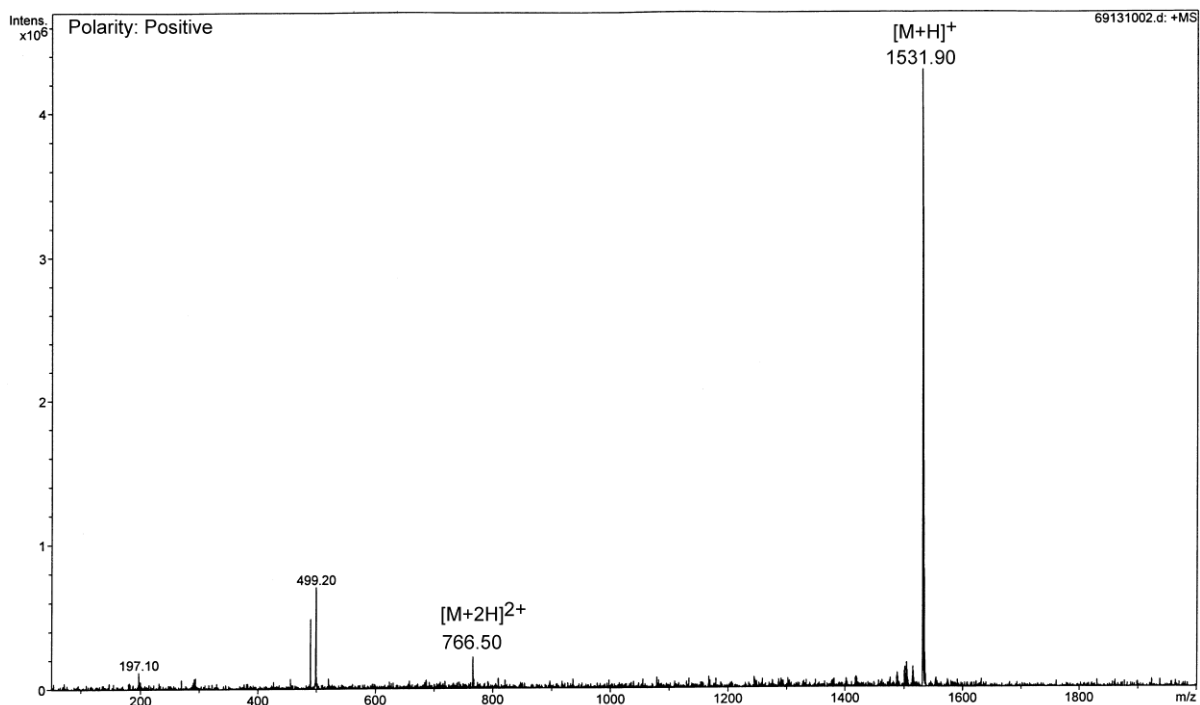
HPLC chromatogram of purified 5 recorded at 220 nm. Gradient: 18→54 % acetonitrile in 0.1% aq. TFA over 20 minutes at flow rate 1 mL/min.

$[Aha^3, Pra^{11}]SFTI-1[1,14]$  (**6**)

HPLC chromatogram of purified **6** recorded at 220 nm. Gradient: 18→40.5 % acetonitrile in 0.1% aq. TFA over 20 minutes at flow rate 1 mL/min.

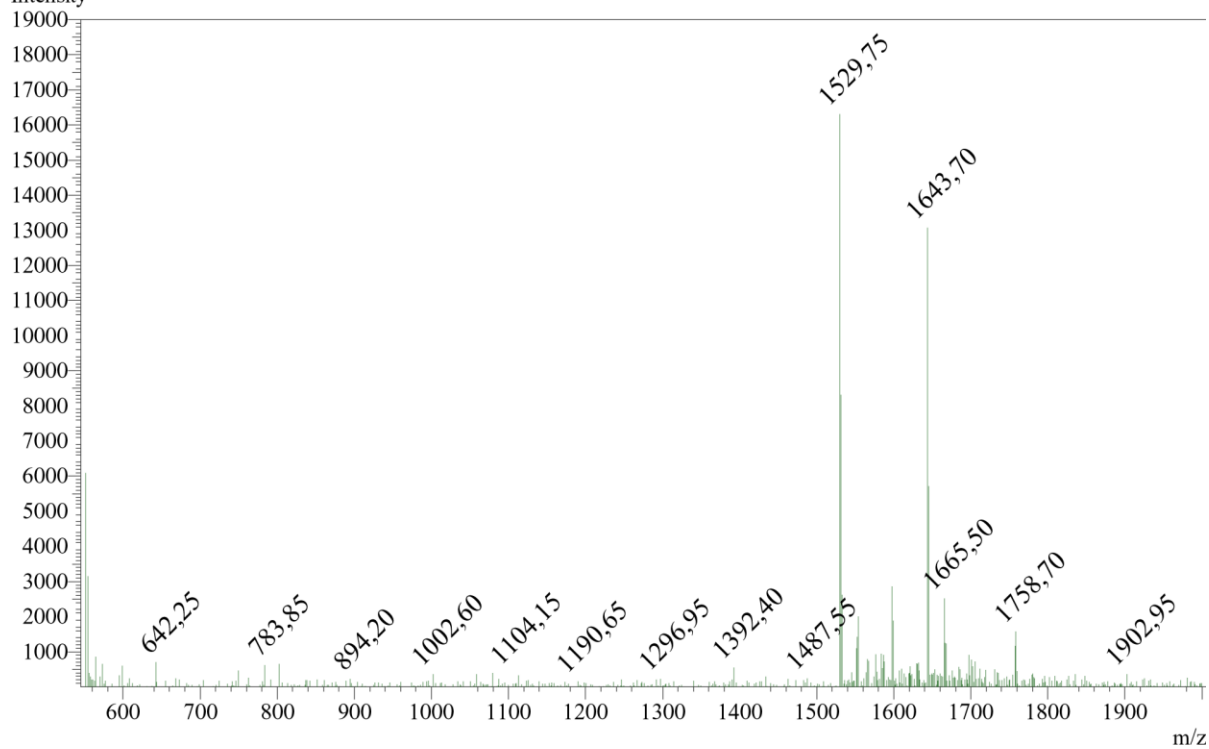
## 6.3.5 ESI-MS

## SFTI-1[1,14] (1)

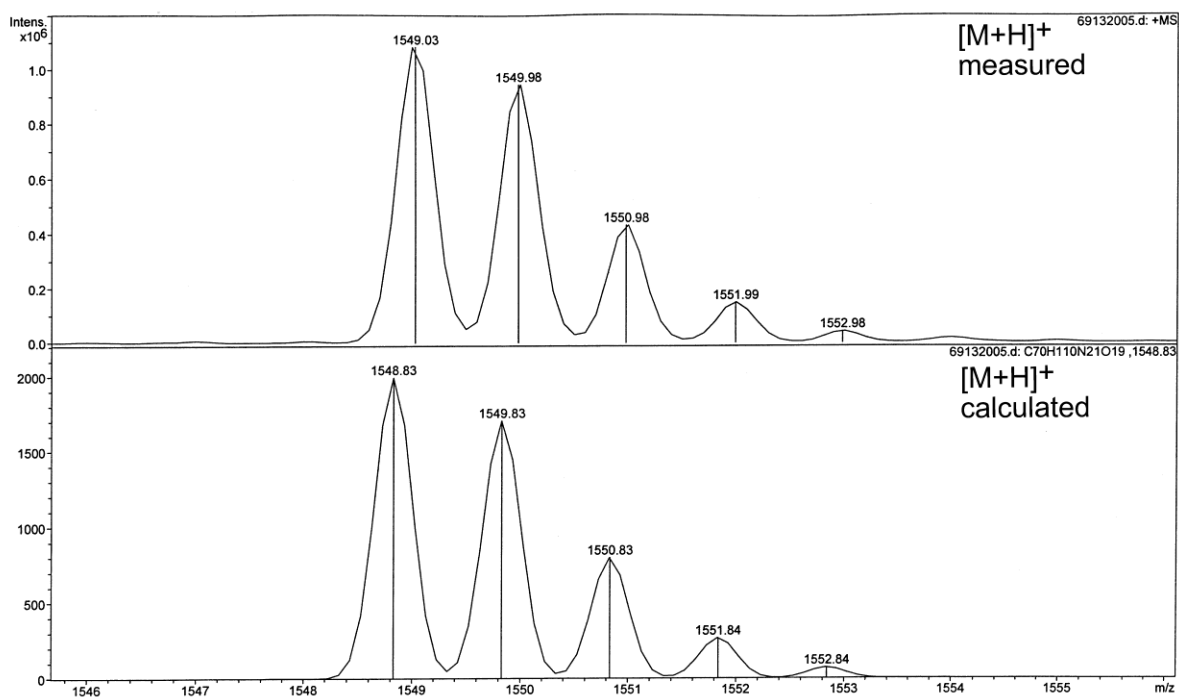
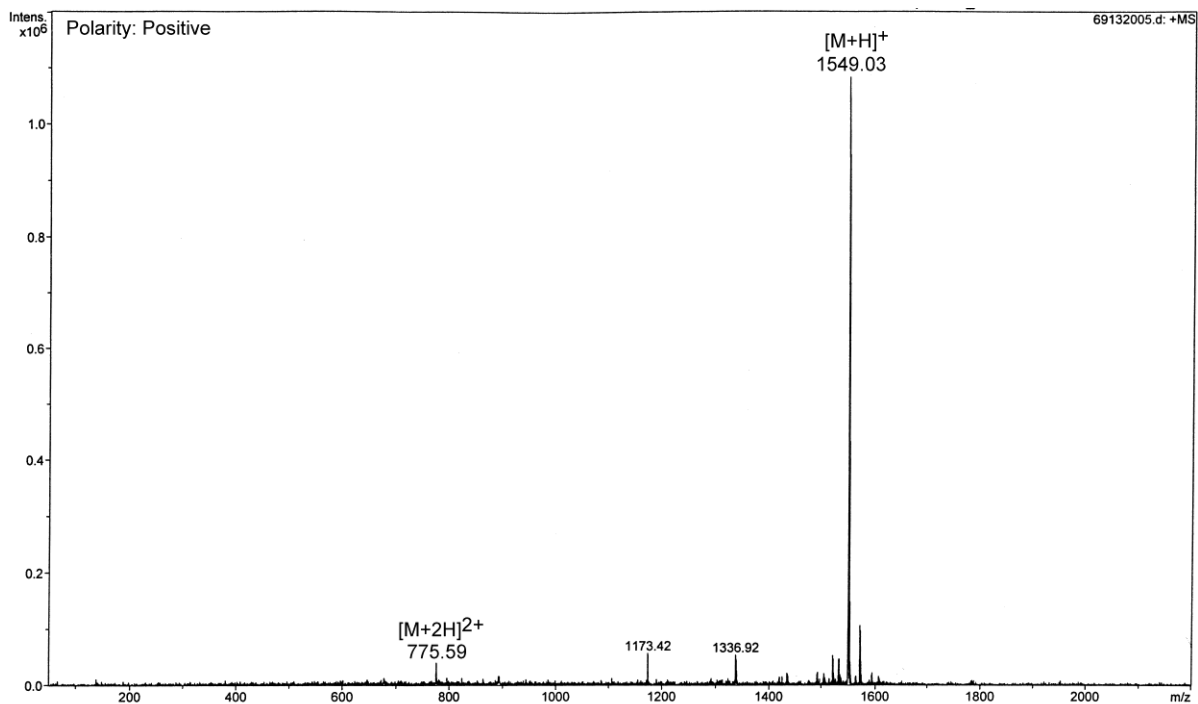


Polarity: Negative

Intensity

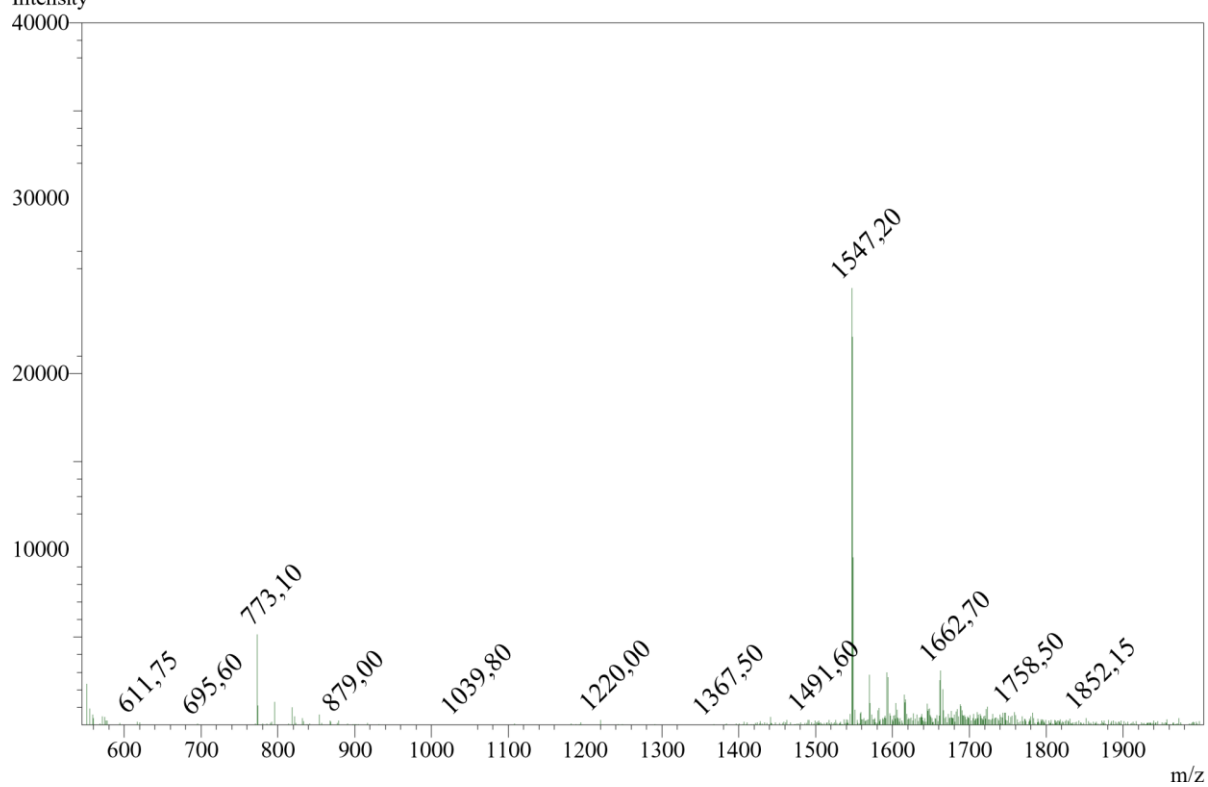


m/z

$[\text{Ala}^3(\&^1), \text{Ala}^{11}(\&^2)]\text{SFTI-1}[1,14][(\&^1\text{-CH}_2\text{-1,5-[1,2,3]\text{triazolyl-}\&^2)] (2)$ 

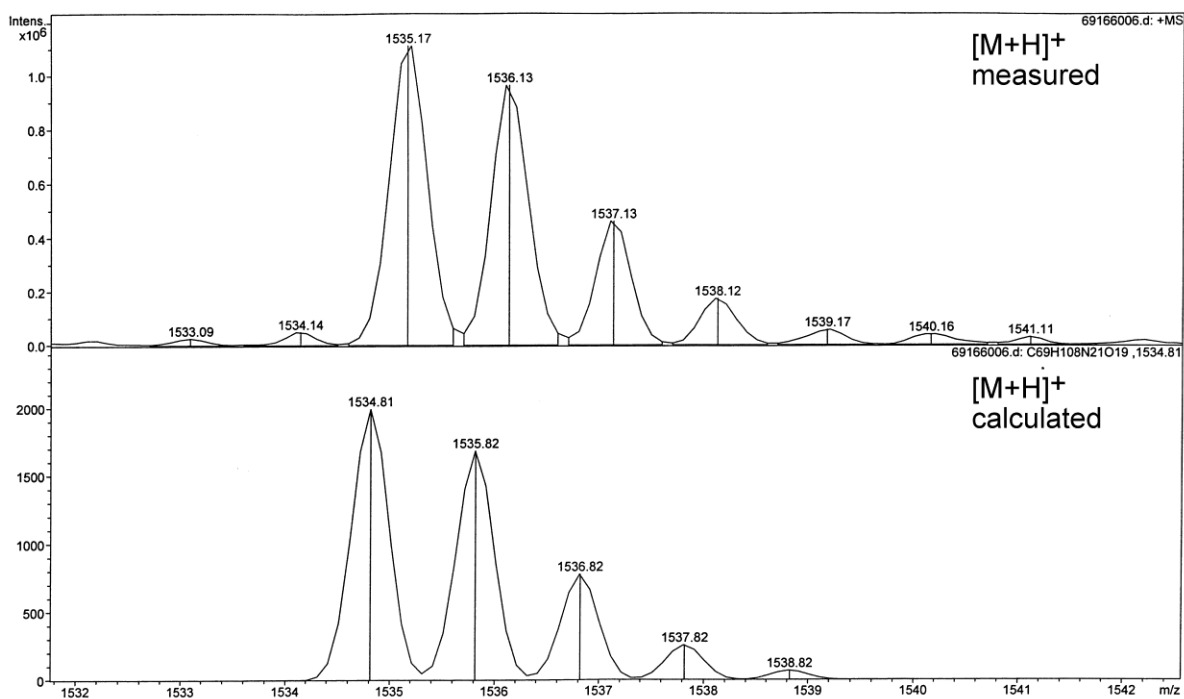
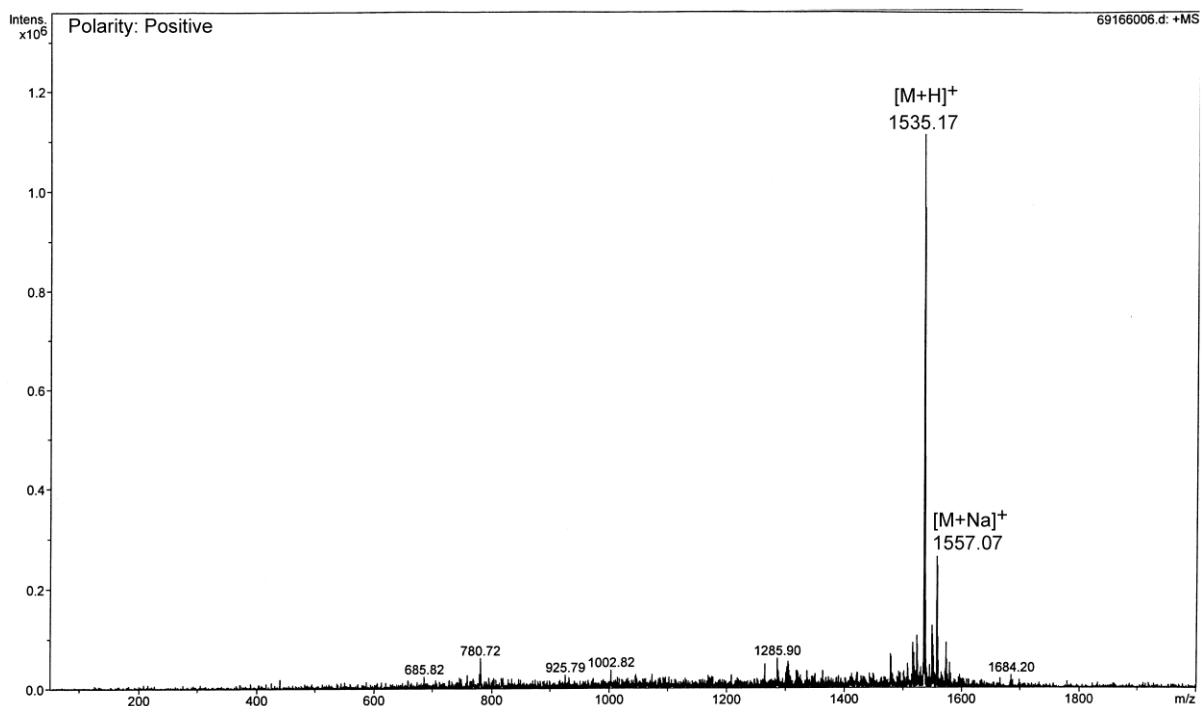
Polarity: Negative

Intensity



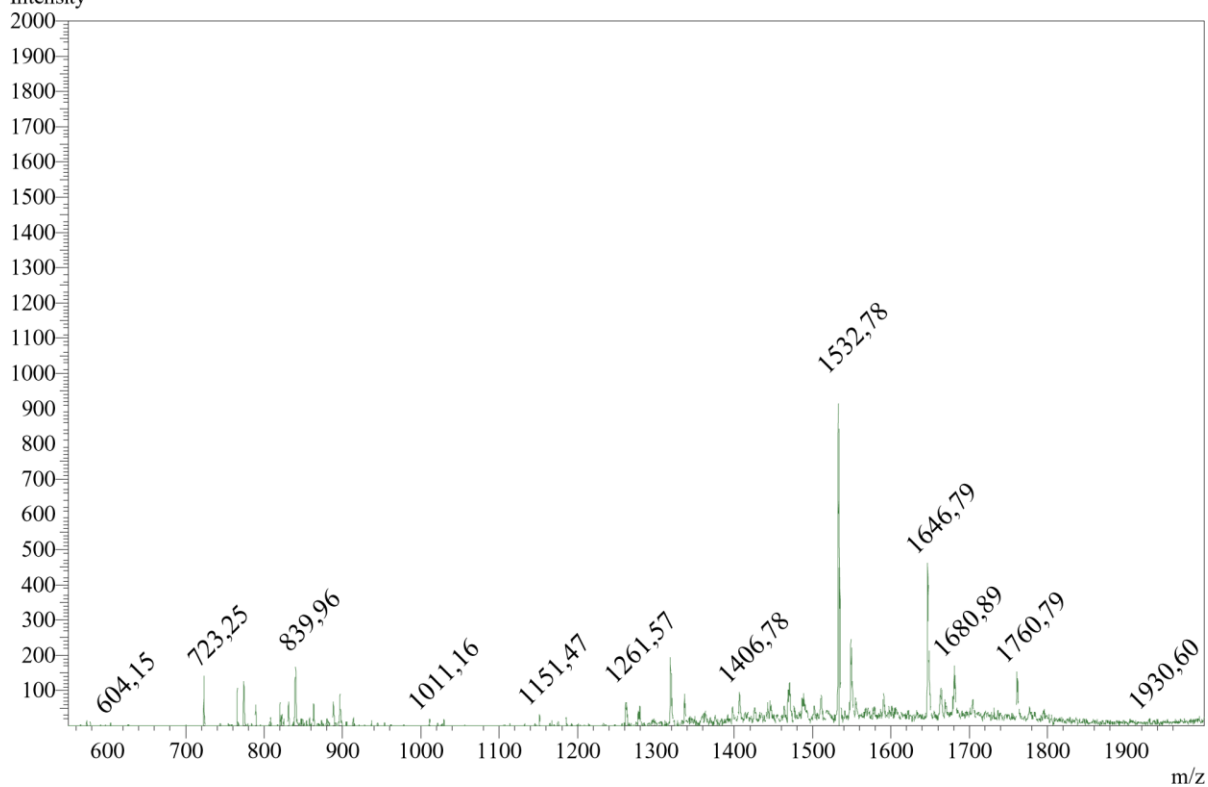
m/z



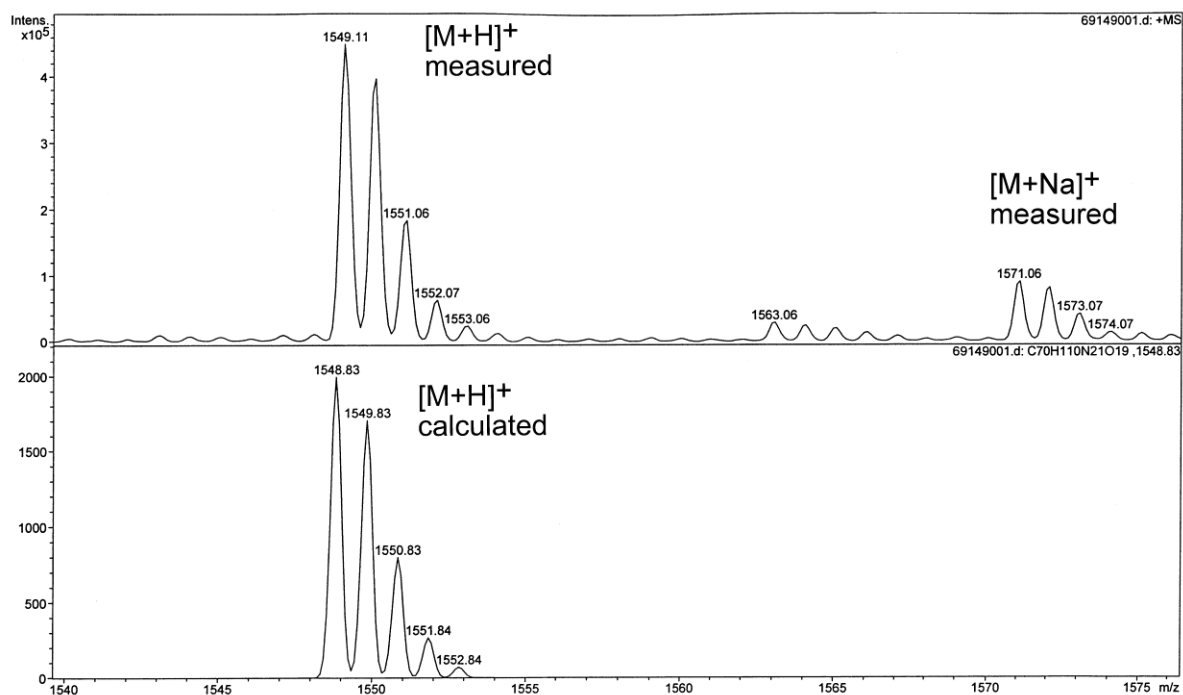
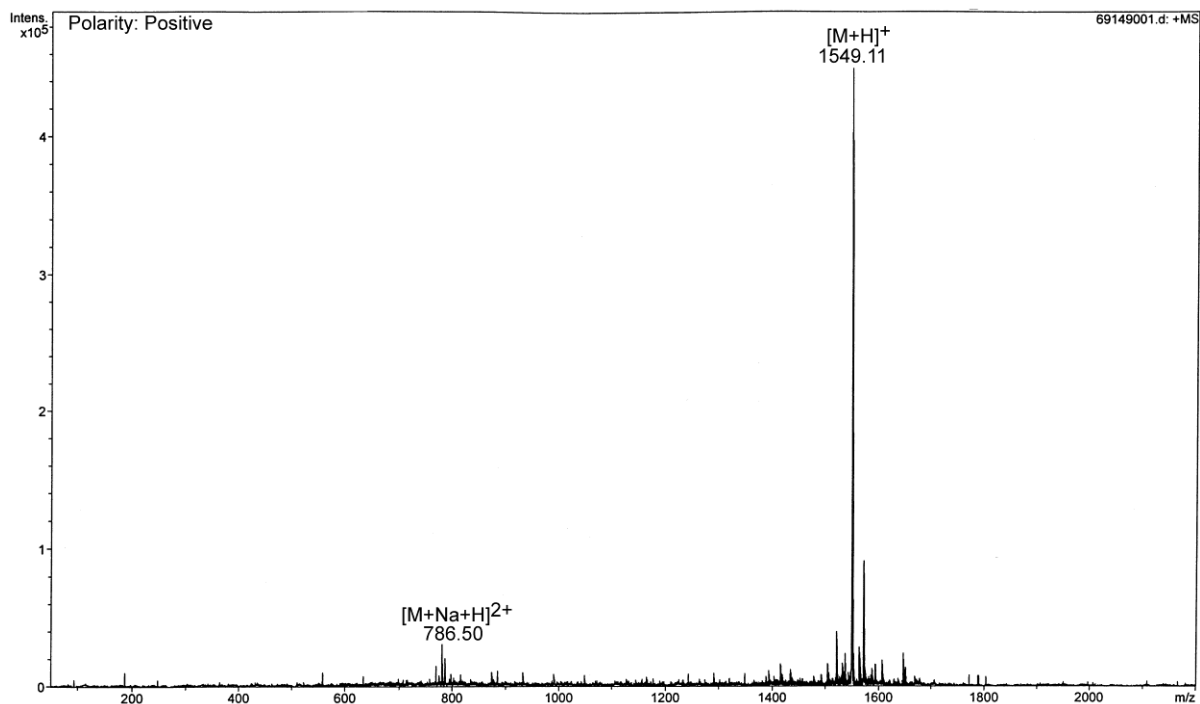
$[\text{Ala}^3(\&^1), \text{Ala}^{11}(\&^2)]\text{SFTI-1}[1,14][(\&^{-1}-1,4-[1,2,3]\text{triazolyl}-\&^2)]$  (3)

Polarity: Negative

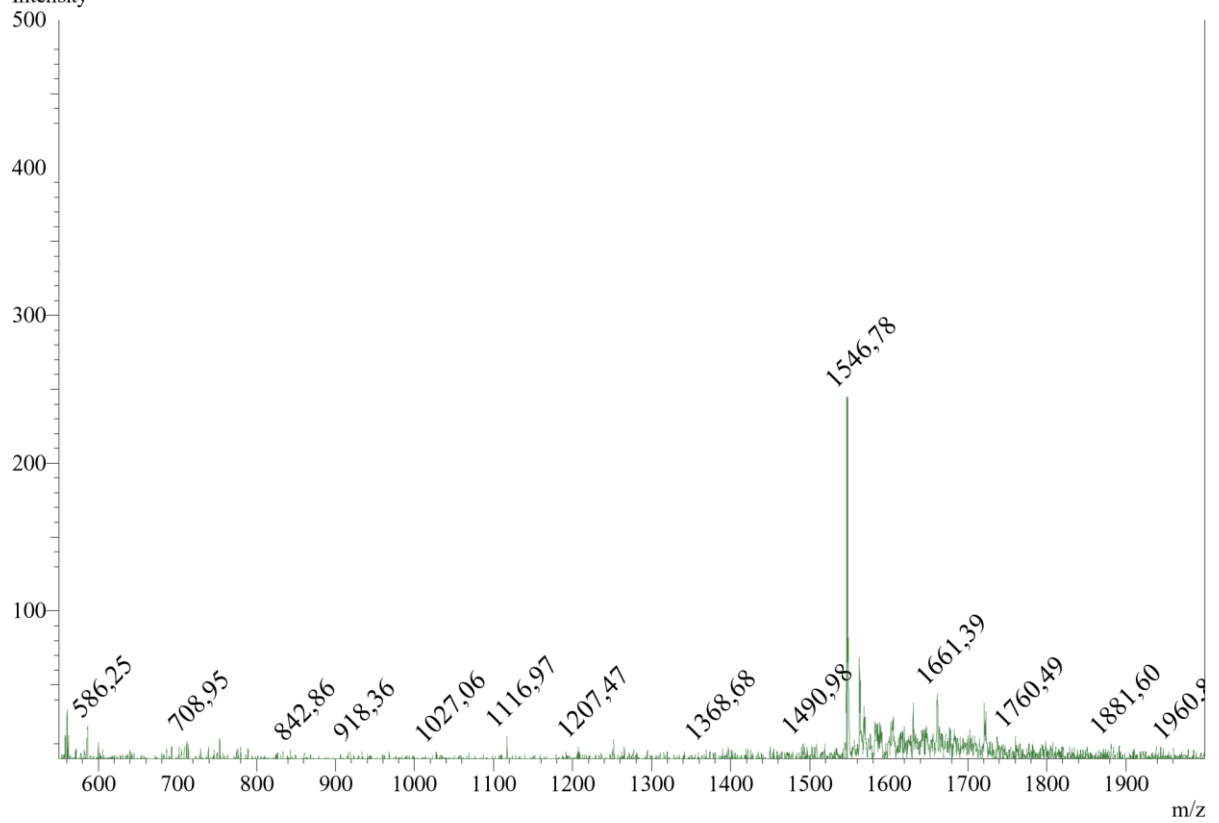
Intensity



[Ala<sup>3</sup>(&<sup>1</sup>),Ala<sup>11</sup>(&<sup>2</sup>)]SFTI-1[1,14][(&<sup>1</sup>-CH<sub>2</sub>-1,4-[1,2,3]triazolyl-&<sup>2</sup>)] (4)



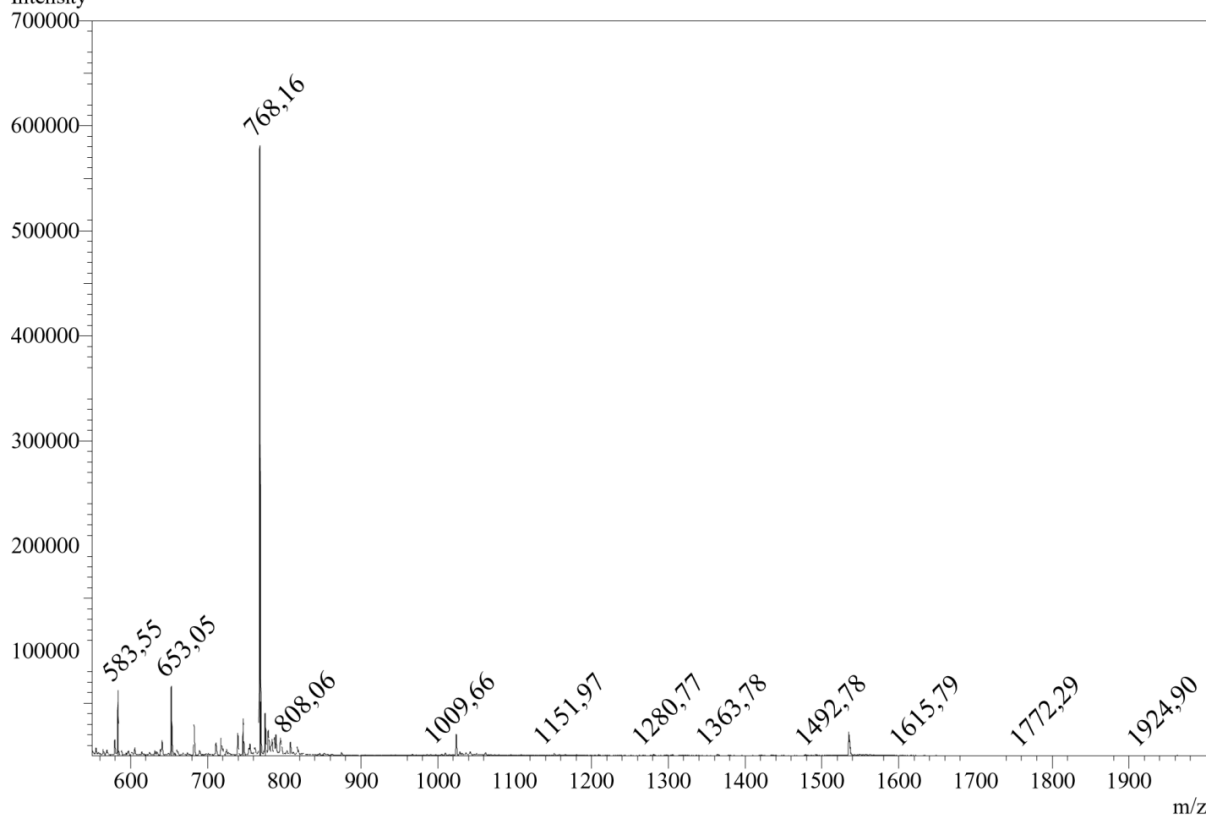
Polarity: Negative  
Intensity



[Aza<sup>3</sup>,Pra<sup>11</sup>]SFTI-1[1,14] (5)

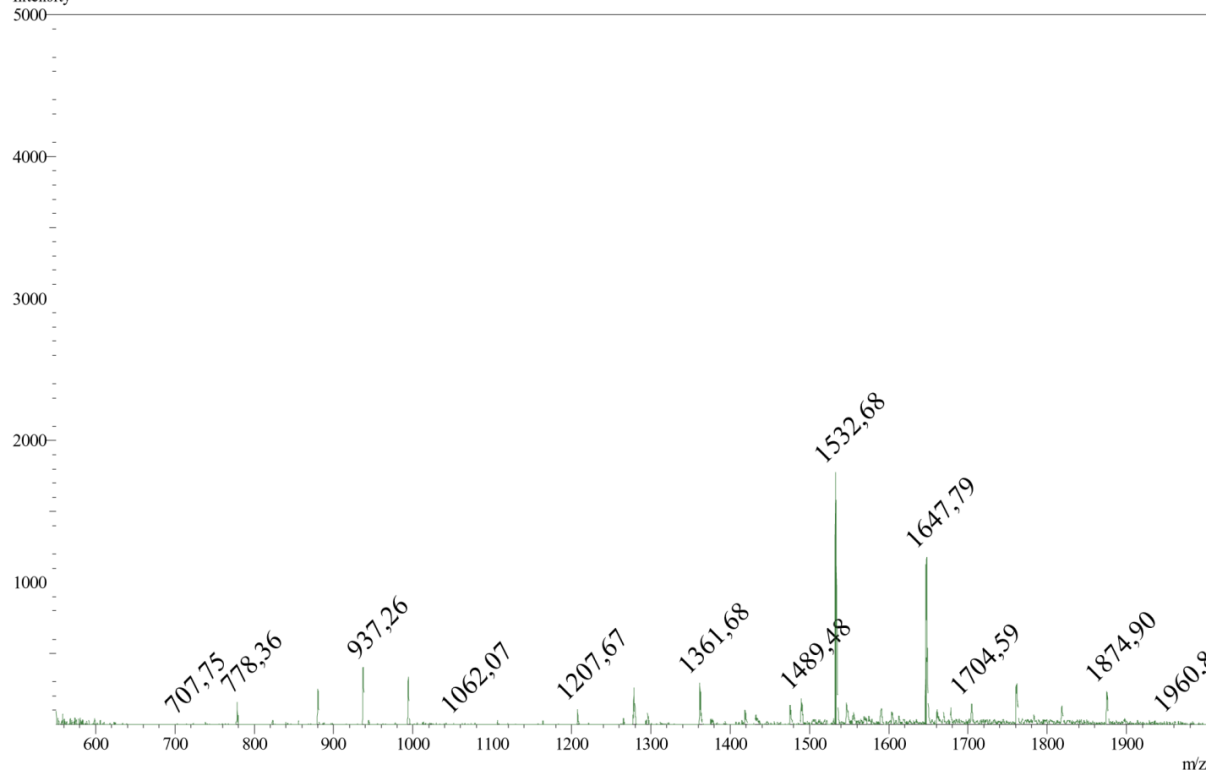
Polarity: Positive

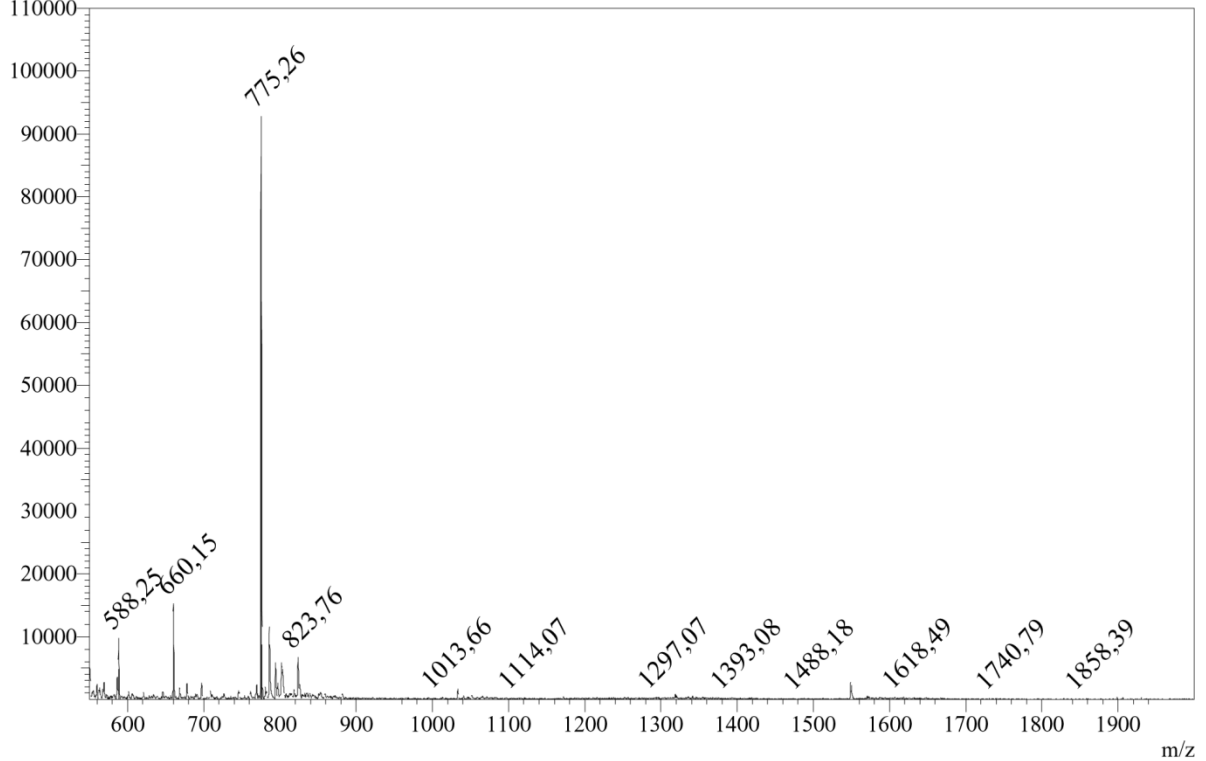
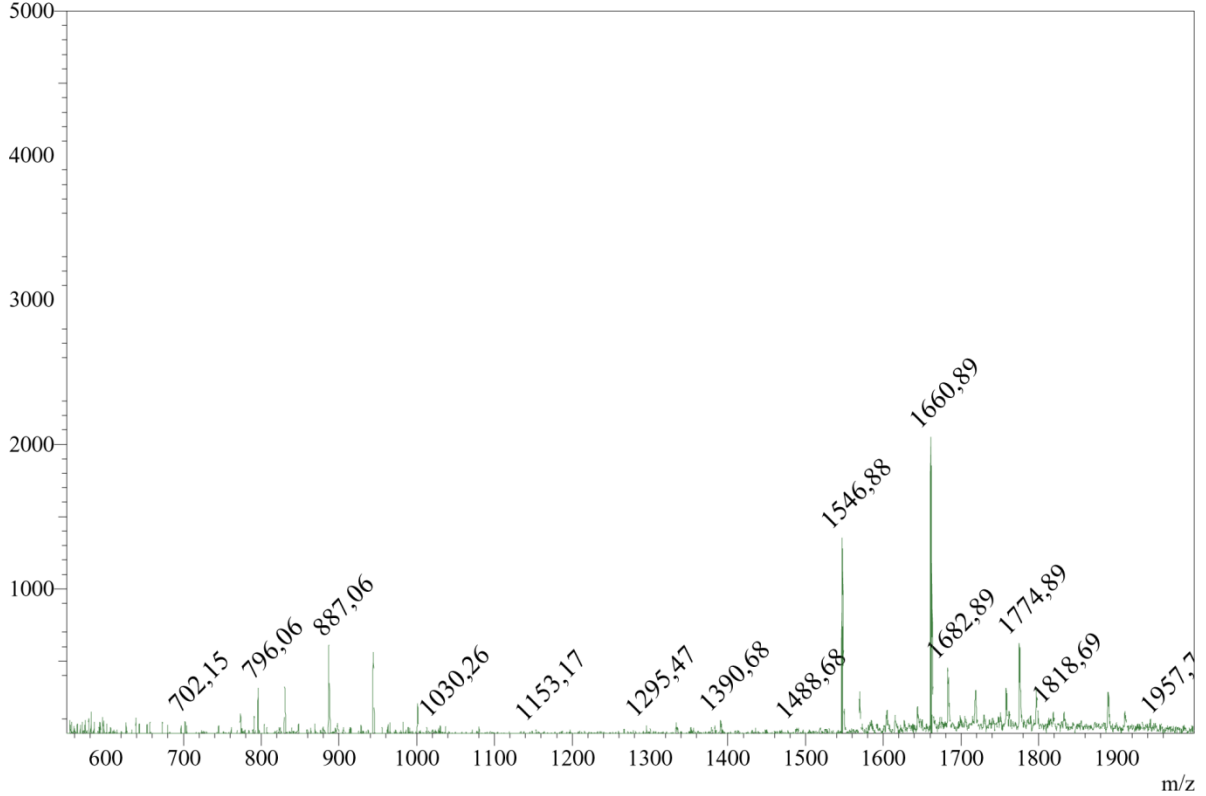
Intensity



Polarity: Negative

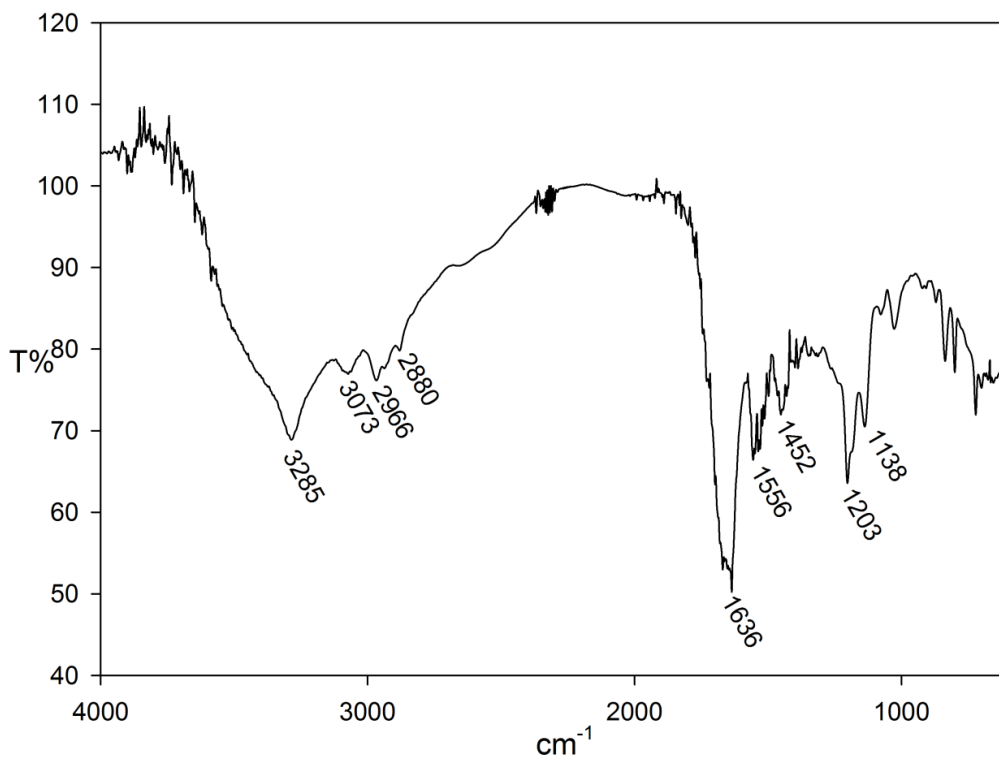
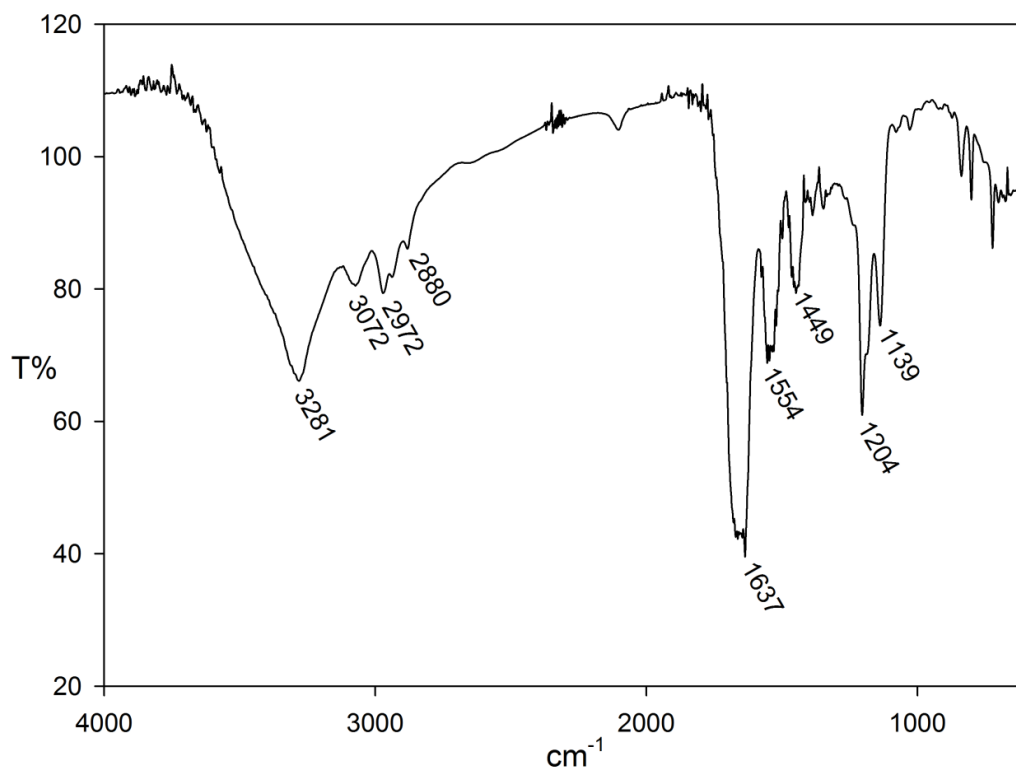
Intensity



[Aha<sup>3</sup>,Pra<sup>11</sup>]SFTI-1[1,14] (6)Polarity: Positive  
IntensityPolarity: Negative  
Intensity

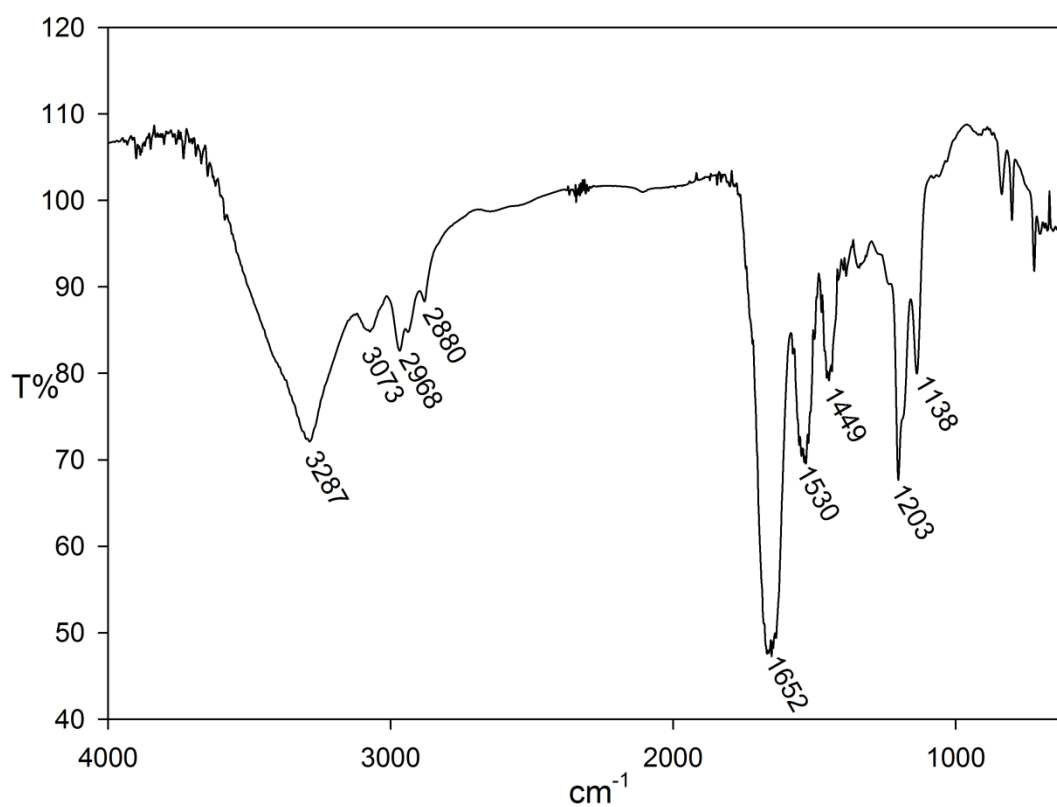
### 6.3.6 IR Spectra

SFTI-1[1,14] (1)

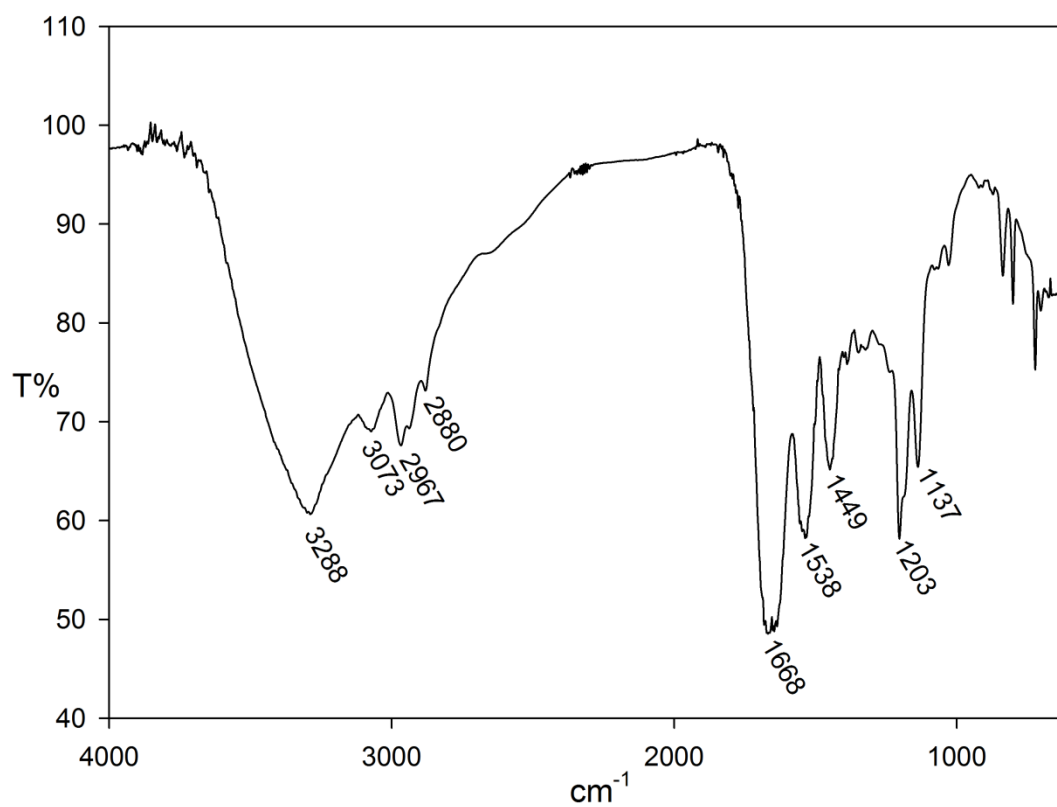
[Ala<sup>3</sup>(&<sup>1</sup>),Ala<sup>11</sup>(&<sup>2</sup>)]SFTI-1[1,14][(&<sup>1</sup>-CH<sub>2</sub>-1,5-[1,2,3]triazolyl-&<sup>2</sup>)] (2)

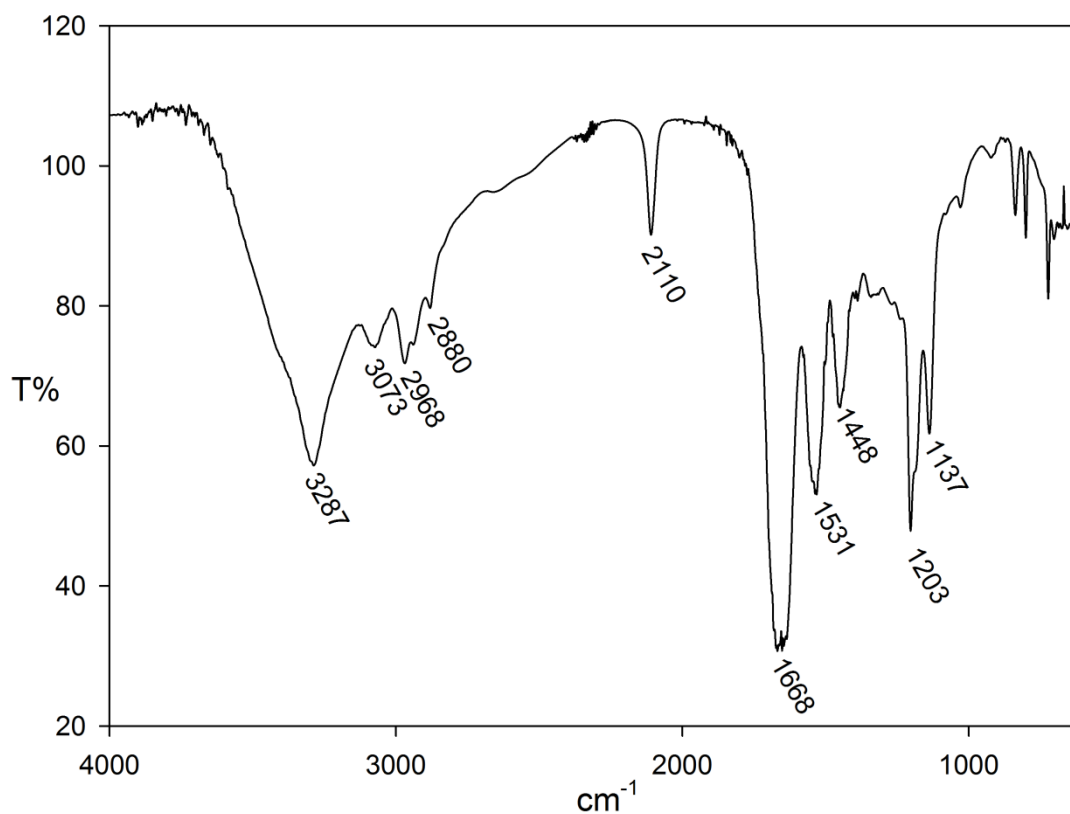
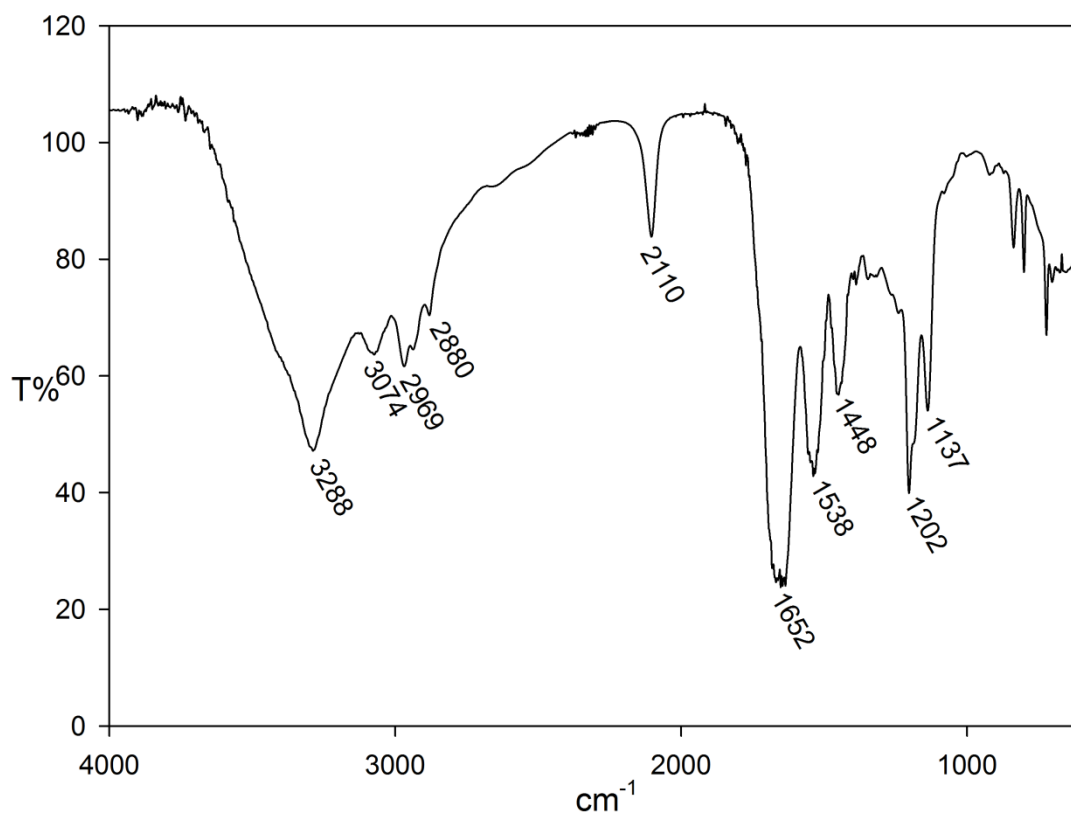


[Ala<sup>3</sup>(&<sup>1</sup>),Ala<sup>11</sup>(&<sup>2</sup>)]SFTI-1[1,14][(&<sup>1</sup>-1,4-[1,2,3]triazolyl-&<sup>2</sup>)] (3)



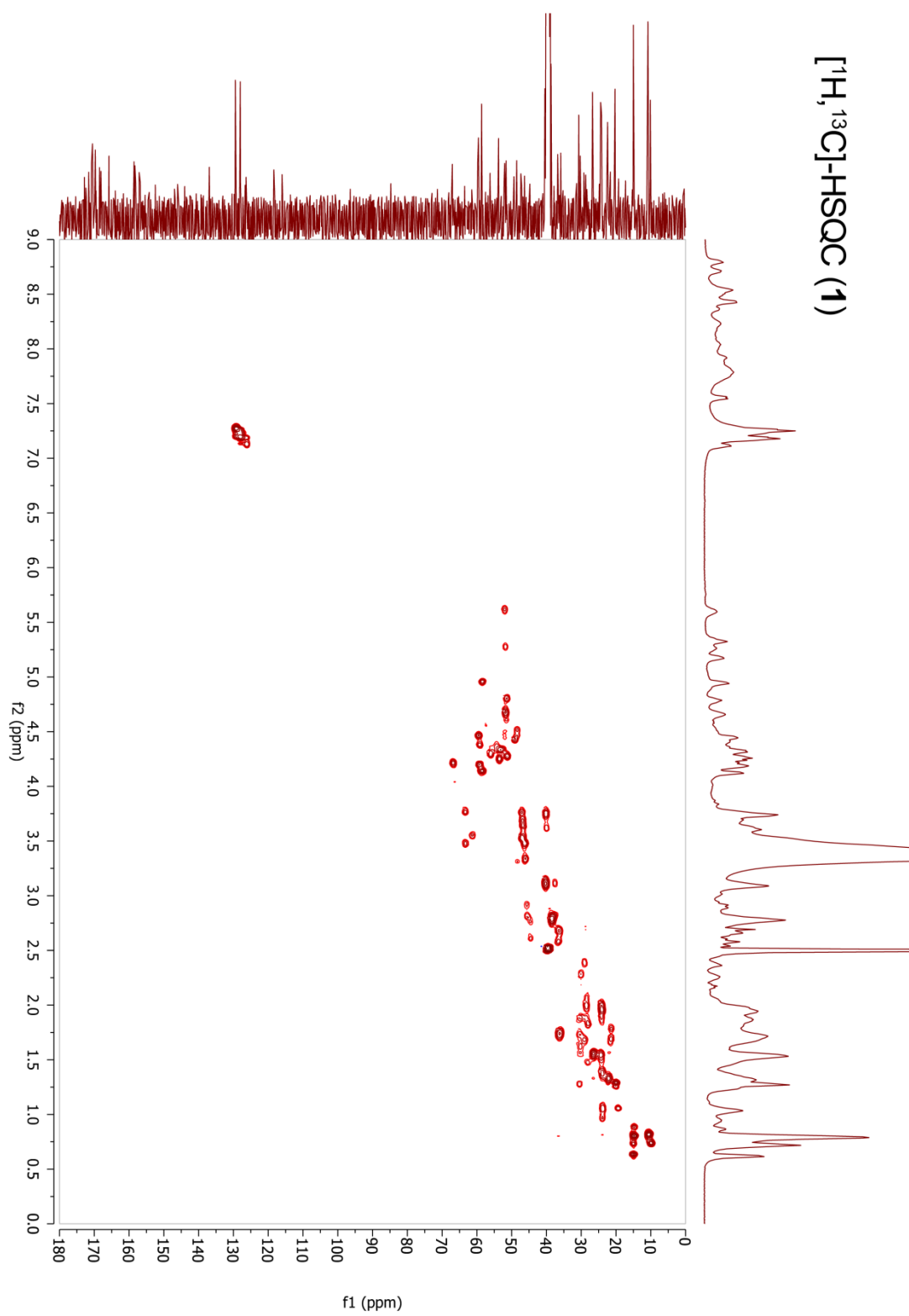
[Ala<sup>3</sup>(&<sup>1</sup>),Ala<sup>11</sup>(&<sup>2</sup>)]SFTI-1[1,14][(&<sup>1</sup>-CH<sub>2</sub>-1,4-[1,2,3]triazolyl-&<sup>2</sup>)] (4)

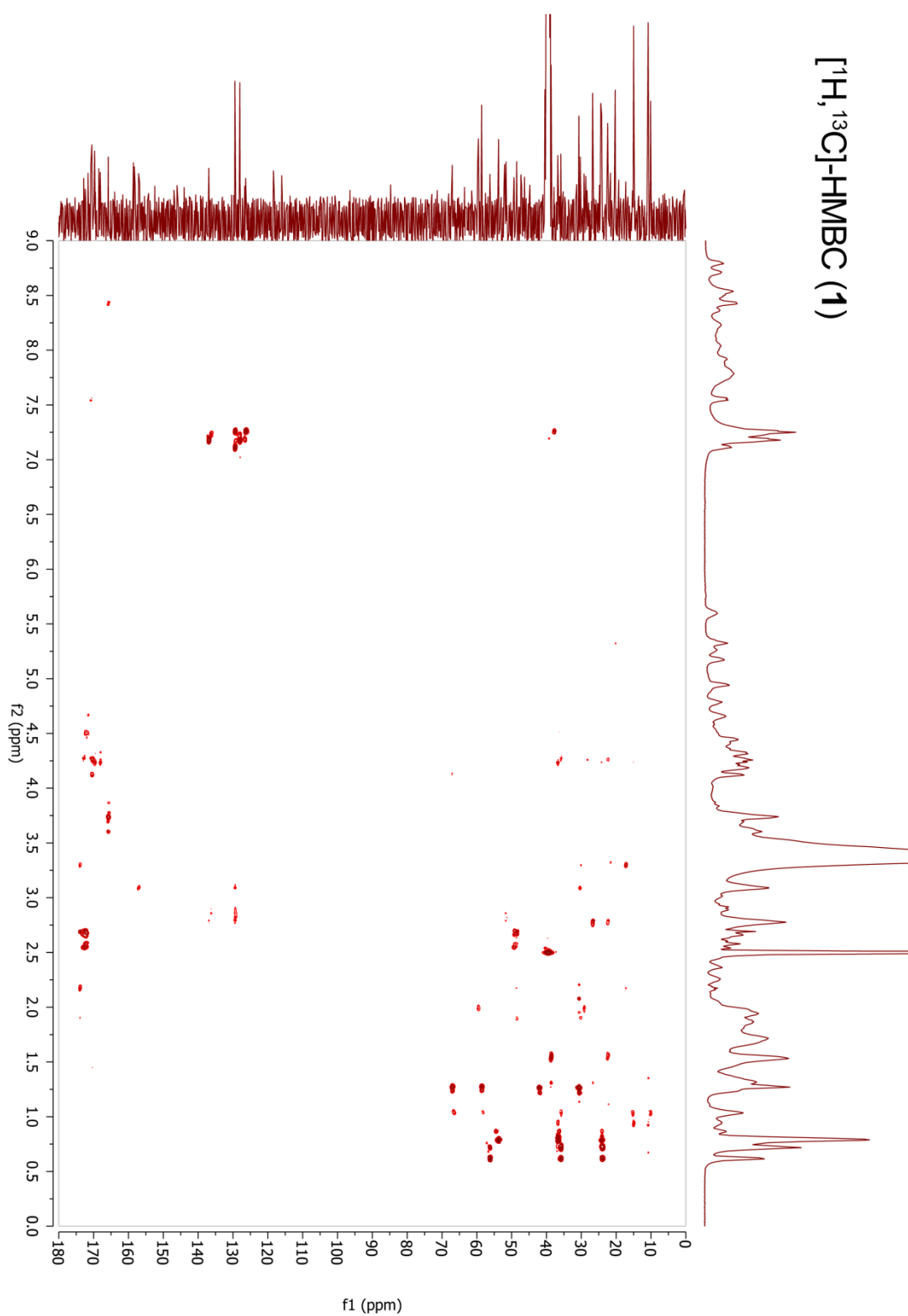


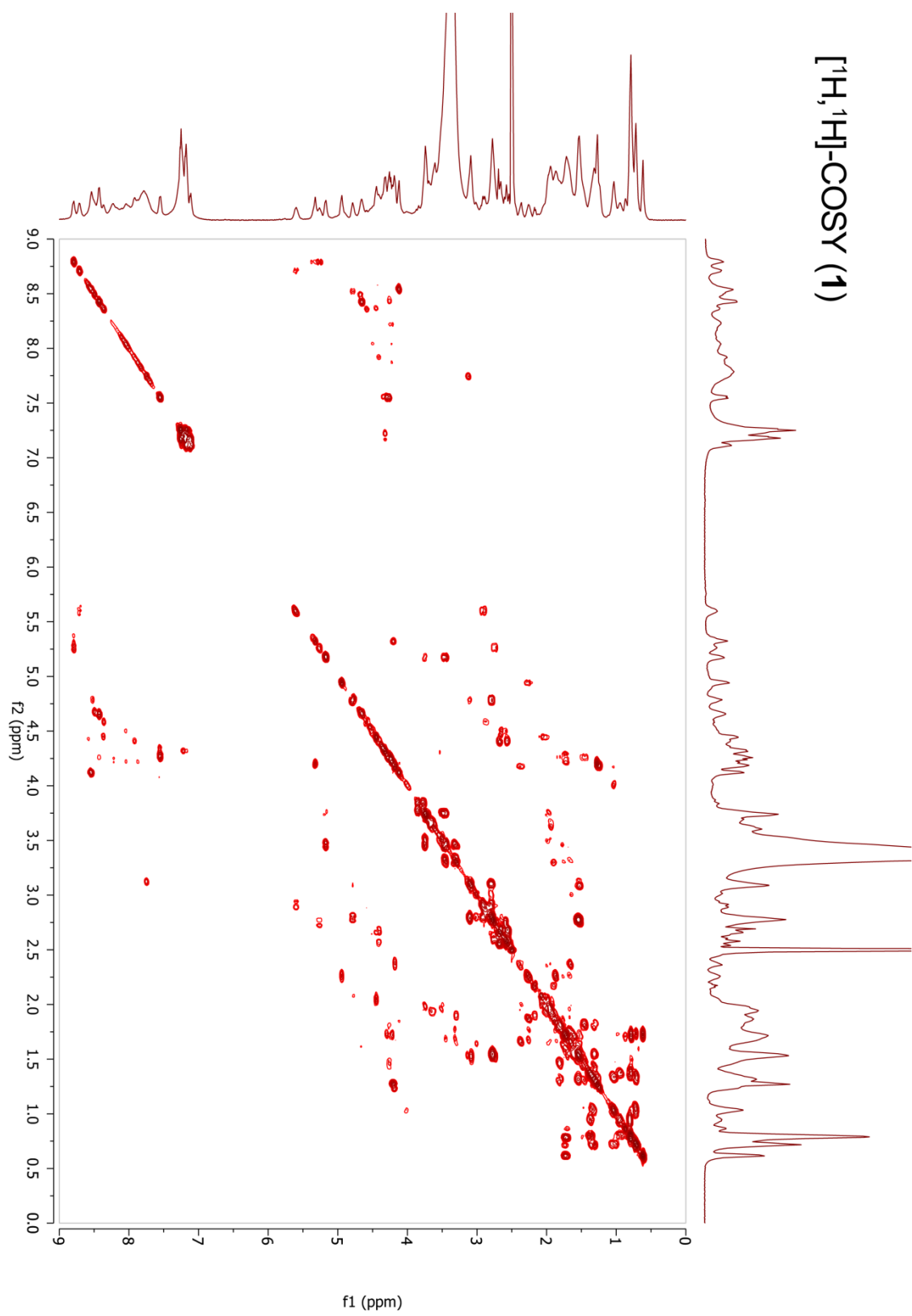
[Aza<sup>3</sup>,Pra<sup>11</sup>]SFTI-1[1,14] (5)[Aha<sup>3</sup>,Pra<sup>11</sup>]SFTI-1[1,14] (6)

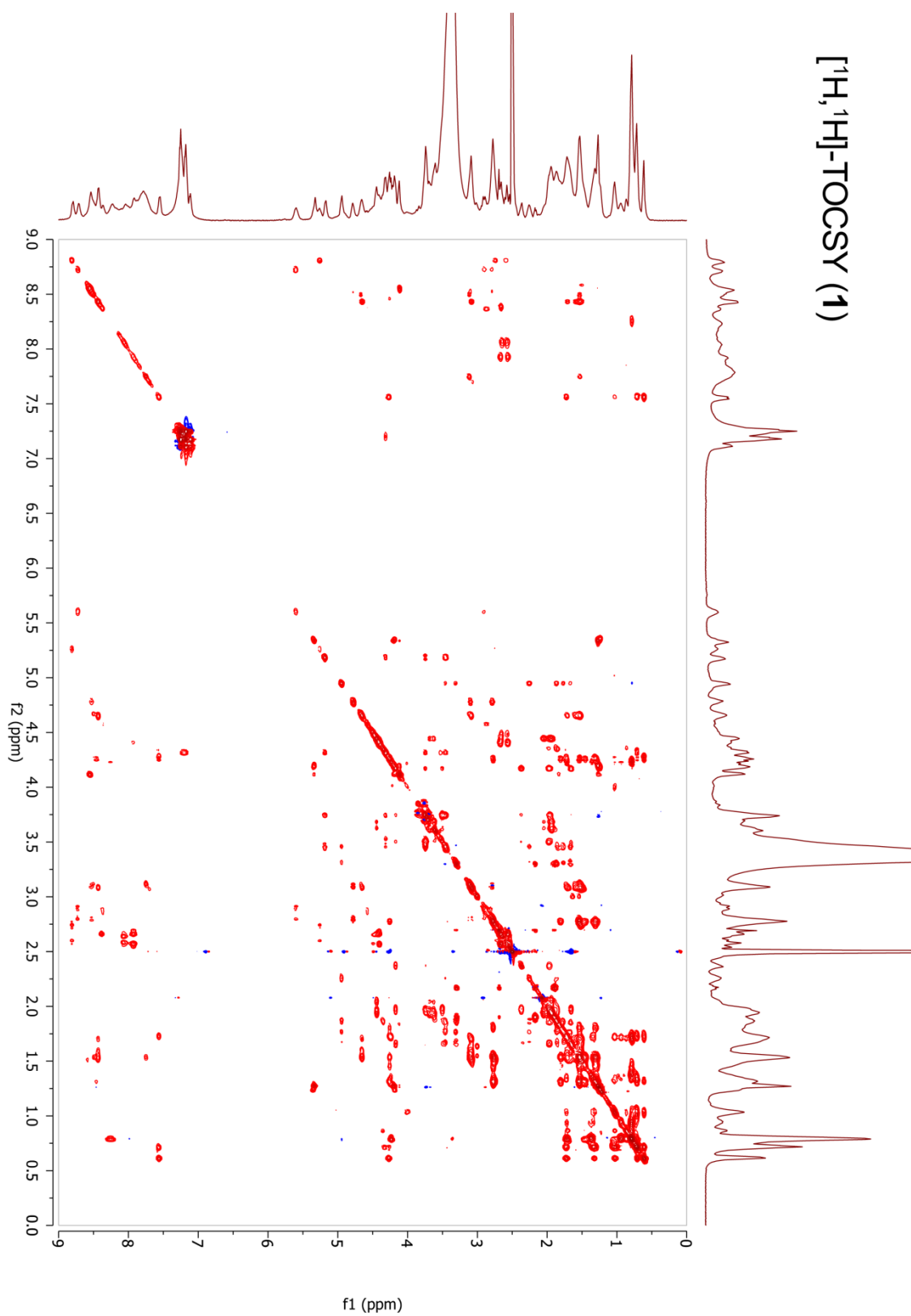
## 6.3.7 NMR Spectra

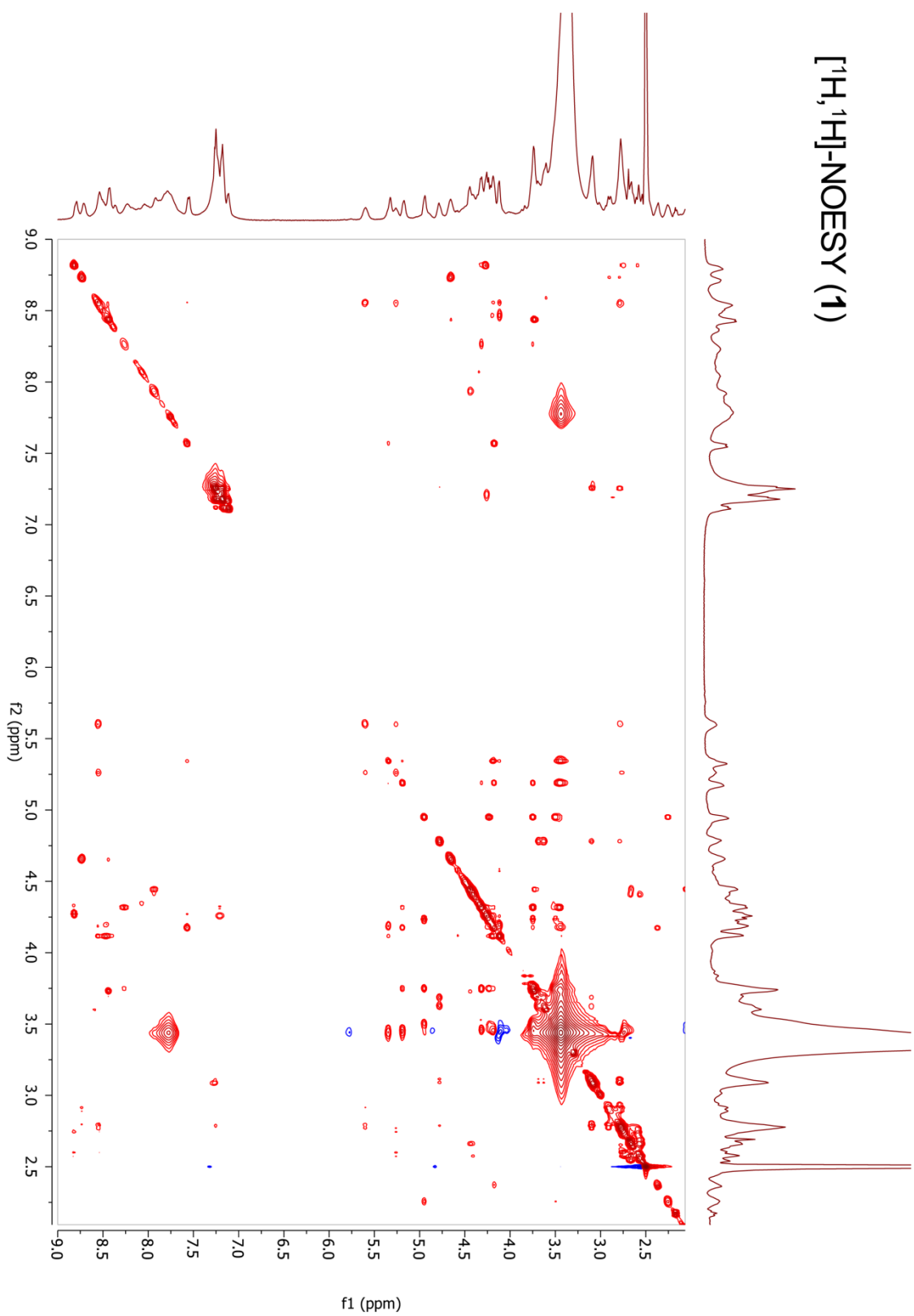
SFTI-1[1,14] (1)





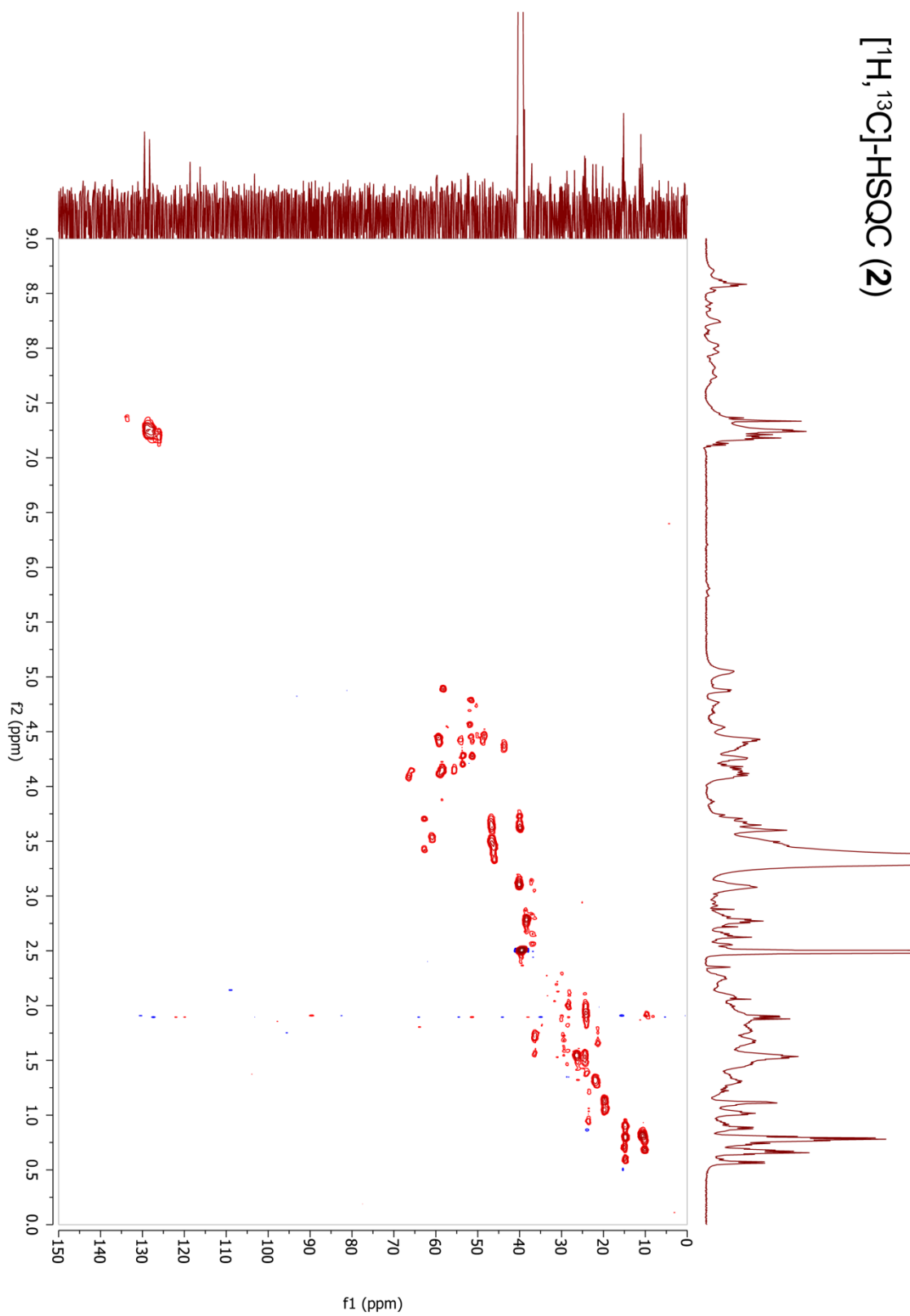
$[^1\text{H}, ^1\text{H}]$ -COSY (1)



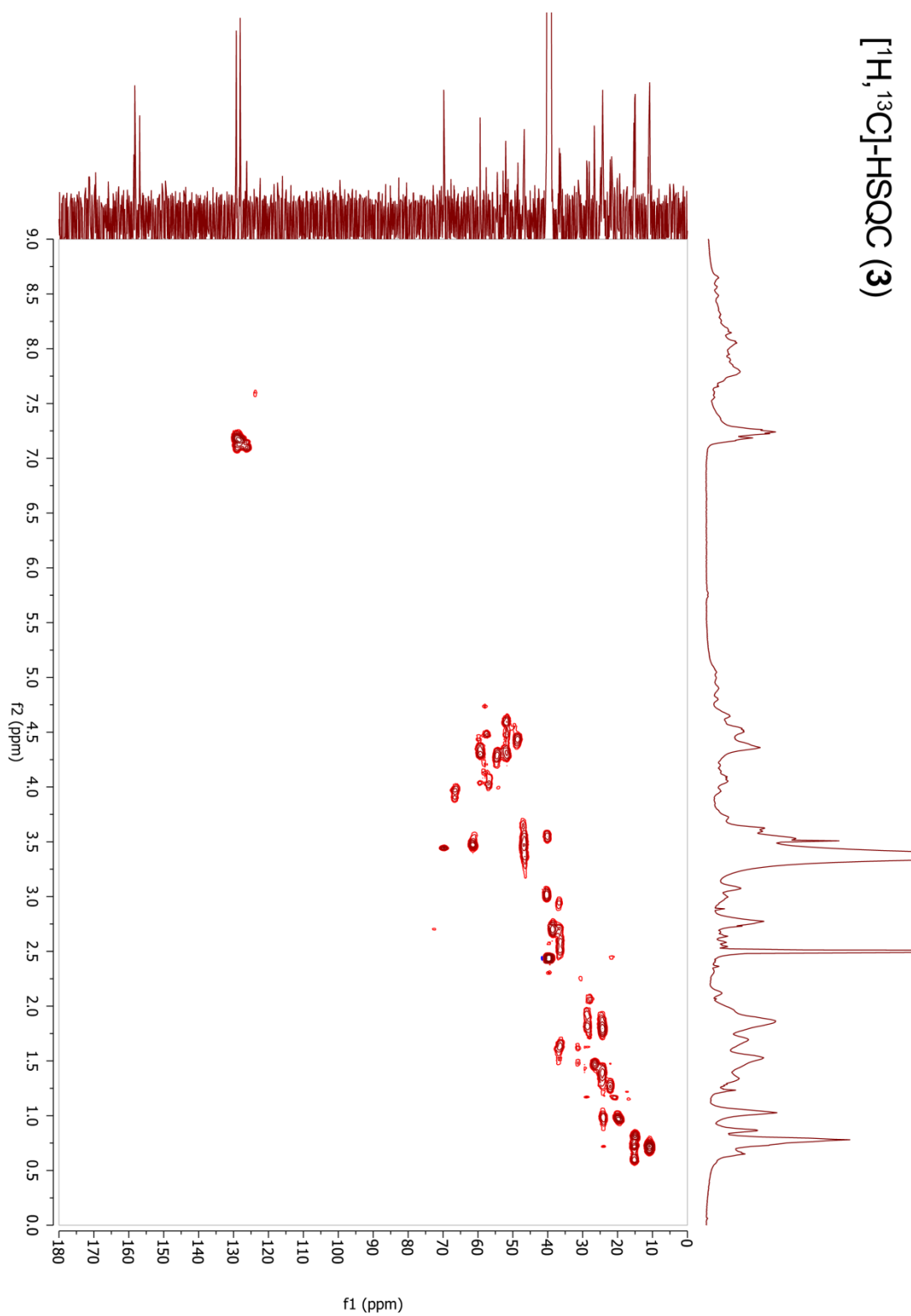
$[^1\text{H}, ^1\text{H}]$ -NOESY (1)



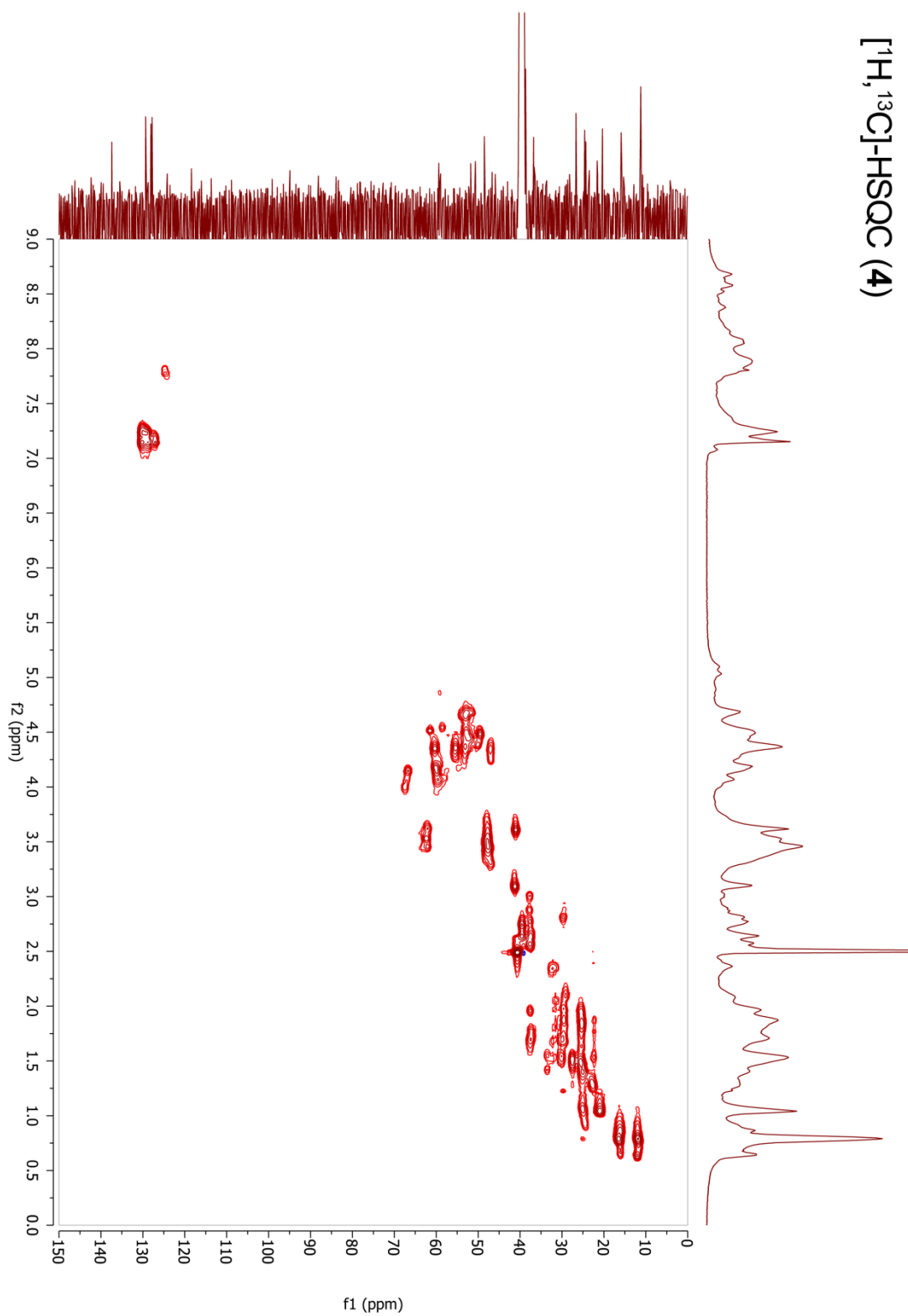
[Ala<sup>3</sup>(&<sup>1</sup>),Ala<sup>11</sup>(&<sup>2</sup>)]SFTI-1[1,14][(&<sup>1</sup>-CH<sub>2</sub>-1,5-[1,2,3]triazolyl-&<sup>2</sup>)] (2)



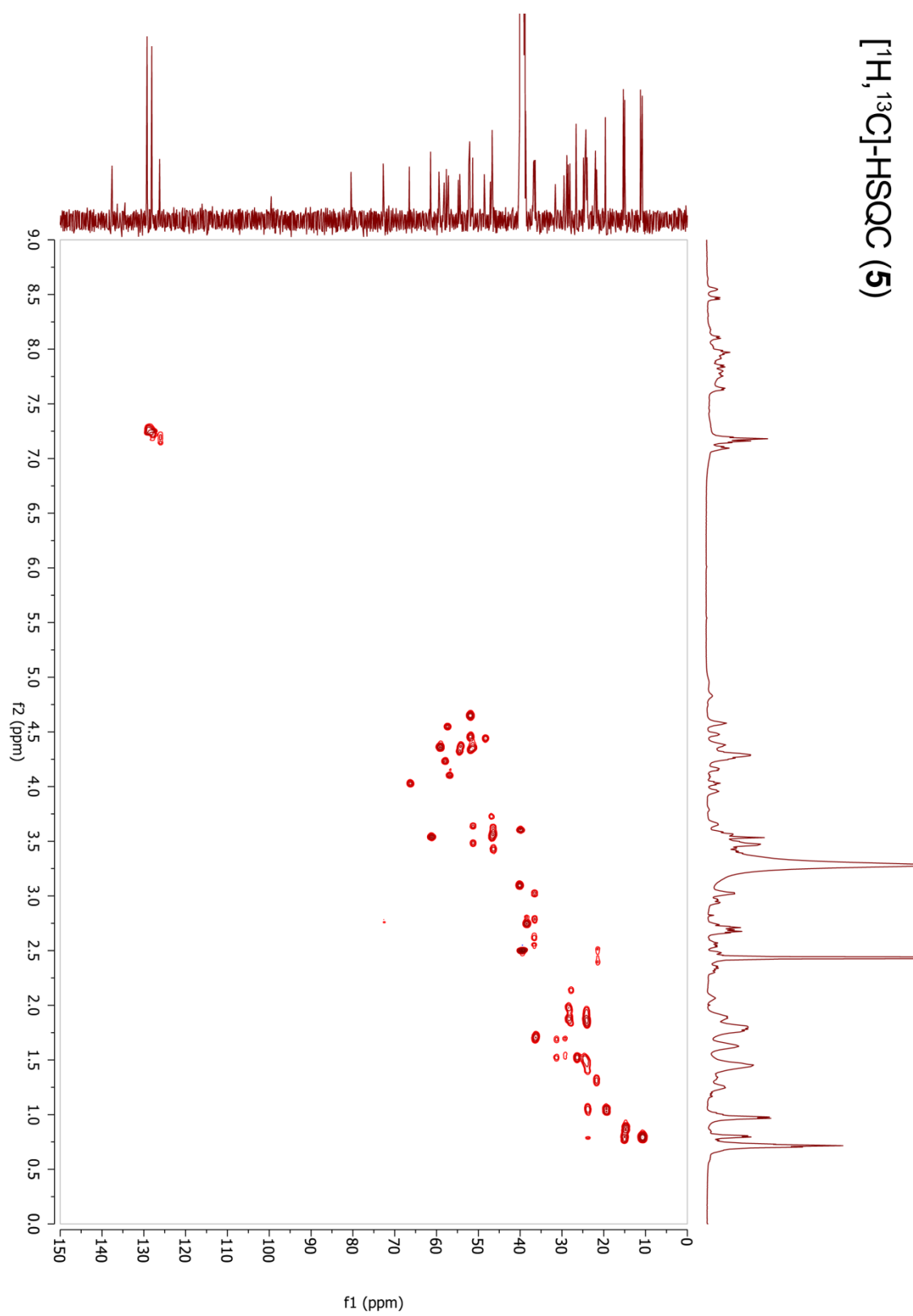
[Ala<sup>3</sup>(&<sup>1</sup>),Ala<sup>11</sup>(&<sup>2</sup>)]SFTI-1[1,14][(&<sup>1</sup>-1,4-[1,2,3]triazolyl-&<sup>2</sup>)] (3)



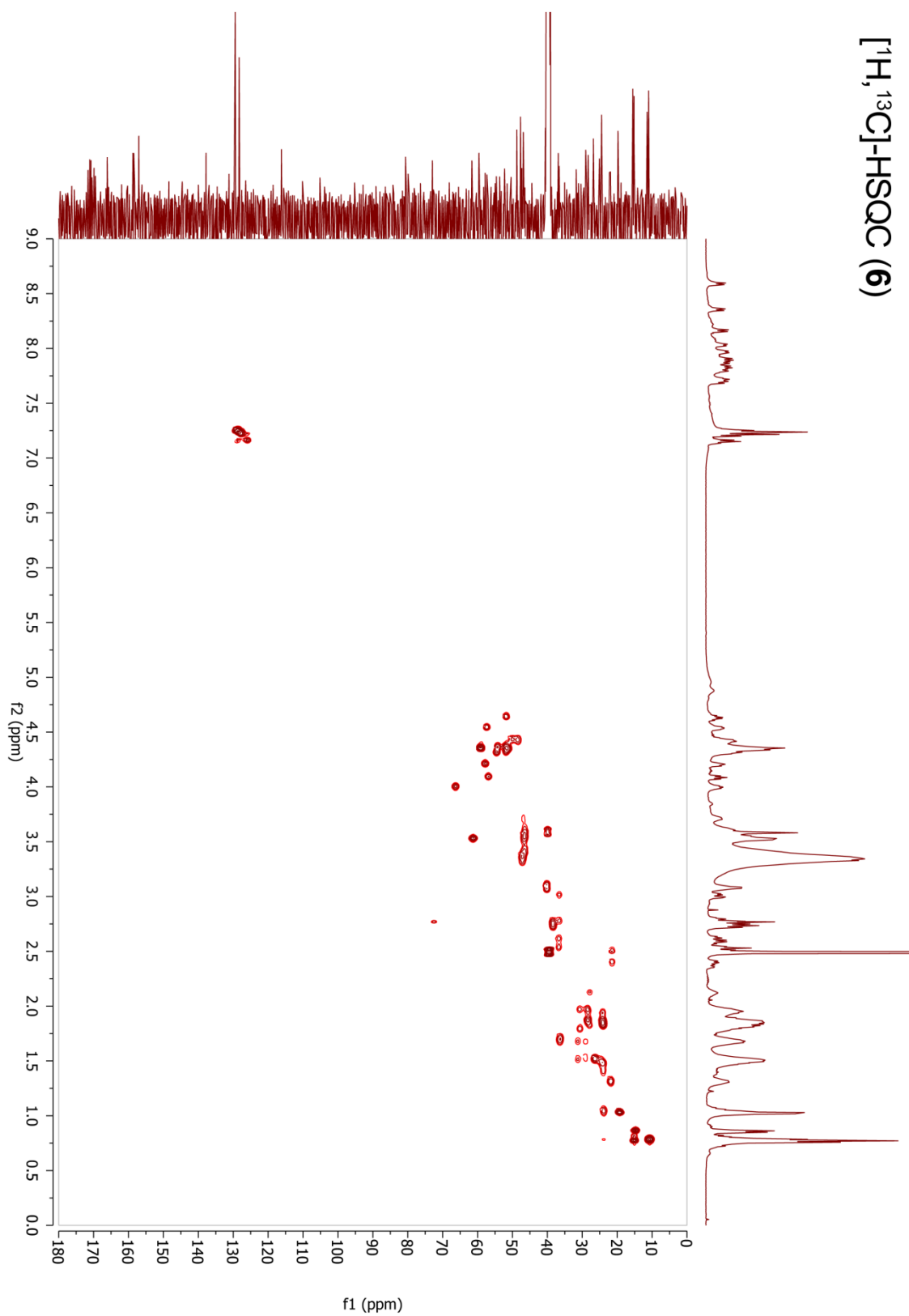
[Ala<sup>3</sup>(&<sup>1</sup>),Ala<sup>11</sup>(&<sup>2</sup>)]SFTI-1[1,14][(&<sup>1</sup>-CH<sub>2</sub>-1,4-[1,2,3]triazolyl-&<sup>2</sup>)] (4)



[Aza<sup>3</sup>,Pra<sup>11</sup>]SFTI-1[1,14] (5)



[Aha<sup>3</sup>,Pra<sup>11</sup>]SFTI-1[1,14] (6)



## 6.4 Supporting Information for Chapter 2.4

### 6.4.1 Experimental Procedures

#### Instrumentation

Analytical HPLC was conducted using a Varian 920-LC system equipped with a Phenomenex Hypersil 5u BDS C18 LC column (150 x 4.6 mm, 5  $\mu\text{m}$ , 130 Å). Semi-preparative RP-HPLC was performed on a Varian modular system comprising a PrepStar 218 Solvent Delivery Module, a ProStar 410 HPLC AutoSampler and a ProStar 325 Dual Wavelength UV-Vis HPLC Detector using a YMC J'sphere ODS-H80 C-18 LC column (250 x 20 mm, 4  $\mu\text{m}$ , 8 nm). The eluent system for analytical and semi-preparative HPLC consisted of eluent A (0.1% aq. TFA) and eluent B (90 % aq. acetonitrile containing 0.1% TFA).

ESI mass spectra were recorded using a Shimadzu LCMS-2020 equipped with a Phenomenex Jupiter 5u C4 LC column (50 x 1 mm, 5  $\mu\text{m}$ , 300 Å). The eluent system consisted of eluent A (0.1% aq. formic acid, LC-MS grade) and eluent B (acetonitrile containing 0.1% formic acid, LC-MS grade).

Fast protein liquid chromatography (FPLC) was conducted using an ÄKTApurifier (Amersham Pharmacia Biotech).

#### General Fmoc-SPPS Procedures

Peptides were synthesized on a Liberty 12-channel automated peptide synthesizer coupled with a Discover SPS microwave peptide synthesizer platform (CEM) using the Fmoc strategy. Amino acids were attached by double or triple coupling employing 4 eq of the corresponding amino acid, 4 eq of 2-(1H-benzotriazol-1-yl)-1,1,3,3-tetramethyluronium hexafluorophosphate (HBTU) and 8 eq of *N,N*-diisopropylethylamine (DIEA), or in case of cysteine 3-4 eq of 2,4,6-trimethylpyridine (collidine). Arginine and cysteine were coupled using a two-step microwave program: 1. RT, 0 W, 25 min; 2. 75 °C, 25 W, 0.5 min (Arg) and 1. RT, 0 W, 2 min; 2. 50 °C, 25 W, 4 min (Cys), respectively. All other amino acids were coupled using a standard microwave program: 75 °C, 21 W, 5 min.

Fmoc deprotection was achieved in two steps by reaction with 20% piperidine in DMF at 75 °C, 42 W for 0.5 min (initial deprotection) followed by a second deprotection step with 20% piperidine in DMF at 75 °C, 42 W for 3 min.

#### Compounds 2 and 4–6

Synthesis and characterization of compounds 2 and 4–6 have already been described in detail in reference 13 from the main text.

#### SFTI-1 (1)

The linear precursor of 1 was synthesized on chlorotriyl resin preloaded with Fmoc-Gly (0.59 mmol/g) at 0.25 mmol scale according to the automated Fmoc-SPPS protocol described above. The peptide was cleaved from the resin under conservation of side chain protection using 5 mL of a mixture of acetic acid, DCM, and methanol (50:40:10, v/v/v) for 2 h at ambient temperature. The solvents were evaporated. To the resulting yellow oil *n*-hexan was added and then evaporated. This step was repeated three times. The residue was dissolved in 20 mL H<sub>2</sub>O/CH<sub>3</sub>CN (1:1, v/v) and lyophilized. 30 mg (0.025 mmol) of the linear peptide were dissolved in 30 mL dry DMF, and 4.4 mg HOBT (5 eq), 17 mg (5 eq) benzotriazol-1-yl-oxytripyrrrolidinophosphonium hexafluorophosphate (PyBOP) as well as 11.3  $\mu\text{L}$  (10 eq) DIEA

were added for backbone macrocyclization. After 16 h of reaction, additional portions of HOBT (4.4 mg, 5 eq), PyBOP (17 mg, 5 eq), and DIEA (11.3  $\mu$ L, 10 eq) were added and the reaction mixture was stirred overnight at ambient temperature. The solvent was evaporated and the protecting groups were removed by acidolytic cleavage using TFA/H<sub>2</sub>O/anisole/triethylsilane (TES) (47:1:1:1, v/v/v/v) and a small amount of dithiothreitol (DTT). The reaction mixture was shaken for 3 h at ambient temperature with subsequent by precipitation and washing (3 $\times$ ) with 30 mL methyl *tert*-butyl ether (MTBE) to yield the crude monocyclic peptide. Oxidative disulfide formation was conducted in 100 mM (NH<sub>4</sub>)<sub>2</sub>CO<sub>3</sub> aq (pH = 8.6) at 1 mg peptide/mL dilution. After complete conversion, the solvent was removed *in vacuo* to yield the crude peptide. Chromatographic isolation by RP-HPLC yielded 4.5 mg of pure **1** (11.9 %).

RP-HPLC: Rt = 15.5 min (18 % acetonitrile over 2 min followed by 18 $\rightarrow$ 40.5 % acetonitrile in 0.1 % TFA over 20 min at flow rate 1 mL/min). ESI-MS: m/z: [M+H]<sup>+</sup> obsd. = 1514.6 (calc = 1513.7), [M+2H]<sup>2+</sup> obsd. = 757.8 (calc = 757.4), [M-H]<sup>-</sup> obsd. = 1511.8 (calc = 1511.7).

### [Ala<sup>3</sup>(&<sup>1</sup>),Ala<sup>11</sup>(&<sup>2</sup>)]SFTI-1[1,14][(&<sup>1</sup>-1,5-[1,2,3]triazolyl-&<sup>2</sup>)] (**3**)

The amino acid sequence Fmoc-Aza-Thr(tBu)-Lys(Boc)-Ser(tBu)-Ile-Pro-Pro-Ile-Pra-Phe-Pro-Asp(tBu) was assembled on an AmphiSpheres 40 HMP resin (0.4 mmol/g, Varian/Agilent) at 0.125 mmol scale using the automated microwave-assisted Fmoc-SPPS procedure described above. Loading of the resin with Fmoc-Asp(tBu)-OH was conducted by triple coupling 2 eq AA, 2 eq 2-(1H-7-azabenzotriazol-1-yl)-1,1,3,3-tetramethyluronium hexafluorophosphate (HATU), 4 eq DIEA and two-step microwave program (1. 60 °C, 30 W, 45 min, 2. 75 °C, 20 W, 5 min). Fmoc-Aza-OH and Fmoc-Pra-OH were attached using double coupling of 2 eq AA, 2 eq HATU, 4 eq DIEA, and two-step microwave program (1. 60 °C, 30 W, 45 min, 2. 75 °C, 20 W, 5 min). On-support ruthenium(II)-catalyzed macrocyclization of linear resin-bound precursor was conducted as previously reported (reference 12 from the main text). *N*-terminal sequence Gly-Arg(Pbf) was assembled using double coupling for each amino acid (4 eq aa, 3.9 eq HBTU, 8 eq DIEA) and microwave irradiation (50 °C, 30 W, 30 min). The peptide resin was dried and subjected to acidolytic cleavage using TFA/H<sub>2</sub>O/anisole/TES (47:1:1:1, v/v/v/v). Ether precipitation, washing, and subsequent purification *via* semi-preparative HPLC yielded 2.1 mg macrocyclic peptide **3** (1.37  $\mu$ mol, 1.1 % according to the initial loading of the resin). RP-HPLC: Rt = 16.2 min (18 % acetonitrile over 2 min followed by 18 $\rightarrow$ 40.5 % acetonitrile in 0.1 % TFA over 20 min at flow rate 1 mL/min). ESI-MS (m/z) [M+2H]<sup>2+</sup> obsd. = 768.56 (calc = 767.9), [M+3H]<sup>3+</sup> obsd. = 512.85 (calc = 512.8), [M-H]<sup>-</sup> obsd. = 1533.29 (calc = 1532.8). IR (cm<sup>-1</sup>) 3424, 2924, 1652, 1538, 1451, 1203, 1132.

### Inhibition Assays

Kinetic curves were recorded by monitoring the absorption of the corresponding samples in 96-well plates (NUNC, flat bottom, clear) at 405 nm in intervals of 60 sec over 30 min at RT using the Tecan GENios microplate reader. All experiments were performed in triplicate. Trypsin from bovine pancreas (Sigma) or matriptase were standardized by active-site titration with *p*-nitrophenyl-*p*'-guanidinobenzoate (NPGb) in phosphate buffered saline (PBS: 137 mM NaCl, 2.7 mM KCl, 10.0 mM Na<sub>2</sub>HPO<sub>4</sub>, 1.76 mM KH<sub>2</sub>PO<sub>4</sub>, pH 7.4).

The normalized residual proteolytic activity  $v/v_0$  of trypsin against the chromogenic substrate Boc-QAR-*p*NA (250  $\mu$ M, Bachem) at different concentrations of bicyclic and monocyclic SFTI-1 analogues **1-6** [I] was determined for  $\sim$  0.5 nM (trypsin) or 0.9 nM (matriptase) active enzyme ([E]) in aqueous buffer (50 mM Tris/HCl, 150 mM NaCl, 0.01% Triton X-100, 0.01% sodium azide, pH 7.6 or 8.5). The apparent inhibition constants ( $K_i^{app}$ ) were calculated by fitting the Morrison equation for tight binding inhibitors (1) onto the resulting kinetic data with the Marquardt-Levenberg algorithm of SigmaPlot 11.



## Determination of Michaelis-Menten Constant ( $K_M$ ) for Boc-QAR-pNA against Matriptase

The initial reaction rate ( $v_i$ ) of the proteolytic degradation of Boc-QAR-pNA (Bachem) by matriptase (1 nM) was determined for a series of concentrations ( $[S]_i$ ) of the chromogenic substrate (1000-75  $\mu$ M for pH 7.6 and 1000-50  $\mu$ M for pH 8.5). The Michaelis-Menten constant ( $K_M$ ) was calculated *via* Lineweaver-Burk plot (reciprocal initial reaction rate  $1/v_i$  versus the reciprocal substrate concentration  $1/[S]_i$ ) and linear regression of the resulting data. The experiment was performed in triplicate yielding  $K_M$  as  $236.8 \pm 56.1$   $\mu$ M (pH 7.6) and  $66.6 \pm 16.0$   $\mu$ M (pH 8.5) (arithmetic mean, standard deviation given as error).

### Transformation of Equation (2) into Equation (3)

$$\frac{v}{v_o} = \frac{([E]-[I]-K_i^{app}) + \sqrt{([I]+K_i^{app}-[E])^2 + 4K_i^{app}[E]}}{2[E]} \quad (2)$$

$$\frac{v}{v_o} = \frac{2[E]-2[E]+[E]-[I]-K_i^{app} + \sqrt{([I]+K_i^{app}-[E])^2 + 4K_i^{app}[E]}}{2[E]} \quad (8)$$

$$\frac{v}{v_o} = \frac{2[E]}{2[E]} + \frac{-[E]-[I]-K_i^{app} + \sqrt{([I]+K_i^{app}-[E])^2 + 4K_i^{app}[E]}}{2[E]} \quad (9)$$

$$\frac{v}{v_o} = 1 - \frac{([E]+[I]+K_i^{app}) - \sqrt{([I]+K_i^{app}-[E])^2 + 4K_i^{app}[E]}}{2[E]} \quad (10)$$

$$\frac{v}{v_o} = 1 - \frac{([E]+[I]+K_i^{app}) - \sqrt{[I]^2 + (K_i^{app})^2 + [E]^2 + 2K_i^{app}[I] - 2[E][I] - 2K_i^{app}[E] + 4K_i^{app}[E]}}{2[E]} \quad (11)$$

$$\frac{v}{v_o} = 1 - \frac{([E]+[I]+K_i^{app}) - \sqrt{[I]^2 + [E]^2 + (K_i^{app})^2 + 2K_i^{app}[E] + 2K_i^{app}[I] + 2[E][I] - 2[E][I] - 2[E][I]}}{2[E]} \quad (12) \quad \text{trinomial theorem}$$

$$\frac{v}{v_o} = 1 - \frac{([E]+[I]+K_i^{app}) - \sqrt{([E]+[I]+K_i^{app})^2 - 4[E][I]}}{2[E]} \quad (3) \quad \blacksquare$$

### Propagation of Errors for $\Delta_B G^{exp}$

$\Delta_B G^{exp}$  for trypsin and matriptase complexes of compounds 1–6 were calculated from *in vitro*  $K_i$  using equation (7). The error of  $\Delta_B G^{exp}$  ( $\Delta \Delta_B G^{exp}$ ) was calculated by propagation of errors of  $K_i$  ( $\Delta K_i$ ) as follows:

$$(\Delta \Delta_B G^{exp})^2 = \left| \frac{\partial \Delta_B G^{exp}}{\partial K_i} \right|^2 (\Delta K_i)^2 \quad (13)$$

$$\Delta \Delta_B G^{exp} = \sqrt{\left| \frac{\partial \Delta_B G^{exp}}{\partial K_i} \right|^2} (\Delta K_i)^2 \quad (14)$$

Finally, differentiation of  $\Delta_B G^{exp}$  with respect to  $K_i$  yields equation (15).

$$\Delta \Delta_B G^{exp} = \sqrt{\left| \frac{-RT}{K_i} \right|^2} (\Delta K_i)^2 \quad (15)$$

## 6.4.2 In Silico Methods

### Instrumentation

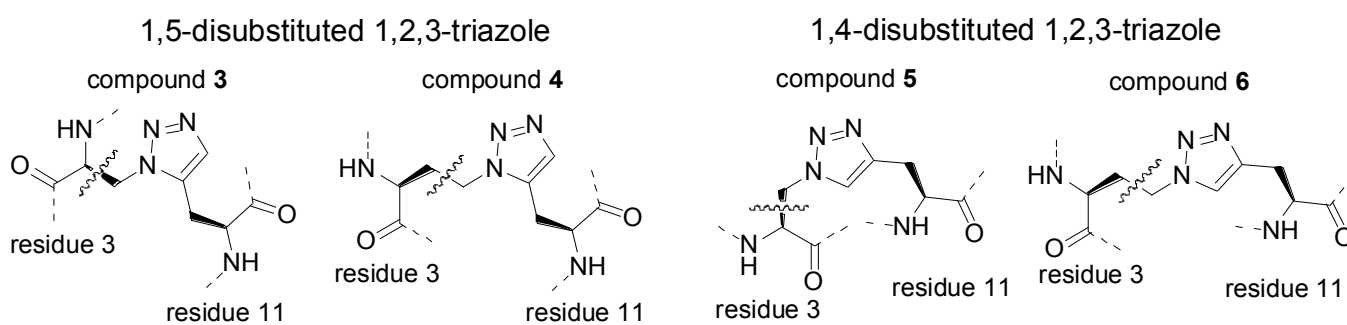
All *in silico* experiments were performed on an Intel® Core™ i7-2600 workstation using 8 virtual cores.

## Graphical Content

Graphical content for Figures 1, 3, 6, S1, and S2 was generated with YASARA ([www.yasara.org](http://www.yasara.org)) and POVray ([www.povray.org](http://www.povray.org)).

### Force Field Parameters for Triazoles within Peptidomimetics 3–6

Each triazolyl moiety was modeled manually into residue 11 of peptidomimetics 3–6 and then connected *via* a single C-C bond to residue 3 as depicted in Scheme S1.



**Scheme S1.** Affiliation of atoms within triazolyl moieties to respective residues within compounds 3–6.

## 6.4.3 Supporting Figures

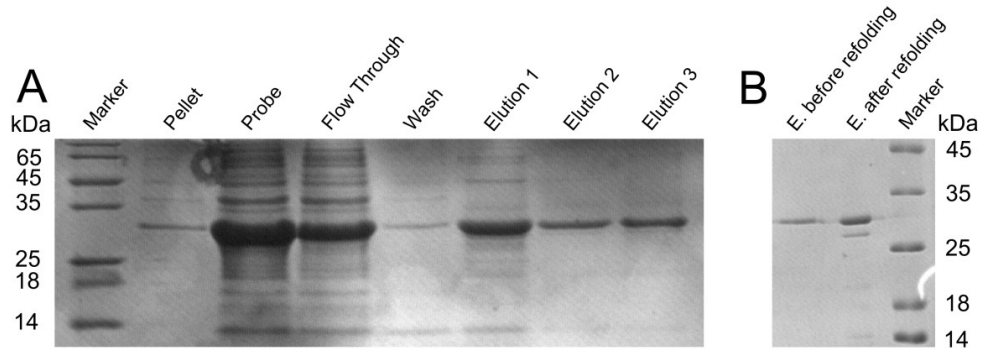


**Fig S1** (A) SDS-PAGE of fractions collected using an immobilized metal ion affinity chromatography (IMAC) column upon purification of human matriptase I under denaturing conditions. Inclusion bodies were produced in *E. coli* BL21-DE3-CodonPlus-RP with the expression vector pET42dest-His-hMatI(cd)596-855 and dissolved in buffer 1 (50 mM Tris-HCl, 100 mM NaCl, 1 mM 2-mercaptoethanol, 6 M urea) after cell disruption. Elution was achieved using buffer 2 (50 mM Tris-HCl, 100 mM NaCl, 1 mM 2-mercaptoethanol, 4.5 M urea). (B) SDS-PAGE of human matriptase I before and after refolding. Refolding was achieved by 3 steps of dialysis for 4-6 hours: 1× against refolding buffer 1 (50 mM Tris-HCl, 100 mM NaCl, 1 mM 2-mercaptoethanol, 3 M urea) and then 2× against refolding buffer 2 (50 mM Tris-HCl, 100 mM NaCl, 1 mM 2-mercaptoethanol).

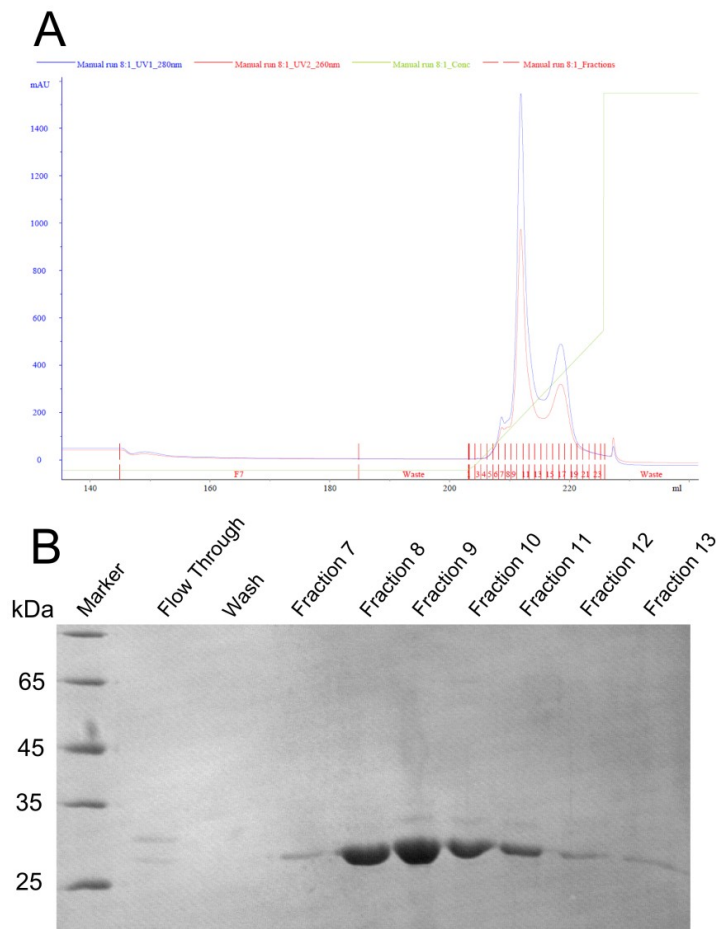


**Fig S2** (A) FPLC trace of refolded/autocatalytically activated human matriptase I using an anion-exchange chromatography column (HiTrap Q HP, GE Healthcare) with detection at 260 nm (red) and 280 nm (blue). Sodium chloride was removed from protein solution before FPLC *via* dialysis against 50 mM Tris-HCl pH 8. Target protease was eluted by an increasing sodium chloride gradient 0→500 mM in 50 mM Tris-HCl (green) at a flow rate of 1 mL/min. Collected fractions are indicated (red lines). (B) SDS-PAGE of the collected fractions.

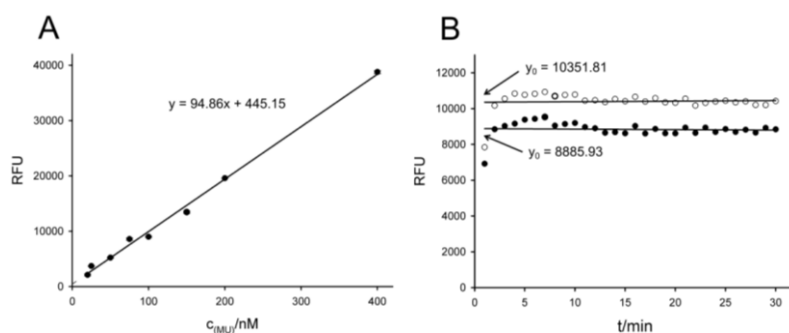


**Fig S3** Analysis of proteolytic activity of the purified matriptase. (A) Calibration curve (linear regression) for fluorophor 4-methylumbelliferone (MU; Sigma) recorded at 465 nM using eight different concentrations and an excitation wavelength of 360 nM. (B) Active-site titration of purified matriptase using fluorogenic 4-methylumbelliferyl-*p*-guanidinobenzoate (MUGB; 1  $\mu$ M; Sigma) in buffer (50 mM Tris/HCl, 150 mM NaCl, 0.01% (v/v) Triton X-100, 0.01% (w/v) sodium azide, pH 7.6). Mean values of two independent measurements over 30 minutes (white circle 250 nM and black circle 200 nM of purified protease) y-intercept of linear regression is given. Protease activity was determined as 43 % of total protein concentration.

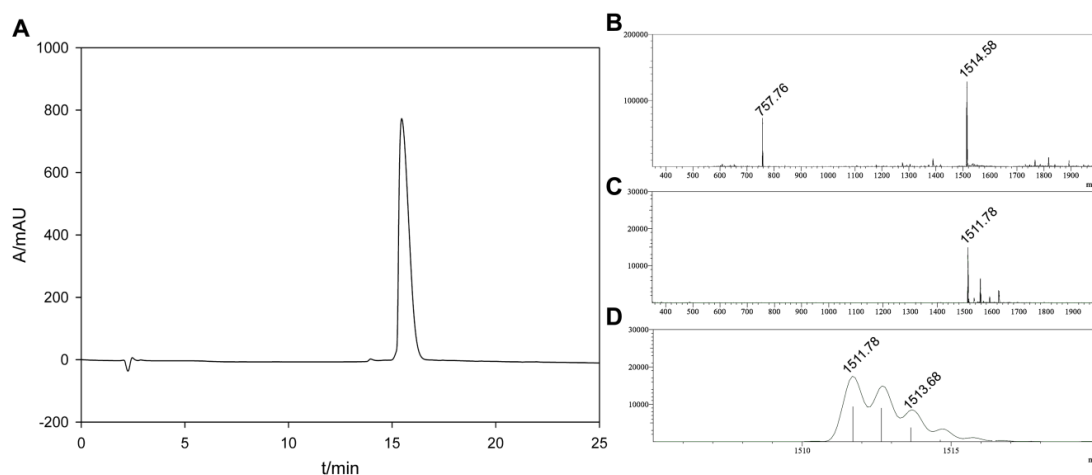


**Fig S4** (A) RP-HPLC trace of bicyclic SFTI-1 (**1**). Conditions: 18 % acetonitrile over 2 min followed by 18→40.5 % acetonitrile in 0.1 % TFA over 20 min at flow rate 1 mL/min. (B) ESI mass spectrum of **1** (positive polarization). (C) ESI mass spectrum of **1** (negative polarization). (D) Section ( $m/z$  1505-1520) of negative ESI mass spectrum showing isotopic pattern of  $[M-H]^-$  signal of **1**.

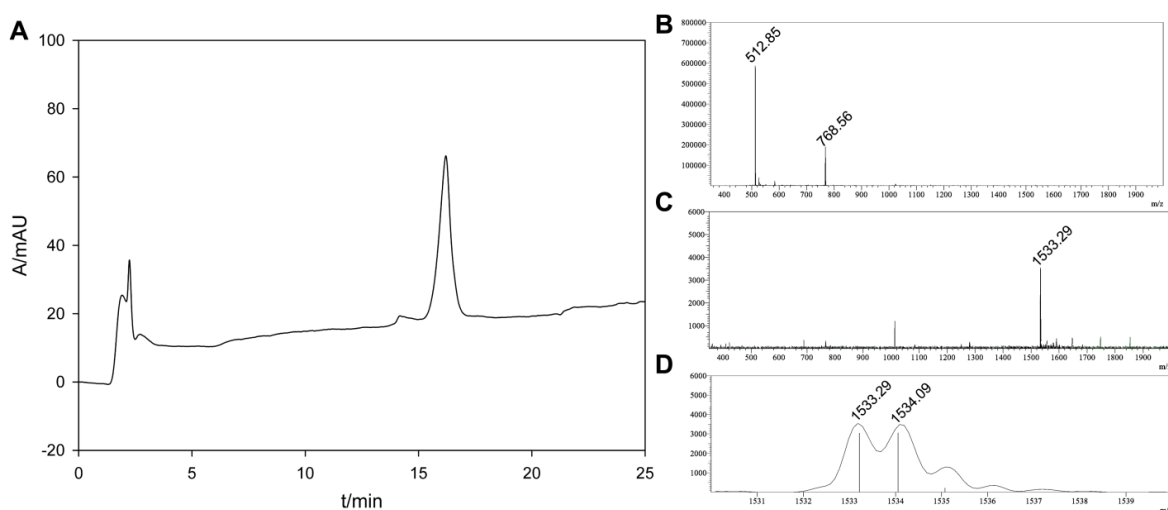


**Fig S5** (A) RP-HPLC trace of peptidomimetic inhibitor (**3**). Conditions: 18 % acetonitrile over 2 min followed by 18→40.5 % acetonitrile in 0.1 % TFA over 20 min at flow rate 1 mL/min. (B) ESI mass spectrum of **3** (positive polarization). (C) ESI mass spectrum of **3** (negative polarization). (D) Section ( $m/z$  1530-1540) of negative ESI mass spectrum showing isotopic pattern of  $[M-H]^-$  signal of **3**.

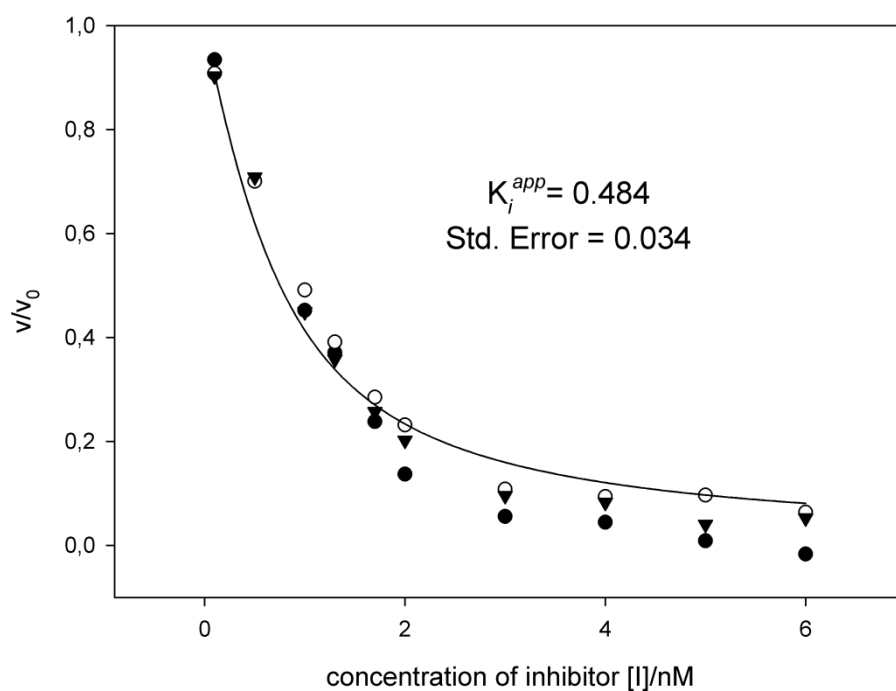


**Fig. S6** Plotted kinetic data for the inhibition of the proteolytic activity of trypsin by bicyclic inhibitor 1 and resulting curve for the global non-linear fit of equation (3) onto the three sets of experimental data (1: white circle, 2: black circle, 3: black triangle). Determined apparent inhibition constant  $K_i^{app}$  and the standard error of the fit are given in nM.

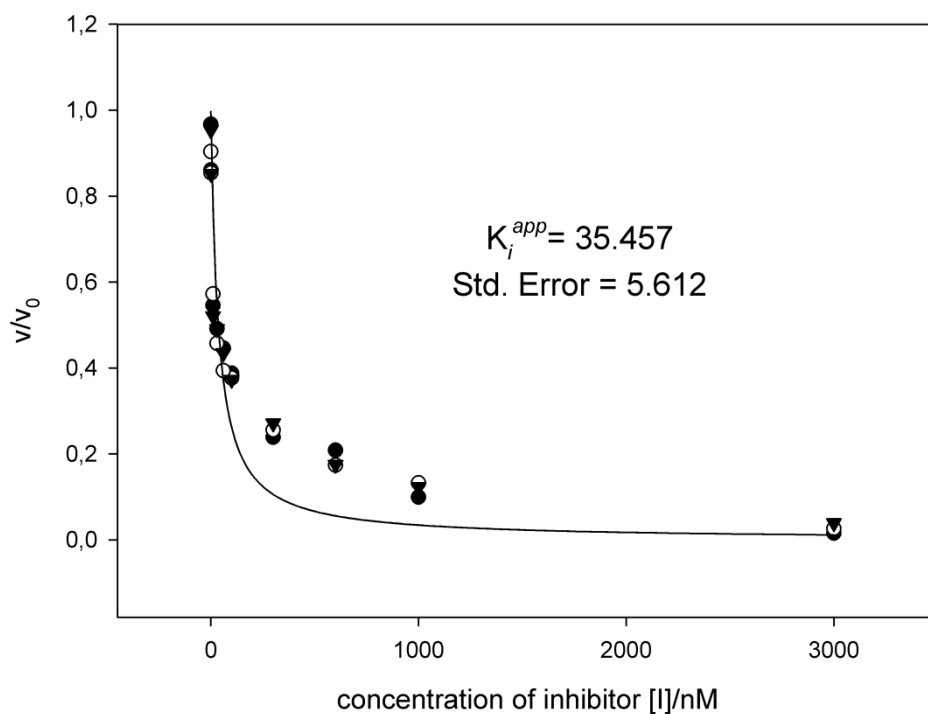


**Fig. S7** Plotted kinetic data for the inhibition of the proteolytic activity of trypsin by peptidomimetic inhibitor 3 and resulting curve for the global non-linear fit of equation (3) onto the three sets of experimental data (1: white circle, 2: black circle, 3: black triangle). Determined apparent inhibition constant  $K_i^{app}$  and the standard error of the fit are given in nM.

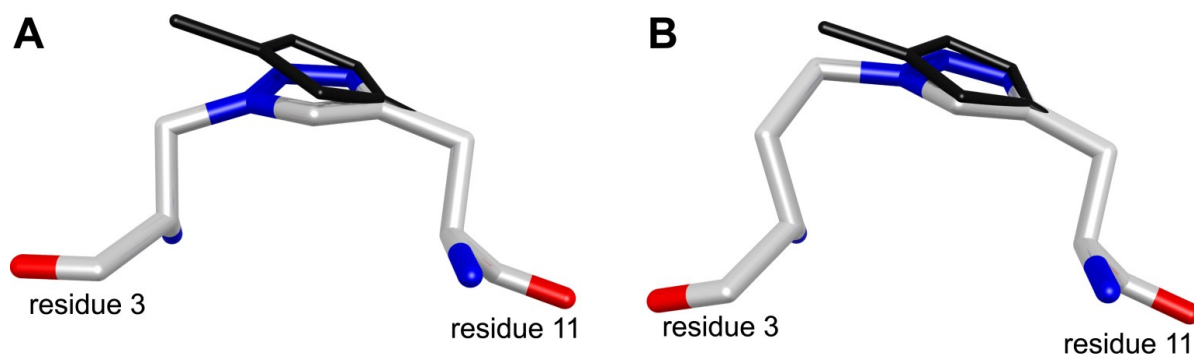


**Fig S8** Bent triazolyl structures within the macrocyclization motif of compounds 5 (A) and 6 (B) resulting after modeling and a singular energy minimization step in an overlay with a corresponding planar triazole structure (thin, black). Blue: nitrogen, red: oxygen, white: carbon, hydrogen omitted for clarity, only residues 3 and 11 are shown.

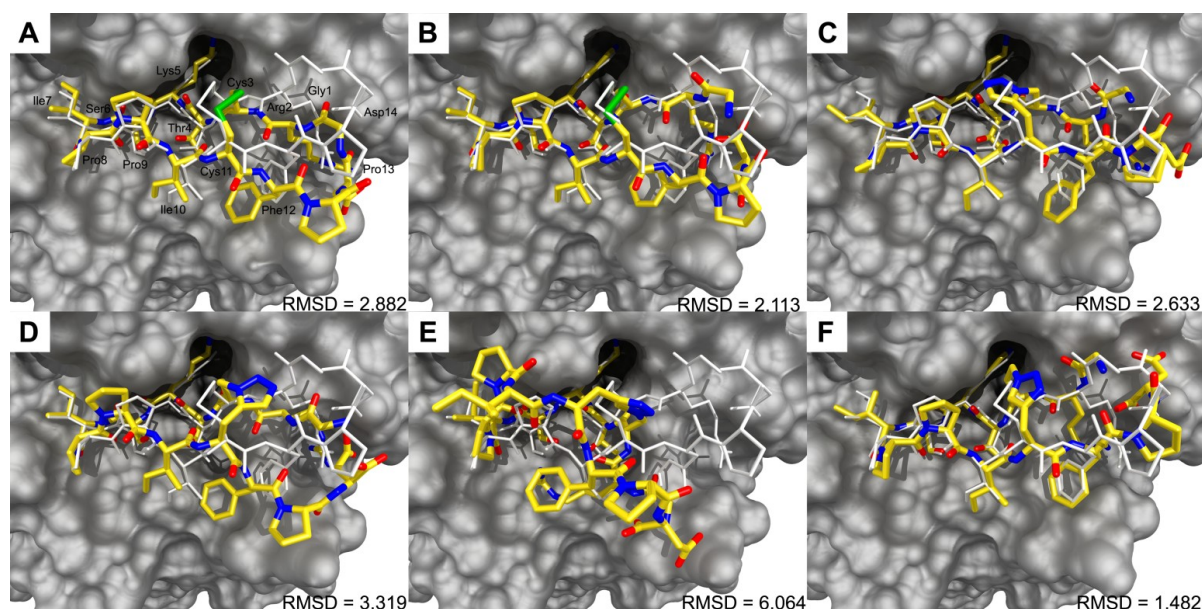


**Fig. S9** Predicted structures of compounds 1 (A), 2 (B), 3 (C), 4 (D), 5 (E), and 6 (F) in complex with trypsin (grey surface) as an overlay with reported crystal structure 1SFI (reference 2 from the main text) (white sticks). Blue: nitrogen, green: sulfur, red: oxygen, yellow: carbon, hydrogen is omitted for clarity. Measured RMSD values for inhibitor backbones compared to 1SFI are given in Å.

#### 6.4.4 Supporting Tables

**Table S1** Determined  $K_i$  for compounds 1-6 against trypsin at pH 7.6 using equations (1) and (4 or 5)<sup>a,b</sup> ( $K_i^1$ ), (2) and (6) ( $K_i^2$ ), as well as (3) and (6) ( $K_i^3$ ).

Entry	$K_i^1/\text{nM}$	$K_i^2/\text{nM}$	$K_i^3/\text{nM}$
1	0.06 <sup>a</sup>	0.07	0.07
2	0.21 <sup>a</sup>	0.21	0.21
3	5.08 <sup>b</sup>	5.07	5.07
4	0.34 <sup>a</sup>	0.34	0.34
5	272.74 <sup>b</sup>	272.72	272.73
6	106.12 <sup>b</sup>	106.09	106.09

<sup>a</sup>Equation (5) was used. <sup>b</sup>Equation (4) was used.

**Table S2** Determined  $K_i$  for compounds 1-6 against matriptase at pH 7.6 using equations (1) and (4) ( $K_i^1$ ), (2) and (6) ( $K_i^2$ ), as well as (3) and (6) ( $K_i^3$ ).

Entry	$K_i^1/nM$	$K_i^2/nM$	$K_i^3/nM$
1	1100.1	1099.9	1099.9
2	702.8	702.5	702.5
3	1236.9	1236.7	1236.7
4	12930.0	12929.1	12929.8
5	285258.8	284749.5	284748.4
6	94092.1	94084.5	94096.2

**Table S3** Determined  $K_i$  for compounds 1 & 2 against matriptase at pH 8.5 using equations (1) and (4) ( $K_i^1$ ), (2) and (6) ( $K_i^2$ ), as well as (3) and (6) ( $K_i^3$ ).

Entry	$K_i^1/nM$	$K_i^2/nM$	$K_i^3/nM$
1	147.5	147.4	147.4
2	100.3	100.2	100.2

**Table S4** Assignment of atom types for investigated 1,5-disubstituted 1,2,3-triazoles and 1,4-disubstituted 1,2,3-triazoles.

Structure	Atom	Atom type
 1,5-disubstituted 1,2,3-triazole	N <sup>1</sup>	N/
	N <sup>2</sup>	N(
	N <sup>3</sup>	N)
	C <sup>4</sup>	C/
	C <sup>5</sup>	C(
	C <sup>6</sup>	C2
	C <sup>7</sup>	C2
	H <sup>4</sup>	H4
	H <sup>6</sup>	HC
	H <sup>7</sup>	HC
 1,4-disubstituted 1,2,3-triazole	N <sup>1</sup>	N\$
	N <sup>2</sup>	N%
	N <sup>3</sup>	N&
	C <sup>4</sup>	C\$
	C <sup>5</sup>	C%
	C <sup>6</sup>	C2
	C <sup>7</sup>	C2
	H <sup>5</sup>	H4
	H <sup>6</sup>	HC
	H <sup>7</sup>	HC

**Table S5** Bond parameters.

Atom1-Atom2	Force constant/(kcal/(mol $\times$ $\text{\AA}^2$ ))	Equilibrium distance/ $\text{\AA}$
C\$-C%	596.25000	1.377
C\$-N&	596.25000	1.363
C2-C\$	396.25000	1.509
C%-H4	458.75000	0.949
C%-N\$	596.25000	1.366
N\$-C2	632.25000	1.467
N&-N%	596.25000	1.293
N%-N\$	596.25000	1.363
C(-C/	596.25000	1.377
C(-N)	596.25000	1.354
C2-C(	396.25000	1.479
C/-H4	458.75000	0.949
C(-N/	596.25000	1.365
N/-C2	632.25000	1.470
N)-N(	596.25000	1.322
N(-N/	596.25000	1.358
C2-h1	425.00000	1.093



Table S6 Angle parameters.

Atom1-Atom2-Atom3	Force constant/(kcal/(mol $\times$ rad $^2$ ))	Equilibrium angle/degrees
C2-C\$-C%	373.02300	125.684
C2-C\$-N&	373.02300	126.776
C\$-C%-H4	95.500000	126.385
C\$-C%-N\$	373.02300	107.231
C\$-N&-N%	373.02300	107.954
C%-N\$-C2	373.02300	131.073
C%-C\$-N&	373.02300	107.540
N&-N%-N\$	373.02300	111.267
C%-N\$-N%	373.02300	105.954
H4-C%-N\$	95.500000	126.385
N%-N\$-C2	373.02300	122.982
C\$-C2-C1	64.700000	108.100
C\$-C2-HC	47.200000	110.860
C1-C2-N\$	65.800000	112.590
N\$-C2-h1	49.900000	109.450
C2-C2-N\$	65.800000	112.590
HC-C2-N\$	49.900000	109.500
C2-C(-C/	373.02300	129.650
C2-C(-N/	373.02300	126.517
C(-C/-H4	95.500000	125.288
C(-C/-N)	373.02300	109.412
C/-N)-N(	373.02300	108.718
C(-N/-C2	373.02300	129.074
N)-N(-N/	373.02300	107.118
C(-N/-N(	373.02300	111.158
H4-C/-N)	95.500000	125.300
N(-N/-C2	373.02300	119.767
C/-C(-N/	373.02300	103.833
C(-C2-C1	64.700000	108.100
C(-C2-HC	47.200000	110.860
C1-C2-N/	65.800000	112.590
N/-C2-h1	49.900000	109.450
C2-C2-N/	65.800000	112.590
HC-C2-N/	49.900000	109.500
h1-C2-h1	39.200000	109.550
HC-C1-N	49.800000	109.500
C -C1-HC	47.200000	109.680
C1-C2-h1	46.400000	110.070
h1-C2-h1	39.200000	109.550
HC-C1-N	49.800000	109.500
C -C1-HC	47.200000	109.680

Table S7 Dihedral angle parameters.

Atom1-Atom2-Atom3-Atom4	Bond paths	Force constant/(kcal/mol)	Phase angle/degrees	periodicity
C2-C\$-N&-N%	2	11.50000	180.00	2
C%-C\$-N&-N%	2	11.50000	180.00	2
C2-C\$-C%-N\$	4	23.69000	180.00	2
C2-C\$-C%-H4	4	23.69000	180.00	2
N&-C\$-C%-N\$	4	23.69000	180.00	2
N&-C\$-C%-H4	4	23.69000	180.00	2
C\$-C%-N\$-C2	2	11.50000	180.00	2
C\$-C%-N\$-N%	2	11.50000	180.00	2
H4-C%-N\$-C2	2	11.50000	180.00	2
H4-C%-N\$-N%	2	11.50000	180.00	2
C2-N\$-N%-N&	2	9.600	180.00	2
C%-N\$-N%-N&	2	9.600	180.00	2
C\$-N&-N%-N\$	1	4.000	180.00	2
X -C\$-C2-X	6	0.000	0.000	3
X -C2-N\$-X	6	0.000	0.000	3
H4-C/-N)-N(	2	11.50000	180.00	2
C(-C/-N)-N(	2	11.50000	180.00	2
N/-C(-C/-H4	4	23.69000	180.00	2
C2-C(-C/-H4	4	23.69000	180.00	2
N/-C(-C/-N)	4	23.69000	180.00	2
C2-C(-C/-N)	4	23.69000	180.00	2
C/-C(-N/-C2	2	11.50000	180.00	2
C/-C(-N/-N(	2	11.50000	180.00	2
C2-C(-N/-C2	2	11.50000	180.00	2
C2-C(-N/-N(	2	11.50000	180.00	2
C2-N/-N(-N)	2	9.600	180.00	2
C(-N/-N(-N)	2	9.600	180.00	2
C/-N)-N(-N/	1	4.000	180.00	2
X -C2-C(-X	6	0.000	0.000	3
X -C2-N/-X	6	0.000	0.000	3



## 6.5 Supporting Information for Chapter 2.5

### 6.5.1 ESI-MS

Table S1 ESI-MS spectral data for compounds 1-22 and 42-44.<sup>a</sup>

Entry	Monoisotopic mass / g·mol <sup>-1</sup>	[M+H] <sup>+</sup>	[M+2H] <sup>2+</sup>	[M+3H] <sup>3+</sup>	[M-2H] <sup>2-</sup>
1	1585.8	-	794.8 (793.9)	530.3 (529.6)	-
2	1599.8	-	800.9 (800.9)	534.2 (534.3)	-
3	1600.8	1601.5 (1601.8)	801.2 (801.4)	534.5 (534.6)	-
4	1614.8	-	808.4 (808.4)	539.3 (539.3)	806.3 (806.4)
5	1614.8	-	808.4 (808.4)	539.3 (539.3)	806.2 (806.4)
6	1628.8	-	815.4 (815.4)	543.9 (543.9)	813.2 (813.4)
7	1632.9	-	818.3 (817.5)	545.9 (545.3)	816.3 (815.5)
8	1646.9	-	824.4 (824.5)	549.9 (550.0)	-
9	1585.8	-	793.9 (793.9)	529.6 (529.6)	791.8 (791.8)
10	1599.8	-	800.7 (800.9)	534.2 (534.3)	-
11	1600.8	-	801.2 (801.4)	534.5 (534.6)	799.0 (799.4)
12	1614.8	1615.3 (1615.8)	808.1 (808.4)	539.1 (539.3)	-
13	1614.8	1615.7 (1615.8)	808.4 (808.4)	539.3 (539.3)	806.2 (806.4)
14	1628.8	1630.0 (1629.8)	815.4 (815.5)	543.9 (543.9)	813.3 (813.4)
15	1632.9	-	817.4 (817.5)	545.3 (545.3)	-
16	1646.9	-	824.5 (824.5)	549.9 (550.0)	-
17	1546.8	-	774.4 (774.4)	516.8 (516.8)	772.5 (772.4)
18	1574.8	-	788.4 (788.4)	526.0 (525.9)	786.2 (786.4)
19	1455.7	1457.0 (1456.7)	728.8 (728.9)	486.2 (486.2)	-
20	1483.8	1484.7 (1484.8)	742.8 (742.9)	495.6 (495.6)	740.8 (740.9)
21	1497.8	-	749.8 (749.9)	500.2 (500.3)	-
22	1521.8	1522.6 (1522.8)	761.8 (761.9)	508.2 (508.3)	508.2 (508.3)
42	1575.8	-	788.9 (788.9)	526.3 (526.3)	786.7 (786.9)
43	1564.8	-	783.4 (783.4)	522.6 (522.6)	781.3 (781.4)
44	1351.6	-	676.7 (676.8)	451.4 (451.5)	674.7 (674.8)

<sup>a</sup> Observed mass-to-charge (m/z) ratio is shown in the table, the calculated m/z ratio is given in brackets.

**6.5.2 RP-HPLC****Table S2** Retention time of compounds **1-22** and **42-44** measured with RP-HPLC.

Entry	R <sub>t</sub> /min	Gradient
1	12.0	18→40.5 % <sup>a</sup>
2	11.8	18→40.5 % <sup>a</sup>
3	12.5	18→40.5 % <sup>a</sup>
4	12.7	18→40.5 % <sup>a</sup>
5	13.3	18→40.5 % <sup>a</sup>
6	12.9	18→40.5 % <sup>a</sup>
7	15.9	18→40.5 % <sup>a</sup>
8	16.7	18→40.5 % <sup>a</sup>
9	7.6	18→40.5 % <sup>a</sup>
10	7.0	18→40.5 % <sup>a</sup>
11	11.6	18→40.5 % <sup>a</sup>
12	13.2	18→40.5 % <sup>a</sup>
13	11.6	18→40.5 % <sup>a</sup>
14	11.7	18→40.5 % <sup>a</sup>
15	16.5	18→40.5 % <sup>a</sup>
16	16.7	18→40.5 % <sup>a</sup>
17	18.2	0→36 % <sup>b</sup>
18	18.5	0→36 % <sup>b</sup>
19	9.8	18→40.5 % <sup>a</sup>
20	12.2	18→40.5 % <sup>a</sup>
21	13.5	18→40.5 % <sup>a</sup>
22	13.9	18→40.5 % <sup>a</sup>
42	11.5	9→45 % <sup>c</sup>
43	12.0	9→45 % <sup>c</sup>
44	11.4	9→45 % <sup>c</sup>

<sup>a</sup> 18 % acetonitrile over 2 min followed by 18→40.5 % acetonitrile in 0.1 % TFA over 20 min at flow rate 1 mL/min <sup>b</sup> 0 % acetonitrile over 2 min followed by 0→36 % acetonitrile in 0.1 % TFA over 20 min at flow rate 1 mL/min. <sup>c</sup> 9 % acetonitrile over 2 min followed by 9→45 % acetonitrile in 0.1 % TFA over 20 min at flow rate 1 mL/min.

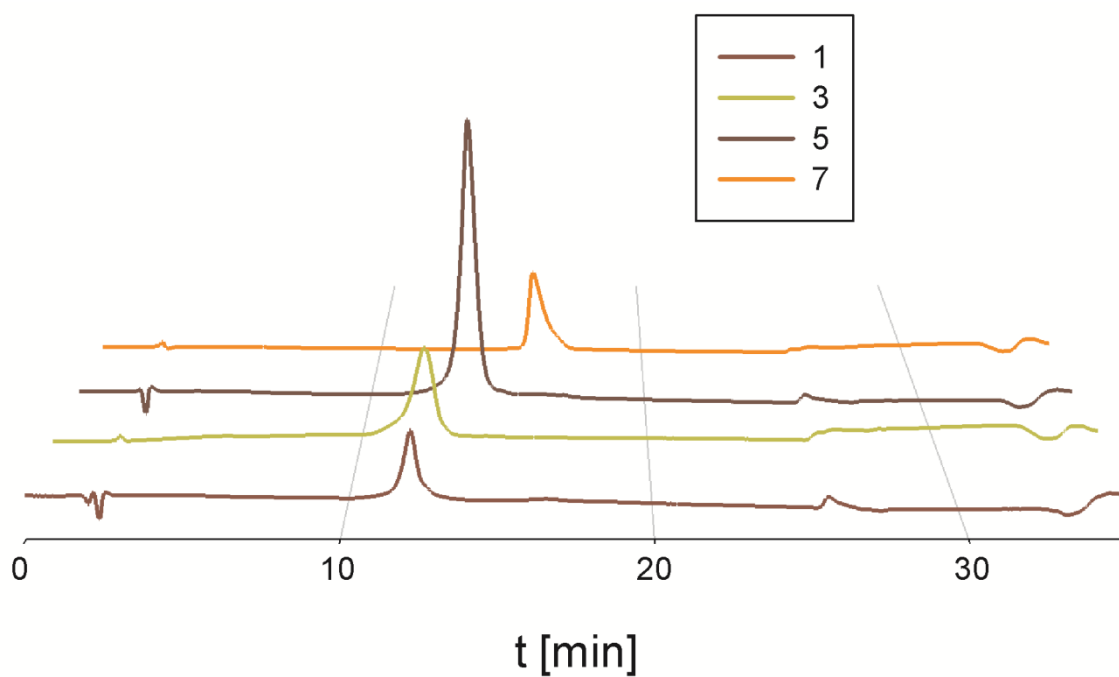


**Fig. S1** HPLC chromatogram of purified **1**, **3**, **5** and **7** recorded at 220 nm. Gradient: 18→40.5 % acetonitrile in 0.1% aq. TFA over 20 minutes at flow rate 1 mL/min.

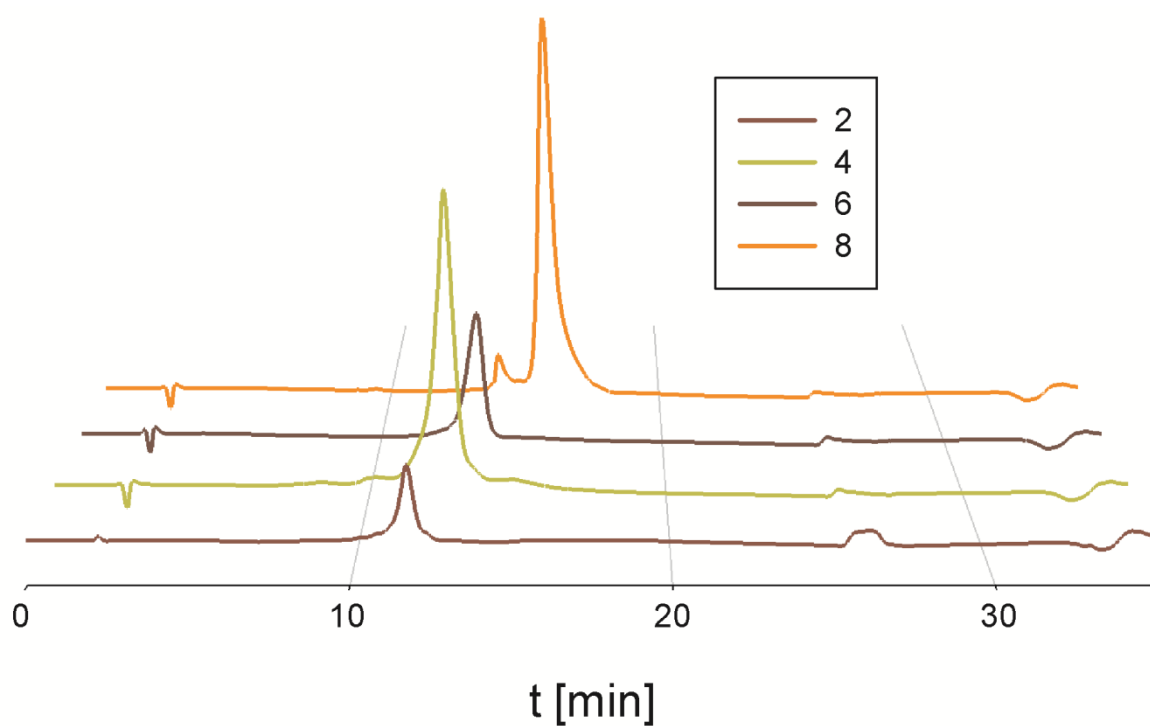


**Fig. S2** HPLC chromatogram of purified **2**, **4**, **6** and **8** recorded at 220 nm. Gradient: 18→40.5 % acetonitrile in 0.1% aq. TFA over 20 minutes at flow rate 1 mL/min.

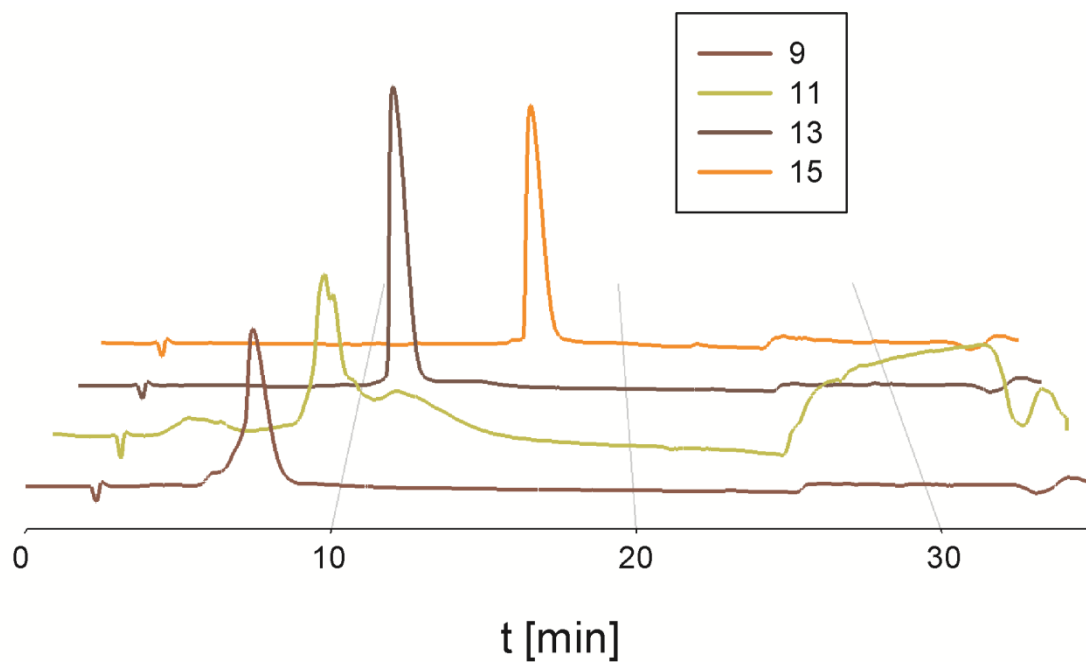


**Fig. S3** HPLC chromatogram of purified 9, 11, 13 and 15 recorded at 220 nm. Gradient: 18→40.5 % acetonitrile in 0.1% aq. TFA over 20 minutes at flow rate 1 mL/min.

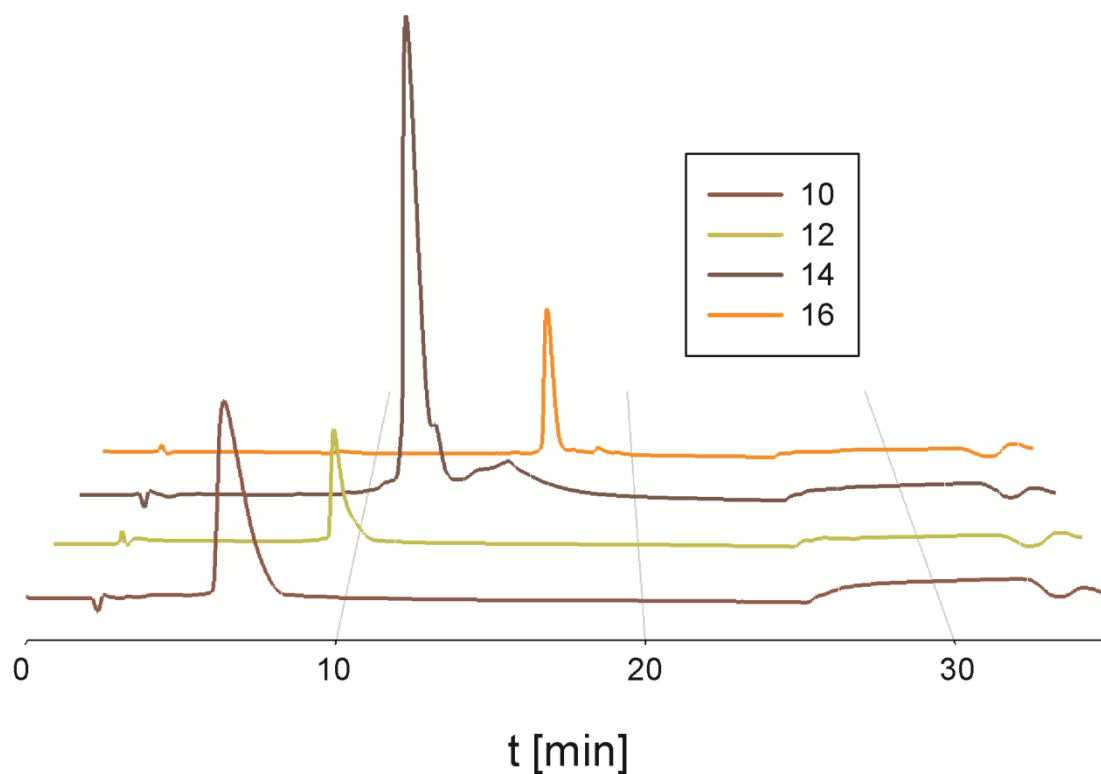


**Fig. S4** HPLC chromatogram of purified 10, 12, 14 and 16 recorded at 220 nm. Gradient: 18→40.5 % acetonitrile in 0.1% aq. TFA over 20 minutes at flow rate 1 mL/min.



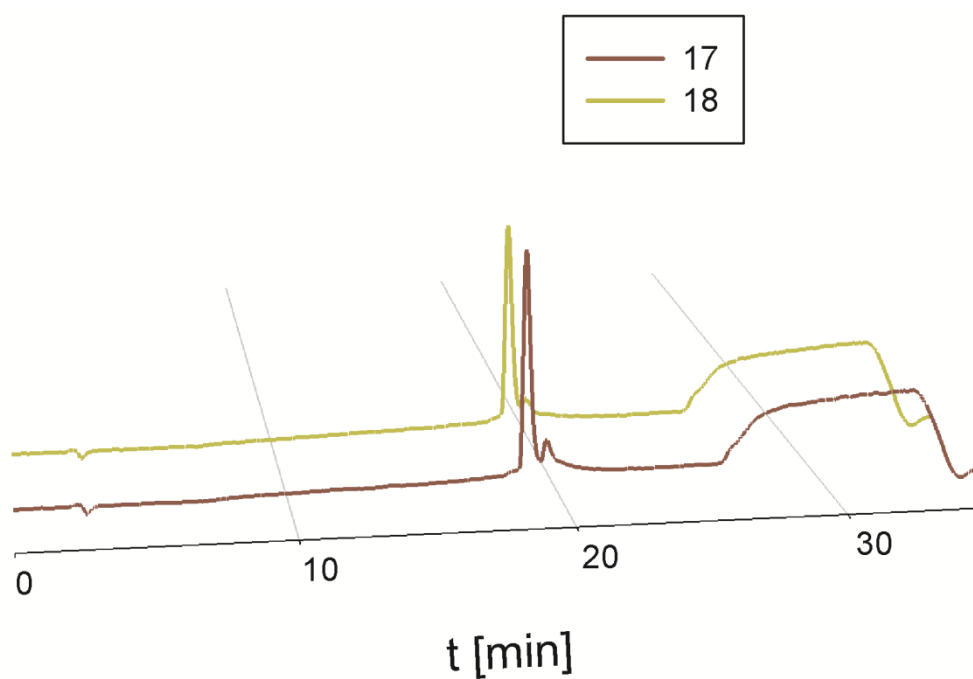


**Fig. S5** HPLC chromatogram of purified **17** and **18** recorded at 220 nm. Gradient: 0→36 % acetonitrile in 0.1% aq. TFA over 20 minutes at flow rate 1 mL/min.

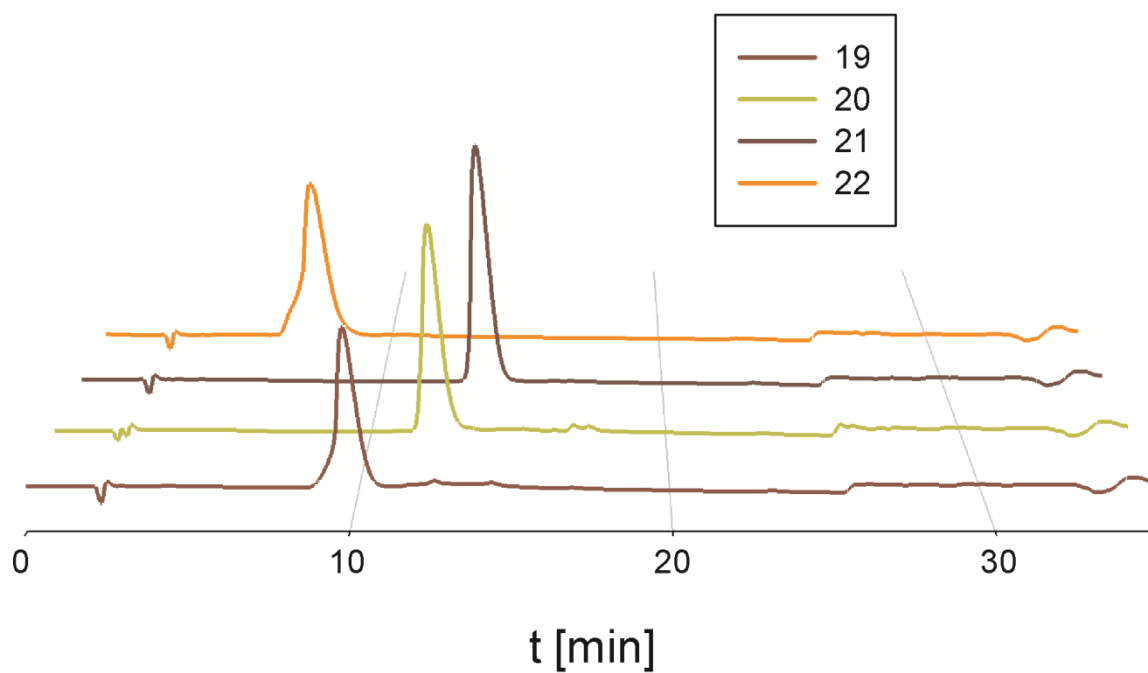


**Fig. S6** HPLC chromatogram of purified **19**, **20**, **21** and **22** recorded at 220 nm. Gradient: 18→40.5 % acetonitrile in 0.1% aq. TFA over 20 minutes at flow rate 1 mL/min.

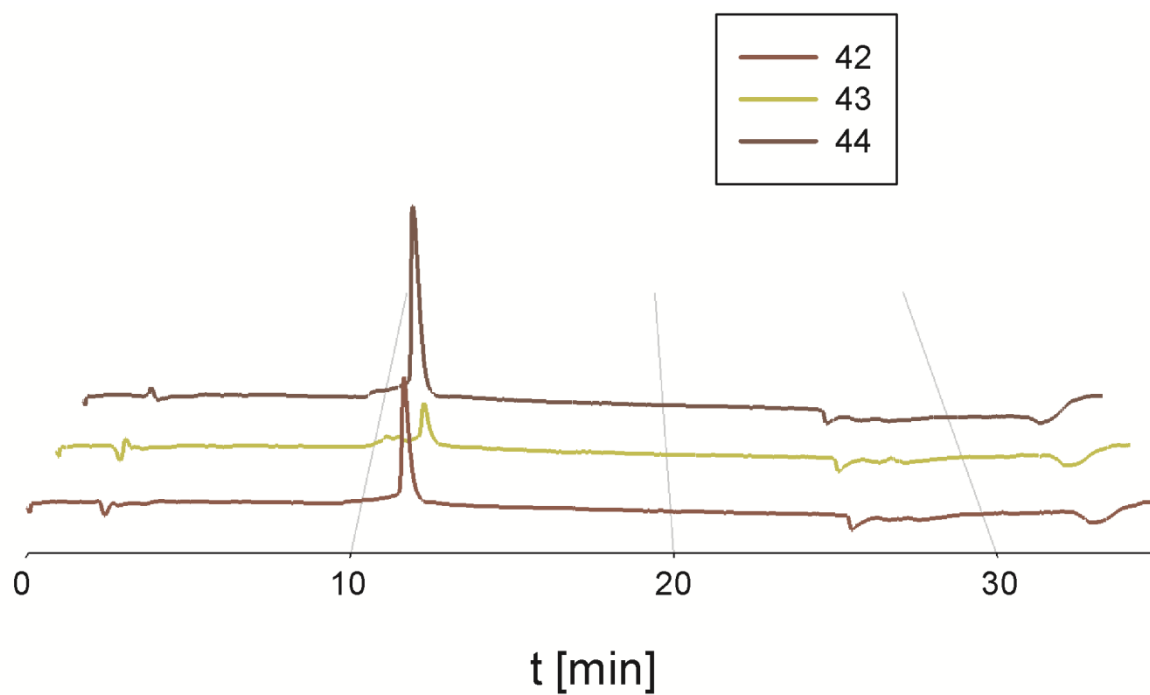


**Fig. S7** HPLC chromatogram of purified **42**, **43** and **44** recorded at 220 nm. Gradient: 9→45 % acetonitrile in 0.1% aq. TFA over 20 minutes at flow rate 1 mL/min.

### 6.5.3 Plotted Kinetic Data

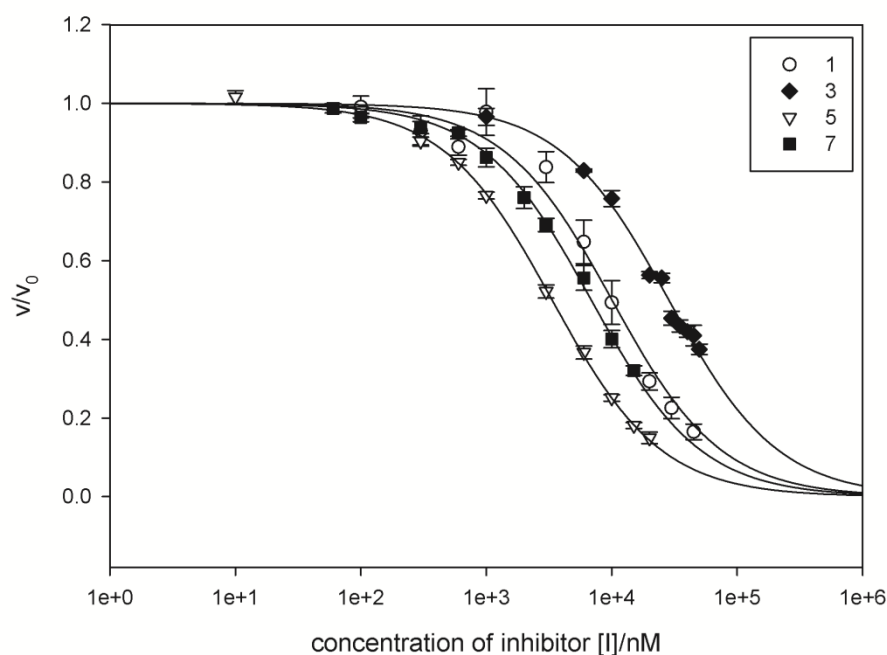


**Fig. S8** Dose-response curves for the inhibition of matriptase-catalyzed proteolysis of chromogenic substrate Boc-QAR-pNA with the X-axis on a logarithmic scale. Comparison of disulfide-bridged inhibitors **1** (white circle), **3** (black diamond), **5** (white triangles) and **7** (black squares) at pH 7.6. Data points are arithmetic means of three experiments and error bars are given as the standard deviation.

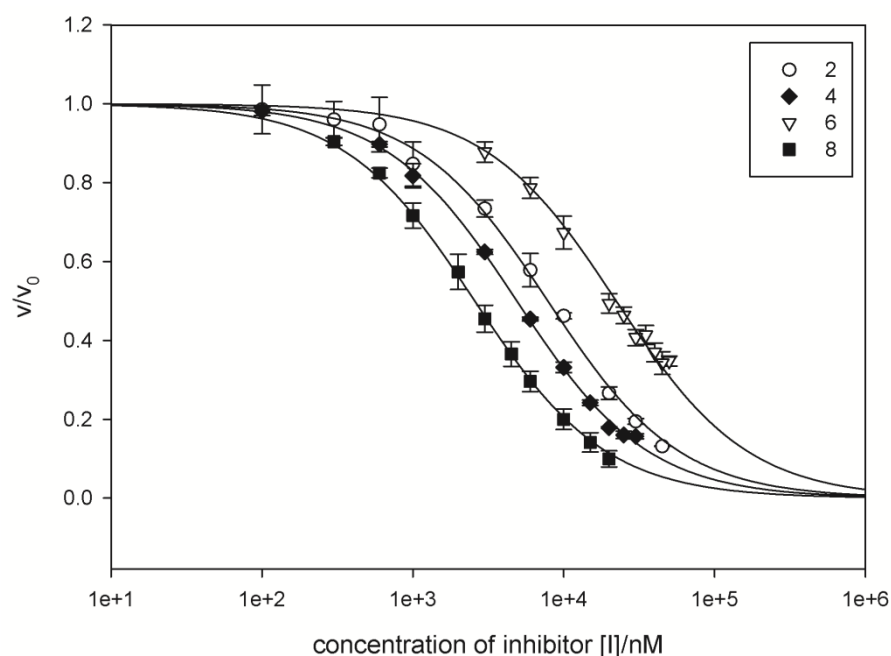


**Fig. S9** Dose-response curves for the inhibition of matriptase-catalyzed proteolysis of chromogenic substrate Boc-QAR-pNA with the X-axis on a logarithmic scale. Comparison of disulfide-bridged inhibitors **2** (white circle), **4** (black diamond), **6** (white triangles) and **8** (black squares) at pH 7.6. Data points are arithmetic means of three experiments and error bars are given as the standard deviation.

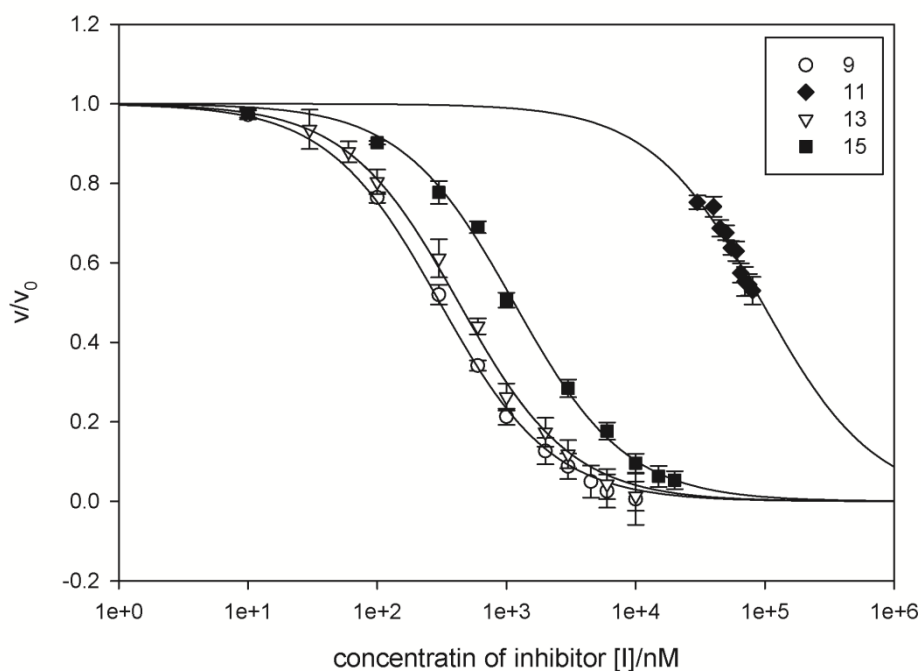


**Fig. S10** Dose-response curves for the inhibition of matriptase-catalyzed proteolysis of chromogenic substrate Boc-QAR-pNA with the X-axis on a logarithmic scale. Comparison of disulfide-bridged inhibitors **9** (white circle), **11** (black diamond), **13** (white triangles) and **15** (black squares) at pH 7.6. Data points are arithmetic means of three experiments and error bars are given as the standard deviation.

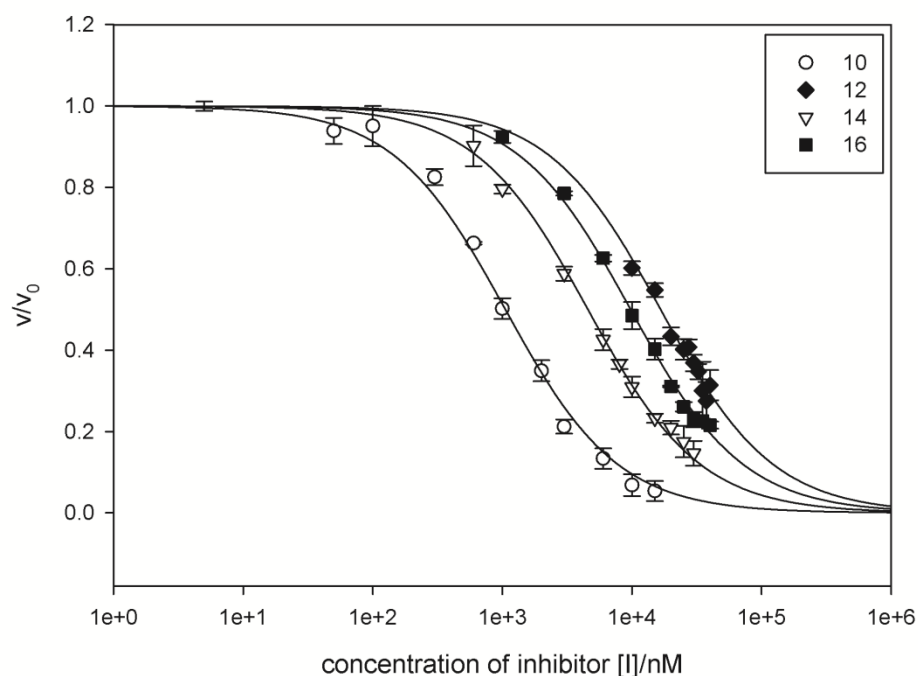


**Fig. S11** Dose-response curves for the inhibition of matriptase-catalyzed proteolysis of chromogenic substrate Boc-QAR-pNA with the X-axis on a logarithmic scale. Comparison of disulfide-bridged inhibitors **10** (white circle), **12** (black diamond), **14** (white triangles) and **16** (black squares) at pH 7.6. Data points are arithmetic means of three experiments and error bars are given as the standard deviation.

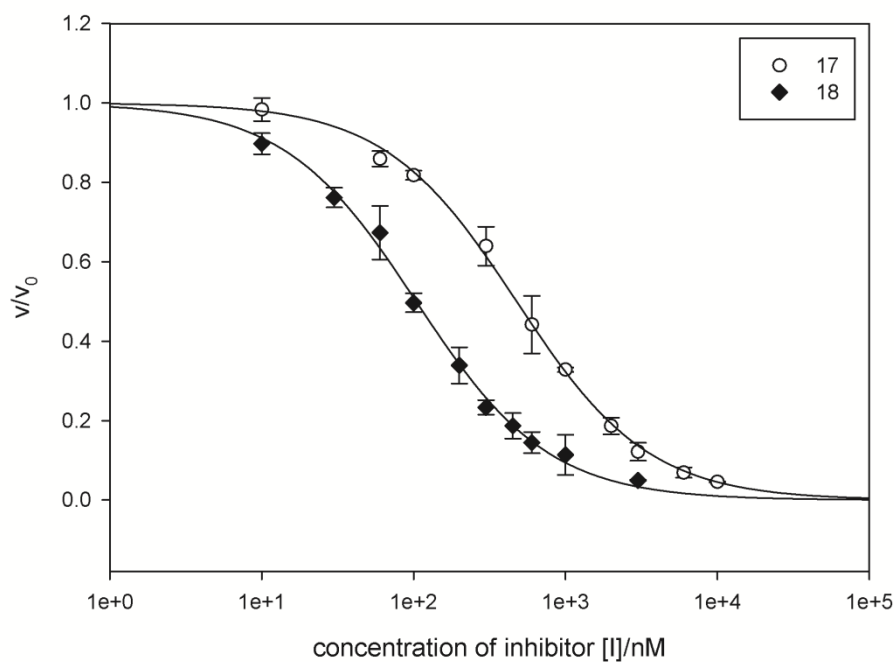


**Fig. S12** Dose-response curves for the inhibition of matriptase-catalyzed proteolysis of chromogenic substrate Boc-QAR-pNA with the X-axis on a logarithmic scale. Comparison of disulfide-bridged inhibitors **17** (white circle) and **18** (black diamond) at pH 7.6. Data points are arithmetic means of three experiments and error bars are given as the standard deviation.

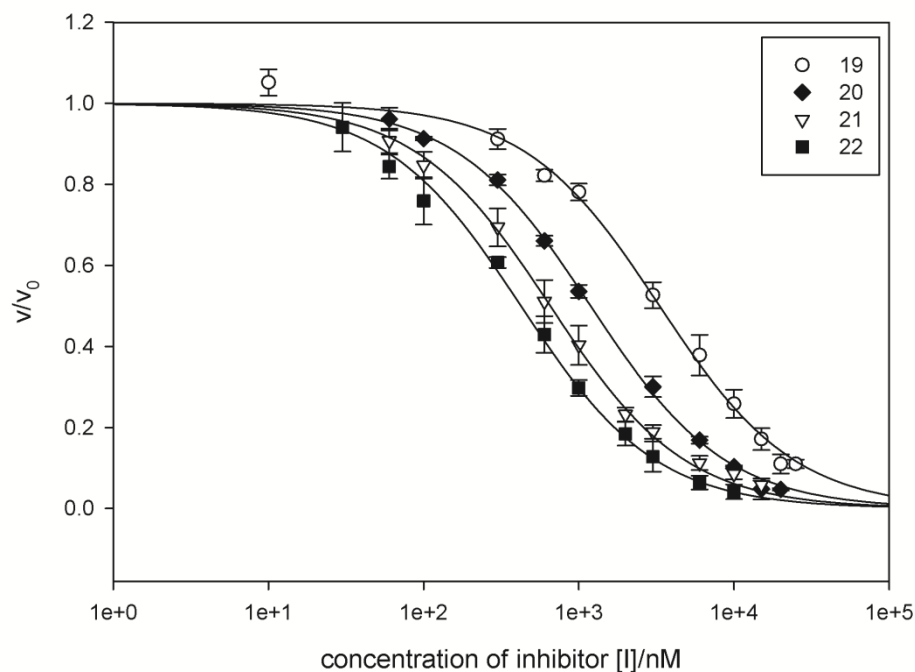


**Fig. S13** Dose-response curves for the inhibition of matriptase-catalyzed proteolysis of chromogenic substrate Boc-QAR-pNA with the X-axis on a logarithmic scale. Comparison of disulfide-bridged inhibitors **19** (white circle), **20** (black diamond), **21** (white triangles) and **22** (black squares) at pH 7.6. Data points are arithmetic means of three experiments and error bars are given as the standard deviation.

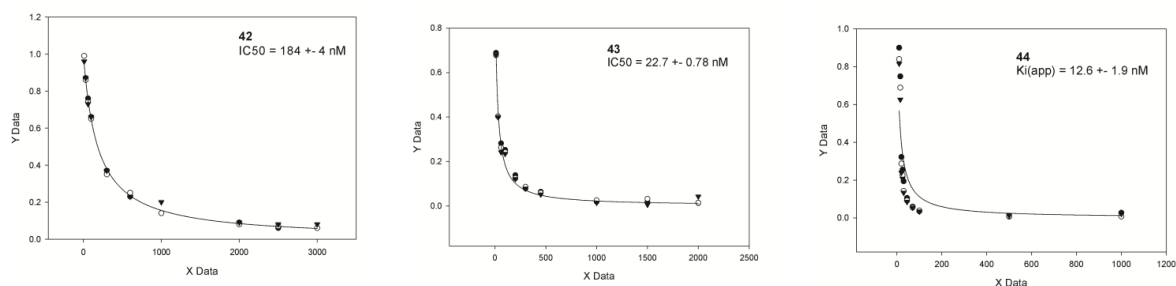


**Fig. S14** Dose-response curves for the inhibition of matriptase-catalyzed proteolysis of chromogenic substrate Boc-QAR-pNA of compound **42** (left), **43** (middle) and **44**(right).

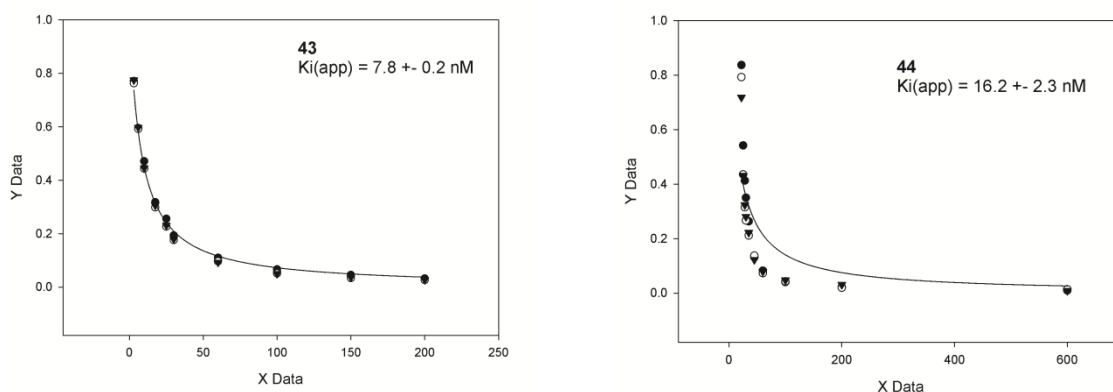


**Fig. S15.** Dose-response curves for the inhibition of matriptase-catalyzed proteolysis of chromogenic substrate Boc-QAR-pNA at pH 8.5 of compound **43** (left) and **44**(right).

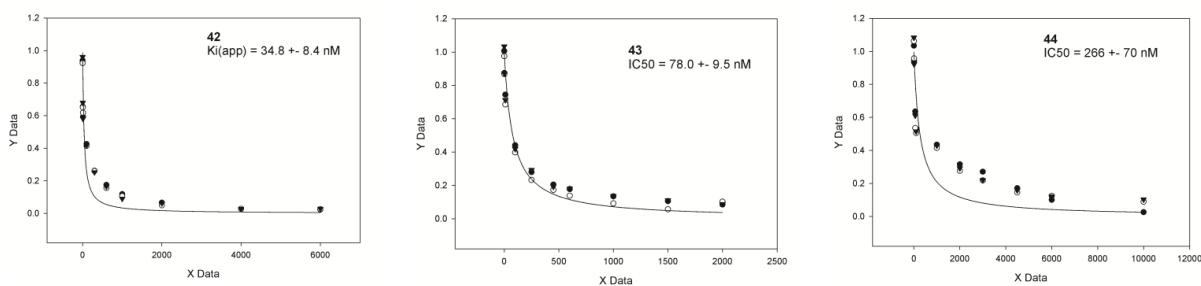
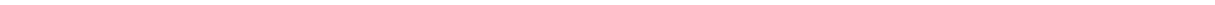


**Fig. S16** Dose-response curves for the inhibition of trypsin-catalyzed proteolysis of chromogenic substrate Boc-QAR-pNA of compound **42** (left), **43** (middle) and **44**(right).







---

Dipl. Ing.  
**Martin Empting**  
Tulpenhofstr. 7  
63067 Offenbach  
0171 – 8389854  
empting@biochemie-TUD.de

Offenbach, den 02.11.2012

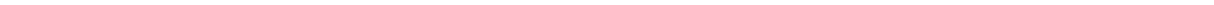
### **Eidesstattliche Erklärung**

Ich erkläre hiermit an Eides Statt, dass ich meine Dissertation selbständig und nur mit den angegebenen Hilfsmitteln angefertigt habe.

---

Dipl. Ing. Martin Empting

---



---

Dipl. Ing.  
**Martin Empting**  
Tulpenhofstr. 7  
63067 Offenbach  
0171 – 8389854  
empting@biochemie-TUD.de

Offenbach, den 02.11.2012

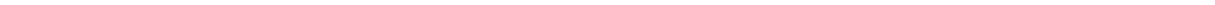
### Erklärung

Ich erkläre hiermit, noch keinen Promotionsversuch unternommen zu haben.

---

Dipl. Ing. Martin Empting

---



---

## LEBENS LAUF

Dipl. Ing.  
**Martin Empting**

Tulpenhofstr. 7  
63067 Offenbach  
0171 – 8389854  
empting@biochemie-TUD.de

### *Persönliche Daten*

---

Geburt: 28. März 1983 in Königs Wusterhausen  
Nationalität: deutsch  
Familienstand: ledig

### *Akademischer Werdegang*

---

März 2009 bis  
Dezember 2012: **Promotion** am Clemens-Schöpf-Institut für Organische Chemie und Biochemie der Technischen Universität Darmstadt unter der Betreuung von Prof. Dr. Harald Kolmar

Oktober 2003 bis  
Februar 2009: **Diplomstudium in Chemie**, Technische Universität Darmstadt.  
Titel der Diplomarbeit:  
*'Application of Copper(I)-Catalyzed Azide Alkyne Cycloaddition to the Synthesis of Template-Assembled Multivalent Peptide Conjugates'*  
Betreuer: Prof. Dr. Harald Kolmar

### *Schulbildung*

---

1994-2002 Kaiserin-Friedrich-Gymnasium, Bad Homburg v. d. Höhe  
Abschluss: Abitur (Note: 1,5)

1989-1994 Grundschule IV, Königs Wusterhausen

---

Dipl. Ing. Martin Empting

---

